UNIVERSITE DE STRASBOURG

ÉCOLE DOCTORALE DES SCIENCES DE LA VIE ET DE LA SANTE (ED 414)
UMR_S 1113 - UNISTRA – INSERM
Interface Recherche Fondamentale Appliquée en Cancérologie

THÈSE présentée par

Aïna VENKATASAMY

Soutenue le 17 décembre 2020

Pour obtenir le grade de : **Docteur de l'Université de Strasbourg**
Discipline/ Spécialité : **Aspects Moléculaires et Cellulaires de la Biologie**

Développement et utilisation d'outils d'analyses précliniques pour le traitement du cancer de l'estomac

---

THÈSE dirigée par :
Mr MELLITZER Georg, Directeur de Recherche, Université de Strasbourg
Mr ROMAIN Benoît, Médecin, Directeur de Recherche, Université de Strasbourg

---

RAPPORTEURS :
Madame Christine HOEFFEL, Professeur de radiologie, Université de Reims Champagne-Ardenne
Monsieur Dominik VON ELVERFELDT, Professeur, Radiologische Klinik Medizin Physik, Universitätsklinikum Freiburg, Allemagne

AUTRES MEMBRES DU JURY :
Mme Eliette TOUATI, Directeur de recherche, Institut Pasteur
Mr Patrice LAQUERRIERE, Professeur, Institut Pluridisciplinaire Hubert Curien, CNRS

REMERCIEMENTS

To my jury members Dr Eliette Touati, Pr Christine Hoeffel, Pr Dominik von Elverfeldt and Pr Patrice Laquerriere, thank you very much for this honor.

A Christian Gaiddon, Georg Mellitzer, Benoit Romain, Eric Guerin, Véronique Devignot, Christophe Orvain et toute la team de l'UMR_S 1113 - UNISTRA – INSERM - Interface Recherche Fondamentale Appliquée en Cancérologie, pour avoir fait le pari d'accueillir une jeune radiologue dans votre équipe et pour avoir su me guider, me soutenir et m'encourager au travers des méandres de la recherche pré-clinique de ces cinq années.

Au Dr Wilfried Reichardt et toute l'équipe de Medizin Physik de Universitätsklinikum Freiburg, pour m'avoir montré l'efficacité et l'organisation à l'allemande, dans un environnement de travail vraiment idéal.

A madame le Professeur Flanagan et monsieur le Professeur Bond, pour les afterworks Londoniens et toute la génomique des cancers glissée entre.

A monsieur le Professeur Veillon, pour m'avoir ouvert les yeux sur un certain nombre de choses que je ne voulais pas forcément voir.

A monsieur le Professeur Gallix, pour cette nouvelle aventure qui commence.

A mes co-doctorants (Gilles, Alex, Anaïs B, Justine, Amandine, Christelle…), compagnons de manips qui marchent très bien – en théorie – *pour l'impossible nous demandons de prévoir 48h de délai*.

A mes amis, Alexandra, Anaïs P., Anne, Nina, Sarah, Robin, Matthieu B., Pouki, Marion, Aurélie B., Samuel, Laure, Antoine, Florence, Aude et tous les autres…, pour votre soutien indéfectible depuis tant d'années.

Aux essentiels : papa, maman, Luc.

Table des matières

Résumé des travaux de thèse – VERSION FRANÇAISE

Introduction

Le cancer gastrique est le 5ème cancer en termes de fréquence et le 3ème en termes de mortalité dans le monde, avec une survie à 5 ans d'environ 36% pour les cancers opérables, qui chute à 5-20% en cas de cancer localement avancé ou métastatique. L'arsenal thérapeutique standard du cancer gastrique est centré sur une prise en charge chirurgicale à visée curative, encadrée par une chimiothérapie néo adjuvante/adjuvante basée sur les dérivés de platine. Cependant, la survie médiane est faible, à environ 11 mois. Le mauvais pronostic des cancers gastriques apparait multifactoriel *i)* leur fréquente (~65%) découverte à un stade tardif (inopérable ou métastatique) du fait de l'absence de moyens de diagnostic précoce non invasif (faible place de l'imagerie, nécessité d'une endoscopie digestive haute avec biopsies pour le diagnostic…), *ii)* la chimiorésistance aux dérivés de platines dans les stades avancés (75% des cas) et *iii)* la survenue conjointe d'une cachexie et d'une atrophie musculaire (=sarcopénie) dans environ 30 à 60% des cas. Cette cachexie/sarcopénie est un facteur reconnu de mauvais pronostic pour de nombreux cancers et serait responsable d'environ 20 à 25% de la mortalité liée au cancer. Elle apparait *i)* indépendante du stade tumoral, *ii)* indépendante des traitements (car présente parfois au diagnostic) et *iii)* indépendante du statut nutritionnel et pourrait représenter un axe thérapeutique potentiel. Récemment, deux nouvelles classifications moléculaires des adénocarcinomes gastriques ont engendré d'importants espoirs de thérapeutiques ciblées. Cependant, la plupart des thérapies ciblées sont pour l'instant restées au stade expérimental car les différents essais (réalisés sans stratification des patients) ont donné des résultats plutôt décevants (excepté le trastuzumab dans les cancers HER2 positifs). De nombreux progrès restent donc à faire dans ce domaine, que ce soit en matière de diagnostic, de traitement, ou de prise en charge des complications liées à la tumeur et/ou au traitements.

Le but de mon travail de thèse est de développer et de caractériser des modèles animaux qui soient représentatifs de la diversité et de la complexité des cancers gastriques. Le but est d'être capable in fine de mettre en place des protocoles expérimentaux permettant le développement et l'étude longitudinale de thérapies innovantes prenant compte de l'ensemble de l'écosystème tumoral dans son ensemble (cellule tumorale, microenvironnement, macro-environnement et tissus environnants notamment les muscles). Pour ce faire, nous avons combiné le développement de modèles de xénogreffes dérivées de patients, la recherche et l'étude moléculaire de potentiel biomarqueurs et l'utilisation des dernières technologies d'imagerie du petit anomal. Ce projet innovant a nécessité des interactions dynamiques et synergiques entre différents services hospitaliers, des laboratoires de biologie moléculaire et d'analyses cellulaires, des laboratoires de chimie et des laboratoires de physique et d'imagerie du petit animal. Au total, mon projet s'articule autour de trois axes

1) Le développement et le maintien de plusieurs xénogreffes dérivés de patients (PDX), qui seraient représentatives de la complexité des cancers gastriques, comme le degré de différenciation des cellules cancéreuses, le statut p53 ou PD-L1…

2) La caractérisation des modèles animaux par différentes méthodes d'imagerie petit animal (échographie, ultrasons, scanner, IRM..) et leur comparaison aux données histologiques et moléculaires appariées

3) L'utilisation de ces modèles PDX pour le développement de nouvelles approches thérapeutiques dans le cancer gastrique, englobant à la fois l'étude de la tumeur, de son microenvironnement et des tissus environnants (comme le muscle).

Résultats

Mise en place de modèles de xénogreffes dérivées de patient de cancer gastrique (ARTICLES 1 et 2)

Si la majorité des modèles utilisés (82%) sont dérivés de lignées de cellules tumorales (cell-derived xenograft), 7% des modèles sont issus de fragments tumeurs humaines (patient-derived xenograft = PDX). Le modèle PDX est le seul modèle capable de refléter la variabilité inter-patient et intra-tumorale, inhérente aux cancers chez l'homme. En effet, ces modèles conservent les caractéristiques histologiques, moléculaires et génétiques des tumeurs primaires desquelles elles dérivent et restent stables au cours des passages dans les différentes générations de souris. En recherche translationnelle pré-clinique oncologique, ces modèles PDX permettent de réaliser des mesures répétées de volume tumoral et un suivi au long cours des réponses tumorales à différentes conditions (traitement anti-tumoral, modifications génétiques…), notamment grâce à une bonne corrélation avec les réponses cliniques présentées par les patients à la chimiothérapie. Dans ma thèse, j'ai créé puis pérennisé 5 modèles de xénogreffes dérivées de patients (PDX) d'adénocarcinome gastrique, en implantant en hétérotopique (sur les flancs de souris immunodéprimées athymique de type NUDE) des biopsies ou des fragments de tissus tumoraux d'adénocarcinome gastrique, avec 21% de succès à la prise de greffe (ARTICLE 1). Si de tels modèles existent déjà dans la littérature, ils sont peu nombreux (deux articles significatifs, 5 publications notables sur le sujet) avec un taux de succès similaire au notre (25 à 34%) et des taux de lymphoprolifération significatifs, en fonction du receveur murin choisi (NOG ou NOD). Cependant, comme dans la littérature, nous n'avons pas réussi à développer de modèles de PDX à cellules isolées, probablement en raison du trop faible pourcentage nombre de cellules tumorales présentes dans les tissus utilisés pour l'implantation initiale. Comme attendu, après vérification histologique, nos tumeurs PDX conservaient les caractéristiques cellulaires, architecturales et génétiques de leur tumeur primaire au fil des passages différentes générations de souris (jusqu'à 10 passages).

Caractérisation des modèles et imagerie du petit animal (ARTICLES 1 et 2)

Une fois les modèles PDX établis nous les avons caractérisés pour pouvoir être plus sélectifs quant à leur utilisation ultérieure pour des expériences *in vivo*. Nous avons souhaité en préciser les caractéristiques morphologiques par imagerie du petit animal. Comme attendu, nos 5 modèles PDX présentaient à la fois des différences en termes d'aspect sur l'imagerie (IRM), histologiques (hématoxyline-éosine), et immuno-histochimiques (p53, H3K9, a-smooth-actine, Ki67, PD-L1…), et morphologiques (signal T2, caractéristiques cellulaires de la tumeur estimées sur l'imagerie de diffusion). Par ailleurs, nous avons pu démontrer l'intérêt de l'échographie avec sonde haute fréquence pour le suivi longitudinal rapproché dans ces modèles PDX**.** En effet, l'échographie permet une mesure du volume tumoral plus précise qu'avec un Caliper manuel, mais également le suivi longitudinal de volume au cours d'une expérience in vivo de traitement. L'avantage indéniable de l'échographie est l'accès en temps réel (et à bas coût) à l'aspect morphologique de la tumeur et à son échostructure interne comme par exemple la présence de remaniements post-thérapeutique comme des kystes.

Utilisation des modèles pour l'étude in vivo de nouvelles thérapies (ARTICLES 2, 3 et 4)

Une fois les modèles PDX caractérisés, nous avons utilisé un de nos modèles - un adénocarcinome bien différencié (GCX-004) - pour des tests *in vivo* de molécules anti-cancéreuses. Nous avons vérifié dans un premier temps que ce modèle choisi répondait bien au traitement de chimiothérapie standard à base de dérivés de platine (cisplatine), ce qui était le cas, avec des différences en termes de volume tumoral, une augmentation de la valeur de l'ADC, des modifications histologiques (prédominance du stroma et diminution de la charge cellulaire) et moléculaires (p53). Nous l'avons ensuite testé in vivo pour évaluer la synergie des dérivés de platines avec un inhibiteur des HDAC (enzymes histones deacetylase exprimées de façon aberrantes dans plusieurs cancers dont le cancer gastrique et leur expression est liée à la cancérogénèse), l'acide suberoylanilide hydroxamic (SAHA, Vorinostat) qui a eu l'agrément de la FDA (Food and Drug Administration américaine) pour le traitement du lymphoma T cutané, avec peu d'effets secondaires sur les cellules saines. Le SAHA apparait donc comme un bon candidat anti-cancéreux dans les cancers gastriques, montrant une inhibition de la croissance cellulaire et une induction de l'apoptose dans les lignées de cellules tumorales gastriques, notamment en cas de co-traitement avec des dérivés de platine, avec une diminution du volume tumoral *in vivo*. Une autre molécule

innovante, un dérivé du ruthénium (RDC 11) est encore en phase de tests précliniques. Il induit *in vitro* une plus forte activité cytotoxique que les dérivés de platine (indépendante de p53, avec une induction d'un stress du réticulum endoplasmique dans les cellules de cancer gastrique). Dans un modèle murin syngénique de xénogreffe (lignée YTN16 de cellules de cancer gastrique de souris), il entraine un diminution plus marquée du volume tumoral comparativement aux dérivés de platine, tout en causant moins d'effets secondaires (notamment hépatiques et neurologiques) chez la souris que les dérivés de platine et apparait également comme un candidat anti-cancéreux prometteur dans le cancer gastrique.

La cachexie et la sarcopénie (ARTICLES 5, 6 et 7)

Le cancer gastrique est complexe biologiquement et moléculairement. Au-delà de la tumeur et du microenvironnement tumoral, le macro-environnement global joue également un rôle pronostic. En effet, un des facteurs de mauvais pronostic est la survenue (parfois dès le stade initial dans 6 à 13% des cas) d'une cachexie-sarcopénie, qui peut être liée à la fois à la tumeur mais aussi favorisée/majorée par les traitements, notamment les chimiothérapies. Elle surviendrait dans 30 à 60% des cas. Dans le cadre de notre approche translationnelle, nous avons étudié le cancer gastrique et la cachexie / sarcopénie, à la fois chez les patients et dans nos modèles animaux. Chez l'homme, nous avons étudié la place de la jéjunostomie dans l'arsenal thérapeutique de la prise en charge des cancers de l'estomac, notamment faciliter la réalisation de l'ensemble des cycles de chimiothérapie et en support nutritionnel quant à la survenue d'une sarcopénie. Nous avons évalué le degré de sarcopénie selon la méthode de Prado et al., sur des mesures de surface des muscles psoas et para-vertébraux à la hauteur du corps vertébral de L3, sur des scanners abdominaux en coupe axiale. Dans le groupe ayant bénéficié de la jéjunostomie d'alimentation, il y avait 13% de patients sarcopéniques avant chimiothérapie contre 22.6% après chimiothérapie néo-adjuvante versus respectivement 6.7% puis 60% dans le groupe contrôle, soulignant l'intérêt d'une prise en charge multifactorielle des cancers, d'autant plus que la jéjunostomie d'alimentation permettait également aux patients atteints de cancer gastrique de parvenir à compléter l'ensemble de leurs cycles de chimiothérapie. Dans notre étude, il était intéressant de noter qu'il n'y avait pas de retour à la normale possible chez les patients sarcopéniques dès le stade initial - et ce malgré la prise en charge nutritionnelle - soulignant l'intérêt d'un dépistage précoce de ces pathologies. La méthode d'estimation de la sarcopénie basée sur l'imagerie abdominale que nous avons utilisée n'a encore jamais été appliquée à l'heure actuelle chez l'animal. Il est possible de créer un modèle animal de souris sarcopénique, en injectant une dose unique de 20mg/kg de doxorubicine en injection intrapéritonéale unique chez la souris C57/BL6. Nous avons donc en parallèle cherché à mieux comprendre la survenue d'une sarcopénie chez l'animal par cette méthode d'induction rapide. En effet, la perte de masse musculaire est rapide, survenant en 3 à 5 jours et définitive. Nous avons également constaté qu'un tel traitement entraine des modifications transcriptomiques, avec la down-régulation de certains gènes et l'up-régulation d'autres. Dans une expérience longitudinale avec un traitement à J1 de souris wild type C57/BL6) par injection intrapéritonéale doxorubicine, une baisse de 20-25% de la masse musculaire au niveau des muscles gastrocnémiens (muscles de la patte) dans le groupe traité, avec une diminution débutant à J3 et se poursuivant jusqu'à J5, corrélée à l'expression d'ubiquitines ligases pro-atrophiques. Cette atrophie musculaire chimio-induite entraine l'induction de l'expression de plusieurs genes (MURF-1 / Trim63 ubiquitine ligase), notamment des gènes impliqués dans l'autophagie, la croissance cellulaire et les dommges à l'ADN, avec activation des gènes cibles TP53 et Tap63. D'autres voies sont down-régulées, notamment celles impliquées dans l'adhésion cellulaire et les composants de la matrice extracellulaire et ceux liés au développement des muscles squelettiques. En imagerie (CT), en appliquant la même méthode d'analyse que chez l'homme (avec une mesure à la hauteur des hiles rénaux), nous retrouvions une diminution d'environ 15% en 5 jours de la surface musculaire des muscles paravertébraux des souris traitées, corrélée à une surexpression de certains marqueurs musculaires comme MURF comparativement aux souris contrôles. Ces constatations TDM ont été par la suite confirmées en IRM imagerie *ex vivo* (diminution 29%). En parallèle, nous avons constaté des différences en termes de surface musculaire para vertébrale entre les différents modèles PDX non traités, suggérant l'implication de facteurs liés à la tumeur dans la survenue de modifications du macro-environnement tumoral. De plus, après traitement d'un modèle PDX par cisplatine, nous retrouvions la même diminution de la surface musculaire para vertébrale (28%)

8

observée avec la doxorubicine, ce qui n'avait encore jamais été décrit pour des dérivés de platine, confirmant le caractère complexe et probablement multifactoriel de la survenue d'une sarcopénie.

Conclusion et perspectives

Mon travail de thèse a permis la mise en place de différents modèles animaux et plusieurs protocoles expérimentaux qui seront utiles pour relever les défis posés par la complexités des cancers, et notamment du cancer gastrique. Les études réalisés posent les prémisses du développement d'outils innovants pour le suivi de la croissance tumorale, l'étude des variations de la constitution du microenvironnement (ex. paysage immunitaire) et l'impact de la tumeur et des traitements sur le macro-environnement (ex. les muscles), qui sont des éléments clés à considérer pour le développement futur de biomarqueurs notamment pour des thérapies plus personnalisées ou pour évaluer l'activité de nouvelles biothérapies ciblées. Nous avons déjà commencé à appliquer ces protocoles pour évaluer l'activité *in vivo* de thérapies anticancéreuses innovantes développées par notre laboratoire (HDACi, RDC11…).

Au final, même si mes travaux de thèse de science sont centrés sur le cancer gastrique, tout ce que j'ai pu apprendre au cours de ces 4 années de thèse et de ma mobilité à Oxford et à Fribourg concernant le développement, l'utilisation et la mise en place de protocole d'imagerie des modèles animaux en recherche pré-clinique pourra *in fine* trouver applications et généralisations à d'autres pathologies cancéreuses – ou non. En tant que radiologue, travailler sur de tels modèles animaux m'a permis d'avoir un accès direct à des changements morphologiques et carcinologiques d'organes et de systèmes, avec la possibilité d'observer le développement de tumeurs à des stades très précoces – avec un suivi rapproché, longitudinal et standardisé – ce qui n'est pas toujours possible chez nos patients. En somme, le développement de nouveaux biomarqueurs, de nouvelles techniques d'imagerie plus rapides et plus précises et l'amélioration de nos outils existants sont essentiels, à l'heure où les thérapies ciblées et des traitements plus personnalisés sont la priorité des médecins d'aujourd'hui. Pour ce faire, nous avons besoin de modèles animaux plus réalistes, plus proches des caractéristiques des patients et de la complexité de leurs tumeurs. Au final, le futur sera sans doute un *diagnostic intégré*, combinant à la fois histologie, imagerie, analyses moléculaires et génétiques, avec le développement de nouveaux biomarqueurs et la possibilité d'offrir des traitements plus personnalisés et plus adaptés à nos patients.

ARTICLES LIES AU TRAVAIL DE THESE :

Publiés:
- Voisinet M., Venkatasamy A., Alratrout H., Delhorme JB, Brigand C., Rohr S, Gaiddon C., Romain B. (2020). How to prevent Sarcopenia Occurrence during Neoadjuvant Chemotherapy for Oesogastric Adenocarcinoma ? Nutrition and Cancer, 1-7
- Licona C., Delhorme JB, Riegel G, Vidimar V, Cerón-Camacho R, Boff B, Venkatasamy A, Tomasetto C, da Silva Figueiredo Celestino Gomese P, Rognan D, Freund JN, Le Lagadec R., Pfeffer M, Gross I, Mellitzer G, and Gaiddon C*. Anticancer activity of Ruthenium and Osmium Cyclometalated compounds: Identification of ABCB1 and EGFR as resistance mechanisms. Inorganic Chemistry Frontier, 2020, DOI: 10.1039/C9QI01148J
- Spaety ME., Gries A., Badie A., Venkatasamy A., Romain B., Orvain C, Pfeffer S. (2019). HDAC4 Levels Controls Sensibility towards Cisplatin in Gastric Cancer via the p53-p73/BIK Pathways. Cancers, 11(11), 1747
- Vidimar V., Licorna C., Ceron-Camacho R., Guerin E., Coliat P., Venkatasamy A., Ali . Guenot D., Le Lagadec R. Jung AC. Freund JN., Pfeffer M. Mellitzer G., Sava G., Gaiddon C. (2019). A redox ruthenium compound directly targets PHD2 and inhibits the HIF1 pathway to reduce tumor angiogenesis independently of p53. Cancer Lett. 2019 Jan;440-441:145-155
- Manfredelli S., Delhorme JB., Venkatasamy A., Gaiddon C., Brigand C., Rohr S., Romain B. (2017). Could a feeding jejunostomy be integrated into a standardized preoperative management of oesogastric junction adenocarcinoma? Annals of Surgical Oncology, 24 (11), 3324-3330

En cours de soumission :
- Venkatasamy A., Guerin E., Blanchet A., Orvain C., Devignot V., …., Chenard MP., Romain B., Mellitzer G., Gaiddon C. Ultrasonic evaluation of gastric cancer patient-derived xenografts shows different impact between cisplatin and suberoylanilide hydroxamic acid (SAHA) on tumor structure.
- Riegel G., Orvain C., Barthe A., Schleiss C., Venkatasamy A., Poschet G., Yamamoto M., Nomura S., Tetsuya T., Pfeffer M., Mellitzer G., Gaiddon C.. Targeting gluthathione metabolism in gastric cancer : A non-conventional target for ruthenium-based compounds.

En préparation :
- Venkatasamy A., Guerin E., Reichardt W, Chenard MP., Romain B., Mellitzer G., Gaiddon C.. Characterization of the immune check-points and sarcopenia in patient-derived xenografts of gastric cancers
- Griess A., Badie A., Venkatasamy A., Spaety ME, Kurtz JE, Romain B. Mellitzer G., Gaiddon C.. Inhibition of HDAC synergies chemotherapy via p53 in gastric cancer.
- De Abreu P, Barthe A, Von Grabowiecky Y, Venkatasamy A, Aberdam D, Mellitzer G, Gaiddon C.. Role of the TAp63 in the regulation of Trim63 in chemotherapy-induced cachexia

1. INTRODUCTION: Gastric cancer: a cancer of poor prognosis. Why?

1.1. Epidemiology and risk factors of gastric cancer

Gastric cancer represents the **5th highest incidence of cancer worldwide and the 3rd highest cause of cancer-related deaths**, with geographical (Asian : Japan, Korea and China, Eastern/Central European and South American predominance), as well as socioeconomical variations in its incidence [1-2]. They are clinically separated between proximal (cardia, close to the oesogastric junction, *Figure 1*) and distal cancers (body, fundus, antrum, pyloric region) based on their anatomical location. Incidence rate and risk factors have showed differences according to the tumor location, with an upward trend for proximal cancer cases [2]. In France, the overall incidence of gastric cancer is decreasing, especially for body and antrum tumors, while an increase of cases of diffuse cancers (linitis) and eso-gastric junction tumors have been observed.
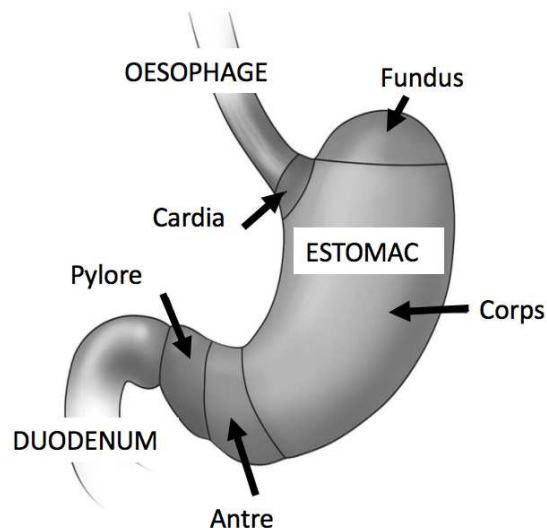
Figure 1. Schematic representation of the different portions of the stomach.

Gastric cancer is a heterogeneous disease, with multiple environmental etiologies and several alternative pathways of carcinogenesis. The major environmental risk factor for gastric cancer is a chronic *Helicobacter Pylori* infection *(Marshall, 1983)* which leads to chronic gastric atrophy [3-5]. Several consecutive lesions induced by a chronic *Helicobacter Pylori* infection may result in the development of sporadic gastric cancers (intestinal type) with a 6-fold increased risk compared to non-infected patients [5]. Chronic *Helicobacter Pylori* may also lead to atrophic gastritis (1.7 to 4.9-fold increased relative cancer risk) and intestinal metaplasia (6.4-fold increased cancer risk) [5]. If *Helicobacter Pylori* represents the most common risk factor of gastric cancer development, it is only accountable of less than 50% of the cases in Western countries [3, 4]. In proximal cancers, the two major risk factors are obesity and gastroesophageal reflux [3]. Additionally, multiple other

environmental risk factors (such as Epstein-bar virus infection, nitrites + salt-rich diet, alcohol consumption, poor diet in fruits and vegetables or low intake of fibers, smoking..) have been described, but additional epidemiological studies are required to confirm them [3]. Apart from environmental risks, other benign diseases (Biermer's disease, history of partial gastrectomy, Menetrier's disease, Gastric adenomatous polyps, Barrett's esophagus, Gastric metaplasia, fundic gland polyps and hyperplasic polyps…) have been described as potentially at risk of gastric cancer [4].

On the other hand, around 3% of gastric cancers, especially those occurring at earlier ages, are related to hereditary cancer-related-syndromes, such as Hereditary diffuse gastric cancer (HDGC), Li-Fraumeni syndrome (LFS), Familial adenomatous polyposis, Lynch syndrome, Hereditary breast and ovarian cancer syndrome or Peutz-Jeghers syndrome [4-5]. For instance, the **Hereditary Diffuse Gastric Cancer (HDGC)** is associated with a germline *CDH1* E-cadherin mutation (autosomal dominant inheritance pattern) in ~ 25 to 30% of the cases [5-7]. Germline *CDH1* mutations confer an increased lifetime risk of developing diffuse gastric cancer, with early age-of-onset (average 38 years) : with a 67 % cumulative cancer risk by age 80 for men (95% confidence interval [95% CI], 39–99) and a 83% for women (95% CI, 58–99)) [5-6]. Additionally, women with this syndrome also carried an increased risk of lobular breast cancer (39%, 95% CI, 12–84). Therefore, the guidelines for the genetic testing for *CDH1* mutation are as follows *"1)* families with ≥2 cases of stomach cancer with at least 1 being diffuse gastric cancer, *2)* diffuse gastric cancer occurring < age 40, *3)* personal or family history of diffuse gastric cancer and lobular breast cancer, if at least 1 case is < age 50, *4)* families with ≥2 cases of lobular breast cancer diagnosed < age 50, 5) multiple different lobular breast cancers < age 50, 6) diffuse gastric cancer + personal or family history of a cleft lip/palate" [5-7]. Similarly, gastric cancer development has been observed in around 4 to 5% of patients with **Li-Fraumeni Syndrome (LFS)**, with an early-onset of tumors (mean age 43) [8-11]. LFS is a rare and autosomal dominant hereditary-cancer-syndrome associated with germline or *de novo* mutations in the *TP53* tumor suppressor gene (on chromosome 17) in 77% of the cases. LFS patients present an increased and risk of early-onset cancers from the LFS spectrum (sarcomas of the soft tissue and bone, brain tumors, leukemia, breast and adrenal cortical carcinomas…) [8-11]. **Familial adenomatous polyposis (FAP)** is hereditary colorectal cancer syndrome with germline mutations in the *APC* gene *(Adenomatous polyposis coli,* which controls β-catenin concentration), with increased risks of colorectal, duodenal, and thyroid cancers [12]. The lifetime risk of gastric cancer is limited (0.6%) and quite similar to the general population risk, but it is to be noted that some studies reported a recent rise of gastric cancer cases in FAP patient registries [12]. The **Lynch syndrome** is related to various germline mutations of the mismatch repair genes *(MMR = MSH2, MSH6, MLH1 and PMS2)*. It is associated with a 13% increased risk of gastric cancer development [13]. Lynch syndrome is associated with an excess of early-onset colorectal cancers, as well as gynecologic cancers (endometrium carcinomas, ovarian cancers) or gastric and small bowel cancers [13]. Additionally, **Hereditary breast and ovarian cancer syndrome** (BRCA1/2) classically carried an increased risk of breast and ovarian cancers. Recent studies showed that germline mutations in the DNA-damage repair genes (*BRCA1 or BRCA2)* were also associated with an up to 4-fold increased cumulative risk of gastric cancer [14]. Finally, a 29% increased gastric cancer risk has also been described in the **Peutz-Jeghers syndrome**, associated with AMPK pathway activator STK11 (or LKB1) mutations [15].

1.2. Clinical symptoms and diagnosis of gastric cancer

The majority of gastric cancer cases are **discovered at advanced (late) stages**, where treatment options are limited, therefore resulting in a poor prognosis. There is no specific tell-tale sign of such cancer and it remains asymptomatic for quite a long time [5, 16]. Gastric cancers usually slowly evolve for years before presenting at advanced stages with non-specific symptoms, such as abdominal pain, abdominal discomfort, dysphagia (difficulties to swallow), nausea or vomiting, weight loss or decreased appetite, hematemesis (vomiting blood) or melena (blood in the stool) [5]. Microcytic anemia (secondary to chronic occult bleeding) may be observed, but otherwise the lab results are usually normal. Additionally, current known cancer blood markers are of little use for gastric cancers.

The diagnosis of gastric tumors requires **quite invasive methods**, by means of a **gastroscopy** (= upper gastrointestinal track endoscopy) **with** histological analysis of **biopsies** samples (*Figure 2*), which have a diagnostic accuracy ~ 95% (when ≥10 biopsies are performed), enabling a direct visualization of the tumor. Gastroscopy also gives information on the size and location (cardia, fundus, body, antrum) of the tumor, as well as on the distance between the tumor and the cardia / pylori. Intestinal-type gastric adenocarcinomas often presents as a budding or ulcerated mass originating the stomach wall and as diffusely thickened stomach wall, which lost its normal plication in in diffuse-type cancers.

The TNM classification, according to the 7th edition of the Union for International Cancer Control (UICC) American Joint Cancer Committee (AJCC) guidelines and staging manual, classifies the gastric cancers according to the depth of tumor infiltration (T), the presence of lymph node involvement (N) and distant metastases (M), (*Figure 2*) [16-17]. Firstly, the primary gastric tumor originates (high grade dysplasia > T *in situ* > cancer stage T1) from the mucosal or the submucosal layers of the stomach and slowly evolves for years. Early-stage gastric cancers are usually small, from 2 to 5 cm, and are often located in the lesser curvature. Then, the tumor grows and reaches the muscle layer (T2), then the serosa (T3) of the stomach wall, before spreading into the surrounding tissues and adjacent organs (T4). Gastric cancer can metastasize at any T-stage either in the surrounding lymph nodes (N+) or in distant organs (M+ : such as liver, lungs, adrenal glands, ovaries, distant lymph node and/or peritoneum) [16-17]. Gastric cancers can be visualized at advanced (T3-T4) and/or metastatic stages (N+/M+) on simple non-invasive imaging modalities such as CT and/or MRI. Nonetheless, the diagnosis would still require a histological analysis of tissue-samples, which can only be obtained by means of invasive techniques, such as gastroscopy + biopsies of the primary tumor or biopsies of a distant metastasis

Stage grouping	T stage	N stage	M stage
Stage 0	Tis	N0	M0
Stage IA	T1	N0	M0
Stage IB	T1	N1	M0
	T2	N0	M0
Stage IIA	T1	N2	M0
	T2	N1	M0
	T3	N0	M0
Stage IIB	T1	N3	M0
	T2	N2	M0
	T3	N1	M0
	T4a	N0	M0
Stage IIIA	T2	N3	M0
	T3	N2	M0
	T4a	N1	M0
Stage IIIB	T3	N3	M0
	T4a	N2	M0
	T4b	N0-1	M1
Stage IIIC	T4a	N3	M0
	T4b	N2-3	M0
Stage IV	Any T	Any N	M1

Figure 3. AJCC/UICC stage grouping (from the 7th Edition)

1.3. Histology of gastric cancer

Three different histological types represent the majority of stomach cancers: the most common one is **adenocarcinoma** (90%), while the remaining 5 to 10% are mostly non-Hodgkin **lymphoma** and **the gastro-intestinal stromal tumor** (GIST, a sort of soft tissue-sarcoma) [3]. Gastric adenocarcinoma is classified using histology and morphology, with either Lauren or WHO classification systems. Lauren's classification separates gastric adenocarcinomas between intestinal (54%), diffuse (32%) and undetermined (15%) types[3]. On the other hand, the WHO 2010 classification distinguishes **papillary**, **mucinous** and **tubular types** of intestinal adenocarcinoma and signet-ring cells + other **poorly cohesive cells** (which corresponds to diffuse adenocarcinoma) [18-20].

Intestinal type adenocarcinoma is classically observed in elderly patients (50-70 years old), with a male predominance, a longer course of the disease and a better prognosis, with higher incidence in high-risk geographic regions (Asia, South America) [3]. Clinically, a localized mucosal tumor mass is often observed (*Figure 3*) and may sometimes be ulcerated [3]. These tumor cells are arranged in tubular/ glandular formations and lymphatic and/or vascular invasion may be observed. Intestinal-type adenocarcinomas are separated between **well-differenciated tumors,** with gland-forming cohesive tumor cells (similar-looking aspect compared to normal cells), **moderately-differentiated** tumors with cells of intermediate appearance and **poorly differentiated** ones, where the tumor cells lose their resemblance to normal cells, with a distorted architecture of the glands (*Figure 4)*.
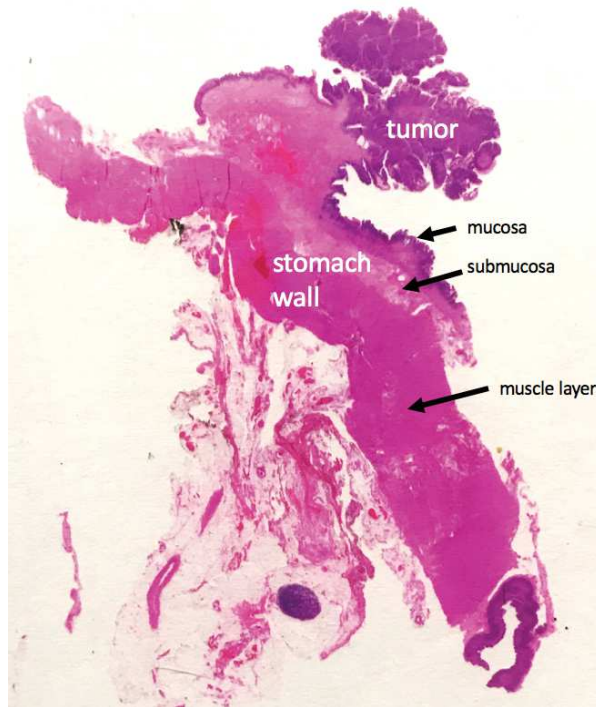
Figure 3. Photography (author's personal collection, no magnification) of a hematoxylin eosin-stained slice, showing a tumor in the mucosa and the other layers of the stomach wall.

| Well differentiated adenocarcinoma | Moderately to poorly differentiated adenocarcinoma |
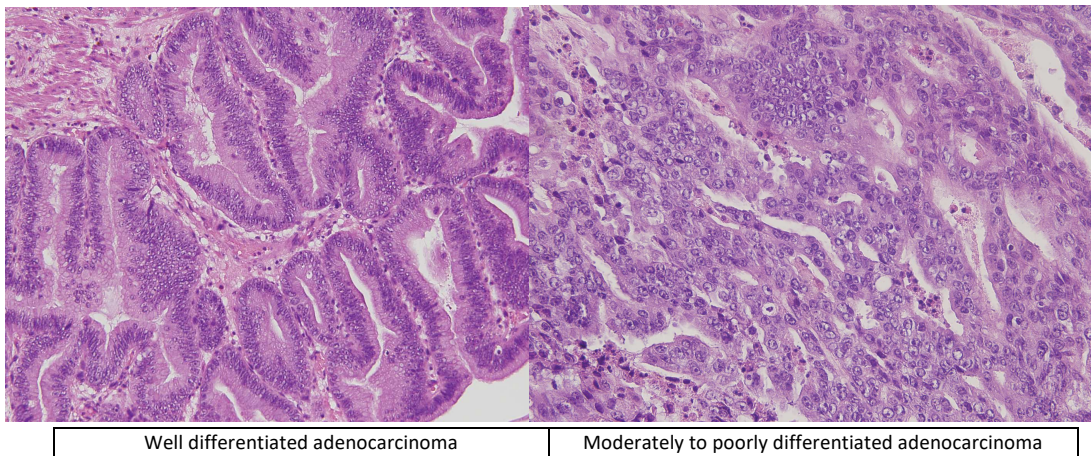
Figure 4. A) Well differentiated intestinal-type adenocarcinoma. Hematoxilin eosin-stained slice, magnification x40 showing cohesive tumor cells form glands. Their aspect is not so different from normal cells. **B) Poorly differentiated intestinal-type adenocarcinoma.** Hematoxilin eosin-stained slice, magnification x40 showing tumor cells that lost their resemblance to normal cells, with distorted architecture of the glands.

On the other hand, **diffuse adenocarcinoma** usually occurs in younger patients, with a female predominance and is associated with a poorer prognosis and shorter course of the disease. The tumor cells are not cohesive, and they do not form glands (Figure 6). Diffuse cancers tumor cells infiltrate the stroma of the stomach wall as **single cells**, from the submucosal layer. This results in a thickening of the stomach walls, with no distinguishable budging/ulcerated mass in the mucosa (*Figure 5*) [18-20]
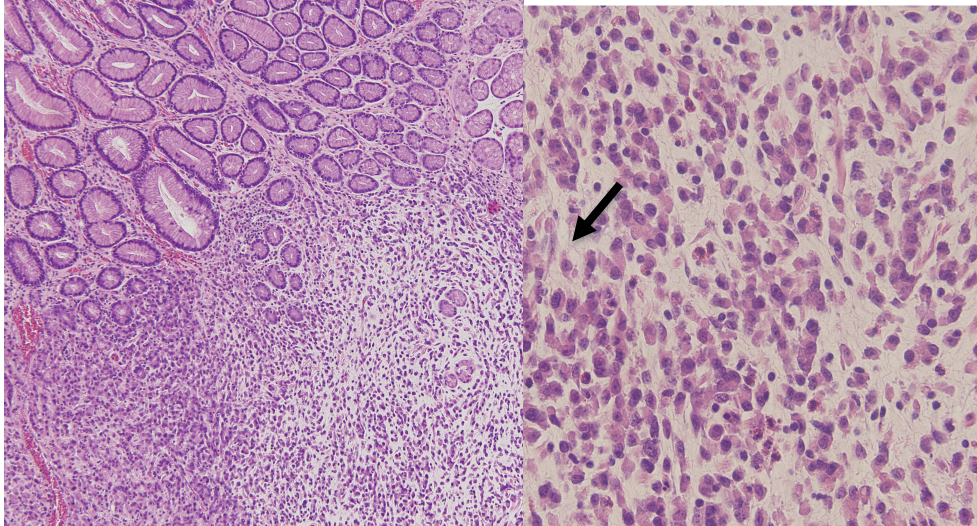
Figure 5. A) Hematoxilin eosin-stained slice (author's personal collection), magnification x20 showing non cohesive tumor cells in the submucosa (arrow) surrounded by normal glands in a diffuse adenocarcinoma. B) Hematoxilin eosin-stained slice, magnification x40 showing the non-cohesive signet ring cells.

Additionally, the HER2 status (positive or negative) is also important in gastric cancer's histological classification. The major interest of HER2 as a biomarker in gastric cancer is that it could be actionable as a targeted therapy (e.g. trastuzumab), but it also appears a potential target for functional imaging (see page 34). The HER2 protein (p185, HER2/neu, ErbB-2) is a 185-kDa transmembrane tyrosine kinase (TK) receptor and a member of the epidermal growth factor receptors (EGFRs) family [21]. Overexpression may be determined by immunohistochemistry (IHC) using monoclonal antibody (HercepTest® positivity, if IHC 2+ or 3+) and/or FISH for gene amplification (HER2+, if FISH+). Multiple studies have highlighted the role of HER2 in the development of various cancers, such as **gastric** (since 1986), colon, breast, bladder, ovarian, lung, endometrial, uterine cervix and head & neck tumors. In breast cancer in particular, researchers showed that HER2 overexpression/amplification was present in 10% to 34% of the cases, were it correlates with a poor response to chemotherapy and endocrine therapies [21]. In **gastric cancers**, for Gravalos et al., the rate of **HER2-positivity ranged from 13 to 22%**, with significant variations according to the histological subtype (predominant in intestinal type 34% vs diffuse 6% vs mixed 20%, in the ToGA trial) and according location the tumor (25 to 34% for the gastroesophageal junction and 9.5 to 18% for other gastric localizations) [21-22]. Additionally, they reported that HER2-positive gastric cancers have a poorer prognosis, with shorter disease-free survival and shorter overall survival (median survival of HER2 - patients 12.7 vs 6.6 months for HER2+ patients, p= 0.37).

1.4. Imaging of gastric cancers: current trends

The diagnosis of gastric cancer always requires tissue-samples analysis (histology and IHC/FISH). Therefore, radiologists are usually already aware of the diagnosis, when they perform various imaging modalities for tumor staging. **CT scans** (thorax, abdomen and pelvis) are used to evaluate the loco-regional extension of the primary tumor as well as distant metastasis, especially efficient at advanced (T3-T4) or metastatic stages (N+/M+), but earlier stage disease may be missed. Radiographs and barium studies (Figure 4) have long been abandoned, as they only had a very limited diagnostic value

(they did not aid in the accurate staging of the tumor and did not allow differentiation between benign and malignant lesions). On the other hand, **endoscopic ultrasound** is very useful to stage (T) the cancer and delineates the depth of tumor invasion through the layers of the stomach wall. This technique (Figure 6) appears to be the most effective way to differentiate localized tumors (stage T1) from more advanced ones (stage T2-T3, overall accuracy = 70.2 – 93% for Lee et al., superior to CT), but poorly performs for larger tumors (>5cm) [23]. Endoscopic ultrasound is mostly performed in specialized centers, in cases of doubt between T1 and T2/T3 stages, or in case of suspicion of linitis and if a neoadjuvant treatment is needed [24]. It appears less effective than CT for nodal involvement for Kwee et al. (43% accuracy for N+ evaluation) and does not evaluate distant metastases [24]. Another downfall of endoscopic ultrasound is that like all ultrasound examinations, it requires a certain level of expertise and is observer-dependent [23].

Current guidelines recommend monitoring the extension of gastric cancer by means of a CT of the chest + abdomen + pelvis, which has a relatively high accuracy (71% for T-staging, 66% for N-staging, and 81% for M-staging) [16-17]. Unfortunately, as explained by Seevaratnam et al. CT does not provide tissue confirmation for tumor grading or histological classification (for instance from adenocarcinomas to lymphomas) compared to gastroscopy or endoscopic ultrasound [25]. To improve the detection of localized tumor, some teams suggested using air, water or barium distension of the stomach or virtual-gastroscopy CT images [26]. Using virtual gastroscopy with air distension on CT, Chen et al. were able to identify gastric cancers in 91% of the cases and overall accuracy in the assessment of tumor invasion of the stomach walls (T stage) was improved using MPR images compared to transverse ones, but in clinical routine, those numbers are probably lower, especially in T1 to T3 tumors [27]. Current French CT protocol requires 6 hours of fasting + 300-500 mL water distension of the stomach prior to the CT, with portal venous phase and MPR reconstructions (*Figure 8*). Staging (T), size and location of the tumor can be estimated on CT, as well as the thickness of the stomach wall, the presence or absence of a fatty plane between the tumor and adjacent organs and distant nodal / vascular / visceral metastatic spread. In early gastric cancer cases, CT is less efficient than endoscopic ultrasound for Shimizu et al. and Kim et al., as it is not able to distinguish the different layers of the gastric wall. Hence the visualization of early lesions (T in situ, T1...) is more difficult than for advanced (T3-T4) ones (accuracy 53-65% vs 66-87% for more advanced lesions) [27-28]. In T1 and T2 tumors, the outer layer of the gastric wall appears regular, while in stage T3 tumors it may appear irregular with dense linear spikes in the surrounding fat. Stage T4 tumors present with a loss of fatty interface between the tumor and the adjacent organs or a decrease in density of the organ. For lymph node invasion (N), CT criteria for involvement of the node are size >8-10 mm (small axis), round shape, necrosis and heterogeneous contrast uptake. Metastasis are commonly observed in the liver, the lungs (bases and periphery), the adrenal glands (heterogeneous masses, wash out), the ovaries (Kruckenberg tumor, bilateral solid masses), distant lymph node (Troisier's node, left subclavicular node) or the peritoneum (bad prognosis, easily missed on CT).

Figure 6 A) Multidetector CT, axial plane, portal venous phase showing a localized mass in the upper part of the stomach in a 55-year-old man (histology: poorly differentiated gastric adenocarcinoma, pT3N0M0). **B)** Multidetector CT, coronal plane, portal venous phase showing a diffuse thickening of the stomach wall (arrows) in a 46 years-old woman. **C)** Multidetector CT, axial plane, portal venous phase (with water distension of the stomach) showing a diffuse thickening of the stomach wall (arrows) and liver metastases (stars). **D)** Multidetector CT, axial plane, portal venous phase showing a diffuse thickening of the stomach wall (arrows) and peritoneal carcinomatosis with liquid effusion in a 49-yearl-old woman with diffuse adenocarcinoma (circled area).

The primary tumor can be missed on abdominal CT (*Figure 7*) and so do 44% of small peritoneal or liver metastasis. Thus, some authors suggested using new texture-analysis method to improve detection, but such methods are still ongoing research and development [29-34]. As imaging techniques perform poorly for peritoneal dissemination, peritoneal extension is usually assessed during **laparoscopic evaluation with washing** [35].
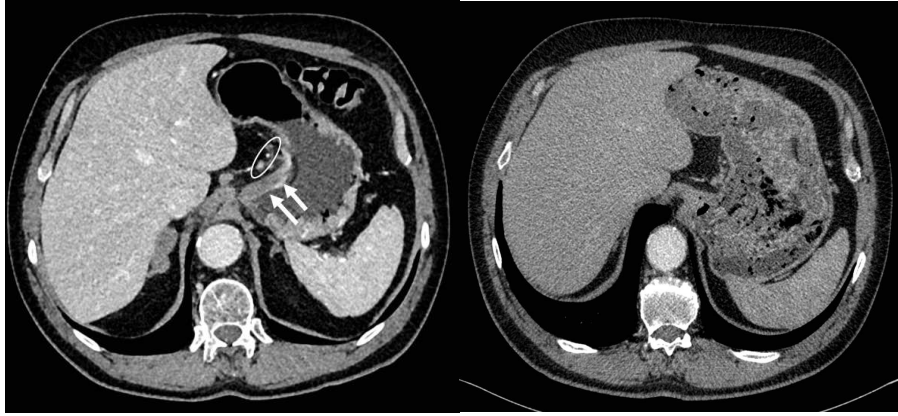
Figure 7. A) Abdominal CT showing a focal thickening of the lesser curvature (arrow) with small lymph nodes (circled). B) Same patient, earlier CT exam performed 2 months earlier for abdominal pain. The tumor was more difficult to visualize and was missed.

Other imaging techniques (such as MRI and functional imaging) are still being evaluated and are not currently part of current diagnosis guidelines (Figure 8) [35].

Procedure	Purpose
Routine blood tests	Check for evidence of iron-deficiency anaemia. Check hepatic and renal function to determine appropriate therapeutic options.
Endoscopy + biopsy	Obtain tissue for diagnosis, histological classification and molecular biomarkers, e.g. HER-2 status.
CT thorax + abdomen ± pelvis	Staging of tumour—particularly to detect local/distant lymphadenopathy and metastatic disease sites.
Endoscopic ultrasound (EUS)	Accurate assessment of T and N stage in potentially operable tumours. Determine proximal and distal extent of the tumour.
Laparoscopy + washings	To exclude occult metastatic disease involving the diaphragm/peritoneum.
Positron emission tomography (PET, if available)	May improve detection of occult metastatic disease in some cases.

Figure 8. Recommendations ESMO–ESSO–ESTRO Clinical Practice Guidelines for gastric cancer diagnosis [35]

Magnetic Resonance Imaging (MRI) is not used in clinical routine for the diagnosis of gastric cancer, as its use is still being investigated. For instance, Joo et al. evaluated the diagnostic performances of 3T MRI for the staging of gastric cancer and found no significant difference compared to MDCT (multidetector CT) in terms of diagnostic accuracy [36]. In most of the published studies, the authors relied on diffusion-weighted MRI (DW-MRI) and dynamic-contrast enhanced images to evaluate the aggressiveness of gastric cancer and its response to treatment [36-42]. The most useful sequence is probably DWI with its apparent diffusion coefficient (ADC value), which appears superior to T2-weighted sequences for the detection of early gastric cancers (pT1) and the staging of advanced cancers (≥pT2) [41]. All in all, the most common indication of MRI in gastric cancer remains the M staging of the tumor, especially in case of liver metastasis.

There is currently no consensus regarding the application of functional imaging (PET-CT and/or PET-MRI) in the management of gastric cancer, as their usefulness remain to be determined and no clear consensus appears between studies [43-46]. According to recent studies, PET-CT should be limited to staging distant metastasis [40-41]. For example, if Ma et al. suggested that ^{18}F-FDG PET-CT could be used for the initial diagnosis of primary gastric cancer with a 92% sensitivity and 75% specificity (p=0.359), Youn et al. judged it insufficient for T and N staging (very low sensitivity for early gastric cancer detection ~ 20.7% which raises to 42.2% in more advanced tumors and 30.7% sensitivity / 94.7% specificity for lymph node metastasis detection) [43-44]. Therefore, Youn et al. suggested to limit its use to the search for a synchronous second primary tumor (37.5%, n=9/24) and the staging distant metastasis (M) [44]. Attempts to improve PET-CT's diagnostic accuracy using gastric distension (using a mixture of milk and Diatriozoate Meglumine) failed, even though the lesions were slightly more clearly displayed [43]. Some authors, such as Chen et al., tried limiting its use HER2+ tumors and described a ^{18}F-FDG uptake associated with HER2 expression in 64 gastric tumors (8.619 ± 5.878 SUV$_{max}$ for HER2- tumors significantly higher than in HER2+ tumors 3.789 ± 2.613, p=0.021), with a 6.2 cut-off SUV value predicting HER2 expression with 64.4% accuracy [45]. All in all, the major problem of functional imaging - which has been highlighted by most authors - is the risk of false negative cases, with a low detection rate for diffuse and mucosecreting tumors, as well as differences in terms of tumor detection rate between the different histological subtypes (47.1% sensitivity for intestinal type tumors vs 39.4% for mixed vs 27.9% for diffuse tumors) [43-45].

1.5. New molecular classifications

Gastric cancer is a **complex and biologically heterogeneous disease**, not only regarding its various imaging and/or histological presentations, but also regarding the presence of an inter-patient and intra-tumor variability, which complicates the stratification of the disease. Genetic, local environmental and host factors altogether play an important role in the pathogenesis. As for other cancers, gastric cancer is the result of accumulated genomic damages, affecting essential cellular functions, which leads to cancer development. Therefore, the current clinical and histological classifications end up being quite complex and probably insufficient to define all the existing tumor subtypes. The tumors biology and clinical outcome vary significantly among different gastric cancer patients, with overall poor prognosis, mainly secondary to different genetic signatures. The current Lauren/WHO classifications are not useful in informing prognosis, do not provide necessary information relevant to clinical utilities or treatment guidelines and therefore are not useful to make personalized treatment decisions. Additionally, existing classifications poorly predict responses to therapy, especially given the little differences in clinical outcomes between the different subgroups. Therefore, there was a need for a new classification system that could change clinical decisions and help in targeting therapy development. For a better understanding of gastric cancers, a recent genomic approach, led by The Cancer Genome Atlas (*TGCA, 2014, Figure 9*) Research Network, studied genomic alterations gastric cancer [47]. They developed a molecular classification system based on gene expression profiling aiming to provide a framework to guide individualized patient therapy and to better predict treatment response. They analyze the molecular composition of gastric cancers (DNA, RNA & protein arrays). Based on this data, they classified gastric cancer into **4 different subtypes**: **EBV infected** (9%), **Microsatellite instable** (MSI, 22%), **Genomic stable** (GS, 20%) and **Chromosomal Instability** (CNI, 49%) [47-48].

Figure 9. Molecular subtypes of gastric cancer (TGCA, 2014) together with their dysregulated pathways issued from publication ref n°18.

As detailed in the TCGA article, EBV-positive gastric adenocarcinomas are predominantly found in the gastric fundus and body (62%) and in males (81%) and currently associated with the best prognosis. If EBV is asymptomatically carried in the circulating blood of around 90% of adults, it is believed that EBV is associated with 2% of all human tumors and observed in tumor cells of 9% of all gastric adenocarcinomas [47]. Programmed Cell Death Ligand 1 and 2 (PD-L1/L2), involved in immune checkpoints (associated with a greater degree of T-well involvement), are amplified. Cyclin-dependent kinase inhibitor 2A (CDKN2A) promoter hypermethylation are also found in all EBV (100%) associated gastric adenocarcinomas and PIK3CA are observed in 80% of the cases. **Microsatellite Unstable gastric adenocarcinomas,** comprising 21% of all gastric adenocarcinomas, are typically diagnosed at older age (~70 yo), with a female predominance (56%) [47]. Defects in the mismatch repair (MMR) genes are observed and lead to widespread replication errors in simple repetitive microsatellite sequences. These MMR defects lead to hypermutation, MLH1 silencing and involvement of mitotic pathways. Such tumors have an intermediate level prognosis with a lower chance of lymph node metastases. Unfortunately, unlike EBV-positive tumors, such tumors lack targetable amplifications [47]. **Chromosomally Unstable gastric adenocarcinomas,** associated with an intermediate prognosis, represent 50% of all gastric cancers and 65% of them involve the gastro-esophageal junction (cardia) [47]. Such tumors involved the unequal distribution of DNA to daughter cells, leading to loss or gain of chromosomes during cells division, associated with amplification of receptor tyrosine kinase (RTKs), EGFR, Cyclin-D1 (CCND1) and Cyclin-dependent kinase 6 (CDK6), which were thought to be potential candidates for future targeted therapies. **Genomically Stable gastric adenocarcinoma**s represent 20% of all gastric cancers, usually diagnosed at an earlier age (~59 yo) and carry the worst prognosis of all four subtypes [47]. Such cancers are associated with diffuse or poorly cohesive histology and mutations in Ras Homolog Family Member A (RHOA, 15%) and CDH1, both involved in cellular adhesion, are observed. Three percent of such cancers show interchromosomal translocation between Claudin 18 (CLDN18) and RhoGTPase-activating Protein 6 (ARH-GAP26).

However, the question of the clinical implications of such findings remains. To address this issue, in 2015 and 2017, the Asian Cancer Research Group (**ACRG***)* performed whole-genome sequencing of 300 primary gastric tumors. They identified four similar groups of gastric cancer, *1)* **microsatellite unstable**

(MSI, 23%), *2)* microsatellite stable and expressing **epithelial mesenchymal transition signatures** (MSS/EMT, 15%), *3)* microsatellite-stable with **intact TP53** (MSS/TP53+, 26%) and *4)* microsatellite stable **with TP53 mutations** (MSS/TP53-, 36%), with distinct clinical outcomes [48-49].

Diffuse adenocarcinomas for instance are included by the ACRG in the **MSS/EMT subtype**, which had worst prognosis, together with an earlier age of onset and the highest recurrence frequency (63%) of the four subtypes. On the contrary, **MSI tumors** were intestinal-subtype tumors (especially in the antrum), with high somatic mutation burden, had the best overall prognosis and the lowest frequency of recurrence (22%). The prognosis and recurrence rate were intermediate for MSS/TP53+ and TP53-types. All in all, epidemiological, genomic and histological data support the fact that gastric cancer is a heterogeneous disease of multiple entities, resulting in distinct clinical outcomes for each, shedding light on the need of new targeted therapies and personalized treatment options. Unfortunately, even though the recent molecular classifications of gastric adenocarcinomas have enabled the identification of **multiple dysregulated pathways**, the resultant targeted therapies have unfortunately proven to be ineffective so far, therefore questioning the relevance of the existing classifications for therapeutic purposes, especially in advanced gastric cancers [48-53].

1.6. Dysregulated pathways in gastric cancer

1.6.1. Pi3 Kinase /Akt/ mTOR pathway

One of the most frequently dysregulated pathways in human cancers is the PI3K/AKT/mTOR signaling pathway, which controls multiple cellular processes including proliferation and cell growth, metabolism, motility, angiogenesis and survival [54-56]. This pathway appears deregulated in gastric cancers, with **overexpression of PI3K, AKT, p-AKT and mTOR**, especially associated with lymph node metastases [54-55]. Through a phosphorylation cascade, the activated (by growth factors and cytokines) PI3 kinase phosphorylates Akt, which induces the activation of mTOR. This promotes cell growth and protein synthesis, while p-Akt inhibits various targets including p21, p27 and BAD (Bcl-2 associated agonist of cell death) and GSK3, which promote cell proliferation and prevents apoptosis 57].

1.6.2. MAP Kinase pathway

The MAPK pathway (mitogen-activated protein kinase) is often deregulated in gastric cancer, with 17% of **KRAS alterations,** especially common in the **MSI** subtype of gastric cancers [47-55]. The MAPK pathway is a molecular cascade regulating several cellular responses, for instance cell adhesion, cell cycle, migration, differentiation, apoptosis and angiogenesis. An activated MAP3K (by growth factors and cytokines) phosphorylates MAP2K, which phosphorylates MAPK (ERK, p38), thus promoting cellular response.

1.6.3. Wnt/ β cathenin pathway

The Wnt/β-catenin signaling pathway can also be deregulated in gastric cancer with somatic mutations (APC gene), promoter hyper-methylations or miRNA expressions. An activated Wnt/β-catenin pathway

can be found in **30% of gastric cancers**, with an overexpression of several components of the Wnt pathway, as well as a loss of Wnt inhibitors [59]. In the absence of Wnt ligands, the cytoplasmic β-catenin binds to a complex composed by Axin+ adenomatous polyposis coli (APC) + glycogen synthase kinase 3β (GSK3β) + casein kinase 1α (CK1α). The kinases of the complex phosphorylate β-catenin, which is then recognized by an E3 ubiquitin ligase (β-TrCP) and targeted to proteasomal degradation (= low cytosolic levels). In the presence of Wnt ligand, Wnt binds to the receptor complex (Frizzled + low-density lipoprotein receptor family LRP5/6), which recruits Disheveled (Dvl) and induces the delocalization of Axin and phosphorylation (CK1α + GSK3β). Therefore, the degradation of β-catenin stops, and it accumulates in the cytoplasm. Active non-phosphorylated ß-catenin then translocate to the nucleus where it acts as a transcriptional co-activator with TCF/LEF for target genes [59].

1.6.4. HIPPO pathway

A deregulation of the HIPPO signaling pathway has been described as strongly associated with the initiation and the development of human gastric cancer, as well as its distant metastasis. According to the TCGA, **an alteration of the Hippo pathway is observed in 71% of gastric cancer cases** [47]. A **downregulation** of the upstream HIPPO pathway is most common, with **alterations in MST1/2** (2.5% and **9%** respectively), **LATS1/2** (6% and 5%) and **RASSF1** (2.5%) [47-60]. Additional data, from other research teams, show that hypermethylation of the promoter RASSF1 activates the HIPPO pathway leading to an increased gastric cancer risk (OR = 12.67) [61]. The HIPPO signaling pathway (short for "MST1/2-WW45-LATS1/2 signaling pathway") is a critical pathway that determines cell growth rate and organ size. In the normal HIPPO pathway, MST1 and MST2 phosphorylate and activate LATS1-2 (large tumor suppressor 1 and 2), which phosphorylate YAP1 (Yes-associated protein 1) and its paralog TAZ (WW-domain-containing transcription regulator), resulting in its cytoplasmic accumulation (Figure 17). On the contrary, in gastric cancer, MST1 and LATS1 are downregulated and this results in a YAP1/TAZ translocation to the nucleus, where they bind with TEAD1-4 (TEA domain DNA-binding transcription factors 1 to 4), therefore inducing transcriptional activity for cell proliferation and differentiation [61]. Additionally, the deregulated Hippo pathway shares crosstalk with Wnt/β-catenin/Notch/TGF-β (transforming growth factor beta) pathways in tumorigenesis.

1.6.5. Nuclear factor-κB pathway

The Nuclear factor kappa B (NFκB) signaling pathway comprised a group of transcription factors (RelA, RelB,c-Rel, NFκB1/p50, NFκB2/p52). This pathway appears overactive in gastric cancer cases, with **1.8%** of RelA alterations, **2.5%** of Relb, **2.8%** of NFκB1 and **5%** of NFκB2 (mostly gain function mutations or gene amplifications) [62-63]. As a response to various microbial compounds, hormones and/or growth factors, the NFκB pathway either upregulates or suppresses the expression of several genes such as cytokines/chemokines (IL-1, TNF), VEGF, MMP (Matrix metalloproteases, promoting cell survival and invasion) or Cyclooxygenase-2 (COX2, promoting cell growth and apoptosis inhibition).

1.6.6. Sonic hedgehog (Shh) pathway

The Sonic hedgehog (Shh) pathway is activated in gastric cancer, leading to cell proliferation, tumor growth and shorter survival [64-67]. The Sonic hedgehog (Shh) pathway is activated by Shh binding to

the Patched (PTCH)-Smoothened (SMO) membrane-receptor complex. Upon activation, SMO promotes nuclear translocation of the GLI family of transcription factors (Gli1, 2 and 3) that subsequently activates target gene expression controlling cell cycle and invasion.

1.6.7.   The p53 family (p53, p63 and p73)

P53, p63 and P73 are members of a family of related transcription factors, frequently mutated in cancers. For instance, according to Levrero et al., ***50 to 70% of gastric tumor cells harbor p53 mutation, around ~4% a p63 one and ~ 1% a p73*** [68]. Additionally, ***p53 status varies according to gastric cancer subtypes***, with p53 mutations commonly found in the **MSI** subtype, while being less common in the EBV subtype (with a strong expression of p53 and a decrease of p53 mRNA levels) as explained by Ribiero et al. [69]. Besides the presence of mutations, the P53 level and activity is controlled by **MDM2**, which is an E3 ubiquitin ligase promoting p53 proteasomal degradation. After DNA damage, MDM2 is inhibited, which disrupts its binding to p53 and accumulates and therefore activates p53. MDM2 **is overexpressed in around 40% of gastric cancer** and MDM2 gene amplification is especially found in diffuse-type cancers. The upregulation of MDM2 results in TP53 inactivation, thus inhibiting the cell cycle arrest and apoptosis, which could result in the promotion of gastric tumorigenesis. Furthermore, upon a genomic stress such as a chemotherapy treatment with platinium-derived compound, p53 maintains genomic integrity by the transcriptional activity of its target genes such as CDKN1A (P21) or PMAIP1 (Noxa). Moreover, p53 appears unable to induce apoptosis in response to DNA damage, without the presence of p63 or p73.

The TAp63 isoforms binds to DNA across p53 response elements and activate the transcription of target genes inducing cell cycle arrest or apoptosis (common functions to p53). TP63 appears altered (gene amplifications) in **9%** of gastric cancer cases in the TCGA (http://www.cbioportal.org/) and is more expressed in gastric tumor tissue samples compared to normal gastric tissue, with an overexpression in advanced diffuse type gastric cancers. Furthermore, Song et al. found that p63 expression was a poor prognosis factor, as it correlated with shorter overall survival and lower 5-year-survival rates [70-71].

Like TP63, TA73 isoforms can bind to DNA across p53 response elements, thus activating the transcription of target genes, which results in a cell cycle arrest or apoptosis induction. The ΔNp73 isoforms can bind DNA across p53 elements and can exert dominant-negative effects over p53, p63 and p73 activities. TP73 is altered (majority of deep deletions) in **3%** of gastric cancers according to the TGCA. Wei J et al. also described an increased level of P73 expression in 94% of their patients (n=37/39) and Vilgem et al. described ΔNp73 as a poor prognosis factor, related to shortened survival (20 months for ΔNp73 + vs 47 months for ΔNp73 -) [72-73]. They also showed that HIC1 (Zinc finger and BTB domain-containing protein 29 or Hypermethylated in cancer 1) targets ΔNp73 promoter reducing its expression [73-74]. HIC1 is hypermethylated in gastric cancer, therefore promoting the upregulation of ΔNp73, which may result in the inhibition of p53 and TAp73 activities and all in all promote gastric tumorigenesis [73-74]. Therefore, ΔNp73 seems to have pro-tumor role in gastric cancer. On the other hand, TAp73 appears to have an antitumor activity by recusing cell proliferation and inducing apoptosis. However, TAp73 overexpression promotes Cyclin D expression, which leads to cell proliferation and Doxorubicin-resistance in gastric cancer cells and reduces the p53-dependent

apoptosis induced by chemotherapeutic drugs in several cell lines (SNU-1, SNU-3, and AGS) [75-76]. All in all, an overexpression of TAp73 can result in drug resistances and seems to have a pro-tumor role in gastric cancer, which highlights the dual role played p73 in gastric cancer tumorigenesis.

1.7. Current treatments of gastric cancer

Unfortunately, those altered pathways in gastric cancer have not yet resulted in usable targeted therapies. The current recommended therapeutic approach relies on a standardized multidisciplinary approach, which involves **surgery** (total or partial gastrectomy +/- lymph node resection) **and perioperative** (neoadjuvant and/or adjuvant) **chemotherapy** in most of the cases (*Figure 10*) [48].
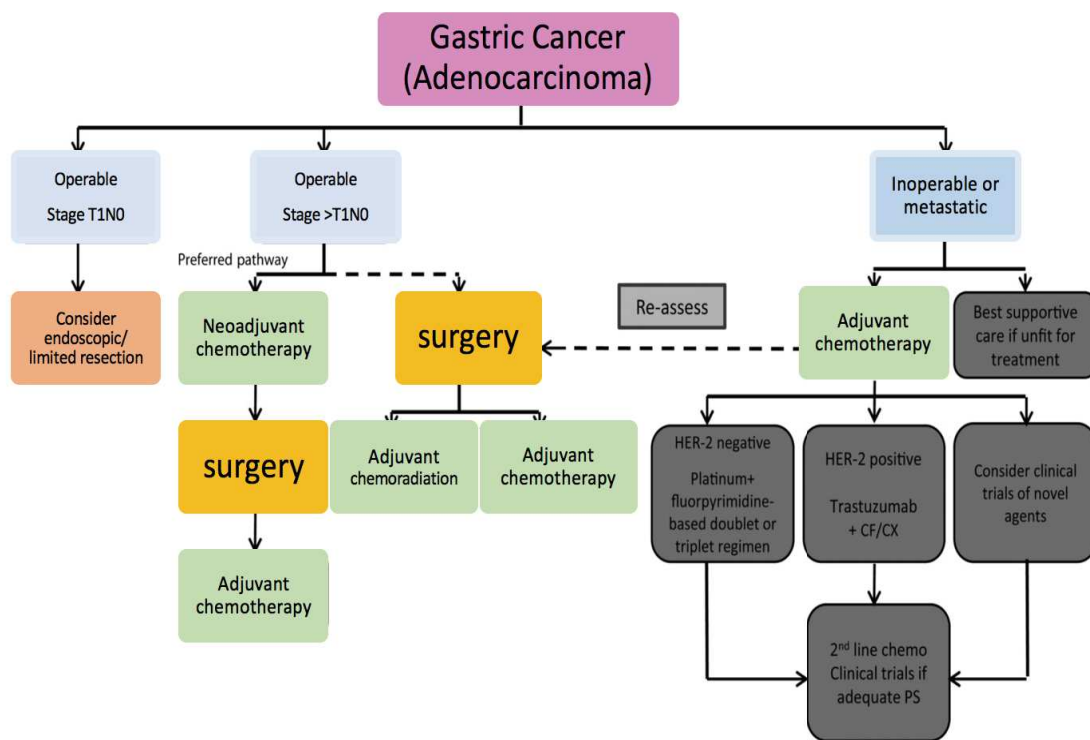
Figure 10. Recommendations ESMO–ESSO–ESTRO Clinical Practice Guidelines for gastric cancer treatment

1.7.1.   Surgical procedure

Adequate surgery by means of a total or subtotal **gastrectomy** (laparoscopic – favored – or open approach) **with lymph node resection** (15 lymph nodes) is the cornerstone of gastric cancer treatment [35, 50]. According to the ESMO–ESSO–ESTRO Clinical Practice Guidelines, total gastrectomy is indicated for resectable stage IB–III disease, while subtotal gastrectomy may be performed if a 5 cm tumor-free proximal margin between the tumor and the oesogastric junction is possible [35]. Minimally invasive techniques, by means of endoscopic resection, can also be curative option early stages (T1a) cancers if : they are well-differentiated, smaller than 2 cm, confined to the mucosa and

not ulcerated [35]. **Curative (R0) resection is the only potentially curative option**, even though its efficacy may be limited, as achievement of loco-regional control in advanced diseases remains very difficult and the majority of patients will relapse following resection.

1.7.2.   Standard chemotherapy protocols +/- radiation therapy

Therefore, combined treatments are standard **for ≥ stage IB disease** (>T1N1/T2N0 or more) [35]. Standard first-line treatment of advanced gastric cancer is based on **neo-adjuvant chemotherapy**, **and combinatory treatments**. Although advanced gastric cancer is sensitive to numerous agents, response rates with monotherapy are generally low (10 to 30% according to Kang et al.) [77]. For years, chemotherapy protocols were based on the combination between fluorinated pyrimidine (5-FU) and a platinum-derived compound (cisplatin or oxaliplatin). This association remains in use, with standardized protocols such as the **EOX protocol** (oxaliplatin + 5-FluoroUracil / capecitabine) and now especially the **FLOT protocol** (Table 1; regimen to be given 2 weekly : 4 cycles before surgery and 4 cycles after, Table 1).

DRUG	DOSE	Administration	FLUID	TIME
Docetaxel	50 mg/m^2	IV	250mL 0.9% sodium chloride	1h
Oxaliplatin	85 mg/m^2	IV	500mL 5% Glucose	2h
Folinic acid	350mg	IV	250mL 5% Glucose	2h
5-FU	2600 mg/m^2	IV	Infusion pump	24h
Dexamethasone	8mg			12h for 3 days *starting 24h before chemo*

Table 1. FLOT protocol with doses

Neoadjuvant systemic chemotherapy +/- radiotherapy is recommended prior to surgery, to increase the loco-regional control, in order to obtain R0 resection [35]. It is followed by adjuvant chemotherapy (after surgery) to maintain the anti-tumor activity. A pooled analysis of 1318 patients from two clinical trials (REAL-2 and ML17032) observed that patients who received capecitabine-containing regimens of chemotherapy had increased overall survival (median 332 vs 285 days, HR 0.87 95% CI [0.77–0.98], p= 0.02) and were more likely to obtain an objective response (OR=1.38, 95% CI [1.10–1.73], p= 0.006) [52]. In France, according to current recommendations (*thesaurus National de Cancérologie Digestive, 2016)* stage I/II tumors (uT1N0, uT2No, uT1N1, uT2N1, uT3N0) should undergo **neoadjuvant and adjuvant chemotherapy (4 cycles) using FLOT**, while **stage III** (T3N1 or T4N0-N1) should undergo either neoadjuvant and adjuvant chemotherapy (4 cycles) using **FLOT** protocol **or chemoradiations** (FOLFOX : oxaliplatine, folinic acid and 5 FU + radiotherapy (50.4Gy) or paclitaxel / carboplatin + radiotherapy (41Gy). In metastatic gastric cancers, current recommendations limit treatment options to chemotherapy +/- radiotherapy as palliative care [51]. However, the overall toxicity of some regimens renders their general use difficult. For instance, the **side effects** of the FLOT chemotherapy include: myelosuppression (neutropenia/thrombocytopenia), alopecia, mucositis, allergic reactions, coronary artery spasm, palmar/plantar erythema, nausea/vomiting/diarrhea, stomatitis, loss of appetite, fatigue, renal impairment, infection, ovarian failure/infertility, auditory impairment, hepatic

impairment and neurological toxicity. Thus, despite many advances made over the past years, the clinical success rate of the existing chemotherapy protocols remain very low (unchanged for >30 years with platinum-derived compounds) and may vary between patients, emphasizing the need of novel, targeted and personalized therapies, aiming at limiting side effects, especially for advanced gastric cancers, where R0 resection may not be achieved with surgery alone [53-78].

1.7.3. Advanced targeted therapies

Unfortunately, most current targeted therapies have unfortunately proven to be ineffective for now [49]. For example, bevacizumab (phase III *AVAGAST* study), a monoclonal antibody, in association with chemotherapy in advanced gastric adenocarcinoma, failed to improve overall survival of treated patients [79]. Similarly, no clear benefit in terms of overall survival was observed with novel agents targeting EGFR (cetuximab, panitumumab), VEGF-A (bevacizumab), or mTOR (everolimus) pathways [35-80].

Recently, **the targeting of the PD-1/PD-L1 immune checkpoint** signaling appeared as a potential cancer treatment strategy. Cytotoxic T-cells task is to detect and destroy infected or tumor cells. To counteract their actions and to limit damage to surrounding tissue, normal cells differentiate themselves by expressing a protein signal called programmed death ligand 1 (PD-L1), which acts as a signal to stop the elimination of normal cells by cytotoxic T cells, as they detect the PD-L1 signal through a receptor called PD-1 (programmed death receptor 1). Some tumors, including gastric cancer ones, can also express the PD-L1 signal to mimic normal cells and escape elimination. In gastric cancer, **PD-L1 expression was found by Böger et al. in 30% of tumor cells** (n=140) **and 60% of their liver metastases** (n=9), **as well as in 88% of immune cells of gastric cancer** (n=411) and 73% of immune cells from their metastases [81]. Therefore, targetting PD-L1 in gastric cancer seemed possible. **Pembrolizumab (*pembro*)** is a humanized monoclonal antibody against PD-1 that prevents PD-1 from interacting with PD-L1 and PD-L2 and permits activation of an antitumor immune response. **A phase 2 clinical trial was conducted and the response rate as 3rd line of treatment of gastric cancer was 11.6% (n=30/259) and complete responses were observed in 2.3% of patients (n=6)** [82]. These results emphasize the need for further development of pembrolizumab for patients with gastric cancer who have received >2 lines of therapy. Unfortunately, during phase 3, Pembrolizumab did not show improved survival compared with paclitaxel as second-line therapy for advanced PD-L1 + gastric cancer [83].

Hopefully, MET targeted therapies (targeting MET receptor), anti-FGFR therapy and other immunotherapy are currently undergoing evaluation and some have promising preclinical trials results. **The targeted therapy currently used in clinical routine is trastuzumab in HER2+ gastric cancers** (IHC3+ or 2+/FISH-positive), **in combination** with capecitabine or 5-fluorouracil and cisplatin, as combined therapy including this monoclonal antibody increased overall survival of HER2+ patients (11.8 vs 16.0 months, phase III *ToGA* trial) [21-22, 84]. Other potential candidates, such as **HDAC inhibitor SAHA (Vorinostat**, with FDA approval for use in treat cutaneous T-lymphoma**)** or **organometallic ruthenium compound RDC11,** are currently being investigated, after giving promising results on gastric cancer cell lines and in phase 1-2 clinical trials.

1.8. Prognosis and sarcopenia

1.8.1.   Poor prognosis, especially at advanced stages

Unfortunately, not much has changed in gastric cancer care over the past years and targeted therapies (apart from trastuzumab) were deceiving. As a resultant of the lack of non-invasive diagnostic methods and the failure of targeted therapies, gastric cancer remains a disease of poor prognosis, with **very low overall survival** (median around **11 months**) and a **5-year mortality rate around 70%** [53-78]. If the 5-year survival is approximately 36% for resectable gastric cancers, it drops to 5-20% in locally advanced or metastatic tumors, with an average survival < 1 year [2]. Intestinal gastric cancers are thought to have a better prognosis than diffuse ones, as the 5-year overall survival rate for **linitis plastica** range from **0 to 20%** despite multimodal therapy [84]. Similarly, according to Schauer et al. patients with well-differentiated intestinal gastric cancer had a higher 5-year survival rate than patient with poorly differentiated tumors (76% vs. 67%; p=0.058), especially for patients with $\geq$ 10 cm tumors (42% vs. 14%; p = 0.017) [85]. However, new contradictory results were obtained recent studies, such as Adachi et al., which showed similar outcomes in patients with intestinal, diffuse and signet-ring cell cancers [86].

All in all, the high mortality of gastric cancers appears to be **multifactorial:** *i)* a **late diagnosis** with a very high proportion of gastric cancer patients (~**65%**) **diagnosed at inoperable or metastatic stages**, where curative surgery is no longer an option : the symptomatology is non-specific and the examinations required for the diagnosis are quite invasive (upper gastrointestinal endoscopy with biopsies) with a weak place of imaging for screening and diagnosis purposes, *ii)* the **variable sensitivity of tumors to perioperative chemotherapy, with up to 75% resistances to platinum-compounds at advanced stages** and *iii)* the joint occurrence of **sarcopenia** (muscular atrophy) in up to **30** to **70%** of cases, which is recognized as a negative prognostic factor [53-78, 86]. This highlights the progress that remain to be made in terms of diagnosis and treatment, including the management of both the tumor itself and the treatment-complications, as well as regarding the occurrence of cachexia / sarcopenia.

1.8.2.   Cachexia in gastric cancer

An increasing number of studies showed that **cachexia**, characterized by a progressive *loss of adipose tissue and skeletal muscle mass*, occurs in around **50%** of cancer patients, especially in *upper digestive tract cancers* (Figure 11) **[87]**.
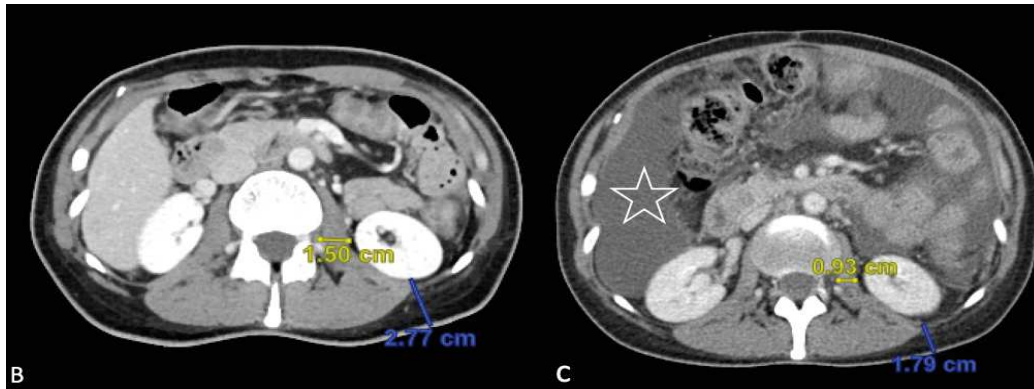
Figure 11. A) Multidetector CR, coronal plane, portal venous phase, showing a diffuse thickening of the stomach wall in a 49-year-old woman with diffuse type gastric cancer (arrows). **B)** Multidetector CR, axial plane, portal venous phase **at diagnosis** (August 2016), **C)** Multidetector CT, axial plane, portal venous phase, same patient **17 months later** (January 2018) at terminal stage (peritoneal carcinomatosis with peritoneal effusion: star). The patient is **cachectic** with muscle atrophy (psoas muscle, yellow measure) with decreased subcutaneous fat (blue measure).

The skeletal muscle loss, or **muscle atrophy**, is associated with loss of muscle strength, which altogether defines **sarcopenia** [86-90]. More specifically, sarcopenia has been defined by the European Working Group on Sarcopenia in Older People (EWGSOP, 2010) as a decrease of muscle mass measured by imaging, impedance or biometrics measurements, associated with decreased performances and/or muscle weakness [91]. Currently in clinical routine, muscle atrophy can only be diagnosed at relatively advanced stages, by means of a CT-based surface & density evaluation of muscles (from abdominal CT, with or without contrast, or CT images of PET-CT). The muscle loss is evaluated through the estimation of a skeletal muscle index, which consists of measuring the surface of the muscles (abdominal wall, psoas and erector spinae muscles) at the level of the 3rd lumbar vertebra (L3) on axial CT images, normalized to the weight and height (BMI) according to the Morsteller formul*a*. The muscles densities (in Housefield Units) are also measured to estimate their fatty infiltration. Most of the studies regarding sarcopenia on imaging, used the following cut-off values for skeletal muscle index (SMI) <52·4 cm²/m² for men and <38·5 cm²/m² for women [91].

Cancer cachexia is also characterized by systemic inflammation and negative protein and energy balance. Sarcopenia has been described in obese patients, elderly patients and patients with various cancers and is a recognized negative prognostic factor [90-91]. It is an insidious syndrome that not only has a dramatic impact on the quality of life but is also associated with poor responses to therapy (chemotherapy and immunotherapy) and decreased survival [92]. Cachexia is estimated to account for around 20 to 25% of cancer-related deaths and is more frequently associated with certain types of cancers. For instance, between 30 to 60% of gastric cancer patients develop cachexia independently of the cancer stage and the incidence of such sarcopenia increases after chemotherapy [93-94]. The available clinical information indicate that muscle atrophy can be *1)* **independent of the tumor stage** (sometimes already present at stage I and II), *2)* **independent of treatments** (sometimes already present at the diagnosis), *3)* **independent of malnutrition** (food supplementation does not restore muscle mass), *4)* a **marker for poor prognosis and response to therapy**.

However, the reasons why only some patients are prone to develop cachexia remain largely unknown. Similarly, the precise part played by the different antitumor treatments, especially chemotherapy agents, in cachexia development is not well understood. Thus, all in all cachexia remains a largely underestimated and untreated condition. One of the main hypothesis is that cancer-related muscle atrophy is caused by inflammatory processes involving interleukins, such as IL6, TNFα and TWEAK, that are often produced by tumors. Hence, the detection of IL6 and TNFα in the serum is one of the techniques used to assess muscle atrophy in patients. However, inflammation is unspecific of muscle atrophy and therefore introduces an important bias. In addition, functional studies and clinical trials aiming at antagonizing IL6 and TNFα using monoclonal antibodies are disappointing and have not clearly confirmed the importance of these interleukins in cancer-related muscle atrophy [95]. If blood levels of IL6 and TNFα could potentially be used as markers for muscle atrophy, they surely are not specific and may present bias. An additional bias is that they can also be induced by infections as well as other pathological afflictions often associated with cancer or anticancer therapies. Therefore, **there is yet no clinically recognized means for unmasking early muscle atrophy or patients at risk of developing it** during the course of the disease. Based on the idea that the catabolism processes associated with muscle atrophy might release proteins outside the muscle, urine markers and blood markers were searched. Several proteins were identified in the urine as markers to identify cancer patients with muscle atrophy, mostly including muscle structural proteins (BPA1, Chromosome 14 open reading frame 78, MIBP1, Maltase-glucoamylase, MACF1, MAP1B, Myosin 5C, Myosin 7A, Myosin heavy polypeptide 7 cardiac muscle ß variant, Myosin 9A, Myosin 10, Nischarin, a-spectrin 1, Zinc finger protein 106 homolog) [96]. Similarly in pancreatic cancer, screening for blood markers led to the identification of 33 circulating proteins associated with muscle atrophy (GRP, S100A7, CCL28, CFH, AFM, MB, TYMS, GHR, PIM1, KLK11, SET, LEP, RSPO3, WFIKKN1, LPO, IL1R2, HRG, HDAC8, MDK, FABP3, COL18A1, LRRTM1, CFH, AKT2, CFD, C5, IMPDH1, IFNA7, IL17B, LILRB2, FCER2, SIGLEC14, LEC1B) [97]. Additionally, single nucleotide polymorphisms in genes (LEPR, TNF, ACE, ACVR2B) that correlates with muscle atrophy have been described in pancreatic cancer patients [98]. Even though these findings are interesting, so far none of them led to clinical protocols that detect muscle atrophy, especially at early stages.

Recently, clinical studies suggest that anticancer treatments based on doxorubicin, taxol or platinum salts (cisplatin, oxaliplatin) could participate in muscle atrophy development in cancer patients compared to non-cancer patients. The downside of such studies is that they did not clearly establish whether it is the anticancer therapy that induced muscle atrophy or the tumor by itself. So far, most of causal studies were performed *in vivo* on murine models focused on the anticancer drug Doxorubicin [99]. Several molecular mechanisms were identified and further investigated in vitro using the myoblastic cell line C2C12 and the production of reactive oxygen species (ROS). The regulation of the NFKB and p53 transcription factors were shown to play a role [100]. The Notch pathway was also impacted by doxorubicin in *in vitro* and *in vivo* models [100]. Additionally, recent studies also showed that p63, the paralog of p53, played a role in muscle atrophy, especially in response to Doxorubicin [101]. Regarding muscle catabolism, TRIM63, and Atrogin1 (ubiquitin ligases inducing muscle protein degradation by the proteasome) have been identified in mouse models and cell cultures, as key mediators of muscle atrophy in different pathological contexts [99]. Molecular mechanisms regulating the expression of these effectors have been characterized, for instance as the expression of TRIM63 is regulated by glucocorticoids or cytokines (IL6, TNFα, TWEAK-TNFRSF12A). Additionally, TRIM63 appears induced in a mouse model of drug-induced (doxorubicin) muscle atrophy, which involves the

Notch signaling pathway and a regulation by the p53 family [101]. MiRNAs were also identified, such as miR-205-5p, as additional mechanisms regulating some key actors of muscle atrophy, including p53 and FOXO3 [102]. Unfortunately, very little evidence has yet been obtained about the existence of these mechanisms in humans, given the difficulty to obtain muscle samples from cancer patients for obvious ethical reasons. Thus, a consensus emerged, highlighting the lack of knowledge on the underlying mechanisms of muscle atrophy and the need to identify, as early as possible, patients at risk of developing severe muscle atrophy. These patients would require adequate early management, while patients considered "not at risk" could avoid heavy, expensive procedures and/or potential procedure-related complications. Despite the fact that multiple mechanisms are reported to be involved in the development of muscle atrophy, with a number of cytokines postulated to play a role in the etiology of the persistent catabolic state (i.e. IL6, TNFα...), **these findings did not lead to a clinically applicable cure yet**.

Preventative measures have been evaluated, such physical activity, dietary supplements (Omega 3, vitamin E), anabolic agents (e.g. selective androgen receptor modulator (SARM)), proteasome inhibitors or antibodies targeting interleukins (TNFα, IL6) [103]. Unfortunately, the preliminary results were disappointing in terms of efficiency, but also because of intrinsic limitations, such as the difficulty to follow-up patients (to ensure good adherence to the physical activity or diet program) or associated side effects. In particular, **no current therapeutic approach can efficiently restore muscle loss and strength**. For instance, food supplementation only restores some adipose tissue mass, but fails to restore muscle mass. Hence, existing therapies for cachexia, including orexigenic appetite stimulants, failed to restore muscle mass and only focused on palliation of symptoms and reduction of the distress of patients and families, rather than the prolongation of life. All in all, there is a clinical need for further development in this field, especially for the development of non-invasive innovative techniques, that would help us stratify patients regarding the risk of developing severe muscle atrophy and to assess more precisely the impact of anticancer therapies on muscles [104-105].

1.9. Animal models of gastric cancer in translational research

In translational cancer research, the use of preclinical mouse models is more and more common, especially for the development of new drug therapies [106-110]. Multiple models are available, from cell-derived or patient-derived xenografts, drug-induced models or murine lines resulting from genetic modifications.

1.9.1. Cell-derived models

Cell line-derived mouse models are being overwhelmingly represented in the literature (up to 82% of the studies until 2016) due to their easy and unexpensive development, but they raised more and more criticism for their distorted tissue architecture, with an altered tumor microenvironment, and the possible occurrence of a loss of genetic heterogeneity, altogether with genetic changes, which has been described after a long-term propagation [107-108]. In gastric cancer, various human cell lines have been used (AGS, NUGC3, MKN45…) and mouse cell lines can also be used to create syngeneic xenografts (such with YTN16 = mouse gastric cancer cells).

1.9.2. Patient-derived xenografts (PDX)

On the contrary, patient-derived xenografts (PDX) are obtained by implanting fresh human tumor fragments, issued from biopsies or surgical specimens, into immune-compromised mice (such as the athymic NMRI NUDE mice for instance), with serial re-transplantations in new mice generations. PDX models are less commonly used (7% of the recent studies) due to higher development costs and the added difficulty of obtaining fresh human tissue samples. in translational cancer research, there is growing interest for such models, as they retain over time the major histological, molecular and genetic characteristics of the primary tumors from which they arose, while remaining stable during the passages in the different mouse generations [107]. Thus, PDX models resemble closely their human counterpart and are able to reflect the vast patient and tumor variability and heterogeneity, that is inherent to human cancer [111-113]. Heterotopic implantation, where the tumor sample is implanted in the flanks of the mouse, is more commonly performed, but its metastatic evolution is unusual [109-113]. On the contrary, orthotopic implantation (= directly in the organ of origin of the primary tumor) may lead to primary and metastatic (especially to the liver) tumor growth mimicking what is seen in patients [115-118]. As animal models, PDX are really useful in translational research, allowing repeated measures and time-course follow-ups of tumor progression in response to various conditions (anticancer drugs, genetic modifications…), as they correlate quite well with clinical responses to chemotherapy. They also enabled the analysis of intratumoral clonal variation. Such models have been established for many cancers, including breast, colon and gastric cancers, with engraftment rates ranging from 25 to 75% [107-110]. **In gastric cancer, the engraftment success rate is quite low (25 to 34%), with a risk of EBV-related lymphoproliferation (33% of the cases) when NOD or NOG mice are used** [109-115]. Importantly, **success rate varies between the histological subtypes** of gastric cancer and **all existing PDX models are of intestinal subtype**. No PDX model was ever successfully developed for diffuse gastric cancer, likely because of the intrinsic properties of the diffuse subtype, characterized by the dispersion of isolated cancer cells in the stroma, insufficient to reach the minimal cancer cells number required to initiate tumor growth, in a similar way as implantation usually fails for low tumor cell percentage biopsies [109].

1.9.3. Genetic engineered mouse models

Tumor-bearing mice can also be genetically engineered to develop cancer. For instance, our collaborators from the University of Pennsylvania (USA) have developed a model of mixed type gastric adenocarcinoma, with both intestinal- and diffuse-type lesions. This model combines conditional oncogenic Kras activation with loss of E-cadherin and p53, specifically in cells of the gastric parietal cell lineage (Atp4b+) and traces these cells with a YFP reporter [119]. The penetrance is reported 100% with a median survival of 2.5 months (90 days) compared to almost a year in other models (Kras wild-type model). One advantage of this genetic engineered model is that the cancer occurs directly in the stomach of the mouse, bearing the same advantages of orthotopic PDX models in terms of loco-regional environment, as well as for lymph node and distant metastasis. In this model, mice develop regional lymph node metastases and lung metastases in 100% of the cases, paratracheal lymph node metastases in 50% of the cases and liver metastases in 20% of the cases. As the tumor develops directly in the stomach of an immunocompetent animal, the tumor ecosystem including both **microenvironment** (blood vessels, immune cells, activated fibroblasts, neuronal infiltration…) and **macroenvironment** (muscle atrophy, fat loos…) is reproduced, while PDX-bearing athymic mice only

have natural killer as immune cells. Additionally, genetic engineered mouse is the only mouse model that develops diffuse-type gastric cancer (~25% of diffuse cells on histology) [109-119].

1.9.4. Mouse model of drug-induced muscle atrophy

If cell-derived, PDX and genetic engineered mouse models are developed more specifically for the tumor they bear, other models were created to reproduce particular side effects of tumor-bearing and/or treatments, such as cachexia and sarcopenia. For instance, muscle atrophy can be induced in C57/BL6 mice by a single intraperitoneal injection of 20 mg/kg of Doxorubicin [118].

1.10. Small animal (rodents) imaging: current trends

1.10.1. Small animal (rodents) imaging in translational research

Recent developments in molecular biology and genomics have boosted the need for laboratory animals, on which longitudinal studies over extended periods of time are conducted. In preclinical studies, one of the most relevant, predictive and easily reproducible way to assess the outcome of a treatment is through the tumor volume and the speed of growth of tumors. Classical measurements of the tumor volume were historically performed by hands-on steel or electronic calipers, which are unexpensive and easy to perform, but lack of precision and interobserver reproducibility [12, 14]. Nowadays, animal models can be imaged (*ex vivo*, *in vivo* and/or longitudinally) by various imaging modalities, such as ultrasound, micro-CT, PET-CT or MRI, enabling a morphological analysis, follow-up and also *in vivo* estimation treatment efficacy. Animal-adapted (coils, probes, devices..) imaging modalities under veterinary supervision in a dedicated facility are required.

1.10.2. Ultrasound

In vivo measurements of the tumor burden are conventionally accepted metrics of the anticancer activity of chemotherapy agents in mouse models and manual hands-on caliper has been the most common way of measuring them. Recently, ultrasound imaging appeared as a radiation-free relatively easy method for tumor measurements in mice (using B-mode), as studies showed that cell-line derived xenografts ultrasound measurements were more accurate than manual caliper ones [94-95-96]. Ultrasound images are based on the propagation of acoustic echoes from high-frequency acoustic waves in various tissues. Unlike CT and MRI, small animal ultrasound studies performed with high frequency probes, are better suited for an easy-to-follow, day-to-day in-real-life assessment of the tumor growth and the tumor volume, while limiting the costs of such evaluation [121]. The vascular network of a tumor can also be assessed using Doppler (observation of blood flow velocity with the B-mode image being overlaid by a color map of either the blood flow = color Doppler, or by its value = power Doppler) and/or gas-filled microbubbles as contrast agent (= contrast-enhanced ultrasound, exploiting the non-linear properties of the bubbles - average diameter of 5 μm and a limited lifespan in the blood flow-) [122].

The major limiting factor is the depth of the tissue that can be imaged through, as ultrasound is most efficient for superficial tumors, with air/bone causing artefacts [122]. Another downside of ultrasound

is observer-dependency of the measure, as its reproducibility relies on the observer's technique (probe movements & experience in recognizing/measuring structures).

1.10.3.   Computed tomography (CT)

Non-invasive imaging techniques, such as micro-CT (= small animal computed tomography) enable a 3D representation of high-density tissue structures needed to monitor therapeutic effects over time, with quite high spatial resolution high (50 μm) and fast imaging times (4-6 minutes) [124]. This method has been used on tumor-bearing mouse models and appeared superior to manual caliper to accurately follow tumor progression. Such longitudinal imaging protocols optimizes intervals between treatment and therefore reduces the number of animals required to get reliable results (especially as images can be post-processed and read by different observers after acquisition) [124]. In small animal oncology, micro-CT is the modality of choice for bone or lungs imaging, where abnormalities can be clearly distinguished from surrounding tissue even without any contrast agent [124]. However, these techniques require a more complex setup of the experiment (machine, mouse sedation..) with increased costs, thus being difficult to apply in large groups of animals. Micro-CT also exposes to animals to ionizing radiations [97].

1.10.4.   Magnetic resonance imaging (MRI)

Magnetic resonance imaging (MRI) appears as the modality of choice and the most morphologically accurate three-dimensional measurement technique for brain and abdomen (liver, kidneys, bladder, prostate, colon, prostate, pancreas, lymphoma…) imaging in rodents, due to its higher spatial and contrast resolution. It is also modality of choice for metastasis imaging - especially to the liver - as well as for muscle studies [97-98]. For rodent imaging, high magnetic fields (7 or 9.4T for instance) with dedicated coils are used. One of its most important role in small animal imaging is its involvement in the development and validation of new animal models of cancers, usually through the measurement of growing tumors [97]. In oncology, MRI enables *1)* the **early detection of tumors**, *2)* a detailed **characterization of the tumor tissue** (liquid, solid, fat…), *3)* the **characterization of the vasculature of the tumor** and *4)* an **analysis distant metastasis sites** (liver, peritoneum…). The major downfall of MR imaging is the length of the examination (for instance : 9 minutes for one sequence on a 9.4T Bruker machine for a T2 sequence with a 28 x 28 mm field of view), resulting in a ~ 20-minute scanning time per animal. Therefore, in order for the mice to remain still, it is anaesthetized with Isoflurane® (Abbott GmbH, Wiesbaden, Germany; 2% vaporized in oxygen) and additional ECG (cardiac) and respiratory gating are required to reduce motion artifacts. The mouse is placed in the MRI, in a dedicated coil, in prone position (head first), dorsal decubitus, on a hot water bed. Contrasts agents (for instance gadolinium) may also be used to aid in the visualization of tumors by enhancing different tissue signal. MRI is not observer-dependent and images are highly reproducible, which makes it a very useful tool for comparison and follow-up of tumors. New imaging methods are currently being developed to be better suited to study the activity of new therapeutic compounds, with in-real time imaging & longitudinal follow-up.

1.10.5. Positron emission tomography–computed tomography (PET-CT)

Even though CT and MRI present with higher spatial resolution, PET-CT permits a more functional approach, with the use of various radionucleotide tracers, such as 18-Fluoxodesoxyglucose or F-MISO [99-102]. Recent studies showed that PDX tumors accurately reproduced the metabolic characteristics of the corresponding parental tumors on PET-CT imaging using ^{18}F-FDG [103]. Gastric adenocarcinomas, as well as other tumor types, showed significant 18-FDG uptake. As PET-CT can monitor both the tumor growth rate and the metabolic uptake of the tumor (by means of SUVmax measurements), it can be a useful tool to assess new therapies and early therapeutic response.

1.11.   Future developments and overall aim of the project

Available recent histological, genetic and molecular data confirmed the heterogeneity of gastric cancers. In the area of precision medicine, recent discoveries (*Figure 27*) regarding biomarkers (for instance HER2 status), together with new generation sequencing genomic data and novel preclinical models of cancers, have increased the hopes of finding new actionable mutations and therefore novel targeted therapies [124].

However, these data have not yet generated significantly help to improve the patients' care. Current failure to obtain more efficient therapeutic approaches have multiple potential explanations, some of them may be *1)* the absence of *ideal* animal model for the *in vivo* preclinical evaluation of such therapies, *2)* the absence of longitudinal molecular signature studies of tumors 'before and after treatment' to better understand treatment-related changes that would provide a more precise and dynamic molecular classification *2)* weaknesses of the diagnostic process and patient selection, especially regarding technical limitations of non-invasive imaging methods together with the absence of patient stratification in the latest phase II/III clinical trials… and *3)* the lack of consideration of co-occurring diseases worsening the prognosis, especially sarcopenia/cachexia.

Indeed, if a certain number of specific effectors of sarcopenia (e.g. TRIM63) have been identified in murine models or cell cultures and molecular mechanisms regulating the expression of these effectors have been characterized (e.g. the expression of TRIM63 is regulated by glucocorticoids, trophic factors - IGF1-AKT, TGFb-SMADs - or cytokines - IL6, TNFα, TWEAK-TNFRSF12A -), the origins and physiopathological mechanisms of sarcopenia/cachexia in cancer in general, and in gastric cancer more specifically, remain unclear. Similarly, the recent molecular classifications (TCGA, ACRG…) of gastric adenocarcinomas have led to the identification of several deregulated pathways, but the resultant targeted therapies were ineffective, which questions the relevance of such classifications for therapeutic purposes. Therefore, there is a need for a more accurate classification, that will take into account the intra-tumor clonal variation, the influence of the tumor microenvironment and the interaction with the macroenvironment (surrounding tissues e.g. muscles), associated with a stratification of patients according to their imaging/molecular/genetic status, to improve the therapeutic care. Thus, the search for new biomarkers or novel actionable targets (which could lead to drugs development), the development of new imaging tools and the improvement of existing diagnostic tools, is essential for a better discrimination of the different subtypes of gastric cancer, each associated with a different prognosis. The heterogeneity of gastric cancers also exists in terms of

response to treatments and the lack of targeted therapy also highlights the need for more personalized treatments. Based on the complexity of cancers, especially gastric ones, and the importance of the microenvironment in their interaction with surrounding tissues (macroenvironment), we need novel and more realistic mouse models - closer to the characteristics of patients and tumors - to be able to better predict treatment responses between "good" and "bad" responders. The future could be an *integrated diagnosis*, combining histological features, imaging data, molecular analyzes and genetic characteristics of cancers, with the aim of eventually offering personalized *à la carte* therapies to cancer patients.

Therefore, the overall aim of my project is to develop and characterize animal models that are representative of the diversity of the gastric cancer complexity. I am to be able to establish a set of experimental protocols allowing the longitudinal and precise testing of novel therapeutic strategies by taking in account to whole tumoral ecosystem (cancer cells, micro-environment, surrounding tissues…). Concerning the surrounding tissues, we have a particular focus on muscle atrophy. To do so, I combined the use of patient-derived xenograft mouse models, molecular characterization of biomarkers, and top of their class imaging tools. By the nature of it objective, this translational project is challenging and highly collaborative, requiring dynamic interactions between different hospital departments, laboratories specialized in small animal imaging a biomedicine laboratory with molecular and cellular analysis tools and chemistry laboratories providing the novel therapeutics.

To reach our final goal, three specific objectives have been identified:

4) **To develop and perpetuate different patient-derived-xenografts (PDX) in gastric cancer that are representative of the gastric cancer complexity, such as different level of cancer cell differentiation, different molecular mutational status for p53….**

5) **To characterize them using various small animal imaging methods (ultrasound, CT, MRI…) compared to their histological samples & molecular characteristics**

6) **To use those PDX models for the development of new therapeutic approaches in gastric cancer and apply imaging methods to longitudinally study the tumor, the microenvironment and the surrounding tissues.**

2. RESULTS

2.1. Development and characterization of gastric cancer patient-derived xenografts models

Most of the recent studies on the development of novel anticancer-drugs or new targeted therapies relied on murine models, such as patient-derived xenografts (PDX) or cell-line-derived xenografts for their *in vivo* validation, as they allow repeated measures of the tumor volume, as well as time-course follow-ups of tumor progression, in response to various conditions (anticancer drugs, genetic modifications…). Compared to cell-line derived xenografts, patient-derived xenograft models are known to remain stable across generations and retain the major traits (architecture, histology and genetic characteristics) of the primary human tumor they derive from, thus resulting in the only murine model able to reflect the patient and tumor variability and heterogeneity, inherent to human cancers. Importantly, Zhu et al. reported that the chemosensitivity of PDX models was comparable with patients and therefore the use of those models appears as the most accurate method to evaluate the efficacy of new anticancer drugs or novel targeted, in preclinical studies [114].

In gastric cancers, there are currently five reports regarding the development and/or use of gastric cancer PDX models [109-110, 113-114, 126-130]. The success rates of such xenografts in the two major papers quite low (25% for Choi et al. et and 34% for Zhu et al.), compared to other cancer types, where it can reach up to 70% (breast, colon…) [109, 114]. Also, Choi et al. and Dieter et al. noted a risk of EBV-related lymphoproliferation (33% of the cases) when NOD or NOG mice were used [109-113]. To create a PDX model, a tumor sample (from a biopsy or a surgical specimen) of gastric cancer is prepared an implanted on the flanks of an immunocompromised mouse (*Figure 12*) We chose athymic NUDE mice, to reduce the lymphoproliferation risk. The tumor then develops over a period of 1 to 6 months, before being harvested and transplanted in another generation of mice.
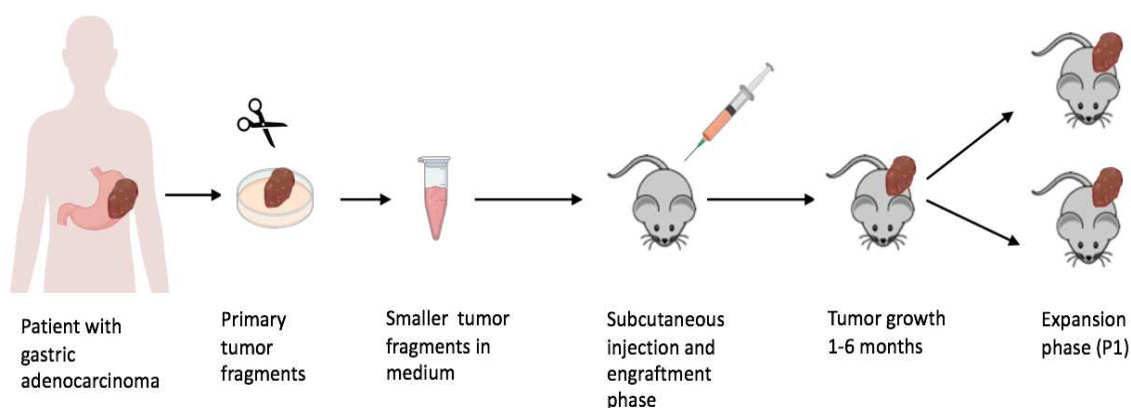
Figure 12. The development of a PDX model of gastric cancer.

Important success factors of such graft appeared to be *i)* the **histological subtype** of gastric cancer, *ii)* the **percentage of tumor cells** on the sample used *iii)* the **use of untreated samples** (success rate 52.1% on naïve tissue versus 21.9% post-treatment - one possible reason could be the higher proportion of

necrotic or scar tissues in treated tumors), while the importance of the **cold ischemic time** (latency before implantation) remains controversial [109, 114]. For now, the few existing PDX models are all of intestinal subtype and no PDX model was ever successfully developed for diffuse gastric cancer. This is probably related to the intrinsic properties of the diffuse subtype, presenting as isolated cancer cells in the stroma of the stomach, therefore insufficient to reach the minimal cancer cells number required to initiate tumor growth, in a similar way as tissue implantation commonly fails in case of biopsies with a too low tumor cells percentage.

In pre-clinical oncology research, most *in vivo* studies using mice are longitudinal ones, conducted over extended periods of time. In such studies, one of the most relevant way to assess the outcome of a treatment is through the tumor volume and the speed of growth of tumors. If the volume of tumors can be estimated using manual caliper, this method lacks precision and inter-observer reproducibility [12, 14]. A more precise way to evaluate the tumor volume, with a direct access to morphological information about the tumor, relies on small animal imaging modalities such as ultrasound, micro-CT, PET-CT and/or MRI. Additionally, small animal imaging enables a morphological analysis as well as a longitudinal follow-up with *in vivo* estimation of treatment efficacy. Choi et al. and Zhu et al. characterized their gastric cancer PDX models histologically and genetically, but they did not perform any morphological imaging correlation (they only used MRI to detect the successful implantation of their fragments implanted in the sub-renal capsule). The other papers did not mention any small animal imaging.

Considering the low success-rate in establishing new PDX models (especially for gastric cancer ~ 25%), the financial burden related to their maintenance and their key-role in pre-clinical cancer research, we thought it that an imaging characterization of our PDX models compared to their corresponding histological slices would help us to better understand them. For a daily usage, we evaluated the performances of ultrasound compared to caliper. We also used magnetic resonance imaging, as it would provide a direct access to information about the tumor size, morphology, sub-structure and to potential treatment-related changes. Additionally, further characterization of the PDX models and especially their stratification according to various status biomolecular (HER2, PD-L1, P53...) status seemed important, in order to be able to be more selective regarding their use in pre-clinical research. Differentiation of gastric cancer PDX models according to their PD-L1 related immune check-point status has never been done before, even though 30% of gastric cancer tumor cells are known to express PD-L1, with pembrolizumab (anti PDL1 with FDA approval) as a potential targeted therapy [81].

*2.1.1. **ARTICLE 1** : Ultrasonic evaluation of gastric cancer patient-derived xenografts shows different impact between cisplatin and suberoylanilide hydroxamic acid (SAHA) on tumor structure*

<div style="border:1px solid blue">

Ultrasonic evaluation of gastric cancer patient-derived xenografts shows different impact between cisplatin and suberoylanilide hydroxamic acid (SAHA) on tumor structure

</div>

Venkatasamy A. [1,2]**, Guerin E.** [1]**, Blanchet A.** [1]**, Orvain C.** [1]**, Devignot V.** [1]**, Chenard MP.** [3]**, Romain B.** [4]**, Gaiddon C.** [1*]**, Mellitzer G**[1*]**.**

Affiliations :

1. Streinth Lab (Stress Response and Innovative Therapies), Inserm UMR_S 1113 IRFAC, Interface Recherche Fondamental et Appliquée à la Cancérologie, 3 avenue Molière, Strasbourg, France
2. Radiology department, Hôpital de Hautepierre, Hôpitaux Universitaires de Strasbourg, 1 avenue Molière, 67098 Strasbourg CEDEX, France
3. Pathology department, Hôpital de Hautepierre, Hôpitaux Universitaires de Strasbourg, 1 avenue Molière, 67098 Strasbourg CEDEX, France
4. Digestive surgery department, Hôpital de Hautepierre, Hôpitaux Universitaires de Strasbourg, 1 avenue Molière, 67098 Strasbourg CEDEX, France
* corresponding authors: Mellitzer G.: Mellitzer@unistra.fr; Gaiddon C.: Gaiddon@unistra.fr

Abstract

Objective. Measurements of tumor burden are conventionally accepted metrics of *in vivo* cytostatic and cytotoxic activity of anticancer drugs. Recently, ultrasound measurements appeared more accurate than manual caliper on cell-line-derived xenografts. The aim of our study was to use ultrasound to evaluate the impact of chemotherapies on gastric tumor growth on patient-derived-xenografts (PDX) and compare its performances to caliper ones.

Material and Methods. For that purpose, we established PDX models of gastric cancer and imaged tumor growth using ultrasound, in response to standard chemotherapy (cisplatin) or targeted therapy (histone acetylase inhibitor SAHA). Manual caliper and ultrasound measurements were compared to macroscopic specimen measurements (gold standard) after resection. Tumors characteristics were also analyzed by immunohistochemistry for relevant makers (Ki67, H3K9ac, p53, -actin).

Results. A selected PDX model responded well to cisplatin, with smaller tumors ($239.8 \text{ mm}^3 \pm 159$) compared to controls ($561.5 \text{ mm}^3 \pm 138.5$, $p = 0.0382$), while there was no significant difference with SAHA ($450.6 \text{ mm}^3 \pm 406.2$, $p=0.6349$). Manual caliper on live mouse globally (90%) overestimated tumor volume compared to gold standard ($p<0.0001$). Ultrasound performed better than caliper with less overestimation (38%) with no significant difference between ultrasonic and gold standard measures. Importantly, ultrasound allowed in-real-time access to the tumor substructure (e.g. cysts), enabling observation of changes (confirmed by immunohistochemistry) in the tumor microenvironment distinctive of the different treatments.

Conclusion. Small animal imaging using ultrasound allowed time-course follow-up of tumor progression with repeated measures, in response to various conditions (anticancer drugs, genetic modifications…), while enabling in-real-time access to tumor volume, morphology and substructure.

Mini abstract (30 words)

Small animal imaging using ultrasound allowed time-course follow-up of tumor progression with repeated measures, in response to various conditions and enables in-real-time access to the tumor volume, morphology and substructure.

Keywords

Gastric Cancer ; ultrasound ; HDAC Inhibitors

Abbreviations

PDX = patient-derived xenografts
HDAC = histone deacetylases
SAHA = suberoylanilide hydroxamic acid
MRI = magnetic resonance imaging
micro CT =small animal computer tomography
IHC = immunohistochemistry
SD = standard deviation
HDACi = HDAC inhibitors

Introduction

Gastric cancer is the 5th most common cancer worldwide and the 3rd in term of mortality, with a 5-year-survival rate around 36% for operable cancers, dropping to 5-20% in locally advanced/metastatic ones and an overall survival <1 year [2]. This highlights the progress that remains to be made for its diagnosis and treatment, including the management of tumor/treatment-related complications. The current standard therapies mainly use platinum-based drugs (cisplatin or oxaliplatin), but the survival rate of patients ongoing palliative therapies remains very low, as the majority (75%) of tumors are chemoresistant at late stages. The recent molecular classification of gastric adenocarcinomas led to the identification of dysregulated pathways, at which targeted therapies attempts have been made, with unsatisfactory results so far [3]. For instance, increased expression of several histone deacetylases (HDAC) have been described in gastric cancers. However, the targeting of HDACs using the pan-HDAC inhibitor Vorinostat (SAHA) showed no gain in patients' survival when administrated without patient stratification [4]. Hence, taking into account the intratumoral clonal variation and/or the influence of the microenvironment might provide crucial information and lead to new targeted therapies or novel treatment combinations, which might improve the therapeutic care. Currently in translational cancer research the use of pre-clinical mouse models, such as patients-derived xenografts (PDX), are more and more common, especially regarding the development of new drug therapies, as PDX models retain the major histological, molecular and genetic characteristics from the primary tumor, which are maintained across passages [1, 5-8]. Therefore, PDX allow time-course follow-up of tumor progression with repeated measures, in response to various conditions and the analysis of the evolution of intra-tumor clonal variation [7]. Unfortunately, in gastric cancer, the success rate for their establishment remains very low (~25%), with only intestinal-type PDX available [6, 8-10].

Measurements of the tumor burden are conventionally accepted metrics of *in vivo* cytostatic and cytotoxic activity of anticancer drugs in mouse models, classically measured by manual calipers [2-3, 6, 9-11]. Non-invasive imaging techniques, such as magnetic resonance imaging (MRI) or micro CT (small animal computered tomography), appeared superior to caliper to accurately follow tumor progression, but require a more complex setup of the experiment with higher costs and are difficult to apply to large groups of animals [13-14]. In recent studies, ultrasound measurements appeared more accurate than manual caliper ones on cell-line derived xenografts [11-12, 14]. Another advantage of the ultrasound is the additional information provided

during the exploration, such as the morphology or the vascularization of the tumor [15]. Accessing this level of information is particularly relevant for PDX models, since their primary interest is to reproduce more closely the structural complexity of the patient's tumor tissue. The aim of our study was to evaluate the performances of ultrasound compared to manual caliper measurements and histology, on gastric cancer PDX mice, treated by cisplatin or suberoylanilide hydroxamic acid (SAHA).

Material and Methods

Establishment of the patient-derived xenograft model

All animal experiments were approved by our Institutional Animal Care and Use Committee (APAFIS#8320). Use of human tissues was approved by the Ethics board. Patients gave their written consent. All protocols adhered to the Declaration of Helsinki. Six weeks-old athymic female Nude mice were acclimated for two weeks and provided with unlimited access to sterilized food and water *ad libitum* and housed with 12h day/night cycles.

Manual (mechanical) Vernier caliper measurement and ultrasound evaluation

For caliper measurements, the thickness of the tumor was extrapolated from the width measure. The volume was calculated as V= (length x width) ^{2}/2 [11]. Ultrasound was performed using B-mode images on a Toshiba Medical Systems Company (Tochigi, Japan) with a superficial transducer (14MHz). Ultrasound measurements: length, width and thickness of the tumor. The volume was calculated using V=((π/6) x Length x Width x Thickness) [14].

We also visually assessed the tumors' morphology with ultrasound :
- presence of solid echoic components, rated 0 (absent) or 1 (present)
- presence of cysts, rated 0 (absent) or 1 (present <50%) or 2 (present >50%)
- location of the cysts (central or peripheric)
- the presence of hyperechoic images, rated 0 (absent) or 1 (present)

Histological evaluation

After the final measurements, the tumor was excised for *ex vivo* macroscopic evaluation. The length, width and thickness of each tumor were measured using the same manual caliper and served as gold standard. The volume was calculated with the same formula as with ultrasound: V=((π/6) x Length x Width x Thickness). Overestimation of the tumor size occurred when the measured volume corresponded to a 10% or higher increase compared to the gold standard volume. Then, all tumors were cut in halves along their greater axis and fixed in 4% paraformaldehyde solution for hematoxylin-eosin (*H&E*) staining. All slices were read at x2 - x20 - x40 magnifications, blinded to the treatment group. The following elements were analyzed:
- necrosis and intraglandular necrosis: 0 (absent) or 1 (present)
- cysts: 0 (absent) or 1 (present <50%) or 2 (present >50%) + location (central or peripheral)
- stroma (normal=0 or more important than in the initial tumor=1)
- glandular papillary tumoral structures

Immunohistochemistry (IHC)

IHC were performed on deparaffinized histological tumor slices (5µm). Unmasking was carried out with NaCitrate in the microwave oven (800W, 10min). After washing once with distilled water and once with PBS the sections were permeabilized with 0.1% PBS-Triton for 5min and the nonspecific sites blocked in 5% NGS-PBS-Triton 0.1% (Normal Goat Serum) during 60min. Subsequently, primary antibodies to P53 DO1 (SC126, 1/200, Santa Cruz®), H3K9 (NB22-0122, 1/300, Netobiotech®), Ki67 (sp6) (RM-9106.S, 1/500, Thermo Fisher RM) and α-actin (aSMA,

1/500) were diluted in PBS + Triton 0.1%, then added and kept at 4°C overnight. After 3 washes with PBS-Triton 0.1% slides were incubated with the secondary antibody (diluted 1:1000 in 1xPBS/5% NGS) specific for the primary antibody for 1 hour at room temperature. Slides were mounted with FluorSafe Reagent Mounting Medium (Calbiochem®) and allowed to dry overnight before observation using a fluorescence microscope (Axio Imager 2 - ZEISS). Ki-67 staining was scored as % of cells showing a positive nuclear staining.

Genetic analysis

We also evaluated tumor tissue ctDNA by parallel next-generation-sequencing (NGS) panel testing. DNA was extracted from the primary tumor from snap-frozen tissue and PDX using phenol/chloroform extraction protocol [16]. Mutation screening was performed on a MiSeq Illumina platform using Tumor Hotspot MASTR Plus assay (Multiplicom-Agilent). Sequencing data were aligned to human genome hg19 using BWA-MEM algorithm (Burrows-Wheeler Aligner-Maximal Exact Matches). Variants were called using three different variant callers: VarScan, GATK Haplotype Caller, and GATK Unified Genotyper. The minimum coverage per base and variant allelic frequency were fixed at 500-fold and 5% respectively. Data were visualized using the Integrative Genomics Viewer. A panel of twenty-six clinically targetable genes were analyzed: ATK1, ALK, BRAF, CDKN2A, CTNNB1, DDR2, EGFR, ERRBB2, ERBB4, FGFR2, FGFR3, H3F3A, HIST1H3B, HRAS, IDH1, IDH2, KIT, KRAS, MAP2K1, MET, NRAS, PDGFRA, PIK3R1, PIK3CA, PTEN and STK11.

Statistical analysis

Continuous variables were expressed as mean ± standard deviation (SD). Categorical variables were expressed in terms of numbers and percentages. Unpaired t-student test with equal SD was performed to compare the tumor volumes between the groups. The significance was set at $p = 0.05$. One-way ANOVA standard tests were used for analysis of significance of the different measures (independent variables). Confidence levels were chosen at 95% confidence-interval. Tukey's Multiple Comparison test was performed to compare caliper, ultrasound and gold standard. All statistical analyses were performed using GraphPad software 6.0 [16].

Results

Patient-derived xenograft (PDX) models are valuable tools in cancer research, especially for anti-cancer drug testing. Considering the low success-rate in establishing new PDX models, the financial cost for maintaining these models and their key-role in cancer research, we thought that in addition to the standard volume measurements of the tumor burden over time, any pre-clinical experiment performed should include an in-real-time access to potential treatment-related changes in the tumor morphology, with limited extra costs. Therefore, ultrasound seamed very appealing, as it would allow the follow-up of tumor growth over time, while providing direct access to information about the tumor structure and treatment-related changes.

Establishment of PDX mouse models.

We established several PDX models, either from gastric cancer biopsies (2x2 mm) or from tumor fragments (4x4mm) of surgical specimens, with limited *ex vivo* time (<25min). The fragment was implanted on the flanks of an anaesthetized immunodeficient mouse (Figure 1a), with close monitoring of their growth (1-3 times/week by caliper). When the implanted tumor reached 500mm³, the engraftment was considered successful, the mouse was anaesthetized and the tumor harvested for serial transplantation into successive mice generations (Figure 1a). We chose to use the *GXC-004* PDX model, originating from a surgical specimen obtained after total gastrectomy of a primary well-differentiated intestinal type HER2-negative gastric adenocarcinoma ypT1aN0, from a 64 years-old man treated with preoperative chemotherapy (EOX: epirubicin + cisplatin + 5-

fluoro-uracil). The implanted fragment reached the 150mm^3 target volume within 15 days. Histology of the different passages of GCX-004 were well-matched with the primary human tumor (Figure 1b) without lymphomatous transformation [2]. In addition to the histological stability over time and passages, the PDX retained the genetic characteristics of the primary tumor, with no potentially pathogenic actionable mutation on the NGS panel of 26 clinically targetable genes.

Effect of anti-cancer drugs on GCX-004 tumor growth: Caliper, ultrasound and Gold standard end-point caliper measurement

For our experiment, several tumor fragments (~3mm^3) from *GCX-004* (passage 8) were implanted subcutaneously on the flanks of 16 NUDE mice, and the mice were split into three groups [4]. Once the tumors reached the target volume, we treated one group (*n*=6) with cisplatin (5mg/kg body weight), a second one (*n*=6) with Vorinostat (SAHA 50mg/kg body weight) and the control group (n=6) with DMSO-PBS-cremofor. Tumor volume was measured every 3-4 days by caliper (Figure 3a) and ultrasound (Figure 3b). At day 23, final measurements were performed. The tumors were dissected and re-measured by caliper (gold standard) (Figure 4a). Unfortunately, for unknown reasons, in the SAHA-treated group four transplanted tumors did not reach 100mm^3 and 2 tumors disappeared after one day of SAHA-treatment. The dissected tumors volumes ranged from 29 to 1444mm^3. The smallest tumor measured V=((π/6) 7x (Length) 4x (Width) 2x (Thickness)) V=29 mm^3, corresponding to approximately 7,000,000 cells (average cell diameter of 20µm) [6]. As expected, cisplatin-treated tumors (*n*=12) were smaller (239.8mm^3±159) than controls (*n*=12, 561.5 mm^3±138.5) (*p*=0.0382). SAHA-treated tumors (*n*=6, 450.6mm^3±406.2) were also slightly smaller than controls (*p*=0.6349). In general, caliper, ultrasound and gold standard measurements showed a similar final tumor volume profile between controls, cisplatin and SAHA-treated groups (Figure 4b, c). Interestingly, when the control group and the cisplatin group are compared, ultrasonic measures gave a better statistical difference than caliper (*p*=0.018 and *p*=0.0243 respectively) showing the relevance of ultrasound for tumor growth evaluation (Figure 4b and c).

Caliper and ultrasound measurements compared to the gold standard

Manual caliper on live mice globally overestimated the volume in 90% (*n*=29) of the cases compared to the gold standard (*p*<0.0001), regardless of the group. For instance, for the same tumors in the control group there was a statistically significant difference between caliper (824.6mm^3±542.2) and gold standard measures (561.5mm^3±479.7, *p* < 0.001) (Figure 5a). The same was also observed with cisplatin (*p* < 0.0001) (Figure 5b) and SAHA (*p* < 0.05) (Figure 5c). Overall, the tumors overestimated by the caliper were in average smaller (368.9mm^3) than those it underestimated (573.8mm^3). On the contrary to caliper, there was no significant difference between ultrasound and gold standard measures within all groups, when measuring the same tumors (Figure 5). For instance, in the control group, there was no significant difference between gold standard (561.5mm^3±479.7) and ultrasound measures (590.9mm^3 ± 425.6, *p*>0.05) (Figure 5a). Hence, ultrasound performed better than caliper and volume overestimation (>10%) was less frequent (38%, *n*=12). Correlation analyses between gold standard and caliper or ultrasound showed in both cases a good *r* (0.95 and 0.94, respectively). The *r* was slightly better for caliper, likely due to one ultrasound measure that was significantly overestimated compared to the gold standard, excluding this specific case we obtained *r*=0.9584 for ultrasound and *r*=0.9520 for caliper. Reanalyzes of this specific case showed that this tumor was the longest and largest one in the cohort, therefore maybe more difficult to measure. Importantly, overestimation or underestimation varied between techniques for each tumor and no specific pattern could be established to explain it.

Ultrasound identifies architectural differences in cisplatin and SAHA treated PDX.

We also observed changes in the tumor structure with ultrasound between groups (Figure 6). For instance, some tumors appeared more solid, with small central hyperechoic punctiform foci with "comet-tail" artifacts. Other tumors appeared more cystic, presenting small (2mm) round anechoic cysts in the periphery,

especially in SAHA-treated tumors. This suggested potential differences regarding the tumor composition and architecture. To confirm this, we performed histological analysis (Figure 6) and IHC staining for the expression of the tumor suppressor p53, the proliferation marker Ki67, α-actin (a marker of cancer-associated fibroblasts, (CAF)) and acetylated H3K9 (Figure 7).

Control group

On ultrasound, all control tumors appeared well defined with regular hyperechoic borders (Figure 6). They were predominantly solid (hypoechoic), with few scattered anechoic cysts in the periphery. The macroscopic specimen was elliptic, regular and sections did not reveal any macroscopic signs of necrosis. This solid aspect was confirmed on histology (Figure 6), as all tumors were similarly predominantly glandular with few scattered peripheral monostratified cysts and no significant architectural changes compared to the human primary tumor. Scarce intraglandular necrosis was also present in some tumors, which could potentially explain some of the comet-tail artifacts we observed. IHC (Figure 7) showed positive nuclear stain for p53 and no apparent p53 expression was detected in the non-neoplastic tissue. All tumor cells presented a 100% positive nuclear stain for Ki67. As one group of GCX-004 bearing mice was treated with the HDAC inhibitor SAHA, we also analyzed for the presence of H3K9 acetylation. As expected, untreated tumors showed positive nuclei staining for acetylated H3K9. In addition, the tumor tissue showed a strong expression of α-actin suggesting a dominant presence of CAFs in the tumor microenvironment.

Cisplatin-treated tumors

On ultrasound, all cisplatin-treated tumors presented a solid hypoechoic central portion, less defined slightly lobulated borders and round anechoic peripheral cysts (>2mm) were more frequent than in controls (Figure 6). The macroscopic specimen appeared solid with slightly irregular external surface. Histology revealed a stromal predominance compared to the primary tumor and controls, with a stroma/gland ratio >50%, thus resulting in a lower tumor burden (cancer cells/mm^2). This stromal predominance did not appear to be correlated to the presence of CAFs (Figure 7), as α-actin staining was less dominant compared to controls. The stroma appeared hypoechoic on ultrasound (Figure 6), in a similar way as glands and tumor tissue, therefore the ultrasound could not differentiate the stroma from the glandular tissue and only detected cysts $\geq$2 mm. Scattered monostratified cysts were frequent in the periphery of the tumor and more common than in controls. IHC also showed that cisplatin treatment resulted in a strong decrease of Ki-67 expression (Figure 7, wide epithelial plaques without significant staining) compared to the controls. In contrast, p53 expression seemed to be increased.

SAHA-treated tumors

On ultrasound, all SAHA-treated tumors appeared far more cystic than cisplatin-treated ones or controls, with a peripheral rim of anechoic cysts (2-3mm) and a solid hypoechoic central portion (Figure 6). Their borders appeared less defined and more hypoechoic, slightly lobulated due to the presence of multiple cysts in the periphery. This lobulated aspect together with the presence of clear peripheral cysts was confirmed on the macroscopic specimen, which appeared partially cystic with very lobulated external surface. Histology also confirmed these findings, as a rim of peripheral monostratified cysts was observed, even though the central portion of the tumor remained glandular, with diminished amount of CAFs in the stroma (Figure 7). IHC showed a loss of Ki-67 staining in around 50% of cells (Figure 7). Additionally, as expected SAHA treatment led to an increase of H3K9 acetylation.

Discussion

In preclinical studies, one of the most relevant approach to assess the outcome of a treatment is through the tumor volume and its speed of growth, using mouse models such as cell-line derived xenografts or patient-

derived ones [12]. Even though cell line-derived models are being overwhelmingly represented in the literature (up to 82% of the studies until 2016), they raised an increasing number of criticisms for their distorted tissue architecture with altered microenvironment and the loss of genetic heterogeneity [17]. On the contrary, PDX models (7% of the recent studies) remain stable across generations and retain the major traits of their originating tumors, thus resulting in the only model able to reflect the vast patient and tumor variability and heterogeneity [17]. In addition, it has been shown that the response of PDX to anti-cancer drugs correlate quite well with clinical responses to chemotherapy [17-24].

Classical tumor-volume measurements are usually performed using a caliper, which are inexpensive and easy to manipulate, but display poor interobserver reproducibility and accuracy [12, 14]. Studies on cell-line derived xenografts have shown that ultrasound was more accurate and reproducible than caliper [11]. In our study using a gastric cancer PDX model, ultrasound also appeared more accurate than caliper. Ultrasound images are based on acoustic echoes from high-frequency acoustic waves. In both cell-line derived and patient-derived xenografts, the tumors are commonly implanted on the flanks of the mouse (=heterotopic implantation), which is well suited for ultrasound imaging with high-frequency probe, as the explored tumor is superficial (the major limiting factor is the depth of the tissue that can be imaged through) and not subject to bone / air artifacts [25]. Overestimation of the tumor size by manual caliper has multiple explanations: (1) dermal or subdermal skin layers' interpositions, (2) irregular non-ellipsoid shapes of the implanted tumors, (3) dependency on the user skills, (4) absence of 'raw dataset' and the impossibility to repeat measurements, as the specimen are no longer available [11, 14]. If ultrasound is somehow also limited by user's skills, it is not limited by interpositions of skin layers or non-ellipsoid tumor shapes, permitting a direct visualization of the tumor and the storage of images of interest. Alternative approaches exist such as micro CT, PET-CT or MRI [13, 18-26]. However, they measurements are more time consuming, limiting the number of animals which can routinely be analyzed, it needs a well-trained operator to run the equipment and a high financial investment for its acquisition. Even though CT and MRI present higher spatial resolution, while PET-CT permits a more functional approach, caliper measures and ultrasound imaging remain better suited for an easy-to-follow, in-real-life assessment of the tumor growth and volume, while limiting the costs of such a day-to-day evaluation [11-14, 24, 26]. Ultrasound, in addition of being an efficient measuring device, with no significant differences compared to macroscopic evaluation, the real-time imaging provides the observer with a direct access to tumor morphology and potential treatment-related structural changes. For instance, in our study, all SAHA-treated tumors appeared far more cystic than controls or cisplatin-treated ones, and peripheral anechoic cysts, described on histological slices, were already visible on live mice ultrasound.

Zhu et al. reported that the chemo-sensitivity of PDX models is comparable with the patient's response and therefore appears to be the most accurate method to evaluate the efficacy of new drugs in preclinical studies [23]. Platinum-derived compounds (cisplatin and oxaliplatin) are the chemotherapy of choice in gastric adenocarcinomas in humans and in tumor-bearing mice models. Their cytotoxic activity is evaluated by the decrease of tumor volume, as we observed with all our measurements. In addition, the decrease of Ki-67 positivity of tumor cells was also a reliable marker of drug efficacy [27]. One of the cytotoxic mechanisms of platinum-based compounds relies on the activation of the p53-dependent apoptosis, as the *p53* gene plays a critical role in cellular response to DNA damage [28-39]. The absence of a wild-type p53 function results in resistance to anticancer-agents such as cisplatin. In gastric cancers overexpression of p53 is strongly linked to its mutational status correlating as well with its resistance to cisplatin [29-30]. In our PDX model, diffuse and homogenous p53 nuclear staining were observed in controls, frequently related with p53 mutation, therefore rendering the little difference in the staining patterns that we observed between treated and non-treated tumors, somehow difficult to analyze. Sequencing of p53 will allow us to verify the mutation status of p53 in our model and possibly provide a model to test p53-reactivating small molecules, as a therapeutic approach [31]. Interestingly, in our PDX model the non-treated tumor tissue also presented strong expression of α-actin, suggesting a dominant presence of cancer-activated fibroblasts in the microenvironment surrounding cancer cells and distorted glands. Platinum-based compounds are known for their activity on gastric cancer cells, but they may also have effects on the tumor microenvironment, which comprises a variety of non-malignant stromal

cells, providing support for tumors progression [32]. Skolenova et al. described a relative resistance of human mesenchymal stromal cells to cisplatin treatment and changes in their secretory phenotype compared to naïve ones in breast cancer [33]. In our study, although we observed changes in the tumor microenvironment (increased stroma/gland ratio with cisplatin), they did not appear correlated to the presence of CAFs (less dominant α-actin staining compared to controls).

HDAC enzymes are aberrantly expressed in various cancers including gastric cancer and HDAC expression is known to be linked to carcinogenesis. For instance, we showed that HDAC4 is a resistant factor against cisplatin in gastric cancer [34]. For this reason, HDAC inhibitors (HDACi) have been developed to counteract pro-oncogenic activity of HDACs [35]. SAHA is one of the most promising HDACi, with FDA approval in cutaneous T-cell lymphoma with limited side effects on normal cells. The inhibition of HDAC activity in our PDX model was present, as the analysis of the acetylation status of the lysine 9 of histone H3 (H3K9, controlled by HDAC3 status, necessary for gene activation) showed a nuclear staining in the control group, which was slightly increased in the SAHA treated group. Even though we failed to observe statistically relevant changes of the volume of SAHA-treated tumors (probably related to a lower *n*, as some tumors disappeared early and the experiment was designed for the evaluation of the measurements methods), we observed treatment-related morphological changes in tumors, with pronounced lobulated contours and the development of small peripheral cysts. In addition, the 50% decrease of Ki-67 positivity in SAHA-treated tumor cells compared to controls was also a sign of drug efficacy. Unfortunately, also previous data obtained on cell-line-xenografts showing that SAHA inhibits cellular growth and induces apoptosis, which our data using our PDX gastric cancer model confirm, it failed phase 2 clinical trials [4, 36]. The exact cause of this failure is yet unknown, but our results may provide novel perspectives about the impact of HDAC inhibition on the tumor structure showing important changes within the microenvironment, which ultimately will impact on the tumor response. Identifying more precisely the molecular relays involved in these structural changes will provide novel insights for novel therapeutic combination or patient stratification, opening the way towards radiomics approaches on small animals.

In preclinical oncology studies, small animal imaging using ultrasound allows repeated measures and time-course follow-ups of tumor progression in response to various conditions (anticancer drugs, genetic modifications...) with limited costs. Ultrasound measurements of the tumor volume is more accurate than caliper ones, especially for non-ellipsoid tumors. But most importantly, the added value of ultrasound imaging is that it enables an in-real-time access to the tumor morphology and substructure, especially useful in patient-derived xenografts to evaluated treatment-related structural changes, such as the presence of cysts in the tumor.

Figure 1

a

b

Figure 1. Establishment of the PDX model of gastric adenocarcinoma and Histological analyses. (A) The primary tumor sample was implanted subcutaneously on the flanks of the mouse (heterotopic implantation). When the tumor reaches the target volume 500-1000mm^3 (photograph left), the tumors were dissected out (photograph middle and right) and 5mm^3 fragment prepared for serial implantation in the next generation of mouse. B) Histological hematoxylin and eosin staining of the primary tumor and after the 1st and 8th passage showing that the PDX tumor retains the architectural and histological characteristics of its primary tumor across passages (40x).

Figure 2
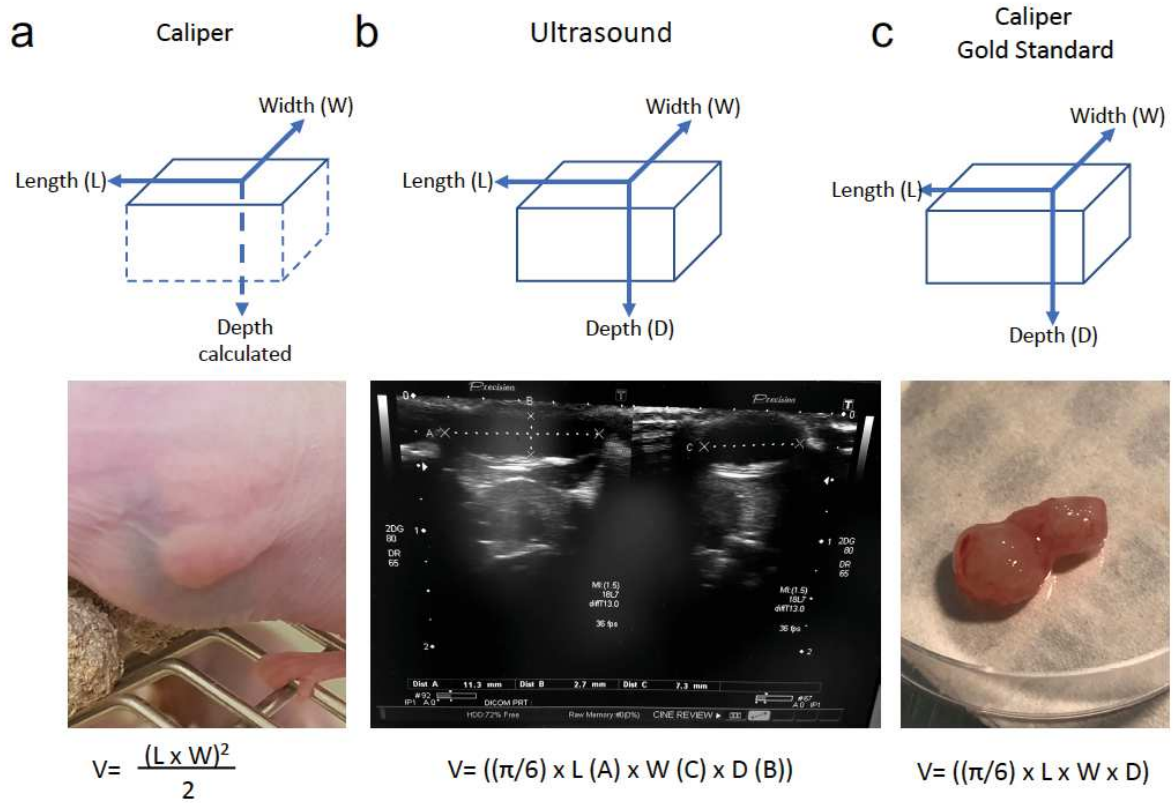
Figure 2. Estimation of the tumor volume with three different methods. Caliper only measures length and width and the depth is estimated (A). On the contrary, ultrasound (B) and gold standard (C) enabled the measurement of all three dimensions of the tumor (length, width and depth) rendering the tumor volume estimation more accurate.

Figure 3
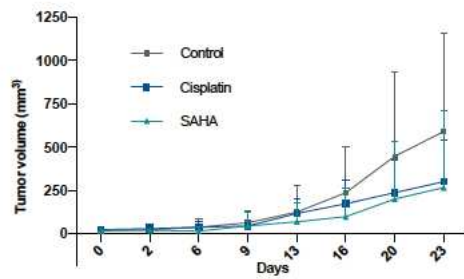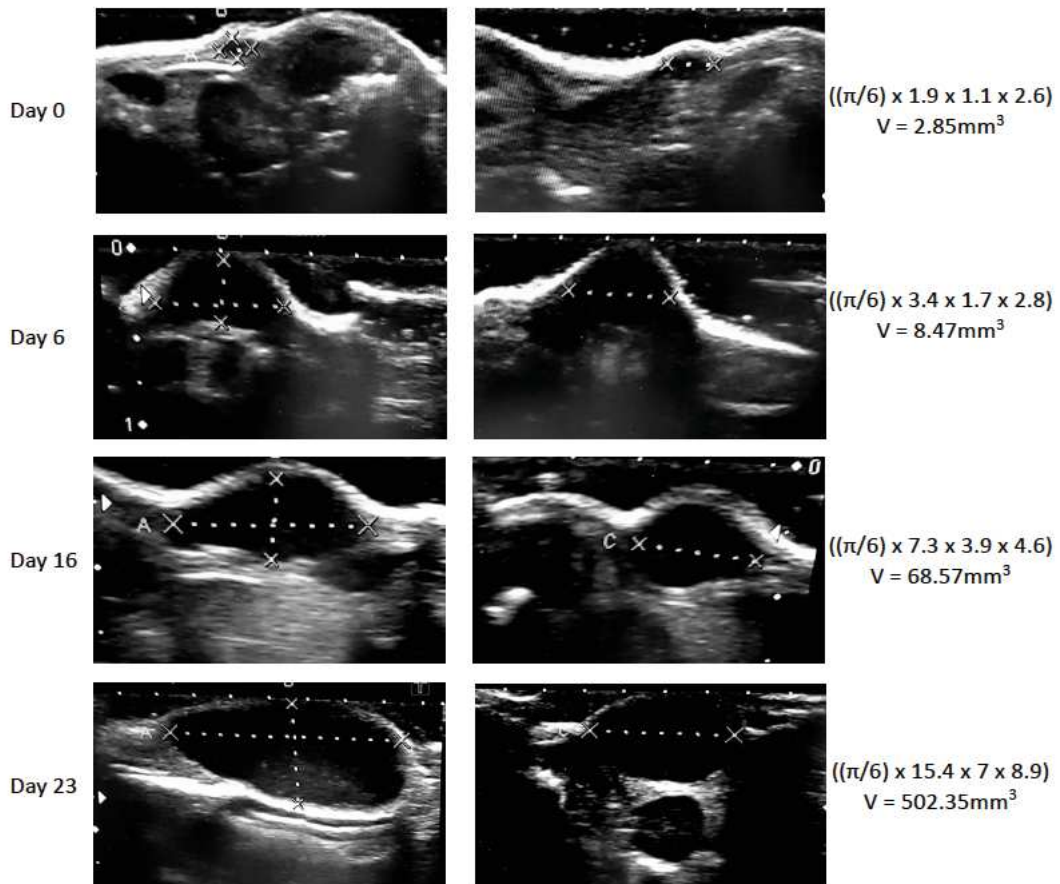
Figure 3. Evolution of the tumor volume (23 days follow-up) between treated and non-treated tumors. (A) Average tumor volume measured by ultrasound at the indicated dates (days 0 - 23). (B) Ultrasound images of a representative GCX-004 tumor in control group taken at the (A) indicated time points a, b, c and d.

Figure 4
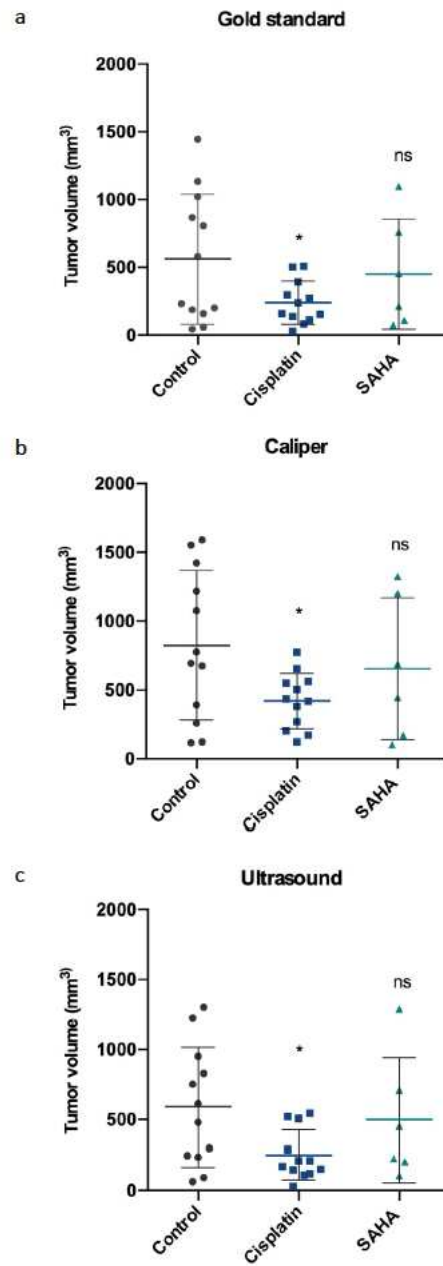
Figure 4. Comparison of the tumor volume between treated (cisplatin or SAHA) and non-treated tumors, for gold standard, caliper and ultrasound.
At day 23, final tumor volumes were measured and compared between each group (control n=12, cisplatin n=12 and SAHA n=6), and each measurement method (gold standard (A), caliper (B) and ultrasound (C)). Data were subjected to statistical analyses using GraphPad software version 6.0 (ns=not significant, *=p<0.05).

Figure 5
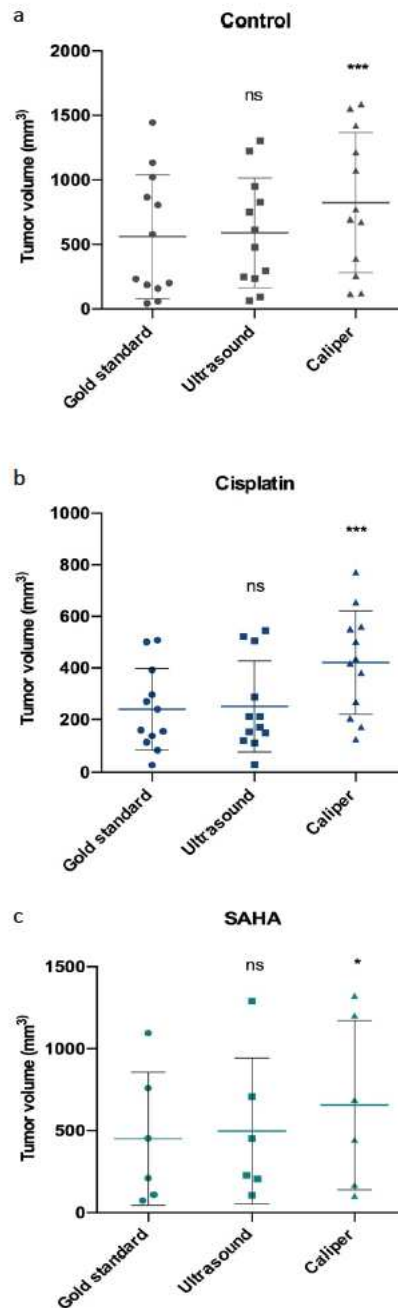
Figure 5. Comparison of the tumor volume between the three measurement modalities (gold standard, ultrasound and caliper) for each group (treated or non-treated).
At day 23, final tumor volumes were taken and compared between each measurement modality gold standard, ultrasound and treatment group control (A, n=12), cisplatin (B, n=12) and SAHA (C, n=6). Data were subjected to statistical analyses using GraphPad software version 6.0 (ns=not significant, *=p<0.05, ***=p<0.001).

51
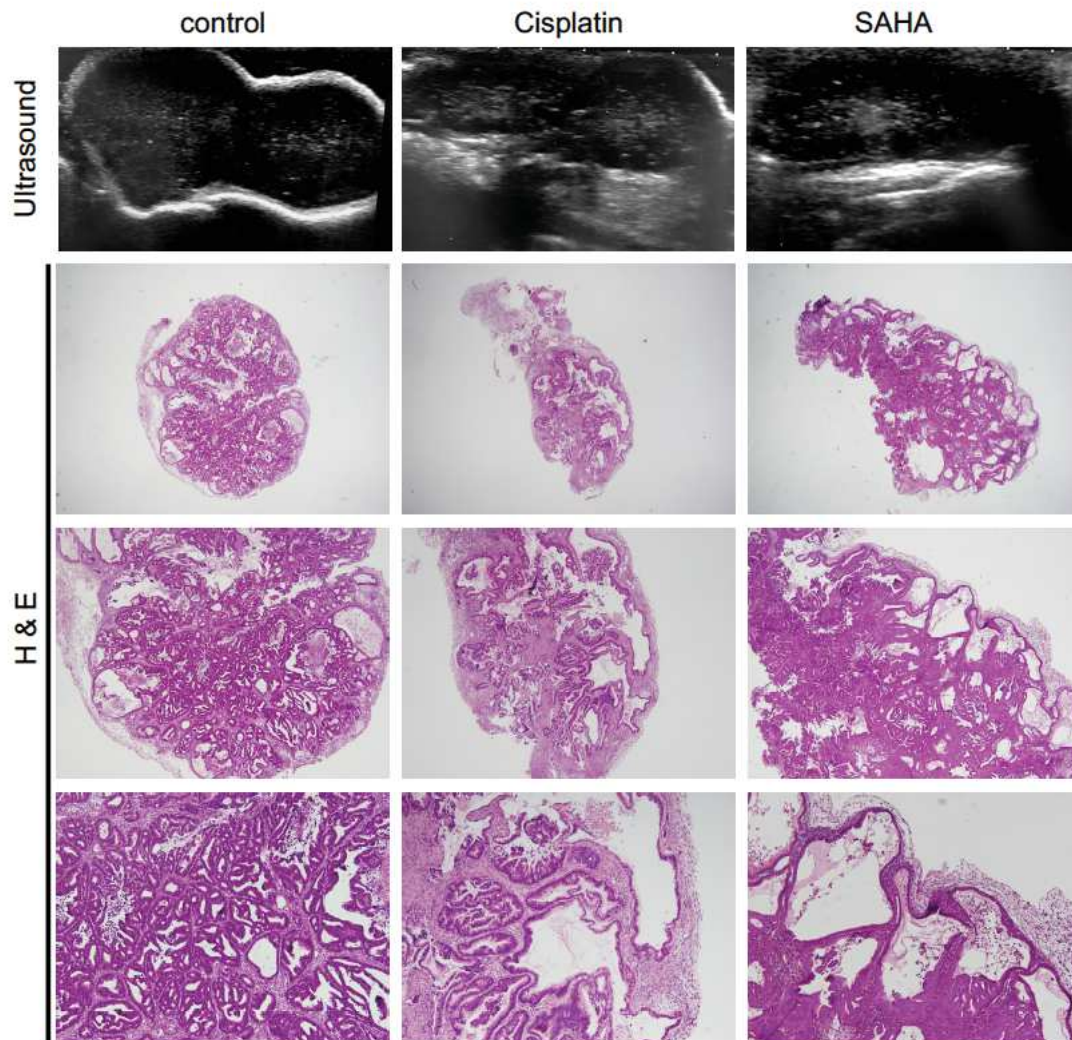
Figure 6

Figure 6. Ultrasound images of the tumor and histological analyses. At day 23, final ultrasound images were taken (top, ultrasound) between controls, cisplatin-treated and SAHA-treated tumors. Lower panel (H&E) histological hematoxilin-eosin staining of a representative GXC-004 tumor for each treatment group magnification x2 (upper), x20 (middle) and x40 (lower). Control tumors had sharper margins, while SAHA-treated tumors were more lobulated. Treated tumors (especially with SAHA) developed cysts in the periphery, which were visible on ultrasound images and confirmed by histology.

Figure 7
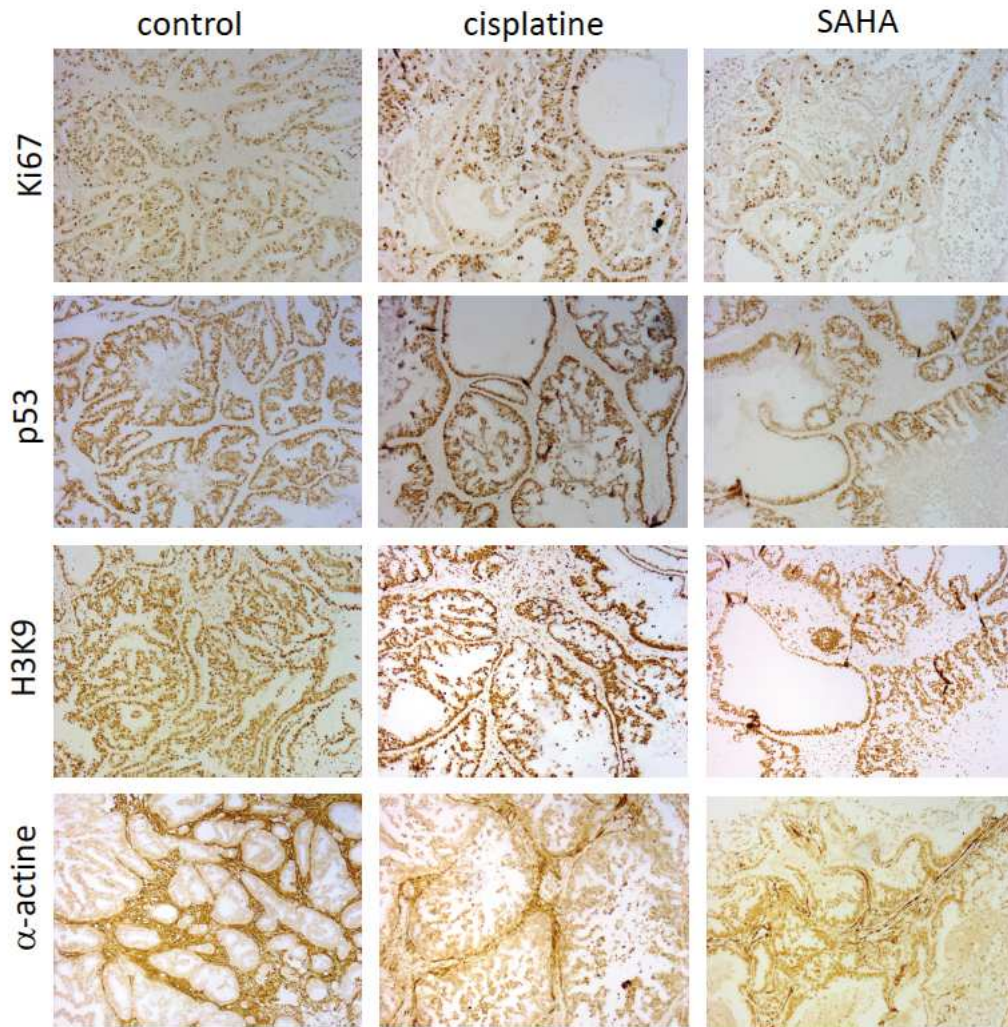
Figure 7. Immunohistochemical staining for Ki67, p53, H3K9 and α-actin.
Comparison of the expression of Ki67, p53, H3K9 and α-smooth-muscle-actin by immunohistochemisty (IHC) on GCX-004 tumors sections of the different treatment groups control, cisplatin and SAHA. Representative photomicrographs of each IHC, for treatment group is shown (magnification=20x).

References

[1]   Hidalgo, M., Amant, F., Biankin, A. V., Budinská, E., Byrne, A. T., Caldas, C., ... & Roman-Roman, S. (2014). Patient-derived xenograft models: an emerging platform for translational cancer research. *Cancer discovery*, *4*(9), 998-1013.

[2]   Bang, Y. J., Van Cutsem, E., Feyereislova, A., Chung, H. C., Shen, L., Sawaki, A., ... & Aprile, G. (2010). Trastuzumab in combination with chemotherapy versus chemotherapy alone for treatment of HER2-positive advanced gastric or gastro-oesophageal junction cancer (ToGA): a phase 3, open-label, randomised controlled trial. *The Lancet*, *376*(9742), 687-697.

[3]   Riquelme, I., Saavedra, K., Espinoza, J. A., Weber, H., García, P., Nervi, B., ... & Bizama, C. (2015). Molecular classification of gastric cancer: Towards a pathway-driven targeted therapy. *Oncotarget*, *6*(28), 24750

[4]   Yoo, C., Ryu, M. H., Na, Y. S., Park, S. R., Lee, C. W., Ryoo, B. Y., & Kang, Y. K. (2015). 2295 Phase 2 study of Vorinostat combined with capecitabine plus cisplatin as first-line chemotherapy in patients with advanced gastric cancer (AGC). *European Journal of Cancer*, *51*, S430.

[5]   Yu, S., Yang, M., & Nam, K. T. (2014). Mouse models of gastric carcinogenesis. *Journal of gastric cancer*, *14*(2), 67-86.

[6]   Choi, Y. Y., Lee, J. E., Kim, H., Sim, M. H., Kim, K. K., Lee, G., ... & Noh, S. H. (2016). Establishment and characterisation of patient-derived xenografts as paraclinical models for gastric cancer. *Scientific reports*, *6*, 22172.

[7]   Siolas, D., & Hannon, G. J. (2013). Patient Derived Tumor Xenografts: transforming clinical samples into mouse models. *Cancer research*, canres-1069.

[8]   Huynh, H., Ong, R., & Zopf, D. (2015). Antitumor activity of the multikinase inhibitor regorafenib in patient-derived xenograft models of gastric cancer. *Journal of Experimental & Clinical Cancer Research*, *34*(1), 132.

[9]   Wang, H., Lu, J., Tang, J., Chen, S., He, K., Jiang, X., ... & Teng, L. (2017). Establishment of patient-derived gastric cancer xenografts: a useful tool for preclinical evaluation of targeted therapies involving alterations in HER-2, MET and FGFR2 signaling pathways. *BMC cancer*, *17*(1), 191.

[10]   Dieter, S. M., Giessler, K. M., Kriegsmann, M., Dubash, T. D., Möhrmann, L., Schulz, E. R., ... & Heger, U. (2017). Patient-derived xenografts of gastrointestinal cancers are susceptible to rapid and delayed B-lymphoproliferation. *International journal of cancer*, *140*(6), 1356-1363.

[11]   Ayers, G. D., McKinley, E. T., Zhao, P., Fritz, J. M., Metry, R. E., Deal, B. C., ... & Manning, H. C. (2010). Volume of preclinical xenograft tumors is more accurately assessed by ultrasound imaging than manual caliper measurements. *Journal of Ultrasound in Medicine*, *29*(6), 891-901.

[12]   Cheung, A. M., Brown, A. S., Hastie, L. A., Cucevic, V., Roy, M., Lacefield, J. C., ... & Foster, F. S. (2005). Three-dimensional ultrasound biomicroscopy for xenograft growth analysis. *Ultrasound in medicine & biology*, *31*(6), 865-870.

[13]   Jensen, M. M., Jørgensen, J. T., Binderup, T., & Kjær, A. (2008). Tumor volume in subcutaneous mouse xenografts measured by micro CT is more accurate and reproducible than determined by 18 F-FDG-micro PET or external caliper. *BMC medical imaging*, *8*(1), 16.

[14]   Pflanzer, R., Hofmann, M., Shelke, A., Habib, A., Derwich, W., Schmitz-Rixen, T., ... & Bereiter-Hahn, J. (2014). Advanced 3D-sonographic imaging as a precise technique to evaluate tumor volume. *Translational oncology*, *7*(6), 681-686.

[15]   Lassau, N., Spatz, A., Avril, M. F., Tardivon, A., Margulis, A., Mamelle, G., ... & Leclere, J. (1997). Value of high-frequency US for preoperative assessment of skin tumors. *Radiographics*, *17*(6), 1559-1565.

[16]   Reita, D., Bour, C., Benbrika, R., Groh, A., Pencreach, E., Guérin, E., & Guenot, D. (2019). Synergistic Anti-Tumor Effect of mTOR Inhibitors with Irinotecan on Colon Cancer Cells. *Cancers*, *11*(10), 1581.

[17]   Choi, Y. Y., Lee, J. E., Kim, H., Sim, M. H., Kim, K. K., Lee, G., ... & Noh, S. H. (2016). Establishment and characterisation of patient-derived xenografts as paraclinical models for gastric cancer. *Scientific reports*, *6*, 22172

[18]   Voisinet, M., Venkatasamy, A., Alratrout, H., Delhorme, J. B., Brigand, C., Rohr, S., ... & Romain, B. (2020). How to Prevent Sarcopenia Occurrence during Neoadjuvant Chemotherapy for Oesogastric Adenocarcinoma?. *Nutrition and Cancer*, 1-7.

[19]   Huynh, H., Ong, R., & Zopf, D. (2015). Antitumor activity of the multikinase inhibitor regorafenib in patient-derived xenograft models of gastric cancer. *Journal of Experimental & Clinical Cancer Research*, *34*(1), 132.

[20]   Gengenbacher, N., Singhal, M., & Augustin, H. G. (2017). Preclinical mouse solid tumor models: status quo, challenges and perspectives. *Nature Reviews Cancer*, *17*(12), 751.

[21]   Lauber, D. T., Fülöp, A., Kovács, T., Szigeti, K., Máthé, D., & Szijártó, A. (2017). State of the art in vivo imaging techniques for laboratory animals. *Laboratory animals*, *51*(5), 465-478.

[22] Dieter, S. M., Giessler, K. M., Kriegsmann, M., Dubash, T. D., Möhrmann, L., Schulz, E. R., ... & Heger, U. (2017). Patient-derived xenografts of gastrointestinal cancers are susceptible to rapid and delayed B-lymphoproliferation. *International journal of cancer*, *140*(6), 1356-1363

[23] Zhu, Y., Tian, T., Li, Z., Tang, Z., Wang, L., Wu, J., ... & Zou, J. (2015). Establishment and characterization of patient-derived tumor xenograft using gastroscopic biopsies in gastric cancer. *Scientific reports*, *5*, 8542.

[24] Dhani, N. C., Lohse, I., Foltz, W. D., Cao, P. J., & Hedley, D. W. (2018). Estimating tumor volume in a primary orthotopic mouse model of human pancreatic cancer using rapid acquisition magnetic resonance imaging. *journal of cancer therapeutics and research*, *3*(1)

[25] Meiburger, K. M. (2017). Quantitative Assessment of Cancer Vascular Architecture by Skeletonization of 3D CEUS Images: Role of Liposomes and Microbubbles. In *Quantitative Ultrasound and Photoacoustic Imaging for the Assessment of Vascular Parameters* (pp. 75-89). Springer, Cham.

[26] Lyons, S. K. (2005). Advances in imaging mouse tumor models in vivo. *The Journal of Pathology: A Journal of the Pathological Society of Great Britain and Ireland*, *205*(2), 194-205.

[27] Cancello, G., Bagnardi, V., Sangalli, C., Montagna, E., Dellapasqua, S., Sporchia, A., ... & Luini, A. (2015). Phase II study with epirubicin, cisplatin, and infusional fluorouracil followed by weekly paclitaxel with metronomic cyclophosphamide as a preoperative treatment of triple-negative breast cancer. *Clinical breast cancer*, *15*(4), 259-265.

[28] Hientz, K., Mohr, A., Bhakta-Guha, D., & Efferth, T. (2017). The role of p53 in cancer drug resistance and targeted chemotherapy. *Oncotarget*, *8*(5), 8921.

[29] Kamoshida, S., Suzuki, M., Shimomura, R., Sakurai, Y., Komori, Y., Uyama, I., & Tsutsumi, Y. (2007). Immunostaining of thymidylate synthase and p53 for predicting chemoresistance to S-1/cisplatin in gastric cancer. *British journal of cancer*, *96*(2), 277-283

[30] Licona, C., Delhorme, J. B., Riegel, G., Vidimar, V., Cerón-Camacho, R., Boff, B., ... & Freund, J. N. (2020). Anticancer activity of ruthenium and osmium cyclometalated compounds: identification of ABCB1 and EGFR as resistance mechanisms. *Inorganic Chemistry Frontiers*, *7*(3), 678-688.

[31] Miller, J. J., Blanchet, A., Orvain, C., Nouchikian, L., Reviriot, Y., Clarke, R. M., ... & Storr, T. (2019). Bifunctional ligand design for modulating mutant p53 aggregation in cancer. *Chemical science*, *10*(46), 10802-10814.

[32] Zheng, P., Chen, L., Yuan, X., Luo, Q., Liu, Y., Xie, G., ... & Shen, L. (2017). Exosomal transfer of tumor-associated macrophage-derived miR-21 confers cisplatin resistance in gastric cancer cells. *Journal of Experimental & Clinical Cancer Research*, *36*(1), 53

[33] Skolekova, S., Matuskova, M., Bohac, M., Toro, L., Durinikova, E., Tyciakova, S., ... & Kucerova, L. (2016). Cisplatin-induced mesenchymal stromal cells-mediated mechanism contributing to decreased antitumor effect in breast cancer cells. *Cell Communication and Signaling*, *14*(1), 1-13.

[34] Spaety, M. E., Gries, A., Badie, A., Venkatasamy, A., Romain, B., Orvain, C., ... & Pfeffer, S. (2019). HDAC4 Levels Control Sensibility toward Cisplatin in Gastric Cancer via the p53-p73/BIK Pathway. *Cancers*, *11*(11), 1747.

[35] Li, Y., & Seto, E. (2016). HDACs and HDAC inhibitors in cancer development and therapy. *Cold Spring Harbor perspectives in medicine*, *6*(10), a026831.

[36] Claerhout, S., Lim, J. Y., Choi, W., Park, Y. Y., Kim, K., Kim, S. B., ... & Cho, J. Y. (2011). Gene expression signature analysis identifies vorinostat as a candidate therapy for gastric cancer. *PloS one*, *6*(9), e24662.

Characterisation of the PDL1-related immune checkpoint and sarcopenia in patient-derived xenografts of gastric cancer

Venkatasamy A. [1,2,3], **Guerin E.**[1], **Reichardt W.**[3], **Chenard MP.**[4], **Romain B.**[5], **Gaiddon C.** [1], **Mellitzer G**[1].

Affiliations :

1　Streinth Lab (Stress Response and Innovative Therapies), Inserm UMR_S 1113 IRFAC, Interface Recherche Fondamental et Appliquée à la Cancérologie, 3 avenue Molière, Strasbourg, France
2　IHU-Strasbourg, Institute of Image-Guided Surgery, Strasbourg, France
3　Medizin Physik, Universitätsklinikum Freiburg, Kilianstr. 5a, 70106 Freiburg, Germany
4　Pathology department, Hôpital de Hautepierre, Hôpitaux Universitaires de Strasbourg, 1 avenue Molière, 67098 Strasbourg CEDEX, France
5　Digestive surgery department, Hôpital de Hautepierre, Hôpitaux Universitaires de Strasbourg, 1 avenue Molière, 67098 Strasbourg CEDEX, France

Abstract

Objectives. Gastric cancer is an aggressive disease. Its poor prognosis can be explained by: i) late diagnosis due the lack of easy/cheap diagnostic tool, ii) resistances to treatments, such as towards immunotherapy due to a frequent low expression of immune check-point ligand PD-L1, or towards chemotherapy due to p53 mutations, iii) comorbidity factors, notably muscle atrophy. To improve our understanding of this complex pathology and develop innovative diagnostic/treatment protocols, we established patient-derived xenograft (PDX) models and characterized them using radio-pathologic correlation, including the expression of two biomarkers relevant to therapy and for the presence of muscle atrophy upon treatment.

Material and Methods. Gastric cancer tissues samples with different characteristics were implanted in nude mice. Established PDX, treated with cisplatin or not, were imaged by MRI and immunohistochemistry for two relevant biomarkers, p53 and PD-L1, was performed.

Results. We obtained 5 different gastric adenocarcinomas PDX (success rate 21%): 3 well-differentiated, 1 moderately-differentiated and 1 poorly-differentiated adenocarcinomas. All models retained the architectural and histological features of their primary tumors across passages. MRI allowed in-real-time evaluation of differences between PDX, in terms of tumors substructure, post-therapeutic changes, including an insight on muscle changes and atrophy. Immunohistochemistry showed differential expression of p53 and PD-L1 between models and upon treatment.

Conclusion. Our PDX represent a complete model of gastric cancer, reproducing quite well the heterogeneity and complexity of human tumors, with differences in structure, histology, PD-L1 status and muscle atrophy, which makes them even more useful for the development of novel drugs and targeted therapies.

Mini abstract (30 words)

A selection of gastric cancer PDX (40%) according to their PD-1/PD-L1 immune checkpoint signaling status is possible, which makes them even more useful for the development of targeted therapies.

Introduction

Third cancer worldwide in terms of mortality, gastric cancer has a very poor prognosis [1-2]. Surgical gastrectomy combined with perioperative chemotherapy with platinum-based compounds (e.g. cisplatin or oxaliplatin) is the cornerstone of current treatments. Even though the use of perioperative chemotherapy has improved the survival rate of patients, the outcome remains unfavorable with a 30 to 40% response-rate to treatments and a median survival of less than a year in advanced or metastatic stages**.** Furthermore, chemotherapy side effects (such as nephrotoxicity, gastro-intestinal toxicity or polyneuropathy…) together with *de novo* or acquired resistances (up to 75%) limit its use and effectiveness*.* Therefore, the development of alternative therapeutic strategies currently represents an absolute necessity.

As other types of cancers, gastric cancer is a morphologically and genetically complex disease. Recently, The Cancer Genome Atlas (TGCA) research network published a classification of gastric cancers according to their molecular characteristics (DNA, RNA, protein and epigenetic changes), which correlated with distinct clinical and histological characteristics, potentially useful for the stratification of patients for targeted therapy [3-4]. Most of the recent studies on the development of novel drugs or targeted therapies used mouse models, such as patient-derived xenografts (PDX), for their *in vivo* validation, as they allowed repeated measures and time-course follow-up of tumor progression in response to various conditions (anticancer drugs, genetic modifications…), as well as an analysis of the evolution of intra-tumoral clonal variation [5-10]. Such models have been developed for various cancer types (including breast, colon and gastric cancer) and retain the major histological, molecular and genetic characteristics of their primary tumor, remaining stable across re-transplantations in successive generations of mice [8-11]. Unfortunately, in gastric cancer, most current targeted therapies have unfortunately proven to be ineffective [11]. However, increasing attention has been recently given to the tumor microenvironment.

Immunotherapy has been a revolution for the treatment strategy of various cancers at advanced stages, including metastatic melanoma. The tumor microenvironment is influenced by the host immune system (T cells, B cells, infiltrating immune cells, neutrophils…), with which tumor cells are known to interact with during development and growth [12]. Cytotoxic T-cells task is to detect and destroy infected or tumor cells. To counteract their actions and to limit damage to surrounding tissue, normal cells differentiate themselves by expressing a protein signal called PD-L1 (programmed death ligand 1), which acts as a signal to stop the elimination of normal cells by cytotoxic T cells, as T cells detect the PD-L1 signal through a receptor called PD-1 (programmed death receptor 1). Some tumors, including gastric cancer ones, can also express the PD-L1 signal to mimic normal cells and escape elimination. For instance, cytotoxic T-lymphocyte associated antigen 4 (CTLA4) and programmed cell death protein 1 (PDA), which are part of the immune checkpoint pathway, can be activated by tumor cells to decrease the immune system reaction by inhibiting T cell response [12]. Thus, targeting the PD-1/PD-L1 immune checkpoint signaling recently appeared as a novel and promising treatment strategy in several tumor entities. For instance, PD-L1 expression was found in 30% of gastric cancer tumors cells and 60% of their liver metastases, as well as in immune cells of gastric cancers (88%) and their liver metastases (73%). Therefore, immune checkpoint inhibitors, such as Pembrolizumab (*pembro*),

which enhances the activity of anti-tumor T-cells through an inhibition of immune checkpoints, such as programmed death 1 (PD-1) receptors and PD-L1 receptors appeared as a potential candidate for targeted therapy in gastric cancer [10]. Pembrolizumab is a humanized monoclonal antibody against PD-1, that prevents PD-1 from interacting with PD-L1 and PD-L2, and permits the activation of an antitumor immune response [11]. A phase 2 clinical trial was conducted and with a promising response rate (as 3rd line of treatment) of 11.6% (n=30/259) and complete responses in 2.3% of the cases (n=6). In 2017, pembrolizumab obtained the FDA-approval for the treatment of recurrent locally advanced or metastatic PD-L1 positive gastric cancer, but favorable results were only obtained for a small subset of tumors [12-15]. In particular, the expression of PD-L1 in the predominant in the intestinal subtype (45% of gastric cancers) of gastric cancers, that largely matches the molecular subgroup of "chromosome instability (CIN)", is relatively low and displays a poor response to immunotherapy, similarly to the "genetic stable subgroup" that is more frequent in younger patients and displays a poorer prognosis [3-16]. Hence, the improvement of immunotherapy response requires a better understanding of the expression and function of PD-L1 in gastric cancer and its consequences on the immune landscape, within the tumor microenvironment.

Similarly, the scientific view of cancers is slowly shifting from organ-centered diseases to a more global and systemic approach. For instance, in gastric cancer, around 30 to 60% of patients are thought to develop cancer cachexia, *presenting as a progressive loss of adipose tissue and skeletal muscle mass,* occurring independently of the cancer stage [17-18]. Additionally, the incidence cachexia / sarcopenia (muscle atrophy) appears to increase after chemotherapy. Cancer cachexia not only has a dramatic impact on *the quality of life,* but is also associated with *poor responses to therapies (chemotherapy and immunotherapy), decreased survival and is estimated to account for around 20 to 25% of cancer-related deaths.* A recurrent question about cancer cachexia is about the respective responsibility of the tumor itself and the treatment in the muscle atrophy.

The retranscription of the gastric cancer complexity, that includes the clonal intra- and inter-tumoral diversity, the role of the microenvironment and the influence of distant tissues (such as the muscle) into adequate and pertinent animal models, is a challenge we face to develop novel diagnostic and therapeutic strategies. It is certainly illusory that a single type of animal model will provide all the required characteristics. In preclinical studies, patient-derived xenografts and cell-line derived mouse models are valuable tools in cancer research, especially for anti-cancer drug testing. Even though cell-line-derived models are being overwhelmingly represented in the literature (up to 82% of the studies until 2016), they raised an increasing number of criticisms for their distorted tissue architecture with altered microenvironment and the loss of genetic heterogeneity, which have been described after long-term propagation [19]. In addition, cell lines are often stably modified or expressing luminescent or fluorescent proteins facilitating the longitudinal evaluation of tumor growth over time. The selection process necessary to make the stable clones has a profound impact on the cell line characteristics. In addition, the luminescent/fluorescent imaging approach used to follow tumor growth is focused on cancer cells. On the contrary, PDX models (7% of the recent studies) remain stable across generations and retain the major traits of their originating tumors, thus resulting in the only model able to reflect the vast patient and tumor variability and heterogeneity, that is inherent to human cancer [19]. PDX models have been developed for various cancers including breast, colon and gastric ones, with success rates ranging from 25 to 75%, especially low for gastric cancers (around 25%), depending on the histological subtype, with a risk of lymphoproliferation when NOG or NOD mice are used [19]. However, these models do not allow an easy to use of luminescent/fluorescent imaging approaches for longitudinal studies.

In this study, we aimed to establish novel gastric cancer PDX models that will allow us to reproduce the intra- and inter-tumoral clonal diversity, a number of characteristics of the microenvironment and the impact on the muscles of different tumors. In addition, we improved small animal imaging abdominal oncology protocols (9.4 Tesla MRI) to accurately characterize them for future longitudinal studies, with a special focus, not only on tumor size, but also on intra- and extra tumoral substructural

variabilities, reflecting differences in the microenvironment and on muscles characteristics. We also correlated this observation with an immunohistological stratification regarding their p53 and PD-L1 immune check-point status, two biomarkers involved in the sensitivity to therapies.

Material and Methods

Establishment of patient-derived xenografts in nude mice

Use of human tissues was approved by the Ethics board. Patients gave their written consent. All protocols adhered to the Declaration of Helsinki. The prospective clinical and histological data included: age, sex, weight, height, type and histology (Lauren's classification), TNM stage, treatment, *p*TNM after gastrectomy, the occurrence of post-operative complications and the patients' clinical evolution. The primary tumor fragment used for implantation was issued from either gastric cancer biopsies (2x2 mm) or tumor fragments (4x4mm) of surgical specimens of gastric adenocarcinomas, either intestinal, diffuse or mixed types, gathered under sterile conditions, with limited cold ischemic time (<25 minutes). All animal experiments were approved by our Institutional Animal Care and Use Committee (APAFIS#8320). The mice were cared according to the Institutional Guidelines for Animal Care. Six weeks-old athymic female NUDE mice were acclimated for two weeks, provided with unlimited access to sterilized food and water *ad libitum,* and housed with 12h day/night cycles. We used NUDE mice instead of NOG/NOD mice because of the risk of lymphoproliferation in NOG/NOD mice that has been described in previous studies but that did not seem to occur in NUDE mice [5, 16]. The primary tumor fragments were implanted on the flanks of anaesthetized (Isoflurane®, Abbott GmbH, Wiesbaden, Germany; 2% vaporized in oxygen) immunodeficient mouse, with close monitoring of their growth (1-3 times/week by caliper). When the implanted tumor reached 500mm^3, the engraftment was considered successful, the mouse was anaesthetized and the tumor harvested for serial transplantation into successive mice generations. To establish the PDX models, tumor implantations were performed in different generations of mice (passage 1 to passage 10), to verify the reproducibility of the implantation, but also the conservation of the tumor major characteristics (architecture, histology, genetics…) between the serial passages.

MRI imaging protocol

Two mice from each established PDX model (> 3 consecutive passages with preserved histological architecture) were imaged using a preclinical 9.4 T MRI (Bruker BioSpin MRI GmbH, BioSpec 94/20, Ettlingen, Germany). The mouse was anaesthetized (Isoflurane®, Abbott GmbH, Wiesbaden, Germany; 2% vaporized in oxygen), then sacrificed. Then, the MR imaging was performed using a mouse body-coil. The mouse was carefully placed in the coil in dorsal decubitus and in a prone position (head first). Firstly, we performed an axial RARE T2-weighted sequence, with the following parameters: TR = 24 ms, TE= 4000 ms, average = 1, slice thickness = 0.5 mm, FOV = 28 x 28, image size = 128 x 128, excitation angle = 90°, duration 4-5 minutes. Then, we performed a diffusion-EPI sequence with ADC map (Apparent Diffusion Coefficient in mm^2/s , which is a measure of the magnitude of diffusion of molecules of water in various tissues, displayed as a parametric map, calculated on the diffusion sequence), using the following parameters : TR = 25.49 ms, TE= 3200 ms, average= 1, flip angle = 90°, slice thickness = 1mm, FOV = 28 x 28, image size = 128 x 128, diffusion directions = 1 (b0 – b200 – b 500 – b1000), duration 4-5 minutes. All data were analyzed using Paravison® 6.1 software. Paravertebral muscle surface have been measured using the open-access dicom viewer Horos ®, by a manual segmentation on axial images of a T2-weighted RARE sequence, at the level of the renal hilum, by an experienced radiologist.

Histological analysis

For each PDX passage, when the implanted tumor reached 500mm^3, it was excised for *ex vivo* macroscopic evaluation, before serial transplantation in a new generation of mice. A fragment of the PDX tumor was implanted in a new mouse and a sample fixed in 4% paraformaldehyde solution for hematoxylin-eosin (*H&E*) staining, for the histological characterisation of the tumor. All slices were read at x10 - x20 - x40 magnifications and compared the histology slices from the different PDX passages across generations and the primary patient's tumor.

Immunohistochemistry (IHC)

IHC were performed on deparaffinized histological tumor slices (5µm). Unmasking was carried out with NaCitrate in the microwave oven (800W, 10min). After washing once with distilled water and once with PBS the sections were permeabilized with 0.1% PBS-Triton for 5min and the nonspecific sites blocked in 5% NGS-PBS-Triton 0.1% (Normal Goat Serum) during 60min. Subsequently, primary antibodies to P53 DO1 (BP53-12, Zytomed), PD-L1 (22-C3) were diluted in PBS + Triton 0.1%, then added and kept at 4°C overnight. After 3 washes with PBS-Triton 0.1% slides were incubated with the secondary antibody (diluted 1:1000 in 1xPBS/5% NGS) specific for the primary antibody for 1 hour at room temperature. Slides were mounted with FluorSafe Reagent Mounting Medium (Calbiochem®) and allowed to dry overnight before observation using a fluorescence microscope (Axio Imager 2 - ZEISS). P53 and PD-L1 staining were scored as % of cells showing a positive staining (nuclear for P53, membranar for PDL1).

Results

Development of the PDX models

We have heterotopically implanted, on the flanks of athymic NUDE mice, 24 different gastric adenocarcinomas samples, 55% (n=13) of which were intestinal type, 42% (n=10) diffuse type and 4% (n=1) mixed type. Seventy-nine percent (n=19) of the samples came from biopsies obtained during diagnostic gastroscopy, while 21% (n=5) came from surgical specimens (primary tumor or metastasis). We have been able to maintain five different gastric adenocarcinomas tumors over time (> 10 passages in serial generations of mice), which corresponds to a success rate of 21%. The clinical characteristics of the patients from whom the successful grafts were issued, are summarized in *Table 1*. Those 5 PDX models comprised 3 well-differentiated intestinal type adenocarcinomas (GCX-001, GCX-004 and GCX-016) and one moderately-differentiated (GCX-018) and one poorly-differentiated (GCX-022) adenocarcinomas. All five models retained the architectural, histological (*Figure 1*) and genetic characteristics of their primary tumors, which were maintained across passages (up to 12 passages for the GCX004 model). The major engraftment limiting factors were the cold ischemic time (below or above 1h) and the percentage of tumor cells in the sample (below 50%). We did not manage to obtain the successful engraftment of any of the purely diffuse type gastric cancer samples, regardless of the sample type (biopsy or surgical specimen), cold ischemic time or percentage of tumor cells in the sample. Hopefully, we did not witness any lymphomatous transformation in any PDX models, even after 8 or more passages [16].

Radiological characterization and correlation with histological differentiation status and muscular atrophy

Considering the low success-rate in establishing new PDX models especially in gastric cancer (~25%), the financial burden related to their maintenance and their key-role in pre-clinical cancer research, we first wanted to characterize them with small-animal imaging, compared to their corresponding

histological slices. In particular, developing small animal imaging oncology protocols suited for PDX models would allow us to perform further longitudinal explorations of the impact of treatment(s) on the tumors, not only regarding their size, but also have a direct access to variations in tumor substructures, indicative of the status of the microenvironment. Therefore, magnetic resonance imaging (MRI) seamed very appealing, as it would provide direct access to information about the tumor size, morphology, sub-structure and to potential treatment-related changes.

We have imaged our five PDX models using a 9.4 Tesla MRI (*Figure 2, left panel*) with a dedicated mouse-coil and using a T2-weighted and a diffusion-weighted sequences, specially improved for murine abdominal oncology, which we analyzed together with their corresponding histological slices (*Figure 2, right panel*). All subcutaneous (heterotopic implantation) tumors, located on the flanks of the mice, had well delineated margins with a signal intensity on T2-weighted images depending on the tumor tissue characteristics and fluid-content. For instance, the PDX model GCX-001, a well-differentiated gastric adenocarcinoma, appeared homogenous (*Figure 2 A and B*), with an intermediate signal on T2-weighted images and well delineated peripheral margins. The left flank tumor (*Figure 2A, right panel*) appears slightly more heterogenous than the other, with central areas of necrosis. As expected due with this papillary subtype, the GCX-004 model presented the classical appearance of a papillary tumor on MRI: lobulated with hypointense fibrous stalk supporting clumps of hyperintense fluid-like oedematous papillae (with a bright signal intensity similar to that of fluid) on T2-weighted images. The GCX-018 model, a moderately to poorly-differentiated gastric adenocarcinoma presented with a heterogenous signal on T2-weighted images, due to large foci of necrosis. The GCX-022 model showed neo-vasculature, especially in the periphery of the tumor, presenting as linear hypointense structures on T2-weighted images. All tumors showed restricted diffusion, related to high cellularity (*Figure 3*: ADC value 0.00113 mm^2/sc for GCX-001, 0.00128 mm^2 /s for GCX018 and 0.00112 mm^2 /s for GCX-022). As expected, the GCX-004 PDX, which showed higher signal on T2-weighted images, also presented with slightly higher ADC values (0.00170 mm^2 /s) than the other PDX tumors, probably due to the fluid-like content of its papillae (*Figure 3*).

To assess the muscle status, we investigated the paravertebral muscles of the PDX mouse models, with the same measurement method used in cancer patients to diagnose muscle atrophy on abdominal images of CT/ PET-CT. Interestingly, the five PDX models presented differences in terms of paravertebral muscle surface. The average paravertebral muscle surface (measured at the level of the renal hilium) was 34 mm^2 ± 6, with up to 28% variations between models. For instance, the paravertebral muscle surface values were higher for GCX-004 and GXC-018 models (36 and 39 mm^2 respectively) compared to GCX-001 and GXC-022 (27 and 32 mm^2 respectively, *Figure 4*).

Characterisation of the p53 status

The tumor suppressor p53 (TP53) is altered in about 50% of gastric adenocarcinomas and these alterations are more common in intestinal type tumors than diffuse ones [17]. Importantly, several studies indicate that the status of p53 impact on patient prognosis and response to treatment. To assess the status of p53, we performed immunohistochemistry. Interestingly, our 5 PDX models, which presented various aspects on MR imaging and in terms of histology, also differed regarding their p53 status (*Figure 5, Left panel).* The majority (80%) of the PDX models (GCX001, GCX-016, GCX018 and GCX-022) showed significant positive nuclear p53 staining. This elevated protein level for p53, in absence of any treatment, strongly suggest that the cancer cells express a p53 mutant, that is not degraded by its negative regulator MDM2. To confirm this, we performed sequencing on p53 hot-spot and are awaiting for the results. In contrast, the naïve GCX-004 model only presented a very weak nuclear staining for P53 (few cells, <5%), suggesting the presence of a wild type p53 protein or a deletion of p53.

Characterization of PD-L1 expression

The tumor microenvironment is influenced by the host immune system (T cells, B cells, infiltrating immune cells, neutrophils…), with which tumor cells are known to interact with during development and growth. Up to 30% of gastric cancer tumor cells and 60% of their liver metastases express PD-L1 to mimic normal cells and escape elimination. Therefore, immune checkpoint inhibitors, such as Pembrolizumab (*pembro*), which enhance the activity of anti-tumor T-cells, by an inhibition of immune checkpoints, such as programmed death 1 (PD-1) receptors and PD-L1 receptors, appeared as a potential candidate for targeted therapy in gastric cancer, but favorable results were only obtained for a small subset of tumors [5]. Thus, a better understanding of the immune contexture of gastric cancer animal models appeared essential, for an optimal usage of immune-based cancer treatments to patients [12].

Therefore, we analyzed by immunohistochemistry the expression of PD-L1, with the same antibody used to characterize the expression of PD-L1 in patients, before prescribing immunotherapy. Interestingly, our 5 PDX models also differed regarding the level of PD-L1 expression. Forty percent of the PDX models (n=2, GCX-001 and GCX-018) presented with a strong membrane PD-L1 staining, respectively 70% and 50% (*Figure 5, right panel*). The other PDX models (n=3, 60%) presented either with no PD-L1 staining (GCX-016) or a low level of staining that would not be looked at positive for the prescription of an immunotherapy (<5%, GXC-004 and GCX-022). It is to note, that we did not see any specific correlation between the expression level of p53 and the one of PD-L1.

Impact of the chemotherapy on p53, PD-L1 and muscular atrophy in PDX models

The overall idea behind the development gastric cancer PDX models and novel oncology imaging protocols was to use them for anti-cancer drug testing in pre-clinical studies during longitudinal studies. For instance, one challenge is to understand how the expression of immune check-points can be impacted over time by treatments and how if may affect the response to immunotherapy.

Therefore, we selected one model (GCX-004), which express low levels of PD-L1, and treated it with the standard platinum-based chemotherapy (cisplatin). Intraperitoneal injections of cisplatin (5 mg/kg body weight) resulted in a decreased tumor size (*Figure 6 A*) and also in an increase of the ADC value (*Figure 6B*). Additionally, to imaging changes, histological modifications were also observed (*Figure 6C*). In absence of treatment, the tumor appeared well-differentiated, predominantly glandular, with no significant architectural changes compared to its human primary tumor on the histological slices with Hematoxylin-eosin staining. The nuclear stain for p53 was very feeble (<5%) with no apparent p53 expression in the non-neoplastic tissue. After cisplatin treatment, histology revealed a stromal predominance *(Figure 5C, left panel),* compared to the primary tumor and controls, with a stroma/gland ratio >50%, thus resulting in a lower tumor burden (cancer cells/mm^2). We also observed a very strong increase in nuclear p53 expression after cisplatin treatment *(Figure 5C, middle panel)*. This indicated that the cancer cells of the GCX-004 PDX likely expressed a wild type p53. On the contrary, only a limited modification was observed with standard platinum-based chemotherapy regarding the PD-L1 staining *(Figure 5C, right panel)* between treated and non-treated tumors. For instance, only few cells across the slides seems to be able to express PD-L1. To note also, there is a slight increase of thePD-L1 staining in the stroma.

Additionally, one of the side effects of chemotherapy is the development of a muscle atrophy as we have observed in gastric cancer patients [18]. Most of the chemotherapies used for gastric cancer patients are based on platinum drugs. However, most of the studies on animal models address this problem using doxorubicin and not platinum drugs [20-21]. Hence, we took the opportunity of our PDX model to investigate how cisplatin impacts muscle physiology, in the presence of a gastric tumor. We observed a decrease of muscle surface after cisplatin chemotherapy in mice (39 mm^2 for controls vs 30.5 mm^2 in cisplatin-treated mice, Figure 6D). This indicates that, as observed in humans, a platinum drug impact negatively on muscle mass

Discussion

In preclinical studies, one of the most relevant approach to assess the outcome of a treatment is through the tumor volume and its speed of growth, using mouse models, such as cell-line derived xenografts or patient-derived ones. PDX tumors remain stable across generations and retain the major traits of their primary human tumors, thus resulting in the only model able to reflect the vast patient and tumor variability and heterogeneity especially compared to cell-line derived tumors, which raised an increasing number of criticisms for their distorted tissue architecture with altered microenvironment [22-23]. Additionally, PDX mouse models are known to respond to anti-cancer drugs in similar ways as the human tumor would respond to chemotherapy, which makes it the most useful tool for novel anticancer drugs or targeted therapies testing.

Regarding gastric cancers, there are currently five significant publications about the development and/or the use of gastric cancer PDX models [7, 9-10, 24-26]. The success rate of such xenografts in the two major papers is similar to ours (21% in our study, 25% for Choi et al. et and 34% for Zhu et al.) and remains quite low compared to other tumor types (it can reach up to 70% especially for breast and colon cancers) [7-26]. If Choi et al. noted also a risk of EBV-related lymphoproliferation (33% of the cases) when NOD or NOG mice were used, which we did not observe such thing after 8 or more passages, as we used athymic NUDE mice [7, 19]. As other authors, we noted that the major engraftment limiting factors were the cold ischemic time (below or above 1h) and the percentage of tumor cells in the sample (below 50%) [5, 7-8, 24-26]. Similarly, the engraftment depended on the histological subtype, as all maintainable PDX models were of intestinal type. All PDX development attempts, including ours, failed to obtain diffuse type gastric cancer PDX, regardless of the sample type (biopsy or surgical specimen), cold ischemic type or percentage of tumor cells in the sample. One potential explanation for this could be the intrinsic properties of the diffuse subtype, with dispersed isolated cancer cells in the stroma of the stomach, insufficient to reach the minimal cancer cells number required to initiate tumor growth, in a similar way as implantation usually fails in case of low tumor cell percentage on implanted biopsies. For that purpose, the only existing mouse models with a limited percentage (around 25%) of diffuse cells are mixed gastric cancer from genetic engineered mice, which directly cancerized its own stomach, with a 100% penetrance, but requires a more complex set-up with either longitudinal MRI studies or mice sacrifice with dissection to follow tumor progression [27].

On the contrary, our PDX models are somehow easier to use, with easily-accessible subcutaneous tumors, which retain the major characteristics of the primary human tumors from which they derived. They confirmed their interesting role for preclinical *in vivo* validation of anti-cancer drugs, as they responded well to standard-of-care platinum-based chemotherapy (cisplatin), showing post-therapeutic changes (size and histological/IHC changes). After cisplatin chemotherapy, GCX004 tumors showed decreased size compared to non-treated ones, with histological changes (stroma predominance and decreased tumor-burden) as well as immunohistochemistry changes, especially a very strong increase in nuclear p53 staining. Additionally, the ADC values of treated tumors was higher than non-treated ones on diffusion images (=an MRI sequence based on the random motion of water molecules in tissue). Images obtained with such sequence depend on the tissue cellularity and the presence of intact cell membranes, which determine the diffusion of the water molecules (using different b values and changing gradient amplitude in the sequence protocol), that can be calculated using the Apparent Diffusion Coefficient value, displayed as a parametric map. An increase of a tumor ADC value as we observed during chemotherapy treatment is a promising sign of therapeutic response, as it is typically associated with cell death [28].

We also took the opportunity of our models to perform the first analysis of PD-L1 expression on gastric cancer PDX tumors. We showed that patient-derived xenograft tumors behaved like human gastric cancers, with 40% strongly expressing PD-L1 (>50% positive membranar staining), which is in agreement with human observations where PD-L1 expression was noted in around 30% of gastric cancer tumor cells [10]. Hence, we showed that the expression of immune-check point inhibitor (i.e.

PD-L1) can be also very different between PDX models, suggesting that the immune landscape might also be different. However, being in immuno-deficient mice, the direct assessment of the immune landscape is limited to macrophages and NK cells. Despites this limitation, these models show that they can be useful tools to investigate how the level of expression of immune-check point ligands in different subclones of cancer cells can be modulated by treatments, such as chemotherapy. This is a crucial information when considering to combine immunotherapy with other types of therapies. For instance, we observed a small increase in PD-L1 expression in some cells, when the GCX004 tumor was treated with cisplatin. Additionally, these models can allow us to explore the possible correlation between the expression of immune check points and other biomarkers relevant for therapy. For instance, we did not see a correlation between p53 expression and PD-L1, in contrast to a recent publication indicating the reverse, but we have to take into account the limited numbers of models we used for the correlation (n=5) [23]. This better understanding of the immune contexture of animal models in gastric cancer is essential, before administering novel targeted therapies, especially immune-based cancer treatments to patients [29]. The radiologic-pathologic correlation of our PDX models and their stratification regarding their PD-L1 immune check-point status will enable us to be more selective regarding use of their use in pre-clinical research. In the future, our PDX MRI data could be integrated in Artificial Intelligence framework based on Machine learning and might be correlated with biologic and/or molecular data (PD-L1 status, transcriptomic analysis…), all in all aiming at the development of future potential imaging biomarkers.

Another important part of the tumor ecosystem is its dynamic interactions with more distant tissues, in particular the muscle, that is affected by a cancer-related atrophy. This is particularly present in gastric cancer, where up to 6 to 13% of patients presented with sarcopenia at diagnosis and 60% developed sarcopenia after chemotherapy [18]. Our study represents the first work that investigates the impact of the human gastric tumors on muscles, using PDX models. We applied the human image-based method to approach muscle atrophy, using a manual delineation of paravertebral muscles at the level of the renal hilum (= approximately L3 vertebra) to our mouse models. With such technique, differences appeared among PDX tumors and also between treated and non-treated ones. This represent the first demonstration that the implantation of human gastric cancer tissues into a mouse can induce muscle atrophy, just by itself. This is quite a critical and fundamental observation still debated in the medical and scientific community, about why gastric cancer patients develop muscle atrophy.

In all cancers, cachexia and sarcopenia probably have complex origins, partially related to the tumor itself and partially induced, or worsened, by treatments. For instance, a single intraperitoneal injection of an anticancer drug, doxorubicin, is known to induce sarcopenia in C57BL/6 mice. However, the reasons why only some patients are prone to develop cachexia, even at an early stage of the pathology, remains largely unknown and additional studies are required, for which our PDX models could offer an interesting animal model in addition to drug-induced mouse models. This is particularly true for gastric cancer, as some clinicians continue to argue that the muscle atrophy is simply due to the fact that patients cannot eat normally, due to their gastric tumor impacting negatively on the capacity of correctly ingesting and digesting food. The results on our PDX models clearly showed that the mechanisms are much more complex and that the muscle atrophy is independent from the mechanical discomfort of food ingestion, since all our PDX tumors were similarly subcutaneously implanted on the flanks of the mice, with no significant compressive effects on internal abdominal organs. Hence, the likely explanation is that certain gastric tumors secrete diffusible molecules, that induces muscle atrophy. As indicated in the literature for other cancers, these molecules can be different cytokines, such as IL6 [30]. In addition, we observed for the first time that a platinum-based drug can also by itself induce muscle atrophy, similarly to what was shown before with doxorubicin.

All in all, our five patient-derived xenografts enabled us to obtain quite complete overview of intestinal-type gastric cancer tumors, reproducing quite well the heterogeneity and the complexity of human tumors, showing differences in terms of tumor structure, histology, P53/PD-L1 status and

muscle atrophy, which makes them even more useful in preclinical research, for the development of novel drugs and targeted therapies.

65

Table 1. Clinical characteristics of the patients from which the successful xenografts are issued

	Histology	Age	Sex	Preoperative treatment	Surgery type	pTNM	Sample type	Cold ischemic time	Percentage of cells on sample	Time to reach ~ 150 mm³	Other
GCX-001	Well-differenciated HER2+ (score 2) gastric adenocarcinoma	76	M	preoperative chemotherapy EOX protoxol (epirubicine + cisplatin + 5-fluoro-uracil)	distal esogastrectomy with Lewis Santy reconstruction	*p*T1b N1(1/30) M0	Pre-therapeutic biopsy	<1h	100%	3 months	
GXC-004	Well-differenciated papillary HER2- gastric adenocarcinoma	64	M	preoperative chemotherapy using EOX protocol	total gastrectomy	ypT1aN0 (0/16) M0	surgical specimen	<1h	100%	15 days	No relapse or recurrence after 3 years
GXC-016	Well-differenciated papillary HER2+ (score 2) gastric adenocarcinoma	74	W	preoperative radio-chemotherapy	total gastrectomy	pT3N0M0	Pre-therapeutic biopsy	>1h	70%	2 months	History of breast cancer. Epidermoid lung cancer diagnosed during follow-up
GXC-018	Moderately-differentiated papillary HER2+ (score 1) gastric adenocarcinoma	59	M	preoperative chemotherapy FLOT protoxol (docetaxel + oxaliplatin + 5-fluoro-uracil+ Folinic acid)	total gastrectomy	ypT4aN1(1/21)M0	surgical specimen	<1h	75%	2 months	No relapse or recurrence after 2 years
GXC-022	Moderately-differentiated papillary HER2 - gastric adenocarcinoma	66	M	preoperative chemotherapy FLOT protoxol (docetaxel + oxaliplatin + 5-fluoro-uracil+ Folinic acid)	Upper pole esogastrectomy with Lewis Santy reconstruction	ypT1N0M0	Pre-therapeutic biopsy	<1h	<30%	1 to 2 months	History of lung cancer. No relapse or recurrence after 3 years

Figure 1
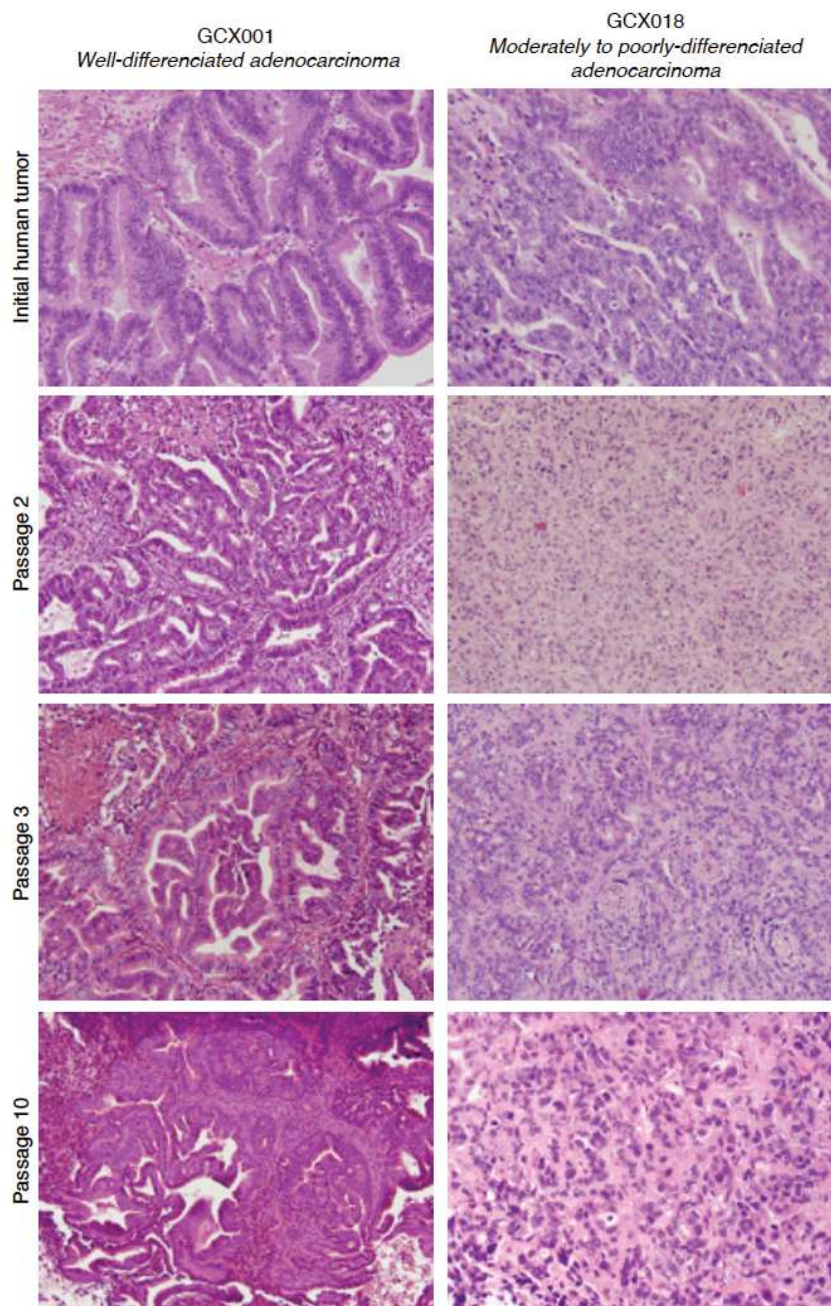
Figure 1. Evolution of tumor characteristics between passages compared to the original tissue. Left panel histological Hematoxilin-eosin (H&E) staining of the primary tumor well-differentiated gastric adenocarcinoma and representative GXC-001 tumors for each passage (2nd, 3rd, 10th) in the mice magnification x20. Right panel histological Hematoxilin-eosin staining of the primary tumor, a poorly differentiated gastric adenocarcinoma and representative GXC-018 tumors for each passage (2nd, 3rd, 10th) in the mice magnification x20, showing no significant difference in terms of architecture of the tumor or tumor differentiation.

Figure 2
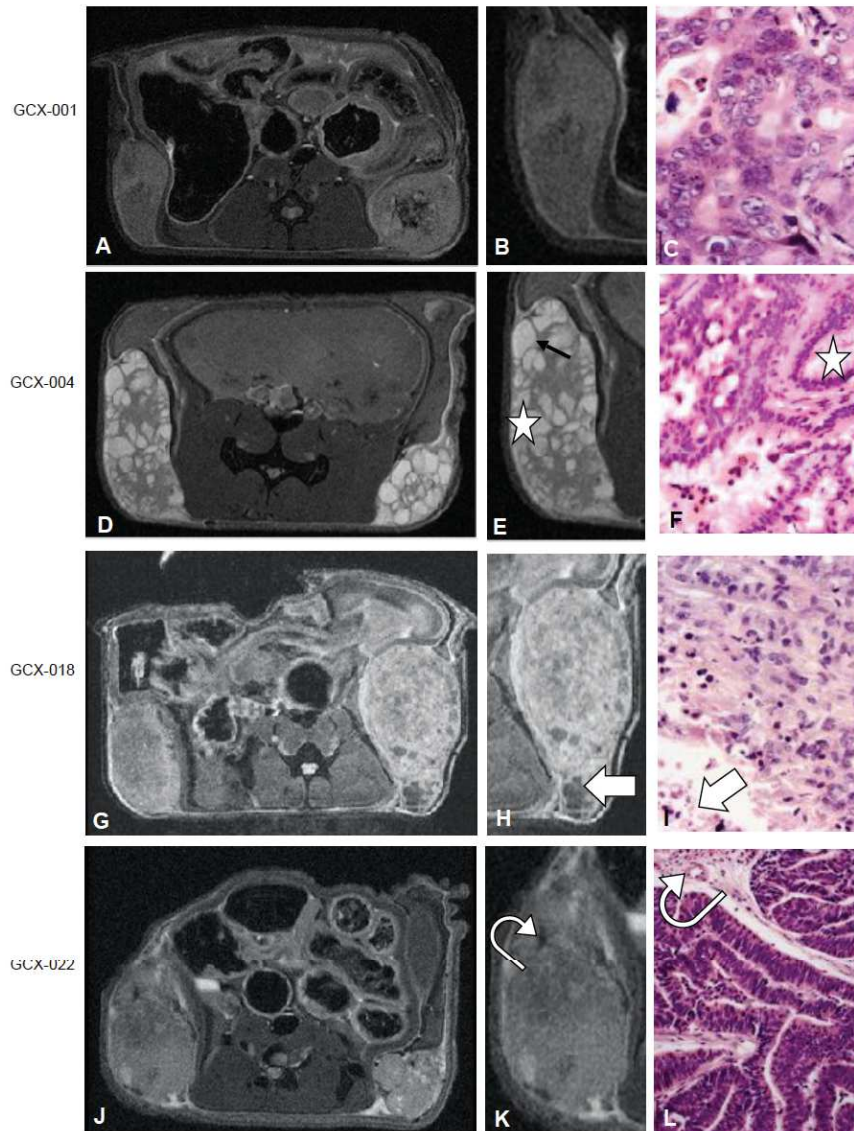
Figure 2. Characterization of tumors' substructures using a 9.4 tesla MRI. **A)** T2-RARE image of a well-differentiated gastric adenocarcinoma, GCX-001 model. There is a tumor on each flank of the mouse, the tumor on the left flank (right side) appearing slightly heterogenous compared to the other. **B)** Close up of the tumor showing a well delineated tumor, with a homogenous signal on T-weighted images. **C)** Corresponding histological slice, Hematoxilin-Eosin staining, magnification x 20. **D)** T2-RARE image of a primary well-differentiated papillary gastric adenocarcinoma, GCX-004 model. **E)** Close-up of the tumor, bearing the classical appearance of a papillary tumor, with hypointense fibrous stalk (arrow) supporting clumps of edematous papillae (star) with fluid like, bright intensity on T2. **F)** Corresponding histological slice, Hematoxilin-Eosin staining, magnification x 20. **H)** T2-RARE image of the GCX-018 model, a poorly-differentiated gastric adenocarcinoma. The subcutaneous tumors appear more heterogenous, with multiple foci of necrosis (thick arrow). **I)** Corresponding histological slice, Hematoxilin-Eosin staining, magnification x 20. **J)** T2-RARE image of a moderately-differentiated gastric adenocarcinoma. K) Close up of the tumor, showing presenting with an intermediate (=light grey) signal on T2-weighted images and with neo-vasculature, predominantly peripheral, presenting as linear hypointense structures on T2-weighted images (curved arrow) **H)** Corresponding histological slice, Hematoxilin-Eosin staining, magnification x 20.

Figure 3
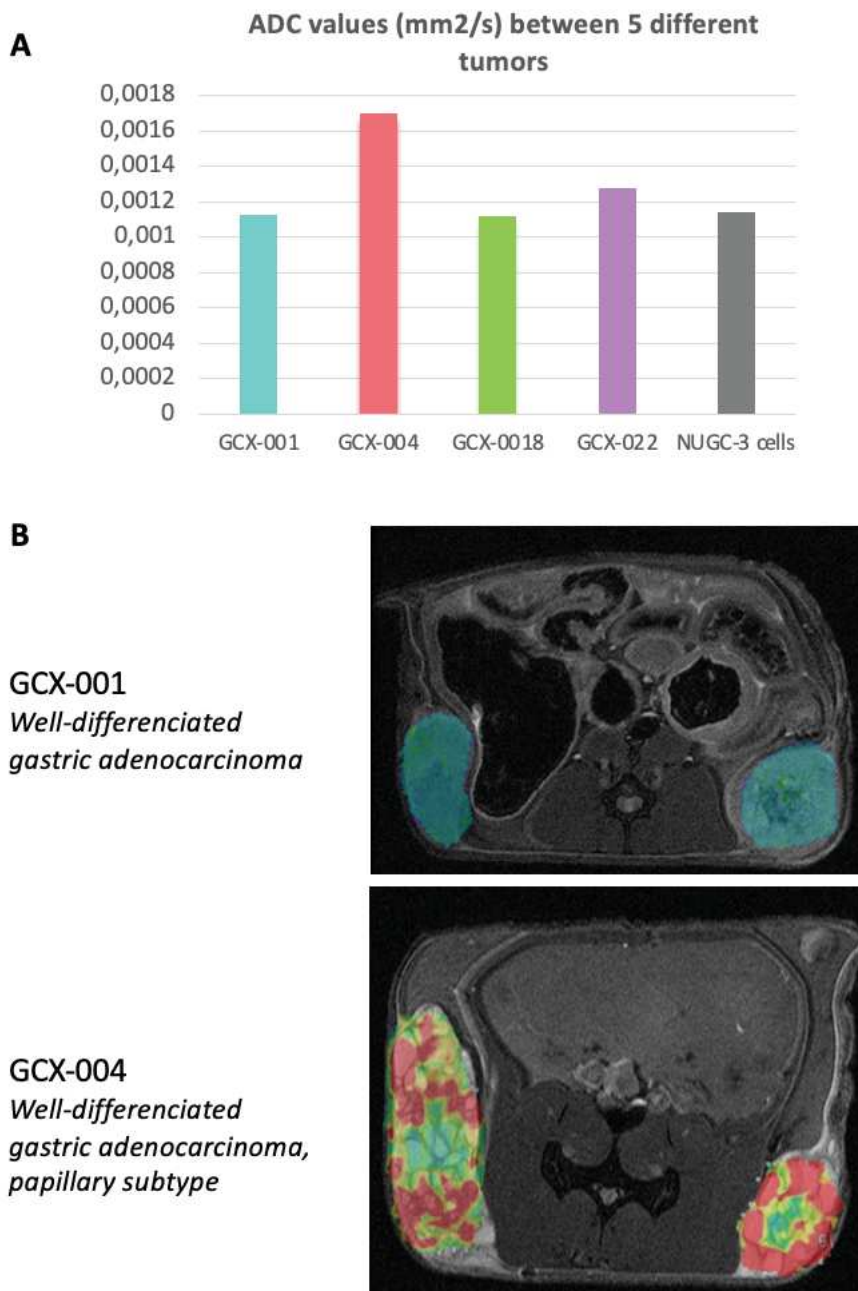
Figure 3. Measure of ADC value in different PDX, indicative of the cellularity of tumors

A) Diffusion (EPI) values showed restricted diffusion in all the subcutaneous tumors, with different ADC values between tumor types (GCX-001, -004, -018, -022) compared to a cell-line-derived tumor obtained from NUGC-3 cells. **B) Upper panel**, fusion image obtained combining a T2-RARE image of a well-differentiated gastric adenocarcinoma (GCX-001) and its corresponding ADC color map. **Lower panel,** fusion image obtained with T2-RARE image of a well-differentiated gastric adenocarcinoma (papillary subtype, GCX-004) and its corresponding ADC color map : the hyperintense clumps of edematous papillae showed higher ADC values, colored in red to yellow on the ADC map.

Figure 4

GCX-001
27.11 mm²

GCX-018
36.02 mm²
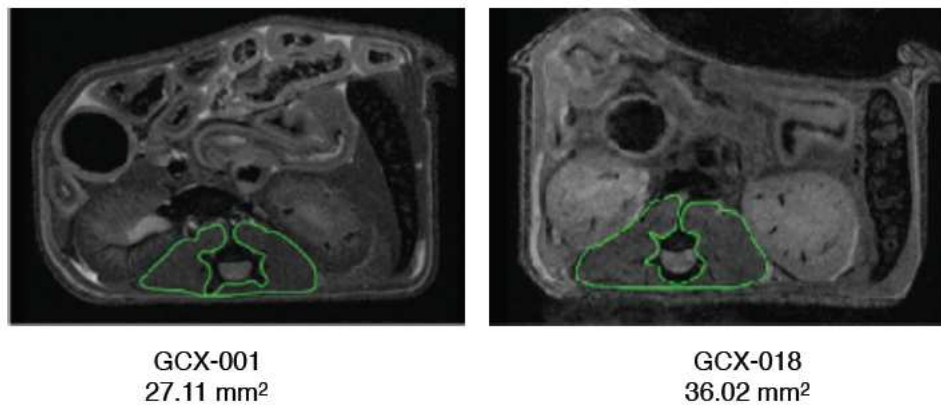
Figure 4. Comparison of muscle volumes between two PDX models. T2-RARE images of four PDX models, with manual delineation (green) of the paravertebral muscles and the corresponding average muscle surface, showing variations between models.

Figure 5
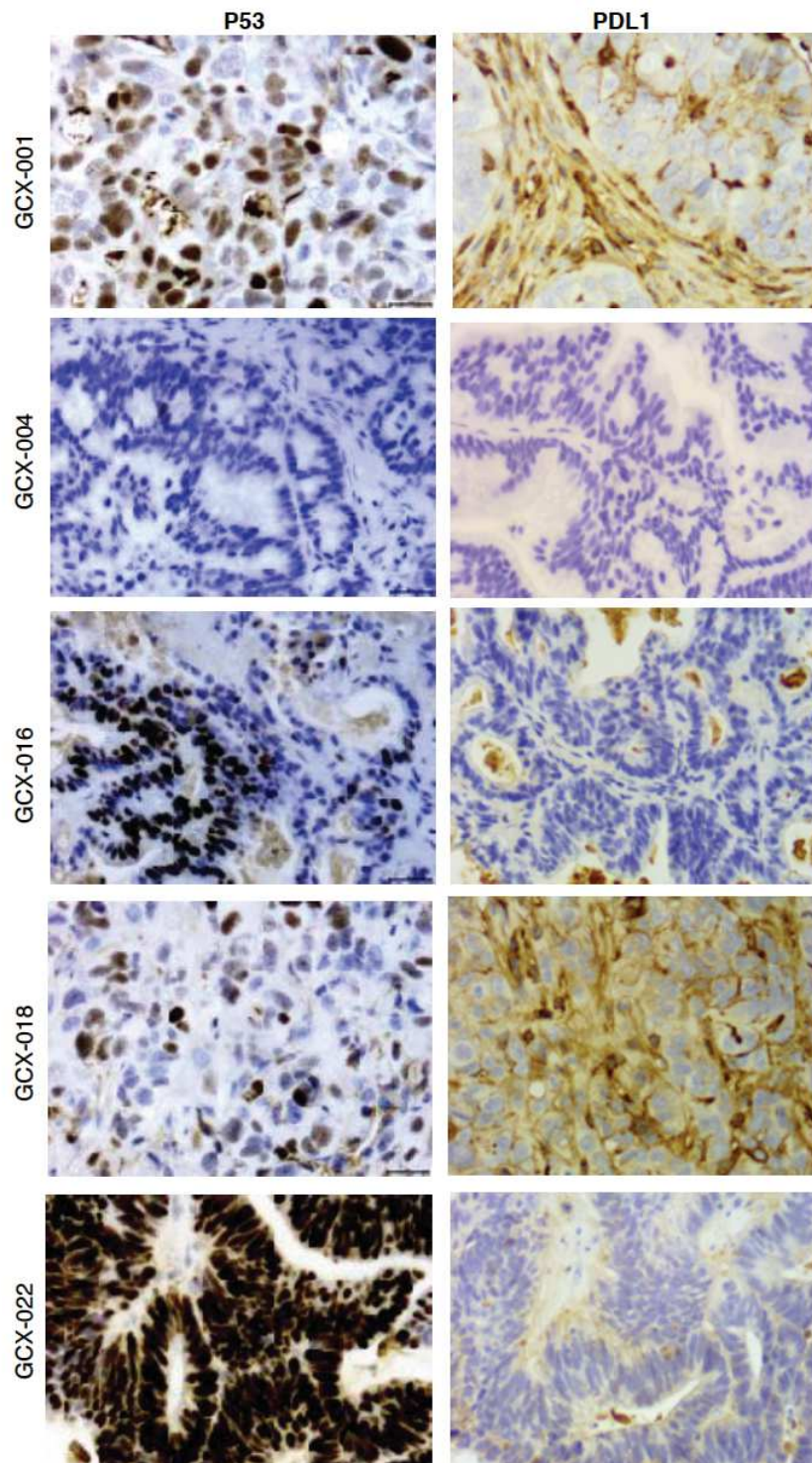
Figure 5. Comparison of the expression of p53 and PD-L1 on tumors sections of the different PDX models. Representative photomicrographs of each IHC, for each PDX model is shown (magnification= x40). Paraffine embedded tissues were used for immunohistochemistry to detect p53 and PD-L1 protein using specific antibodies. Labelling was revealed using DAB. Slides were also labelled using H&E to identify nuclei.

Figure 6
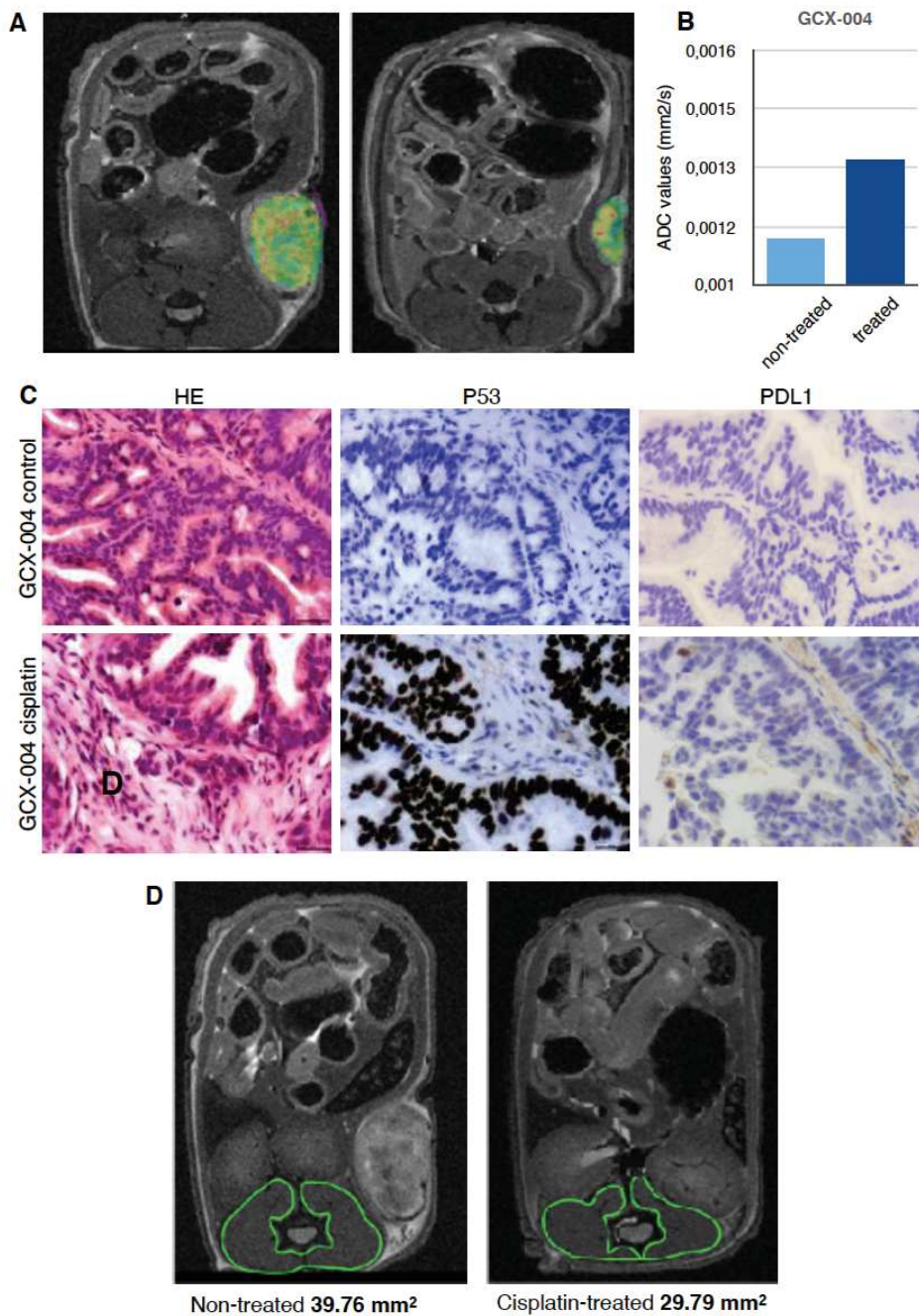
Figure 6. Impact of cisplatin on tumor substructure characteristics, p53 and PD-L1 expression and muscle atrophy.

A) Fusion image obtained combining a T2-RARE image of a well-differentiated gastric adenocarcinoma (GCX-001) and its corresponding ADC color map on a 9.4T MRI of a control mouse showing a non-treated subcutaneous tumor (left panel) or treated by cisplatin (right panel), showing a clear decrease in tumor size. **B)** Diffusion (EPI) values showed restricted diffusion in the subcutaneous tumors non-treated tumor and increased ADC value after cisplatin treatment. **C)** Representative photomicrographs for each histological (Hematoxilin-eosin, magnification x40, left panel) and immunohistochemical slice (P53, middle panel and PD-L1 right panel, magnification x40) showing treatment-related changes. **D)** T2-RARE images, axial plane, with manual delineation (green) of the paravertebral muscles showing differences between non-treated (left) and treated (cisplatin, right) tumors.

References

[1] Hidalgo, M., Amant, F., Biankin, A. V., Budinská, E., Byrne, A. T., Caldas, C., ... & Roman-Roman, S. (2014). Patient-derived xenograft models: an emerging platform for translational cancer research. *Cancer discovery*, *4*(9), 998-1013.

[2] Bang, Y. J., Van Cutsem, E., Feyereislova, A., Chung, H. C., Shen, L., Sawaki, A., ... & Aprile, G. (2010). Trastuzumab in combination with chemotherapy versus chemotherapy alone for treatment of HER2-positive advanced gastric or gastro-oesophageal junction cancer (ToGA): a phase 3, open-label, randomised controlled trial. *The Lancet*, *376*(9742), 687-697.

[3] Cancer Genome Atlas Research Network. (2014). Comprehensive molecular characterization of gastric adenocarcinoma. *Nature*, *513*(7517), 202-209.

[4] Sohn, B. H., Hwang, J. E., Jang, H. J., Lee, H. S., Oh, S. C., Shim, J. J., ... & Cheong, J. H. (2017). Clinical significance of four molecular subtypes of gastric cancer identified by the cancer genome atlas project. *Clinical Cancer Research*, *23*(15), 4441-4449.

[5] Shitara, K., Özgüroğlu, M., Bang, Y. J., Di Bartolomeo, M., Mandalà, M., Ryu, M. H., ... & Muro, K. (2018). Pembrolizumab versus paclitaxel for previously treated, advanced gastric or gastro-esophageal junction cancer (KEYNOTE-061): a randomized, open-label, controlled, phase 3 trial. *The Lancet*, *392*(10142), 123-133.

[6] Yu, S., Yang, M., & Nam, K. T. (2014). Mouse models of gastric carcinogenesis. *Journal of gastric cancer*, *14*(2), 67-86.

[7] Choi, Y. Y., Lee, J. E., Kim, H., Sim, M. H., Kim, K. K., Lee, G., ... & Noh, S. H. (2016). Establishment and characterisation of patient-derived xenografts as paraclinical models for gastric cancer. *Scientific reports*, *6*, 22172.

[8] Siolas, D., & Hannon, G. J. (2013). Patient Derived Tumor Xenografts: transforming clinical samples into mouse models. *Cancer research*, canres-1069.

[9] Huynh, H., Ong, R., & Zopf, D. (2015). Antitumor activity of the multikinase inhibitor regorafenib in patient-derived xenograft models of gastric cancer. *Journal of Experimental & Clinical Cancer Research*, *34*(1), 132.

[10] Wang, H., Lu, J., Tang, J., Chen, S., He, K., Jiang, X., ... & Teng, L. (2017). Establishment of patient-derived gastric cancer xenografts: a useful tool for preclinical evaluation of targeted therapies involving alterations in HER-2, MET and FGFR2 signaling pathways. *BMC cancer*, *17*(1), 191.

[11] Riquelme, I., Saavedra, K., Espinoza, J. A., Weber, H., García, P., Nervi, B., ... & Bizama, C. (2015). Molecular classification of gastric cancer: Towards a pathway-driven targeted therapy. *Oncotarget*, *6*(28), 24750

[12] Kim, J. Y., Kim, W. G., & Kwon, C. H. (2019). Differences in immune contextures among different molecular subtypes of gastric cancer and their prognostic impact. *Gastric Cancer*, *22*(6), 1164-1175.

[13] Böger, C., Behrens, H. M., Mathiak, M., Krüger, S., Kalthoff, H., & Röcken, C. (2016). PD-L1 is an independent prognostic predictor in gastric cancer of Western patients. *Oncotarget*, *7*(17), 24269.

[14] Fuchs, C. S., Doi, T., Jang, R. W., Muro, K., Satoh, T., Machado, M., ... & Garrido, M. (2018). Safety and efficacy of pembrolizumab monotherapy in patients with previously treated advanced gastric and gastroesophageal junction cancer: phase 2 clinical KEYNOTE-059 trial. *JAMA oncology*, *4*(5), e180013-e180013.

[15] Ni, X., Xing, Y., Sun, X., & Suo, J. (2020). The safety and efficacy of anti-PD-1/anti-PD-L1 antibody therapy in the treatment of previously treated, advanced gastric or gastro-oesophageal junction cancer: A meta-analysis of prospective clinical trials. *Clinics and Research in Hepatology and Gastroenterology*, *44*(2), 211-222.

[16] Riquelme, I., Saavedra, K., Espinoza, J. A., Weber, H., García, P., Nervi, B., ... & Bizama, C. (2015). Molecular classification of gastric cancer: Towards a pathway-driven targeted therapy. *Oncotarget*, *6*(28), 24750

[17] Huang, D. D., Chen, X. X., Chen, X. Y., Wang, S. L., Shen, X., Chen, X. L., ... & Zhuang, C. L. (2016). Sarcopenia predicts 1-year mortality in elderly patients undergoing curative gastrectomy for gastric cancer: a prospective study. *Journal of cancer research and clinical oncology*, *142*(11), 2347-2356.

[18] Voisinet, M., Venkatasamy, A., Alratrout, H., Delhorme, J. B., Brigand, C., Rohr, S., ... & Romain, B. (2020). How to Prevent Sarcopenia Occurrence during Neoadjuvant Chemotherapy for Oesogastric Adenocarcinoma?. *Nutrition and Cancer*, 1-7.

[19] Dieter, S. M., Giessler, K. M., Kriegsmann, M., Dubash, T. D., Möhrmann, L., Schulz, E. R., ... & Heger, U. (2017). Patient-derived xenografts of gastrointestinal cancers are susceptible to rapid and delayed B-lymphoproliferation. *International journal of cancer*, *140*(6), 1356-1363.

[20] von Grabowiecki, Y., Licona, C., Palamiuc, L., Abreu, P., Vidimar, V., Coowar, D., ... & Gaiddon, C. (2015). Regulation of a Notch3-Hes1 pathway and protective effect by a tocopherol-omega alkanol chain derivative in muscle atrophy. *Journal of Pharmacology and Experimental Therapeutics*, *352*(1), 23-32.

[21] Ribeiro, N., Thuaud, F., Bernard, Y., Gaiddon, C., Cresteil, T., Hild, A., ... & Désaubry, L. (2012). Flavaglines as potent anticancer and cytoprotective agents. *Journal of medicinal chemistry*, *55*(22), 10064-10073.

[22] Cerami, E., Gao, J., Dogrusoz, U., Gross, B. E., Sumer, S. O., Aksoy, B. A., ... & Antipin, Y. (2012). The cBio cancer genomics portal: an open platform for exploring multidimensional cancer genomics data.

[23] Gengenbacher, N., Singhal, M., & Augustin, H. G. (2017). Preclinical mouse solid tumour models: status quo, challenges and perspectives. *Nature Reviews Cancer*, *17*(12), 751.

[24] Lauber, D. T., Fülöp, A., Kovács, T., Szigeti, K., Máthé, D., & Szijártó, A. (2017). State of the art in vivo imaging techniques for laboratory animals. *Laboratory animals*, *51*(5), 465-478.

[25] Dieter, S. M., Giessler, K. M., Kriegsmann, M., Dubash, T. D., Möhrmann, L., Schulz, E. R., ... & Heger, U. (2017). Patient-derived xenografts of gastrointestinal cancers are susceptible to rapid and delayed B-lymphoproliferation. *International journal of cancer*, *140*(6), 1356-1363

[26] Zhu, Y., Tian, T., Li, Z., Tang, Z., Wang, L., Wu, J., ... & Zou, J. (2015). Establishment and characterization of patient-derived tumor xenograft using gastroscopic biopsies in gastric cancer. *Scientific reports*, *5*, 8542.

[27] Yoshiyuki, T. et al. Immunohistochemical demonstration of epidermal growth factor in human gastric cancer xenografts of nude mice. Cancer 65, 953–7 (1990).

[28] Galban, C. J., Hoff, B. A., Chenevert, T. L., & Ross, B. D. (2017). Diffusion MRI in early cancer therapeutic response assessment. *NMR in biomedicine*, *30*(3), e3458.

[29] iang, Z., Liu, Z., Li, M., Chen, C., & Wang, X. (2018). Immunogenomics analysis reveals that TP53 mutations inhibit tumor immunity in gastric Cancer. *Translational oncology*, *11*(5), 1171-1187.

[30] Miyamoto, Y.; Hanna, D. L.; Zhang, W.; Baba, H.; Lenz, H. J., Molecular Pathways: Cachexia Signaling-A Targeted Approach to Cancer Treatment. Clin Cancer Res 2016, 22 (16), 3999-4004.

2.2. The use of PDX models to test new therapeutic approaches in gastric cancer

2.2.1. ARTICLE 3: Inhibition of HDAC synergies chemotherapy via p53 in gastric cancer

The histone desacetylase enzymes (HDAC, 4 different classes : class I, IIa, IIb and IV) are known to be expressed **aberrantly** in different cancers, including **gastric ones.** Additionally, the expression of **HDAC** is known to be **linked to carcinogenesis** [131]. The cytotoxic activity of platinum-based drugs (e.g. cisplatin/oxaliplatin) depends on the formation of DNA adducts, which results in a cell cycle arrest and the induction of apoptosis, but this requires an access to DNA, which can be altered by DNA-associated proteins, like histones for instance. One of the possible resistance mechanism to chemotherapies is the presence of various epigenetic alterations (such as histone/DNA methylation or histone deacetylation/ acetylation) and post-transcriptional regulations (with microRNAs). All in all, such deregulations are potentially related to cancer progression and resistance against chemotherapy drugs, eventually resulting in a poorer outcome. Hence, **inhibitors of histone desacetylase enzymes** (HDACi) have been developed to counteract their pro-oncogenic activity [132]. For instance, SAHA (Vorinostat), which is a a pan-HDAC inhibitor targeting class I-II-IV of HDACs has obtained the FDA approval for the treatment of cutaneous T-cell lymphoma and showed a promising antitumor *in vitro* (gastric cancer cell lines) and *in vivo* (animal models) activity, with almost no side effects on normal cells [133]. SAHA induces a p53 independent apoptosis through the mitochondria pathway but acts synergistically with p63/p73 (ARTICLE 3). HDACi have been described as chemosensitizers for cisplatin and **combination between HDACi and standard chemotherapy** have been already been successfully evaluated in ovarian cancer, oral squamous cell carcinoma and osteosarcoma, demonstrating its ability to **bypass resistance mechanisms, with reduced side effects**.

For this work, I performed the in vivo experiment for SAHA/platinium-compound chemotherapy evaluation and I participated in the redaction of the manuscript.

Inhibition of HDAC synergies chemotherapy via p53 in gastric cancer

Gries A.[1], Badie A. [1], Spaety M.E.[1,2], Venkatasamy A.[1,3], Pfeffer S. [2], Benoit R.[1,4], Mellitzer G.[1,c], and Gaiddon C.[1,c]

[1] Université de Strasbourg – Inserm UMR_S1113, IRFAC, Streinth Laboratory (Stress Response and Innovative Therapies), ITI InnoVec, 3 av. Molière, Strasbourg, France

[2] ARN, CNRS UPR 9002, Université de Strasbourg, Strasbourg France

[3] IHU-Strasbourg, Institute of Image-Guided Surgery, Strasbourg, France
[4] Digestive surgery department, CHU Hautepierre, Strasbourg, France

[c] Corresponding authors: gaiddon@unistra.fr; mellitzer@unistra.fr

Abstract

In personalized medicine, the developments of combinatory therapies associating drugs that target different pathways, specifically deregulated in patient's tumors, drives hope to treat resistant cancers while reducing side effects. The prerequisite to optimize this strategy is a precise understanding of the molecular basis of combinatory therapies, which can be different from monotherapies. In this study, we analyzed the molecular mechanisms involved in combinatory treatments of gastric cancer cells, associating a platinum-based standard treatment, cisplatin or oxaliplatin, with a histone deacetylase inhibitor (HDACi), the suberoylanilide hydroxamic acid (SAHA). We showed that SAHA potentiated the cytotoxicity of both cisplatin and oxaliplatin in gastric cancer cells and their anticancer activity on a model of patient-derived xenografts of gastric cancer. This increased activity correlates with a reprograming of the cellular response toward apoptosis as indicated by Caspase 3 cleavage. Simultaneously, SAHA surprisingly counteracted the induction of the tumor suppressor gene *TP53* at the protein level through an inhibition of its transcription. In addition, SAHA impacted on the transcription of two other members of the p53 family: TAp63 and TAp73. However, functional studies using siRNA showed that despite having its expression diminished, p53 was necessary for the induction of the cleavage of Caspase 3 by SAHA and platinum drugs combined. Importantly, the restoration of p53 activity by treatment with PRIMA-1 on gastric cancer cells expressing a mutated p53 (NUGC3) increases the synergy of SAHA with platinum drugs. Altogether, these results indicate that combinatory therapies associating SAHA and platinum drugs are promising strategies in gastric cancer treatment, but efficiency might be dependent upon the presence of functional p53 proteins, opening new perspective of tri-therapies with reactivator of p53 mutants.

Keywords: HDACI, SAHA, Vorinostat, p53, p63, p73, gastric cancer, Cisplatin, Oxaliplatin, apoptosis, autophagy, MEF2A, CDX2, HDAC4

Introduction

Gastric cancer (GC) is the fourth most common cancer for men, the fifth for women in the World, and represents the third cause of cancer-related death worldwide *(Michel P et al. 2017)*. Surgical resection combined with perioperative chemotherapy using platinum-derivative compounds (PDC: cisplatin, oxaliplatin) is the cornerstone of current treatments. Although the use of chemotherapy has improved the survival rate of patients, the outcome remains unfavorable with a 30 to 40% response-rate to treatment and a median survival of only 6-9 months in advanced GC**.** Furthermore, significant side effects of platinum derivatives (e.g. nephrotoxicity, emetic activity, polyneuropathy) associated with the frequent development of resistances (innate or acquired), limit their use and effectiveness *(Florea AM et al. 2011).* All in all, the identification of early prognosis markers and the development of alternative therapeutic strategies currently represent an absolute necessity.

One of the mechanisms of tumorigenesis and resistance to chemotherapies involves epigenetic modifications (histone acetylation/deacetylation, histone/DNA methylation) and post-transcriptional regulations (microRNAs). Fraga and co-workers have reported a loss in acetylation of the histone H4K16 and trimethylation H4K20 at repeated DNA sequences of tumor cells at early stage in tumorigenesis (*Fraga MF et al. 2005)*. Histone deacetylase enzymes (HDAC) are aberrantly expressed in various cancers such as gastric or colon cancer. The HDAC family is composed of 4 classes: class I (HDAC 1, 2, 3 and 8), IIa (HDAC 4, 5, 7 and 9), IIb (HDAC 6 and 10) and IV (HDAC11) which are Zn^{2+} dependent and class III (Sirtuins) which is NAD^+ dependent *(Li Y and Seto E. 2017).* HDACs remove the acetyl group of lysine residues from histone and non-histone substrates, leading to chromatin compaction and decreasing gene transcription. They can also target non-histone substrates, such as the tumor suppressor gene p53, the Hypoxia Inducible Factor A (HIF1A) and the α-tubulin, impacting on DNA affinity, transcriptional activity, protein stability and protein interactions, thus having a key role in different cellular pathways *(Zhang J and Zhong Q. 2014; Li Y and Seto E. 2017).* Moreover, HDAC expression is known to be linked to carcinogenesis *(Marks P et al. 2001).* HDAC1 can interact with p53, which reduces its binding capacity to the promoter of the pro-apoptotic gene *BAX*, thus favoring cancer cell survival, which is correlated with poor prognosis (*West AC et al. 2014).* For this reason, HDAC inhibitors (HDACIs) have been developed to counteract the pro-oncogenic activity of HDACs *(West AC et al. 2014; Li Y and Seto E. 2017).*

The HDACIs are classified in five groups, according to their chemical structures. These anticancer agents can induce different phenotypes including growth arrest, differentiation and apoptosis *(Li Y and Seto E. 2017).* Among them, one of the most promising HDACI, a pan-inhibitor targeting class I-II-IV of HDACs called SAHA was approved by the FDA in 2006 for the treatment of cutaneous T-cell lymphoma. SAHA treatment shows an anticancer activity in a variety of tumor cell lines and tumor-bearing animals, with relatively no side effects on normal cells *(Kelly WK et al. 2005).* SAHA has not a massive effect on gene expression, as less than 2% of genes are hyperacetylated *(Komatsu N et al. 2006).* However, it has a specific action on genes involved in apoptosis, cell cycle, tumor suppression and differentiation *(Rikiishi H et al. 2007).* SAHA induces a p53-independent apoptosis through the mitochondria pathway *(Vrana JA et al. 1999)* but acts synergistically with p63/p73 *(Shim SH et al. 2010)* and is thought to overcome multidrug resistance in various cancer cell lines *(Lee MJ et al. 2008).* A gene signature analysis performed by Claerhout and co-workers suggests that SAHA is a good potential drug candidate in GC treatment, as it inhibits cellular growth and induces cellular death in gastric cancer cell lines

(Mutze K et al. 2010; Claerhout S et al. 2011; Yoon C et al. 2014), involving RUNX3 *(Huang C et al. 2007),* MYC *(Labisso WL et al. 2012)* or SRC *(Zhou C et al. 2014).* In addition, the use of SAHA potentiated the activity of taxane anticancer drugs in gastric cancer cells *(Chang H et al. 2010).*

Cisplatin cytotoxicity depends on the formation of DNA adducts, which results in cell cycle arrest and the induction of apoptosis *(Florea AM et al. 2011).* The formation of these adducts requires a DNA accessibility, which can be altered by DNA-associated proteins such as histones. HDACIs are described as chemosensitizers for cisplatin, through a reduction of chromatin condensation and therefore an improvement of DNA platination *(Kim MS et al. 2003; Lin CT et al. 2008; Davies NP et al. 2000).* The use of a combination of HDACI with currently-used chemotherapies, such a SAHA + cisplatin / oxaliplatin has been described in various types of cancers such as oral squamous cell carcinoma (OSCC), ovarian cancer or osteosarcoma *(Kim MS et al. 2003; Ong PS et al. 2012, Pettke A et al. 2016; Rikiishi H et al. 2007; Sato T et al. 2006).* In OSCC, the combination of SAHA and cisplatin was associated with increased expression of markers (Caspase-4/12, eIF2a) involved in the endoplasmic reticulum stress pathway *(Suzuki M et al. 2009).* Some of the molecular mechanisms involved in the synergistic effect of these two drugs - especially regarding their combined influence on p53 - are still controversial. For instance, in gastric cancer cells, the combination of SAHA with oxaliplatin reverses the oxaliplatin-induced activation of the tyrosine kinase Src and decreases the phosphorylation of AKT, which is a major factor for cellular growth and survival *(Zhou C et al. 2014).* More recently, a phase I trial of SAHA combined with cisplatin and capecitabine in patients with advanced gastric cancer showed an increased median overall survival time of 18 months, with manageable side effects *(Yoo C et al. 2014).* Surprisingly, the results of a more recent Phase II study that did not show any significant gain in patient survival, discouraging the use of the combination between SAHA and oxaliplatin in clinical routine *(Yoo C. et al. 2016).*

In an effort to understand these conflicting and disappointing results and find novel strategies for treating gastric cancer, we decided to investigate more thoroughly the molecular mechanisms induced by a co-treatment between SAHA and platinum drugs in gastric tumors. Our study performed *in vitro* and *in vivo* show that the synergistic activity of SAHA with platinum drugs causes a reprograming towards apoptosis that is significantly dependent upon the activity of tumor suppressor gene p53. Hence, this study suggests that the p53 status might represent a biomarker for a personalized therapy of gastric cancer patient treated with a combination between SAHA and platinum drugs. It also shows the potential of p53 re-activating drugs to improve the SAHA-platinum drugs combination.

Material and Methods

Cell culture

AGS cells (ATCC CRL-1739™), KATOIII cells (ATCC HTB-103™), and NUGC3 cells (JCRB Cell Bank, JCRB0822) are grown in RPMI (Roswell Park Memorial Institute medium, Dominique Dutscher) with 10% fetal bovine serum (FBS; Gibco, Life technologies) and 1% penicillin/streptomycin (P/S; PAN-Biotech) at 37°C in a humidified atmosphere and 5% CO_2. Mycoplasma contamination has been tested negatively using PlasmoTest (Invivo gene).

Cellular treatments

Cisplatin (Accord Health Care) and oxaliplatin (Hospira) were used in saline solution as used in clinic. The pan-HDAC inhibitors, SAHA (Vorinostat, Tocris) was solubilized at 20mM in DMSO (VWR Chemicals).

MTT survival test

10.000 cells (AGS) or 20.000 cells (KATOIII, NUGC3) were seeded per wells in 96-well plates (Falcon Multiwell) 24h prior to any treatment. Drugs (PDC, HDACI) were diluted in RPMI+FBS+P/S and 100µL/well were deposited on cells for 48h. MTT survival test was performed as previously described *(Benosman S et al. 2011)*. Briefly, MTT was realized by replacing the culture medium with 100µL/well of new culture medium completed with 5mg/mL of MTT product (Sigma Aldrich) for 1h30 at 37°C. Then, cells were lysed, and the colored formazan product was solubilized in 100µL/well of DMSO. Coloration is an indicator of cellular viability. Optic density (DO) was measured at 590nm with Tristar² Mutlimode Reader® (Berthold Technologies). Experiments were done with four technical replicates and realized at least in three independent times. Cellular viability was evaluated by taking the untreated cells (NT) as control. IC_x represents the concentration where a reduction of cellular viability of X% is measured. IC_x were determined graphically with Prism Graphpad 5 software; curves are generated as log(inhibitor) vs. response -- Variable slope (four parameters).

Isobologram assay

10.000 cells (AGS) or 20.000 cells (KATOIII, NUGC3) were seeded per wells in 96-well plates (Falcon Multiwell) 24h prior to any treatment. Combined treatments (PDC + HDACI), or each concentration of drug alone were diluted in RPMI+FBS+P/S and 100µL/well were deposited on cells for 48h. MTT survival tests were realized as described before. Cellular viability and treatment efficiencies were evaluated by taking the untreated cells (NT) as control (100% of cellular viability; 0% of treatment efficiency). Combined treatment efficiencies were compared to drug alone efficiencies with Compusyn program software (ComboSyn, Inc), which determines mathematically the combination indexes *(Chou TC. 2006 and 2010)*. We arbitrarily and conservatively considered antagonist effect on cell survival between the drugs when combination indexes corresponded to value superior to 1.20, additive effect between 0.80 and 1.20 and synergistic effect when combination indexes were inferior to 0.80. For each drug or combined treatment, experiments were done in height technical replicates and at least realized in three independent times.

Silencing RNA

250.000 cells were seeded per well in 6-well plates (Falcon, Multiwell) 24h prior any treatment in an antibiotic free RPMI+FBS medium. Transfections were performed with the Lipofectamine® RNAiMAX Reagent. SiRNA and 4µL of Lipofectamine® RNAiMAX Reagent were diluted separately in Opti-MEM® Medium (respectively 150µL/product for 1 well). Diluted siRNA was added to the diluted Lipofectamine® RNAiMAX Reagent and the mix was incubated 5min at room temperature. The 300µL of the mix (siRNA-lipid complex) were added to cells (drip throughout the well) with a total volume of 2mL/well (1700µL of fresh RPMI+FBS medium + 300µL siRNA-lipid complex) for 7h at 37°C. Then, the culture medium was replaced with fresh medium RPMI + FBS. After 48h, cells were treated with the different described experimental conditions by replacing the culture medium (always no antibiotics).

The different siRNA used were: **sip53** (30nM, Eurogentech) 5'-GGA AAC UAC UUC CUG AAA A-3'; **Control siRNA duplex pGL3 luciferase** (30nM, Eurgoentech); SR-CL011-005;

Quantitative PCR

500.000 cells were seeded per well in 6-well plates (Falcon, Multiwell) 24h prior any treatment. Then cells were treated with the described drugs at indicated concentrations and times by replacing the culture medium. Total RNA was extracted with TRIzol® Reagent. RNA reverse transcription was performed with the High Capacity cDNA Reverse Transcription Kit® (Applied Biosystems) in a total reaction mix of 20µL as described by the provider during 2h at 37°C. qPCR were performed with the FastStart Universal SYBR Green PCR Master Mix® or the FastStart Universal Probe Master Mix TaqMan® (Roche) in 20µL total volume per reaction containing 4µL of diluted cDNA, 10 µL of FastStart Reagent and 500nM of primers. qPCR was carried out in 7500 Real Time PCR System® (Applied Biosystems). Relative expressions were normalized with TBP according to the method $2^{(-\Delta\Delta Ct)}$ *(Livak KJ and Schmittgen TD. 2001).*

Western blot

500.000 cells were seeded per well in 6-well plates (Falcon Multiwell), 24h prior to any treatment. Then, cells were treated to indicated drugs and times by replacing the culture medium. Adherent and supernatant cells were lysed with Laemmli® 1x (Biorad) added of Dithiothreitol 50mM (DTT; Sigma-Aldrich) at the rate of 100µL/condition. Total proteins were sonicated and denatured before being put on an SDS-PAGE gel (10-20µL/sample). Western blots were performed using Polyvinylidene fluoride (PVDF) membranes and primary antibodies directed against **p53** (mouse anti-p53 DO-1, sc-126, Santa Cruz, 1:1000 in PBS-Milk1%-Tween1‰ [Fisher Bioreagents]), **CLEAVED CASPASE 3** (rabbit anti-cleaved caspase 3, #9661, Cell Signaling, 1:1000 in PBS-Milk1%-Tween1‰), **LC3B** (rabbit anti-LC3B, NB100-2220, Novus Biological, 1:1000 in TBS [152,3mM Tris-HCl; 46,2mM Tris-Base; 1,5M NaCl [Sigma] pH 7.6)-BSA5%-Tween1‰]), **Acetylated H3K9** (rabbit anti-histone H3 [Acetyl K9], ab61231, Abcam, France, 1:500 in PBS-Milk1%-Tween1‰), **HISTONE H3** (rabbit anti-histone H3, #4499, Cell Signaling, 1:1000 in PBS-Milk1%-Tween1‰), **Phosphorylated AKT** (rabbit anti-phospho-Akt [Ser 473], #4060, Cell Signaling, 1:2000 in TBS-BSA5%-Tween1‰), **AKT** (rabbit anti-Akt, #9272, Cell Signaling, 1:1000 in TBS-BSA5%-Tween1‰), **HIF1 ALPHA** (anti-HIF1-alpha, BD Biosciences, 1:1000 in PBS-Milk1%-Tween1‰), **Acetylated ALPHA TUBULIN** (rabbit anti-acetyl [Lys40] alpha tubulin, #5335, Cell Signaling, 1:1000 in TBS-BSA5%-Tween1‰) and **ALPHA TUBULIN** (rabbit anti-alpha tubulin, #2144, Cell Signaling, 1:1000 in TBS-BSA5%-Tween1‰). Secondary antibodies **anti-rabbit NA934V**, **anti-rat NA935** and **anti-mouse NXA931V** (Horseradish linked, ECL GE Healthcare, 1:10.000) were incubated 1h at room temperature. Protein levels were normalized to **ACTIN** (mouse anti-actin Clone C4, Chemicon, 1:10.000). Western blot revelations were done with ECL reagent® (GE Healthcare) and observed with PXi® Syngene. Finally, relative quantification to ACTIN was carried out with Genetools software (Syngene). Western blots were performed three times independently.

Patient derived xenograft

We used an in-house developed patient-derived xenograft mouse model (GCX-004), which is a well-differentiated gastric adenocarcinoma, intestinal type. The tissue sample used was issued from a surgical specimen obtained after total gastrectomy of a primary well-differentiated intestinal type

HER2-negative gastric adenocarcinoma (ypT1aN0, a 64 years-old man). The fragments were implanted on the flanks of an anaesthetized immunodeficient mouse, with close monitoring of their growth (1-3 times/week by manual caliper). When the implanted tumor reached 500mm^3, the engraftment was considered successful, the mouse was anaesthetized and the tumor harvested for serial transplantation into successive mice generations. The implanted fragments reached a 150mm^3 target volume within 15 days. Histology of the different passages were well-matched with the primary human tumor, with no lymphomatous transformation.

Graphical representation and statistical tests

Box plots and histograms represent sample fold inductions compared to the indicated control. Box plots and histograms were obtained by the quantification of three technical replicates of _n_ biological replicates. Normality distribution was checked by Shapiro-Wilk test and homoscedasticity was checked by Bartlett test. Statistical differences were calculated with ANOVA and Tukey post-test or with Mann-Whitney test with a p-value corrected using Prism Graphpad 5 software. * $p < 0.05$; ** $p < 0.01$; *** $p < 0.001$.

Results

Synergy between platinum derivative compounds and SAHA

The gold standard for the treatment of gastric cancer is chemotherapy using platinum derivative compounds (PDC: Cisplatin, Oxaliplatin). We studied the PDC effect on cancer cells for a better understanding of cellular resistance to treatment, to optimize it. We performed the present study on different gastric cancer cell lines with different status for the tumor suppressor gene _TP53_ as it is mutated or inactivated in more than 50% of the tumors. We used the AGS (p53 WT), NUGC3 (p53 mutated Y220C) and KATOIII (p53 deleted) cell lines **(Table S1).** The response of cell lines to platinum compounds and HDAC inhibitor (SAHA) was first assessed by monitoring their survival using an MTT assay after 48 hours of treatment with increasing concentrations of cisplatin or oxaliplatin **(Figure 1).** Viability curves allowed us to determine the IC_{25}, IC_{30} IC_{50} IC_{60}, and IC_{75} which are drug concentrations that respectively induced 25%, 30%, 50%, 60% and 75% of a complete loss of cell viability and are reported in table S1. AGS cells **(Figure 1A)** are more sensitive to oxaliplatin than to cisplatin whereas NUGC3 **(Figure 1B)** are more sensitive for cisplatin and possess higher IC_{50} for oxaliplatin. KATOIII cells **(Figure 1C)** are considered sensitive to cisplatin and oxaliplatin because they possess an IC_{50} inferior or equal to 10µM.

First, in order to establish the impact of HDACI on the cytotoxicity of platinum-based drugs in gastric cancer cells, we performed isobologram assays _(Chou TC. 2006; 2010)._ AGS cells were treated for 48h with different concentrations of either cisplatin or oxaliplatin, combined with SAHA, followed by an isobologram assay to mathematically determine the combination index **(Figure 1D, E).** The combined treatments with both PDC and SAHA had in majority combinatory index below 1. These results indicated that combined treatments had synergistic effect on AGS cell survival **(Figure 1D, E).** Synergistic activities between cisplatin and SAHA were obtained in others GCC KATOIII and NUGC3 **(Supplementary figure 1).** However, in KATOIII cells, the results were more heterogeneous with oxaliplatin showing antagonistic effects when combined with SAHA except for IC_{50}. In NUGC3 cells,

synergistic effects between cisplatin + SAHA and between oxaliplatin + SAHA were only observed at low concentrations of both drugs **(Supplementary figure 1).**

To verify the correct HDAC inhibition activity of SAHA in our conditions, we analyzed the acetylation status of the lysine 9 of histone H3 and on non-histone targets α-tubulin and HIF1A. The acetylation level of H3K9 is controlled by HDAC3 status *(Bhaskara S et al. 2010; Vecera J et al. 2018)* and is necessary for gene expression *(Gates LA et al. 2017).* As expected, SAHA induced a strong increase of H3K9 acetylation **(Figure 1F),** reflecting its HDAC inhibitor activity. Interestingly, PDC alone or combined with SAHA had not a strong influence H3K9 acetylation levels. Moreover, HDAC6 is required for EGFR-induced β-catenin nuclear localization *(Li Y et al. 2008),* HDAC6 controls autophagosome maturation *(Li JY et al. 2010)* and α-tubulin acetylation level *(Li G et al. 2011).* As expected, SAHA induced a strong increase of α-tubulin acetylation **(Figure 1F),** reflecting its HDAC inhibitor activity on HDAC6. Interestingly, PDC alone or combined with SAHA had not a strong influence on α-tubulin acetylation levels as well. Furthermore, HIF1A is an important transcription factor involved in tumor metabolic switch, invasion and drug resistance *(Kitajima Y and Miyazaki K. 2013; Rohwer N and Cramer T. 2011).* HIF1A is regulated among other by HDAC enzymes modifying its stability and its activity (*Geng H et al. 2011; Joo HY et al. 2015).* Indeed, HDAC1 and HDAC3 enhance HIF1A stability and its transactivation function in hypoxic conditions and inhibition of these HDACs decreases HIF1A protein level and its transcriptional activity in human and mouse tumor cell lines *(Kim SH et al. 2007).* Similarly, HDAC4 controls HIF1A stability and activity, since HDAC4 silencing (shRNA) inhibits HIF1A protein stability *(Geng H et al. 2011, Geng H et al. 2012).* As expected, SAHA reduced HIF1A stability promoting HIF1A protein level reduction **(Figure 1G).** And SAHA decreased HIF1A activity on its target genes *VEGF* and *GLUT-1* **(Supplementary figure 2).**

Altogether, these results indicated that SAHA inhibits HDAC enzymes and that SAHA acts synergistically with PDC on gastric cancer cell survival, but this depends on the PDC and the concentrations used in the different cell lines.

Combination between SAHA and cisplatin reduces the tumor volume and induces in vivo treatment-related structural changes within the tumors

The combinatory *in vitro* cytotoxicity observed above indicated that a combinatory treatment of cisplatin and SAHA might be beneficial in gastric cancer. Therefore, we decided to evaluate *in vivo* the effectiveness of combined cisplatin + SAHA treatment on a tumor derived from a patient with gastric cancer xenografted in nude mice that we have established in our laboratory in collaboration with the Digestive Surgery department of the Strasbourg University Hospital of Hautepierre. This patient-derived xenograft model, GCX-004, was established from a well-differentiated gastric adenocarcinoma. For our experiment, several tumor fragments (~3mm^3) from the 8th passage of GCX-004 were subcutaneously implanted on both flanks of NUDE mice, and the mice were split into four groups. Once the tumors reached the target volume (150 mm^3), we treated one group (*n*=6) with cisplatin (5mg/kg body weight), a second one (*n*=6) with Vorinostat (SAHA 50mg/kg body weight), a third one (n=7) with both cisplatin (5mg/kg body weight) + Vorinostat (50mg/kg body weight). The 4th group (n=6) served as controls (DMSO-PBS-cremofor). For each group, the volume of the tumors was measured every 3-4 days by means of a manual caliper. The mice were treated and followed-up for 23 days for their weight **(Figure 2A)** and the tumor volume **(Figure 2B, C)**. **Figure 2B** shows the tumor growth kinetic in all conditions. The combined treatment significantly decreased the growth speed

compared to control or the individual treatment. At final day (= day 23), an ultrasound evaluation of the tumor size and substructure was performed and the tumor was dissected for final examination and histological/ immunohistochemistry analysis. SAHA alone, as well as combined with cisplatin, was well tolerated by the animals, with no significant difference in terms of final weight of the mouse ($p>0.05$, **Figure 2A).** At day 23, the final tumor volumes were the lowest with the combinatory SAHA + cisplatin treatment with an average 490% decrease compared to controls (n=12, p= 0.0002) **(Figure 2C).** The decrease of volume observed with the combinatory treatments was higher than the one observed with cisplatin (125% decrease, n=12, p<0.01 compared to controls) and with SAHA alone (n=6, p<0.05). Tumors also presented treatment-related changes on histology and immunohistochemistry **(Figure 2D, E).** First, we verified that the tumor was presenting a p53 response towards cisplatin. As expected, immunohistochemistry showed that cisplatin treatment resulted in a strong increase of p53 expression compared to the controls, a typical response of a tumor with wild type p53 **(Figure 2D)**. In addition, cisplatin-treated tumors showed a stromal predominance compared to the primary tumor and controls, with a stroma/gland ratio >50%, thus resulting in a lower tumor burden (cancer cells/mm^2) **(Figure 2E).** Additionally, in cisplatin-treated tumors, scattered mono-stratified cysts were frequent in the periphery of the tumor and more common than in controls. Similarly, all SAHA-treated tumors appeared more cystic than cisplatin-treated ones or controls, with a peripheral rim of peripheral mono-stratified cysts (2-3mm, **Figure 2E, SAHA, right panel**) and a solid glandular central portion **(Figure 2E, SAHA left panel)**. The cystic morphology was the majority in the combinatory treatment **(Figure 2E, C+S)**. IHC showed strong decrease of Ki-67 expression in around 50% of cells in cisplatin-treated tumors compared to controls, while p53 expression seemed to be increased (data not shown). Additionally, as expected, SAHA treatment led to an increase of H3K9 acetylation (data not shown).

Combinatory treatments PDC + SAHA reduce AGS cell proliferation and promote apoptosis

To understand the molecular basis of the synergistic activity of SAHA combined with PDC in GC cells, we analyzed the activation of markers for cellular death and cellular survival pathways. Thus, we looked at the level of cleaved Caspase 3, which reflects apoptosis **(Figure 3A)**. AGS cells were chosen as they present relatively the same characteristic as GCX4, being a gastric adenocarcinoma of intestinal subtype with a wild-type p53. The cells were treated for 24h with SAHA, cisplatin and oxaliplatin used individually or combined at a synergistic concentration (combinatory index = 0.5 corresponding to cisplatin = 15µM; oxaliplatin = 0.5µM and SAHA = 2.75µM). Individual doses of oxaliplatin or cisplatin did not have a significant effect on the cleavage of Caspase 3 (Cleaved Casp 3) and SAHA alone only induced a very small increase of Caspase 3 cleavage after 24h of treatment. On the contrary, the combination of SAHA with either cisplatin or oxaliplatin strongly induced the cleavage of Caspase 3, suggesting that combinatory treatments favored a pro-apoptotic program in AGS cells. In parallel, we analyzed the expression of the pro-apoptotic genes, *NOXA, PUMA* and *BAX* involved *(Shibue T et al. 2003; Yee KS et al. 2009; Liu YL et al. 2014).* The combinatory treatment induced more strongly the expression of the pro-apoptotic gene *NOXA* than each treatment alone **(Figure 3B)**. Surprisingly, SAHA alone or combined with PDC reduced other pro-apoptotic gene *PUMA* and *BAX* expression at 8h of treatment **(Supplementary figure 3).** However, SAHA alone or combined with PDC reduced pAkt level suggesting a decrease of pro-survival signaling pathway in AGS cells **(Figure 3A).** This correlated with the study of *Zhou et al.* indicating that AKT was downregulated when using combinatory treatment of oxaliplatin and SAHA in gastric cancer cells *(Zhou C et al. 2014).*

In parallel, we analyzed the expression of genes related to the cell cycle after 8h or 24h of treatment. The mRNA levels of the cell cycle inhibitor p21 were significantly induced at 8h and 24h by the treatments when applied separately or in combination **(Figure 3C)**. Inversely, the mRNA levels of the cell cycle activator Cyclin B2 were significantly repressed upon the treatment. Importantly, the repression was more severe with the combinatory treatments, oxaliplatin + SAHA or cisplatin + SAHA **(Figure 3D)**. Otherwise, CDC2, which is associated with CYCLIN B during the cell cycle *(Guadagno TM and Newport JW. 1996) (Ogasawara T. 2013)*, had its lowest expression level observed at 24h of combinatory treatment cisplatin and SAHA (~ 50% decreased) **(Supplementary figure 3).** To illustrate the impact of combinatory treatments on cell proliferation we performed an immunocyto-staining of the proliferation marker Ki67. Combined treatments PDC + SAHA also reduced the proliferation marker Ki67 in AGS cells and the number of cells **(Supplementary figure 4).** These results indicated that PDC + SAHA reduce AGS cell proliferation and induce apoptosis reducing AGS cell survival.

We were also interested in the potential role of autophagy, another key mechanism in cancer that can play a pro-survival or a pro-death role in gastric cancer *(Qian HR and Yang Y. 2016)*. We investigated the impact of the treatment on ATG8 (LC3B) **(Figure 4A)**, which is involved in the biosynthesis of autophagosomes, and p62, which is in a ubiquitin binding complex that serves as a selective autophagy substrate **(Figure 4B)** *(Qian HR and Yang Y. 2016).* We also looked NRF2 expression which is involved in radical oxidizing species response, endoplasmic reticulum stress response and crosstalk to promote autophagy *(Digaleh H et al. 2013).* Combined treatments PDC + SAHA increased the protein level of LC3B active form (lower band) at 8h **(Figure 4A; Supplementary figure 5).** However, we remarked that SAHA alone or combined with PDC reduces significantly *p62* and *NRF2* expression **(Figure 4B, C).** On the contrary, cisplatin alone increased *NRF2* expression but SAHA had dominant effect on PDC. These results suggested that that the combined treatment did not induced a complete autophagy response.

The combinatory SAHA-PDC treatment reduces p53 protein level and impact on TAp63 and TAp73

The tumor-suppressor gene *TP53* often mutated in gastric cancer, is a key regulator of cellular death and Caspase 3 activation *(Grabsch HI and Tan P. 2013; Mahu C et al. 2014)* and is known to be induced in response to cisplatin *(Oren M et al. 2010; Osman AA et al. 2015; Rivlin N et al. 2011).* We previously showed that p53 is induce in AGS cells by cisplatin *(Speaty et al. 2019)*. Hence, we analyzed *p53* expression in AGS cells to verify if the increased apoptosis caused by the combinatory treatment was mediated by p53. AGS cells were treated with the synergic concentrations of the different drugs for 24h. As expected, cisplatin and oxaliplatin induced p53 at protein level **(Figure 5A).** SAHA used alone slightly reduced the protein level of p53, but surprisingly, the combination of SAHA with cisplatin or oxaliplatin strongly inhibited the platinum-induced induction of p53 at protein level. TP53 expression is mainly regulated at post-translational level through ubiquitination and proteasome degradation. Therefore, we used the proteasome inhibitor MG132, to understand if this repression was due to a destabilization of p53 proteins. Unexpectedly, MG132 did not restore p53 protein levels in the presence of SAHA (alone or combined) **(Figure 5A)**. Hence, we analyzed p53 mRNA levels using RT-qPCR. AGS cells were treated for 8h and 24h under the same experimental conditions **(Figure 5B).** mRNA levels for *TP53* were not affected by cisplatin and oxaliplatin. On the contrary, SAHA reduced *TP53* mRNA level at 8h and strongly decreased *TP53* mRNA level after 24h of treatment, a repression

which was also observed with the combined treatment. These results indicated that the loss of p53 proteins with the combinatory treatments, involved a transcriptional regulation of the *TP53* gene.

We hypothesized that the reduction of p53 mRNA level was due to miRNAs targeting p53 expression. According to miRTarBase *(http://mirtarbase.mbc.nctu.edu.tw/php/index.php)* and the literature *(Ishiguro H et al. 2014; Rokavec M et al. 2014; Liu J et al. 2017)* we analyzed the expression of potential miRNAs targeting p53 (miR-25, miR-30d, miR-125a, and miR-222) and a miRNA targeted by p53 (miR-22), as a positive control *(Tsuchiya N et al. 2011; Lin J et al. 2014).* Cells were treated for 4h **(Supplementary figure 6)** and 8h **(Supplementary figure 6)** . We chose 4h as an additional time point expecting to see the induction of miRNA that would be able to explain the loss of p53 mRNA level that we observed at 8h of treatment **(Figure 4b).** To quantify miRNA expressions by the method $2^{(-\Delta\Delta Ct)}$ we tested the expression of reference miRNA (RNU6, SNORD65, and SNORD95) **(Supplementary figure 6).** Unfortunately, none of the reference miRNAs could be used because each treatment strongly reduced their expressions. We arbitrarily decided to use an identic Ct to calculate the relative expression **(Supplementary figure 6, 7).** We did not find a miRNA targeting p53 and selectively induced by SAHA alone, which would explain the reduction of *TP53* level at 8h **(Figure 4b).** miR-22 a target of p53 was induced at 4h of treatment of oxaliplatin but was reduced with other treatments or combinations **(Supplementary figure 6).** At 8h, miR-22 seemed to be induce by all treatments but a variation was still present **(Supplementary figure 7).** Hence, so far, we did not identify a miRNA candidate that may explain the loss of p53 mRNA upon SAHA treatment in GC cells.

This surprising decrease of p53 protein level upon the combinatory treatment raised the question whether p53 was involved or whether its homologues may take over. TP53 is the founding member of the p53 family that also contains p63 and p73, which are also known to induce apoptosis *(Arrosmith CH, 1999; Pietsch EC et al. 2008).* We have previously shown that these transcription factors are induced and can mediate the response to anticancer drug *(Benosman S et al. 2011; Von Grabowiecki Y et al. 2016).* These three genes encode two classes of isoforms either containing a transactivation domain in the N terminus (p53, TAp63, TAp73) or not (Δp53, ΔNp63, ΔNp73). These proteins are thought to be involved in many aspects of the digestive system cancers *(Zaika AI and El-Rifai W. 2006)* and TAp63 and TAp73 isoforms are commonly seen as pro-apoptotic transcription factors *(Wei J et al. 2012).* Thus, we decided to assess whether the combinatory treatment SAHA/platinum drugs would impact on the expression of these isoforms in AGS cells. At 8h of treatment, cisplatin and oxaliplatin alone did not induce TAp63 and TAp73 mRNA levels in AGS cells **(Figure 5C, D).** On the contrary (compared to its effect on p53) SAHA increased *TAp73* mRNA level when combined with oxaliplatin after 8h of treatment, while the combination with cisplatin did not significantly impact on p73 mRNA expression level. SAHA alone and combined with oxaliplatin and cisplatin induced TAp63 mRNA level after 8h of treatment, while the single use of cisplatin did not significantly impact on p63 mRNA expression level. At 24h of treatment the same effects were observed for *TAp63*, whereas for *TAp73* we observed an increase with platinum compounds alone, but none with SAHA and a decrease with cisplatin + SAHA combination **(Figure 5C, D).** As expected, TAp73 target genes *AQP3* and *p57* had their expression increased when *p73* expression were higher. Interestingly, the combination cisplatin with SAHA significantly up-regulated *AQP3* and *p57* while it was not the case for p73. SAHA alone induced AQP3 expression at 24h **(Supplementary figure 12).** Altogether, these results indicated that cisplatin, oxaliplatin, SAHA and the combined treatments of SAHA and platinum compounds had different impacts on the expression of the various members of

the p53 family which may promote apoptosis. It also indicates that the combinatory treatment did not induced strongly the mRNA level or neither TAp63 nor TAp73, which did not support a key role of these transcription factors in the synergistic induction of apoptosis observed.

TP53 status drives the apoptotic pathway in combined treatments in gastric cancer cells

Hence, for a clarification of the role of p53 in the activation of caspase 3 induced by combinatory treatment using SAHA and platinum drugs in gastric cancer, we used siRNA directed against TP53 (sip53) and assessed the protein level for p53 and the cleavage of Caspase 3 **(Figure 6A)**. Surprisingly, the extinction of p53 expression strongly reduced the level of cleaved Caspase 3 suggesting that even if combinations PDC + SAHA reduced p53 expression, p53 was necessary to induce AGS cell apoptosis. To understand this contradictory result opposing the downregulation of p53 protein and its necessity for co-treatment induced apoptosis, we investigated the acetylation of p53 at lysin 120, which constitute an activating post-translational modification for p53. AGS cells were treated for 8h and 24h with two concentrations of PDC and SAHA. As observed previously, inhibition of HDAC by treatment with SAHA diminished the protein level of p53. However, SAHA increased drastically the acetylation of p53 at K120, when used alone or in combination with PDC **(Figure 6B)**. Interestingly, the acetylation of p53 at K120 induced by SAHA is not sufficient to cause Caspase 3 cleavage, indicating that additional mechanism induced by PDC are required to fully induced caspase 3 cleavage. In addition, the co-treatment did induce Caspase 3 cleavage, but without a significantly increase in K120 acetylation. Hence, these results suggest that the acetylation in K120 is permissive for p53 to induce apoptosis but not sufficient.

As p53 is often mutated in gastric cancer, we wanted to study the effects of the combined treatment on KATOIII cells with a p53 deletion and on p53 mutated NUGC3 cells (Y220C$^{+/+}$) *(Liu X et al. 2013)*. We first performed an isobologram assay on both cell lines to determine the synergic concentration for platinum derivative compounds and SAHA **(Supplementary figure 1)**. We found a strong synergy of the combination of SAHA with cisplatin on cell survival in KATOIII cells and more heterogeneous effects when combined with oxaliplatin. We were interested in the mechanisms involved in the reduction of KATOIII cell survival. Again, we focused study on synergistic combined treatments PDC + SAHA (combinatory index = 0.5). KATOIII cells were treated 24h or 48h with cisplatin = 10µM; oxaliplatin = 10µM and SAHA = 3µM. As hypothesized, we didn't observe a cleavage of caspase 3 neither at 24h nor at 48h of treatment in p53-deleted KATOIII cells **(Figure 6C)** validating our hypothesis that p53 is necessary for the co-treatment to induce apoptosis. Then, to understand how the co-treatment can caused a synergistic cytotoxicity we looked on proliferation marker Ki67 **(Supplementary figure 8)** and LC3B autophagic marker **(Supplementary figure 9)**. Observations of Ki67 at 24h of treatment didn't clearly indicate a decrease of cell number (DAPI intensity) or Ki67. Ki67 intensity seemed to increase with oxaliplatin or SAHA alone **(Supplementary figure 9)**. Otherwise, SAHA neither combined to oxaliplatin nor to cisplatin induced the autophagic active form of LC3B (bottom band) **(Supplementary figure 10)**. These results indicate that in KATOIII cells (p53 deleted), the combinatory treatments did not induce a caspase-dependent apoptosis but reduce cell survival by an undetermined pathway.

Afterwards, we compared the effects of combinatory treatments between AGS p53 WT cells and NUGC3 p53-mutated cells **(Figure 6D)**. Again, we focused our study on synergistic combined treatments PDC + SAHA (combinatory index = 0.5). NUGC3 cells were treated 24h with cisplatin = 2.5µM; oxaliplatin = 14µM and SAHA = 3.5µM. In this case, SAHA alone induced a cleavage of Caspase 3, which was significantly stronger when combined to platinum compounds, as we have observed on AGS cells. As seen in AGS cells, SAHA diminished p53 protein level. Interestingly, the silencing of p53 by the siRNA only slightly reduced the cleavage of Caspase 3 **(Figure 6D)**. This result indicated that the presence of the Y220C p53 mutant in NUGC3 cells is mostly not necessary for the induction of apoptosis by the combinatory treatment, suggesting that the cells use an alternative pathway to respond. However, we wondered whether the ability of the NUGC3 to respond to the combinatory treatment can be improved by restoring the function of the p53 mutant. To do so, we used PRIMA-1 compound to reactivate p53 mutant *(Lambert JMR et al. 2009)*. We performed the same experiment with combined drug concentrations for 24h with or without a pre-treatment with PRIMA-1 during 8h **(Figure 6E).** We used a PRIMA-1 concentration of 44µM corresponding to IC_{50} determined by MTT survival test (data not shown). As expected, the p53 restauration mediated by PRIMA-1 compound increased the level of cleaved caspase 3 suggesting a reactivation of p53-mediated apoptosis in NUGC3 cells. Moreover, we also performed an immunostaining on Ki67 showing SAHA reduced cell number (less DAPI signal) and cell proliferation (less Ki67 signal) alone or combined with PDC illustrating the synergistic activity of combined treatments on NUGC3 cells **(Supplementary figure 10).** Altogether, these results indicated that combined treatments reduce gastric cancer cell survival by p53 dependent and independent manners. TP53 status drives the apoptotic pathway in response to combined treatments in gastric cancer cells.

Discussion

Alterations affecting HDAC expression and histones acetylation have been described in various types of cancers, including gastric cancers. These deregulations are thought to be related to cancer progression as well as resistance against cytotoxic anticancer drugs, thus resulting in a poorer outcome. The chemical pan-inhibitors of HDAC have been developed and two HDACI drugs recently received FDA-approval for routine-usage: SAHA (Vorinostat, 2006) in cutaneous T cell lymphoma and hydroxamic acid variants (f.e. Farydak, Panobinostat 2015) in multiple myeloma. Unfortunately, the two major clinical studies evaluating SAHA on gastric cancer patients treated with oxaliplatin, showed no significant beneficial outcome *(Yoo C. et al. 2015, Yoo C. et al 2016*). To try to understand the reasons why the combinatory treatment between SAHA and oxaliplatin did not produce satisfactory results in patients with gastric cancer, we decided to investigate the molecular mechanisms induced. Our hypothesis is that a better stratification of the patients using molecular biomarkers might allow to identify a subpopulation of patient that might have a better response or a clue allowing to optimize the treatment. Therefore, we studied the combinatory treatment in gastric cancer cells using the standardly-used in clinical routine platinum-based drugs in combination with SAHA. We have identified some of the molecular mechanisms involved in the synergistic effect of combinatory treatment on AGS cells, which highlights the necessity for a better characterization of the molecular specificities of the tumors treated with these combinations.

The synergistic effect of SAHA on cell survival is observed in association with cisplatin or oxaliplatin in different cell lines, as well as *in vivo* on a patient-derived xenograft tumor. *In vivo*, the cotreatment

induces an almost complete stop of the tumor growth associated with severe alterations in the tumor structure. These encouraging results questioned the results of the Phase I and II studies indicating a poor advantage in patient survival *(Yoo C. et al. 2015, Yoo C. et al 2016)*. The discrepancy with our preclinical results may be explained possibly by a lack of patient stratification in the clinical studies since our result suggest that the cellular and molecular response toward the combinatory treatment depends for a significant part on the p53 status and apoptosis.

Indeed, we observed that this combination triggered a marked cleavage of Caspase 3, a reduced marker of cell cycle progression, but no complete indication of autophagy. Interestingly, no significant activation of Caspase 3 was observed in AGS cells treated with cisplatin or oxaliplatin in monotherapies at these concentrations and only a weak activation was observed with SAHA alone. This demonstrated that the SAHA/platinum combination induced a reprogramming, leading to cellular death by apoptosis. It is likely that higher doses of cisplatin, oxaliplatin and SAHA, or longer time of treatment will also induce Caspase 3 activation and cellular death, as previously described, but we show here that the combination of SAHA with either cisplatin or oxaliplatin provides a significant efficacy a lower dose, which might reduce the risk of side effects *(Florea AM et al. 2011; Manal M et al. 2016)*.

The absence of a complete set of autophagic markers indicates that the combinatory therapy does not seem to induce autophagy. Therefore, autophagy cannot account for the apoptosis induced by the co-treatment, as previously described in other conditions *(Xie B et al. 2013; Wang Y et al. 2017)*. It cannot account either for the lack of apoptosis upon cisplatin treatment, as previously described *(Zhang HQ et al. 2013)*. In AGS cells, SAHA was not able to induce an autophagy. This is the contrary of a previous study by Vrana *et al.* showing that cisplatin-induced apoptosis is stimulated in renal tubular epithelial cells in presence of autophagy inhibitors *(Vrana JA et al. 1999)*.

Surprisingly, the apoptosis stimulation by combinatory SAHA/platinum treatments was correlated with the absence of an increase of p53 at protein levels, and rather a diminution of p53 protein level upon SAHA treatment. This was highly unexpected as the pro-apoptotic properties of cytotoxic anticancer drugs often are associated with increased p53 expression *(Florea AM et al. 2011)*. Hence, in our study, we observed an uncoupling between the p53 expression level and the stimulation of apoptosis. Previous studies have shown contradictory results regarding the role of p53 in the cellular response to the combination of SAHA and platinum drugs. For instance, *Dong G et al.* showed that SAHA had a cytoprotective effect on renal tubular cells treated with cisplatin, through the suppression of p53 activation *(Dong G et al. 2010)*. On the contrary, *Hacker S et al.* suggested that the synergistic activity of SAHA with anticancer drugs in medulloblastoma cells was mediated by p53 *(Hacker S et al. 2011)*. In addition, we show that SAHA induces the expression of TAp63 in gastric cancer cells, suggesting that this p53 family member is somehow involved in the anticancer mechanism of SAHA in gastric cancer, which has only been described in head and neck cancer in the literature *(Finzer P et al. 2004)*. Similarly, Shim *et al.* enhanced SAHA anticancer effects by adding p63/p73 in head and neck squamous cell carcinoma *(Shim SH et al. 2010)*. However, in the absence of a specific TAp63 antibody, the nature proteinic expression remains to be established and functional experiment are required before a conclusion could be drawn on the role of TAp63 in apoptosis in gastric cancer cells.

Despites the diminished expression of p53 upon SAHA co-treatment, p53 appears to be essential for the SAHA-PDC combinatory treatments to induce apoptosis in the AGS gastric cancer cells.

The key role of p53 is demonstrated by the abolition of apoptosis when p53 is silenced, but also by the lack of apoptosis in the gastric cancer cells where p53 is deleted, the KATOIII cells. However, the situation is not that simple as in the NUGC3 cells, which have a Y220C p53 mutant, SAHA and PDC can synergize to induce apoptosis. Interestingly, the silencing of the mutant slightly reduces the apoptosis observed, and the reactivation of the mutant with PRIMA-1 enhances it. Multiple interpretations can be provided, starting with the fact that the overall genetic alterations affecting NUGC3 cells led to a relative independence towards p53 in this particular situation. But this is also a perfect illustration of the complex role played by a mutant p53 in cancer cells. For instance, the fact that the silencing of mutant p53 slightly diminished the apoptosis suggests that part of the p53 is playing a role, likely because the mutant retains some wild type activity. It also indicates that the mutant does not interfere negatively with the apoptotic process in this particular case, as its removal do not improve the apoptosis. Hence, in NUGC3 cells the Y220C p53 mutant do not display any gain of function properties towards these treatments, in contrast to what has been described for other mutants in other cell types *(Gaiddon et al. 2001)*. However, the fact that PRIMA-1 improved the apoptosis, indicates also that if more wild-type p53 like protein are present, the efficacy of the treatment is improved.

These complex results illustrate well the contradictory documented results of the influence of HDACi (such as SAHA) in monotherapy or combined with platinum derivate compounds on p53. Early studies showed that cellular growth arrest and induction of p21 mediated by SAHA were independent from p53 *(Huang L et al. 2000; Vrana JA et al. 1999)* and another study by *Sonneman et al.* demonstrates that SAHA did not require p53 for its anticancer effects *(Sonnemann J et al. 2014). Li et al.* also showed that SAHA appeared more active on cancer cells with a p53 mutation *(Li D et al. 2011).* However, these observations are balanced by other studies based on different cells lines, indicating the important role of p53 for the biological activity of SAHA *(Henderson C et al. 2003).* Similarly, to the use of SAHA in monotherapy, the implication of p53 in combinatory treatments, which associate SAHA with DNA-damaging anticancer drugs, is also unclear. As stated above, SAHA appeared protective against Cisplatin in renal tubular cells through a suppression of p53 activation *(Dong G et al. 2010)* and SAHA acted synergistically with doxorubicin in colon cancer cells independently of p53 *(Alzoubi S et al. 2016).* Inversely, SAHA combined with anticancer drugs in medulloblastoma cells *(Hacker S et al. 2011)* and combined with doxorubicin on cervical cancer cells *(Lee SJ et al. 2014)* appeared to act synergistically on p53. Therefore, it seems that the contribution of p53 in the synergistic activity of SAHA with DNA damaging drugs, such as cisplatin and oxaliplatin, might be dependent on the cellular context, including the cancer type and especially the molecular markers, as well as the exact mode of action of the individual drugs. In the case of the gastric cancer, p53 seems to play a key role.

At the molecular level, we observed that the diminution of p53 protein level coincides with an increase in p53 acetylation at K120. We tried to identify the molecular mechanisms responsible for the loss of p53 mRNA, so far without success. Importantly, despite that the p53 protein level drops, the overall activity of p53 seems to be maintained or even induced due to this acetylation. However, the acetylation by itself is not enough to drive apoptosis, as SAHA by itself does not induces it. Hence, additional post-translational modifications of p53 seem to be required and induced by the PDC. It is also to note that only selected p53 pro-apoptotic target genes are induced, such as *NOXA* and *BIK*, while others are repressed, such as *BAX and PUMA*. Again, this highlights the complexity of the regulation of p53 activity and that the combinatory treatment likely induces a specific combination of p53 post-translational modifications, which might affect the selectivity of p53 for certain target genes.

All in all, this study illustrates the importance of the development of combinatory therapies associating standard cisplatin/oxaliplatin drugs with HDACIs such as SAHA, for the perioperative treatment of gastric cancers. It also pinpoints the necessity a better characterization of the molecular specificities of the treated tumor for an optimized choice and use of drug combinations based on selected markers, such the expression of a functional p53 protein. Another important point which should be considered is the differences observed between the first (cisplatin) and the second (oxaliplatin) generations of platinum drugs, as the newly developed HDAC inhibitors might act differently depending on the associated drug. These results could open new treatment possibilities especially in resistant cancers, with a reduction of side effects.
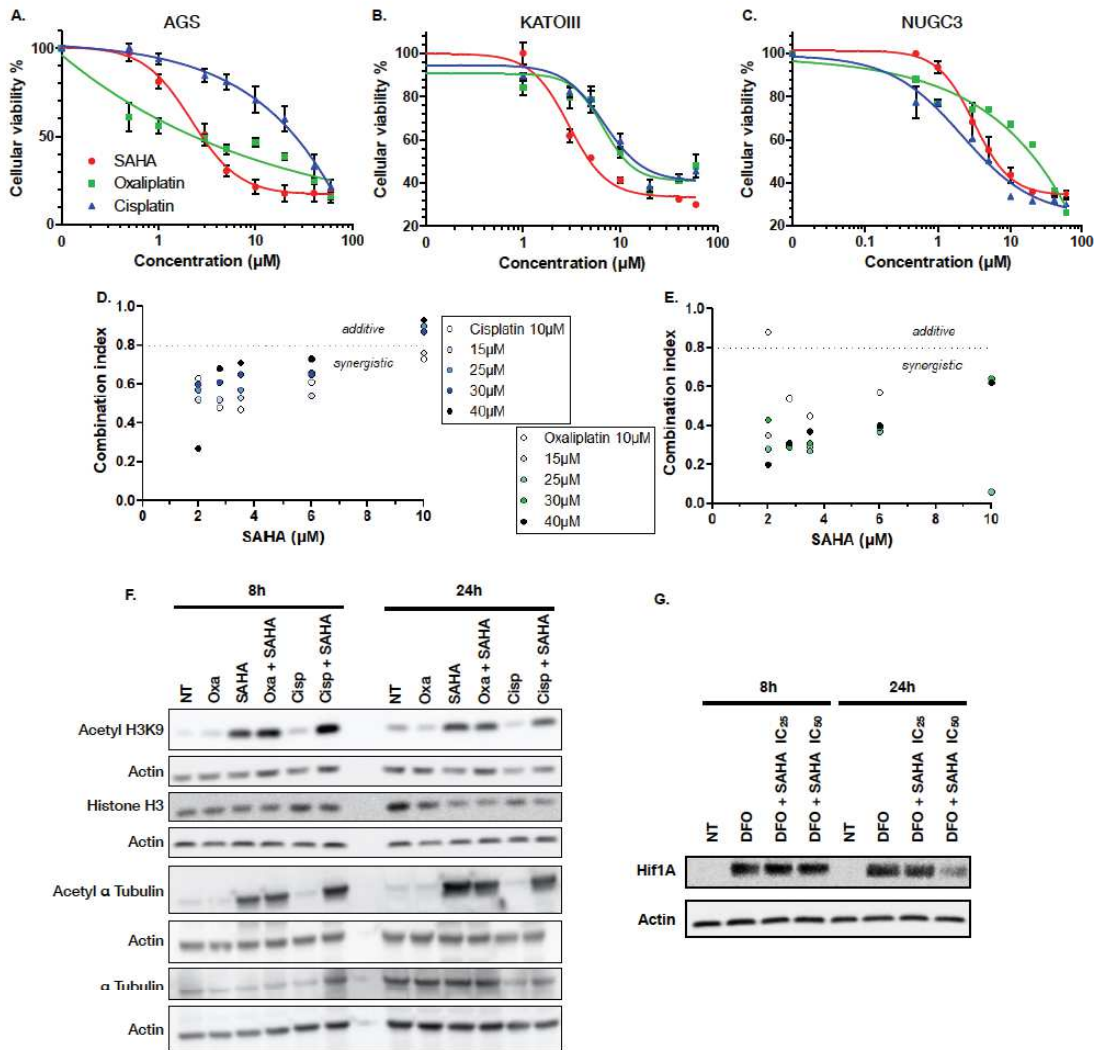
Figure 1

Figure 1. SAHA and platinium compounds impact gastric cancer cell survival.

A. B. C. Gastric cancer cells, AGS (**A**), KATO III (**B**), and NUGC3 (**C**) cells were seeded in 96-wells and treated 48h with cisplatin, oxaliplatin or SAHA (Vorinostat). Viability of the cells was evaluated using MTT tests. Curves represent the log (inhibitor) vs. response – Variable slope (four parameters). Data are represented in % compared to the non-treated condition (n=3). **D. E.** AGS cells were treated with cisplatin (**D**.) or oxaliplatin (**E**.) and SAHA (Vorinostat) for 48h followed by an isobologram assay to determine mathematically the combination index. We arbitrarily and conservatively considered than antagonist effect between the drugs corresponded to the value > 1.20, additive effect between 0.80 and 1.20 and synergistic effect <0/80. **F.** AGS cells were treated or not (NT) with the synergistic concentrations of cisplatin (Cisp), oxaliplatin (Oxa) and SAHA for 8h and 24h. Western blot experiments were performed using antibodies against acetylated Lysine K9 on Histone H3, against Histone H3 protein and antibodies against acetylated-alpha Tubulin and alpha Tubulin. **G.** AGS cells were treated with Deferoxamin (DFO; 100 μM) to mimic hypoxia condition and stabilize HIF1A. Additive treatment with SAHA for 8h or 24h or without (NT). Western blot was performed with antibodies against HIF1A.

Figure 2
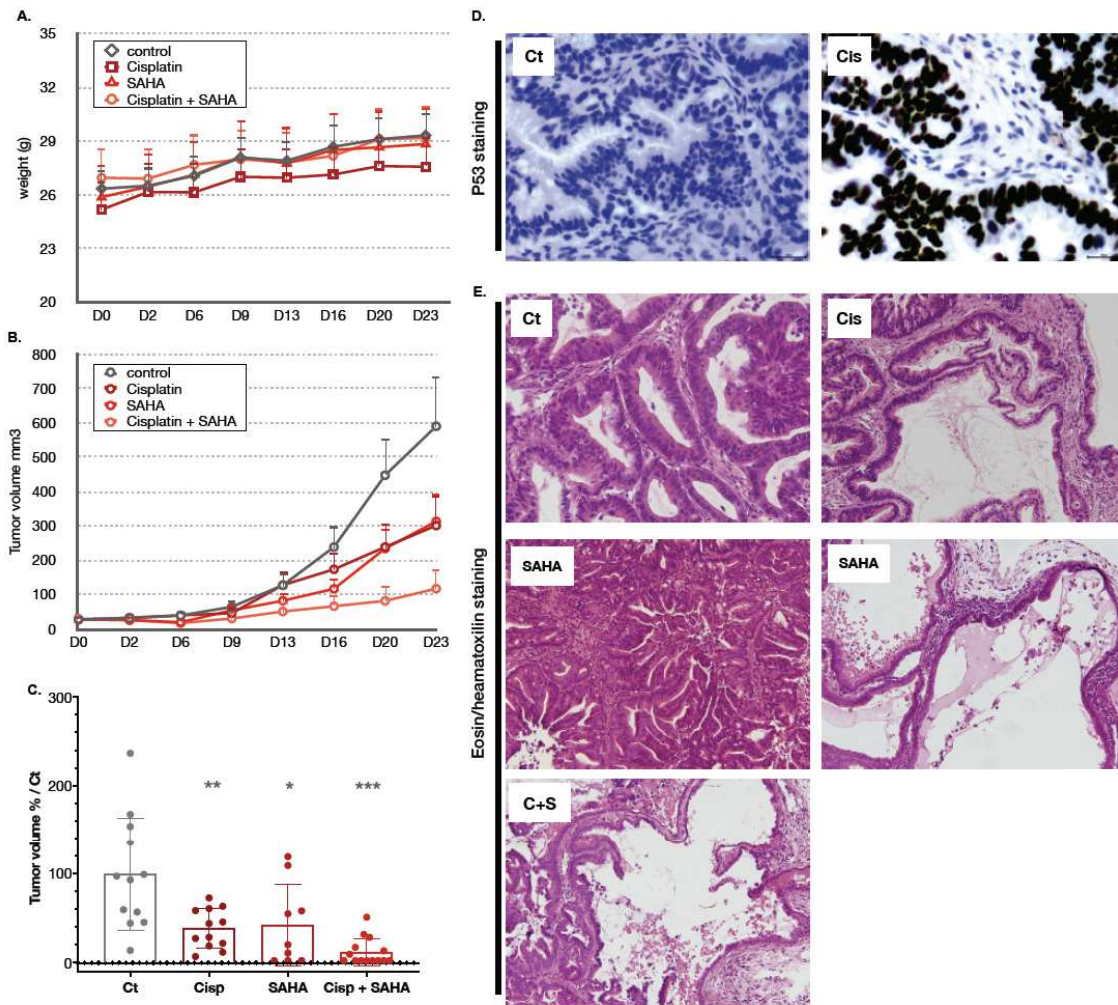
Figure 2. SAHA and combinatory treatment (SAHA + cisplatin) reduce tumor volume and induce treatment-related changes

A. Evolution (23 days follow-up) of the weight of the mice between treated (cisplatin, n=12; SAHA, n = 6; SAHA + cisplatin, n=12) and non-treated tumors (n=12). Graph indicates means with standard deviation. **B.** Evolution (23 days follow-up) of the volume of the tumors between treated (cisplatin, SAHA and SAHA+ cisplatin) and non-treated mice, as measured using caliper. **C.** Box plot representing the final tumor volumes between controls (Ct), cisplatin (Cisp), SAHA and combinatory treatment (Cisp + SAHA). *** p<0.001, ** p<0.01, * p<0.05 were calculated with Mann-Whitney test. **D.** Upper panel, representative photomicrographs of immunohistochemical slices labeled for p53 (magnification x40) in non-treated mice (Ct) and cisplatin (Cis) treated mice. **E**. Immunohistological hematoxilin-eosin (H&E) staining showing changes in tumors between control, cisplatin, SAHA, and SAHA + cisplatin treatments (magnification x20). For SAHA, two location are shown representative of the center of the tumor (left panel) and the periphery (right panel).

Figure 3
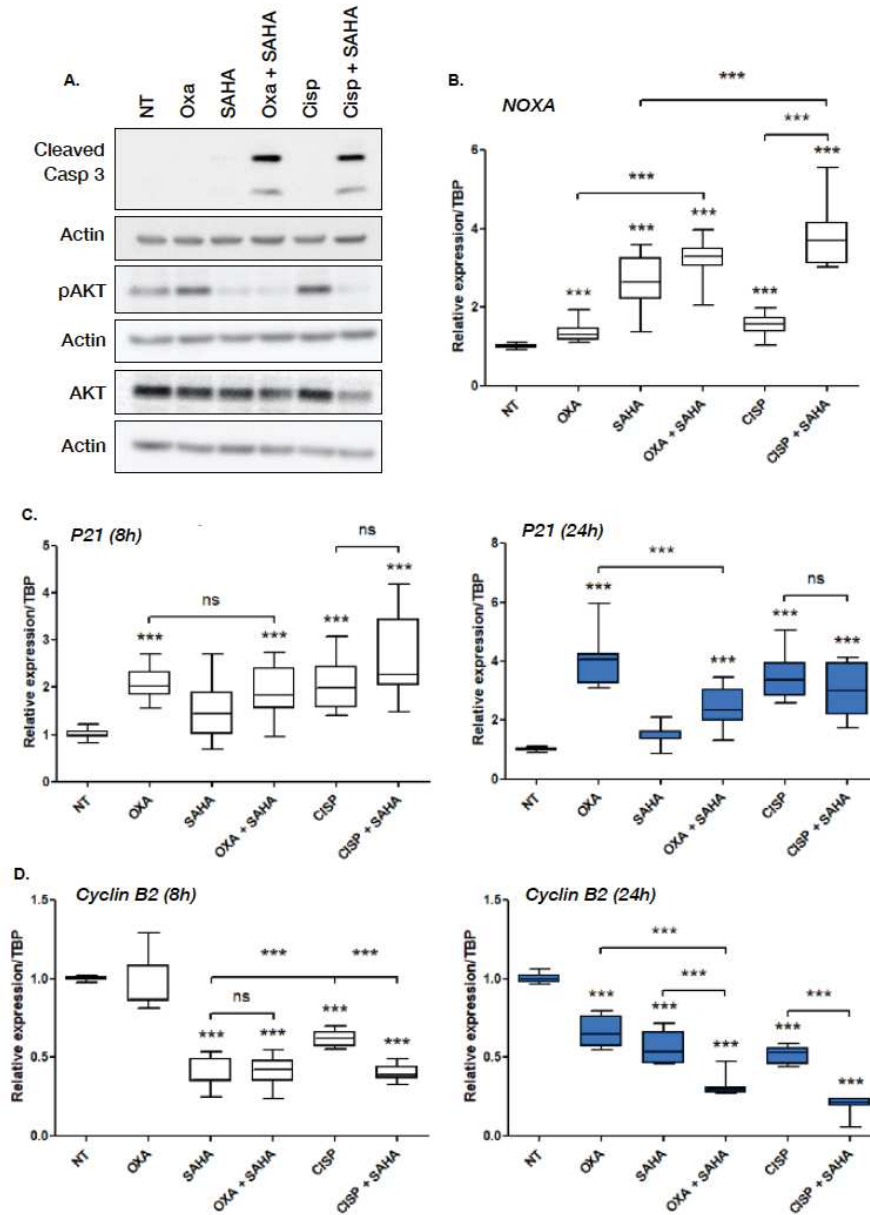
Figure 3. Combinatory treatments reduce AGS cell survival and proliferation and induce an apoptosis.

A. Western blot experiment was performed after 24h of treatment of AGS cells with the indicated drugs. Cellular extracts were probed using antibodies against the cleaved Caspase 3, Akt protein or the phosphorylated Akt protein at serine 473 (pAkt). Actin was used as loading control. **B.** RT-qPCR were assayed after 8h of treatment. Blot plots represent the fold induction of NOXA mRNA for each condition versus the control (NT). **(d-e)** RT-qPCR were assayed after 8h (white) or 24h (blue) of treatment. Box plots represent the fold induction of *p21* and *CYCLIN B2* mRNA normalized to the control (NT). *** p<0.001 are calculated by Mann-Whitney test (p-value limit = 0.001).

Figure 4
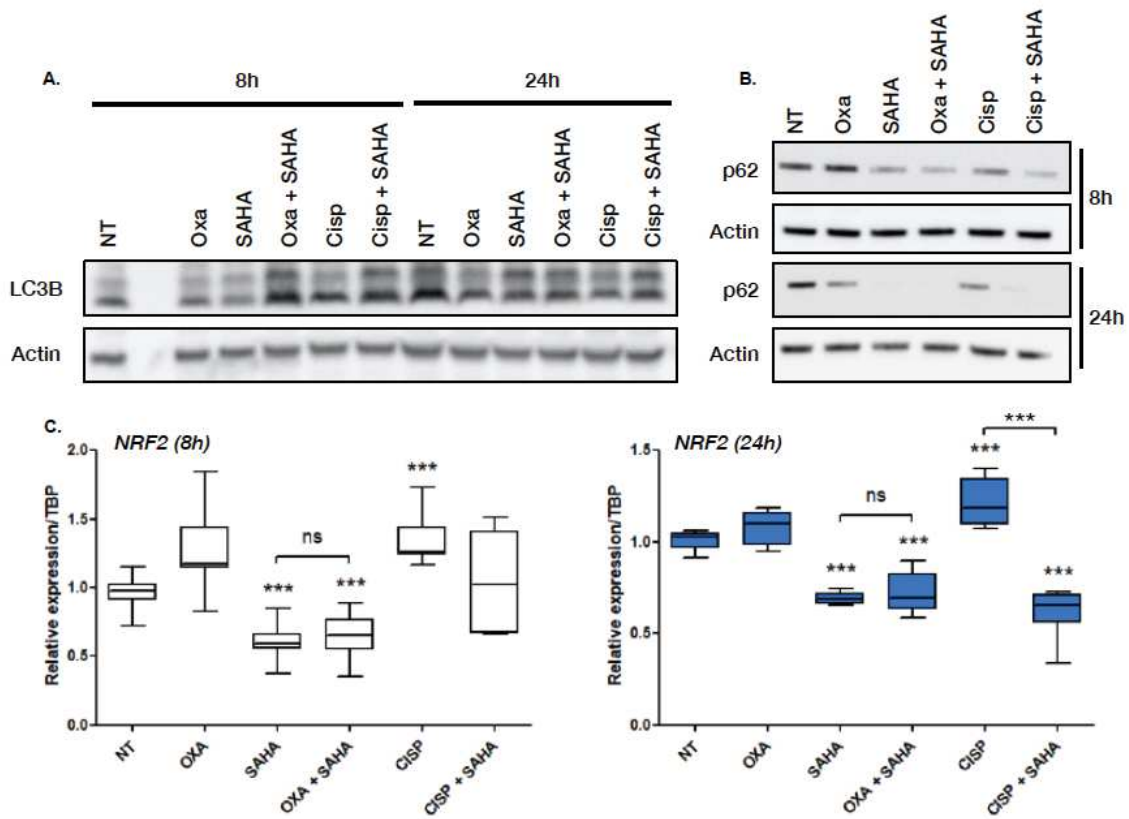
Figure 4: Combinatory treatments do not promote autophagy in AGS cells

A. AGS cells were treated or not (NT) with the synergistic concentrations of cisplatin (CISP), oxaliplatin (OXA) and SAHA (Vorinostat). Western blot experiment was performed after 8h or 24h of treatment using antibodies against the LC3B protein. The active form of LC3B (LC3B-II) is the bottom band and its quantification is represented in supplementary data. **B**. Western blot experiment was performed after 8h or 24h of treatment using antibodies against p62. **C.** RT-qPCR were assayed after 8h (white) or 24h (blue) of treatment. Box plots represent the fold induction of NRF2 mRNA normalized to the control (NT). *** p< 0.001 are calculated by Mann-Whitney test (p-value limit = 0,001).

Figure 5
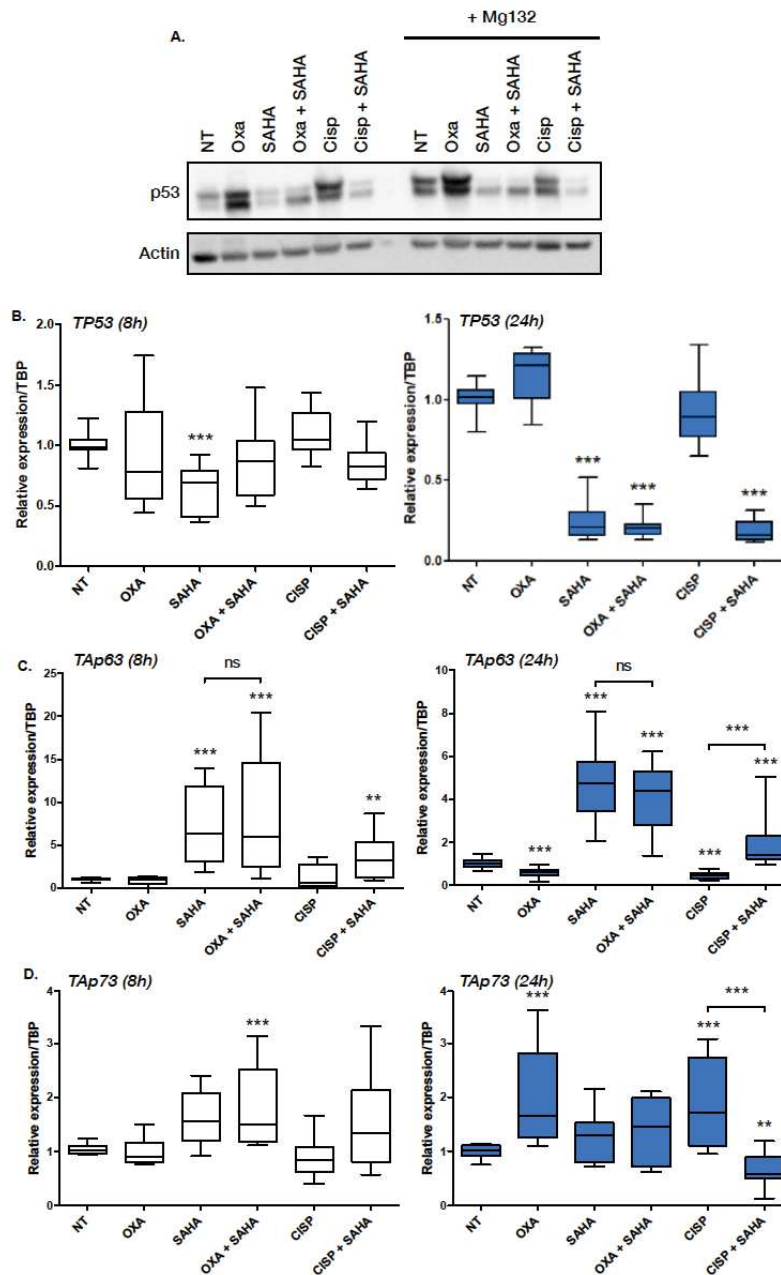
Figure 5. SAHA and the combinatory treatments modulate the expression of the members of the p53 family.

A. Cells were treated 24h with synergistic combinations and with or without 10µM of Mg132 a proteasome inhibitor during 6h. Western blot experiment was performed using antibodies against p53. **B. C. D.** RT-qPCR were assayed after 8h (white) or 24h (blue) of treatment. Box plots represent the fold induction of p53 (B), TAp63 (C), and TAp73 (D) mRNA for each condition versus the control (NT) (n=5). *** p< 0,001 are calculated by Mann-Whitney test (p-value limit = 0,001).
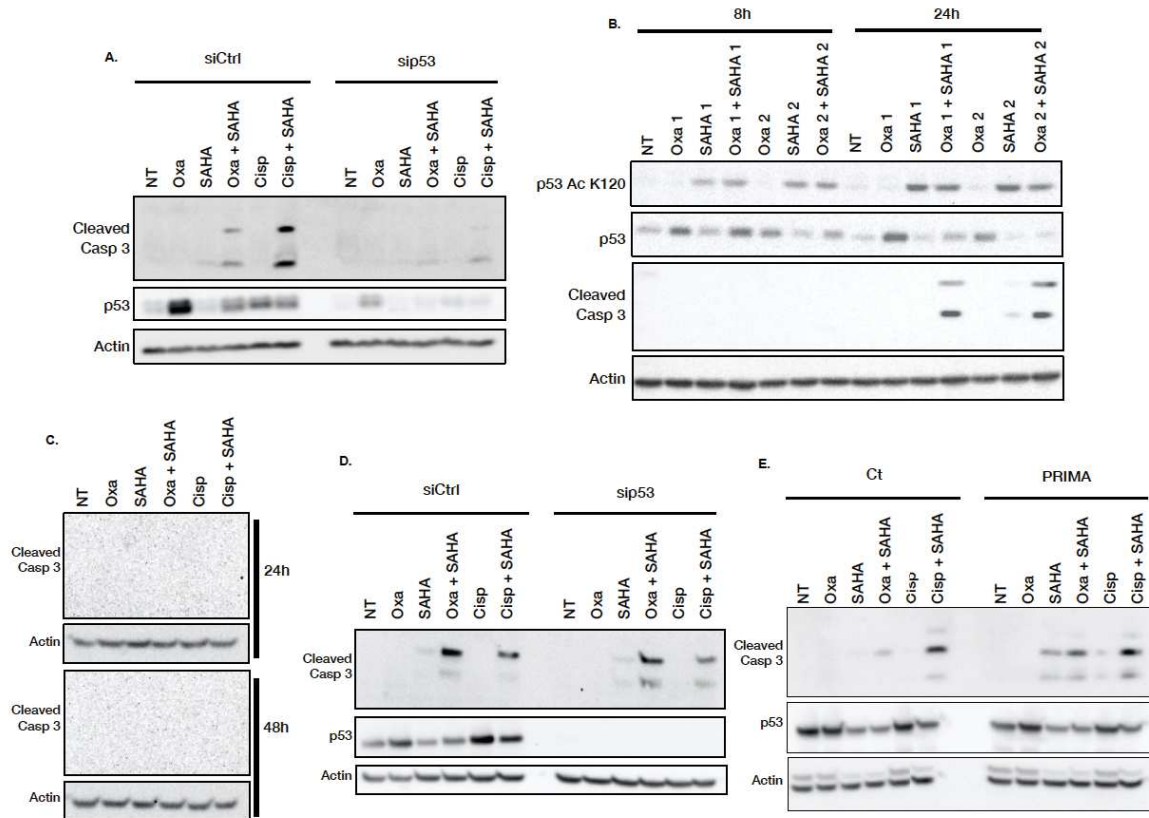
Figure 6. The induced apoptosis is p53 dependent in AGS cells

A. AGS cells were transfected with control siRNA (siCtrl) or siRNA directed against p53 (sip53) for 48h. Cells were then treated or not (NT) with the synergistic concentrations of cisplatin (CISP), oxaliplatin (OXA) and SAHA (Vorinostat) for 24h. Western blot experiment was performed using antibodies against p53 and Cleaved Caspase 3. **B**. AGS cells were treated or not (NT) with the synergistic concentrations of Cisplatin (CISP), Oxaliplatin (OXA) and SAHA (Vorinostat). Western blot experiment was performed after 8h or 24h of treatment using antibodies against the p53, the acetylated form of p53 at lysine 120 (p53 Ac K120), and cleaved caspase 3. **C.** KATOIII cells were treated 24h or 48h. Then, western blots were performed using antibodies against Cleaved Caspase 3. **D**. NUGC3 cells were transfected 48h with a siRNA directed to p53 (sip53) or with a scramble siRNA (siCtrl). Then, cells were treated 24h with the synergistic combined treatments and western blot experiments were performed using antibodies against Cleaved Caspase 3 and p53. **E**. NUGC3 cells were pretreated or not with PRIMA-1MET (44µM) during 8h. After, cells were treated with Cisplatin (CISP) or Oxaliplatin (OXA) and SAHA (Vorinostat) for 24h at the synergistic concentrations. Western blot experiments were performed using antibodies against Cleaved Caspase 3 and p53.

Name	Characteristics*	Drugs	IC$_{25}$ (µM)	IC$_{30}$ (µM)	IC$_{50}$ (µM)	IC$_{60}$ (µM)	IC$_{75}$ (µM)
AGS	Adenocarcinoma Diploid p53 WT MDM2 mutated/WT (bi-allelic) APC silent Kras mutated/WT (bi-allelic) CDH1 (G579fs9) homozygous CTNNB1 mutated/WT (bi-allelic) PIK3CA mutated/WT (bi-allelic)	SAHA	2	2,75	3,5	6	10
		Oxaliplatin	0,5	2,5	5	30	40
		Cisplatin	10	15	25	30	40
NUGC3	Adenocarcinoma Hypotriploid p53 mutated (Y220C)	SAHA	3	3,5	4	9,5	13
		Oxaliplatin	2,7	3,7	14	24	85
		Cisplatin	1	1,5	2,5	10	56
KATOIII	Pleural effusion Hypotetraploid p53 deleted K-sam amplification c-met amplification ERK amplification Cyclin E amplification APC deletion	SAHA	1	2	3	5	10
		Oxaliplatin	0,5	2	10	15	20
		Cisplatin	5	7,5	10	20	40

KATOIII cells isobologram

KATOIII cells isobologram

NUGC3 cells isobologram
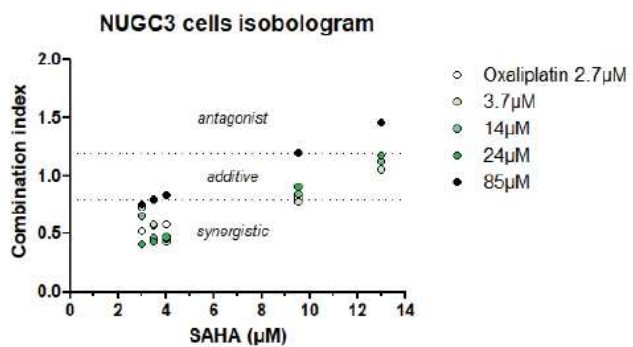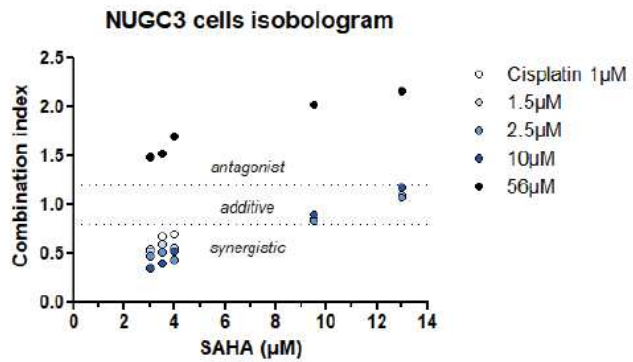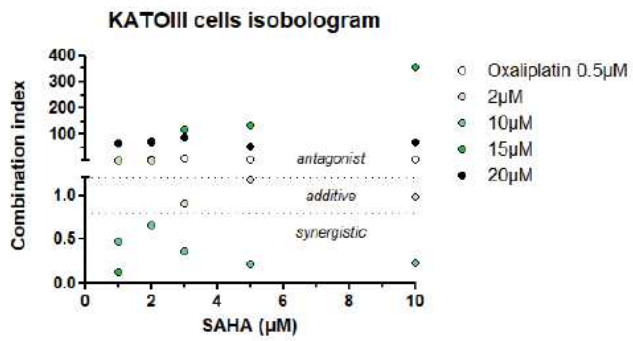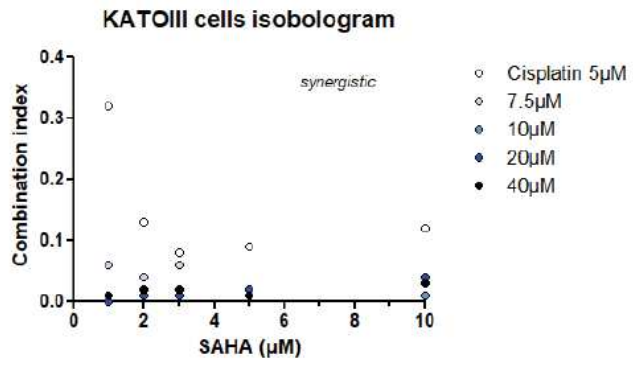
Supplementary figure 1: Combinatory treatments impact differently gastric cancer cells

Gastric cancer cells were treated at the indicated concentrations of Cisplatin (CISP) or Oxaliplatin (OXA) and SAHA (Vorinostat) for 48h followed by an isobologram assay to determine mathematically the combination index. We arbitrarily and conservatively considered antagonist effect between the drugs correspond to value > 1.20, additive effect between 0.80 and 1.20 and synergistic effect <0.80.

NUGC3 cells isobologram

VEGF

GLUT-1
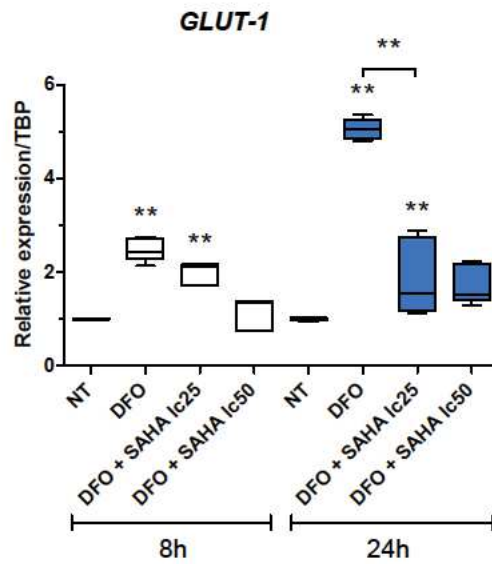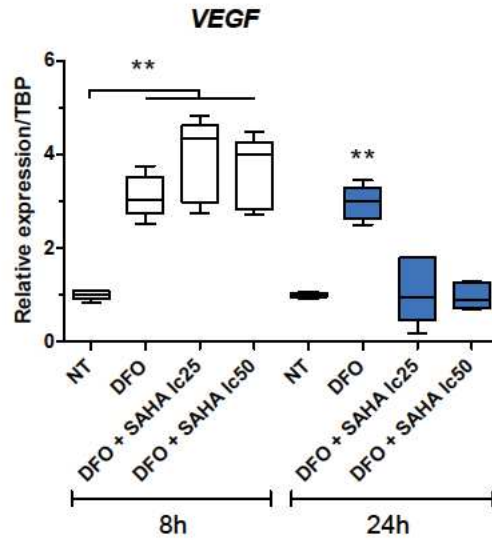
<u>**Supplementary figure 2**</u>: **SAHA reduces HIF1alpha protein level and its activity on gene expression in AGS cells**

AGS cells were treated or not (NT) with Deferoxamine (DFO; 100µM) added or not with SAHA (Vorinostat). RT-qPCR were assayed after 8h (white) or 24h (blue) of treatment. Box plots represent the fold induction of *VEGF*, and *GLUT-1* mRNA for each condition versus the control (NT) (n=2). ** p< 0,0083 are calculated by Mann-Whitney test (corresponding to p-value limit).
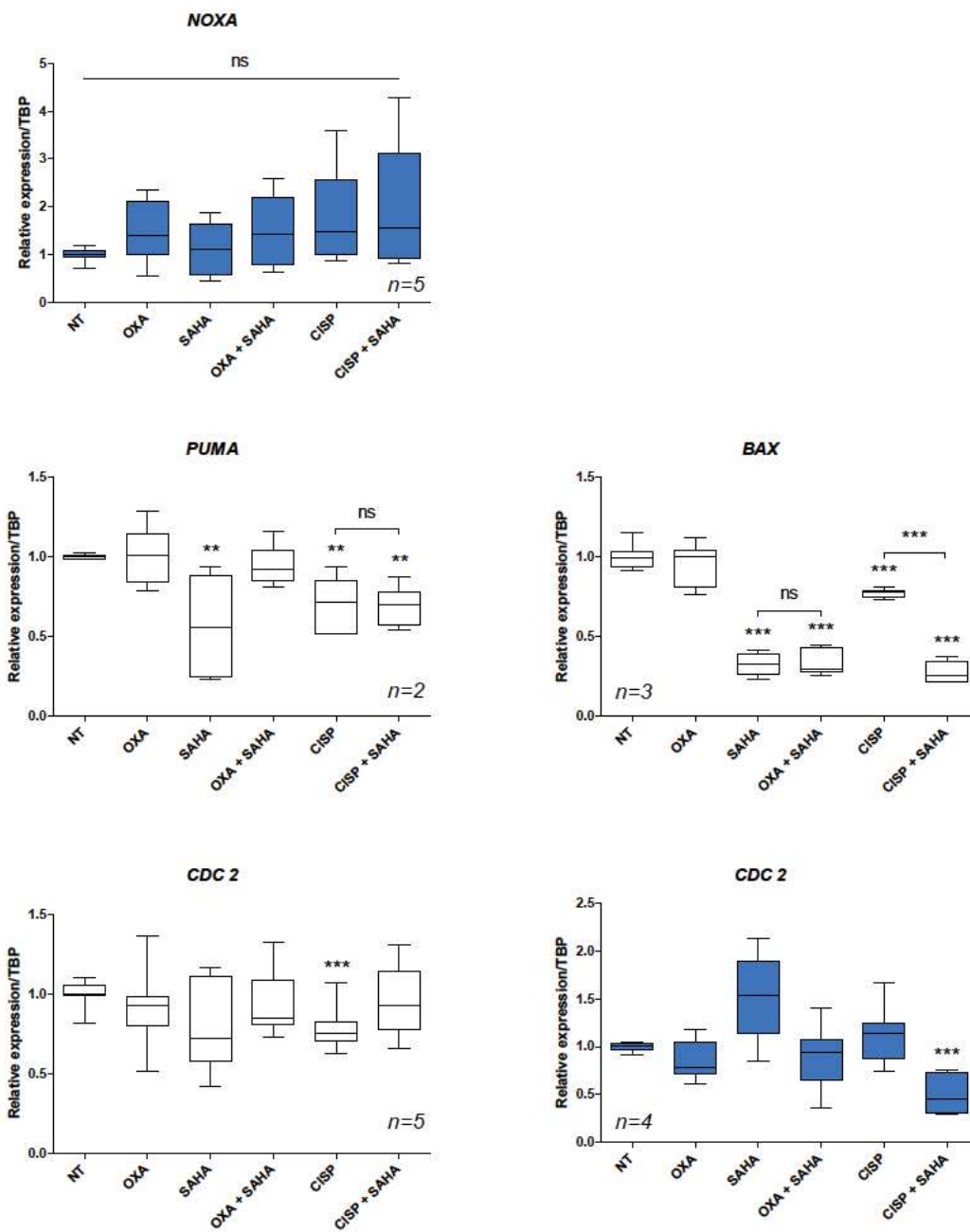
Supplementary figure 3: Combinatory treatments impact apoptosis and proliferation pathways in AGS cells

AGS cells were treated or not (NT) with the synergistic concentrations of Cisplatin (CISP), Oxaliplatin (OXA) and SAHA (Vorinostat). RT-qPCR were assayed after 8h (white) or 24h (blue) of treatment. Box plots represent the fold induction of *NOXA, PUMA, BAX* and *CDC2* mRNA normalized to the control (NT). ** p< 0,0033 ; *** p< 0.001 are calculated by Mann-Whitney test (p-value limit = 0,0033).
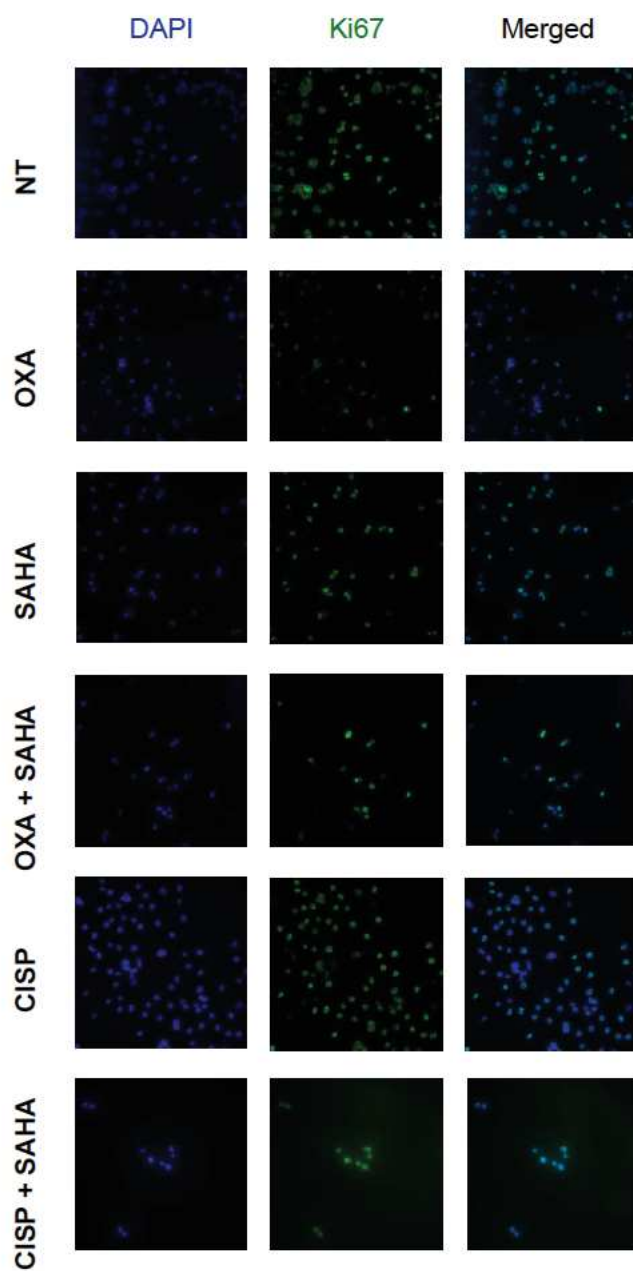
Supplementary figure 4: Impact of combinatory treatments on AGS cell proliferation

Immunocytology on AGS cells were performed after 24h of treatment to reveal Ki67 (Alexa 488 – Green) and DNA (DAPI – Blue). Observations are done with the ApoTome 2® microscope (Zeiss) and Zen Blue software x40.

LC3B-II

Supplementary figure 5: LC3B quantification in response to combinatory treatments in AGS cells

Quantification normalized to ACTIN of the Wetsern blot of LC3B presented in Figure 3.
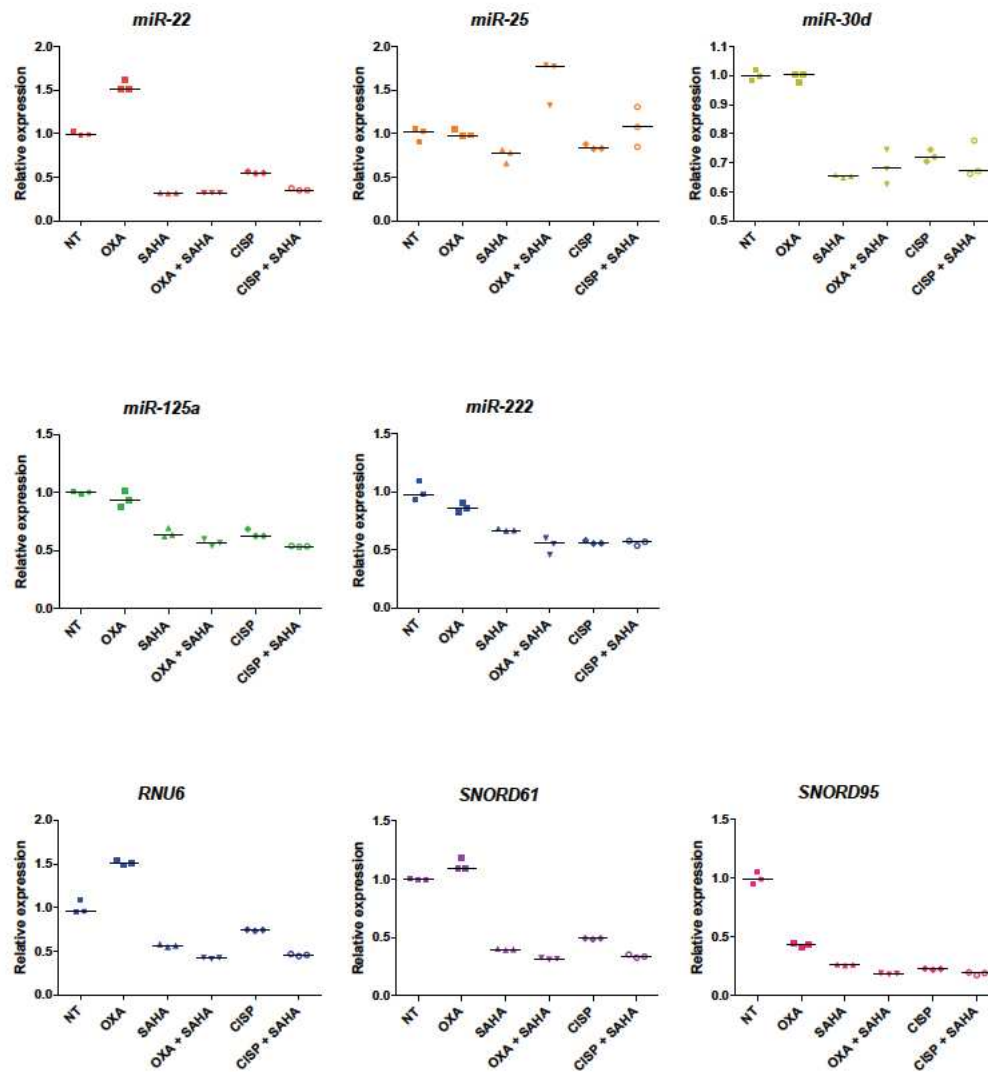
Supplementary figure 6: PDC and SAHA impact miRNA targeting and targeted by p53 expression

AGS cells were treated 4h with Oxaliplatin (OXA; 0,5µM), Cisplatin (CISP; 15µM), SAHA (Vorinostat ; 2,75µM) alone or combined or were untreated (NT). microRNA level were analyzed by Rt-qPCR. Points represent relative expression of each technical replicates. RNU6, SNORD61, SNORD95 are reference miRNA for quantification. Because of treatment impact on their expressions, the relative quantification were done with an arbitrarily Ct and calculated with $2^{(-\Delta\Delta Ct)}$.
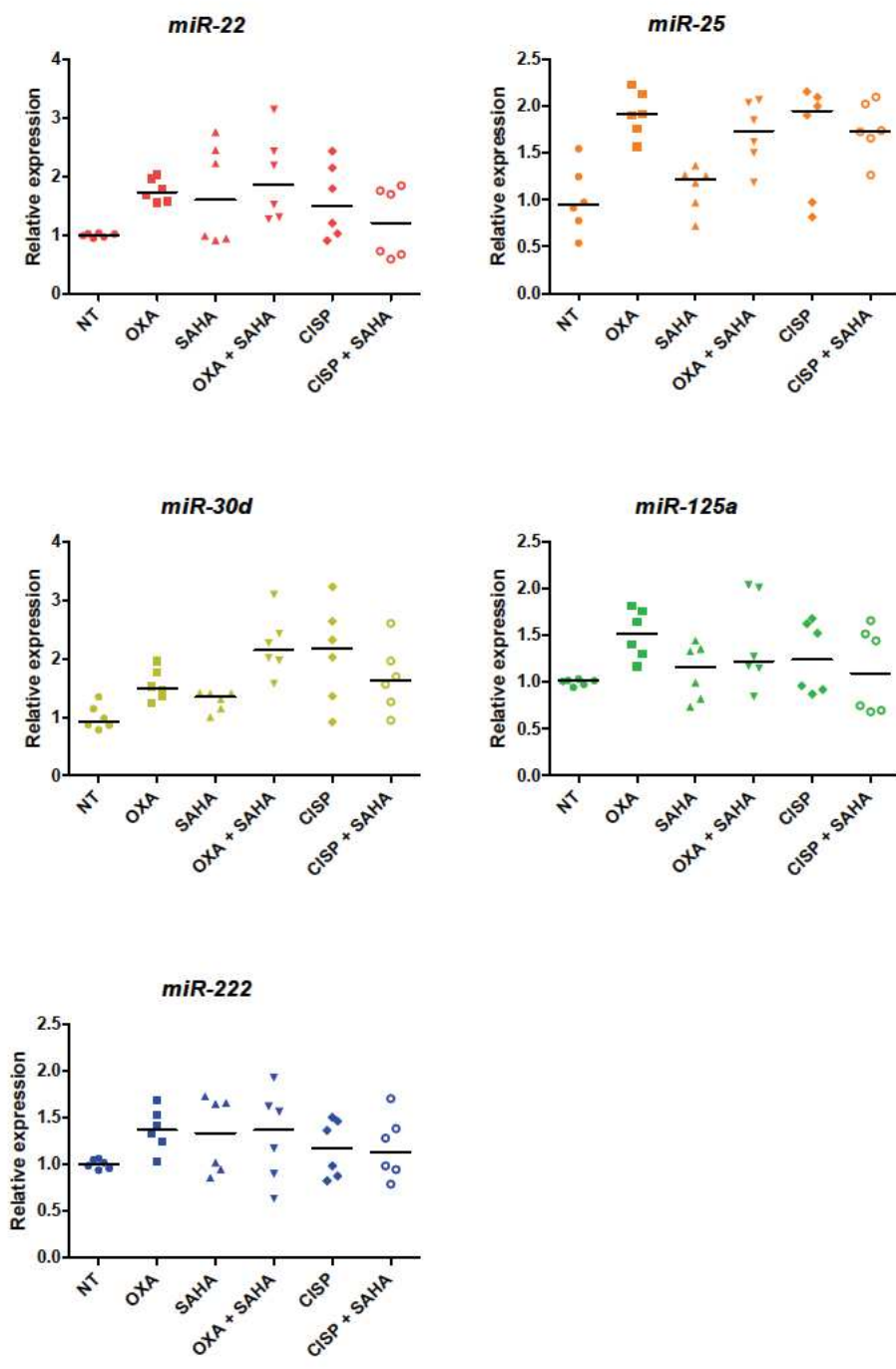
Supplementary figure 7: PDC and SAHA impact miRNA targeting and targeted by p53 expression

AGS cells were treated 8h with Oxaliplatin (OXA; 0,5µM), Cisplatin (CISP; 15µM), SAHA (Vorinostat ; 2,75µM) alone or combined or were untreated (NT). microRNA level were analyzed by Rt-qPCR. Points represent relative expression of each technical replicates (n=2). The relative quantification were done with an arbitrarily Ct and calculated with $2^{(-\Delta\Delta Ct)}$.
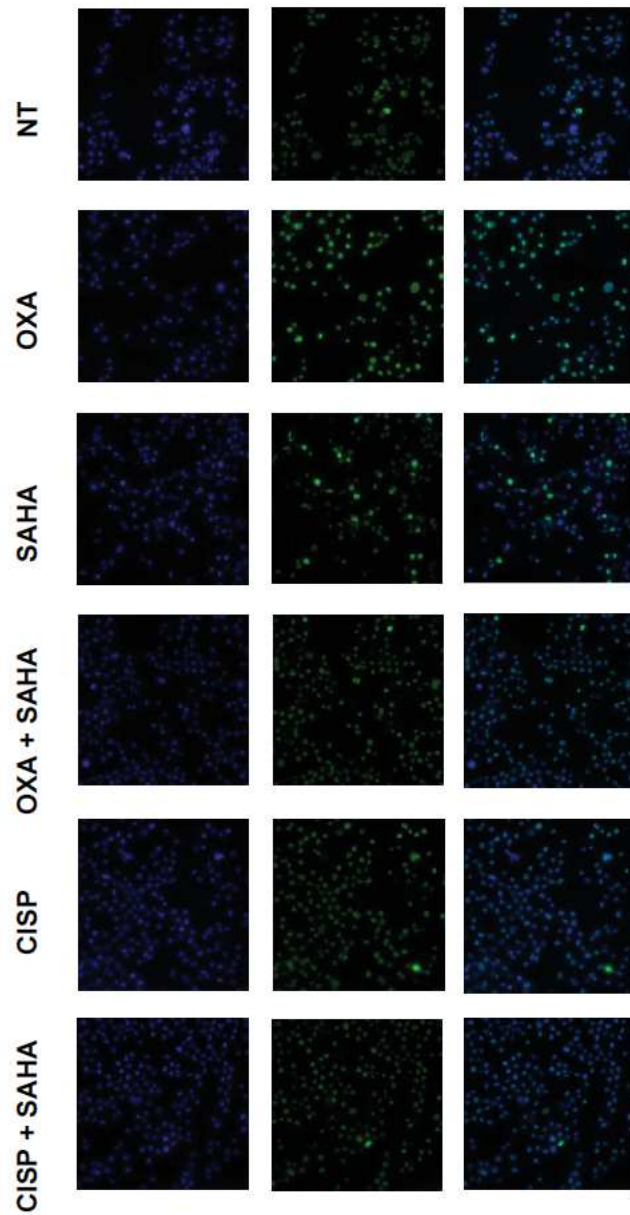
Supplementary figure 8: Impact of combinatory treatments on KATOIII cell proliferation

Immunocytology on KATOIII cells were performed after 24h of treatment to reveal Ki67 (Alexa 488 – Green) and DNA (DAPI – Blue). Observations are done with the ApoTome 2® microscope (Zeiss) and Zen Blue software x40.

8h   **24h**

LC3B

ACTIN

NT
OXA

LC3B-II/LC3B-I

□ 8h
■ 24h
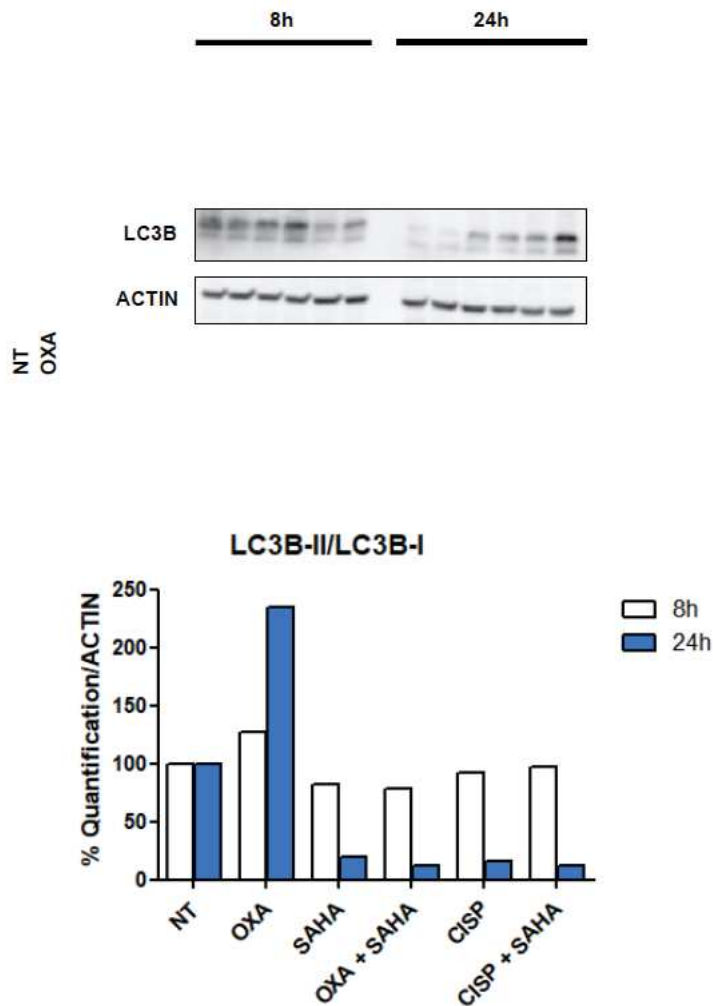
Supplementary figure 9: Combinatory treatments do not induce autophagy in KATOIII cells

KATOIII cells were treated or not (NT) with the synergistic concentrations of Cisplatin (CISP), Oxaliplatin (OXA) and SAHA (Vorinostat) for 8h or 24h. Wetsern blot were perfomed using antobosies against LC3B. The active form of LC3B (LC3B-II) is the bottom band. The relative quantification of the ratio LC3B-II/LC3B-I (active/non-active form) are represented and obtained by a normalization to Actin.
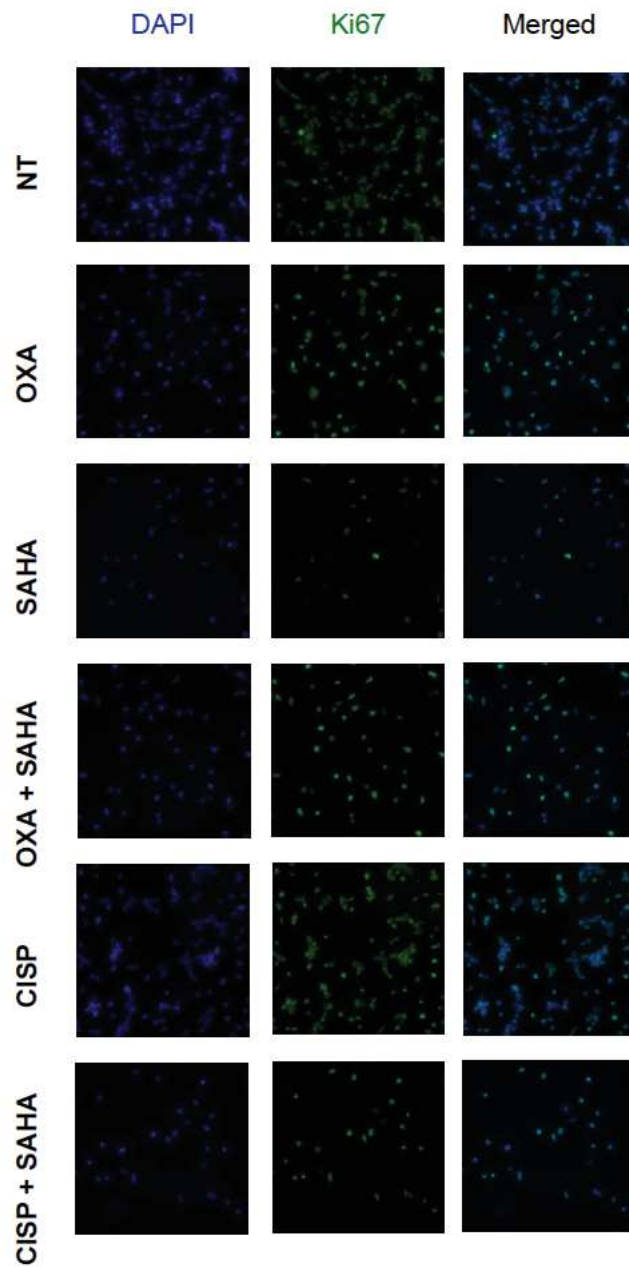
Supplementary figure 10: Impact of combinatory treatments on NUGC3 cell proliferation

Immunocytology on NUGC3 cells were performed after 24h of treatment to reveal Ki67 (Alexa 488 – Green) and DNA (DAPI – Blue). Observations are done with the ApoTome 2® microscope (Zeiss) and Zen Blue software x40.

(a)

(b)

(c)

(d)
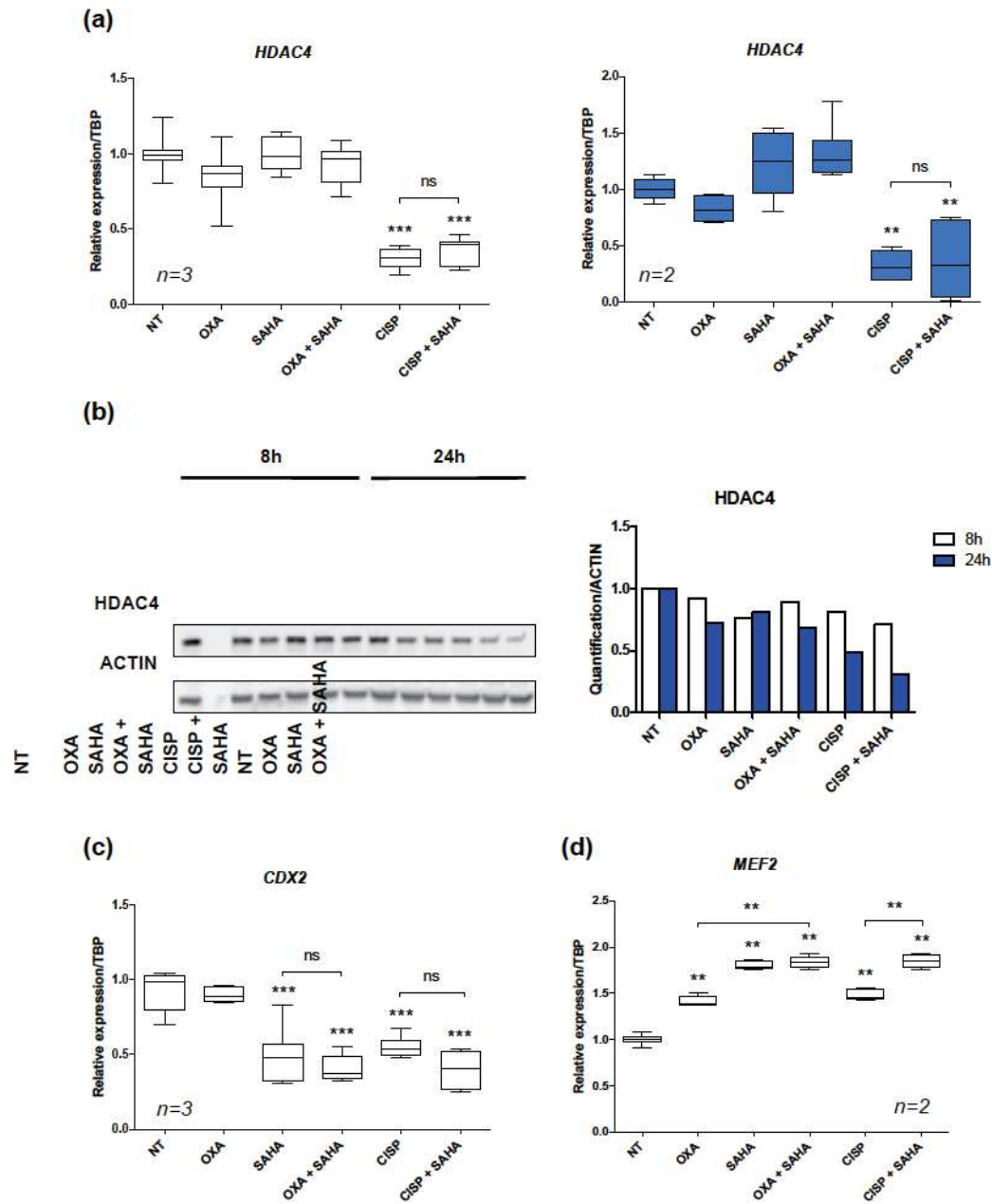
<u>**Supplementary figure 11**</u>: Combinatory treatments impact *HDAC4, CDX2* and *MEF2* expression in AGS cells

AGS cells were treated or not (NT) with the synergistic concentrations of Cisplatin (CISP), Oxaliplatin (OXA) and SAHA (Vorinostat). **(a)** RT-qPCR were assayed after 8h (white) or 24h (blue) of treatment. Box plots represent the fold induction of *HDAC4* mRNA normalized to the untreated (NT) control. **(b)** Western blot was performed using antibodies against HDAC4. The relative quantification was normalized to Actin. **(c-d)** RT-qPCR were assayed after 8h of treatment. Box plots represent the fold induction of *CDX2* and *MEF2* mRNA normalized to the control (NT). ** $p < 0,0033$; *** $p < 0.001$ are calculated by Mann-Whitney test (p-value limit = 0,0033).
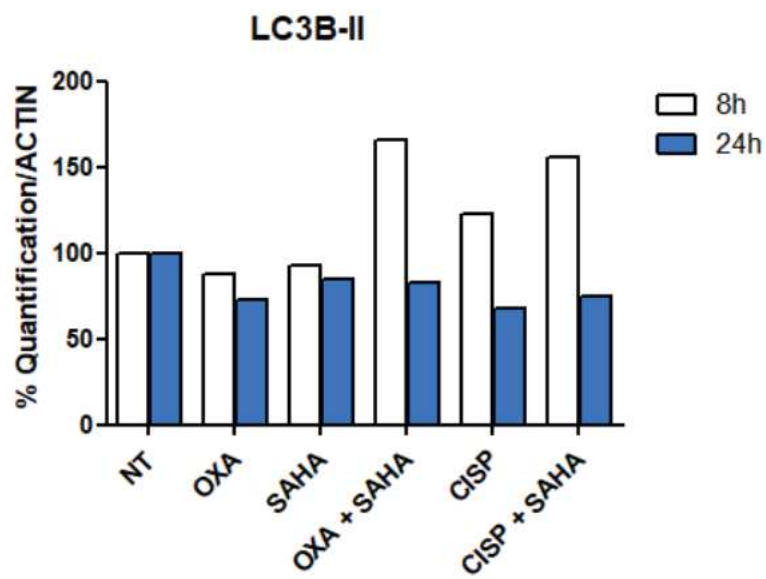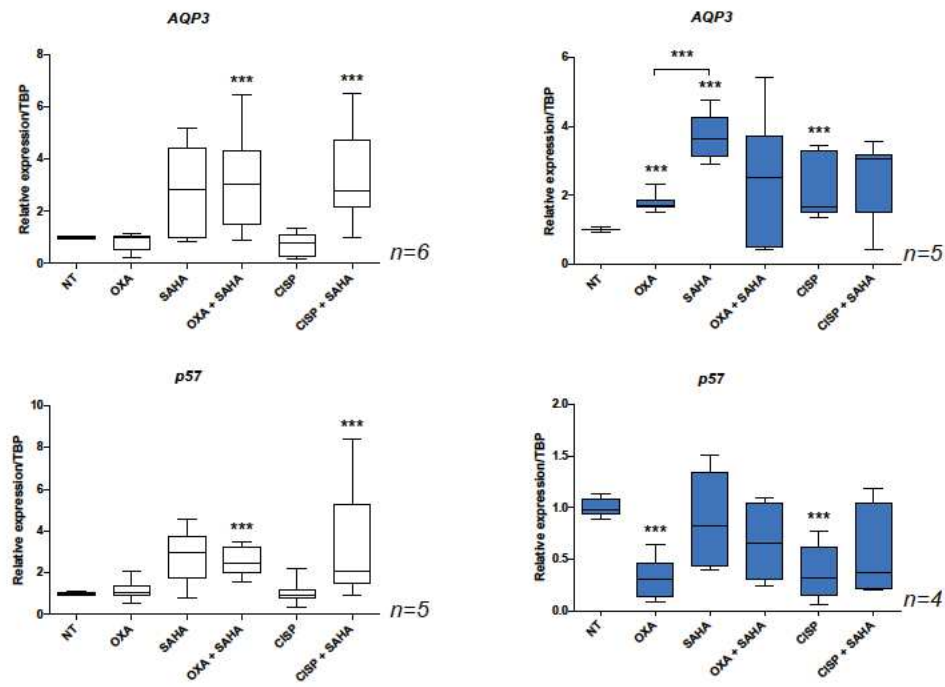
Supplementary figure 12: Combinatory treatments impact p53 and AQP3 expression in AGS cells

AGS cells were treated or not (NT) with the synergistic concentrations of Cisplatin (CISP), Oxaliplatin (OXA) and SAHA (Vorinostat). RT-qPCR were assayed after 8h (white) or 24h (blue) of treatment. Box plots represent the fold induction *AQP3* and *p57* mRNA normalized to the control (NT). ** p< 0,0033; *** p< 0.001 are calculated by Mann-Whitney test (p-value limit = 0,0033).

MKN45 cells isobologram

MKN45 cells isobologram
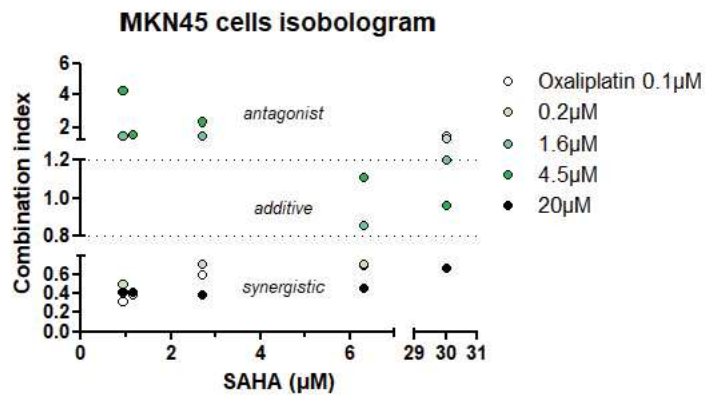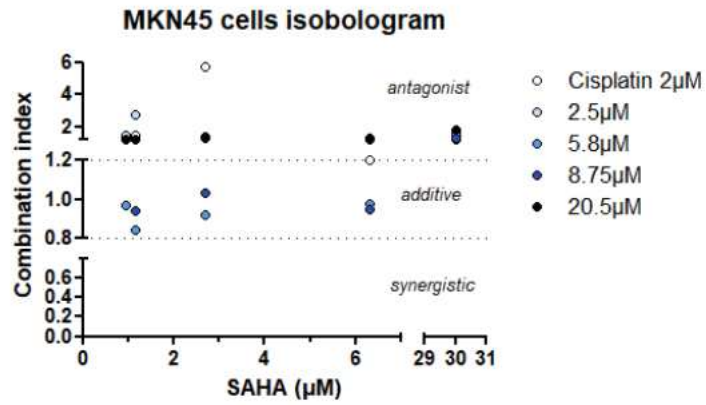
Complementary figure II-2: **Combinatory treatments impact differently MKN45 cells**

MKN45 cells were treated at the indicated concentrations of Cisplatin (CISP) or Oxaliplatin (OXA) and SAHA (Vorinostat) for 48h followed by an isobologram assay to determine mathematically the combination index. We arbitrarily and conservatively considered antagonist effect between the drugs correspond to value > 1.20, additive effect between 0.80 and 1.20 and synergistic effect <0.80.

MKN45 cells

Name	Characteristics*	Drugs	IC$_{25}$ (µM)	IC$_{30}$ (µM)	IC$_{50}$ (µM)	IC$_{60}$ (µM)	IC$_{75}$ (µM)
MKN45	Liver metastasis Near diploid p53 WT/mutated bi-allelic c-met amplification ERK mRNA amplification Cyclin E amplification	SAHA	0,95	1,15	2,7	6,30	30
		Oxaliplatin	0,1	0,20	1,6	4,5	20
		Cisplatin	2	2,5	5,8	8,75	20,5

<u>**Complementary figure II-1**</u>: **SAHA and platinum compounds impact MKN45 cell survival**

MKN45 cells were seeded in 96-wells and treated 48h with Cisplatin, Oxaliplatin or SAHA (Vorinostat). Viability of the cells was evaluated using MTT tests (n=3). The table summarizes the different concentrations for each drug graphical determined. For example, IC$_{25}$ represents the concentration where we have 25% of the total effect on cell survival. *ATCC ; Yokozaki H. Pathology International, 2000 ; Cancer Cell Lines, Part 2, Human Cell Culture, 2002 ; portals.broadinstitute.org/ccle*
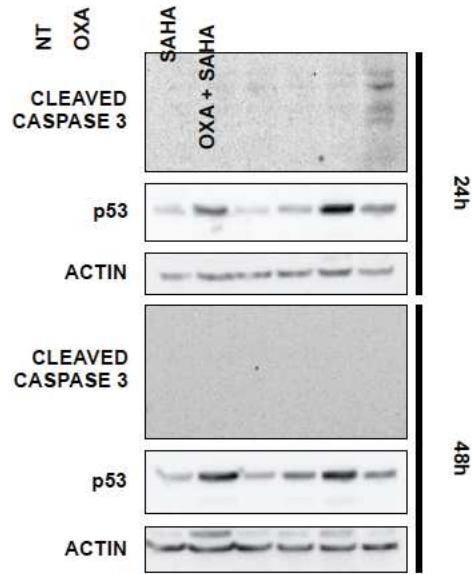
Complementary figure II-3: Combined treatments PDC + SAHA do not induce a caspase dependent apoptosis in MKN45 cells

MKN45 cells were treated or not (NT) with combined drugs or drugs alone for 24h or 48h; Cisplatin (CISP) or Oxaliplatin (OXA) and SAHA (Vorinostat). Then, western blots were performed using antibodies against Cleaved Caspase 3 and p53.
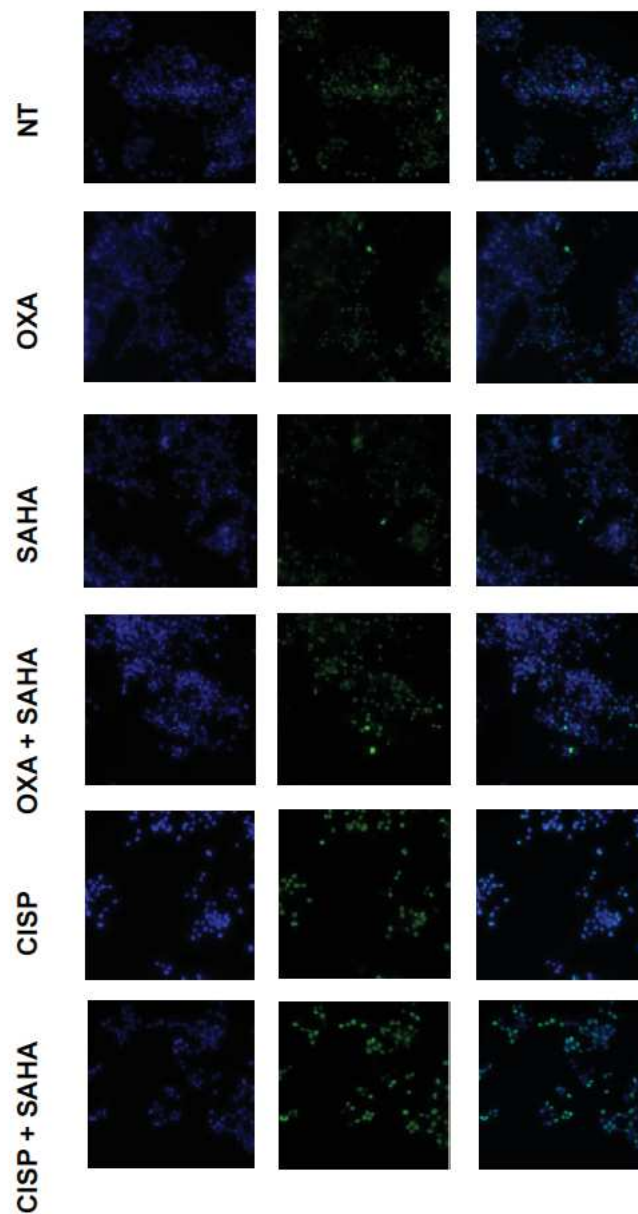
Complementary figure II-4: Impact of combinatory treatments on MKN45 cell proliferation

Immunocytology on MKN45 cells were performed after 24h of treatment to reveal Ki67 (Alexa 488 – Green) and DNA (DAPI – Blue). Observations are done with the ApoTome 2® microscope (Zeiss) and Zen Blue software x40.

p53

p21

CYCLIN B2

Complementary figure II: Impact of p53 on apoptotic pathway

NOXA

PUMA

BIK

DIABLO
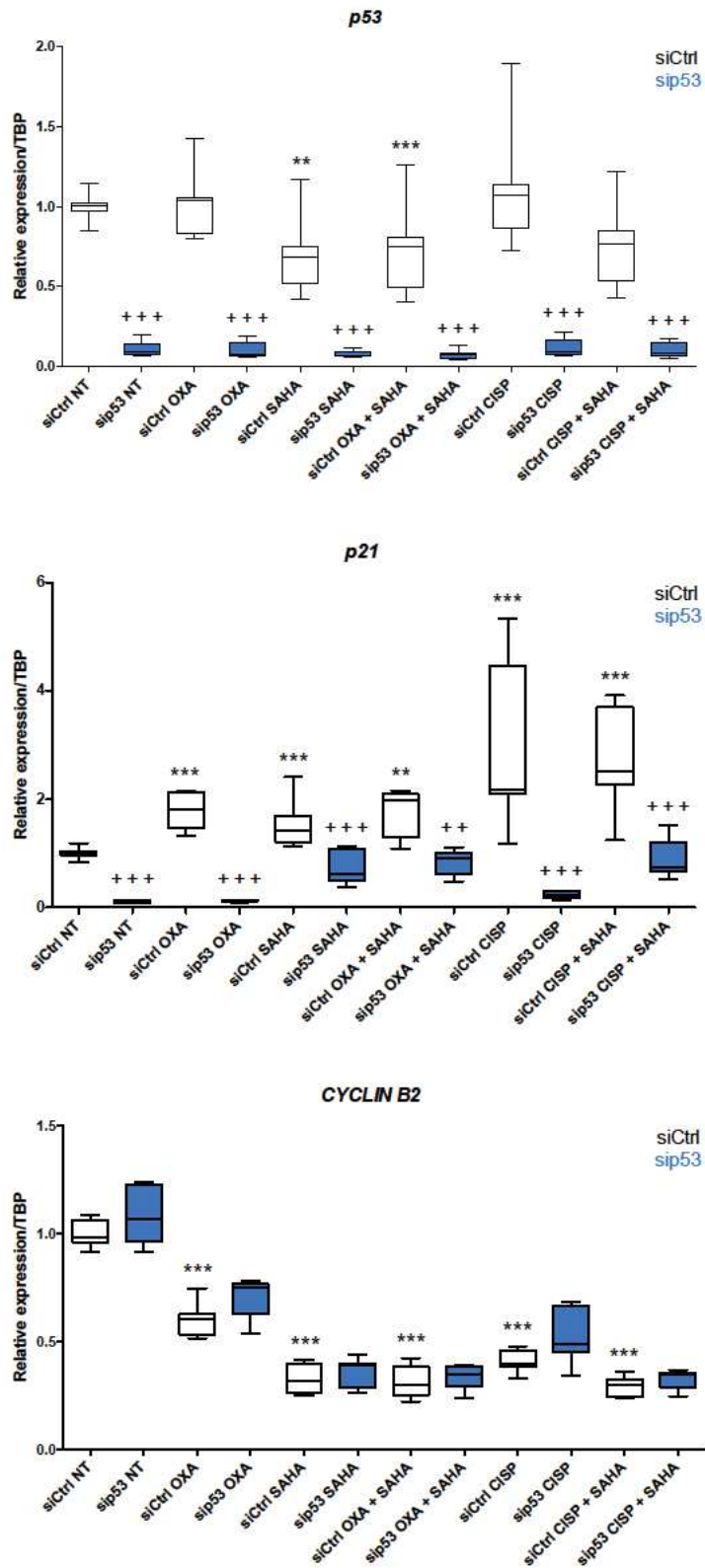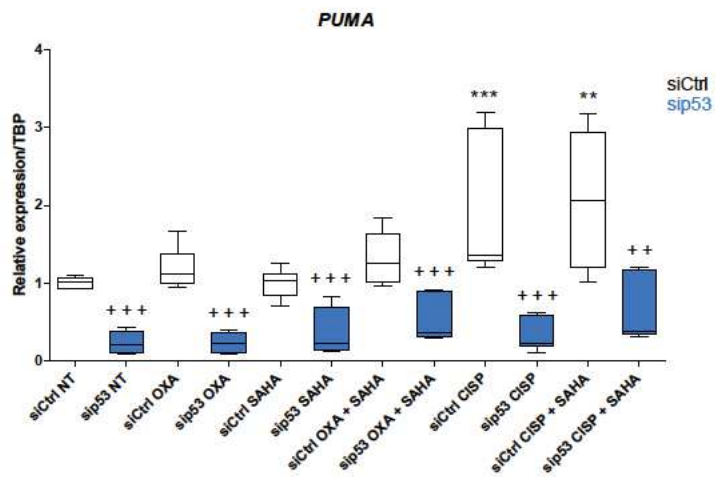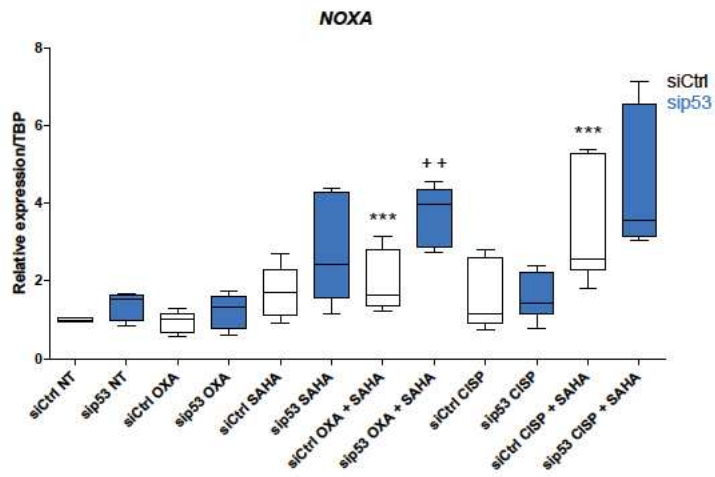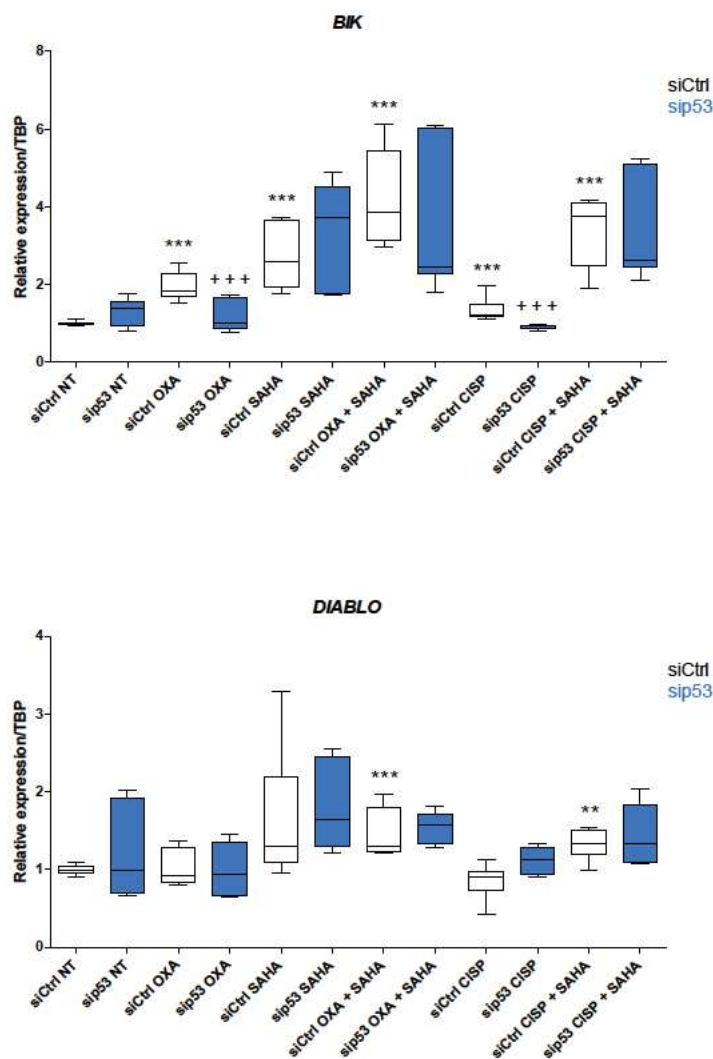
Continuation complementary figure II: Impact of p53 on apoptotic pathway

AGS cells were transfected with 30nM of a scramble siRNA (siCtrl) or of a siRNA against TP53 (sip53) for 48h. Then, cells were treated 8h with SAHA (Vorinostat), Oxaliplatin (OXA) and Cisplatin (CISP) at synergistic concentrations. *TP53, CYCLIN B2, p21, PUMA, NOXA, BIK,* and *DIABLO* (n=3) mRNA levels were analyzed by RT-qPCR. Box plots represent the fold induction of mRNA for each condition normalized to the control (siCtrl NT). Statistical differences were calculated by Mann-Whitney test with a correction as p-value limit p=0,0045. * vs siCtrl NT ; + siCtrl vs siHDAC4. ** p< 0,0045 ; *** p< 0,001

References

Abdelfatah, E., Kerner, Z., Nanda, N., and Ahuja, N. (2016). Epigenetic therapy in gastrointestinal cancer: the right combination. Therap Adv Gastroenterol *9*, 560–579.

Abrahao-Machado, L.F., and Scapulatempo-Neto, C. (2016). HER2 testing in gastric cancer: An update. World J Gastroenterol *22*, 4619–4625.

Ajani, J.A., Lee, J., Sano, T., Janjigian, Y.Y., Fan, D., and Song, S. (2017). Gastric adenocarcinoma. Nature Reviews Disease Primers *3*, 17036.

Akiyoshi, S., Fukagawa, T., Ueo, H., Ishibashi, M., Takahashi, Y., Fabbri, M., Sasako, M., Maehara, Y., Mimori, K., and Mori, M. (2012). Clinical significance of miR-144-ZFX axis in disseminated tumour cells in bone marrow in gastric cancer cases. Br. J. Cancer *107*, 1345–1353.

Alcindor, T., and Beauger, N. (2011). Oxaliplatin: a review in the era of molecularly targeted therapy. Curr Oncol *18*, 18–25.

Alzoubi, S., Brody, L., Rahman, S., Mahul-Mellier, A.-L., Mercado, N., Ito, K., El-Bahrawy, M., Silver, A., Boobis, A., Bell, J.D., et al. (2016). Synergy between histone deacetylase inhibitors and DNA-damaging agents is mediated by histone deacetylase 2 in colorectal cancer. Oncotarget *7*, 44505–44521.

Amodio, N., Stamato, M.A., Gullà, A.M., Morelli, E., Romeo, E., Raimondi, L., Pitari, M.R., Ferrandino, I., Misso, G., Caraglia, M., et al. (2016). Therapeutic Targeting of miR-29b/HDAC4 Epigenetic Loop in Multiple Myeloma. Mol. Cancer Ther. *15*, 1364–1375.

Arrowsmith CH. (1999). Structure and function in the p53 family [see comments]. Cell Death Differ; 6: 1169-1173.

Azarkhazin, F., and Tehrani, G.A. (2018). Detecting promoter methylation pattern of apoptotic genes Apaf1 and Caspase8 in gastric carcinoma patients undergoing chemotherapy. J Gastrointest Oncol *9*, 295–302.

Backert, S., and Blaser, M.J. (2016). The Role of CagA in the Gastric Biology of Helicobacter pylori. Cancer Res. *76*, 4028–4031.

Bannister, A.J., Miska, E.A., Görlich, D., and Kouzarides, T. (2000). Acetylation of importin-alpha nuclear import factors by CBP/p300. Curr. Biol. *10*, 467–470.

Bär, C., Chatterjee, S., and Thum, T. (2016). Long Noncoding RNAs in Cardiovascular Pathology, Diagnosis, and Therapy. Circulation *134*, 1484–1499.

Basile, V., Mantovani, R., and Imbriano, C. (2006). DNA damage promotes histone deacetylase 4 nuclear localization and repression of G2/M promoters, via p53 C-terminal lysines. J. Biol. Chem. *281*, 2347–2357.

Basourakos, S.P., Li, L., Aparicio, A.M., Corn, P.G., Kim, J., and Thompson, T.C. (2017). Combination Platinum-based and DNA Damage Response-targeting Cancer Therapy: Evolution and Future Directions. Curr Med Chem *24*, 1586–1606.

Benosman S, Meng X, Von Grabowiecki Y, Palamiuc L, Hritcu L, Gross I *et al*. (2011). Complex regulation of p73 isoforms after alteration of amyloid precursor polypeptide (APP) function and DNA damage in neurons. J Biol Chem; 286: 43013-43025.

Bhaskara, S., Knutson, S.K., Jiang, G., Chandrasekharan, M.B., Wilson, A.J., Zheng, S., Yenamandra, A., Locke, K., Yuan, J., Bonine-Summers, A.R., et al. (2010). Hdac3 is essential for the maintenance of chromatin structure and genome stability. Cancer Cell *18*, 436–447.

Bhat, S.A., Ahmad, S.M., Mumtaz, P.T., Malik, A.A., Dar, M.A., Urwat, U., Shah, R.A., and Ganai, N.A. (2016). Long non-coding RNAs: Mechanism of action and functional utility. Non-Coding RNA Research *1*, 43–50.

Boland, C.R., and Yurgelun, M.B. (2017). Historical Perspective on Familial Gastric Cancer. Cell Mol Gastroenterol Hepatol *3*, 192–200.

Bosch-Presegué, L., and Vaquero, A. (2011). The Dual Role of Sirtuins in Cancer. Genes Cancer *2*, 648–662.

Boyes, J., Byfield, P., Nakatani, Y., and Ogryzko, V. (1998). Regulation of activity of the transcription factor GATA-1 by acetylation. Nature *396*, 594–598.

Buas, M.F., and Vaughan, T.L. (2013). Epidemiology and Risk Factors for Gastroesophageal Junction Tumors: Understanding the Rising Incidence of This Disease. Seminars in Radiation Oncology *23*, 3–9.

Budillon, A., Di Gennaro, E., Bruzzese, F., Rocco, M., Manzo, G., and Caraglia, M. (2007). Histone deacetylase inhibitors: a new wave of molecular targeted anticancer agents. Recent Pat Anticancer Drug Discov *2*, 119–134.

Busuttil, R.A., Zapparoli, G.V., Haupt, S., Fennell, C., Wong, S.Q., Pang, J.-M.B., Takeno, E.A., Mitchell, C., Di Costanzo, N., Fox, S., et al. (2014). Role of p53 in the progression of gastric cancer. Oncotarget *5*, 12016–12026.

Cancer Genome Atlas Research Network (2014). Comprehensive molecular characterization of gastric adenocarcinoma. Nature *513*, 202–209.
Cao, G., Chen, K., Chen, B., and Xiong, M. (2017). Positive prognostic value of HER2-HER3 co-expression and p-mTOR in gastric cancer patients. BMC Cancer *17*.

Cao, L.-L., Yue, Z., Liu, L., Pei, L., Yin, Y., Qin, L., Zhao, J., Liu, H., Wang, H., and Jia, M. (2017). The expression of histone deacetylase HDAC1 correlates with the progression and prognosis of gastrointestinal malignancy. Oncotarget *8*, 39241–39253.

Catalanotto, C., Cogoni, C., and Zardo, G. (2016). MicroRNA in Control of Gene Expression: An Overview of Nuclear Functions. Int J Mol Sci *17*.

Cavanagh, H., and Rogers, K.M.A. (2015). The role of BRCA1 and BRCA2 mutations in prostate, pancreatic and stomach cancers. Hereditary Cancer in Clinical Practice *13*, 16.

CDU-HGE. (2014). *The fundamentals of digestive pathology.* Elsevier-Masson Editions [French].

CDU-HGE. (2015). *Abbreviated hepato-gastro-enterology and digestive surgery.* Elsevier-Masson 3rd Editions [French].

Chang H, Rha SY, Jeung HC, Jung JJ, Kim TS, Kwon HJ *et al*. (2010). Identification of genes related to a synergistic effect of taxane and suberoylanilide hydroxamic acid combination treatment in gastric cancer cells. J Cancer Res Clin Oncol; 136: 1901-1913.

Chen, X., Gao, B., Ponnusamy, M., Lin, Z., and Liu, J. (2017). MEF2 signaling and human diseases. Oncotarget *8*, 112152–112165.
Cheung, K.-S., and Leung, W.K. (2018). Risk of gastric cancer development after eradication of Helicobacter pylori. World J Gastrointest Oncol *10*, 115–123.

Chia, N.-Y., and Tan, P. (2016). Molecular classification of gastric cancer. Annals of Oncology *27*, 763–769.

Chiurillo, M.A. (2015). Role of the Wnt/β-catenin pathway in gastric cancer: An in-depth literature review. World J Exp Med *5*, 84–102.

Cho, S.Y., Park, J.W., Liu, Y., Park, Y.S., Kim, J.H., Yang, H., Um, H., Ko, W.R., Lee, B.I., Kwon, S.Y., et al. (2017). Sporadic Early-Onset Diffuse Gastric Cancers Have High Frequency of Somatic CDH1 Alterations, but Low Frequency of Somatic RHOA Mutations Compared With Late-Onset Cancers. Gastroenterology *153*, 536-549.e26.

Choi, H.-K., Choi, Y., Park, E.S., Park, S.-Y., Lee, S.-H., Seo, J., Jeong, M.-H., Jeong, J.-W., Cheong, J.-H., Lee, P.C.W., et al. (2015). Programmed cell death 5 mediates HDAC3 decay to promote genotoxic stress response. Nature Communications *6*, 7390.

Choi, J.-H., Kim, Y.-B., Ahn, J.M., Kim, M.J., Bae, W.J., Han, S.-U., Woo, H.G., and Lee, D. (2018). Identification of genomic aberrations associated with lymph node metastasis in diffuse-type gastric cancer. Experimental & Molecular Medicine *50*, 6.

Choi, W., Kim, J., Park, J., Lee, D.-H., Hwang, D., Kim, J.-H., Ashktorab, H., Smoot, D., Kim, S.-Y., Choi, C., et al. (2018). YAP/TAZ Initiates Gastric Tumorigenesis via Upregulation of MYC. Cancer Res *78*, 3306–3320.

Chou, T.-C. (2006). Theoretical basis, experimental design, and computerized simulation of synergism and antagonism in drug combination studies. Pharmacol. Rev. *58*, 621–681.

Chou, T.-C. (2010). Drug combination studies and their synergy quantification using the Chou-Talaly method. Cancer Research. *70*, 440-446

Cisło, M., Filip, A.A., Arnold Offerhaus, G.J., Ciseł, B., Rawicz-Pruszyński, K., Skierucha, M., and Polkowski, W.P. (2018). Distinct molecular subtypes of gastric cancer: from Laurén to molecular pathology. Oncotarget *9*, 19427–19442.

Claerhout S, Lim JY, Choi W, Park YY, Kim K, Kim SB *et al*. (2011). Gene expression signature analysis identifies vorinostat as a candidate therapy for gastric cancer. PLoS One; 6: e24662.

Cohen, A.L., Piccolo, S.R., Cheng, L., Soldi, R., Han, B., Johnson, W.E., and Bild, A.H. (2013). Genomic pathway analysis reveals that EZH2 and HDAC4 represent mutually exclusive epigenetic pathways across human cancers. BMC Med Genomics *6*, 35.

Cohen, H.Y., Lavu, S., Bitterman, K.J., Hekking, B., Imahiyerobo, T.A., Miller, C., Frye, R., Ploegh, H., Kessler, B.M., and Sinclair, D.A. (2004). Acetylation of the C terminus of Ku70 by CBP and PCAF controls Bax-mediated apoptosis. Mol. Cell *13*, 627–638.

Colarossi, L., Memeo, L., Colarossi, C., Aiello, E., Iuppa, A., Espina, V., Liotta, L., and Mueller, C. (2014). Inhibition of histone deacetylase 4 increases cytotoxicity of docetaxel in gastric cancer cells. Proteomics Clin Appl *8*, 924–931.

Correa, P., and Piazuelo, M.B. (2011). Helicobacter pylori Infection and Gastric Adenocarcinoma. US Gastroenterol Hepatol Rev *7*, 59–64.

Correa, P., and Piazuelo, M.B. (2012). The gastric precancerous cascade: The gastric precancerous cascade. Journal of Digestive Diseases *13*, 2–9.

Costanzo, A., Pediconi, N., Narcisi, A., Guerrieri, F., Belloni, L., Fausti, F., Botti, E., and Levrero, M. (2014). TP63 and TP73 in cancer, an unresolved "family" puzzle of complexity, redundancy and hierarchy. FEBS Lett. *588*, 2590–2599.
Cross, A.J., Pollock, J.R.A., and Bingham, S.A. (2003). Haem, not protein or inorganic iron, is responsible for endogenous intestinal N-nitrosation arising from red meat. Cancer Res. *63*, 2358–2360.

Curtin, N.J. (2012). DNA repair dysregulation from cancer driver to therapeutic target. Nature Reviews Cancer *12*, 801–817.

Dar, A.A., Belkhiri, A., and El-Rifai, W. (2009). The Aurora kinase A Regulates GSK-3β in Gastric Cancer Cells. Oncogene *28*, 866–875.

Dasari, S., and Tchounwou, P.B. (2014). Cisplatin in cancer therapy: molecular mechanisms of action. Eur J Pharmacol *0*, 364–378.

Davies NP, Hardman LC, Murray V. (2000). The effect of chromatin structure on Cisplatin damage in intact human cells. Nucleic Acids Res; 28: 2954-2958.

De Dosso, S., Zanellato, E., Nucifora, M., Boldorini, R., Sonzogni, A., Biffi, R., Fazio, N., Bucci, E., Beretta, O., Crippa, S., et al. (2013). ERCC1 predicts outcome in patients with gastric cancer treated with adjuvant cisplatin-based chemotherapy. Cancer Chemother. Pharmacol. *72*, 159–165.

de Ruijter, A.J.M., van Gennip, A.H., Caron, H.N., Kemp, S., and van Kuilenburg, A.B.P. (2003). Histone deacetylases (HDACs): characterization of the classical HDAC family. Biochem. J. *370*, 737–749.

Di Giorgio, E., Clocchiatti, A., Piccinin, S., Sgorbissa, A., Viviani, G., Peruzzo, P., Romeo, S., Rossi, S., Dei Tos, A.P., Maestro, R., et al. (2013). MEF2 is a converging hub for histone deacetylase 4 and phosphatidylinositol 3-kinase/Akt-induced transformation. Mol. Cell. Biol. *33*, 4473–4491.

Di Giorgio, E., Hancock, W.W., and Brancolini, C. (2018). MEF2 and the tumorigenic process, hic sunt leones. Biochim. Biophys. Acta.

Digaleh, H., Kiaei, M., and Khodagholi, F. (2013). Nrf2 and Nrf1 signaling and ER stress crosstalk: implication for proteasomal degradation and autophagy. Cell. Mol. Life Sci. *70*, 4681–4694.

Ding, J. (Diane), Ri, M., Narita, T., Masaki, A., Mori, F., Ito, A., Kusumoto, S., Ishida, T., Komatsu, H., Shiotsu, Y., et al. (2012). Reduced Expression of HDAC3 Contributes to the Resistance Against HDAC Inhibitor, Vorinostat (SAHA) in Mature Lymphoid Malignancies. Blood *120*, 1342–1342.

Diyabalanage, H.V.K., Granda, M.L., and Hooker, J.M. (2013). Combination therapy: histone deacetylase inhibitors and platinum-based chemotherapeutics for cancer. Cancer Lett. *329*, 1–8.

Dong G, Luo J, Kumar V, Dong Z. (2010). Inhibitors of histone deacetylases suppress Cisplatin-induced p53 activation and apoptosis in renal tubular cells. Am J Physiol Renal Physiol; 298: F293-300.

Dong, J., Zheng, N., Wang, X., Tang, C., Yan, P., Zhou, H.-B., and Huang, J. (2018). A novel HDAC6 inhibitor exerts an anti-cancer effect by triggering cell cycle arrest and apoptosis in gastric cancer. Eur. J. Pharmacol. *828*, 67–79.

Duan, S., Yin, J., Bai, Z., and Zhang, Z. (2018). Effects of taxol resistance gene 1 on the Cisplatin response in gastric cancer. Oncol Lett *15*, 8287–8294.

Dunne, C., Dolan, B., and Clyne, M. (2014). Factors that mediate colonization of the human stomach by Helicobacter pylori. World Journal of Gastroenterology *20*, 5610–5624.

Duong, V., Bret, C., Altucci, L., Mai, A., Duraffourd, C., Loubersac, J., Harmand, P.-O., Bonnet, S., Valente, S., Maudelonde, T., et al. (2008). Specific activity of class II histone deacetylases in human breast cancer cells. Mol Cancer Res *6*, 1908–1919.

Duquet, A., Polesskaya, A., Cuvellier, S., Ait-Si-Ali, S., Héry, P., Pritchard, L.L., Gerard, M., and Harel-Bellan, A. (2006). Acetylation is important for MyoD function in adult mice. EMBO Rep *7*, 1140–1146.

Eckschlager, T., Plch, J., Stiborova, M., and Hrabeta, J. (2017) Histone Deacetylase Inhibitors as Anticancer Drugs. International Journal of Molecular Sciences. Review. *18*, 1414

Ellis, L., Atadja, P.W., and Johnstone, R.W. (2009). Epigenetics in cancer: targeting chromatin modifications. Mol. Cancer Ther. *8*, 1409–1420.

Ertao, Z., Jianhui, C., Chuangqi, C., Changjiang, Q., Sile, C., Yulong, H., Hui, W., and Shirong, C. (2016). Autocrine Sonic hedgehog signaling promotes gastric cancer proliferation through induction of phospholipase Cγ1 and the ERK1/2 pathway. J Exp Clin Cancer Res *35*.

Espinosa-Parrilla, Y., Muñoz, X., Bonet, C., Garcia, N., Venceslá, A., Yiannakouris, N., Naccarati, A., Sieri, S., Panico, S., Huerta, J.M., et al. Genetic association of gastric cancer with miRNA clusters including the cancer-related genes MIR29, MIR25, MIR93 and MIR106: Results from the EPIC-EURGAST study. International Journal of Cancer *135*, 2065–2076.

Falkenberg, K.J., and Johnstone, R.W. (2014). Histone deacetylases and their inhibitors in cancer, neurological diseases and immune disorders. Nature Reviews Drug Discovery *13*, 673–691.

Fang, D., Hawke, D., Zheng, Y., Xia, Y., Meisenhelder, J., Nika, H., Mills, G.B., Kobayashi, R., Hunter, T., and Lu, Z. (2007). Phosphorylation of β-Catenin by AKT Promotes β-Catenin Transcriptional Activity. J. Biol. Chem. *282*, 11221–11229.

Fang, Z., Yin, S., Sun, R., Zhang, S., Fu, M., Wu, Y., Zhang, T., Khaliq, J., and Li, Y. (2017). miR-140-5p suppresses the proliferation, migration and invasion of gastric cancer by regulating YES1. Mol Cancer *16*.

Feng, L., Pan, M., Sun, J., Lu, H., Shen, Q., Zhang, S., Jiang, T., Liu, L., Jin, W., Chen, Y., et al. (2013). Histone deacetylase 3 inhibits expression of PUMA in gastric cancer cells. J. Mol. Med. *91*, 49–58.

Finzer P, Krueger A, Stohr M, Brenner D, Soto U, Kuntzen C *et al*. (2004). HDAC inhibitors trigger apoptosis in HPV-positive cells by inducing the E2F-p73 pathway. Oncogene; 23: 4807-4817.

Fischle, W., Dequiedt, F., Fillion, M., Hendzel, M.J., Voelter, W., and Verdin, E. (2001). Human HDAC7 histone deacetylase activity is associated with HDAC3 in vivo. J. Biol. Chem. *276*, 35826–35835.

Fischle, W., Dequiedt, F., Hendzel, M.J., Guenther, M.G., Lazar, M.A., Voelter, W., and Verdin, E. (2002). Enzymatic activity associated with class II HDACs is dependent on a multiprotein complex containing HDAC3 and SMRT/N-CoR. Mol. Cell *9*, 45–57.

Florea AM, Busselberg D. (2011). Cisplatin as an anti-tumor drug: cellular mechanisms of activity, drug resistance and induced side effects. Cancers (Basel); 3: 1351-1371.

Fox, J.G., Dangler, C.A., Taylor, N.S., King, A., Koh, T.J., and Wang, T.C. (1999). High-salt diet induces gastric epithelial hyperplasia and parietal cell loss and enhances Helicobacter pylori colonization in C57BL/6 mice. Cancer Res. *59*, 4823–4828.

Fraga MF, Ballestar E, Villar-Garea A, Boix-Chornet M, Espada J, Schotta G *et al*. (2005). Loss of acetylation at Lys16 and trimethylation at Lys20 of histone H4 is a common hallmark of human cancer. Nat Genet; 37: 391-400.

Freund, J.-N., Duluc, I., Reimund, J.-M., Gross, I., and Domon-Dell, C. (2015). Extending the functions of the homeotic transcription factor Cdx2 in the digestive system through nontranscriptional activities. World J. Gastroenterol. *21*, 1436–1443.

Fushida, S., Kinoshita, J., Kaji, M., Oyama, K., Hirono, Y., Tsukada, T., Fujimura, T., and Ohta, T. (2016). Paclitaxel plus valproic acid versus paclitaxel alone as second- or third-line therapy for advanced gastric cancer: a randomized Phase II trial. Drug Des Devel Ther *10*, 2353–2358.

Gaiddon C, de Tapia M, Loeffler JP. (1999). The tissue-specific transcription factor Pit-1/GHF-1 binds to the c-fos serum response element and activates c-fos transcription. Mol Endocrinol; 13: 742-751.

Gaiddon, C., Lokshin, M., Ahn, J., Zhang, T., and Prives, C. (2001). A subset of tumor-derived mutant forms of p53 down-regulate p63 and p73 through a direct interaction with the p53 core domain. Mol. Cell. Biol. *21*, 1874–1887.

Gaiddon, C., et al. (2001). "A Subset of Tumor-Derived Mutant Forms of p53 Down-Regulate p63 and p73 through a Direct Interaction with the p53 Core Domain." <u>Mol Cell Biol</u> **21**(5): 1874-1887.

Gates, L.A., Shi, J., Rohira, A.D., Feng, Q., Zhu, B., Bedford, M.T., Sagum, C.A., Jung, S.Y., Qin, J., Tsai, M.-J., et al. (2017). Acetylation on histone H3 lysine 9 mediates a switch from transcription initiation to elongation. J. Biol. Chem. jbc.M117.802074.

Ge, S., Xia, X., Ding, C., Zhen, B., Zhou, Q., Feng, J., Yuan, J., Chen, R., Li, Y., Ge, Z., et al. (2018). A proteomic landscape of diffuse-type gastric cancer. Nature Communications *9*, 1012.

Geng, H., Harvey, C.T., Pittsenbarger, J., Liu, Q., Beer, T.M., Xue, C., and Qian, D.Z. (2011). HDAC4 protein regulates HIF1α protein lysine acetylation and cancer cell response to hypoxia. J. Biol. Chem. *286*, 38095–38102.

Geng, H., Liu, Q., Xue, C., David, L.L., Beer, T.M., Thomas, G.V., Dai, M.-S., and Qian, D.Z. (2012). HIF1α protein stability is increased by acetylation at lysine 709. J. Biol. Chem. *287*, 35496–35505.

Ghaleb, A.M., Elkarim, E.A., Bialkowska, A.B., and Yang, V.W. (2016). KLF4 Suppresses Tumor Formation in Genetic and Pharmacological Mouse Models of Colonic Tumorigenesis. Mol Cancer Res *14*, 385–396.

Gigek, C.O., Chen, E.S., Calcagno, D.Q., Wisnieski, F., Burbano, R.R., and Smith, M.A.C. (2012). Epigenetic mechanisms in gastric cancer. Epigenomics *4*, 279–294.

Gomceli, I., Demiriz, B., and Tez, M. (2012). Gastric carcinogenesis. World J Gastroenterol *18*, 5164–5170.

Grabsch HI, Tan P. (2013). Gastric cancer pathology and underlying molecular mechanisms. Dig Surg; 30: 150-158.

Greene, W.C., and Chen, L. (2004). Regulation of NF-kappaB action by reversible acetylation. Novartis Found. Symp. *259*, 208–217; discussion 218-225.

Griffiths, E.A., Pritchard, S.A., Valentine, H.R., Whitchelo, N., Bishop, P.W., Ebert, M.P., Price, P.M., Welch, I.M., and West, C.M.L. (2007). Hypoxia-inducible factor-1α expression in the gastric carcinogenesis sequence and its prognostic role in gastric and gastro-oesophageal adenocarcinomas. British Journal of Cancer *96*, 95–103.

Gross, I., Duluc, I., Benameur, T., Calon, A., Martin, E., Brabletz, T., Kedinger, M., Domon-Dell, C., and Freund, J.-N. (2008). The intestine-specific homeobox gene Cdx2 decreases mobility and antagonizes dissemination of colon cancer cells. Oncogene *27*, 107–115.

Gu, L., Chen, M., Guo, D., Zhu, H., Zhang, W., Pan, J., Zhong, X., Li, X., Qian, H., and Wang, X. (2017). PD-L1 and gastric cancer prognosis: A systematic review and meta-analysis. PLoS ONE *12*, e0182692.

Guadagno, T.M., and Newport, J.W. (1996). Cdk2 Kinase Is Required for Entry into Mitosis as a Positive Regulator of Cdc2–Cyclin B Kinase Activity. Cell *84*, 73–82.

Günther, T., Schneider-Stock, R., Häckel, C., Kasper, H.-U., Pross, M., Hackelsberger, A., Lippert, H., and Roessner, A. (2000). *Mdm2* Gene Amplification in Gastric Cancer Correlation with Expression of Mdm2 Protein and *p53* Alterations. Modern Pathology *13*, 621–626.

Hacker S, Karl S, Mader I, Cristofanon S, Schweitzer T, Krauss J *et al*. (2011). Histone deacetylase inhibitors prime medulloblastoma cells for chemotherapy-induced apoptosis by enhancing p53-dependent Bax activation. Oncogene; 30: 2275-2281.

Hagelkruys, A., Sawicka, A., Rennmayr, M., and Seiser, C. (2011). The biology of HDAC in cancer: the nuclear and epigenetic components. Handb Exp Pharmacol *206*, 13–37.

Hatakeyama, M. (2004). Oncogenic mechanisms of the Helicobacter pylori CagA protein. Nat. Rev. Cancer *4*, 688–694.

Hayashi, M., Inokuchi, M., Takagi, Y., Yamada, H., Kojima, K., Kumagai, J., Kawano, T., and Sugihara, K. (2008). High expression of HER3 is associated with a decreased survival in gastric cancer. Clin. Cancer Res. *14*, 7843–7849.

He, Q., Li, G., Wang, X., Wang, S., Hu, J., Yang, L., He, Y., Pan, Y., Yu, D., and Wu, Y. (2017). A Decrease of Histone Deacetylase 6 Expression Caused by Helicobacter Pylori Infection is Associated with Oncogenic Transformation in Gastric Cancer. Cell. Physiol. Biochem. *42*, 1326–1335.

Heim, S., and Lage, H. (2005). Transcriptome analysis of different multidrug-resistant gastric carcinoma cells. In Vivo *19*, 583–590.

Henderson C, Mizzau M, Paroni G, Maestro R, Schneider C, Brancolini C. (2003) Role of caspases, Bid, and p53 in the apoptotic response triggered by histone deacetylase inhibitors trichostatin-A (TSA) and suberoylanilide hydroxamic acid (SAHA). J Biol Chem; 278: 12579-12589.

Hong, L., Yang, Z., Ma, J., and Fan, D. (2013). Function of miRNA in controlling drug resistance of human cancers. Curr Drug Targets *14*, 1118–1127.

Hu, B., El Hajj, N., Sittler, S., Lammert, N., Barnes, R., and Meloni-Ehrig, A. (2012). Gastric cancer: Classification, histology and application of molecular pathology. J Gastrointest Oncol *3*, 251–261.

Hu, X.-F., Yao, J., Gao, S.-G., Wang, X.-S., Peng, X.-Q., Yang, Y.-T., and Feng, X.-S. (2013). Nrf2 overexpression predicts prognosis and 5-FU resistance in gastric cancer. Asian Pac. J. Cancer Prev. *14*, 5231–5235.

Huang C, Ida H, Ito K, Zhang H, Ito Y. (2007). Contribution of reactivated RUNX3 to inhibition of gastric cancer cell growth following suberoylanilide hydroxamic acid (vorinostat) treatment. Biochem Pharmacol; 73: 990-1000.

Huang L, Sowa Y, Sakai T, Pardee AB. (2000). Activation of the p21WAF1/CIP1 promoter independent of p53 by the histone deacetylase inhibitor suberoylanilide hydroxamic acid (SAHA) through the Sp1 sites. Oncogene; 19: 5712-5719.

Huang, D., Duan, H., Huang, H., Tong, X., Han, Y., Ru, G., Qu, L., Shou, C., and Zhao, Z. (2016). Cisplatin resistance in gastric cancer cells is associated with HER2 upregulation-induced epithelial-mesenchymal transition. Sci Rep *6*, 20502.

Huang, G., and Zhu, G. (2018). Sirtuin-4 (SIRT4), a therapeutic target with oncogenic and tumor-suppressive activity in cancer. Onco Targets Ther *11*, 3395–3400.
Huang, K.-H., Hsu, C.-C., Fang, W.-L., Chi, C.-W., Sung, M.-T., Kao, H.-L., Li, A.F.-Y., Yin, P.-H., Yang, M.-H., and Lee, H.-C. (2014). SIRT3 expression as a biomarker for better prognosis in gastric cancer. World J Surg *38*, 910–917.

Human cell culture Volume II Cancer cell lines Part 2. (2002). Klumwer Academic Publishers. Masters, J.R.W., and Palsson B. Editors.

Humar, B., Graziano, F., Cascinu, S., Catalano, V., Ruzzo, A.M., Magnani, M., Toro, T., Burchill, T., Futschik, M.E., Merriman, T., et al. (2002). Association of *CDH1* haplotypes with susceptibility to sporadic diffuse gastric cancer. Oncogene *21*, 8192–8195.

Imbriano, C., Gurtner, A., Cocchiarella, F., Di Agostino, S., Basile, V., Gostissa, M., Dobbelstein, M., Del Sal, G., Piaggio, G., and Mantovani, R. (2005). Direct p53 Transcriptional Repression: In Vivo Analysis of CCAAT-Containing G2/M Promoters. Mol Cell Biol *25*, 3737–3751.

Ishiguro, H., Kimura, M., and Takeyama, H. (2014). Role of microRNAs in gastric cancer. World J Gastroenterol *20*, 5694–5699.

Jang, S.-H., Kim, K.-J., Oh, M.-H., Lee, J.-H., Lee, H.J., Cho, H.D., Han, S.W., Son, M.W., and Lee, M.S. (2016). Clinicopathological Significance of Elevated PIK3CA Expression in Gastric Cancer. J Gastric Cancer *16*, 85–92.

Jencks, D.S., Adam, J.D., Borum, M.L., Koh, J.M., Stephen, S., and Doman, D.B. (2018). Overview of Current Concepts in Gastric Intestinal Metaplasia and Gastric Cancer. Gastroenterol Hepatol (N Y) *14*, 92–101.

Jin, Z., Jiang, W., Jiao, F., Guo, Z., Hu, H., Wang, L., and Wang, L. (2014). Decreased expression of histone deacetylase 10 predicts poor prognosis of gastric cancer patients. Int J Clin Exp Pathol *7*, 5872–5879.

Joo, H.-Y., Yun, M., Jeong, J., Park, E.-R., Shin, H.-J., Woo, S.R., Jung, J.K., Kim, Y.-M., Park, J.-J., Kim, J., et al. (2015). SIRT1 deacetylates and stabilizes hypoxia-inducible factor-1α (HIF-1α) via direct interactions during hypoxia. Biochem. Biophys. Res. Commun. *462*, 294–300.

Juan, L.J., Shia, W.J., Chen, M.H., Yang, W.M., Seto, E., Lin, Y.S., and Wu, C.W. (2000). Histone deacetylases specifically down-regulate p53-dependent gene activation. J. Biol. Chem. *275*, 20436–20443.

Jung, K.H., Noh, J.H., Kim, J.K., Eun, J.W., Bae, H.J., Chang, Y.G., Kim, M.G., Park, W.S., Lee, J.Y., Lee, S.-Y., et al. (2012). Histone deacetylase 6 functions as a tumor suppressor by activating c-Jun NH2-terminal kinase-mediated beclin 1-dependent autophagic cell death in liver cancer. Hepatology *56*, 644–657.

Kandel, C., Leclair, F., Bou-Hanna, C., Laboisse, C.L., and Mosnier, J.-F. (2014). Association of HER1 amplification with poor prognosis in well differentiated gastric carcinomas. J. Clin. Pathol. *67*, 307–312.

Kang, W., Tong, J.H., Chan, A.W., Zhao, J., Dong, Y., Wang, S., Yang, W., Sin, F.M., Ng, S.S., Yu, J., et al. (2014). Yin Yang 1 contributes to gastric carcinogenesis and its nuclear expression correlates with shorter survival in patients with early stage gastric adenocarcinoma. J Transl Med *12*, 80.

Kang, Y.-K., Boku, N., Satoh, T., Ryu, M.-H., Chao, Y., Kato, K., Chung, H.C., Chen, J.-S., Muro, K., Kang, W.K., et al. (2017). Nivolumab in patients with advanced gastric or gastro-esophageal junction cancer refractory to, or intolerant of, at least two previous chemotherapy regimens (ONO-4538-12, ATTRACTION-2): a randomized, double-blind, placebo-controlled, phase 3 trial. The Lancet *390*, 2461–2471.

Kang, Z.-H., Wang, C.-Y., Zhang, W.-L., Zhang, J.-T., Yuan, C.-H., Zhao, P.-W., Lin, Y.-Y., Hong, S., Li, C.-Y., and Wang, L. (2014). Histone Deacetylase HDAC4 Promotes Gastric Cancer SGC-7901 Cells Progression via p21 Repression. PLOS ONE *9*, e98894.

Katoh, Y., and Katoh, M. (2005). Hedgehog signaling pathway and gastric cancer. Cancer Biology & Therapy *4*, 1050–1054.

Kelly WK, Marks PA. (2005). Drug insight: Histone deacetylase inhibitors--development of the new targeted anticancer agent suberoylanilide hydroxamic acid. Nat Clin Pract Oncol; 2: 150-157.

Kim MS, Blake M, Baek JH, Kohlhagen G, Pommier Y, Carrier F. (2003). Inhibition of histone deacetylase increases cytotoxicity to anticancer drugs targeting DNA. Cancer Res; 63: 7291-7300.

Kim, E., H. Bisson, W., V. Löhr, C., E. Williams, D., Ho, E., H. Dashwood, R., and Rajendran, P. (2015). Histone and Non-Histone Targets of Dietary Deacetylase Inhibitors. Current Topics in Medicinal Chemistry *16*, 714–731.

Kim, G.R., Cho, S.-N., Kim, H.-S., Yu, S.Y., Choi, S.Y., Ryu, Y., Lin, M.Q., Jin, L., Kee, H.J., and Jeong, M.H. (2016). Histone deacetylase and GATA-binding factor 6 regulate arterial remodeling in angiotensin II-induced hypertension. J. Hypertens. *34*, 2206–2219.

Kim, H.S., Shen, Q., and Nam, S.W. (2015). Histone Deacetylases and Their Regulatory MicroRNAs in Hepatocarcinogenesis. J Korean Med Sci *30*, 1375–1380.

Kim, J., Kim, N., Park, J.H., Chang, H., Kim, J.Y., Lee, D.H., Kim, J.M., Kim, J.S., and Jung, H.C. (2013). The Effect of Helicobacter pylori on Epidermal Growth Factor Receptor-Induced Signal Transduction and the Preventive Effect of Celecoxib in Gastric Cancer Cells. Gut Liver *7*, 552–559.

Kim, J.K., Noh, J.H., Eun, J.W., Jung, K.H., Bae, H.J., Shen, Q., Kim, M.G., Chang, Y.G., Kim, S.-J., Park, W.S., et al. (2013). Targeted inactivation of HDAC2 restores p16INK4a activity and exerts antitumor effects on human gastric cancer. Mol. Cancer Res. *11*, 62–73.

Kim, K.-J., Jung, H.Y., Oh, M.-H., Cho, H., Lee, J.-H., Lee, H.J., Jang, S.-H., and Lee, M.S. (2015). Loss of ARID1A Expression in Gastric Cancer: Correlation with Mismatch Repair Deficiency and Clinicopathologic Features. J Gastric Cancer *15*, 201–208.

Kim, M.-G., Pak, J.H., Choi, W.H., Park, J.-Y., Nam, J.-H., and Kim, J.-H. (2012). The relationship between cisplatin resistance and histone deacetylase isoform overexpression in epithelial ovarian cancer cell lines. Journal of Gynecologic Oncology *23*, 182.

Kim, S.-H., Jeong, J.-W., Park, J.A., Lee, J.-W., Seo, J.H., Jung, B.-K., Bae, M.-K., and Kim, K.-W. (2007). Regulation of the HIF-1alpha stability by histone deacetylases. Oncol. Rep. *17*, 647–651.

Kim, Y.-K., Yu, J., Han, T.S., Park, S.-Y., Namkoong, B., Kim, D.H., Hur, K., Yoo, M.-W., Lee, H.-J., Yang, H.-K., et al. (2009). Functional links between clustered microRNAs: suppression of cell-cycle inhibitors by microRNA clusters in gastric cancer. Nucleic Acids Res *37*, 1672–1681.

Kitajima, Y., and Miyazaki, K. (2013). The Critical Impact of HIF-1α on Gastric Cancer Biology. Cancers (Basel) *5*, 15–26.

Komatsu N, Kawamata N, Takeuchi S, Yin D, Chien W, Miller CW *et al*. (2006). SAHA, a HDAC inhibitor, has profound anti-growth activity against non-small cell lung cancer cells. Oncol Rep; 15: 187-191.

Kovacs, J.J., Murphy, P.J.M., Gaillard, S., Zhao, X., Wu, J.-T., Nicchitta, C.V., Yoshida, M., Toft, D.O., Pratt, W.B., and Yao, T.-P. (2005). HDAC6 regulates Hsp90 acetylation and chaperone-dependent activation of glucocorticoid receptor. Mol. Cell *18*, 601–607.

Kufe, D.W. (2009). Mucins in cancer: function, prognosis and therapy. Nat. Rev. Cancer *9*, 874–885.

Kulić, A., Sirotković-Skerlev, M., Dedić Plavetić, N., Belev, B., Kralik-Oguić, S., Ivić, M., and Vrbanec, D. (2014). Sirtuins in tumorigenesis. Periodicum Biologorum *116*, 381–386.

Kupcinskaite-Noreikiene, R., Ugenskiene, R., Noreika, A., Rudzianskas, V., Gedminaite, J., Skieceviciene, J., and Juozaityte, E. (2016). Gene methylation profile of gastric cancerous tissue according to tumor site in the stomach. BMC Cancer *16*.

Labisso WL, Wirth M, Stojanovic N, Stauber RH, Schnieke A, Schmid RM *et al*. (2012). MYC directs transcription of MCL1 and eIF4E genes to control sensitivity of gastric cancer cells toward HDAC inhibitors. Cell cycle (Georgetown, Tex; 11: 1593-1602.

Lambert, J.M.R., Gorzov, P., Veprintsev, D.B., Söderqvist, M., Segerbäck, D., Bergman, J., Fersht, A.R., Hainaut, P., Wiman, K.G., and Bykov, V.J.N. (2009). PRIMA-1 reactivates mutant p53 by covalent binding to the core domain. Cancer Cell *15*, 376–388.

Lambert, R. (2010). Épidémiologie du cancer gastrique dans le monde. Cancéro digest II. [French]

Lee MJ, Kim YS, Kummar S, Giaccone G, Trepel JB. (2008). Histone deacetylase inhibitors in cancer therapy. Curr Opin Oncol; 20: 639-649.

Lee, J.-H., Choy, M.L., and Marks, P.A. (2012). Mechanisms of resistance to histone deacetylase inhibitors. Adv. Cancer Res. *116*, 39–86.

Lee, J.-H., Jeong, E.-G., Choi, M.-C., Kim, S.-H., Park, J.-H., Song, S.-H., Park, J., Bang, Y.-J., and Kim, T.-Y. (2010). Inhibition of histone deacetylase 10 induces thioredoxin-interacting protein and causes accumulation of reactive oxygen species in SNU-620 human gastric cancer cells. Mol. Cells *30*, 107–112.

Lee, S.H., Lee, J.W., Soung, Y.H., Kim, H.S., Park, W.S., Kim, S.Y., Lee, J.H., Park, J.Y., Cho, Y.G., Kim, C.J., et al. (2003). *BRAF* and *KRAS* mutations in stomach cancer. Oncogene *22*, 6942–6945.

Lee, S.-J., Hwang, S.-O., Noh, E.J., Kim, D.-U., Nam, M., Kim, J.H., Nam, J.H., and Hoe, K.-L. (2014). Transactivation of bad by vorinostat-induced acetylated p53 enhances doxorubicin-induced cytotoxicity in cervical cancer cells. Exp. Mol. Med. *46*, e76.

Lee, Y.-C., Chiang, T.-H., Chou, C.-K., Tu, Y.-K., Liao, W.-C., Wu, M.-S., and Graham, D.Y. (2016). Association Between Helicobacter pylori Eradication and Gastric Cancer Incidence: A Systematic Review and Meta-analysis. Gastroenterology *150*, 1113-1124.e5.

Lerin, C., Rodgers, J.T., Kalume, D.E., Kim, S., Pandey, A., and Puigserver, P. (2006). GCN5 acetyltransferase complex controls glucose metabolism through transcriptional repression of PGC-1alpha. Cell Metab. *3*, 429–438.

Lévy, L., Wei, Y., Labalette, C., Wu, Y., Renard, C.-A., Buendia, M.A., and Neuveut, C. (2004). Acetylation of β-Catenin by p300 Regulates β-Catenin-Tcf4 Interaction. Mol. Cell. Biol. *24*, 3404–3414.

Li D, Marchenko ND, Moll UM. (2011). SAHA shows preferential cytotoxicity in mutant p53 cancer cells by destabilizing mutant p53 through inhibition of the HDAC6-Hsp90 chaperone axis. Cell Death Differ; 18: 1904-1913.

Li, A., Liu, Z., Li, M., Zhou, S., Xu, Y., Xiao, Y., and Yang, W. (2016). HDAC5, a potential therapeutic target and prognostic biomarker, promotes proliferation, invasion and migration in human breast cancer. Oncotarget *7*.

Li, G., Jiang, H., Chang, M., Xie, H., and Hu, L. (2011). HDAC6 α-tubulin deacetylase: a potential therapeutic target in neurodegenerative diseases. J. Neurol. Sci. *304*, 1–8.

Li, J., Zou, K., Yu, L., Zhao, W., Lu, Y., Mao, J., Wang, B., Wang, L., Fan, S., Song, B., et al. (2018). MicroRNA-140 Inhibits the Epithelial-Mesenchymal Transition and Metastasis in Colorectal Cancer. Molecular Therapy - Nucleic Acids *10*, 426–437.

Li, L., and Yang, X.-J. (2015). Tubulin acetylation: responsible enzymes, biological functions and human diseases. Cell. Mol. Life Sci. *72*, 4237–4255.

Li, N., Xie, C., and Lu, N.-H. (2016). p53, a potential predictor of Helicobacter pylori infection-associated gastric carcinogenesis? Oncotarget *7*, 66276–66286.

Li, Q., Yao, Y., Eades, G., Liu, Z., Zhang, Y., and Zhou, Q. (2014). Downregulation of miR-140 promotes cancer stem cell formation in basal-like early stage breast cancer. Oncogene *33*, 2589–2600.

Li, S., Wang, F., Qu, Y., Chen, X., Gao, M., Yang, J., Zhang, D., Zhang, N., Li, W., and Liu, H. (2017). HDAC2 regulates cell proliferation, cell cycle progression and cell apoptosis in esophageal squamous cell carcinoma EC9706 cells. Oncol Lett *13*, 403–409.

Li, Y., and Seto, E. (2017). HDACs and HDAC Inhibitors in Cancer Development and Therapy. Cold Spring Harb Perspect Med *6*, a026831.

Li, Y., Liang, J., and Hou, P. (2015). Hypermethylation in gastric cancer. Clinica Chimica Acta *448*, 124–132.

Li, Y., Peng, L., and Seto, E. (2015). Histone Deacetylase 10 Regulates the Cell Cycle G2/M Phase Transition via a Novel Let-7–HMGA2–Cyclin A2 Pathway. Mol. Cell. Biol. *35*, 3547–3565.

Li, Y., Zhang, X., Polakiewicz, R.D., Yao, T.-P., and Comb, M.J. (2008). HDAC6 Is Required for Epidermal Growth Factor-induced β-Catenin Nuclear Localization. J. Biol. Chem. *283*, 12686–12690.

Li, Z., and Zhu, W.-G. (2014). Targeting Histone Deacetylases for Cancer Therapy: From Molecular Mechanisms to Clinical Implications. Int J Biol Sci *10*, 757–770.

Licona, C., Spaety, M.-E., Capuozzo, A., Ali, M., Santamaria, R., Armant, O., Delalande, F., Van Dorsselaer, A., Cianferani, S., Spencer, J., et al. (2017). A ruthenium anticancer compound interacts with histones and impacts differently on epigenetic and death pathways compared to Cisplatin. Oncotarget *8*.

Lin CT, Lai HC, Lee HY, Lin WH, Chang CC, Chu TY *et al.* (2008). Valproic acid resensitizes Cisplatin-resistant ovarian cancer cells. Cancer Sci; 99: 1218-1226.

Lin, J., Huo, R., Xiao, L., Zhu, X., Xie, J., Sun, S., He, Y., Zhang, J., Sun, Y., Zhou, Z., et al. (2014). A novel p53/microRNA-22/Cyr61 axis in synovial cells regulates inflammation in rheumatoid arthritis. Arthritis & Rheumatology (Hoboken, N.J.) *66*, 49–59.

Lin, L., Jiang, H., Huang, M., Hou, X., Sun, X., Jiang, X., Dong, X., Sun, X., Zhou, B., and Qiao, H. (2015). Depletion of histone deacetylase 1 inhibits metastatic abilities of gastric cancer cells by regulating the miR-34a/CD44 pathway. Oncol. Rep. *34*, 663–672.

Liu X., Wilcken R., Joerger AC., Chuckowree IS., Amin J., Spencer J., and Fersht AR. (2013). Small molecule induced reactivation of mutant p53 in cancer cells. Nucleic Acids Research; 41: 6034-6043

Liu, G., Xin, Z.-C., Chen, L., Tian, L., Yuan, Y.-M., Song, W.-D., Jiang, X.-J., and Guo, Y.-L. (2007). Expression and localization of CKLFSF2 in human spermatogenesis. Asian J. Androl. *9*, 189–198.

Liu, J., Wen, D., Fang, X., Wang, X., Liu, T., and Zhu, J. (2015). p38MAPK Signaling Enhances Glycolysis Through the Up-Regulation of the Glucose Transporter GLUT-4 in Gastric Cancer Cells. Cell. Physiol. Biochem. *36*, 155–165.

Liu, J., Zhang, C., Zhao, Y., and Feng, Z. (2017). MicroRNA Control of p53. J. Cell. Biochem. *118*, 7–14.

Liu, Q., Teh, M., Ito, K., Shah, N., Ito, Y., and Yeoh, K.G. (2007). CDX2 expression is progressively decreased in human gastric intestinal metaplasia, dysplasia and cancer. Mod. Pathol. *20*, 1286–1297.

Liu, Y., Xia, R., Lu, K., Xie, M., Yang, F., Sun, M., De, W., Wang, C., and Ji, G. (2017). LincRNAFEZF1-AS1 represses p21 expression to promote gastric cancer proliferation through LSD1-Mediated H3K4me2 demethylation. Mol Cancer *16*.

Liu, Y.L., Lai, F., Wilmott, J.S., Yan, X.G., Liu, X.Y., Luan, Q., Guo, S.T., Jiang, C.C., Tseng, H.-Y., Scolyer, R.A., et al. (2014). Noxa upregulation by oncogenic activation of MEK/ERK through CREB promotes autophagy in human melanoma cells. Oncotarget *5*, 11237–11251.

Liu, Y.-P., Ling, Y., Qi, Q.-F., Zhang, Y.-P., Zhang, C.-S., Zhu, C.-T., Wang, M.-H., and Pan, Y.-D. (2013). The effects of ERCC1 expression levels on the chemosensitivity of gastric cancer cells to platinum agents and survival in gastric cancer patients treated with oxaliplatin-based adjuvant chemotherapy. Oncol Lett *5*, 935–942.

Liu, Z., Shao, Y., Tan, L., Shi, H., Chen, S., and Guo, J. (2014). Clinical significance of the low expression of FER1L4 in gastric cancer patients. Tumour Biol. *35*, 9613–9617.

Livak, K.J., and Schmittgen, T.D. (2001). Analysis of relative gene expression data using real-time quantitative PCR and the 2(-Delta Delta C(T)) Method. Methods *25*, 402–408.

Lledo, G., Mariette, C., Raoul, JL., Dahan, L., Landi, B., Conroy, T., Piessen, G., Tougeron, D., Créhange, G., Lepillez, V., Artru, P., Drouillard, A., Bosset. JF. « Cancer de l'œsophage ». Thésaurus National de Cancérologie Digestive, 09-2016, [En ligne] http://www.tncd.org

Loh, J.T., Torres, V.J., and Cover, T.L. (2007). Regulation of Helicobacter pylori cagA expression in response to salt. Cancer Res. *67*, 4709–4715.

López, I., Tournillon, A.-S., Prado Martins, R., Karakostis, K., Malbert-Colas, L., Nylander, K., and Fåhraeus, R. (2017). p53-mediated suppression of BiP triggers BIK-induced apoptosis during prolonged endoplasmic reticulum stress. Cell Death Differ. *24*, 1717–1729.

Lu, H., Yang, X.-F., Tian, X.-Q., Tang, S.-L., Li, L.-Q., Zhao, S., and Zheng, H.-C. (2016). The in vitro and vivo anti-tumor effects and molecular mechanisms of suberoylanilide hydroxamic acid (SAHA) and MG132 on the aggressive phenotypes of gastric cancer cells. Oncotarget *7*, 56508–56525.

Lu, W., You, R., Yuan, X., Yang, T., Samuel, E.L.G., Marcano, D.C., Sikkema, W.K.A., Tour, J.M., Rodriguez, A., Kheradmand, F., et al. (2015). The microRNA miR-22 inhibits the histone deacetylase HDAC4 to promote T(H)17 cell-dependent emphysema. Nat. Immunol. *16*, 1185–1194.

Ma, G., Wang, Y., Li, Y., Cui, L., Zhao, Y., Zhao, B., and Li, K. (2015). MiR-206, a Key Modulator of Skeletal Muscle Development and Disease. Int J Biol Sci *11*, 345–352.

Ma, J., Shen, H., Kapesa, L., and Zeng, S. (2016). Lauren classification and individualized chemotherapy in gastric cancer. Oncology Letters *11*, 2959–2964.

Ma, K., Baloch, Z., He, T.-T., and Xia, X. (2017). Alcohol Consumption and Gastric Cancer Risk: A Meta-Analysis. Med Sci Monit *23*, 238–246.

Ma, Q. (2013). Role of Nrf2 in Oxidative Stress and Toxicity. Annu Rev Pharmacol Toxicol *53*, 401–426.

Ma, Y., Shi, Y., Li, W., Sun, A., Zang, P., and Zhang, P. (2014). Epigallocatechin-3-gallate regulates the expression of Kruppel-like factor 4 through myocyte enhancer factor 2A. Cell Stress Chaperones *19*, 217–226.

Machado, J.C., Nogueira, A.M., Carneiro, F., Reis, C.A., and Sobrinho-Simões, M. (2000). Gastric carcinoma exhibits distinct types of cell differentiation: an immunohistochemical study of trefoil peptides (TFF1 and TFF2) and mucins (MUC1, MUC2, MUC5AC, and MUC6). J. Pathol. *190*, 437–443.

Machado, J.C., Oliveira, C., Carvalho, R., Soares, P., Berx, G., Caldas, C., Seruca, R., Carneiro, F., and Sobrinho-Simöes, M. (2001). E-cadherin gene (*CDH1*) promoter methylation as the second hit in sporadic diffuse gastric carcinoma. Oncogene *20*, 1525–1528.

Mahu C, Purcarea AP, Gheorghe CM, Purcarea MR. (2014). Molecular events in gastric carcinogenesis. J Med Life; 7: 375-378.

Mal, A., Sturniolo, M., Schiltz, R.L., Ghosh, M.K., and Harter, M.L. (2001). A role for histone deacetylase HDAC1 in modulating the transcriptional activity of MyoD: inhibition of the myogenic program. EMBO J *20*, 1739–1753.

Manal M, Chandrasekar MJ, Gomathi Priya J, Nanjan MJ. (2016). Inhibitors of histone deacetylase as antitumor agents: A critical review. Bioorg Chem; 67: 18-42.

Manal, M., Chandrasekar, M.J.N., Gomathi Priya, J., and Nanjan, M.J. (2016). Inhibitors of histone deacetylase as antitumor agents: A critical review. Bioorganic Chemistry *67*, 18–42.

Marek, L., Hamacher, A., Hansen, F.K., Kuna, K., Gohlke, H., Kassack, M.U., and Kurz, T. (2013). Histone deacetylase (HDAC) inhibitors with a novel connecting unit linker region reveal a selectivity profile for HDAC4 and HDAC5 with improved activity against chemoresistant cancer cells. J. Med. Chem. *56*, 427–436.

Mariadason, J.M., Corner, G.A., and Augenlicht, L.H. (2000). Genetic reprogramming in pathways of colonic cell maturation induced by short chain fatty acids: comparison with trichostatin A, sulindac, and curcumin and implications for chemoprevention of colon cancer. Cancer Res. *60*, 4561–4572.

Markham, D., Munro, S., Soloway, J., O'Connor, D.P., and La Thangue, N.B. (2006). DNA-damage-responsive acetylation of pRb regulates binding to E2F-1. EMBO Rep *7*, 192–198.

Marks P, Rifkind RA, Richon VM, Breslow R, Miller T, Kelly WK. (2001). Histone deacetylases and cancer: causes and therapies. Nat Rev Cancer; 1: 194-202.

Martínez-Balbás, M.A., Bauer, U.M., Nielsen, S.J., Brehm, A., and Kouzarides, T. (2000). Regulation of E2F1 activity by acetylation. EMBO J. *19*, 662–671.

Martinez-Balibrea, E., Martínez-Cardús, A., Ginés, A., Porras, V.R. de, Moutinho, C., Layos, L., Manzano, J.L., Bugés, C., Bystrup, S., Esteller, M., et al. (2015). Tumor-Related Molecular Mechanisms of Oxaliplatin Resistance. Mol Cancer Ther *14*, 1767–1776.

Masood, M.A., Loya, A., and Yusuf, M.A. (2016). CDX2 as a prognostic marker in gastric cancer. Acta Gastroenterol. Belg. *79*, 197–200.

Matsumoto, Y., Marusawa, H., Kinoshita, K., Endo, Y., Kou, T., Morisawa, T., Azuma, T., Okazaki, I.-M., Honjo, T., and Chiba, T. (2007). Helicobacter pylori infection triggers aberrant expression of activation-induced cytidine deaminase in gastric epithelium. Nat. Med. *13*, 470–476.

Matsuoka, T., and Yashiro, M. (2014). The Role of PI3K/Akt/mTOR Signaling in Gastric Carcinoma. Cancers (Basel) *6*, 1441–1463.

Matsuzaki, H., Daitoku, H., Hatta, M., Aoyama, H., Yoshimochi, K., and Fukamizu, A. (2005). Acetylation of Foxo1 alters its DNA-binding ability and sensitivity to phosphorylation. Proc. Natl. Acad. Sci. U.S.A. *102*, 11278–11283.

McClure, J.J., Li, X., and Chou, C.J. (2018). Chapter Six - Advances and Challenges of HDAC Inhibitors in Cancer Therapeutics. In Advances in Cancer Research, K.D. Tew, and P.B. Fisher, eds. (Academic Press), pp. 183–211.

Meng, Y., Gao, R., Ma, J., Zhao, J., Xu, E., Wang, C., and Zhou, X. (2017). MicroRNA-140-5p regulates osteosarcoma chemoresistance by targeting HMGN5 and autophagy. Scientific Reports *7*, 416.
Meng, Y., Gao, R., Ma, J., Zhao, J., Xu, E., Wang, C., and Zhou, X. (2017). MicroRNA-140-5p regulates osteosarcoma chemoresistance by targeting HMGN5 and autophagy. Sci Rep *7*, 416.

Messenger, S.W., Falkowski, M.A., Thomas, D.D.H., Jones, E.K., Hong, W., Giasano, H.Y., Boulis, N.M., and Groblewski, G.E. (2014). Vesicle Associated Membrane Protein 8 (VAMP8)-mediated Zymogen Granule Exocytosis Is Dependent on Endosomal Trafficking via the Constitutive-Like Secretory Pathway. J Biol Chem *289*, 28040–28053.

Michel, P., Buecher, B., Chapelle, N., Dubreuil, O., Meilleroux, J., Granger, V., Fares, N., Baumann, A., Benhaim, L., Lefort, C., Pezet, D., Vendrely, V., Zaanan, A. « Cancer de l'estomac » Thésaurus National de Cancérologie Digestive, Octobre 2017, en ligne [http://www.tncd.org]

Micheli, L., D'Andrea, G., Leonardi, L., and Tirone, F. (2017). HDAC1, HDAC4, and HDAC9 Bind to PC3/Tis21/Btg2 and Are Required for Its Inhibition of Cell Cycle Progression and Cyclin D1 Expression. J. Cell. Physiol. *232*, 1696–1707.

Mihmanli M, Ilhan E, Idiz UO, Alemdar A, Demir U. (2016). Recent developments and innovations in gastric cancer. World journal of gastroenterology: WJG; 22: 4307-4320.

Mihmanli, M., Ilhan, E., Idiz, U.O., Alemdar, A., and Demir, U. (2016). Recent developments and innovations in gastric cancer. World J Gastroenterol *22*, 4307–4320.

Mitsuda, Y., Morita, K., Kashiwazaki, G., Taniguchi, J., Bando, T., Obara, M., Hirata, M., Kataoka, T.R., Muto, M., Kaneda, Y., et al. (2018). RUNX1 positively regulates the ErbB2/HER2 signaling pathway through modulating SOS1 expression in gastric cancer cells. Sci Rep *8*, 6423.

Mohammadi Saravle, S., Ahmadi Hedayati, M., Mohammadi, E., Sheikhesmaeili, F., and Nikkhou, B. (2018). Sirt1 Gene Expression and Gastric Epithelial Cells Tumor Stage in Patients with Helicobacter pylori Infection. Asian Pac. J. Cancer Prev. *19*, 913–916.

Moll, U.M., and Slade, N. (2004). p63 and p73: Roles in Development and Tumor Formation11National Cancer Institute. Mol Cancer Res *2*, 371–386.

Moore G. (2012). *221B Baker Street.* Le Cherche Midi Editions [Selection of Sir Arthur Conan Doyle quotes].

Mottamal, M., Zheng, S., Huang, T.L., and Wang, G. (2015). Histone deacetylase inhibitors in clinical studies as templates for new anticancer agents. Molecules *20*, 3898–3941.

Mu, Y.-P., Tang, S., Sun, W.-J., Gao, W.-M., Wang, M., and Su, X.-L. (2014). Association of miR-193b down-regulation and miR-196a up-regulation with clinicopathological features and prognosis in gastric cancer. Asian Pac. J. Cancer Prev. *15*, 8893–8900.

Murray-Zmijewski, F., Lane, D.P., and Bourdon, J.-C. (2006). p53/p63/p73 isoforms: an orchestra of isoforms to harmonise cell differentiation and response to stress. Cell Death and Differentiation *13*, 962–972.

Mutze K, Langer R, Becker K, Ott K, Novotny A, Luber B *et al*. (2010). Histone deacetylase (HDAC) 1 and 2 expression and chemotherapy in gastric cancer. Ann Surg Oncol; 17: 3336-3343.

Mutze, K., Langer, R., Becker, K., Ott, K., Novotny, A., Luber, B., Hapfelmeier, A., Göttlicher, M., Höfler, H., and Keller, G. (2010). Histone Deacetylase (HDAC) 1 and 2 Expression and Chemotherapy in Gastric Cancer. Ann Surg Oncol *17*, 3336–3343.

Negmeldin, A.T., Padige, G., Bieliauskas, A.V., and Pflum, M.K.H. (2017). Structural Requirements of HDAC Inhibitors: SAHA Analogues Modified at the C2 Position Display HDAC6/8 Selectivity. ACS Med. Chem. Lett. *8*, 281–286.

Nishizawa, T., and Suzuki, H. (2015). Gastric Carcinogenesis and Underlying Molecular Mechanisms: Helicobacter pylori and Novel Targeted Therapy.

Noguchi, A., Kikuchi, K., Zheng, H., Takahashi, H., Miyagi, Y., Aoki, I., and Takano, Y. (2014). SIRT1 expression is associated with a poor prognosis, whereas DBC1 is associated with favorable outcomes in gastric cancer. Cancer Med *3*, 1553–1561.

Ogasawara, T. (2013). Cell cycle control factors and skeletal development. Japanese Dental Science Review *49*, 79–87.

Ong PS, Wang XQ, Lin HS, Chan SY, Ho PC. (2012). Synergistic effects of suberoylanilide hydroxamic acid combined with Cisplatin causing cell cycle arrest independent apoptosis in platinum-resistant ovarian cancer cells. International journal of oncology; 40: 1705-1713.

Oren M, Rotter V. (2010). Mutant p53 gain-of-function in cancer. Cold Spring Harb Perspect Biol; 2: a001107.

Osada, H., Tatematsu, Y., Saito, H., Yatabe, Y., Mitsudomi, T., and Takahashi, T. Reduced expression of class II histone deacetylase genes is associated with poor prognosis in lung cancer patients. International Journal of Cancer *112*, 26–32.

Osman AA, Neskey DM, Katsonis P, Patel AA, Ward AM, Hsu TK *et al*. (2015). Evolutionary Action Score of TP53 Coding Variants Is Predictive of Platinum Response in Head and Neck Cancer Patients. Cancer Res; 75: 1205-1215.

Ozawa, Y., Towatari, M., Tsuzuki, S., Hayakawa, F., Maeda, T., Miyata, Y., Tanimoto, M., and Saito, H. (2001). Histone deacetylase 3 associates with and represses the transcription factor GATA-2. Blood *98*, 2116–2123.

Padmanabhan, N., Ushijima, T., and Tan, P. (2017). How to stomach an epigenetic insult: the gastric cancer epigenome. Nat Rev Gastroenterol Hepatol *14*, 467–478.

Park, J.-H., Kim, T.-Y., Jong, H.-S., Kim, T.Y., Chun, Y.-S., Park, J.-W., Lee, C.-T., Jung, H.C., Kim, N.K., and Bang, Y.-J. (2003). Gastric epithelial reactive oxygen species prevent normoxic degradation of hypoxia-inducible factor-1alpha in gastric cancer cells. Clin. Cancer Res. *9*, 433–440.

Park, J.W., Kim, M.-S., Voon, D.C., Kim, S.-J., Bae, J., Mun, D.-G., Ko, S.-I., Kim, H.K., Lee, S.-W., and Kim, D.-Y. (2018). Multi-omics analysis identifies pathways and genes involved in diffuse-type gastric carcinogenesis induced by E-cadherin, p53, and Smad4 loss in mice. Mol. Carcinog.

Park, S., Lee, J., Kim, Y.H., Park, J., Shin, J.-W., and Nam, S. (2016). Clinical Relevance and Molecular Phenotypes in Gastric Cancer, of *TP53* Mutations and Gene Expressions, in Combination With Other Gene Mutations. Scientific Reports *6*, 34822.

Parker, J.P., Nimir, H., Griffith, D.M., Duff, B., Chubb, A.J., Brennan, M.P., Morgan, M.P., Egan, D.A., and Marmion, C.J. (2013). A novel platinum complex of the histone deacetylase inhibitor belinostat: Rational design, development and in vitro cytotoxicity. Journal of Inorganic Biochemistry *124*, 70–77.

Patel, J.H., Du, Y., Ard, P.G., Phillips, C., Carella, B., Chen, C.-J., Rakowski, C., Chatterjee, C., Lieberman, P.M., Lane, W.S., et al. (2004). The c-MYC Oncoprotein Is a Substrate of the Acetyltransferases hGCN5/PCAF and TIP60. Mol. Cell. Biol. *24*, 10826–10834.

Pejanovic, N., Hochrainer, K., Liu, T., Aerne, B.L., Soares, M.P., and Anrather, J. (2012). Regulation of Nuclear Factor κB (NF-κB) Transcriptional Activity via p65 Acetylation by the Chaperonin Containing TCP1 (CCT). PLOS ONE *7*, e42020.

Pettke A, Hotfilder M, Clemens D, Klco-Brosius S, Schaefer C, Potratz J *et al*. (2016). Suberanilohydroxamic acid (vorinostat) synergistically enhances the cytotoxicity of doxorubicin and Cisplatin in osteosarcoma cell lines. Anti-cancer drugs.

Pflaum, J., Schlosser, S., and Müller, M. (2014). p53 Family and Cellular Stress Responses in Cancer. Front. Oncol. *4*.

Pietrantonio, F., Fucà, G., Morano, F., Gloghini, A., Corso, S., Aprile, G., Perrone, F., Vita, F.D., Tamborini, E., Tomasello, G., et al. (2018). Biomarkers of Primary Resistance to Trastuzumab in HER2-Positive Metastatic Gastric Cancer Patients: the AMNESIA Case-Control Study. Clin Cancer Res *24*, 1082–1089.

Pietsch, E.C., Sykes, S.M., McMahon, S.B., and Murphy, M.E. (2008). The p53 family and programmed cell death. Oncogene *27*, 6507–6521.
Platet, N., Hinkel, I., Richert, L., Murdamoothoo, D., Moufok-Sadoun, A., Vanier, M., Lavalle, P., Gaiddon, C., Vautier, D., Freund, J.-N., et al. (2017). The tumor suppressor CDX2 opposes pro-metastatic biomechanical modifications of colon cancer cells through organization of the actin cytoskeleton. Cancer Lett. *386*, 57–64.

Polakovicova, I., Jerez, S., Wichmann, I.A., Sandoval-Bórquez, A., Carrasco-Véliz, N., and Corvalán, A.H. (2018). Role of microRNAs and Exosomes in Helicobacter pylori and Epstein-Barr Virus Associated Gastric Cancers. Front Microbiol *9*, 636.

Polom, K., Das, K., Marrelli, D., Roviello, G., Pascale, V., Voglino, C., Rho, H., Tan, P., and Roviello, F. (2017). KRAS Mutation in Gastric Cancer and Prognostication Associated with Microsatellite Instability Status. Pathol. Oncol. Res.

Praud, D., Rota, M., Pelucchi, C., Bertuccio, P., Rosso, T., Galeone, C., Zhang, Z.-F., Matsuo, K., Ito, H., Hu, J., et al. (2018). Cigarette smoking and gastric cancer in the Stomach Cancer Pooling (StoP) Project. Eur. J. Cancer Prev. *27*, 124–133.
Qian, H., and Yang, Y. (2016). Functional role of autophagy in gastric cancer. Oncotarget *7*, 17641–17651.

Qiang, L., Ji, Z., and Wang, X. (2018). Expression of TAp73α affects the therapy effect of chemotherapy drugs in gastric cancer. Oncol. Res.

Qiao, Y., Li, T., Zheng, S., and Wang, H. (2018). The Hippo pathway as a drug target in gastric cancer. Cancer Lett. *420*, 14–25.

Qu, Y., Dang, S., and Hou, P. (2013). Gene methylation in gastric cancer. Clinica Chimica Acta *424*, 53–65.

Quadri, H.S., Smaglo, B.G., Morales, S.J., Phillips, A.C., Martin, A.D., Chalhoub, W.M., Haddad, N.G., Unger, K.R., Levy, A.D., and Al-Refaie, W.B. (2017). Gastric Adenocarcinoma: A Multimodal Approach. Front Surg *4*.

Ree, A.H., Dueland, S., Folkvord, S., Hole, K.H., Seierstad, T., Johansen, M., Abrahamsen, T.W., and Flatmark, K. (2010). Vorinostat, a histone deacetylase inhibitor, combined with pelvic palliative radiotherapy for gastrointestinal carcinoma: the Pelvic Radiation and Vorinostat (PRAVO) phase 1 study. Lancet Oncol. *11*, 459–464.
Reed, S.M., and Quelle, D.E. (2014). p53 Acetylation: Regulation and Consequences. Cancers (Basel) *7*, 30–69.

Reinhardt, H.C., and Schumacher, B. (2012). The p53 network: cellular and systemic DNA damage responses in aging and cancer. Trends Genet. *28*, 128–136.

Ribeiro, J., Malta, M., Galaghar, A., Silva, F., Afonso, L.P., Medeiros, R., and Sousa, H. (2017). P53 deregulation in Epstein-Barr virus-associated gastric cancer. Cancer Letters *404*, 37–43.

Rikiishi H, Shinohara F, Sato T, Sato Y, Suzuki M, Echigo S. (2007). Chemosensitization of oral squamous cell carcinoma cells to Cisplatin by histone deacetylase inhibitor, suberoylanilide hydroxamic acid. International journal of oncology; 30: 1181-1188.

Riley, T., Sontag, E., Chen, P., and Levine, A. (2008). Transcriptional control of human p53-regulated genes. Nature Reviews Molecular Cell Biology *9*, 402–412.

Riquelme, I., Letelier, P., Riffo-Campos, A.L., Brebi, P., and Roa, J.C. (2016). Emerging Role of miRNAs in the Drug Resistance of Gastric Cancer. Int J Mol Sci *17*.

Rivas-Ortiz, C.I., Lopez-Vidal, Y., Arredondo-Hernandez, L.J.R., and Castillo-Rojas, G. (2017). Genetic Alterations in Gastric Cancer Associated with Helicobacter pylori Infection. Front. Med. *4*.

Rivlin N, Brosh R, Oren M, Rotter V. (2011). Mutations in the p53 Tumor Suppressor Gene: Important Milestones at the Various Steps of Tumorigenesis. Genes Cancer; 2: 466-474.

Rohwer, N., and Cramer, T. (2011). Hypoxia-mediated drug resistance: Novel insights on the functional interaction of HIFs and cell death pathways. Drug Resistance Updates *14*, 191–201.

Rokavec, M., Li, H., Jiang, L., and Hermeking, H. (2014). The p53/microRNA connection in gastrointestinal cancer. Clin Exp Gastroenterol *7*, 395–413.

Romeo, M.M., Ko, B., Kim, J., Brady, R., Heatley, H.C., He, J., Harrod, C.K., Barnett, B., Ratner, L., Lairmore, M.D., et al. (2015). Acetylation of the c-MYC oncoprotein is required for cooperation with the HTLV-1 p30II accessory protein and the induction of oncogenic cellular transformation by p30II/c-MYC. Virology *476*, 271–288.

Rowland, B.D., and Peeper, D.S. (2006). KLF4, p21 and context-dependent opposing forces in cancer. Nature Reviews Cancer *6*, 11–23.

Rufini, A., Agostini, M., Grespi, F., Tomasini, R., Sayan, B.S., Niklison-Chirou, M.V., Conforti, F., Velletri, T., Mastino, A., Mak, T.W., et al. (2011). p73 in Cancer. Genes Cancer *2*, 491–502.

Saadat, I., Higashi, H., Obuse, C., Umeda, M., Murata-Kamiya, N., Saito, Y., Lu, H., Ohnishi, N., Azuma, T., Suzuki, A., et al. (2007). Helicobacter pylori CagA targets PAR1/MARK kinase to disrupt epithelial cell polarity. Nature *447*, 330–333.

Saeki, N., Sakamoto, H., and Yoshida, T. (2014). Mucin 1 Gene (MUC1) and Gastric-Cancer Susceptibility. International Journal of Molecular Sciences *15*, 7958–7973.

Saju, P., Murata-Kamiya, N., Hayashi, T., Senda, Y., Nagase, L., Noda, S., Matsusaka, K., Funata, S., Kunita, A., Urabe, M., et al. (2016). Host SHP1 phosphatase antagonizes Helicobacter pylori CagA and can be downregulated by Epstein-Barr virus. Nat Microbiol *1*, 16026.

Sato T, Suzuki M, Sato Y, Echigo S, Rikiishi H. (2006). Sequence-dependent interaction between Cisplatin and histone deacetylase inhibitors in human oral squamous cell carcinoma cells. International journal of oncology; 28: 1233-1241.

Sehdev, V., Katsha, A., Arras, J., Peng, D., Soutto, M., Ecsedy, J., Zaika, A., Belkhiri, A., and El-Rifai, W. (2014). HDM2 Regulation by AURKA Promotes Cell Survival in Gastric Cancer. Clinical Cancer Research *20*, 76–86.

Sekar, D., Krishnan, R., Thirugnanasambantham, K., Rajasekaran, B., Islam, V.I.H., and Sekar, P. (2016). Significance of microRNA 21 in gastric cancer. Clin Res Hepatol Gastroenterol *40*, 538–545.

Shaaban, S., Negm, A., Ibrahim, E.E., and Elrazak, A.A. (2014). Chemotherapeutic Agents for the Treatment of Hepatocellular Carcinoma: Efficacy and Mode of Action. Oncol Rev *8*.

Shah, M.A., Khanin, R., Tang, L., Janjigian, Y.Y., Klimstra, D.S., Gerdes, H., and Kelsen, D.P. (2011). Molecular classification of gastric cancer: a new paradigm. Clin. Cancer Res. *17*, 2693–2701.

Shen, D.-W., Pouliot, L.M., Hall, M.D., and Gottesman, M.M. (2012). Cisplatin Resistance: A Cellular Self-Defense Mechanism Resulting from Multiple Epigenetic and Genetic Changes. Pharmacol Rev *64*, 706–721.

Shen, X., Li, P., Xu, Y., Chen, X., Sun, H., Zhao, Y., Liu, M., and Zhang, W. (2017). Association of sirtuins with clinicopathological parameters and overall survival in gastric cancer. Oncotarget *8*, 74359–74370.

Shen, Y.-F., Wei, A.-M., Kou, Q., Zhu, Q.-Y., and Zhang, L. (2016). Histone deacetylase 4 increases progressive epithelial ovarian cancer cells via repression of p21 on fibrillar collagen matrices. Oncol. Rep. *35*, 948–954.

Shi, D.-T., Han, M., Gao, N., Tian, W., and Chen, W. (2014). Association of RASSF1A promoter methylation with gastric cancer risk: a meta-analysis. Tumor Biol. *35*, 943–948.

Shi, J. (2014). Pathogenetic mechanisms in gastric cancer. World Journal of Gastroenterology *20*, 13804.

Shi, J., Yao, D., Liu, W., Wang, N., Lv, H., Zhang, G., Ji, M., Xu, L., He, N., Shi, B., et al. (2012). Highly frequent PIK3CA amplification is associated with poor prognosis in gastric cancer. BMC Cancer *12*, 50.

Shi, W.-J., and Gao, J.-B. (2016). Molecular mechanisms of chemoresistance in gastric cancer. World Journal of Gastrointestinal Oncology *8*, 673.

Shibue, T., Takeda, K., Oda, E., Tanaka, H., Murasawa, H., Takaoka, A., Morishita, Y., Akira, S., Taniguchi, T., and Tanaka, N. (2003). Integral role of Noxa in p53-mediated apoptotic response. Genes Dev *17*, 2233–2238.

Shim SH, Lee CT, Lee JJ, Kim SY, Hah JH, Heo DS *et al*. (2010). A combination treatment with SAHA and ad-p63/p73 shows an enhanced anticancer effect in HNSCC. Tumour Biol; 31: 659-666.

Shinozaki-Ushiku, A., Kunita, A., and Fukayama, M. (2015). Update on Epstein-Barr virus and gastric cancer (Review). International Journal of Oncology *46*, 1421–1434.

Shirakawa, K., Chavez, L., Hakre, S., Calvanese, V., and Verdin, E. (2013). Reactivation of latent HIV by histone deacetylase inhibitors. Trends Microbiol. *21*, 277–285.

Silberg, D.G., Sullivan, J., Kang, E., Swain, G.P., Moffett, J., Sund, N.J., Sackett, S.D., and Kaestner, K.H. (2002). Cdx2 ectopic expression induces gastric intestinal metaplasia in transgenic mice. Gastroenterology *122*, 689–696.

Simonsson, M., Heldin, C.-H., Ericsson, J., and Grönroos, E. (2005). The balance between acetylation and deacetylation controls Smad7 stability. J. Biol. Chem. *280*, 21797–21803.

Spaety, M. E., et al. (2019). "HDAC4 Levels Control Sensibility toward Cisplatin in Gastric Cancer via the p53-p73/BIK Pathway." <u>Cancers (Basel)</u> **11**(11).

Sokolova, O., and Naumann, M. (2017). NF-κB Signaling in Gastric Cancer. Toxins (Basel) *9*.

Son, M.W., Song, G.J., Jang, S.-H., Hong, S.A., Oh, M.-H., Lee, J.-H., Baek, M.J., and Lee, M.S. (2017). Clinicopathological Significance of Large Tumor Suppressor (LATS) Expression in Gastric Cancer. J Gastric Cancer *17*, 363–373.

Song, B., Wang, Y., Xi, Y., Kudo, K., Bruheim, S., Botchkina, G.I., Gavin, E., Wan, Y., Formentini, A., Kornmann, M., et al. (2009). Mechanism of chemoresistance mediated by miR-140 in human osteosarcoma and colon cancer cells. Oncogene *28*, 4065–4074.

Song, C., Zhu, S., Wu, C., and Kang, J. (2013). Histone Deacetylase (HDAC) 10 Suppresses Cervical Cancer Metastasis through Inhibition of Matrix Metalloproteinase (MMP) 2 and 9 Expression. J Biol Chem *288*, 28021–28033.

Song, S., Song, S., Wang, Y., Wang, Y., Xu, P., Xu, P., Yang, R., Yang, R., Ma, Z., Ma, Z., et al. (2015). The inhibition of histone deacetylase 8 suppresses proliferation and inhibits apoptosis in gastric adenocarcinoma. International Journal of Oncology *47*, 1819–1828.

Song, Y., Liu, D., and He, G. (2015). TKTL1 and p63 are biomarkers for the poor prognosis of gastric cancer patients. Cancer Biomark *15*, 591–597.

Sonnemann, J., Marx, C., Becker, S., Wittig, S., Palani, C.D., Krämer, O.H., and Beck, J.F. (2014). p53-dependent and p53-independent anticancer effects of different histone deacetylase inhibitors. Br. J. Cancer *110*, 656–667.

Stronach, E.A., Alfraidi, A., Rama, N., Datler, C., Studd, J.B., Agarwal, R., Guney, T.G., Gourley, C., Hennessy, B.T., Mills, G.B., et al. (2011). HDAC4-Regulated STAT1 Activation Mediates Platinum Resistance in Ovarian Cancer. Cancer Research *71*, 4412–4422.

Sukawa, Y., Yamamoto, H., Nosho, K., Kunimoto, H., Suzuki, H., Adachi, Y., Nakazawa, M., Nobuoka, T., Kawayama, M., Mikami, M., et al. (2012). Alterations in the human epidermal growth factor receptor 2-phosphatidylinositol 3-kinase-v-Akt pathway in gastric cancer. World J. Gastroenterol. *18*, 6577–6586.

Sulahian, R., Casey, F., Shen, J., Qian, Z.R., Shin, H., Ogino, S., Weir, B.A., Vazquez, F., Liu, X.S., Hahn, W.C., et al. (2014). An integrative analysis reveals functional targets of GATA6 transcriptional regulation in gastric cancer. Oncogene *33*, 5637–5648.

Sun, H., Huang, D., Liu, G., Jian, F., Zhu, J., and Zhang, L. (2018). SIRT4 acts as a tumor suppressor in gastric cancer by inhibiting cell proliferation, migration, and invasion. Onco Targets Ther *11*, 3959–3968.

Suzuki M, Endo M, Shinohara F, Echigo S, Rikiishi H. (2009). Enhancement of Cisplatin cytotoxicity by SAHA involves endoplasmic reticulum stress-mediated apoptosis in oral squamous cell carcinoma cells. Cancer Chemother Pharmacol; 64: 1115-1122.

Tahara, T., Shibata, T., Okamoto, Y., Yamazaki, J., Kawamura, T., Horiguchi, N., Okubo, M., Nakano, N., Ishizuka, T., Nagasaka, M., et al. (2016). Mutation spectrum of TP53 gene predicts clinicopathological features and survival of gastric cancer. Oncotarget *7*.
Takagi, T., Iio, A., Nakagawa, Y., Naoe, T., Tanigawa, N., and Akao, Y. (2009). Decreased Expression of MicroRNA-143 and -145 in Human Gastric Cancers. OCL *77*, 12–21.

Takata, A., Otsuka, M., Yoshikawa, T., Kishikawa, T., Hikiba, Y., Obi, S., Goto, T., Kang, Y.J., Maeda, S., Yoshida, H., et al. (2013). MicroRNA-140 acts as a liver tumor suppressor by controlling NF-κB activity by directly targeting DNA methyltransferase 1 (Dnmt1) expression. Hepatology *57*, 162–170.

Tan, P., and Yeoh, K.-G. (2015). Genetics and Molecular Pathogenesis of Gastric Adenocarcinoma. Gastroenterology *149*, 1153-1162.e3.

Tannapfel, A., Schmelzer, S., Benicke, M., Klimpfinger, M., Kohlhaw, K., Mössner, J., Engeland, K., and Wittekind, C. (2001). Expression of the p53 homologues p63 and p73 in multiple simultaneous gastric cancer. J. Pathol. *195*, 163–170.

Tao, X., Yan, Y., Lu, L., and Chen, B. (2017). HDAC10 expression is associated with DNA mismatch repair gene and is a predictor of good prognosis in colon carcinoma. Oncol Lett *14*, 4923–4929.

Terada, T. (2013). An immunohistochemical study of primary signet-ring cell carcinoma of the stomach and colorectum: II. expression of MUC1, MUC2, MUC5AC, and MUC6 in normal mucosa and in 42 cases. 9.

To, K.K.-W., Tong, W.-S., and Fu, L. (2017). Reversal of platinum drug resistance by the histone deacetylase inhibitor belinostat. Lung Cancer *103*, 58–65.

Tomkova, K., Belkhiri, A., El-Rifai, W., and Zaika, A.I. (2004). p73 isoforms can induce T-cell factor-dependent transcription in gastrointestinal cells. Cancer Res. *64*, 6390–6393.

Tomkova, K., El-Rifai, W., Vilgelm, A., Kelly, M.C., Wang, T.C., and Zaika, A.I. (2006). The gastrin gene promoter is regulated by p73 isoforms in tumor cells. Oncogene *25*, 6032–6036.
Tortora, G.J., and Derrickson, B.H. (2008). *Principles of Anatomy and Physiology.* John Wiley & Sons Editions.

Truong, C., Feng, W., Li, W., Alrawi, S., Khoury, T., Yao, J., Xie, K., and Tan, D. (2008). Expression of SOX9 and p63: A study of 200 cases to determine their role in human gastric cancer. Cancer Res *68*, 2197–2197.

Tsai, M.-M., Wang, C.-S., Tsai, C.-Y., Huang, H.-W., Chi, H.-C., Lin, Y.-H., Lu, P.-H., and Lin, K.-H. (2016). Potential Diagnostic, Prognostic and Therapeutic Targets of MicroRNAs in Human Gastric Cancer. Int J Mol Sci *17*.

Tsuchiya, N., Izumiya, M., Ogata-Kawata, H., Okamoto, K., Fujiwara, Y., Nakai, M., Okabe, A., Schetter, A.J., Bowman, E.D., Midorikawa, Y., et al. (2011). Tumor suppressor miR-22 determines p53-dependent cellular fate through post-transcriptional regulation of p21. Cancer Res. *71*, 4628–4639.

Ung, M., Dubot, C., and Coussy, F. (2015). Mécanismes de résistance au trastuzumab dans les cancers du sein. La lettre du Cancérologue. *8*, Septembre

Ushiku, T., Chong, J.-M., Uozaki, H., Hino, R., Chang, M.-S., Sudo, M., Rani, B.R., Sakuma, K., Nagai, H., and Fukayama, M. (2007). p73 gene promoter methylation in Epstein-Barr virus-associated gastric carcinoma. International Journal of Cancer *120*, 60–66.

Vallabhapurapu, S.D., Noothi, S.K., Pullum, D.A., Lawrie, C.H., Pallapati, R., Potluri, V., Kuntzen, C., Khan, S., Plas, D.R., Orlowski, R.Z., et al. (2015). Transcriptional repression by the HDAC4-RelB-p52 complex regulates multiple myeloma survival and growth. Nat Commun *6*, 8428.

Van Cutsem, E., Sagaert, X., Topal, B., Haustermans, K., and Prenen, H. (2016). Gastric cancer. Lancet *388*, 2654–2664.

Večeřa, J., Bártová, E., Krejčí, J., Legartová, S., Komůrková, D., Rudá-Kučerová, J., Štark, T., Dražanová, E., Kašpárek, T., Šulcová, A., et al. (2018). HDAC1 and HDAC3 underlie dynamic H3K9 acetylation during embryonic neurogenesis and in schizophrenia-like animals. J. Cell. Physiol. *233*, 530–548.

Vidimar V, Meng X, Klajner M, Licona C, Fetzer L, Harlepp S *et al*. (2012) Induction of caspase 8 and reactive oxygen species by ruthenium-derived anticancer compounds with improved water solubility and cytotoxicity. Biochem Pharmacol; 84: 1428-1436.

Vilgelm, A.E., Hong, S.-M., Washington, M.K., Wei, J., Chen, H., El-Rifai, W., and Zaika, A.I. (2010). Characterization of ΔNp73 expression and regulation in gastric and esophageal tumors. Oncogene *29*, 5861–5868.

Vilgelm, A.E., Washington, M.K., Wei, J., Chen, H., Prassolov, V.S., and Zaika, A.I. (2012). Interactions of the p53 protein family in cellular stress response in gastrointestinal tumors. Mol. Cancer Ther. *9*, 693–705.

von Grabowiecki Y, Abreu P, Blanchard O, Palamiuc L, Benosman S, Meriaux S *et al*. (2016). Transcriptional activator TAp63 is upregulated in muscular atrophy during ALS and induces the pro-atrophic ubiquitin ligase Trim63. eLife; 5.

Vrana JA, Decker RH, Johnson CR, Wang Z, Jarvis WD, Richon VM *et al*. (1999). Induction of apoptosis in U937 human leukemia cells by suberoylanilide hydroxamic acid (SAHA) proceeds through pathways that are regulated by Bcl-2/Bcl-XL, c-Jun, and p21CIP1, but independent of p53. Oncogene; 18: 7016-7025.

Wada, Y., Takemura, K., Tummala, P., Uchida, K., Kitagaki, K., Furukawa, A., Ishige, Y., Ito, T., Hara, Y., Suzuki, T., et al. (2018). Helicobacter pylori induces somatic mutations in TP53 via overexpression of CHAC1 in infected gastric epithelial cells. FEBS Open Bio *8*, 671–679.

Wade, M., Wang, Y.V., and Wahl, G.M. (2010). The p53 orchestra: Mdm2 and Mdmx set the tone. Trends Cell Biol *20*, 299–309.

Wan, J., Zhou, J., Zhao, H., Wang, M., Wei, Z., Gao, H., Wang, Y., and Cui, H. (2014). Sonic hedgehog pathway contributes to gastric cancer cell growth and proliferation. Biores Open Access *3*, 53–59.

Wang, B., Zhao, M., Cui, N., Lin, D., Zhang, A., Qin, Y., Liu, C., Yan, W., Shi, J., and Chen, B. (2015). Krüppel-like factor 4 induces apoptosis and inhibits tumorigenic progression in SK-BR-3 breast cancer cells. FEBS Open Bio *5*, 147–154.

Wang, H., Holloway, M.P., Ma, L., Cooper, Z.A., Riolo, M., Samkari, A., Elenitoba-Johnson, K.S.J., Chin, Y.E., and Altura, R.A. (2010). Acetylation Directs Survivin Nuclear Localization to Repress STAT3 Oncogenic Activity. J Biol Chem *285*, 36129–36137.

Wang, H., Liu, Z., Li, J., Zhao, X., Wang, Z., and Xu, H. (2012). ΔNp63α mediates proliferation and apoptosis in human gastric cancer cells by the regulation of GATA-6. Neoplasma *59*, 416–423.

Wang, J., Zhou, X.-Q., Li, J.-Y., Cheng, J.-F., Zeng, X.-N., Li, X., and Liu, P. (2014). Prognostic significance of ERCC1 expression in postoperative patients with gastric cancer. Chin. J. Cancer Res. *26*, 323–330.

Wang, L., Wang, W.-Y., and Cao, L.-P. (2015). SIRT3 inhibits cell proliferation in human gastric cancer through down-regulation of Notch-1. Int J Clin Exp Med *8*, 5263–5271.

Wang, L., Xiang, S., Williams, K.A., Dong, H., Bai, W., Nicosia, S.V., Khochbin, S., Bepler, G., and Zhang, X. (2012). Depletion of HDAC6 enhances cisplatin-induced DNA damage and apoptosis in non-small cell lung cancer cells. PLoS ONE *7*, e44265.

Wang, X., Hu, S., and Liu, L. (2017) Phosphorylation and acetylation modifications of FOXO3a: Independently or synergistically? Oncol Lett. *13*, 2867–2872.

Wang, Y., Xie, J., Wang, H., Huang, H., and Xie, P. (2017). Beclin-1 suppresses gastric cancer progression by promoting apoptosis and reducing cell migration. Oncol Lett *14*, 6857–6862.

Wei, J., Zaika, E., and Zaika, A. (2012). p53 Family: Role of Protein Isoforms in Human Cancer.

Weichert, W. (2009). HDAC expression and clinical prognosis in human malignancies. Cancer Lett. *280*, 168–176.

Weichert, W., Röske, A., Gekeler, V., Beckers, T., Ebert, M.P.A., Pross, M., Dietel, M., Denkert, C., and Röcken, C. (2008). Association of patterns of class I histone deacetylase expression with patient prognosis in gastric cancer: a retrospective analysis. Lancet Oncol. *9*, 139–148.

West AC, Johnstone RW. (2014). New and emerging HDAC inhibitors for cancer treatment. The Journal of clinical investigation; 124: 30-39.

West, A.C., and Johnstone, R.W. (2014). New and emerging HDAC inhibitors for cancer treatment. J. Clin. Invest. *124*, 30–39.

Willers, H., Azzoli, C.G., Santivasi, W.L., and Xia, F. (2013). Basic Mechanisms of Therapeutic Resistance to Radiation and Chemotherapy in Lung Cancer. Cancer J *19*, 200–207.

Wilson, A.J., Byun, D.-S., Nasser, S., Murray, L.B., Ayyanar, K., Arango, D., Figueroa, M., Melnick, A., Kao, G.D., Augenlicht, L.H., et al. (2008). HDAC4 promotes growth of colon cancer cells via repression of p21. Mol. Biol. Cell *19*, 4062–4075.

Wisnieski, F., Calcagno, D.Q., Leal, M.F., Chen, E.S., Gigek, C.O., Santos, L.C., Pontes, T.B., Rasmussen, L.T., Payão, S.L.M., Assumpção, P.P., et al. (2014). Differential expression of histone deacetylase and acetyltransferase genes in gastric cancer and their modulation by trichostatin A. Tumor Biol. *35*, 6373–6381.

Wu, T., Chen, J., Shi, Y., Shen, R., and Chen, M. (2016) Expression of HDAC9 in gastric. Int J Clin Exp Pathol. *9*, 12829-12835

Wu, Z., Zhang, R., Chao, C., Zhang, J., and Zhang, Y. (2007). Histone deacetylase inhibitor trichostatin A induced caspase-independent apoptosis in human gastric cancer cell. Chin. Med. J. *120*, 2112–2118.

Xia, L., Zhang, D., Du, R., Pan, Y., Zhao, L., Sun, S., Hong, L., Liu, J., and Fan, D. (2008). miR-15b and miR-16 modulate multidrug resistance by targeting BCL2 in human gastric cancer cells. Int. J. Cancer *123*, 372–379.
Xia, T., Chen, S., Jiang, Z., Shao, Y., Jiang, X., Li, P., Xiao, B., and Guo, J. (2015). Long noncoding RNA FER1L4 suppresses cancer cell growth by acting as a competing endogenous RNA and regulating PTEN expression. Sci Rep *5*.
Xiao, Z.-Y., Ru, Y., Sun, J.-T., Gao, S.-G., Wang, Y.-F., Wang, L.-D., and Feng, X.-S. (2012). Expression of CDX2 and villin in gastric cardiac intestinal metaplasia and the relation with gastric cardiac carcinogenesis. Asian Pac. J. Cancer Prev. *13*, 247–250.

Xie, B., Zhou, J., Shu, G., Liu, D.-C., Zhou, J., Chen, J., and Yuan, L. (2013). Restoration of klotho gene expression induces apoptosis and autophagy in gastric cancer cells: tumor suppressive role of klotho in gastric cancer. Cancer Cell Int. *13*, 18.

Xie, W.-B., Liang, L.-H., Wu, K.-G., Wang, L.-X., He, X., Song, C., Wang, Y.-Q., and Li, Y.-H. (2018). MiR-140 Expression Regulates Cell Proliferation and Targets PD-L1 in NSCLC. CPB *46*, 654–663.
Xu, G., Zhu, H., Zhang, M., and Xu, J. (2018). Histone deacetylase 3 is associated with gastric cancer cell growth via the miR-454-mediated targeting of CHD5. Int J Mol Med *41*, 155–163.
Xu, K., and Zhao, Y.-C. (2016). MEF2D/Wnt/β-catenin pathway regulates the proliferation of gastric cancer cells and is regulated by microRNA-19. Tumour Biol. *37*, 9059–9069.
Xu, S., Zhu, X., Huang, W., Zhou, Y., and Yan, D. (2017). Supramolecular cisplatin-vorinostat nanodrug for overcoming drug resistance in cancer synergistic therapy. Journal of Controlled Release *266*, 36–46.

Yamaguchi, T., Cubizolles, F., Zhang, Y., Reichert, N., Kohler, H., Seiser, C., and Matthias, P. (2010). Histone deacetylases 1 and 2 act in concert to promote the G1-to-S progression. Genes Dev. *24*, 455–469.
Yamamoto, H., Watanabe, Y., Maehata, T., Morita, R., Yoshida, Y., Oikawa, R., Ishigooka, S., Ozawa, S.-I., Matsuo, Y., Hosoya, K., et al. (2014). An updated review of gastric cancer in the next-generation sequencing era: insights from bench to bedside and vice versa. World J. Gastroenterol. *20*, 3927–3937.

Yan, J., Zhang, M., Zhang, J., Chen, X., and Zhang, X. (2011). Helicobacter pylori infection promotes methylation of WWOX gene in human gastric cancer. Biochem. Biophys. Res. Commun. *408*, 99–102.

Yan, L.-H., Wei, W.-Y., Cao, W.-L., Zhang, X.-S., Xie, Y.-B., and Xiao, Q. (2014). Overexpression of CDX2 in gastric cancer cells promotes the development of multidrug resistance. Am J Cancer Res *5*, 321–332.

Yang C, Kaushal V, Shah SV, Kaushal GP. (2008). Autophagy is associated with apoptosis in Cisplatin injury to renal tubular epithelial cells. Am J Physiol Renal Physiol; 294: F777-787.

Yang, J., Wei, X., Wu, Q., Xu, Z., Gu, D., Jin, Y., Shen, Y., Huang, H., Fan, H., and Chen, J. (2011). Clinical significance of the expression of DNA methyltransferase proteins in gastric cancer. Mol Med Rep *4*, 1139–1143.

Yang, L., Lu, X., Nossa, C.W., Francois, F., Peek, R.M., and Pei, Z. (2009). Inflammation and intestinal metaplasia of the distal esophagus are associated with alterations in the microbiome. Gastroenterology *137*, 588–597.

Yang, M., and Huang, C.-Z. (2015). Mitogen-activated protein kinase signaling pathway and invasion and metastasis of gastric cancer. World J Gastroenterol *21*, 11673–11679.

Yang, Y.-H., Zhao, M., Li, W.-M., Lu, Y.-Y., Chen, Y.-Y., Kang, B., and Lu, Y.-Y. (2006). Expression of programmed cell death 5 gene involves in regulation of apoptosis in gastric tumor cells. Apoptosis *11*, 993–1001.
Yao, Y., Suo, A.-L., Li, Z.-F., Liu, L.-Y., Tian, T., Ni, L., Zhang, W.-G., Nan, K.-J., Song, T.-S., and Huang, C. (2009). MicroRNA profiling of human gastric cancer. Mol Med Rep *2*, 963–970.

Yao, Y.-L., Yang, W.-M., and Seto, E. (2001). Regulation of Transcription Factor YY1 by Acetylation and Deacetylation. Mol Cell Biol *21*, 5979–5991.

Yee, K.S., Wilkinson, S., James, J., Ryan, K.M., and Vousden, K.H. (2009). PUMA- and Bax-induced autophagy contributes to apoptosis. Cell Death Differ. *16*, 1135–1145.
Yokozaki, H. Molecular characteristics of eight gastric cancer cell lines established in Japan (2000). Pathology International. *50*, 767-777.

Yoo, C., Ryu, M.-H., Na, Y.-S., Ryoo, B.-Y., Lee, C.-W., and Kang, Y.-K. (2016). Vorinostat in combination with capecitabine plus cisplatin as a first-line chemotherapy for patients with metastatic or unresectable gastric cancer: phase II study and biomarker analysis. Br J Cancer *114*, 1185–1190.

Yoo, C., Ryu, M.-H., Na, Y.-S., Ryoo, B.-Y., Lee, C.-W., Maeng, J., Kim, S.-Y., Koo, D.H., Park, I., and Kang, Y.-K. (2014). Phase I and pharmacodynamic study of vorinostat combined with capecitabine and cisplatin as first-line chemotherapy in advanced gastric cancer. Invest New Drugs *32*, 271–278.

Yoo, C., et al. (2016). "Vorinostat in combination with capecitabine plus cisplatin as a first-line chemotherapy for patients with metastatic or unresectable gastric cancer: phase II study and biomarker analysis." Br J Cancer **114**(11): 1185-1190.

Yoon, H.S., Chen, X., and Yang, V.W. (2003). Krüppel-like Factor 4 Mediates p53-dependent G1/S Cell Cycle Arrest in Response to DNA Damage. J. Biol. Chem. *278*, 2101–2105.

Yoon, J.H., Choi, W.S., Kim, O., and Park, W.S. (2014). The Role of Gastrokine 1 in Gastric Cancer. J Gastric Cancer *14*, 147–155.

Yu, B., Gu, D., Zhang, X., Liu, B., and Xie, J. (2017). The role of GLI2-ABCG2 signaling axis for 5Fu resistance in gastric cancer. Journal of Genetics and Genomics *44*, 375–383.

Yu, L., Lu, Y., Han, X., Zhao, W., Li, J., Mao, J., Wang, B., Shen, J., Fan, S., Wang, L., et al. (2016). microRNA -140-5p inhibits colorectal cancer invasion and metastasis by targeting ADAMTS5 and IGFBP5. Stem Cell Research & Therapy *7*.

Yu, Y., Cao, F., Yu, X., Zhou, P., Di, Q., Lei, J., Tai, Y., Wu, H., Li, X., Wang, X., et al. (2017). The expression of HDAC7 in cancerous gastric tissues is positively associated with distant metastasis and poor patient prognosis. Clin Transl Oncol *19*, 1045–1054.

Zaika AI, El-Rifai W. (2006). The role of p53 protein family in gastrointestinal malignancies. Cell Death Differ; 13: 935-940.

Zandi, S., Hedayati, M.A., Mohammadi, E., and Sheikhesmaeili, F. (2018). Helicobacter pylori infection increases sirt2 gene expression in gastric epithelial cells of gastritis patients. Microb. Pathog. *116*, 120–123.

Zeng, L.-S., Yang, X.-Z., Wen, Y.-F., Mail, S.-J., Wang, M.-H., Zhang, M.-Y., Zheng, X.F.S., and Wang, H.-Y. (2016). Overexpressed HDAC4 is associated with poor survival and promotes tumor progression in esophageal carcinoma. Aging (Albany NY) *8*, 1236–1249.

Zeng, L.-S., Yang, X.-Z., Wen, Y.-F., Mail, S.-J., Wang, M.-H., Zhang, M.-Y., Zheng, X.F.S., and Wang, H.-Y. (2016). Overexpressed HDAC4 is associated with poor survival and promotes tumor progression in esophageal carcinoma. Aging (Albany NY) *8*, 1236–1249.

Zhang J, Zhong Q. (2014). Histone deacetylase inhibitors and cell death. Cell Mol Life Sci; 71: 3885-3901.

Zhang, C., Richon, V., Ni, X., Talpur, R., and Duvic, M. (2005). Selective Induction of Apoptosis by Histone Deacetylase Inhibitor SAHA in Cutaneous T-Cell Lymphoma Cells: Relevance to Mechanism of Therapeutic Action. Journal of Investigative Dermatology *125*, 1045–1052.

Zhang, H., and Xue, Y. (2008). Wnt pathway is involved in advanced gastric carcinoma. Hepatogastroenterology *55*, 1126–1130.

Zhang, H.-H., Gu, G.-L., Zhang, X.-Y., Li, F.-Z., Ding, L., Fan, Q., Wu, R., Shi, W., Wang, X.-Y., Chen, L., et al. (2015). Primary analysis and screening of microRNAs in gastric cancer side population cells. World J Gastroenterol *21*, 3519–3526.

Zhang, H.-Q., He, B., Fang, N., Lu, S., Liao, Y.-Q., and Wan, Y.-Y. (2013). Autophagy inhibition sensitizes cisplatin cytotoxicity in human gastric cancer cell line SGC7901. Asian Pac. J. Cancer Prev. *14*, 4685–4688.

Zhang, Q., Feng, Y., Liu, P., and Yang, J. (2017). MiR-143 inhibits cell proliferation and invasion by targeting DNMT3A in gastric cancer. Tumour Biol. *39*, 1010428317711312.

Zhang, S., Chen, P., Huang, Z., Hu, X., Chen, M., Hu, S., Hu, Y., and Cai, T. (2015). Sirt7 promotes gastric cancer growth and inhibits apoptosis by epigenetically inhibiting miR-34a. Sci Rep *5*, 9787.

Zhang, S., Huang, S., Deng, C., Cao, Y., Yang, J., Chen, G., Zhang, B., Duan, C., Shi, J., Kong, B., et al. (2017). Co-ordinated overexpression of SIRT1 and STAT3 is associated with poor survival outcome in gastric cancer patients. Oncotarget *8*, 18848–18860.

Zhang, Y., Cai, X., Chai, N., Gu, Y., Zhang, S., Ding, M., Cao, H., Sha, S., Yin, J., Li, M., et al. (2015). SIRT1 Is Reduced in Gastric Adenocarcinoma and Acts as a Potential Tumor Suppressor in Gastric Cancer. GAT *2*, 109–123.

Zhao, Y., Li, Y., Ma, Y., Wang, S., Cheng, J., Yang, T., Sun, Z., Kuang, Y., Huang, H., Fan, K., et al. (2016). Myocyte enhancer factor 2D promotes tumorigenicity in malignant glioma cells. Tumour Biol. *37*, 601–610.

Zheng, L., Chen, Y., Ye, L., Jiao, W., Song, H., Mei, H., Li, D., Yang, F., Li, H., Huang, K., et al. (2017). miRNA-584-3p inhibits gastric cancer progression by repressing Yin Yang 1- facilitated MMP-14 expression. Sci Rep *7*.

Zhou, C., Ji, J., Shi, M., Yang, L., Yu, Y., Liu, B., Zhu, Z., and Zhang, J. (2014). Suberoylanilide hydroxamic acid enhances the antitumor activity of oxaliplatin by reversing the oxaliplatin-induced Src activation in gastric cancer cells. Mol Med Rep *10*, 2729–2735.

Zhuang, M., Shi, Q., Zhang, X., Ding, Y., Shan, L., Shan, X., Qian, J., Zhou, X., Huang, Z., Zhu, W., et al. (2015). Involvement of miR-143 in cisplatin resistance of gastric cancer cells via targeting IGF1R and BCL2. Tumour Biol. *36*, 2737–2745.

Zhuang, S. (2013). Regulation of STAT Signaling by Acetylation. Cell Signal *25*, 1924–193

2.2.2. **ARTICLE 4:** Targeting glutathione metabolism in gastric cancer: A non-conventional target for ruthenium-based compounds

In gastric cancer, as well as in several other cancers (lung, breast, colon...) platinium-derived compounds are the chemotherapy of choice, targeting DNA, to induce cell cycle arrest and apoptosis. Unfortunately, they are flawed by their non-specific mode of action, inducing strong side effects in normal healthy tissue, as well as intrinsic or acquired resistance. For instance, the activity of platinium-based compounds is mediated by the presence of p53, which is problematic as around 50% of gastric tumors harbor a p53 mutation [68]. To overcome these flaws, a new generation of anticancer drugs, based on transition-metal such as gold, osmium or ruthenium are being investigated. **Ruthenium-based** compounds *i)* can hold 6 covalent bonds giving the possibilities to attach a multitude of ligands increasing the library that can be synthetized, *ii)* have a wide range of redox state, *iii)* can be under different charges (from 0 to +3), *iv)* can form prodrugs according to their capacity to exchange ligands and *v)* can be transported into cancer cells through iron transportation mechanism [134]. In our lab, a special family of ruthenium-based compound, possessing a C-Ru covalent bond, is under investigation. The lead compound of this family is RDC11. **RDC11**, induces **stronger cytotoxic activity than platinium based anticancer drugs on cell lines**, with a **diminished tumor growth in a syngeneic mouse model of gastric cancer** (YTN16 mouse gastric cancer cell line), while inducing lower or no side effects in the treated mice. On the contrary to platinium compounds, RDC11 **induces a p53-independent and caspase 3-independent apoptosis**, interacting with other targets than DNA like histones or PDH2. Its cytotoxic activity is based on the induction of endoplasmic reticulum stress pathway (also shown in colon cancer, glioblastoma and lymphoblastoma), impacting negatively on key enzymes of the transsulfuration pathway (via ATF4), and also increase Ros production.

For this article, I performed the qPCR analysis for genes targeted by RDC11, as well as the MTT cell survival assay and I participated in the redaction of the manuscript.

Targeting glutathione metabolism in gastric cancer: A non-conventional target for ruthenium-based compounds

Riegel G.,[1] Orvain C.,[1] Barthe A.,[1] Schleiss C.,[1] Venkatasamy A.,[1] Poschet G.,[2] Yamamoto M.,[3] Nomura S.,[4] Tetsuya T.,[5] Pfeffer M.,[6] Mellitzer G.,[1$] Gaiddon Christian.,[1$]

[1] Université de Strasbourg, Inserm, UMR_S1113 IRFAC, Laboratory "Streinth" (Stress Response and Innovative Therapies), Strasbourg, France

[2] Centre for Organismal Studies (COS), University of Heidelberg, Heidelberg, Germany
[3] Department of Pathology, Nippon Veterinary and Life Science University, Tokyo, Japan
[4] Department of Gastrointestinal Surgery, Graduate School of Medicine, The University of Tokyo, Tokyo, Japan
[5] Department of Pathology, Graduate School of Medicine, Fujita Health University, Toyoake, Japan
[6] Institut de Chimie, UMR7177, Laboratoire de Synthèses Métallo-Induites, Strasbourg, France

Keywords: RDC11, ER stress, Transsulfuration, Glutathione, Caspase-independent apoptosis, Metabolism

$Corresponding authors: Christian Gaiddon, Gaiddon@unistra.fr; Georg Mellitzer, mellitzer@unistra.fr
The authors declare no potential conflicts of interest.

Abstract

Ruthenium-based compounds are considered as promising candidates to replace gold standard platinum-based drugs known to be resistant prone and induce strong side effects. Unfortunately, their clinical development is slowed down due to still poorly characterized mode of action. The lead compound of the RDC family, RDC11 was demonstrated to induce stronger cytotoxic activity than platinum-based drugs while inducing lower or no side effects in mice. In addition, previous studies provided the evidence that RDC11, display different mode of action than classical platinum-based compound like it was shown that RDC11 display a P53 independent mode of action and interacts with other targets than DNA like PHD2 and histones. Furthermore, RDC11 induces its cytotoxic activity through the induction of the ER stress pathway. However, it has not been demonstrated yet through which type of cell death RDC11 display its cytotoxic activity. In this study we could confirm RDC11 mediated ER stress induction in gastric cancer cells and further characterized an ER stress dependent effect on cancer metabolism participating to its activity. Here, we highlighted an RDC11 mediated ATF4 induction resulting in a CBS repression, which is the rate limiting enzyme of the transsulfuration pathway. In response to lower flux through the transsulfuration pathway, glutamate levels were strongly reduced in order to supply cysteine content, further leading to a drastic decrease of GSH production. Low GSH content cooccurs with RDC11 mediated ROS production ultimately leading to nuclear AIF translocation demonstrating the induction of caspase independent apoptosis in response to RDC11. Interestingly, we provided the evidence of similar effect mediated by structurally different ruthenium-based compounds suggesting that these regulations could be a more general mode of action for other ruthenium-based compounds. This study provides a more precise understanding about RDC11 mode of action regarding its effect on central metabolic pathway namely transsulfuration and GSH biosynthesis.

Introduction

For several years, the implication of transition metal in the development of anticancer compounds prepared the way for the development of a whole new generation of drugs. The most well-known are cisplatin and oxaliplatin use for the treatment of many different cancer including lung, breast, colon, and gastric cancers. The principal mode of action of the platinum-based compounds is to target DNA inducing cell cycle arrest and apoptosis (Puigvert et al., 2016). However, although this mode of action is frequently very efficient in killing cancer cells it is flawed by its mode of action as it is not specific for cancer cells targeting also normal healthy tissues. Consequently, platinum base anti-cancer drugs are known to induce strong side effects, like neuro- and/or renal-toxicity or bone marrow-suppression, forcing sometimes clinicians to stop the treatment. Another drawback of platin-anti-cancer drug is that their efficacy is often defied by cancer cells through intrinsic or acquired resistance. These resistances can be due to several mechanism including reduce cellular drug uptake, enhance DNA damage repair mechanism, or overproduction of glutathione for detoxification (Galluzzi et al., 2012; Hatem et al., 2017). To overcome these flaws of platinum-based anti-cancer drugs other transition-metals like gold, osmium, or ruthenium are investigated (Bergamo et al., 2012) and have entered clinical trials. For example, the ruthenium-based compounds NAMI-A, KP1019, or RM175 have entered phase I/II clinical trials, showing high anti metastatic activity, and a high cytotoxic effect against different cancers (Bergamo et al., 2012, Zeng et al., 2017). When compared to platinum ruthenium-based compounds have completely different characteristics i) they can hold 6 covalent bonds giving the possibilities to attach a multitude of ligands increasing the library that can be synthetized, ii) they have a wide range of redox states, iii) they can be under different charges (from 0 to +3), iv) and can form prodrugs according to their capacity to exchange ligands, v) and they can be transported into cancer cells through iron transportation mechanism (Bergamo et al., 2012; Klajner et al., 2014). Nevertheless, the progression of new ruthenium-based anti-cancer drugs into clinal trials has been slowed down mainly due to their still poorly characterized mode of action. In this respect, over the past years we have developed and studied in our lab a new family of ruthenium compounds called RDCs, which are characterised by a C-RU (Leyva et al., 2007). These compounds also display the ability to interact with some redox enzymes impacting on cellular metabolism (Meng et al., 2009; Ryabov et al., 2005). One of our lead compound RDC11 displays a greater cytotoxicity in comparison to cisplatin (IC_{50} between 1 and 5µM), does not generate cross resistance with platinum compounds and diminished tumor growth in a xenograft mouse model, without inducing liver, or neurologic side effects (Bergamo et al., 2012; Meng et al., 2009; Vidimar et al., 2019). Our subsequent studies to characterise its mode of action showed that RDC11 can in U87 (glioblastoma cells), TK6 and NH32 (lymphoblastoid cells) (Meng et al., 2009) induces some markers of the endoplasmic reticulum (ER) stress pathway like BiP, XBP1s and Chop (Meng et al., 2009), which correlated with the cytotoxicity of the compound. Additionally, we also have shown than RDC11 induces the production of oxygen reactive species, which participates to its cytotoxic effect (Vidimar et al., 2019). However, this mode of actions cannot totally give account for the cytotoxic activity of the compound. To get further into the mode of action of RDC11 we have recently performed on RDC11 treated U87 cells a transcriptomic analysis revealing the ability of RDC11 to regulate the transsulfuration pathways, a metabolic pathway implicated in the synthesis of cysteine and glutathione (Licona et al., 2017; Sbodio et al., 2019). In this study we provide the evidence that RDC11 and Oxaliplatin differently impact on the transsulfuration pathway regulating glutathione production. We demonstrate that the impact of RDC11 on the transsulfuration pathway is specifically mediated by the repressive effect of the transcription factor ATF4 (ER stress pathway) on CBS resulting in low cellular glutathione levels, increased ROS production and induction of an AIF linked caspase independent apoptosis.

Materials and Methods

<u>Chemicals</u>

RDC11 was synthesized and purified according to a previously described technique (Gaiddon et al., 2005). Tunicamycin was purchased from Santa Cruz Biotechnology. Cisplatin and oxaliplatin were purchased from Accord Healthcare France SAS and Hospira France respectively.

<u>Cell cultures</u>

Both intestinal types of gastric cancer cells AGS, and KATOIII cells were obtained from ATCC. The diffuse type cells MKN45 cells were acquired by Riken® (RCB1001). These cells were cultured in RPMI medium with 10% FBS (Dominique Dutcher™) and 1% Penicillin + Streptomycin (Sigma) at 37°C with 5% CO2 atmosphere. YTN16 cells were obtained from Dr Tsukamoto in Japan. These cells were cultured in DMEM medium with 10% FBS, 1% Penicillin, 1% Glutamine and MITO+ on collagen coated culture dishes. All experiments were conducted by comparing the treatments conditions with cells treated without any active compound (RDC11, tunicamycin, oxaliplatin, cisplatin).

<u>In vivo tumor growth</u>

C57BL/6 mice (6-weeks old) were injected subcutaneously with 15×10^6 YTN16 cells and matrigel solution. After tumor formation, tumors were harvested and reinjected into a new group of mice. Injections of RDC11 (8μmole/kg), Oxa+5FU (10mg/kg) and RDC11+BSO (8μmole/kg and 600mg/kg) started when tumors were palpable (100 mm3) and were performed intraperitoneally once a week. Tumor volumes were measured using caliper. Solutions were prepared in PBS/5% Cremophore. Data are representing the difference between the beginning and the end of the experiment in percentage. Control group were injected only with vehicle (PBS/5% Cremophore). Drugs effect were statistically different ($p < 0.05$) compared to control, as calculated by a student t-test. Animal experiments have been approved by the regional ethic and animal welfare committee, are performed by authorized and trained personnel, and hosted in an animal facility with the necessary mandatory administrative authorizations.

<u>siRNA silencing</u>

ATF4 and P53 siRNAs against human ATF4 and P53 were purchased form Invitrogen ID n°122372 and designed from Eurogenetec respectively. SiRNAs were transfected in cells using Lipofectamine RNAimax (Invitrogen) as described by invitrogen.

<u>MTT cell survival assay</u>

1.10^5 cells were seeded per well in 96-well microplates (Falcon Multiwell) 24h prior to any treatment. RDC11, Tunicamycin, Oxaliplatin, and Cisplatin were applied for 48h in fresh medium. MTT assay was performed as previously described, by replacing medium with fresh one for 2h, supplemented with 5 mg/mL MTT (Sigma). MTT medium was removed, and the formazan crystal was then dissolved with an adjunction of 100μl of DMSO (dimethyl sulphoxide VWR Chemicals) per well. Measurements were performed at 590 nm with Tristar² Multimode Reader LB942 (Berthold Technologies®).

<u>Clonogenic assay</u>

AGS cells were plate in 6-well plates 24h prior to any treatment. RDC11, Tunicamycin, Oxaliplatin, and Cisplatin were applied for 24h in fresh medium. After the treatment cells in every condition are counted and 1.10^3 cells were seeded in 3004 plates for 8 days. After this delay, cells were fixed with 4% PFA during 20min. After one PBS wash, cells were incubated with violet crystal (0,1% filtered) during 20 min. Colonies were counted manually and reported to the control condition.

Flow cytometry of cell death

Cell apoptosis was evaluated using FITC annexin-V Apoptosis detection kit and propidium iodide (PI) (both from BD Pharmingen, BD Bioscience, San Jose, CA, USA). Cells (10^6) were washed in phosphate-buffered saline (PBS) and re-suspended in annexin buffer before the addition of FITC annexin-V and incubated for 20 min on ice in the dark. PI was then added for 5 min before flow cytometry analysis. DAPI (Sigma-Aldrich; Missouri, USA) was also used to analyse cell viability.

Quantitative reverse transcription PCR

Cultured cells were lysed with 1ml of TRIzol (Invitrogen), and RNA was extracted according to the manufacturer's instructions. RNA samples were isopropanol-precipitated and ethanol-washed twice. 2 µg was used for reverse transcription (High-Capacity cDNA Reverse Transcription Kit, Applied Biosystems). qPCR was performed with cDNA previously diluted 10X and SYBR Green mix (SYBR Green PCR Master Mix, Applied Biosystems) and with 400 µM of each primer according to the manufacturer's instructions. The relative expression was calculated using the ΔΔCt method. Expression levels were normalized using average of TBP.

Western blotting

Cells were lysed with NP40 Lysis Buffer (125mM TrisHCl pH 6.7, NaCl 150 mM, NP40 0.5%, 10% Glycerol). 30µg of proteins were denatured and deposited into a SDS-PAGE gel. Western blotting was performed using antibodies against CTH (clone F-1, Santa Cruz Biotechnology®, 1/1000), ATF4 (clone W16016A, BioLegend ®, 1/500), CHOP (L63F7, Cell Signaling, 1/1000) and XBP1s (Clone 143F BioLegend). Secondary antibodies (anti-rabbit, anti-rat, anti-mouse: Sigma, MA) were incubated at 1:1000, or 1:5000 depending on the primary antibody. Loading was controlled with GAPDH (purified at the lab).

Glutathione production measurement

AGS cells were seeded in 6-well plates and treated for 24h. After the treatment cells were harvest and the glutathione production was measured with the glutathione detection kit provided by enzo life sciences. The experiment was performed as described by the providers.

Ros production measurement

AGS cells were seeded in black 96-well plates and treated for 6h. After the treatment cells were incubated with a solution of PBS, 10% FBS and 50µM of dihydroethidine for 30min. Photos are taken with a fluorescent microscope and positive celles were counted.

Immunofluorescent staining

Cells were seeded in 6-well plates and treated the day after with the indicated agents for 6h. Cells were stained with a rabbit anti-AIF (H-300 sc-5586 Santa Cruz) antibody 1:1000 and a mouse anti-phospho-Histone-H2AX (05-636 Merck) 1:250. Cells were stained with secondary antibodies goat anti-rabbit Alexa 488 and with a goat anti-mouse Alexa 565 1:1000. Nuclei were labeled with a DAPI solution (1/40000) for 10 min. Pictures of cells were taken with a Zeiss Axio Imager M2-Apotome2 fluorescence microscope.

Analysis of metabolites

Free amino acids and thiols were extracted from 4 x 10^6 cells starting material with 0.35 ml of 0.1 M HCl in an ultrasonic ice-bath for 10 min. The resulting extracts were centrifuged twice for 10 min at 4°C and 16.400 g to remove cell debris. Amino acids were derivatized with AccQ-Tag reagent (Waters) and determined as described in Weger et al., 2016. Free Cys was quantified by reducing disulfides with DTT followed by thiol derivatization with the fluorescent dye monobromobimane (Thiolyte, Calbiochem). Derivatization was performed as described in Wirtz et al., 2004. UPLC-FLR analysis was carried out using an Acquity H-class UPLC system. Separation was achieved with a binary gradient of buffer A (100 mM potassium acetate, pH 5.3) and solvent B (acetonitrile) with the following gradient: 0 min 2.3 % buffer B; 0.99 min 2.3 %, 1 min 70 %, 1.45 min 70 %, and re-equilibration to 2.3 % B in 1.05 min at a flow rate of 0.85 ml min^{-1}. The column (Acquity BEH Shield RP18 column, 50 mm x 2.1

mm, 1.7 μm, Waters) was maintained at 45°C and sample temperature was kept constant at 14 °C. Monobromobimane conjugates were detected by fluorescence at 480 nm after excitation at 380 nm and quantified using ultrapure standards (Sigma). Data acquisition and processing was performed with the Empower3 software suite (Waters).

<u>Statistical analysis</u>
All statistical analyses were performed by using Prism 6 (GraphPad Software). Statistical significance was determined by the Student t test and the minimal level of significance was P < 0.05.

Results

<u>RDC11 induces cell death in a p53 and caspase 3 independent manner in gastric cancer cells.</u>

Previous results of our lab suggested that RDC11 induces the ER-stress pathway but the underlying mechanism and its importance in the cytotoxicity has not been studied. To address these questions, we first tested the cytotoxicity of RDC11 on different human gastric cancer cells lines and compared it to tunicamycin and oxaliplatin (Fig. 1A). The latter is frequently used in clinics for the treatment of gastric cancer patients. In general, in all three tested cells lines the IC_{50} of RDC11 was lower than the IC_{50} of oxaliplatin. In addition, in MKN45 and KATOIII its IC_{50} was similar to that of tunicamycin whereas it was higher in AGS cells (Fig 1A). Interestingly, in a clonogenic survival assay RDC11 was as efficient as oxaliplatin in inhibiting colony formation whereas tunicamycin only let to a decrease in colony size (Fig 1B). To test it in vivo anti-cancer activity we used a syngeneic gastric cancer mouse model (Fig 1D), namely YTN16 cell line, which was derived from a mouse gastric tumor (Yamamoto et al., 2018). We firstly assess the cytotoxic potential of RDC11 and oxaliplatin on the YTN16 cell line. RDC11 displays again a lower IC_{50} than oxaliplatin (Fig 1C). YTN16 cells were injected subcutaneously and when tumors reached $50mm^3$ mice were treated with RDC11, the standard treatment protocol for gastric cancer oxaliplatin together with 5FU. When tumors of the untreated control group reached a tumor volume of around $500mm^3$ the experiment was stopped, and tumor volume compared in the three groups. This showed that RDC11 drastically inhibited tumor growth, with even a complete disappearance of the tumor in two cases (Fig 1D). We performed then FACS (Fig 1E) and Western blot analyses for the expression of cleaved caspase 3 (Fig 1F) to further pinpoint down the cell death pathway induced by RDC11. RDC11 and tunicamycin treatment induced a strong accumulation of cells being in an early apoptotic phase (annexin V positive) when compared to oxaliplatin (Fig 1E). Interestingly, whereas tunicamycin and cisplatin induced cleaved caspase 3 expression already after 24h and more strongly after 48h of treatment, cleaved caspase 3 expression was almost undetectable in RDC11 treated cells even after a high concentration (IC_{75}) after 48h (Fig 1F). In addition, RDC11 induce cell death seemed to be independently of p53 induction (Fig 1G). Taken together, these results suggest that RDC11 mostly induces a p53 – caspase 3 independent cell death pathway.

<u>RDC11 induces the expression of ATF4</u>

We have previously shown that RDC11 induces the expression of components of the ER stress pathway IRE1α, XBP1 and CHOP respectively, in the mouse melanoma cell line B16F10 similarly to tunicamycin a known induction of ER stress (Chow et al., 2018; Licona et al., 2017; Meng et al., 2009). In the human gastric cancer cell line AGS RDC11 strongly induced the expression of XBP1s and CHOP whereas oxaliplatin and cisplatin had no effect (Fig 2A). Importantly, RDC11, like the ER stress inducer tunicamycin, strongly induced the expression of ATF4 (Fig 2B, C), which regulates the expression of CHOP, whereas oxaliplatin and cisplatin again failed to do so. Taken together, these data confirming our previous observation that RDC11 is a strong inducer of the different components of the ER stress pathway.

<u>RDC11 inversely regulates the expression of CBS and CTH two enzymes in the transsulfuration pathway.</u>

ATF4 is known to regulate several genes involved in amino acid transport and metabolism in order to induce the integrated stress response (ISR). Notably, ATF4 was shown to directly regulate the expression of the cystathionine γ-lyase (CTH) linking the activation of the ER-stress pathway to the transsulfuration pathway responsible for the de-novo production of cysteine and glutathione production. To investigate if RDC11 via the activation of ATF4 impacts on the transsulfuration pathway we first analyzed for the expression of CTH by RT-qPCR and Western blot in AGS cell which were treated with different concentrations of RDC11, tunicamycin, oxaliplatin and cisplatin for 6h or 24h (Fig 3B, C). This showed that RDC11, like tunicamycin, strongly increased the expression of CTH at the RNA and protein level, whereas oxaliplatin and cisplatin had only a very minor (6h) or even repressive (24h) effect (Fig 3B, C). These results suggest that RDC11 via the activation of ATF4 impacts on the expression of CTH and consequently increasing glutathione production (Fig 3A). However, in the transsulfuration pathway the "rate limiting step" is the conversion of homocysteine to cystathionine by the cystathionine beta synthase (CBS) (Fig 3A). AGS cells were treated with RDC11, tunicamycin, oxaliplatin and cisplatin at the indicated concentrations for 6h or 24h and expression of CBS was then analyzed by RT-QPCR and Western blot. Interestingly, in contrast to CTH expression, CBS protein expression was completely lost after 6h of RDC11 treatment and maintained to be undetectable after 24h (Fig 3D, E). In contrast CBS expression was induced by tunicamycin, oxaliplatin and cisplatin at the RNA and protein level (Fig 3D, E). Taken together, this suggests that also RDC11 increases the level of CTH expression it at the same time represses the expression of CBS, which is the "rate limiting" enzyme in the transsulfuration pathway.

ATF4 and p53 are differently involved in the regulation of CTH and CBS mRNA expression

To further study the role of ATF4 in the transsulfuration pathway, AGS cells were transfected with a siRNA targeting ATF4 and then treated with RDC11, tunicamycin or oxaliplatin for 24h at the IC_{50} (Fig 4A), and CTH and CBS expression analyzed by RT-QPCR (Fig 4B, C). The loss of ATF4 expression in AGS cells clearly reduced the capacity of RDC11 and tunicamycin to induce CTH mRNA expression (Fig 4C). Interestingly, loss of ATF4 rescued the repressive effect of RDC11 on CBS mRNA expression and let also to a weak increase of its expression induced by oxaliplatin. In contrast, tunicamycin slightly lost its capacity to induce CBS mRNA expression in ATF4 negative AGS cells (Fig 4C). Taken together, these data supporting published data showing CTH to be a direct target gene of ATF4, but they also suggest that ATF4 might also be directly involved, also differently, in the transcriptional regulation of CBS in response to RDC11, tunicamycin and oxaliplatin. Although oxaliplatin does not induce ER stress pathways markers like XBP1s, CHOP (Fig 2A) and ATF4 (Fig 2B, C) it induced the expression of the CBS (Fig 3D, E) the rate limiting enzyme of the transsulfuration pathway. In contrast to RDC11, oxaliplatin strongly induces the expression of p53 (Fig 1G and Fig 4D) and as p53 is also implicated in the regulation of different metabolic pathways we investigated its role in the expressional regulation of CTH and CBS mRNA expression in response to the different drug treatments (Fig 4E, F). Inhibition of p53 expression, using a specific siRNA, slightly reduced the capacity of tunicamycin to induced mRNA expression of CTH, whereas it did not alter the inductive or repressive effect of RDC11 and oxaliplatin, respectively (Fig 4E). Interestingly, loss of p53 clearly diminished oxaliplatin induced expression of CBS mRNA, whereas it did not alter the effect of RDC11 or tunicamycin (Fig 4F).

RDC11 lowers glutathione production possibly via enhanced cellular glutamate expulsion.

Our results show that RDC11 specifically down regulated the expression of CBS, the "rate limiting" enzyme in the transsulfuration pathway (Fig 3D, E), which should consequently lead to a reduction in cellular glutathione levels (Fig 5 A) the end-point product of this pathway. To investigate this, we treated AGS cells with RDC11, tunicamycin or oxaliplatin at the indicated concentrations and times and measured the cellular concentration of glutathione but also of Glutamate and Cysteine, two amino acids upstream necessary for its production (Fig 5B – D). As expected RDC11 lead to a strong reduction in the cellular glutathione concentration (Fig 5B). In contrast, tunicamycin and oxaliplatin treatment slightly increased cellular glutathione concentration, which is consistent with their positive effect on CBS expression (Fig 3D, E). In addition, inhibition of ATF4 rescued the repressive

effect of RDC11 on cellular glutathione concentration and further stimulated it in the case of tunicamycin (Suppl Fig 1), whereas inhibition of p53 had no effect except for oxaliplatin (Suppl Fig 1). Furthermore, RDC11 treatment led also to a strong reduction in Glutamate levels where as tunicamycin and oxaliplatin had no effect (Fig 5C). Likewise, tunicamycin and oxaliplatin had no effect on cysteine levels (Fig 5D). But surprisingly, RDC11 treatment did also not reduce the cellular cysteine levels, which we would have expected as it strongly reduces CBS expression (Fig 5D). It is well known that cellular cysteine levels can be replenished from outside the cells via expulsion of glutamate through the anti-porter xCT, which is encoded by the SLC7A11 gene (Fig 5A). To investigate this, we analyzed the expression of SLC7A11 mRNA by RT-qPCR after treatment of AGS cells with RDC11, tunicamycin or oxaliplatin (Fig 5E). This showed that RDC11 and tunicamycin treatment increases the expression of SLC7A11 (Fig 5E) in AGS cells. This suggest, that although RDC11 decreases the expression of CBS, the rate limiting enzyme in the transsulfuration pathway, cellular homeostasis of cysteine is established by the up-regulation of the anti-porter xCT, which however leads to a decrease of glutamate concentration resulting in a decrease in glutathione. In addition, we also analyzed the expression of Glutamate Cysteine Ligase (GCL), which ligates glutamate to cysteine to produce γ-glutamylcysteine (Fig 5A). This showed that RDC11 and tunicamycin treatment increases the expression of GCL whereas oxaliplatin decreased it.

RDC11 treatment leads to a strong increase in Ros production

It is well known that increased glutathione levels serve to lower oxidative stress. To investigate if RDC11 increases Ros concentrations AGS cells were treated with either RDC11, tunicamycin, oxaliplatin at the indicated concentration or with H_2O_2 know to strongly induce Ros production. Ros production was then analyzed by dihydroethidine staining and positive cells counted. This showed that RDC11 strongly induced the percentage of Ros positive cells whereas tunicamycin and oxaliplatin had no effect (Fig 6A B). This strong increase in Ros positive cells is specific to RDC11 as BSO, an inhibitor of GCL, did not significantly increase Ros positive staining in tunicamycin and oxaliplatin treated AGS cells (Fig 6C).

Inhibiting the negative effect of RDC11 on the transsulfuration pathway partially blocks its cytotoxic effect.

The strong effect of RDC11 on the transsulfuration pathway prompted us to investigate its contribution in its cytotoxicity we performed a series of clonogenic assays. In the first assay, we transfected AGS with an ATF4 specific or control siRNA and then treated cells prior to the clonogenic assay with RDC11 or oxaliplatin (Fig 7A). As expected, in the siCTL transfected cells RDC11 drastically decreased colony formation even stronger than oxaliplatin. Inhibition of ATF4 expression significantly increased colony formation of the RDC11 treated AGS whereas it did not alter the cytotoxicity of oxaliplatin. Similarly, supplementing the cell culture medium with glutathione rescued colony formation of RDC11 treated AGS cells (Fig 7B). Furthermore, co-treatment of AGS cells with the glutamate-cysteine-ligase (GCL) inhibitor BSO further increased the cytotoxicity of RDC11 (Fig 7C). In contrast, inhibition of p53 expression did not alter the cytotoxicity of RDC11 but decreased the efficiency of oxaliplatin (Fig 7D).

RDC11 does not induce ferroptosis but caspase independent apoptosis.

Our observations that RDC11 does not induce cleaved caspase 3 expression (Fig 1F) but induces ER stress, as well as strong reduction of intracellular GSH concentrations and an increase in ROS production suggests that it might either induce cell death through ferroptosis or caspase independent apoptosis. To address the first possibility, we treated AGS cells with increasing doses of RDC11 with or without ferrostatin-1 a known inhibitor of ferroptosis and performed MTT survival assay (Fig 8A). Co-treatment of RDC11 with ferrostatin-1 did not diminish the cytotoxic effect of RDC11 at all concentration tested. This data suggests that RDC11 does not induce ferroptosis but rather caspase independent apoptosis.
Induction of caspase independent apoptosis is marked by the nuclear translocation of AIF leading to DNA damage. To address this, AGS cells were treated with RDC11 or H_2O_2, a known strong inducer of nuclear

translocation of AIF, and analyzed by immunofluorescence staining for the nuclear translocation of AIF and the expression of p-γH2AX a marker for DNA damage (Fig 8B). As seen in immunofluorescence staining (Fig 8B) and confirmed by our cell counts (Fig 8C) RDC11 treatment led to a marked increase in cells showing a nuclear expression of AIF and p-γH2AX staining. Taken together, these results suggest that RDC11 induces cell death via caspase independent apoptosis.

Other ruthenium-based compounds also impact on the transsulfuration pathway

To investigate if only RDC11 impacts on the transsulfuration pathway or if it might also hold true for other ruthenium-based compounds (RDC) we treated cells with structurally different RDCs compounds and analyzed by RT-QPCR and Western blot for their impact on the expression of ATF4, CBS and CTH. When compared to RDC11, from the 3 tested ruthenium compounds 2 showed a similar effect on the transsulfuration pathway. For example, similar to RDC11 treatment of AGS cells with RDC60 (Fig 8A) led to an increase in ATF4 and CTH but a decrease in CBS expression at the mRNA and protein level (Fig 9B, C).

Discussion

Unravelling the mode of action of anticancer drugs still represents a great challenge in oncology. Platinum-based gold standard treatment displays good anticancer activity against several cancer types, including gastric cancer. Unfortunately, due to side effects, and frequent resistance mechanism, they do not completely fulfil the needs of clinicians for save and efficient anti-cancer drug. However, their long-lasting success encourages the development new metal-based anticancer drugs with the aim of avoiding side effects induction and resistances. In this respect, ruthenium- and osmium-based compounds are good candidates due to their interesting cytotoxic capacities and the variety of compounds that can be synthetized. Some ruthenium-based compounds enter clinical trials like NAMI-A and KP1019 (Bergamo et al., 2012; Zeng et al., 2017), however, their clinical development was stopped due to lack of knowledge about their mode of action. A better understanding of their mode of action and the chemical structure responsible for it would ultimately lead to the development of more active and supportable anticancer drugs. In this study we demonstrate the impact of RDC11 on metabolic pathways including transsulfuration and GSH biosynthesis and describe their role for RDC11 mediated cytotoxicity. The repression of these two metabolic pathways observed in response to RDC11 leads to a mitochondrial-dependent induction of apoptosis in gastric cancer.

RDC11 induces a strong ER stress response in gastric cancer cells

We firstly demonstrate that RDC11 displays higher cytotoxic potential in gastric cancer cells correlating with a higher apoptosis induction when compared to oxaliplatin. More importantly, RDC11 decreases more strongly the tumor volume in syngeneic gastric xenograft models as oxaliplatin/5FU demonstrating the potential application benefits provided by RDC11. Interestingly, in contrast to classical anticancer drugs like cisplatin and oxaliplatin, RDC11 doesn't induces strong cleavage of caspase-3 nor strong P53 expression suggesting that the classical DNA/P53 dependent mechanism is not its principal mode of action. However, and in contrast to oxaliplatin, RDC11 was seen to induce another pathway important for cell survival called ER stress pathway. We could demonstrate that RDC11 induces the expression of XBP1s and CHOP, which are central actors and markers of ER stress activation. This result is in line with previous work of our group demonstrating an induction of ER stress pathway in response to RDC11 in other cancer cell lines including colon cancer, glioblastoma, and lymphoblastoma (Licona et al., 2017; Meng et al., 2009). This highlights the important role of ER stress induction for the mode of action of RDC11, and an ER stress induction mediated by RDC11 in cancer cell lines of different origin. Together with published data showing the activation of the ER stress pathway by structurally different ruthenium compounds clearly suggest that induce of the ER stress pathway (Chow et al., 2016, 2018; Meng et al., 2009; Xu et al., 2019) might be a general mode of action of these type of anti-cancer drugs. More importantly,

we could also validate that RDC11 can induce the expression of the transcription factor ATF4 the upstream regulator of CHOP expression suggesting that the Perk-ATF4 axis is an important branch of ER stress pathway induced by RDC11. Moreover, platinum-based compounds did not induce the ER stress pathway but required the presence of a functional P53 for their cytotoxic activity confirming data published by others (Dasari and Tchounwou, 2014). In contrast, RDC11 did not induce P53 and further P53 silencing didn't impact on the cytotoxic activity of RDC11 confirming the P53 independent mode of action of RDC11. Interestingly, in contrast to RDC11, the activity of platinum-based compound is dictated by the presence of P53 as well as most of the resistance mechanisms implicate DNA repair mechanisms (Galluzzi et al., 2012; Martinez-Balibrea et al., 2015). Furthermore, it is important to note that RDC11 can induce the expression of CHOP, XBP1s as strongly as tunicamycin a known strong inducer of ER stress markers. However, even if both drugs are able to induce apparently the same type of ER stress, they don't have the same effect on metabolism. According to the literature, the outcome of ER stress activation can differ strongly due to differences in kinetics, and branche(s) of ER stress activated (Hetz, 2012). The ER stress pathway is tightly regulated by the interaction partners of the ER stress sensor. The cytosolic domains of the sensors enable interaction with several activator or inhibitor leading to the formation of a regulation platform called UPRosome. This platform can differ from one situation to another leading to differences in the effects observed by the ER stress induction. In addition, the way of activation of ER stress including misfolded protein accumulation or changes in ER calcium loads can also determine which sensor will be preferentially activated and further decide the cellular outcome (Hetz, 2012). However, how RDC11 induces ER stress has still to be elucidated and knowledge of it would help to dictate the further development of these type of anti-cancer compounds.

RDC11 impacts on cellular metabolism

Our results show that RDC11 induce strong expression of ATF4, a transcription factor known to be implicated in amino acids import and synthesis including cystathionine gamma-lyase, a central actor of the transsulfuration pathway (Dickhout et al., 2012; Mistry et al., 2016). This suggests that RDC11 might impact via ATF4 on the transsulfuration and indeed found that RDC11 increases CTH and represses CBS expression, two key enzymes of the transsulfuration pathway, whereas oxaliplatin showed an opposite effect. Importantly we could demonstrate that ATF4 silencing rescued the repressive effect of RDC11 on CBS expression. Although ATF4 is most commonly known as a transcriptional activator Horiguchi and coworkers demonstrate that when ATF4 interacts with C/EBPα it has a transrepresionnal activity (Horiguchi et al., 2012). Furthermore, the homologous form of ATF4 found in california sea hare, Aplysia CREB2, was also described to have a rather transcriptional repressor function in the nervous system (Bartsch et al., 1995). These published data suggest that in our condition where RDC11 induces ATF4 expression and represses CBS expression in an ATF4 dependent many, ATF4 functions as a transcriptional repressor. Despite the repressionnal activity on CBS, the induction of ATF4 by RDC11 results in an upregulation of CTH expression, as it was shown that ATF4 silencing reduces RDC11 mediated CTH induction. This result is in line with the literature as CTH is known to be a transcriptional target gene of ATF4 (Dickhout et al., 2012; Mistry et al., 2016), and further suggest that depending on the interaction partners of ATF4, the target genes can be upregulated or repressed. In addition, these results demonstrate the importance of ATF4 in RDC11 mediated regulation of the transsulfuration pathway.

CBS is the limiting enzyme of the transsulfuration pathway, and repression of it leads to a lower flux through this pathway (Zhu et al., 2018). Furthermore, transsulfuration is the only way for de novo cysteine production (Combs and DeNicola, 2019; Sbodio et al., 2019) suggesting that RDC11 treatment result in a lower cysteine production. However, metabolomic analysis of AGS cells treated with RDC11 and oxaliplatin didn't confirm this as we found no change in cellular cysteine content after RDC11 treatment. However, this could be explained by our finding that RDC11 increased the expression of xCT antiporter. This antiporter is known to be responsible for cysteine supply, by continuously importing this amino acid from the culture medium while exporting glutamate (Hatem et al., 2017). Interestingly, we demonstrate that RDC11 induces the level of this anti-porter correlating with a strong decrease in glutamate content in gastric cancer cells. Importantly, low levels of glutamate are known to

reduce glutathione (GSH) production (Hatem et al., 2017). It is exactly what we see, RDC11 treatment not only reduces glutamate concentrations in the gastric cancer cells but also leads to a dramatic decrease in GSH production. In addition, oxaliplatin induces the GSH production in the same cells. It is well known that high levels of GSH results in a more efficient drug detoxification (Balendiran et al., 2004; Traverso et al., 2013) correlating with the resistance of cancer cells to the treatment with platinum drugs. Therefore, the differences observed for GSH production between RDC11 and oxaliplatin could explain the difference observed in the cytotoxic effect of these two drugs. Importantly, we could demonstrate that reintroduction of synthetic GSH in the culture medium reduced the cytotoxicity of RDC11 whereas inhibition of CBS activity with BSO increased it. Altogether, the functional analysis demonstrates that the reduction of GSH by RDC11 participates to its cytotoxic activity and the induction mediated by oxaliplatin represents a resistance mechanism toward this drug. Reduction of GSH production is known to correlated with a Ros insults. Indeed, RDC11 induces high levels of Ros suggesting that due to its ability to decrease GSH production, RDC11, in contrast to oxaliplatin, is able to induce a strong oxidative stress. This result is in line with previous studies demonstrating that oxidative stress is induced by different ruthenium-based compounds like RDC34, RAS-1T, and RAS-1H (Chow et al., 2016; Vidimar et al., 2019). Ros production is an early process already induced at 6h by RDC11 whereas the decrease in glutathione production is only observed after 24h. Several studies, as reviewed by (Hatem et al., 2017; Liu et al., 2014), demonstrate that GSH homeostasis is also controlled by Ros levels due to the detoxification role of GSH. More precisely, GSH in consumed by the cells in order to lower oxidative stress and avoid cell death induction, resulting in lower GSH levels. This might also give account for the GSH reduction mediated by RDC11 as Ros induction is already observed after 6h inducing GSH consumption resulting in GSH reduction later on. The absence of Ros induction by oxaliplatin in AGS cells could be explained by the higher GSH levels induction. However, cotreatment of AGS cells with oxaliplatin and the GSH inhibitor buthionine sulfoximine (BSO) didn't results in a higher Ros production further suggesting an absence of Ros induction by platinum-based drugs in gastric cancer cells. Interestingly, we could confirm the same type of regulation of ATF4, CBS and CTH expression by structurally different ruthenium-based compounds suggesting that it might be a more general mode of action of these types of drugs further demonstrating the strength of our findings.

RDC11 induces caspase independent cell death

The ability of RDC11 to impact on the transsulfuration pathway and to induce high levels of Ros suggested that it might induce cell death known as ferroptosis (Dixon et al., 2012; Yang et al., 2014). However, when we cotreated AGS cells with RDC11 and ferrostatin-1, a ferroptosis inhibitor, we didn't observe changes in its cytotoxicity. This suggested RDC11 does not induce cell death via induction of ferroptosis. Interestingly, ferroptosis depends on iron and some links between iron and ruthenium import have already been described as it was shown that ruthenium interacts with the transferrin system. For example, Klajner and co-workers (Klajner et al., 2014) demonstrated that RDC34 lowers the expression of transferrin and induces the expression of ferritin, an iron packaging protein. This suggests that RDC34 can impact directly on the iron metabolism. Furthermore, RDC34 was shown to be imported inside the cells through iron transporter and probably taking over the place of normal iron. The effect of RDC11 on iron metabolism should therefore be further investigated in order to understand why RDC11 did not induce ferroptosis and its difference to RDC34. Importantly, in contrast to cisplatin and oxaliplatin RDC11 didn't induce caspase-3 cleavage prompting us to the investigation caspase independent apoptosis, a cell death pathway characterized by the nuclear translocation of the mitochondrial factor AIF (apoptosis inducing factor) (Bano and Prehn, 2018). Indeed, treatment of AGS cells with RDC11 promoted nuclear translocation of AIF suggesting that this cell death pathway is implicated in RDC11 cytotoxic activity. In addition, we could observe in the same conditions, the phosphorylation of the histone γH2AX known to be a DNA damage marker. In accordance with the literature, when AIF is imported in the nucleus it activates non-specific endonucleases leading to DNA condensation and fragmentation (Bano and Prehn, 2018; Elmore, 2007). It is noteworthy that RDC11 did not induce strong P53 levels suggesting that DNA damage is not the principal mode of action of RDC11. However, in our case where RDC11 treatment leads to AIF nuclear translocation, DNA damage seems more to be the outcome of apoptosis induction. Despite the fact that

induction of DNA damage is known to correlate in some cases with induced cell death, more precise analysis are required in order to determine if RDC11 induces, in an AIF dependent manner, endonuclease and if this results in DNA fragmentation contributing to its mode of action or not. Altogether, this study provides new insides into the mode of action of RDC11 anticancer compound. We highlighted the higher cytotoxic potential of RDC11, correlating with lower side effect as described in previous studies (Meng et al., 2009), demonstrating the potential benefits of RDC11 over platinum-based compounds. Through the ER stress induction and more precisely through ATF4, RDC11 is able to regulate the transsulfuration pathways leading to amino acids deregulation in glutamate content. Therefore, RDC11 was seen to decrease strongly glutathione levels and induce strong Ros levels participating in its cytotoxic activity. Furthermore, we provided the evidence of caspase independent apoptosis induction showing unconventional cell death pathway activation for RDC11.

Conclusion

Here we demonstrate that the ruthenium-based anti-cancer compound RDC11 displays a higher cytotoxicity in gastric cancer cells than classical gold-standard chemotherapeutic agents like oxaliplatin. We show that it induces a strong ER stress response and that via induction of ATF4 expression it impacts negatively on one of the key enzymes of the transsulfuration pathway. Furthermore, we demonstrate that RDC11 strongly up-regulates the expression of cystine/glutamate exchanger (xCT) correlating with reduction of cellular glutamate concentrations. The loss of glutamate, a precursor of glutathione (GSH) synthesis, results in a strong reduction of GSH production. Importantly, the negative effect of RDC11 on cell survival can be rescued with the supplementation of glutathione showing that the negative impact of RDC11 on the transsulfuration pathway is one of its principle mode of action. Moreover, RDC11 was able to induce strong levels of ROS correlating with a strong nuclear translocation of AIF. This leads to the activation of DNA cleavage correlating with DNA damage observed by phosphorylation of the histone γH2AX. Altogether, this work highlights the role of ER stress pathway and its interconnection with cellular metabolism for the cytotoxic activity of the RDC11.

References

Balendiran, G.K., Dabur, R., and Fraser, D. (2004). The role of glutathione in cancer. Cell Biochem. Funct. *22*, 343–352.

Bano, D., and Prehn, J.H.M. (2018). Apoptosis-Inducing Factor (AIF) in Physiology and Disease: The Tale of a Repented Natural Born Killer. EBioMedicine *30*, 29–37.

Bartsch, D., Ghirardi, M., Skehel, P.A., Karl, K.A., Herder, S.P., Chen, M., Bailey, C.H., and Kandel, E.R. (1995). Aplysia CREB2 represses long-term facilitation: relief of repression converts transient facilitation into long-term functional and structural change. Cell *83*, 979–992.

Bergamo, A., Gaiddon, C., Schellens, J.H.M., Beijnen, J.H., and Sava, G. (2012). Approaching tumor therapy beyond platinum drugs: status of the art and perspectives of ruthenium drug candidates. J. Inorg. Biochem. *106*, 90–99.

Chow, M.J., Licona, C., Pastorin, G., Mellitzer, G., Ang, W.H., and Gaiddon, C. (2016). Structural tuning of organoruthenium compounds allows oxidative switch to control ER stress pathways and bypass multidrug resistance. Chem Sci *7*, 4117–4124.

Chow, M.J., Babak, M.V., Tan, K.W., Cheong, M.C., Pastorin, G., Gaiddon, C., and Ang, W.H. (2018). Induction of the Endoplasmic Reticulum Stress Pathway by Highly Cytotoxic Organoruthenium Schiff-Base Complexes. Mol. Pharm. *15*, 3020–3031.

Combs, J.A., and DeNicola, G.M. (2019). The Non-Essential Amino Acid Cysteine Becomes Essential for Tumor Proliferation and Survival. Cancers (Basel) *11*.

Dasari, S., and Tchounwou, P.B. (2014). Cisplatin in cancer therapy: molecular mechanisms of action. Eur. J. Pharmacol. *740*, 364–378.

Dickhout, J.G., Carlisle, R.E., Jerome, D.E., Mohammed-Ali, Z., Jiang, H., Yang, G., Mani, S., Garg, S.K., Banerjee, R., Kaufman, R.J., et al. (2012). Integrated stress response modulates cellular redox state via induction of cystathionine γ-lyase: cross-talk between integrated stress response and thiol metabolism. J. Biol. Chem. *287*, 7603–7614.

Dixon, S.J., Lemberg, K.M., Lamprecht, M.R., Skouta, R., Zaitsev, E.M., Gleason, C.E., Patel, D.N., Bauer, A.J., Cantley, A.M., Yang, W.S., et al. (2012). Ferroptosis: an iron-dependent form of nonapoptotic cell death. Cell *149*, 1060–1072.

Elmore, S. (2007). Apoptosis: a review of programmed cell death. Toxicol Pathol *35*, 495–516.

Gaiddon, C., Jeannequin, P., Bischoff, P., Pfeffer, M., Sirlin, C., and Loeffler, J.P. (2005). Ruthenium (II)-derived organometallic compounds induce cytostatic and cytotoxic effects on mammalian cancer cell lines through p53-dependent and p53-independent mechanisms. J. Pharmacol. Exp. Ther. *315*, 1403–1411.

Galluzzi, L., Senovilla, L., Vitale, I., Michels, J., Martins, I., Kepp, O., Castedo, M., and Kroemer, G. (2012). Molecular mechanisms of cisplatin resistance. Oncogene *31*, 1869–1883.

Hatem, E., El Banna, N., and Huang, M.-E. (2017). Multifaceted Roles of Glutathione and Glutathione-Based Systems in Carcinogenesis and Anticancer Drug Resistance. Antioxid. Redox Signal. *27*, 1217–1234.

Hetz, C. (2012). The unfolded protein response: controlling cell fate decisions under ER stress and beyond. Nat. Rev. Mol. Cell Biol. *13*, 89–102.

Horiguchi, M., Koyanagi, S., Okamoto, A., Suzuki, S.O., Matsunaga, N., and Ohdo, S. (2012). Stress-Regulated Transcription Factor ATF4 Promotes Neoplastic Transformation by Suppressing Expression of the INK4a/ARF Cell Senescence Factors. Cancer Res *72*, 395–401.

Klajner, M., Licona, C., Fetzer, L., Hebraud, P., Mellitzer, G., Pfeffer, M., Harlepp, S., and Gaiddon, C. (2014). Subcellular localization and transport kinetics of ruthenium organometallic anticancer compounds in living cells: a dose-dependent role for amino acid and iron transporters. Inorg Chem 53, 5150–5158.

Leyva, L., Sirlin, C., Rubio, L., Franco, C., Lagadec, R.L., Spencer, J., Bischoff, P., Gaiddon, C., Loeffler, J.-P., and Pfeffer, M. (2007). Synthesis of Cycloruthenated Compounds as Potential Anticancer Agents.

Licona, C., Spaety, M.-E., Capuozzo, A., Ali, M., Santamaria, R., Armant, O., Delalande, F., Van Dorsselaer, A., Cianferani, S., Spencer, J., et al. (2017). A ruthenium anticancer compound interacts with histones and impacts differently on epigenetic and death pathways compared to cisplatin. Oncotarget 8, 2568–2584.

Liu, Y., Hyde, A.S., Simpson, M.A., and Barycki, J.J. (2014). Emerging regulatory paradigms in glutathione metabolism. Adv. Cancer Res. 122, 69–101.

Martinez-Balibrea, E., Martínez-Cardús, A., Ginés, A., Ruiz de Porras, V., Moutinho, C., Layos, L., Manzano, J.L., Bugés, C., Bystrup, S., Esteller, M., et al. (2015). Tumor-Related Molecular Mechanisms of Oxaliplatin Resistance. Mol. Cancer Ther. 14, 1767–1776.

Meng, X., Leyva, M.L., Jenny, M., Gross, I., Benosman, S., Fricker, B., Harlepp, S., Hébraud, P., Boos, A., Wlosik, P., et al. (2009). A ruthenium-containing organometallic compound reduces tumor growth through induction of the endoplasmic reticulum stress gene CHOP. Cancer Res. 69, 5458–5466.

Mistry, R.K., Murray, T.V.A., Prysyazhna, O., Martin, D., Burgoyne, J.R., Santos, C., Eaton, P., Shah, A.M., and Brewer, A.C. (2016). Transcriptional Regulation of Cystathionine-γ-Lyase in Endothelial Cells by NADPH Oxidase 4-Dependent Signaling. J. Biol. Chem. 291, 1774–1788.

Puigvert, J.C., Sanjiv, K., and Helleday, T. (2016). Targeting DNA repair, DNA metabolism and replication stress as anti-cancer strategies. FEBS J. 283, 232–245.

Ryabov, A.D., Kurova, V.S., Ivanova, E.V., Le Lagadec, R., and Alexandrova, L. (2005). Redox Mediation and Photomechanical Oscillations Involving Photosensitive Cyclometalated Ru(II) Complexes, Glucose Oxidase, and Peroxidase. Anal. Chem. 77, 1132–1139.

Sbodio, J.I., Snyder, S.H., and Paul, B.D. (2019). Regulators of the transsulfuration pathway. Br. J. Pharmacol. 176, 583–593.

Traverso, N., Ricciarelli, R., Nitti, M., Marengo, B., Furfaro, A.L., Pronzato, M.A., Marinari, U.M., and Domenicotti, C. (2013). Role of glutathione in cancer progression and chemoresistance. Oxid Med Cell Longev 2013, 972913.

Vidimar, V., Licona, C., Cerón-Camacho, R., Guerin, E., Coliat, P., Venkatasamy, A., Ali, M., Guenot, D., Le Lagadec, R., Jung, A.C., et al. (2019). A redox ruthenium compound directly targets PHD2 and inhibits the HIF1 pathway to reduce tumor angiogenesis independently of p53. Cancer Letters 440–441, 145–155.

Weger, B.D., Weger, M., Görling, B., Schink, A., Gobet, C., Keime, C., Poschet, G., Jost, B., Krone, N., Hell, R., et al. (2016). Extensive Regulation of Diurnal Transcription and Metabolism by Glucocorticoids. PLOS Genetics 12, e1006512.

Wirtz, M., Droux, M., and Hell, R. (2004). O-acetylserine (thiol) lyase: an enigmatic enzyme of plant cysteine biosynthesis revisited in Arabidopsis thaliana. J. Exp. Bot. 55, 1785–1798.

Xu, L., Zhang, P.-P., Fang, X.-Q., Liu, Y., Wang, J.-Q., Zhou, H.-Z., Chen, S.-T., and Chao, H. (2019). A ruthenium(II) complex containing a p-cresol group induces apoptosis in human cervical carcinoma cells through endoplasmic reticulum stress and reactive oxygen species production. J. Inorg. Biochem. 191, 126–134.

Yamamoto, M., Nomura, S., Hosoi, A., Nagaoka, K., Iino, T., Yasuda, T., Saito, T., Matsushita, H., Uchida, E., Seto, Y., et al. (2018). Established gastric cancer cell lines transplantable into C57BL/6 mice show fibroblast growth factor receptor 4 promotion of tumor growth. Cancer Sci. 109, 1480–1492.

Yang, W.S., SriRamaratnam, R., Welsch, M.E., Shimada, K., Skouta, R., Viswanathan, V.S., Cheah, J.H., Clemons, P.A., Shamji, A.F., Clish, C.B., et al. (2014). Regulation of ferroptotic cancer cell death by GPX4. Cell *156*, 317–331.

Zeng, L., Gupta, P., Chen, Y., Wang, E., Ji, L., Chao, H., and Chen, Z.-S. (2017). The development of anticancer ruthenium(ii) complexes: from single molecule compounds to nanomaterials. Chem Soc Rev *46*, 5771–5804.

Zhu, H., Blake, S., Chan, K.T., Pearson, R.B., and Kang, J. (2018). Cystathionine β-Synthase in Physiology and Cancer. Biomed Res Int *2018*, 3205125.

Figure 1
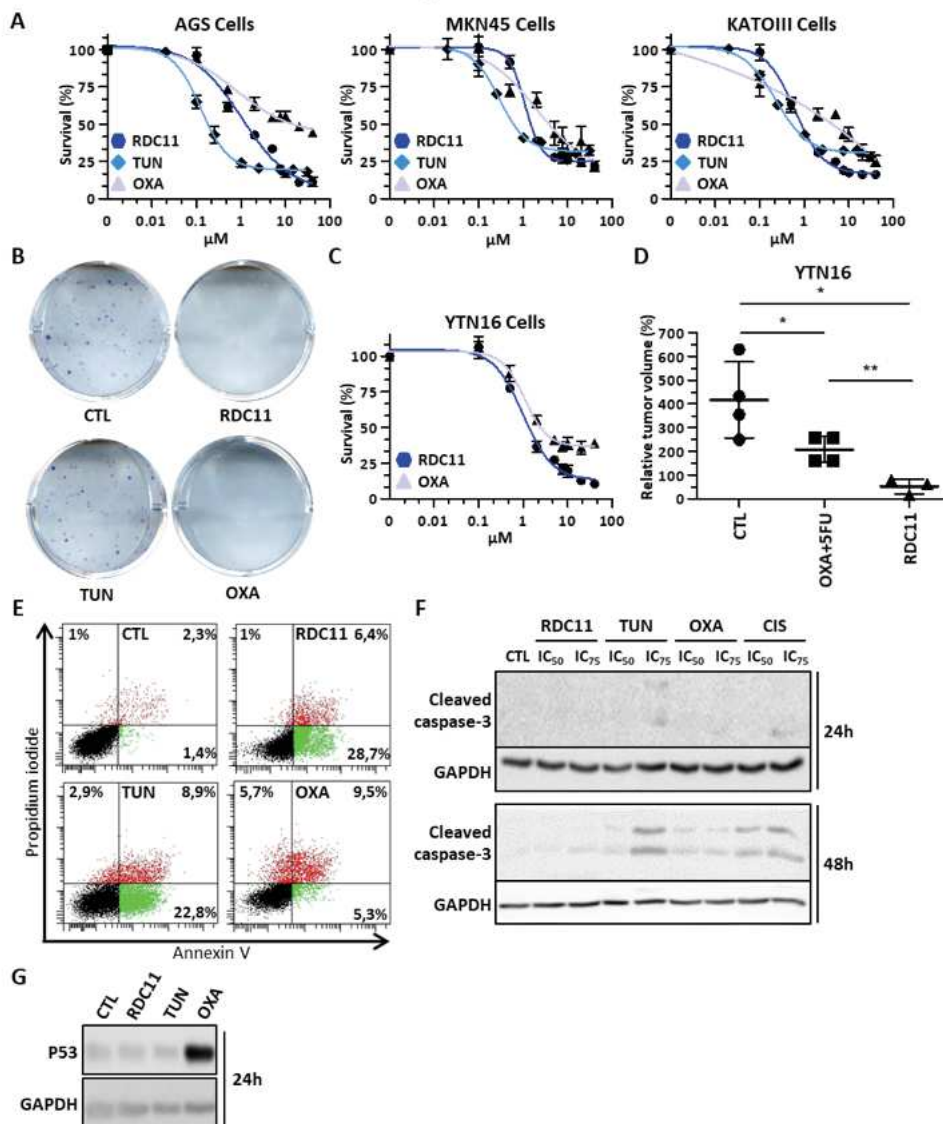
Cytotoxic characteristics of RDC11 in gastric cancer cells: (A) AGS, MKN45, and KATOIII cells were treated with growing concentrations of RDC11, Tunicamycin (TUN) and Oxaliplatin (OXA) for 48h and cell survival was assessed by MTT in each cell line. (B) AGS cells were treated with RDC11, TUN, and OXA at the IC_{50} for 24h or non treated (CTL) and survival was assessed by clonogenic assay 8 days after plating. (C) YTN16 cells were treated with growing concentrations of RDC11 and Oxaliplatin (OXA) for 48h and cell survival was assessed by MTT. (D) YTN16 syngenique xenograft mouse models treated once per week with vehicule (CTL) oxaliplatin + 5-fluorouracile (OXA+5FU), and RDC11 for 4 weeks. Tumor volume after the 4 weeks are represented. (E) AGS cells were treated with RDC11, TUN, and OXA at the IC_{75} for 48h or non treated (CTL) and apoptosis was assessed by flow cytometry. (F) AGS cells were treated for 24h and 48h with RDC11, TUN, and OXA at the IC_{50} and IC_{75} or non treated (CTL) and western blot analysis revealed the caspase-3 cleavage. (G) AGS cells were treated for 24h with RDC11, TUN, and OXA at the IC_{50} or non treated (CTL) and western blot analysis revealed P53 expression. Representative experiments are shown and statistics were performed on technical replicates. Student t-test are considered as significatif with $\alpha<0,5$. *=0,05, **=0,01, ***=0,001

Figure 2

A   ER Stress marker protein expression

B   ATF4 mRNA

C   ATF4 protein expression
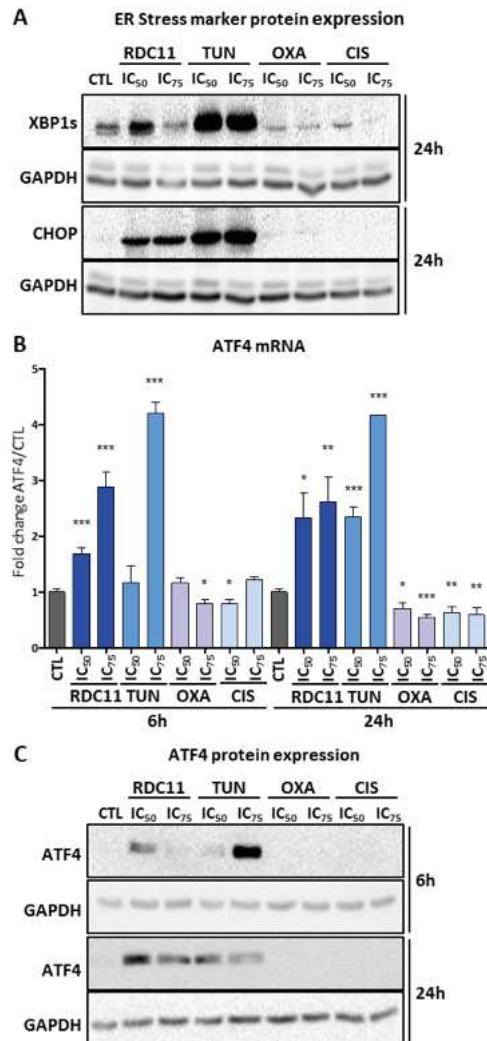
ER Stress pathway activation in gastric cancer: (A) Protein of AGS cells treated with RDC11, Tunicamycin (TUN), Oxaliplatin (OXA) Cisplatin (CIS) at the IC_{50} and IC_{75} for 6h and 24h or non treated (CTL) were obtained and western Blot analysis revealed XBP1s, CHOP, and GAPDH protein expression level. (B-C) Protein and RNA were extracted from AGS cells treated with the same conditions and RT-qPCR analysis revealed the relative mRNA expression level of ATF4 (B), and Western Blot analysis revealed ATF4 protein expression (C). Representative experiments are shown and statistics were performed on technical replicates. Student t-test are considered as significatif with α<0,5.   *=0,05, **=0,01, ***=0,001

Figure 3
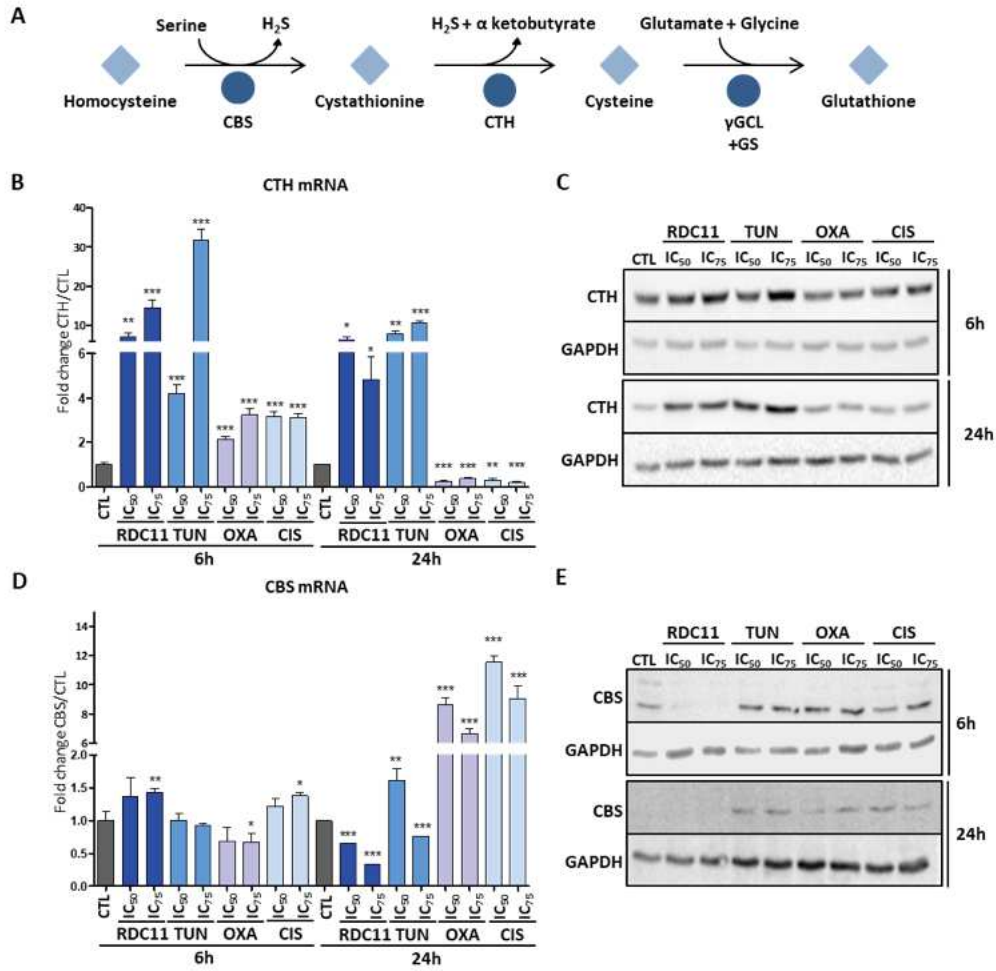
Regulation of the transsulfuration pathway by the RDC11: (A) Schematic representation of the transsulfuration and glutathione biosynthtic pathway. (B&D) RNA of AGS cells treated with RDC11, tunicamycine (TUN), Oxaliplatin (OXA) and cisplatin (CIS) at the IC50 and IC75 for 6h and 24h or non treated (CTL) were obtained and RT-qPCR analysis revealed CTH (B) and CBS (D) expression. (C&E) Protein extraction of AGS cells in the same conditions were obtained and western blot analysis revealed the protein expression of CTH (C) and CBS (E). Representative experiments are shown and statistics were performed on technical replicates. Student t-test are considered as significatif with α<0,5. *=0,05, **=0,01, ***=0,001

154

Figure 4
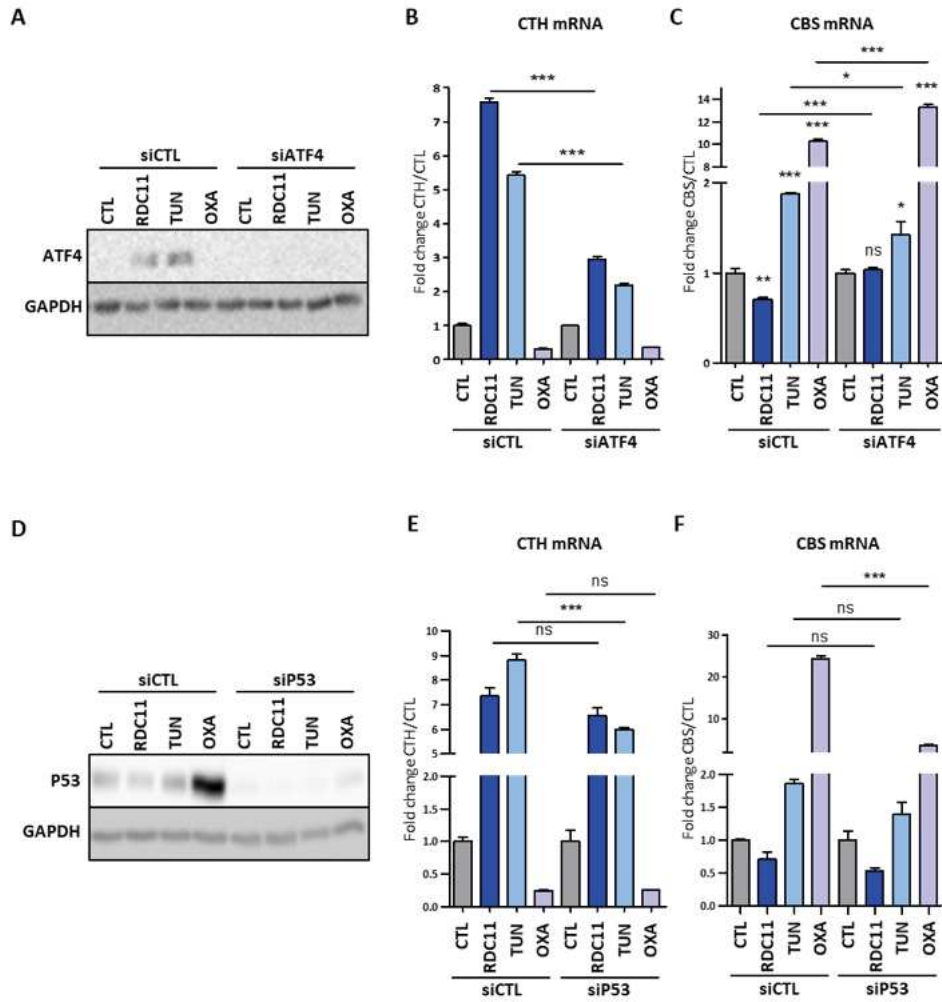
Implication of ATF4 and P53 in the regulation of the transsulfuration pathway: (A&D) Proteins were extracted from AGS cells transfected with silencer RNA control (siCTL) or specific for ATF4 (siATF4) or P53 (siP53) for 48h and then treated with RDC11, Tunicamycin (TUN) and Oxaliplatine (OXA) at the IC_{50} or non treated (CTL) for 24h. Western Blot analysis revealed the efficient silencing of ATF4 and P53 in these conditions. (B,C,E,F) RNA were extracted from AGS cells in the same conditions, and RT-qPCR analysis show the expression of CTH (B&E) and CBS (C&F). Representative experiments are shown and statistics were performed on technical replicates. Student t-test are considered as significatif with α<0,5. *=0,05, **=0,01, ***=0,001

Figure 5
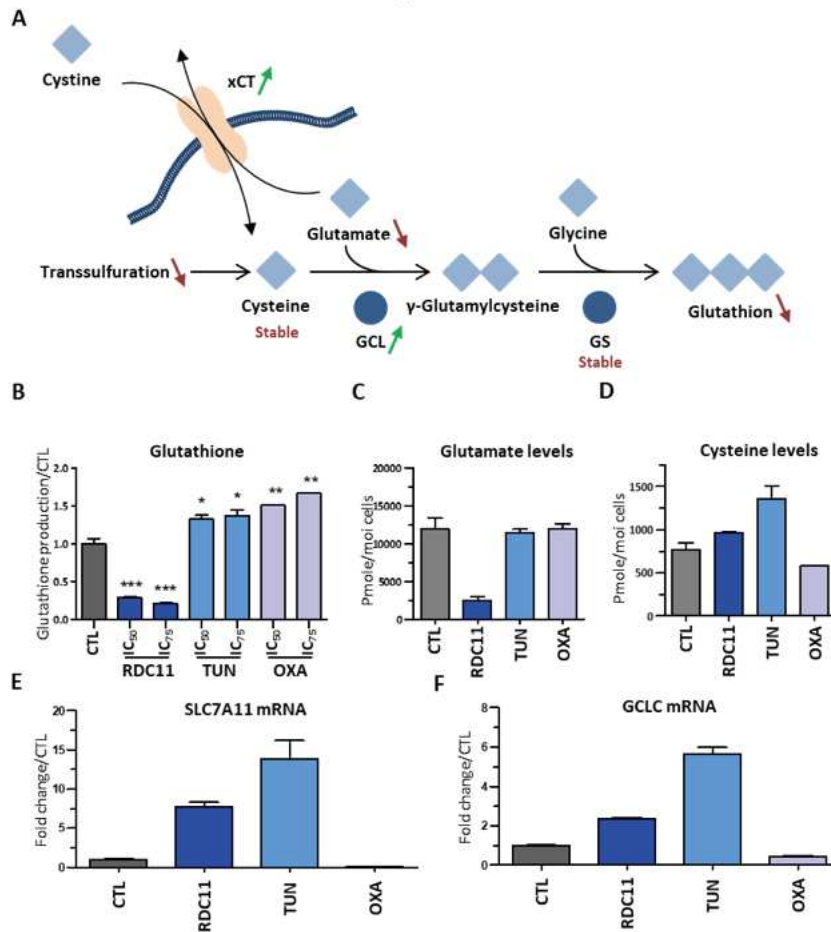
Metabolic changes induced by RDC11 in gastric cancer: (A) Schematic represntation of glutathione biosynthetic pathway Modulations induced by RDC11 are representend with green arrows for the upregulations and in red for the repressions. (B) AGS cells were treated with RDC11, Tunicamycin (TUN), Oxaliplatin (OXA) at the IC_{50} and IC_{75} for 24h or non treated (CTL) and glutathione production was measured using a glutathione kit (enzo lifescience). (C&D) AGS cells were treated with RDC11, Tunicamycin (TUN), Oxaliplatin (OXA) at th IC_{50} for 6h and 24h or non treated (CTL) and metabolomic analysis revealed the cellular content of glutamate (C) and cysteine (D). (E&F) AGS cells were treated with the same conditions and RT-qPCR analysis show the expression level of SLC7A11 (E) and GCLC (F). Representative experiments are shown and statistics were performed on technical replicates. Student t-test are considered as significatif with α<0,5. *=0,05, **=0,01, ***=0,001

156

Figure 6
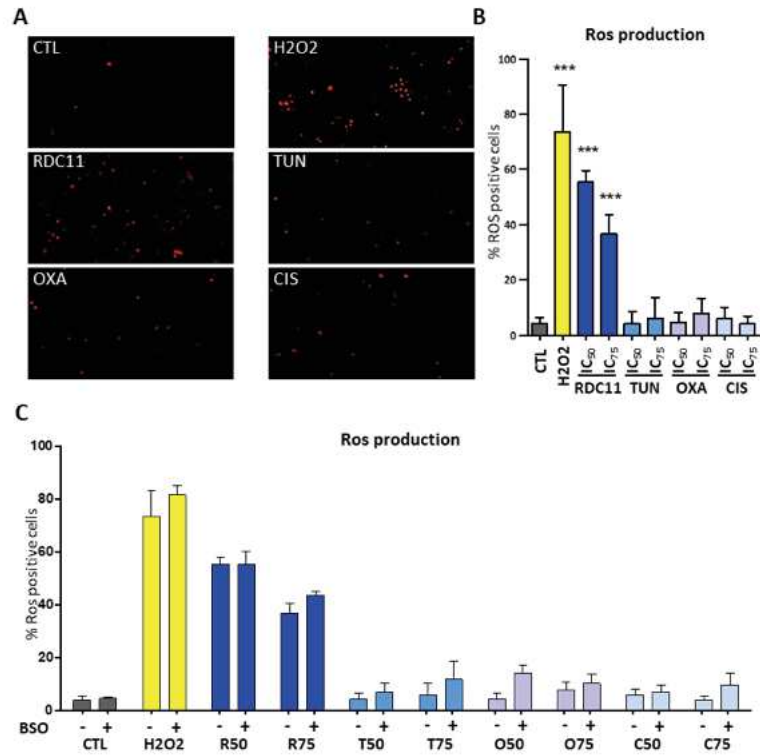
**Oxydative stress induced by RDC11:** (A&B) AGS cells were treated with H_2O_2 at 100µM, RDC11, Tunicamycin (TUN), Oxaliplatin (OXA and Cisplatin (CIS) at the the IC_{50} or the IC_{75} for 6h or non treated (CTL) and Ros production was assessed by dihydroethidine. (A) Fluorescence microcopic photos of these cells are shown, and Ros positive cells were counted (B). (C) AGS cells were treated with the same conditions and or cotreatment with buthionine sulfoximide (BSO) and Ros production was assessed and counted following the same method. Biological replicates are represented and statistics were performed on technical replicates. Student t-test are considered as significatif with α<0,5. *=0,05, **=0,01, ***=0,001

157

Figure 7
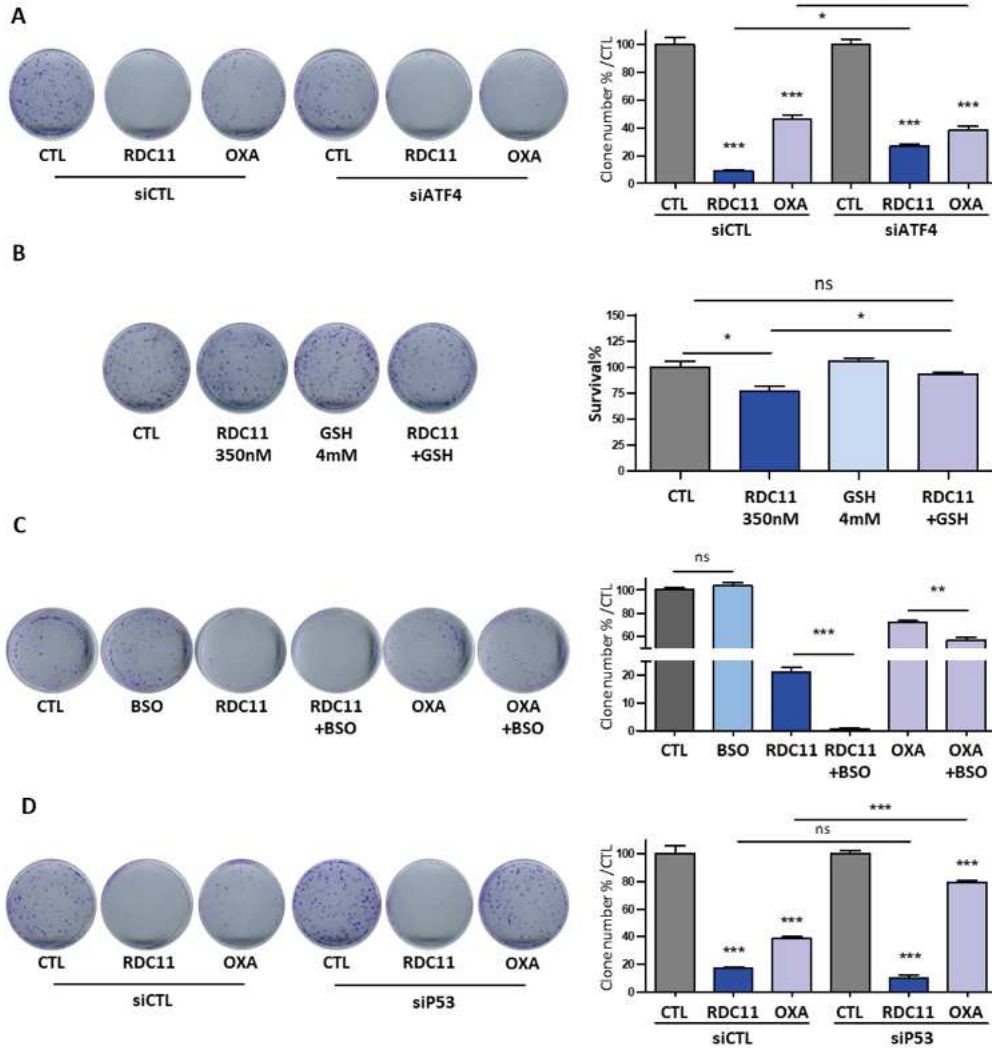
(A-D) Clonogenic assay were performed on AGS cells. (A&D) AGS cells were transfected with silencer RNA control (siCTL) or specific for ATF4 (siATF4) or P53 (siP53) for 24h and treated with RDC11 and Oxaliplatin (OXA) at 250nM for 24h. (B) AGS cells were treated with RDC11 at 350nM, Glutathione at 4mM (GSH) and RDC11 combined with Glutathione for 24h. (C) AGS cells were treated with RDC11 and Oxaliplatin (OXA) at the IC_{30}, or BSO at 1mM or in combinaison with BSO for 24h. The number of colony is counted manually 8 days after plating. Representative experiments are shown and statistics were performed on technical replicates. Student t-test are considered as significatif with α<0,5. *=0,05, **=0,01, ***=0,001

Figure 8
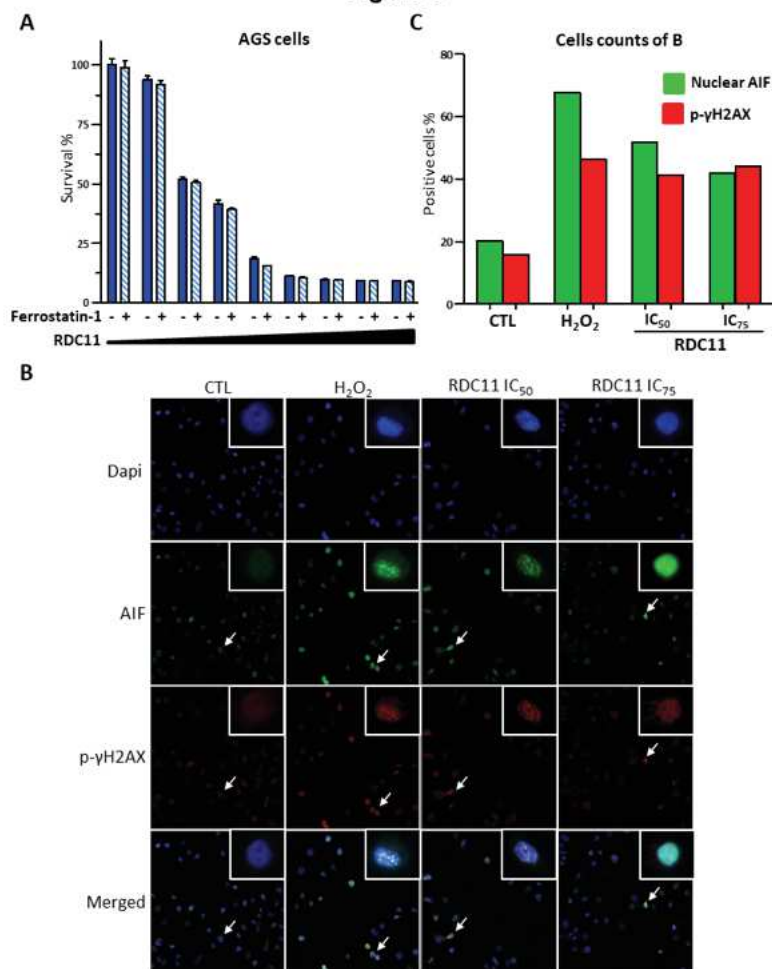
(A) AGS cells were treated with growing concentrations of RDC11 with or without ferrostatin-1 for 48h and cell survival was assessed by MTT survival assay. (B) Fluorescence micropic photos of AGS cells treated with H_2O_2 at 100μM, RDC11 at the IC_{50} and IC_{75} for 6h or non treated (CTL) are shown. (C) AGS cells treated with the same conditions and positive cells for nuclear AIF and p-γH2AX expression were counted.

159

Figure 9
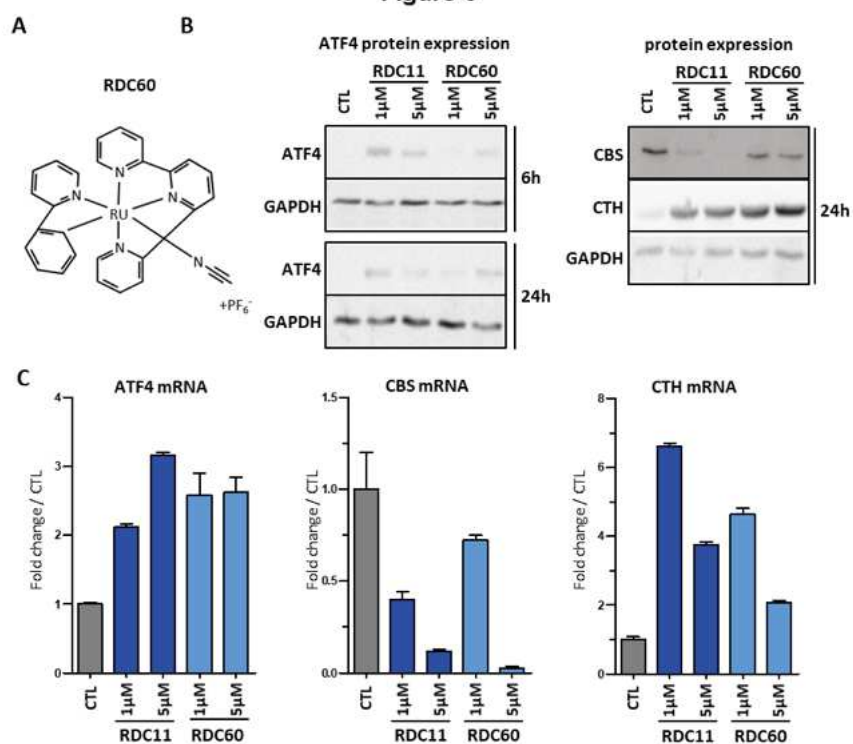
(A) Chemical structure of RDC60. (B) AGS cells were treated with RDC11 and RDC60 at 1μM or 5μM for 6h and 24h and western blot analysis show the expression of ATF4, CBS, CTH, and GAPDH. (C) AGS cells were treated with the same conditions and RT-qPCR analysis revealed the mRNA level of ATF4, CBS, and CTH.

Supplemental Figure 1
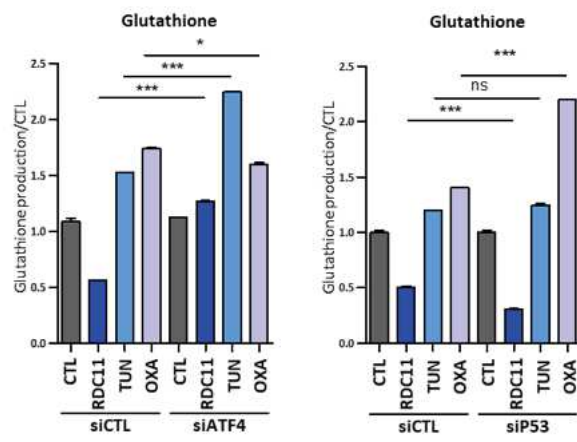
(A&B) AGS cells were transfected with silencer RNA control (siCTL) or specific for ATF4 (siATF4) or P53 (siP53) for 48h and then treated with RDC11, Tunicamycin (TUN), and Oxaliplatin (OXA) at the IC_{50} or non treated (CTL) for 24h and glutathione production was measured using a glutathione kit (enzo lifescience).

2.3. Cachexia and sarcopenia in gastric cancer

The scientific view of all cancers is slowly shifting from organ-centered diseases, to a more global and systemic approach. For instance, recent focus has been made on **cachexia**, which occurs in approximately **50% of cancer patients** - especially digestive tract cancers - presenting as a progressive loss of adipose tissue and skeletal muscle mass*,* associated with a worsened prognosis [87]*.* Cancer cachexia not only has a dramatic impact on the quality of life, but is also associated with poor responses to therapies (chemotherapy and immunotherapy), decreased survival and is estimated to account for around 20 to 25% of cancer-related deaths [92]. Cancer cachexia can be *1)* independent of the tumor stage, *2)* independent of treatments and sometimes already present at diagnosis, *3)* independent of malnutrition, *4)* a marker of poor prognosis and poor response to therapies.

However, the reasons why only some patients are prone to develop cachexia remains largely unknown. In gastric cancer, around **30 to 60%** of patients are thought to develop cachexia, independently of the cancer stage and the incidence cachexia / sarcopenia appear to increase after chemotherapy [93-94]. **Sarcopenia**, often associated with cachexia, is defined by skeletal muscle loss, or **muscle atrophy**, can currently be estimated at relatively advanced stages, by a measure of the muscles surface (abdominal wall, psoas and erector spinae muscles) at the level of the 3rd lumbar vertebra on axial CT images, normalized to weight and height (BMI). Currently, no therapeutic approach can efficiently restore muscle loss and strength. Therefore, we wanted to evaluate the clinical impact of a feeding jejunostomy on gastric cancer patients, before and after chemotherapy cycles and its influence on muscle atrophy and the completion of chemotherapy cycles. Additionally, in a cohort of gastric cancer patients, we evaluated the muscle status (normal or atrophic) at diagnosis and the occurrence of any treatment-related changes after chemotherapy with platinum-based compounds. Furthermore, we also wanted to approach the underlying origins of chemotherapy-induced cachexia and muscle atrophy at a genomic and molecular levels and on imaging.

For these articles, I have participated in the study design, performed the radiology-related measures on CT, micro-CT and MRI and participated in the manuscript preparation & review.

Annals of
SURGICAL ONCOLOGY
OFFICIAL JOURNAL OF THE SOCIETY OF SURGICAL ONCOLOGY

CrossMark

ORIGINAL ARTICLE – GASTROINTESTINAL ONCOLOGY

Could a Feeding Jejunostomy be Integrated into a Standardized Preoperative Management of Oeso-gastric Junction Adenocarcinoma?

Simone Manfredelli, MD[1], Jean-Baptiste Delhorme, MD[1,2], Aïna Venkatasamy, MD[2,3], Christian Gaiddon, PhD[2], Cécile Brigand, MD, PhD[1], Serge Rohr, MD, PhD[1], and Benoît Romain, MD, PhD[1,4]

[1]Department of Digestive Surgery, Strasbourg University Hospital, Strasbourg, France; [2]Inserm U1113, Strasbourg University, FMTS, Strasbourg, France; [3]Department of Radiology, Strasbourg University Hospital, Strasbourg, France; [4]EA3430, Strasbourg University, FMTS, Strasbourg, France

ABSTRACT

Purpose. To evaluate the impact of a feeding jejunostomy (FJ) on the preoperative management of patients with an oesogastric adenocarcinoma (OGA).

Methods. From January 2007 to December 2014, patients with potentially resectable OGA were enrolled in a perioperative chemotherapy protocol. FJ was performed before starting perioperative treatments in patients presenting with dysphagia or with a nutritional risk index (NRI) <97.5. The patients who did not require a FJ served as a control group.

Results. Among the 114 patients with OGA consecutively admitted in our surgical department, 88 (77.2%) were enrolled for neoadjuvant treatment. A FJ was placed in 50 patients (56.8%) before the neoadjuvant treatment (FJ group), whereas 38 patients (43.2%) started neoadjuvant treatments without FJ (control group). Ninety-six percent of patients ($n = 48$) in the FJ group successfully completed the neoadjuvant treatment but only 81.6% of patients without FJ ($n = 31$; $p = 0.004$). The FJ group was divided between responders: 37 patients with a weight response (74%), and nonresponders: 13 patients without weight response (26%). In the FJ group, the nutritional response during preoperative chemotherapy was a significant predictive factor for the achievement of second stage oesogastric resection ($p = 0.002$).

Conclusions. FJ with enteral nutritional support during the preoperative management of OGA is a safe and effective support for the completion of the preoperative chemotherapy. The weight response to the enteral support is a predictor factor for a completion of the preoperative chemotherapy and could identify a group of patients who would have a better chance of reaching radical surgery.

During the past 20 years, the incidence of oesogastric adenocarcinoma (OGA) has increased in the western world.[1–3] Preoperative neoadjuvant chemotherapy decreases tumor activity, increases its resectability, and improves disease-free and overall survival. Thus, preoperative treatment is designed to eradicate micrometastatic disease and potentially downstage cancers to obtain a curative surgery.[2,4] One of the factors limiting the survival in patients with OGA is the small number of patients eligible for a curative surgery, because some might not be able to receive the planned perioperative therapy, especially because of their poor performance status.

Nutritional management and accurate preoperative tumor staging are crucial for the patient's care, especially with this type of tumor. Patients with OGA have an estimated weight loss around 60%, which is a factor of poor prognosis, as a weight loss exceeding 15% of the usual body weight is known to be associated with significantly higher morbidity and mortality.[4–17] Patients presenting with weight loss at the time of diagnosis also have a decreased overall survival.[6,8,9,16–18] While a postoperative nutritional support is becoming a well-established part of the patient's care, preoperative nutritional support is still not a standardized option. In locally advanced OGA, aggressive combined oncologic therapies using cytotoxic agents (such as cisplatin, 5-fluoruracil, epirubicin, irinotecan) that are known to be associated with gastrointestinal

side effects may worsen an already deteriorated nutritional status. Furthermore, preoperative oral nutritional support is not always possible in OGA, especially in case of dysphagia. The purpose of this study was to investigate the impact of a preoperative feeding jejunostomy (FJ) in the management of potentially resectable OGA.

METHODS

Study Setting and Selection of Participants

The Ethics Committee of our institution approved the study, and all patients gave their written consent for their participation in this monocentric study. Patients presenting with OGA were consecutively and retrospectively included in the database between January 2007 and December 2014. All patients were classified according to sex, age, World Health Organization (WHO) score, tumor location according to the Siewert classification, tumor staging, comorbidities, usual body mass index (BMI), BMI at diagnosis, percentage of weight loss and nutritional risk index (NRI) (Tables 1, 2).[19]

Patients presenting with a nonmetastatic OGA, with WHO score 0–2, and treated with a perioperative chemotherapy protocol were included in our study. The exclusion criteria were: confirmed metastatic disease on noninvasive staging techniques [total-body computed tomography or positron-emission tomography (PET scan)], WHO score 3 or 4, positive macroscopic peritoneal carcinomatosis or positive peritoneal cytology in staging laparoscopy (SL), and the absence of perioperative chemotherapy.

For all study population patients, a nutritional assessment was conducted by measurement of BMI, serum albumin and prealbumin, NRI score, oral intake, and daily caloric requirements. According to the literature, NRI score was used to assess initial nutritional status and to monitor the impact of nutritional interventions.[20–28] All patients presenting with dysphagia or insufficient oral intake and NRI < 97.5 underwent a staging laparoscopy with peritoneal washing associated with the placement of a FJ during the same operating time. If NRI > 97.5, patients only underwent the SL with the peritoneal washing. All patients without liquid dysphagia in the group with and

TABLE 1 Baseline demographic and clinical characteristics

	Total study population ($n = 88$)	Control group ($n = 38$)	FJ group ($n = 50$)	p value
Mean age ± SD (year)	59.83 ± 10.5	59.5 ± 10.1	60.08 ± 10.9	0.80
Gender				
Female	21 (23.86%)	42.86%	57.14%	0.97
Male	67 (76.14%)	43.28%	56.72%	
WHO score				
0	58 (65.91%)	46.55%	53.45%	0.58
1	27 (30.68%)	37.04%	62.96%	
2	3 (3.41%)	33.33%	66.67%	
Siewert classification				
1	45 (51.14%)	33.33%	66.67%	0.42
2	18 (20.45%)	38.89%	61.11%	
3	25 (28.41%)	64.00%	36.00%	
Isolated cells				
Yes	13 (14.77%)	30.77%	69.23%	0.33
No	75 (85.23%)	45.33%	54.67%	
Grading				
1	45 (51.14%)	46.67%	53.33%	0.91
2	28 (31.82%)	39.29%	60.71%	
3	13 (14.77%)	38.46%	61.54%	
4	2 (2.27%)	50%	50%	
T stage				
T2	26.14%	52.17%	47.83%	0.39
T3	64.77%	42.11%	57.89%	
T4	9.09%	25.00%	75.00%	
Mean BMI ± SD at admission (kg/m²)	26.18 ± 5.41	26.57 ± 5.07	25.87 ± 5.70	0.56

TABLE 2 Nutritional risk index before and after chemotherapy

Nutritional Risk Index (NRI)	Control group (n = 38)	FJ group (n = 50)	p value	Responders group (n = 37)	Nonresponders group (n = 13)	p value
Mean NRI before chemotherapy ± SD	93.66 ± 8.01	96.47 ± 8.03	0.053	95.47 ± 8.19	99.29 ± 7.09	0.07
Mean NRI after chemotherapy ± SD	95.23 ± 8.71	94.61 ± 9.28	0.75	96.63 ± 7.65	88.85 ± 11.30	0.003

without FJ had a supplementary oral intake (Fresubin® Jucy Drink, Fresenius Kabi; Fresubin® 2 kcal Fibre Drink, Fresenius Kabi). Oral intake was evaluated by the nutritionist during preoperative period every 15 days to adapt total intake (enteral and oral).

Outcomes and results were evaluated and compared between patients with NRI < 97.5 who underwent the preoperative placement of a FJ (FJ group) versus a control group (NRI > 97.5). Weight response to the enteral nutritional support during neoadjuvant treatment was evaluated to classify patients between those who gained weight or stabilized their weight (responders group) and those who did not (nonresponders group). Postoperative complications of SL, FJ, and oesogastric resection were defined according to the Clavien-Dindo score.[29]

Surgical Technique of the Feeding Jejunostomy

Once the SL with peritoneal washing was performed and any required biopsies were taken, we identified the first jejunal loop 20 to 30 cm away from the Treitz ligament. Then, we performed a mid-line incision approximately 10 cm above the umbilicus and exteriorized the first jejunal loop. Afterwards, we introduced a jejunal catheter through abdominal wall of the left subcostal area, using a needle kit for jejunostomy (Kangaroo™, Covidien™) and performed a jejunostomy according to Witzel technique.[30] At the end of this procedure, we routinely fixed the jejunal loop to the posterior part of the abdominal wall with four stitches (3/0 Vicryl™, Ethicon®) at cardinal points around the site of introduction of the catheter. An additional stitch was placed in caudal position and two stitches in ventral position to stabilize the jejunal loop and avoid twists. The permeability of the jejunal catheter was tested during all phases of the procedure. The patient was fed through the FJ within the first 24 h of the immediate post-operative period, with a gradual increase of the volume and concentration of the nutrition to achieve the targeted calories required for the patient. The patient was then fed through the jejunostomy continuously during the neoadjuvant treatment, until the surgical resection according to the nutritionist's prescriptions, which were reevaluated every

15 days to ensure adequate calorie intake. Immunonutrition was prescribed the week before surgical resection according to French recommendations.[18]

Statistical Analysis

Chi-square and Fisher's exact tests were used to determine the association between nominal variables. Student's t test was used to evaluate differences in means between two groups of continuous variables. Planned subset analysis between FJ group and control group and between responders and nonresponders also was performed. A multivariate logistic regression analysis was performed to assess the independency of the association between the FJ and the completion of the neoadjuvant treatment and the rate of radical surgical resections. A difference was considered significant when p value < 0.05. Only variables with p value < 0.20 on univariate analysis were included in the multivariate analysis. All statistical calculations were performed using SPSS 10.0 (SPSS Inc., Chicago, IL).

RESULTS

Cohort Demographics

We included 114 consecutive patients presenting with OGA. Twenty-six patients were excluded: 12 patients (10.5%) whose tumor was staged less than IB, who underwent surgical oncological resection without any neoadjuvant treatment, and 14 patients (12.3%) who presented with a positive peritoneal washing on the staging laparoscopy.

Eighty-eight patients were analyzed. The FJ group comprised 50 patients (56.8%) who underwent the placement of a FJ, and 38 patients (43.2%) were included in the control group, because they only received perioperative chemotherapy without enteral nutritional support. Demographic, clinical and nutritional characteristics of the two groups are reported in Tables 1 and 2. There was no difference between the clinical data of the two groups. The complication rate related to the surgical FJ procedure was 6%: 1 patient (2%) presented with an abdominal wall

abscess (Grade IIIA) and 2 patients (4%) with intestinal occlusion (Grade IIIB) treated with surgery.

Predictive Factors for Preoperative Chemotherapy

FJ was an independent predictive factor for the achievement of the preoperative chemotherapy cycles in both the uni- and the multi-variate analysis (Tables 3, 4; $p = 0.04$). The neoadjuvant treatment was successful completed in 96% of patients with a FJ ($n = 48$), but it was only completed by 81.6% of the patients of the control group, without a FJ ($n = 31$). In patients with a FJ, the neoadjuvant treatment was only interrupted in two patients (4%). Only one of the interruption was related to the FJ; one patient (2%) developed an intolerance to the enteral

nutrition compound (association of nausea and vomiting) at the end of the second cycle of chemotherapy out of the three planned. The other cause of interruption was not related to the FJ; one patient (2%) needed a change of chemotherapy due to a metastatic progression of the disease. On the contrary, the neoadjuvant treatment was interrupted in patients without FJ mostly because of an intolerance to the chemotherapy associated with excess weight loss (6/7 patients, 85.7%).

According to the nutritional response to enteral nutrition (weight gain or stabilization), during the neoadjuvant treatment, the FJ patients were divided into responders group: 37 patients (74%) and nonresponders group: 13 patients (26%). All responders have completed the preoperative chemotherapy cycles. An interruption of the

TABLE 3 Univariate analysis with logistic regression reporting odds ratio (OR) and 95% CI

	All cycles of preoperative chemotherapy completed	*p* value	Radical surgery performed	*p* value
Age	1.00 (0.96–1.07)	0.987	0.90 (0.82–0.99)	0.046
Gender				
Female	Reference		Reference	
Male	0.97 (0.21–5.79)	0.903	2.39 (0.61–9.45)	0.214
WHO score				
0	Reference		Reference	
1	0.58 (0.11–3.01)	0.520	0.92 (0.21–4.00)	0.915
2	1.00		0.23 (0.01–2.94)	0.259
Siewert classification				
1	Reference		Reference	
2	0.47 (0.05–4.33)	0.51	0.77 (0.17–3.47)	0.733
3	1.09 (0.23–5.00)	0.91	3.69 (0.41–32.57)	0.240
Isolated cells				
0	Reference		Reference	
1	1.00		1.00	
Grading				
1	Reference		Reference	
2	2.33 (0.48–11.31)	0.293	0.58 (0.15–2.20)	0.419
3	2.55 (0.37–17.16)	0.337	1.00	0
4	1.00		1.00	
T stage				
T2	Reference		Reference	
T3	0.36	0.175	0.68 (0.13–3.54)	0.175
T4	0.68	0.747	0.67 (0.05–8.52)	0.755
N stage				
N0	Reference		Reference	
N+	0.56 (0.17–1.94)	0.367	0.21 (0.03–1.75)	0.149
BMI at admission	0.98 (0.86–1.12)	0.792	1.08 (0.93–1.24)	0.296
Jejunostomy				
No	Reference	0.043	Reference	0.829
Yes	0.19 (0.04–0.95)		0.86 (0.23–3.30)	

166

TABLE 4 Multivariate analysis with primary and secondary endpoints

	All cycles of preoperative chemotherapy completed	At least one cycle of chemotherapy interrupted	p value	Radical surgery performed	Radical surgery not performed	p value
Control group (n = 38)	31 (81.6%)	7 (18.4%)	0.04	34 (89.5%)	4 (10.5%)	0.97
FJ group (n = 50)	48 (96%)	2 (4%)		41 (82%)	9 (18%)	
FJ group: Responders group (n = 37)	37 (100%)	0 (0%)	0.01	34 (91.9%)	3 (8.1%)	0.002
FJ group: nonresponders group (n = 13)	11 (84.6%)	2 (15.4%)		7 (53.85%)	6 (46.15%)	

neoadjuvant treatment was only observed in the nonresponders group where 15.4% of the patients were not able to complete the full cycles of chemotherapy (15.4% in nonresponders vs. 0% in responders, $p = 0.01$). The NRI difference at the beginning of chemotherapy was at the limit of the statistical significance ($p = 0.053$) between control group and FJ group (Table 2). After chemotherapy, there were no statistical differences between control and FJ groups ($p = 0.75$).

Predictive Factors to Achieve Oesogastric Radical Resection

The performance of the oesogastric radical resection was not associated with the presence or the absence of a preoperative FJ on the uni- and multi-variate analysis (Tables 3, 4). A radical oncological surgical resection was obtained in 41 patients with a FJ (82%) compared with 34 patients without FJ (89.5%; $p = 0.32$). However, when analyzing the subgroups of patients with a FJ, a nutritional response during preoperative chemotherapy was a significant predictive factor for the achievement of the oesogastric resection. A surgical radical resection was obtained in 91.9% of the patients ($n = 34$) who responded to the FJ (responders group), but only in 53.85% of the nonresponder patients ($n = 7$; $p = 0.002$). A progressive disease was observed in 16% of FJ group ($n = 8$) and 5.26% of control group ($n = 2$; $p = 0.11$). Among FJ group, 38.5% of nonresponders ($n = 5$) had a progressive disease compared with 8.1% of responders ($n = 3$; $p = 0.01$). FJ did not decrease the postoperative morbidity after the oesogastric resection. A major morbidity with a Clavien-Dindo score superior or equal to grade 3 was observed in 21.9% in the FJ group ($n = 9$) compared with 20.6% in the control group ($n = 7$; $p = 0.88$).[20]

DISCUSSION

The purpose of this study was to evaluate the impact of a preoperative FJ during the neoadjuvant treatment of patients with OGA. Preoperative FJ enabled significantly more the patients to achieve all the full cycles of preoperative chemotherapy compared to control group without FJ (96% vs. 81.6%; $p = 0.004$). Considering patients with a FJ, the rate of radical surgical resection also was significantly higher in patients who presented a nutritional response to the FJ (responders group, 91.9%) than in patients who did not (no responders, 53.85%). Our results indicated a positive and decisive impact of FJ for the outcome of surgical resection procedures of cancer patients with OGA. This impact was observed at the level of the ability of the patients to sustain a full chemotherapeutic protocol when responding to the FJ, which favors the rate of second-stage surgical resection. These results are an important step into the patient care of OGA cancers that often are associated with body weight loss and allow a better definition of the recommendations for FJ.

Indeed, OGA are aggressive tumors with a poor prognosis even when completely resectable.[31–35] When diagnosed, almost two thirds of the patients with a gastric cancer present with a locally advanced disease.[33] In western countries, with surgery alone, a R0 resection (macroscopic and microscopic complete resection according to the International Union Against Cancer) is only obtained in 41.1% of the cases, and the median overall survival is only of 16.4 months.[34] Thus, perioperative chemotherapy is the "gold standard" for the managment of OGA.[35–38] The MAGIC trial evaluated the effect of a combination of pre- and postoperative chemotherapy compared with surgery alone in patients with resectable adenocarcinoma of the stomach or lower oesophagus. The overall and progression-free survivals were significantly improved in the chemotherapy-containing arm.[35] The 5-year survival rate was 36% in the perioperative chemotherapy group compared with only 23% in the group without perioperative chemotherapy.[35] However, it is difficult to assess the relative contribution of the pre- and postoperative components of the chemotherapy on the patient's survival rate in both the MAGIC and ACCORD-07 trials.[35–38]

To receive a neoadjuvant chemotherapy, patients need to be fit enough and not in a degraded physical condition. A loss of bodyweight is almost inevitable and causes serious

problems in the pre- and postoperative management of OGA. Supplementation through preoperative nutritional support and immunonutrition has already proven to benefit critically ill patients with acute respiratory distress or patients undergoing a major abdominal surgery.[39–47] Evidence-based guidelines recommend a preoperative nutritional intervention lasting for 7 to 14 days in moderately or severely malnourished patients undergoing major gastrointestinal surgery.[45–47] In OGA, dysphagia may be the limiting factor of the oral administration of preoperative nutritional support. Furthermore, the patient's adherence to this type of nutritional support may not be optimal. An early preoperative nutritional support using a FJ could be an alternative for the improvement of the preoperative nutritional status, while minimizing the impact of the patient's adherence to the nutritional program. In our series, the FJ group had a 74% nutritional response during preoperative management, and this effect was significantly correlated to the achievement of all cycles of preoperative chemotherapy (96 vs. 81.6%), but also the achievement of the oesogastric surgery (91.1 vs. 89.5%). The achievement of the oesogastric surgery is limited to the patient that responded to the FJ, indicating clearly that the critical factors are the physiological impact of the FJ and not the surgical procedure by itself. However, the exact physiological factors responsible for the better outcome have not been identified. They might be overall body weight, BMI, muscle mass, or blood components. It also remains unknown why a significant fraction of the patients with FJ did not respond properly. This might be a critical point for further improvement.

The benefits from a nutritional support in well-nourished subjects are still controversial.[48,49] In our cohort, patients in the control group did not have dysphagia or any criteria of denutrition at the time of diagnosis. However, more patients with FJ achieved the full length of the neoadjuvant chemotherapy treatment than patients without FJ. Despite a higher rate of progressive disease observed in FJ group than in control group (respectively, 16% vs. 5.26%; $p = 0.11$), the completion rate of chemotherapy was higher (respectively, 96% vs. 81.6%; $p = 0.04$). Thus, these results suggest that a FJ could be useful in all patients with OGA, even those without denutrition at diagnosis. These positive results need to be counterbalanced with few potential postoperative complications that might occur after the placement of a FJ. In our study, the complications rate was very low (6%). This low rate of complications is in accordance with the literature, and it is observed even when the feeding catheter is used for a longer period of time.[46,47,50–52] In a series of more than 500 esophagectomies, the Witzel tube jejunostomy was found to be safe with a low complication rate (2.1%) and to be an efficient way to provide enteral nutrition.[47,51]

Few studies have been perfomed to assess the impact of a FJ on the preoperative management of OGA. Our monocentric study, with a limited population has inherent limitations and sources of bias. A multicentric, randomized trial with a large population is necessary for a more thorough analysis of the impact of a FJ on the preoperative managment of OGA.

CONCLUSIONS

Feeding jejunostomy with enteral nutritional support during the preoperative management of oesogastric adenocarcinomas is a safe and effective support for the completion of the preoperative chemotherapy. The weight response to the enteral support is a predictor factor for a completion of the preoperative chemotherapy and could identify a group of patients with a higher nutritionally risk that would have better chance of reaching radical surgery.

DISCLOSURE None.

REFERENCES

1. Brown LM, Swanson CA, Gridley G, et al. Adenocarcinoma of the esophagus: role of obesity and diet. *J Natl Cancer Inst.* 1995;87:104–9.
2. Chow WH, Blot WJ, Vaughan TL, et al. Body mass index and risk of the esophagus and gastric cardia. *J Natl Cancer Inst.* 1990;90:150–5.
3. Lagergen J, Bergstrom R, Nyren O. Association between body mass index and adenocarcinoma of the esophagus and gastric cardia. Ann Intern Med. 1999;130:883-90.
4. Daly JM, Fry WA, Little AG et al. Esophageal cancer: results of an American College of Surgeons patient care evaluation study. *J Am Coll Surg.* 2000;190:562–72.
5. Martin CA, Walsh GL, Morelan K. Relationship of weight loss and postoperative nutritional complications in esophagoastric surgery. *J Parenter Enteral Nutr.* 1999;23:S20.
6. Burden S, Todd C, Lal S. Preoperative nutrition support in patients undergoing gastrointestinal surgery. *Cochrane Database Syst Rev.* 2012;11:CD008879.
7. Schiesser M, Müller S, Kirchhoff P, et al. Assessment of a novel screening score for nutritional risk in predicting complications in gastrointestinal surgery. *Clin Nutr.* 2008;27:565–70.
8. Christein JD, Hollinger EF, Millikan KW. Prognostic factors associated with resectable carcinoma of the esophagus. *Am Surg.* 2002;68:258–62.
9. Ikeda M, Natsugoe S, Ueno S, et al. Significant host- and tumor-related factors for predicting prognosis in patients with esophageal carcinoma. *Ann Surg.* 2003;238:197–202.
10. Windsor A, Braga M, Martindale R, et al. Fit for surgery: an expert panel review on optimizing patients prior to surgery, with a particular focus on nutrition. *Surgeon.* 2004;2:315–9.
11. O'Gormann RB, Feliciano DV, Matthews KS, et al. Correlation of immunologic and nutritional status with infectious complications after major abdominal trauma. *Surgery.* 1986;99:549–56.
12. Gibbs J, Cull W, Henderson WC, et al. Preoperative serum albumin level as predictor of operative mortality and morbidity: results from national VA surgical risk study. *Arch Surg.* 1999;134:36–42.

13. Bailey SH, Bull DA, Harpole DH, et al. Outcomes after esophagectomy: a ten years prospective cohort. *Ann Thorac Surg.* 2003;75:217–22.

14. Belghiti J, Langonnet E, Bourstiyn E, et al. Surgical implications of malnutrition and immunodeficiency in patients with carcinoma of the esophagus. *Br J Surg.* 1983;70:339–41.

15. Conti S, West J, Fitzpatrick HF. Mortality and morbidity after esophagogastrectomy for cancer of the esophagus and cardia. *Am Surg.* 1997;43:92–6.

16. Nozoe T, Kimura Y, Ishida M, et al. Correlation of preoperative nutritional condition with postoperative complications in surgical treatment for esophageal carcinoma. *Eur J Surg Oncol.* 2002;28:396–400.

17. Pedersen H, Hansen HS, Cederqvist C, et al. The prognostic significance of weight loss and its integration in stage-grouping of esophageal cancer. *Acta Chir Scand.* 1982;148:363–6.

18. Mariette C, De Botton ML, Piessen G. Surgery in esophageal and gastric cancer patients: what is the role for nutrition support in your daily practice? *Ann Surg Oncol.* 2012;19:2128–34.

19. Siewert JR, Stein HJ, Feith M. Adenocarcinoma of the esophago-gastric junction. *Scand J Surg.* 2006;95:260–9.

20. Van Cutsem E, Arends J. The causes and consequences of cancer-associated malnutrition. *Eur J Oncol Nurs.* 2005;9 Suppl 2:S51–63.

21. Sungurtekin H, Sungurtekin U, Balci C, et al. The influence of nutritional status on complications after major intraabdominal surgery. *J Am Coll Nutr.* 2004;23:227–32.

22. Fruchtenicht AV, Poziomyck AK, Kabke GB, et al. Nutritional risk assessment in critically ill cancer patients: systematic review. *Rev Bras Ter Intensiva.* 2015;27:274–83.

23. Faramarzi E, Mahdavi R, Mohammad-Zadeh M, et al. Validation of nutritional risk index method against patient-generated subjective global assessment in screening malnutrition in colorectal cancer patients. *Chin J Cancer Res.* 2013;25:544–8.

24. Ottery FD. Definition of standardized nutritional assessment and interventional pathways in oncology. *Nutrition.* 1996;12:S15–9.

25. Poziomyck AK, Fruchtenicht AV, Kabke GB, et al. Reliability of nutritional assessment in patients with gastrointestinal tumors. *Rev Col Bras Cir.* 2016;43:189–97.

26. Abe Vicente M, Barão K, Silva TD, et al. What are the most effective methods for assessment of nutritional status in outpatients with gastric and colorectal cancer? *Nutr Hosp.* 2013;28:585–91.

27. Caccialanza R, Klersy C, Cereda E, et al. Nutritional parameters associated with prolonged hospital stay among ambulatory adult patients. *CMAJ.* 2010;23;182:1843–9.

28. Cox S, Powell C, Carter B, et al. Role of nutritional status and intervention in oesophageal cancer treated with definitive chemoradiotherapy: outcomes from SCOPE1. *Br J Cancer.* 2016;115:172–7.

29. Dindo D, Demartines N, Clavien PA. Classification of surgical complications a new proposal with evaluation in a cohort of 6336 patients and results of a survey. *Ann Surg.* 2004;240:205–13.

30. Harbinson SP. Intubation of the stomach and small intestine. In: Surgery of the alimentary tract, vol 1, 6th edn. Philadelphia: Saunders Elsevier. P. 749–59.

31. Chau I, Norman AR, Cunningham D, et al. Multivariate prognostic factor analysis in locally advanced and metastatic esophago-gastric cancer: pooled analysis from three multicenter, randomized, controlled trials using individual patient data. *J Clin Oncol.* 2004;22:2395–403.

32. Gertler R, Stein HJ, Langer R, et al. Long-term outcome of 2920 patients with cancers of the esophagus and esophagogastric junction: evaluation of the New Union Internationale Contre le Cancer/American Joint Cancer Committee staging system. *Ann Surg.* 2011;253:689–98.

33. Greenlee RT, Murray T, Bolden S, et al. Cancer statistics, 2000. *CA Cancer J Clin.* 2000;50:7–33.

34. Roder JD, Böttcher K, Siewert JR, et al. Prognostic factors in gastric carcinoma. Results of the german gastric carcinoma study 1992. *Cancer.* 1993;72:2089–97.

35. Cunningham D, Allum WH, Stenning SP, et al. Perioperative chemotherapy versus surgery alone for resectable gastro-sophageal cancer. *N Engl J Med.* 2006;355:11–20.

36. Ychou M, Boige V, Pignon JP, et al. Perioperative chemotherapy compared with surgery alone for resectable gastroesophageal adenocarcinoma: an FNCLCC and FFCD multicenter phase III trial. *J Clin Oncol.* 2011;29:1715–21.

37. Schuhmacher C, Gretschel S, Lordick F, et al. Neoadjuvant chemotherapy compared with surgery alone for locally advanced cancer of the stomach and cardia: European Organisation for Research and Treatment of Cancer randomized trial 40954. *J Clin Oncol.* 2010;28:5210–8.

38. Marrelli D, Polom K, de Manzoni G, et al. Multimodal treatment of gastric cancer in the west: Where are we going? *World J Gastroenterol.* 2015;21:7954–69.

39. Braga M, Gianotti L, Vignali A, et al. Preoperative oral arginine and n-3 fatty acid supplementation improves the immunometabolic host response and outcome after colorectal resection for cancer. *Surgery.* 2002;132:805–14.

40. Rice TW, Wheeler AP, Thompson BT, et al. Enteral omega-3 fatty acid, gamma-linolenic acid, and antioxidant supplementation in acute lung injury. *JAMA.* 2011;306:1574–81.

41. Ryan AM, Reynolds JV, Healy L, et al. Enteral nutrition enriched with eicosapentaenoic acid (EPA) preserves lean body mass following esophageal cancer surgery: results of a double-blinded randomized controlled trial. *Ann Surg.* 2009;249:355–63.

42. Perinel J, Mariette C, Dousset B, et al. Early enteral versus total parenteral nutrition in patients undergoing pancreaticoduodenectomy: a randomized multicenter controlled trial (Nutri-DPC). *Ann Surg.* 2016;264:731–7.

43. Beale RJ, Bryg DJ, Bihari DJ. Immunonutrition in the critically ill: a systematic review of clinical outcome. *Crit Care Med.* 1999;27:2799–805.

44. Heyland DK, Novak F, Drover JW, et al. Should immunonutrition become routine in critically ill patients? A systematic review of the evidence. *JAMA.* 2001;286:944–53.

45. Heys SD, Walker LG, Smith I, et al. Enteral nutritional supplementation with key nutrients in patients with critical illness and cancer: a metaanalysis of randomized controlled clinical trials. *Ann Surg.* 1999;229:467–77.

46. Gianotti L, Braga M, Nespoli L, et al. A randomized controlled trial of preoperative oral supplementation with a specialized diet in patients with gastrointestinal cancer. *Gastroenterology.* 2002;122:1763–70.

47. Zheng Y, Li F, Qi B, et al. Application of perioperative immunonutrition for gastrointestinal surgery: a meta-analysis of randomized controlled trials. *Asia Pac J Clin Nutr.* 2007;16:253–7.

48. Bower MR, Martin RC. Nutritional management during neoadjuvant therapy for esophageal cancer. *J Surg Oncol.* 2009;100:82–7.

49. Bozzetti F. Nutritional support in patients with oesophageal cancer. *Support Care Cancer.* 2010;18:S41–50.

50. Jenkinson AD, Lim J, Agrawal N, et al. Laparoscopic feeding jejunostomy in esophagogastric cancer. *Surg Endosc.* 2007;21:299–302.

51. Gerndt SJ, Orringer MB. Tube jejunostomy as an adjunct to esophagectomy. *Surgery.* 1994;115:164–9.

52. Bueno JT, Schattner MA, Barrera R, et al. Endoscopic placement of direct percutaneous jejunostomy tubes in patients with complications after esophagectomy. *Gastrointest Endosc.* 2003;57:536–40.

169

Check for updates

How to Prevent Sarcopenia Occurrence during Neoadjuvant Chemotherapy for Oesogastric Adenocarcinoma?

Marlène Voisinet[a], Aïna Venkatasamy[b,c], Hefzi Alratrout[a], Jean-Baptiste Delhorme[a,c], Cécile Brigand[a,c], Serge Rohr[a,c], Christian Gaiddon[c], and Benoît Romain[a,c]

[a]Department of Digestive Surgery, Strasbourg University Hospital, Strasbourg, France; [b]Department of Radiology, Strasbourg University Hospital, Strasbourg, France; [c]Inserm IRFAC UMR_S1113, Laboratory STREINTH, Université de Strasbourg, Strasbourg, France

ABSTRACT

The aim of this study was to evaluate the impact of a preoperative feeding jejunostomy (FJ) on the occurrence of sarcopenia before and after preoperative chemotherapy for patients with an oesogastric adenocarcinoma (OGA). Forty-six patients with potentially resectable OGA were enrolled in a perioperative chemotherapy protocol. Sarcopenia was evaluated by measuring muscle surfaces (psoas, paraspinal and abdominal wall muscles) on abdominal CT images at the level of the 3rd lumbar vertebra. A FJ was placed in 31 patients (67.4%) before the neoadjuvant treatment (FJ group), while 15 patients (32.6%) started neoadjuvant treatments without FJ (control group). After preoperative chemotherapy, there were significantly more sarcopenic patients in the control group, compared to the FJ group. In the FJ group, 13% of the patients ($n = 4$) were sarcopenic before treatment and 22.6% of them ($n = 7$) became sarcopenic after preoperative chemotherapy ($p = 0.3$). In the control group, if initially only 6.7% ($n = 1$) of patients were sarcopenic, the majority of the patients (60%, $n = 9$) became sarcopenic after chemotherapy ($p = 0.012$). The FJ was an independent risk factor of sarcopenia after neoadjuvant chemotherapy. FJ with enteral nutritional support during the preoperative management of OGA seemed to efficiently counteract sarcopenia occurrence during preoperative chemotherapy.

Introduction

Sarcopenia, is an age-related syndrome, characterized by a progressive and generalized loss of skeletal muscle mass and strength [1]. Over the past years, sarcopenia has been gradually recognized as a negative prognosis factor after colorectal, pancreatic, hepatic, and gastric surgery [2–4]. In the recent article of Kawamura et al [2], gastric cancer patients with sarcopenia were more prone to have a reduced surgery and less likely to be treated with adjuvant chemotherapy. They also showed that in terms of long term outcomes, the overall survival was significantly shorter and deaths (from both gastric cancer as well as other causes) were more frequent in patients with sarcopenia.

Nutritional management and accurate pre-operative tumor staging are crucial for the patient's care, especially with oesogastric adenocarcinoma (OGA). Patients with OGA have an estimated weight loss around 60% which is a factor of poor prognosis [3,

4], as a weight loss exceeding 15% of the usual body weight is known to be associated with significantly higher morbidity and mortality [5]. Patients presenting with weight loss at the time of diagnosis also have a decreased overall survival [3–5]. While a post-operative nutritional support is becoming a well-established part of the patient's care, a pre-operative nutritional support is still not a standardized option. In locally advanced OGA, aggressive combined anticancer therapies using cytotoxic agents (such as cisplatin, 5-fluoruracil, epirubicin, irinotecan) are known to be associated with gastrointestinal side effects andmay worsen an already deteriorated nutritional status. Furthermore, pre-operative oral nutritional support is not always possible in OGA, especially in case of dysphagia. A preoperative feeding jejunostomy (FJ) is frequently used when denutrition is diagnosed or in case of dysphagia. Manfredelli et al. [6] have shown that preoperative FJ significantly enabled more patients to achieve all cycles of preoperative chemotherapy

CONTACT Benoît Romain ✉ benoit.romain@chru-strasbourg.fr 🏥 Department of Digestive Surgery, Strasbourg University, 3 av. Molière, 67000 Strasbourg, France

Table 1. Baseline demographic and clinical characteristics.

	Total Study Population (n = 46)	FJ group (n = 31)	Control group (n = 15)	p-value
Mean age ± SD (years)	61.6 ± 10.6	61.1 ± 11.8	62.6 ± 7.7	0.66
Gender				1.00
Female	10	7	3	
Male	36	24	12	
WHO Score				0.44
0	32	22	10	
1	13	9	4	
2	1	0	1	
Siewert Classification				0.29
1	24	17	7	
2	10	8	2	
3	12	6	6	
Isolated cells				1.00
Yes	11	8	3	
No	35	23	12	
T Stage				0.33
T2	17	13	4	
T3	27	16	11	
T4	2	2	0	
Mean BMI ± SD at admission (kg/m^2)	26.0 ± 6.1	25.6 ± 6.4	26.7 ± 5.5	0.58

compared to the control group without FJ (96% vs. 81.6%; $p = 0.004$). Considering patients with a FJ, the rate of radical surgical resection was also significantly higher in patients who presented a nutritional response to the FJ (responders group, 91.9%) than in patients who did not (no- responders, 53.85%). These results indicated a positive and decisive impact of FJ for the outcome of surgical resection procedures of cancer patients with OGA. The objective of our study was to elucidate the impact of a preoperative FJ on sarcopenia in patients with OGA after preoperative chemotherapy.

Material and Methods

Study Setting and Selection of Participants

The Ethics Committee of our institution approved the study and all patients gave their written consent for their participation in this monocentric study. Patients presenting with OGA were consecutively and retrospectively included in the database between January 2007 and March 2017. All patients were classified according to sex, age, World Health Organization (WHO) score, tumor location according to the Siewert classification [7], tumor staging, comorbidities, usual Body Mass Index (BMI), and Nutritional Risk Index (NRI) (Table 1).

Patients presenting with a non-metastatic OGA, with a WHO score 0–2, treated with a perioperative chemotherapy protocol and who underwent an abdominal computed tomography (CT) before and after chemotherapy were included in our study. The exclusion criteria were: confirmed metastatic disease on noninvasive staging techniques (total-body computed tomography or positron-emission tomography

(PET-Scan)), WHO score 3 or 4, positive macroscopic peritoneal carcinomatosis or positive peritoneal cytology in staging laparoscopy (SL), the absence of perioperative chemotherapy. We also excluded patients with missing imaging data (CT) either before and/or after preoperative chemotherapy, and patients did not have second stage surgical resection of the primitive tumor. In the analyze of factors influencing the occurrence of sarcopenia after preoperative chemotherapy, we excluded patients with preexistent sarcopenia before preoperative chemotherapy. Complications were graded according to Clavien-Dindo classification [8]. Major complications were defined as a complication with a grade superior or equal to 3a.

For all study population patients, a nutritional assessment was conducted by measurement of BMI, serum albumin and prealbumin, NRI score, oral intake, daily caloric requirements. According to the literature, NRI score was used to assess initial nutritional status and to monitore the impact of nutritional interventions [9, 10]. From January 2010 to December 2014, only patients presenting with dysphagia or insufficient oral intake and a NRI < 97.5 underwent a staging laparoscopy with peritoneal washing associated with the placement of a FJ during the same operating time. If the NRI was above 97.5, the patients only underwent the SL with the peritoneal washing. Since January 2015, all patients have had a SL with a FJ performed. We have compared patients without FJ (control group) to patients with a FJ.

All patients without or with liquid dysphagia had a supplementary oral intake (Fresubin® Jucy Drink, Fresenius Kabi; Fresubin® 2 kcal fiber Drink, Fresenius Kabi). Oral intake was evaluated by a

Table 2. Nutritional risk index before and after chemotherapy.

Nutritional Risk Index (NRI)	FJ Group (n = 31)	Control Group (n = 15)	p-value
Mean NRI before chemotherapy ± SD	76.3 ± 25.1	86.7 ± 21.8	0.16
Mean NRI after chemotherapy ± SD	94.5 ± 9.7	91.8 ± 11.3	0.43

nutritionist during preoperative period, every 15 day, in order to adapt total intake (enteral and oral).

Sarcopenia Evaluation

Each patient's record was reviewed for abdominal CT images, acquired before and after the chemotherapy cycles, in both FJ and control groups. Muscle mass was evaluated on electronically stored images, which were taken for routine diagnosis purposes. According to the literature [11, 12], the third lumbar vertebrae (L3) served as a landmark for the choice of the segmented CT slice used for the measurement of the muscle cross-sectional area. The skeletal muscle comprised the psoas muscle, paraspinal muscles (erector spinae, quadratus lomborum) and abdominal wall muscles (rectus abdominus, internal and external obliques and transversus abdominus), which were identified and quantified using Housefield units (HU) thresholds from −30 to +110 HU. Surfaces were measured with Image J ® software. The muscles cross-sectional areas was segmented automatically and manually corrected if needed and cross sectional areas (cm^2) of the sum of all these muscles were computed for each patient. The obtained value was normalized for stature through body-surface area (by the use of the Mosteller formula [body-surface area (m^2) = (height (cm) × weight (kg)/3600) × 0.5]. Cutoffs for sarcopenia were based on CT-based guidelines by Prado et al. [11] (ie., L3 skeletal muscle index < 38.5 cm2/m2 for women and < 52.4 cm2/m2 for men).

Follow-Up

All patients were followed every 3 to 6 mo, with a physical examination. The diagnosis of recurrences was based on postoperative examination, imaging, tumor markers, or biopsy.

Statistical Analysis

Chi-square and Fisher's exact tests were used to determine the association between nominal variables. Student's t-test was used to evaluate differences in means between two groups of continuous variables. A univariate and multivariate logistic regressions were also performed. A difference was considered significant when p-value was < 0.05. Only variables with a p-value < 0.20 on univariate analysis were included in

the multivariate analysis. Kaplan-Meier survival was calculated from the date of liver resection and significant differences were determined with a log-rank test. All statistical calculations were performed using SPSS 10.0 (SPSS Inc., Chicago, IL).

Results

Cohort Demographics

We included 46 consecutive patients presenting with OGA imaged by abdominal CT before and after preoperative chemotherapy. The FJ group comprised 31 patients who underwent the placement of a FJ and 15 patients were included in the control group, as they only received perioperative chemotherapy without enteral nutritional support. Demographic, clinical and nutritional characteristics of the 2 groups are reported in Tables 1 and 2. There was no difference between the two groups in terms of demographics data. Nutritional status was decreased in the FJ group compared to control group before preoperative chemotherapy, but the difference between the two groups was not significant (p = 0.16) (Table 2).

Sarcopenia Incidence

In the control group, only 6.7% (n = 1) of the patients were initially sarcopenic, but the majority of them (60%, n = 9) became sarcopenic after preoperative chemotherapy (p = 0.002). In the FJ group, 13% of the patients (n = 4) were sarcopenic at inclusion, but only seven of them (22.6%) became sarcopenic after preoperative chemotherapy (p = 0.3). More patients became sarcopenic in the control group (without FJ) after preoperative chemotherapy than in the FJ group (respectively 60% vs 22.6%; p = 0.012).

Factors Influencing Radiologic Sarcopenia

We have studied different factors which might significantly influence the occurrence of sarcopenia after preoperative chemotherapy. For this purpose, we excluded patients (n = 5) with preexistent sarcopenia (before preoperative chemotherapy). Age and preoperative feeding jejunostomy were significant risk factors of sarcopenia (p = 0.02 and p = 0.006 respectively; Table 3). In the multivariate analysis factors, age

Table 3. Risk factors of sarcopenia occurrence. Patients with sarcopenia at the diagnosis were excluded ($n = 5$).

	Sarcopenia	p-value
Age (years)		
≤59	2	0.02
≥60	12	
Gender		
Female	3	1.00
Male	11	
WHO Score		
0	9	0.32
1	4	
2	1	
Siewert Classification		
1	10	0.06
2	0	
3	4	
Signet ring cells		
0	10	0.69
1	4	
T stage		
T2	6	0.82
T3	8	
T4	0	
Preoperative chemotherapy interruption		
Yes	1	0.34
BMI at admission		
<20	2	0.23
20-<25	4	
25-<30	6	
≥30	2	
Jejunostomy		
No	9 (64.3%)	0.006
Yes	5 (18.5%)	

≥ 60 years old and preoperative feeding jejunostomy were independent risk factors of sarcopenia ($p = 0.02$ and 0.006 respectively; Table 4).

Impact of Sarcopenia on Postoperative Morbidity, Oeso-Gastric Radical Resection Achievement and Survival

After resection of the primary tumor, if we consider sarcopenic patients together ($n = 14$; 14.3%), there were two patients with major complications (Dindoclavien ≥3a) while complications occurred in 7 patients without sarcopenia (regardless of the group, $n = 27$; 25.6%) ($p = 0.7$). Thus, sarcopenia did not appear as a significant risk factor of major postoperative complication in our study.

Sarcopenia also did not appear as a significant risk factor of prolonged length of stay after primitive tumor resection, as the mean length of stay was 18 day [7–52] in patients without sarcopenia compared to 17.5 day [9–39] in patients with sarcopenia.

The mean follow-up was 3 ± 2.2 years (range: 0.1–8.7). After gastric resection, 31 patients died during follow-up. For the two patients who died after 2 years, we have no information about a potential recurrence or the cause of death. Among the 46 studied patients, the overall survival rates, including the postoperative death, were 80%, 70.1%, 63.1%, 43.1%, and 24.6% at 1-, 2-, 3-, 4-, and 5-yearrespectively (Figure 1A). The median survival was 4.1 years in the non-sarcopenic group compared to 3.9 years in the sarcopenic group. The 1-, 3-, and 5-year overall survival of sarcopenic patients ($n = 16$) did not differ from those observed in non-sarcopenic patients ($n = 30$; $p = 0.7$). The disease-free survival rates were 69.2%, 67%, 59.7%, 56.2%, and 52% at 1-, 2-, 3-, 4-, and 5-year, respectively (Figure 1B). The disease-free survival of sarcopenic patients did not differ from those observed in non-sarcopenic patients ($p = 0.8$).

Discussion

Sarcopenia was traditionally defined as an age-related decline in muscle mass [1, 13]. The European Working Group on Sarcopenia in Older People (EWGSOP) recently proposed that the sarcopenic phenotype should also include impaired muscular strength and/or physical function [13]. In the literature, sarcopenia - irrespective of definition- is independently associated with poor prognosis across a wide range of cancers [11] suggesting that muscle dysfunction is an important factor in the cancers' history [14]. However, sarcopenia is preferentially associated with certain cancers, such as lung, pancreatic and gastric cancer, but the exact reason for this specificity remains unclear. Studies have also suggested that sarcopenia is independent of the cancer stage and the therapeutic protocols used [15], although doxorubicin induces severe sarcopenia in animal models. Importantly, it has been proposed that, in contrast to fat loss, muscle atrophy is not restored by nutritional complements [13, 16].

The purpose of this study was to further investigate the occurrence of sarcopenia in patients with OGA, and more precisely to evaluate the impact of a preoperative FJ on sarcopenia occurrence during neoadjuvant treatment. We have shown that preoperative FJ significantly decreased the occurrence of sarcopenia during the preoperative chemotherapy: 22.6% vs 60% of sarcopenia occurrence in the FJ and control groups respectively ($p = 0.012$). The absence of a preoperative FJ and age ≥ 60 years old were independent significant risk factors of sarcopenia occurrence after preoperative chemotherapy. However, sarcopenia was not a significant risk factor of major postoperative complications and prolonged length of stay after primitive tumor resection. Sarcopenia did not influence overall and disease-free survivals in our study. This differs from previous studies showing that sarcopenia is of

Table 4. Multivariate analysis with logistic regression reporting odds ratio (OR) and 95% CI.

		Crude OR	95% CI	p	Adjusted OR	95% CI	p
Preoperative FJ	No	1 (ref)	–	0.004	1 (ref)	–	0.010
	Yes	0.13	0.03-0.54		0.10	0.02-0.68	
Gender	Female	1 (ref)	–	0.954	1 (ref)	–	0.593
	Male	1.05	0.22-5.02		0.55	0.06-4.74	
Age (years)	≤59	1 (ref)	–	0.015	1 (ref)	–	0.007
	≥60	6.46	1.21-34.55		13.4	1.45-123.95	
BMI	<20	2.17	0.26-17.90	0.224	2.98	0.18-49.28	0.463
	20-<25	1 (ref)	–		1 (ref)	–	
	25-<30	4.88	0.90-26.42		3.32	0.41-27.27	
	≥30	0.93	0.13-6.40		0.49	0.03-7.00	
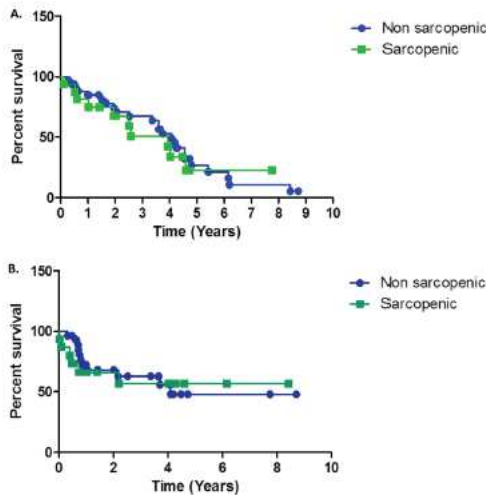
Figure 1. Overall survival (A) and disease free survival (B) (Kaplan-Meier test).

bad prognostic for overall survival [2–4]. The cause of this difference might be due to the limited size of our cohort that did not allow enough statistical power.

Sarcopenic patients are also prone to have an increased propensity for nosocomial infections and other complications during their hospital stay [12]. Tan et al have shown that sarcopenia could increase chemotherapy toxicity and intolerance [12]. Many of the preoperative risk profiles and known risk factors (age, diabetes, or other chronic diseases ...) are not changeable nor is it not possible to improve them during the short preoperative period. Nowadays perioperative chemotherapy is the gold-standard for the management of OGA [17]. In order to receive a neoadjuvant chemotherapy, patients need to be fit enough and not in a degraded physical condition. A loss of body weight is almost inevitable and causes serious problems in the pre- and postoperative management of OGA. In their study, Mirkin et al have shown that one third of their study population was sarcopenic

after neoadjuvant chemotherapy [18]. In our study, there was a high incidence of sarcopenia in the control group of patients without FJ after preoperative chemotherapy. Sarcopenia occurrence was influenced by an age ≥ 60 years old and the need of a nutritional support by means of a preoperative FJ, while the tumor stage or the presence of signet ring cells were not risk factors.

Supplementation through preoperative nutritional support and immunonutrition has already proven to benefit critically ill patients with acute respiratory distress or patients undergoing a major abdominal surgery [19]. In our case, the period of time during the preoperative chemotherapy permitted to improve the preoperative nutritional status of patients with OGA. We have shown in a previous publication that preoperative FJ enabled a better completion of all cycles of preoperative chemotherapy [6]. Although it is admitted that nutritional supplementation alone cannot restore muscle mass, the reversal of an observed decline in muscle mass and particularly in physical function has been achieved in a number of clinical settings [20, 21]. Several strategies have been described as combination of pharmacological/nutritional [22] and exercise-based countermeasures. The role of 'prehabilitation' is rapidly emerging in surgical oncology and holds major potential targeting sarcopenic patients undergoing gastrointestinal cancer surgery, by improving physiological status, enabling to increase the patient's ability to cope with surgical stress [14]. In our article, we have shown that preoperative FJ could significantly counteract sarcopenia settling during the preoperative chemotherapy. Thus, a preoperative FJ could improve the preoperative nutritional status and prevent the occurrence of sarcopenia during neoadjuvant chemotherapy. This highlights the importance of early actions on patient care, before any deleterious impact of the tumor on the general physiology occurs. It also clearly points to the fact that cancer should be considered as a systemic pathology. It remains to establish if the gain observed with preoperative FJ could be further improved with more

174

specific nutritional support. For instance, we previously showed that vitamin E derivatives could counteract efficiently muscle atrophy in animal models [23]. In addition, the molecular mechanisms involved in the limitation of sarcopenia caused by FJ has to be investigated, to understand how early nutritional support may limit muscle atrophy. Several critical molecular mechanisms for muscle atrophy have been described. Tumor-induced inflammation leading to cytokine production have been proposed as essential mediators of muscle atrophy [24]. Similarly, activation of p53-dependent signaling have been proposed as common effectors in patients and animal models [25]. Hence, additional investigations are needed to establish how early nutritional support antagonizes inflammation mediators or the p53 signaling pathway.

Although technological advances for tumor resection and improved surgical techniques are developed, postoperative morbidity burden remains a significant clinical challenge in gastrointestinal cancer care. We failed to show a significant impact of sarcopenia on major postoperative complications, the length of stay and overall and disease free survivals, despite the fact that many articles have demonstrated that sarcopenia was associated with approximately 30% to 40% increased risk of major and total complications after gastrointestinal [14]. Furthermore, postoperative complications not only affect the patient's symptoms and recovery, but also have detrimental implications for long-term risk of disease progression and mortality [14, 26]. Since preoperative FJ could decrease the risk of sarcopenia occurrence, FJ might be a critical point for further improvement of preoperative OGA management in order to decrease postoperative complications.

Few studies have been performed in order to assess the impact of a FJ on the preoperative management of OGA. Our monocentric study, with a limited population has inherent limitations and sources of bias. The interpretation of the sarcopenic status by means of a radiologic assessment (CT-based abdominal muscle evaluation) alone, such as proposed by Prado et al and used by many authors afterwards may also be a source of bias [14]. For these reasons, a multicentric, randomized trial with a large population is necessary for a more thorough analysis of the impact of a FJ on the preoperative management of OGA.

Preoperative FJ seems to efficiently counteract sarcopenia occurrence during preoperative chemotherapy for patient with OGA. Preoperative FJ could be a crucial factor in the preoperative management of OGA, independently of tumor stage, improving the preoperative nutritional status and long term outcome, while decreasing postoperative complications.

Authorship and contributions

Conception and design: BR, CD; Data acquisition: BR, HA, MV, AV; Drafting or revising: BR, SR, CB, CD, JBD; Final approval: MV, AV, JBD, SR, CB, CD, HA, BR

ORCID

Benoît Romain   http://orcid.org/0000-0002-8315-1079

References

1. Cruz-Jentoft AJ, Baeyens JP, Bauer JM, Boirie Y, Cederholm T, Landi F, Martin FC, Michel J-P, Rolland Y, Schneider SM, et al. Sarcopenia: European consensus on definition and diagnosis: Report of the European Working Group on Sarcopenia in Older People. Age Ageing. 2010;39(4):412–23. doi:10.1093/ageing/afq034

2. Kawamura T, Makuuchi R, Tokunaga M, Tanizawa Y, Bando E, Yasui H, Aoyama T, Inano T, Terashima M. Long-term outcomes of gastric cancer patients with preoperative sarcopenia. Ann Surg Oncol. 2018;25(6): 1625–32. doi:10.1245/s10434-018-6452-3

3. Daly JM, Fry WA, Little AG, Winchester DP, McKee RF, Stewart AK, Fremgen AM. Esophageal cancer: results of an American College of Surgeons Patient Care Evaluation Study. J. Am. Coll. Surg. 2000;190(5): 562–72; discussion 572–573. doi:10.1016/S1072-7515(00)00238-6

4. Burden S, Todd C, Hill J, Lal S. Pre-operative nutrition support in patients undergoing gastrointestinal surgery. Cochrane Database Syst Rev. 2012;11: CD008879. doi:10.1002/14651858.CD008879.pub2

5. Christein JD, Hollinger EF, Millikan KW. Prognostic factors associated with resectable carcinoma of the esophagus. Am Surg. 2002;68:258–62, discussion 262–263

6. Manfredelli S, Delhorme J-B, Venkatasamy A, Gaiddon C, Brigand C, Rohr S, Romain B. Could a feeding jejunostomy be integrated into a standardized preoperative management of oeso-gastric junction adenocarcinoma? Ann Surg Oncol. 2017;24(11): 3324–30. doi:10.1245/s10434-017-5945-9

7. Siewert JR, Stein HJ, Feith M. Adenocarcinoma of the esophago-gastric junction. Scand J Surg. 2006;95(4):260–9. doi:10.1177/145749690609500409

8. Clavien PA, Barkun J, de Oliveira ML, Vauthey JN, Dindo D, Schulick RD, de Santibañes E, Pekolj J, Slankamenac K, Bassi C, et al. The Clavien-Dindo classification of surgical complications: five-year experience. Ann Surg. 2009;250(2):187–96. doi:10.1097/SLA.0b013e3181b13ca2

9. Faramarzi E, Mahdavi R, Mohammad-Zadeh M, Nasirimotlagh B. Validation of nutritional risk index method against patient-generated subjective global assessment in screening malnutrition in colorectal cancer patients. Chin J Cancer Res. 2013;25(5):544–8. doi:10.3978/j.issn.1000-9604.2013.10.04

10. Ottery FD. Definition of standardized nutritional assessment and interventional pathways in oncology. Nutr Burbank Los Angel Cty Calif. 1996;12(1):S15–S19. doi:10.1016/0899-9007(96)90011-8

11. Prado CMM, Lieffers JR, McCargar LJ, Reiman T, Sawyer MB, Martin L, Baracos VE. Prevalence and clinical implications of sarcopenic obesity in patients with solid tumours of the respiratory and gastrointestinal tracts: a population-based study. Lancet Oncol. 2008;9(7):629–35. doi:10.1016/S1470-2045(08)70153-0

12. Tan BHL, Brammer K, Randhawa N, Welch NT, Parsons SL, James EJ, Catton JA. Sarcopenia is associated with toxicity in patients undergoing neo-adjuvant chemotherapy for oesophago-gastric cancer. Eur J Surg Oncol. 2015;41(3):333–8. doi:10.1016/j.ejso.2014.11.040

13. Cruz-Jentoft AJ, Landi F, Schneider SM, Zúñiga C, Arai H, Boirie Y, Chen L-K, Fielding RA, Martin FC, Michel J-P, et al. Prevalence of and interventions for sarcopenia in ageing adults: a systematic review. Report of the International Sarcopenia Initiative (EWGSOP and IWGS). Age Ageing. 2014;43(6):748–59. doi:10.1093/ageing/afu115

14. Simonsen C, de Heer P, Bjerre ED, Suetta C, Hojman P, Pedersen BK, Svendsen LB, Christensen JF, et al. Sarcopenia and postoperative complication risk in gastrointestinal surgical oncology: a meta-analysis. Ann Surg. 2018;268:58–69. doi:10.1097/SLA.0000000000002679

15. Levolger S, van Vugt JLA, de Bruin RWF, IJzermans JNM. Systematic review of sarcopenia in patients operated on for gastrointestinal and hepatopancreatobiliary malignancies. Br J Surg. 2015;102(12):1448–58. doi:10.1002/bjs.9893

16. Denison HJ, Cooper C, Sayer AA, Robinson SM. Prevention and optimal management of sarcopenia: a review of combined exercise and nutrition interventions to improve muscle outcomes in older people. Clin Interv Aging. 2015;10:859–69. doi:10.2147/CIA.S55842

17. Cunningham D, Allum WH, Stenning SP, Thompson JN, Van de Velde CJH, Nicolson M, Scarffe JH, Lofts FJ, Falk SJ, Iveson TJ, et al. Perioperative chemotherapy versus surgery alone for resectable gastroesophageal cancer. N Engl J Med. 2006;355(1):11–20. doi:10.1056/NEJMoa055531

18. Mirkin KA, Luke FE, Gangi A, Pimiento JM, Jeong D, Hollenbeak CS, Wong J. Sarcopenia related to neoadjuvant chemotherapy and perioperative outcomes in resected gastric cancer: a multi-institutional analysis. J. Gastrointest. Oncol. 2017;8(3):589–95. doi:10.21037/jgo.2017.03.02

19. Wischmeyer PE, Carli F, Evans DC, Guilbert S, Kozar R, Pryor A, Thiele RH, Everett S, Grocott M, Gan TJ, et al. American Society for enhanced recovery and perioperative quality initiative joint consensus statement on nutrition screening and therapy within a surgical enhanced recovery pathway. Anesth Analg. 2018;126(6):1883–95. doi:10.1213/ANE.0000000000002743

20. Phillips SM. Nutritional supplements in support of resistance exercise to counter age-related sarcopenia. Adv Nutr. 2015;6(4):452–60. doi:10.3945/an.115.008367

21. Adams SC, Segal RJ, McKenzie DC, Vallerand JR, Morielli AR, Mackey JR, Gelmon K, Friedenreich CM, Reid RD, Courneya KS, et al. Impact of resistance and aerobic exercise on sarcopenia and dynapenia in breast cancer patients receiving adjuvant chemotherapy: a multicenter randomized controlled trial. Breast Cancer Res Treat. 2016;158(3):497–507. doi:10.1007/s10549-016-3900-2

22. Anandavadivelan P, Lagergren P. Cachexia in patients with oesophageal cancer. Nat Rev Clin Oncol. 2016;13(3):185–98. doi:10.1038/nrclinonc.2015.200

23. von Grabowiecki Y, Licona C, Palamiuc L, Abreu P, Vidimar V, Coowar D, Mellitzer G, Gaiddon C. Regulation of a Notch3-Hes1 pathway and protective effect by a tocopherol-omega alkanol chain derivative in muscle atrophy. J Pharmacol Exp Ther. 2015;352(1):23–32. doi:10.1124/jpet.114.216879

24. Bonaldo P, Sandri M. Cellular and molecular mechanisms of muscle atrophy. Dis Model Mech. 2013;6(1):25–39. doi:10.1242/dmm.010389

25. von Grabowiecki Y, Abreu P, Blanchard O, Palamiuc L, Benosman S, Mériaux S, Devignot V, Gross I, Mellitzer G, Gonzalez de Aguilar JL, et al. Transcriptional activator TAp63 is upregulated in muscular atrophy during ALS and induces the proatrophic ubiquitin ligase Trim63. eLife. 2016;5:e10528. doi:10.7554/eLife.10528

26. Cho H, Yoshikawa T, Oba MS, Hirabayashi N, Shirai J, Aoyama T, Hayashi T, Yamada T, Oba K, Morita S, et al. Matched pair analysis to examine the effects of a planned preoperative exercise program in early gastric cancer patients with metabolic syndrome to reduce operative risk: the Adjuvant Exercise for General Elective Surgery (AEGES) study group. Ann. Surg. Oncol. 2014;21(6):2044–50. doi:10.1245/s10434-013-3394-7

176

2.3.3. ARTICLE 7: *Role of the TAp63 in the regulation of Trim63 in chemotherapy-induced cachexia*

<div style="border:1px solid blue">

Role of the TAp63 in the regulation of Trim63 in chemotherapy-induced cachexia

</div>

Paula Abreu[1], Anais Barthe[1], Yannick von Grabowiecki[1], Aina Venkatasamy[1,4], Véronique Devignot[1],

Huiqing Zhou[3], Wilfried Reichardt[5], Daniel Aberdam[2], Georg Mellitzer[1] *, Christian Gaiddon[1] *

[1]Université de Strasbourg-Inserm (Institut de la Santé et de la Recherche Médicale) UMR_S U1113, IRFAC, Laboratory STREINTH (Stress Response and Innovation Therapeutic in Cancer), ITI InnoVec, Fédération de Médecine Translationnelle, Strasbourg, France

[2]Université de Paris, INSERM UMR_S976, F75010, Paris

[3]Department of Human Genetics, Nijmegen Centre for Molecular Life Sciences, Radboud University Nijmegen Medical Centrum, The Netherlands

[4]IHU-Strasbourg, Institute of Image-Guided Surgery, Strasbourg, France

[5]Universitatsklinikum Freiburg, Medizin Physic, Freiburg, Germany

Running title: Role of TAp63 in the chemotherapy-induced muscle atrophy

Keywords: p53, p63, muscle atrophy, chemotherapy, trim63

Highlights:

• The doxorubicin-based chemotherapy induces TAp63 in skeletal muscles

• Transcriptomic analysis of skeletal muscles treated with doxorubicin highlights activation of p53-related target genes

• Skeletal muscle cells express TAp63

• TAp63 and p53 control the expression of trim63

$Corresponding authors: Christian Gaiddon, Gaiddon@unistra.fr; Georg Mellitzer, mellitzer@unistra.fr

The authors declare no potential conflicts of interest

Abstract

Muscle atrophy is a severe syndrome associated with certain types of cancers and chemotherapies that worsen the prognosis for patients. We performed a transcriptomic analysis on skeletal muscle of mice treated with the chemotherapeutic drug doxorubicin to identify the deregulated pathways that may play a role in muscle atrophy. Beside increase in muscle atrophy mechanisms, such as *trim63*, we observed an activation of cell death (i.e. *puma*) and DNA damage (i.e. *gadd45b*) mechanisms, and of p53 and TAp63 target genes (i.e. *peg3*) or regulators (i.e. *aen*), as well as a putative YAP inhibitor, *arrdc2*. We first validated the deregulate genes and characterized the expression of p53 and TAp63 in muscle treated with doxorubicin. We then showed that p53 as well as TAp63 are involved in the regulation of the expression of the pro-atrophic gene *trim63* via a direct interaction on its promoter. Finally, we showed that the YAP transcription factor participates in the regulation of *trim63* expression and is regulated by doxorubicin. Altogether, our results characterize novel molecular mechanisms induced by the chemotherapeutic drug doxorubicin in skeletal muscle that may account for atrophy observed in cancer patients.

Introduction

Muscle atrophy can occur as part of many diseases and is often an indicator of bad prognosis, impairing quality of life and increasing mortality [1, 2]. In addition, several conditions like aging, starvation, disuse and immobilization can lead to muscle loss and, depending on the cause, different molecular pathways can be involved in the muscle atrophy process. However, the imbalance between protein synthesis and degradation mediated by the proteasome pathway and modulated by the muscle specific ubiquitin ligases Trim63 (Murf1) and Atrogin-1 (MAFbx) is a common feature among the diverse causes of muscle loss [3]. These muscle specific ubiquitin ligases - Trim63 and Atrogin-1 - are described to be consistently upregulated in a range of skeletal muscle atrophy models.

Cancer cachexia is a multifactorial syndrome characterized by pronounced muscle atrophy, systemic inflammation and metabolic alterations [4-6]. Importantly, cachexia affects between 50 to 80% of cancer patients and is responsible for about 20% of their death [7]. Increasing evidences point out the impact of the tumors and/or the therapies on muscle function and integrity in cancer patients. Studies suggest that the tumor itself plays an active role in muscle wasting due to its ability to secrete pro-inflammatory cytokines and the large requirement of nutrients to maintain cell growth, creating a tumor-host interaction that aggravates the condition of the patient [4]. At the same time, cancer chemotherapy presents side effects that could contribute to cachexia, like anorexia, nausea and diarrhea. But more than that, it has been shown that chemotherapeutic agents have a direct negative effect on protein metabolism leading to cachexia [8] [9]. In this context, the anticancer drug doxorubicin is well recognized for having negative muscle catabolic effects [10]. Some works suggest that its atrophic effect would be due to production of ROS [11], TNF-α [12] or ceramides [13]. In addition, it was shown that doxorubicin is able to induce p53 accumulation in cardiac myocytes, which can contribute to muscle wasting [14].

However, despite the identification of these different mechanisms involved in muscle atrophy, no efficient therapy has been yet developed to prevent muscle mass loss or restore it in cancer patients. Hence, we used a transcriptomic approach on muscle of mice treated with doxorubicin to identify novel mechanisms that might account for skeletal muscle atrophy and that could represent therapeutic targets. Among the deregulated pathways, this approach pointed to an activation of p53 and its homologue TAp63.

In addition to the classical roles of the p53 family of transcription factors (p53, p63 and p73) in tumorigenesis, cell cycle, apoptosis regulation, epithelial and neuronal development, numerous

elements in the literature suggest that the p53 family modulates myogenesis and differentiation [15] [16]. For example, recently it has been shown that the key muscle factor MyoD coregulates the pro-apoptotic gene PUMA along with p53 [17]. Furthermore, p63 is particularly important during heart development [18], and transdifferentiation of fibroblasts into cardiomyocytes-like cells [19]. p73 modulates myoblast differentiation [20]. In addition, p53 and p63 play a role during muscle regeneration and metabolism by controlling Sirt1, TIGAR and AMPK expression [21] [22] [23]. Within the p53 family distinct promoters generate two classes of isoforms containing (TA) or not (ΔN) the N-terminal transactivation domain generally recognized for having antagonist function [24]. Importantly, within skeletal muscles, the balance between TA and ΔN-isoform expression influences on developmental and differentiation processes [25].

However, despites recent studies, the exact role and importance of p53 in muscle physiopathology is still difficult to apprehend, due to contradictory results. For instance, p53 has been shown to be induced during limb immobilization [26]. Overexpression of p53 in muscle is sufficient to induce muscle atrophy and loss of p53 reduces muscle atrophy cause by limb immobilization [26]. However, the loss of p53 does not impact on muscle endurance or adaptation, despite the activation of p53 during exercise [27]. Similarly, loss of p53 does not affect age-related cachexia in mice, despite that induction of p53 in atrophic muscle is observed [28] [29]. Interestingly, p53 could have a regenerative function for the muscle, but this is inhibited by deficiency of the Notch pathway in the aged muscle [30].

Some of the discrepancies observed while studying the function of p53 in muscle physiopathology might be due to compensation mechanisms by p53 family members. For instance, we underlined the p53 family relation with muscle atrophy showing that p63 is upregulated in amyotrophic lateral sclerosis (ALS) and able to directly modulate *Trim63* (Murf1) expression [31].

Hence, in this work, we investigate whether the p53 and TAp63 can modulate muscle wasting in a cancer-associated cachexia model induced by doxorubicin and if it could be a common regulatory mechanism of muscle atrophy associated to diseases.

Materials and Methods

Cell culture

C2C12 cells were obtained from ATCC (ATCC CRL-1772) and grown in DMEM (Dulbecco's modified Eagle's medium; Life Technology, Carlsbad, CA) with 10% fetal bovine serum (Life Technology) at 37°C in a humidified atmosphere and 5% CO_2. Mycoplasma contamination has been tested

negatively using PlasmoTest (Invivogene, San Diego, CA). Cells and animals were treated with doxorubicin (Pfizer 50mg).

Quantitative PCR

TRIzol (Invitrogen, Carlsbad, CA) was used to extract RNA. One µg of RNA was used for reverse transcription (iScript cDNA kit, Bio-Rad, France) and qPCR was carried out (iQ SYBR Green, Bio-Rad). Expression levels were normalized TBP as previously described [32].

Western blotting

Cells or tissue were lysed with LB (125 mM Tris-HCl pH 6.7, NaCl 150 mM, NP40 0.5%, 10% glycerol). Proteins were denatured and deposited directly (35 µg of proteins) onto a SDS-PAGE gel. Western blotting was performed using antibodies raised against p53 (mouse monoclonal anti-p53, 1C12, Cell Signaling Technology, France), p63 (mouse anti-p63, 4A4, Santa Cruz Biotechnology; p63, Abcam, France), p73 (rabbit monoclonal anti-p73, EP436Y, Epitomics Abcam Company, France), TAp63 (rabbit polyclonal anti-Tap63, 618901, Biolegend), Trim63 (rabbit anti-Trim63, D01, Abnova; Taipei, Taiwan), Yap (mouse monoclonal anti-Yap, sc-101199, Santa Cruz) and phospo-Yap (rabbit monoclonal anti-pYap, 13008, Cell Signaling). Secondary antibodies (anti-rabbit, anti-mouse: Sigma, France) were incubated at 1:1000. Loading was controlled with actin (mouse anti-beta-actin, Sigma, 1:10000) (Antoine *et al.,* 1996).

Transfection assays

Cells were transfected by JetPrim (Polyplus, Strasbourg, France) as previously described [33]. SiRNA transfection was performed using 10 nM of siRNA against p63-pan (Trp63 Stealth RNAi MSS212111, Invitrogen), 50 nM of siRNA against p53 (Trp53 s75474, Ambion) and 30 nM of siRNA against Yap (Yap s76160, Ambion), using RNAiMAX or Dharmafect as described by the protocol provider (Life Technology and Dharmacon™ respectively).

Trp53 sequence: GCU UCG AGA UGU UCC GGG Att

Trp63-pan sequence: CCG AGG UUG UGA AAC GAU GCC CUA A

Yap sequence: GGA UGA AAU GGA UAC AGG Att

Chromatin immunoprecipitation (ChIP) assay

ChIP assays were performed using the standard protocol from the Magna ChIP G kit (Millipore). C2C12 lysates were sonicated 12 times at 10% power (Bioruptor™ UCD-200, Diagenode). For each 1 million cells, 1 μg of antibody was used. P53 and p73 were immunoprecipitated with a mouse antibody raised against total p53 (mouse monoclonal anti-p53, 1C12, Cell Signaling Technology, France) and p73 (mouse monoclonal anti-p73, E-3, Santa Cruz Biotechnology; Abcam, France). Mouse-anti-RAB11A was used as negative control (Santa Cruz Biotechnology).

RNA sequencing

Sequencing was performed by the Sequencing platform of the IGBMC (Strasbourg) and results were first analyzed using AltAnalysis software [34]. Deregulated gene were identified based on two-fold change expression and t-test p-value <0.05. Deregulated genes were then analyzed for over-representation in selected biological processes in several resources: Gene Ontology, MPhenoOntology, Disease Ontology, GOSlim, PathwayCommons, KEGG, Transcription Factor Targets, miRNA Targets, Domains, BioMarkers, RVista Transcription Sites, DrugBank, BioGrid.

Wild-type mice and doxorubicin treatment

In total forty wild-type (WT) male mice C57BL/6 background 5 months old were randomly assigned to four groups of 10 mice each. The animals received a single intraperitoneal injection of doxorubicin (Pfizer 50mg) diluted at 18mg/kg in 0.9% NaCl, during 1, 3 or 5 days. Vehicle-treated littermates received the same formulation without doxorubicin. In vivo experiments were repeated twice with a number of animals recommended to optimize statistical analyses according to the regional and national animal ethics committee. All animal manipulations were performed under appropriate supervision and observing protocols validated by the regional and national animal ethics committee.

Animals underwent an abdominal micro-CT at day 0 – day 3 – day 5 (Institut Pluridisciplinaire Hubert Curien). We also performed, *ex vivo* magnetic resonance imaging using a preclinical 9.4 T MRI (Bruker BioSpin MRI GmbH, BioSpec 94/20, Ettlingen, Germany) and a mouse body-coil. The mice were placed carefully in the coil in dorsal decubitus in a prone position (head first). We performed an axial RARE T2-weighted sequence, with the following parameters: TR = 24 ms, TE= 4000 ms, average = 1, slice thickness = 0.5 mm, FOV = 28 x 28, image size = 128 x 128, excitation angle = 90°, duration 4-5 minutes. Then, we performed a diffusion-EPI sequence with ADC map, using the following parameters : TR = 25.49 ms, TE= 3200 ms, average= 1, flip angle = 90°, slice thickness = 1mm, FOV = 28 x 28, image size = 128 x 128, diffusion directions = 1 (b0 – b200 – b 500 – b1000), duration 4-5 minutes. We performed a T1-weighted in / out of phase sequence, using the following

parameters: TR = 300ms, TE= 1,43/1,79 ms, average= 2, flip angle = 30°, slice thickness = 1mm, FOV = 28, image size = 140x140, duration 1m 24 sec. We also performed a T1-weighted sequence (with and without FS), using the following parameters: TR = 300 ms, TE= 3 ms, average= 2, flip angle = 30°, slice thickness = 1mm, FOV = 28, image size = 140x140, duration 1min 3 sec.

Surface measurements of paravertebral muscles were measured on an axial plane at the level of the renal hilum and signal intensity were measured on the T1-weighted sequences using Region of Interest (ROI) with the free DICOM viewer Horos ™ and Paravison® 6.1 software.

TAp63[+/Cre]ROSA26[Tomato] reporter mouse line

TAP63[CRE/+] mice were generated by the Clinique de la Souris (Strasbourg) by introducing the CRE recombinase cDNA after the TAp63 promoter. The ROSA26-tomato mice contain the cDNA for the fluorescence protein Tomato after a LoxP flanked STOP cassette. By crossing these two mouse lines TAp63[CRE/+]:ROSA26[Tomato] mice were generated in house. Wild type C57BL/6, TAp63[CRE/CRE] or TAp63[CRE/+]:ROSA26[Tomato] C57BL/6 mice of 10 weeks were weighed and intraperitoneally injected with 18 mg/kg doxorubicin in 200 µl 0.009% saline. Mice were weighed on a regular basis. Treated mice were sacrificed either 1, 3 and 5 days after treatment. Gastrocnemius muscles were dissected out for immunofluorescent staining or RTqPCR. All animal experiments were approved by the Regional and National ethical committees.

Statistical Analyses

Statistical analyses were performed using a one-way analysis of variance followed by a Tuckey post-test to allow a comparison between all the conditions. In the graphs, an asterisk indicates a statistically significant difference. Tests confirmed a statistically significant difference between control and treated mice. Statistical analyses were performed using Prism (GraphPad Software, San Diego, CA).

Results

RNA sequencing of doxorubicin-treated skeletal muscles shows multiple deregulated pathways

To better understand and study chemotherapy-related changes in cancer patients' muscle, a frequently used model consists in treating mice with doxorubicin and follow the size and weight of gastrocnemius skeletal muscles [35]. In order to identify novel molecular mechanisms involved in chemotherapy-induced muscle atrophy, we used this model and analyzed the gastrocnemius skeletal

muscles by RNA sequencing (Figure 1). Mice were treated (n=3) with doxorubicin and three days after their muscle mass was measured after dissection, showing a 20% decrease in gastrocnemius weight compared to controls (Figure 1A, B) [35]. In clinical routine, muscle atrophy can currently only be diagnosed at relatively advanced stages using imaging, by means of a CT-based surface & density evaluation (abdominal CT with or without contrast, or CT images of PET-CT) of muscle loss, which consists in measuring the surface and the density (in Housefield units) of the paravertebral muscles (psoas and erector spinae muscles) on an axial plane at the level of the 3rd lumbar vertebra (L3), then normalized to weight and height (BMI). We applied the same measurement method to our drug-induced muscle atrophy mouse model at the level of the renal hilium on micro-CT (Figure 1C, D) and MRI (Figure 1E), for a better reproducibility of the measurement method. We compared our groups of mice: one treated with doxorubicin and the other with only vehicle, and followed them longitudinally at day 0, day 3 and day 5. We observed that doxorubicin induced a progressive diminution in paravertebral muscle surface that could be observed on micro-CT from the 3rd day after the beginning of the experiment (Figure 1D). There was an average decrease in paravertebral muscle surface between day 1 and day 5 of 15.3% ± 0.90, compared to 1.23% ± 0.64 for controls, but we did no see significant differences in terms of muscle density. Similarly, using the same surface-measurement method on MRI, we observed of a lower paravertebral muscle surface in doxorubicin-treated mice (n=5, 25.14mm^2 ± 1.72) compared to controls (n=3, 32.33 mm^2 ± 3.21, 29% decrease p=0.0357 (Figure 1E). MRI showed signal intensity changes in paravertebral muscles between treated-tumors and controls. For instance, the signal intensity ratio between fat saturated T1-weighed images and non-fat saturated T1-weighted images was lower in doxorubicin-treated tumors (54.31 units ± 2.18) compared to controls (61.76 units ± 2.54, p=0.0357 (Figure 1E), but signal intensity ratio between in and out of phase sequences showed no significant differences between groups (p=0,3929). This means that the composition of the muscles has changed, with an increase of fatty-like structures. It may indicate infiltration of fat or increase in conjunctive tissue upon doxorubicin treatment.

Once muscular atrophy was established, we purified RNA from treated and un-treated control muscles and and sequenced it. Sequencing results were analyzed by Altanalysis software to establish a list of genes deregulated by 2-fold with an *adjp* value < 0.05. Then, pathways analyses were performed using multiple databases (ex. DAVID, STRING, Reactome, TRAP). Deregulated processes or pathways were selected when the false discovery rate was bellow 0.05 or the z score above 2.

As expected, muscle atrophy related pathways were identified as induced, which included the Murf-1/Trim63 ubiquitin ligase (Figure 1F). In addition, pathways related to cell death, autophagy, cell

growth, and DNA damage, were also activated. Activation of these pathways correlated with induction of target genes for the Tp53 and TAp63 transcription factors (Figure 1G). Target genes for other transcription factors, such as Nfkb and Fox3p, were also induced. In particular, target genes for MyoD1 were induced, indicating that muscle plasticity mechanisms leading to precursor proliferation are activated upon doxorubicin treatment [36].

Inversely, several mechanisms, such as cell adhesion and extracellular matrix components, skeletal muscle development and pro-survival mechanisms (AKT-Pi3K and PDGF signaling), were strongly downregulated (Figure 1F). Similarly, target genes for several transcription factors, such as SP1, NFAT3, and Myogenin were also downregulated, suggesting that the activity of these transcription factors was downregulated in muscle upon doxorubicin treatment (Figure 1). Interestingly, these transcription factors are also part of the molecular mechanisms of muscle cell differentiation processes [36, 37].

TAp63 is induced during atrophy of skeletal muscle

The pathway analyses in skeletal muscles upon doxorubicin treatment identified the upregulation of several target genes and regulators of Tp53 and TAp63, such as *gadd45*, *nqo1*, *aen*, *eda2r*, *ddit4* and *peg3* (Figure 2A). This observation suggested that Tp53 and TAp63 were involved in the process leading to muscle atrophy induced by doxorubicin. This was previously shown for p53 but never so far for TAp63 [14]. However, as we previously showed that TAp63 expression was induced during skeletal muscle atrophy in amyotrophic lateral sclerosis (ALS) [31], we decided to investigate further the role of TAp63 in the response of muscle to doxorubicin.

Mice were treated with doxorubicin and gastrocnemius muscles were analyzed after 1, 3 and 5 days of treatment. Under these conditions muscle mass decreased of about 25% after 3 days and stayed diminished at 5 days (Figure 2B). As expected, expression of the two major pro-atrophic ubiquitin ligases, *trim63* and *atrogin1*, was strongly upregulated at 3 days of treatment, with a significant but small increase at 1 day and 5 days of treatment (Figure 2C and D). As expected, protein level of P53 increased upon 5 days pf doxorubicin treatment, without changes at the mRNA level. In contrast TAp63 mRNA level was already increased at 3 days of treatment (Figure 2E and F).

We also attempted to visualize TAp63 protein expression in the muscles. Despite the use of multiple antibodies, we never were able to detect TAp63 expression by western blot or immuno-histochemistry (personal data). Hence, we used a genetic approach to assess the existence and the role of the expression of TAp63 in skeletal muscles. Mice with CRE recombinase knock in located in

the promoter of TAp63 (TAP63$^{CRE/+}$) were breaded with ROSA26^{Tomato} mice that contains a LoxP flanked STOP cassette before the cDNA for the fluorescence protein Tomato (Figure 3A). The generated compound mice (TAp63$^{CRE/+}$:Rosa26^{Tomato}) expressed the fluorescent Tomato proteins in cells that have or have had an active TAp63 promoter. Expression of Tomato proteins was present in myotubes of the compound mice (TAp63$^{CRE/+}$:Rosa26^{Tomato}) but not in the Rosa26^{Tomato} mice (Figure 3B). Tomato expression was also observed in nuclei. Interestingly the number of tomato-positive nuclei was increased upon doxorubicin treatment (Figure 3B and C). These results suggested that TAp63 was expressed in muscle cells and that its expression is activated by doxorubicin in some nuclei.

To analyze the possible role of TAp63 in muscles, we inter-crossed TAp63$^{CRE/+}$ mice to generate TAp63$^{CRE/CRE}$ mice that do not express TAp63 protein. TAp63$^{CRE/+}$ and TAp63$^{CRE/CRE}$ mice were treated with doxorubicin for 3 days and compared to non-treated mice. No significant changes in morphology was observed. However, analysis of *trim63* expression showed that doxorubicin induced more strongly *trim63* in TAp63 KO mice (Figure 3D). This result was surprising as we previously reported that TAp63 was capable of inducing *trim63* expression [31]. Hence, we analyzed under the same condition other genes that might be impacted by either doxorubicin treatment or TAp63 expression. Interestingly, under the same conditions atrogin-1 induction by doxorubicin is not changed. In contrast, *sirt1* that has previously been shown to be regulated by TAp63 [23] is induced in WT mice but not in TAp63 KO mice (Supplementary figure 1). These results indicate that TAp63 is expressed in muscles and participates in the regulation of specific genes involved in muscle atrophy.

TAp63 is induced by doxorubicin in myoblastic cells

To clarify the role of TAp63 in the response of skeletal muscle to doxorubicin, we used the murine myoblastic cell line C2C12. In these cells, doxorubicin treatment induced also the mRNA levels of several p53/TAp63 target genes (i.e. *nqo1*, *noxa*) (Figure 4A) that we also found upregulated in the RNA sequencing experiment, indicating that the change in mRNA level was also occurring in muscle cells of the gastrocnemius muscle and not only in some other cell types that might be present in this muscle. We then analyzed the expression level of p53 and TAp63 in C2C12 cells treated with two concentration of doxorubicin (0.4 and 0.6 μM) over different time. This time course experiment revealed that doxorubicin strongly induced the mRNA level of TAp63 at 18h, which was maintained at 24h of treatment (Figure 4B). P63 proteins were also induced although with less intensity (Figure 4C). p53 protein level was also induced by doxorubicin, in a time and dose dependent manner. The induction of p53 protein expression and nuclear localization was confirmed by immunohistochemistry (Supplementary Figure 2).

Interestingly, the doxorubicin-induced expression of p53 and TAp63 correlated with *trim63* (Figure 4D) and *atrogin-1* upregulation (Figure 4E), similarly to what was observed *in vivo* (Figure 2C and F). These results showed that doxorubicin induces the expression of p53 and TAp63 and atrogenes in myoblast cells in a similar time and dose dependent manner, suggesting that they might act in the same pathway.

Functional interaction between p53/TAp63 and Trim63

Based on the correlation existing between the expression of the different p53 family members and atrogenes, we aimed at investigating whether the different members of the p53 family could regulate the expression of *trim63* and *atrogin-1*. To do so, we performed gain of function experiments in murine myoblastic cells (C2C12), treated or not treated with 0.6 μM of doxorubicin for 24 hours, and subsequently analyzed for the expression of *trim63* and *atrogin-1* mRNA by RT-qPCR. The results showed that overexpression of TAp63 strongly induces the expression of *trim63*, which was further potentiated by the treatment with doxorubicin (Figure 5A). Interestingly, ΔNp63, normally described for having a dominant negative effect, also stimulated Trim63 expression. Overexpression of p53 also induced *trim63* expression, but with less intensity than TAp63. Importantly, overexpression of the different p53 family members did not affect *atrogin-1* expression (data not shown). These results confirmed our previous data suggesting that the p53 family regulates *trim63* expression [31].

To investigate if the expression of *trim63* is not only induced but also depends on the expression of the p53 and TAp63, we transfected C2C12 cells with p53 or p63 specific siRNA, treated cells or not with 0.6 μM of doxorubicin for 24 hours and analyzed again for the expression of *trim63* by RT-qPCR (Figure 5B-E). The efficacy of the p53 and p63 siRNAs was confirmed by RT-qPCR (Figure 5B and C) and Western blot (Supplementary Figure 3A and B). Importantly, transfection of siRNA against p53 or p63 strongly decreased Trim63 expression in the presence of doxorubicin (Figure 5D and E) suggesting that doxorubicin induced expression of *trim63* in part depends on p53 and p63 in C2C12. Hence, it is possible that in TAp63 KO mice p53 compensate for the lack of TAp63 in regulating *trim63*.

Physical interaction between the p53/TAp63 and Trim63.

Our results support the hypothesis that p53 family members may participate in the regulation of *trim63* expression during muscle atrophy induced by doxorubicin. Indeed, we have previously shown that TAp63 can bind and transactivate *trim63* promoter [31]. In order to evaluate if doxorubicin might influence the p53 family binding to the *trim63* promoter we performed Chromatin

immunoprecipitation (ChIP) assays covering two possible p53 binding sites in the *trim63* promoter in presence of doxorubicin (Figure 6A). These binding sites were identified using both the "Eukaryotic promoter database" and the "p53FamTAG" bioinformatic tools. One of the sites is located at 660/-690 bp (RE1/2) and the second at 2015/2045 bp (RE3/4). The ChIP assay demonstrated that both p53 and TAp63 bind to the *trim63* promoter (Figure 6B). However, it showed also that although doxorubicin strongly induced *trim63* expression, it does not seem to further increase the binding of p53 or p63 to the *trim63* promoter. The binding of p63 on the trim63 promoter is also observed in the cardiomyocyte ENO2 cells when a TAp63gamme chromatin immunoprecipitation and sequencing of the bound sequences (ChIP seq) was performed [38]. The binding site is close to the start site at a position similar to the RE1/2 sites (Supplementary Figure 3C). It is to note that the CHIP seq was done in non-treated cells, indicating that TAp63gamme is bound to the trim6 promoter at least inn some cells even in absence of treatment, as supporting our observation in C2C12 cells.

Role of YAP in the expression of trim63

One of the most induced genes in the RNA seq experiment was arrdc2 (fold change = 7.2) (Figure 7A). Interestingly, two family members of *arrdc2*, *arrdc1* and *arrdc3*, are negative regulators of YAP [39] [40]. YAP is an important cofactor that belongs to the Hippo pathway, insuring the conversion of mechanical stimuli into biological activity [41]. YAP participates in multiple processes through the interaction with different transcription factors, such as TEAD1-4 and p73, which leads to the expression of different types of target genes, such as *ctgf*, *cyr61*, *igfbp5*, *puma*, or *ankrd1*. In addition, p53 regulates the Hippo pathway by interfering with upstream regulators, such as Lats1/2 [42], and it has been shown that TAp63 can induce the Hippo pathway [43]. Interestingly, YAP has been shown to inhibit *trim63* expression [44], and the Hippo pathway seems to play an important role in controlling muscle plasticity [45]. Hence, we decided to analyze the impact of doxorubicin on the activity of YAP in the skeletal muscle and if YAP participated in the activation of trim63 expression.

Interestingly, analysis of the RNA sequencing data showed that several genes that are coregulated by YAP, such as *cyr61*, *puma* of *ankrd1* are upregulated following doxorubicin treatment. However, other YAP co-regulated genes are downregulated, such as *axl* or *igfbp5* (Figure 7A). The deregulation of two of the most canonical targets genes of the Hippo pathway, *cyr61* and *ctgf*, was validated by RT-qPCR in an independent experiment (Figure 7B). Similarly, upregulation of *cyr61* and *puma*, other YAP target genes, was also observed in C2C12 cells treated with doxorubicin, while *ctgf*

and *igfbp5* were downregulated (Figure 7C). These results further suggested that YAP might be regulated upon doxorubicin treatment.

To analyze YAP regulation, we performed immunofluorescence staining on C2C12 cells treated with doxorubicin using a specific YAP phospho-antibody that recognizes YAP phosphorylated at s127. This phosphorylation sequesters YAP in the cytoplasm into an inactive form. C2C12 cells at confluence and in control condition showed a cytoplasmic and nuclear localization of YAP (Figure 7D). Treatment with doxorubicin induced a nuclear re-localization of YAP without a significant decrease of YAP phosphorylation. These results suggested that doxorubicin induced YAP capacity to induce gene expression by its nuclear localization.

To investigate the role of YAP in *trim63* expression, we used loss of function experiments using the YAP pharmacological inhibitor verteporfin and a siRNA towards YAP. Treatment of C2C12 with verteporfin blocked the induction of *trim63* expression by doxorubicin without affecting the basal expression of *trim63* (Figure 7E). Under the same conditions, verteporfin diminished the expression of two YAP target genes, *cyr61* and *ctgf*, both in basal and doxorubicin-treated conditions. This result suggested that YAP might be involved in the induction of *trim63* expression by doxorubicin but not in its basal expression. Similarly, YAP siRNA diminished the expression of *cyr61* in doxorubicin-treated cells (Figure 7F). However, the effect of YAP siRNA on *trim63* was less marked compared to verteporfin. To gain further understanding on how inhibition of the YAP and Hippo pathway might be impacting on *trim63* expression, we analyzed the expression of the TAp63 and one of its target gene, *aen*. YAP siRNA diminished their mRNA level after doxorubicin treatment, suggesting that YAP might control in part the expression of *trim63* through TAp63.

Discussion

Despites numerous studies and the identification of several molecular mechanisms involved in muscle atrophy, including when it is caused by anticancer treatment, no efficient cure exists yet to restore muscle mass and strength. This lack of therapeutic solution is significantly impairing the quality of life and survival of cancer patients, and highlights the necessity to improve our understanding of the signaling pathways that cause muscle atrophy. To do so, we performed, to our knowledge, the first transcriptomic analysis on skeletal muscles of mice treated with an anticancer drug. This allowed us to identify several pathways and processes that were deregulated, either induced or repressed, upon treatment of mice with doxorubicin. Among them, target genes and regulators of TP53 and TAp63 were identified as being significantly over-represented. Based on this observation and our previous findings that TAp63 was induced in muscle atrophy during ALS and

regulates trim63, we further analyzed the role of TAP63 in the response of muscle to doxorubicin.

Doxorubicin deregulates multiple pathways in skeletal muscle

The transcriptomic analysis identified multiple pathways that were deregulated in the muscle of doxorubicin treated mice. Some of them were expected, such as the activation of the *trim63/atrogin-1* muscle protein degradation program [46] or the induction of apoptosis [47] and autophagy [48], that were previously described in this context. In addition, our transcriptomic analyzes found negative regulation of pro-survival pathways, such as AKT and MAPK pathways, which is consistent with the activation of the apoptosis and autophagy events. However, several deregulated processes or pathways were never connected to doxorubicin-induced skeletal muscle toxicities, such as activation of glycogen and lipid metabolism, or inhibition of enzymes involved in remodeling of the extracellular matrix.

The implication of these processes in the muscle toxicity of anticancer drugs makes sense as they have been shown to be important in muscle homeostasis and plasticity. For instance, dysregulation of lipid homeostasis or glycogen synthesis (i.e. *gbe1* fold change = 2.27) have been shown to be involved in muscle atrophy in various pathologies [49] [50] [51] [23]. Obviously, loss of extracellular matrix and cell adhesion may also participate into muscular atrophy as these components are essential for the structure and the function of the muscle [52]. Interestingly, this loss of interaction with the matrix or adjacent cell may contribute to the complex regulation of the Hippo pathway and YAP that we also observed. Indeed, the Hippo pathway and YAP are essential effectors of the mechanotransduction processes that are often initiated at the membrane by interaction with the extracellular matrix [41].

In addition to these deregulated pathways, the activity of several transcription factors is modulated by doxorubicin in the muscle. For instance, a complex regulation of muscle developmental and differentiation processes seems to take place as MyoD1, which favors proliferation of myoblasts, is induced, while MyoG, which induced differentiation into myotube, is repressed [36, 37]. NFKB and FOXP3 are induced which could be expected as they are nuclear effectors for the signaling pathway induced by cytokines that are often association with cancer-related muscular atrophy [4, 53]. More surprisingly, HIF1A pathway appears to be both induced and repressed. Although we cannot exclude that it may represent an artefact of the bioinformatics analyses, it may also be explained by a complex regulation of the specificity of HIF1A to target selected genes.

Use of MRI and micro-CT imaging technique to support molecular results on muscle atrophy

Interestingly, the changes in lipid metabolism pathways is also supported by our MRI experiment showing a significant change in muscle lipid content upon doxorubicin treatment. Indeed, the changes observed at a molecular and genomic level, we have also been able to observe *in vivo* morphological and composition changes in paravertebral muscles, using small animal imaging. Our results on mice is similar to those observed in patient when analyzed with the method of Prado et al stipulating that measurements of paravertebral muscle surface on an axial plane at the level of the 3rd lumbar vertebra in humans (and the renal hilum in mice, for more reproducible measures) can estimate sarcopenia [54]. Indeed, we observed that doxorubicin induced a progressive decrease of paravertebral muscle surface, which we could observe on micro-CT from the 3rd day on after the beginning of the experiment. In addition, with this method, we have been able to observe doxorubicin-changes in muscle signal intensity on MRI between fat saturated and non-fat saturated images. Our results supports other studies showing the potential of this methods in muscle or other organs changes in animal models [55] [56]. For instance, MRI could be used, in both humans and mice, to detect changes in the liver composition, such as steatosis (=fatty infiltration) of the liver, with specific sequences such as the T1-weighted multi-echo DIXON sequence [57] [58]. Similarly, MRI can also be used to detect changes in muscles morphology and composition, such as injured muscle changes in mouse models of rotator cuff tears or to image age-related sarcopenia in mice and rats [55]. All in all, doxorubicin induced in vitro and in vivo changes in muscles, which we can easily visualize and quantify with small animal imaging studies.

Doxorubicin induces Trim63 (Murf1) expression via the p53 and TAp63.

The transcriptomic approach showed an enrichment of p53/TAp63 target genes and regulators in response to doxorubicin in the skeletal muscle. The induction of p53 was previously shown and is consistent with activation of apoptosis and autophagy [14]. Similarly, activation of p53 was shown in muscle atrophy in other contexts, such as limb immobilization [26], ALS [31], muscle unloading [59], or spinal muscular myopathy [60]. However, abolishing p53 function by gene inactivation did not rescue muscle atrophy, suggesting that compensatory mechanisms may exist [61]. Hence, the activation of TAp63 by doxorubicin we described here, and that we previously showed in ALS [31], could represent a such compensatory mechanism by inducing pro-apoptotic genes in place of p53. In this context, it is interesting to note that pifithrin that has been shown to inhibit the activity of several p53 family members can reduce the muscle atrophy induced by anticancer drugs [62].

In addition, activation of p53 and TAp63 could also explain some of the deregulation of the muscle metabolism. For instance, p63 has been shown to be involved in lipid metabolism [63], for example by inducing *apod* [64], which is a gene that is induced by doxorubicin in our experiments.

In addition to this function of p53 and TAp63 in apoptosis, we also provide evidence that the expression of the pro-atrophic ubiquitin ligase Trim63 is controlled by p53 and TAp63 in the skeletal muscle upon treatment with doxorubicin. Both transcription factors bind to the *trim63* promoter and are involved in *trim63* mRNA upregulation caused by doxorubicin in C2C12 cells. In addition, the deletion of TAP63 in mice impact on the expression of *trim63* by increasing it. This suggests that a compensatory mechanism induced by the loss of TAp63 ends up to favor *trim63* expression upon doxorubicin treatment. For instance, TAp73 could be also part of these compensatory mechanisms as we observed its upregulation in TAp63 KO mice (data not shown). Interestingly, p53 or TAp63 do not play a role in *atrogin-1* expression, neither *in vitro* nor *in vivo*, demonstrating a selective role of these two transcription factors on the ubiquitin ligase that induces degradation of the muscle structural proteins and not on the one targeting the muscle specific transcription factors [46].

This selective effect on trim63 and not atrogin-1 may also explain why we did not observe significant differences in muscle structure and mass between the WT and the TAp63 KO mice upon doxorubicin treatment. However, this can also be due to the intervention of p53 or even TAp73, which would be consistent with our results and the previous studies showing that p53, p63 and p73 proteins play a role in muscle cell proliferation and differentiation [20].

Role of YAP in muscle atrophy and expression of trim63

Doxorubicin causes a differential regulation of YAP co-regulated genes. For instance, *cyr61*, *puma* and *ankrd1* are being upregulated, while *ctgf*, *igfbp5* and *axl* are downregulated. This complex regulation can be partly explained by the fact that YAP interacts with multiple transcription factors that control the expression of these different target genes. For instance, *puma* and *bax* are co-regulated by YAP and TAp73 [65]. Additional interaction between the p53 family and YAP have been shown [66]. More precisely, activation of YAP leads to increased TAp63 activity with production of ROS [67]. This latter study might explain our results showing that the expression of TAp63 and its target gene *aen* is downregulated by YAP silencing upon doxorubicin treatment in myoblastic cells. The mechanisms leading to YAP selective activation are yet to identified, but modulation of cell stiffness by doxorubicin via interaction with DNA or other cellular components might account for part of it. In this sense, some interesting co-factors, the VGLL proteins that interact with the TEAD transcription factors, have been shown to negatively regulate YAP [68]. In particular, VGLL4 has been

described to be important during muscle regeneration because of its knock-down avoids TEAD-4 related transactivation of MyoD, that consequently induces impairments in myoblast contraction and differentiation. Another VGLL family members, Vgll3, is weakly expressed in mouse skeletal muscle while its expression increased in response to hypertrophy or regeneration [69]. Interestingly, Vgll3 silencing suppresses myoblast proliferation, while Vgll3 overexpression promotes myogenic differentiation by reducing the activity of the Hippo pathway. These complex regulations indicate that additional studies will be necessary to understand the mechanism that regulates the association of YAP with its different partners and how it impacts on the expression of selected genes in response to doxorubicin. As YAP is an essential component of the Hippo mechano-transduction pathway, it is possible that the modulation of cell stiffness by doxorubicin via the interaction with different cellular component (DNA, membrane lipids, actin) might impact on YAP activity [70].

This complex regulation might also explain why the role of YAP and the Hippo pathway in skeletal muscle is still controversial [71]. For instance, a dominant active form of YAP, that cannot be phosphorylated at serine 127 and be sequestered into the cytoplasm, reduces the expression of MyoG during myogenesis. This is consistent with our finding of an increase in YAP nuclear localization upon doxorubicin treatment in myoblastic cells. Furthermore, transgenic mice with such a dominant active mutant display muscle atrophy with elevated expression of trim63 [72], supporting our findings that upon doxorubicin YAP participates into the activation of trim63 transcription. However, overexpression of a normal YAP in mouse muscles produces the inverse phenotype [73], and even upon denervation that causes muscle atrophy, its expression was induced. Similarly, muscles with dystrophin mutation associated with Duchenne muscular dystrophy or mutation LMNA associated with LMNA-related congenital muscular dystrophy have a constitutively activated YAP and YAP target genes [74] [75].

Interestingly, it was also found in this study a decrease in phosphorylation at serine 112 of YAP during myoblast maturation. Hence, it appears that the function of YAP in muscle plasticity involves its tight regulation by phosphorylation events that will also mitigate its association with different transcription factors.

In conclusion, our study highlights the complexity of the signaling pathways involved in muscle atrophy caused by anticancer treatments and point to the importance of the p53 family in this process, including via the regulation of the pro-atrophic gene trim63. Our results also provide evidence of possible interactions between the p53 family and the Hippo pathway via the YAP co-

activator during muscle atrophy, shaping a complex network linking mechanotransduction events with metabolism and cell survival processes.

Acknowledgments

References

[1] K. Mukund, S. Subramaniam, Skeletal muscle: A review of molecular structure and function, in health and disease, Wiley Interdiscip Rev Syst Biol Med, (2019) e1462.

[2] R.Y. Cao, J. Li, Q. Dai, Q. Li, J. Yang, Muscle Atrophy: Present and Future, Advances in experimental medicine and biology, 1088 (2018) 605-624.

[3] O. Rom, A.Z. Reznick, The role of E3 ubiquitin-ligases MuRF-1 and MAFbx in loss of skeletal muscle mass, Free Radic Biol Med, 98 (2016) 218-230.

[4] J.M. Argiles, S. Busquets, F.J. Lopez-Soriano, The pivotal role of cytokines in muscle wasting during cancer, Int J Biochem Cell Biol, 37 (2005) 1609-1619.

[5] J.M. Argiles, F.J. Lopez-Soriano, B. Stemmler, S. Busquets, Novel targeted therapies for cancer cachexia, Biochem J, 474 (2017) 2663-2678.

[6] J.M. Argiles, B. Stemmler, F.J. Lopez-Soriano, S. Busquets, Inter-tissue communication in cancer cachexia, Nat Rev Endocrinol, 15 (2018) 9-20.

[7] W.D. Dewys, C. Begg, P.T. Lavin, P.R. Band, J.M. Bennett, J.R. Bertino, M.H. Cohen, H.O. Douglass, Jr., P.F. Engstrom, E.Z. Ezdinli, J. Horton, G.J. Johnson, C.G. Moertel, M.M. Oken, C. Perlia, C. Rosenbaum, M.N. Silverstein, R.T. Skeel, R.W. Sponzo, D.C. Tormey, Prognostic effect of weight loss prior to chemotherapy in cancer patients. Eastern Cooperative Oncology Group, Am J Med, 69 (1980) 491-497.

[8] T. Le Bricon, S. Gugins, L. Cynober, V.E. Baracos, Negative impact of cancer chemotherapy on protein metabolism in healthy and tumor-bearing rats, Metabolism, 44 (1995) 1340-1348.

[9] V.E. Baracos, Management of muscle wasting in cancer-associated cachexia: understanding gained from experimental studies, Cancer, 92 (2001) 1669-1677.

[10] D.S. Hydock, C.Y. Lien, B.T. Jensen, C.M. Schneider, R. Hayward, Characterization of the effect of in vivo doxorubicin treatment on skeletal muscle function in the rat, Anticancer Res, 31 (2011) 2023-2028.

[11] L.A. Gilliam, J.S. Moylan, E.W. Patterson, J.D. Smith, A.S. Wilson, Z. Rabbani, M.B. Reid, Doxorubicin acts via mitochondrial ROS to stimulate catabolism in C2C12 myotubes, Am J Physiol Cell Physiol, 302 (2012) C195-202.

[12] V. Adams, N. Mangner, A. Gasch, C. Krohne, S. Gielen, S. Hirner, H.J. Thierse, C.C. Witt, A. Linke, G. Schuler, S. Labeit, Induction of MuRF1 is essential for TNF-alpha-induced loss of muscle function in mice, J Mol Biol, 384 (2008) 48-59.

[13] J. De Larichaudy, A. Zufferli, F. Serra, A.M. Isidori, F. Naro, K. Dessalle, M. Desgeorges, M. Piraud, D. Cheillan, H. Vidal, E. Lefai, G. Nemoz, TNF-alpha- and tumor-induced skeletal muscle atrophy involves sphingolipid metabolism, Skeletal muscle, 2 (2012) 2.

[14] M. Schwarzkopf, D. Coletti, D. Sassoon, G. Marazzi, Muscle cachexia is regulated by a p53-PW1/Peg3-dependent pathway, Genes Dev, 20 (2006) 3440-3452.

[15] A. Porrello, M.A. Cerone, S. Coen, A. Gurtner, G. Fontemaggi, L. Cimino, G. Piaggio, A. Sacchi, S. Soddu, p53 regulates myogenesis by triggering the differentiation activity of pRb, J Cell Biol, 151 (2000) 1295-1304.

[16] G. Fontemaggi, A. Gurtner, S. Strano, Y. Higashi, A. Sacchi, G. Piaggio, G. Blandino, The transcriptional repressor ZEB regulates p73 expression at the crossroad between proliferation and differentiation, Mol Cell Biol, 21 (2001) 8461-8470.

[17] T.J. Harford, G. Kliment, G.C. Shukla, C.M. Weyman, The muscle regulatory transcription factor MyoD participates with p53 to directly increase the expression of the pro-apoptotic Bcl2 family member PUMA, Apoptosis : an international journal on programmed cell death, 22 (2017) 1532-1542.

[18] M. Paris, M. Rouleau, M. Puceat, D. Aberdam, Regulation of skin aging and heart development by TAp63, Cell Death Differ, 19 (2012) 186-193.

[19] V. Patel, V.P. Singh, J.P. Pinnamaneni, D. Sanagasetti, J. Olive, M. Mathison, A. Cooney, E.R. Flores, R.G. Crystal, J. Yang, T.K. Rosengart, p63 Silencing induces reprogramming of cardiac fibroblasts into cardiomyocyte-like cells, J Thorac Cardiovasc Surg, 156 (2018) 556-565 e551.

[20] H. Cam, H. Griesmann, M. Beitzinger, L. Hofmann, R. Beinoraviciute-Kellner, M. Sauer, N. Huttinger-Kirchhof, C. Oswald, P. Friedl, S. Gattenlohner, C. Burek, A. Rosenwald, T. Stiewe, p53 family members in myogenic differentiation and rhabdomyosarcoma development, Cancer Cell, 10 (2006) 281-293.

[21] K. Bensaad, A. Tsuruta, M.A. Selak, M.N. Vidal, K. Nakano, R. Bartrons, E. Gottlieb, K.H. Vousden, TIGAR, a p53-inducible regulator of glycolysis and apoptosis, Cell, 126 (2006) 107-120.

[22] P.S. Pardo, A.M. Boriek, The physiological roles of Sirt1 in skeletal muscle, Aging (Albany NY), 3 (2011) 430-437.

[23] X. Su, Y.J. Gi, D. Chakravarti, I.L. Chan, A. Zhang, X. Xia, K.Y. Tsai, E.R. Flores, TAp63 is a master transcriptional regulator of lipid and glucose metabolism, Cell Metab, 16 (2012) 511-525.

[24] F. Murray-Zmijewski, D.P. Lane, J.C. Bourdon, p53/p63/p73 isoforms: an orchestra of isoforms to harmonise cell differentiation and response to stress, Cell Death Differ, 13 (2006) 962-972.

[25] R.A. Romano, K. Smalley, C. Magraw, V.A. Serna, T. Kurita, S. Raghavan, S. Sinha, DeltaNp63 knockout mice reveal its indispensable role as a master regulator of epithelial development and differentiation, Development, 139 (2012) 772-782.

[26] D.K. Fox, S.M. Ebert, K.S. Bongers, M.C. Dyle, S.A. Bullard, J.M. Dierdorff, S.D. Kunkel, C.M. Adams, p53 and ATF4 mediate distinct and additive pathways to skeletal muscle atrophy during limb immobilization, American journal of physiology. Endocrinology and metabolism, 307 (2014) E245-261.

[27] K. Beyfuss, A.T. Erlich, M. Triolo, D.A. Hood, The Role of p53 in Determining Mitochondrial Adaptations to Endurance Training in Skeletal Muscle, Scientific reports, 8 (2018) 14710.

[28] S.M. Ebert, J.M. Dierdorff, D.K. Meyerholz, S.A. Bullard, A. Al-Zougbi, A.D. DeLau, K.C. Tomcheck, Z.P. Skopec, G.R. Marcotte, S.C. Bodine, C.M. Adams, An investigation of p53 in skeletal muscle aging, Journal of applied physiology, 127 (2019) 1075-1084.

[29] Y. Kim, M. Triolo, D.A. Hood, Impact of Aging and Exercise on Mitochondrial Quality Control in Skeletal Muscle, Oxid Med Cell Longev, 2017 (2017) 3165396.

[30] L. Liu, G.W. Charville, T.H. Cheung, B. Yoo, P.J. Santos, M. Schroeder, T.A. Rando, Impaired Notch Signaling Leads to a Decrease in p53 Activity and Mitotic Catastrophe in Aged Muscle Stem Cells, Cell stem cell, 23 (2018) 544-556 e544.

[31] Y. von Grabowiecki, P. Abreu, O. Blanchard, L. Palamiuc, S. Benosman, S. Meriaux, V. Devignot, I. Gross, G. Mellitzer, J.L. Gonzalez de Aguilar, C. Gaiddon, Transcriptional activator TAp63 is upregulated in muscular atrophy during ALS and induces the pro-atrophic ubiquitin ligase Trim63, eLife, 5 (2016).

[32] V. Vidimar, C. Licona, R. Ceron-Camacho, E. Guerin, P. Coliat, A. Venkatasamy, M. Ali, D. Guenot, R. Le Lagadec, A.C. Jung, J.N. Freund, M. Pfeffer, G. Mellitzer, G. Sava, C. Gaiddon, A redox ruthenium compound directly targets PHD2 and inhibits the HIF1 pathway to reduce tumor angiogenesis independently of p53, Cancer Lett, 440-441 (2019) 145-155.

[33] C. Gaiddon, Y. Larmet, E. Trinh, A.L. Boutillier, B. Sommer, J.P. Loeffler, Brain-derived neurotrophic factor exerts opposing effects on beta2- adrenergic receptor according to depolarization status of cerebellar neurons, J Neurochem, 73 (1999) 1467-1476.

[34] D. Emig, N. Salomonis, J. Baumbach, T. Lengauer, B.R. Conklin, M. Albrecht, AltAnalyze and DomainGraph: analyzing and visualizing exon expression data, Nucleic Acids Res, 38 (2010) W755-762.

[35] Y. von Grabowiecki, C. Licona, L. Palamiuc, P. Abreu, V. Vidimar, D. Coovar, G. Mellitzer, C. Gaiddon, Regulation of a Notch3-Hes1 pathway and protective effect by a tocopherol-omega alkanol chain derivative in muscle atrophy, J Pharmacol Exp Ther, (2014).

[36] B.D. Harfmann, E.A. Schroder, K.A. Esser, Circadian rhythms, the molecular clock, and skeletal muscle, J Biol Rhythms, 30 (2015) 84-94.

[37] Y.Y. Cho, K. Yao, A.M. Bode, H.R. Bergen, 3rd, B.J. Madden, S.M. Oh, S. Ermakova, B.S. Kang, H.S. Choi, J.H. Shim, Z. Dong, RSK2 mediates muscle cell differentiation through regulation of NFAT3, J Biol Chem, 282 (2007) 8380-8392.

[38] Z. Wolchinsky, S. Shivtiel, E.N. Kouwenhoven, D. Putin, E. Sprecher, H. Zhou, M. Rouleau, D. Aberdam, Angiomodulin is required for cardiogenesis of embryonic stem cells and is maintained by a feedback loop network of p63 and Activin-A, Stem Cell Res, 12 (2014) 49-59.

[39] J. Xiao, Q. Shi, W. Li, X. Mu, J. Peng, M. Li, M. Chen, H. Huang, C. Wang, K. Gao, J. Fan, ARRDC1 and ARRDC3 act as tumor suppressors in renal cell carcinoma by facilitating YAP1 degradation, Am J Cancer Res, 8 (2018) 132-143.

[40] X. Shen, X. Sun, B. Sun, T. Li, G. Wu, Y. Li, L. Chen, Q. Liu, M. Cui, Z. Zhou, ARRDC3 suppresses colorectal cancer progression through destabilizing the oncoprotein YAP, FEBS Lett, 592 (2018) 599-609.

[41] Z. Meng, T. Moroishi, K.L. Guan, Mechanisms of Hippo pathway regulation, Genes Dev, 30 (2016) 1-17.

[42] Y. Aylon, M. Oren, Tumor Suppression by p53: Bring in the Hippo!, Cancer Cell, 32 (2017) 397-399.

[43] X. Su, M. Napoli, H.A. Abbas, A. Venkatanarayan, N.H. Bui, C. Coarfa, Y.J. Gi, F. Kittrell, P.H. Gunaratne, D. Medina, J.M. Rosen, F. Behbod, E.R. Flores, TAp63 suppresses mammary tumorigenesis through regulation of the Hippo pathway, Oncogene, (2016).

[44] C.A. Goodman, J.M. Dietz, B.L. Jacobs, R.M. McNally, J.S. You, T.A. Hornberger, Yes-Associated Protein is up-regulated by mechanical overload and is sufficient to induce skeletal muscle hypertrophy, FEBS Lett, 589 (2015) 1491-1497.

[45] K.I. Watt, C.A. Goodman, T.A. Hornberger, P. Gregorevic, The Hippo Signaling Pathway in the Regulation of Skeletal Muscle Mass and Function, Exerc Sport Sci Rev, 46 (2018) 92-96.

[46] A.N. Kavazis, A.J. Smuder, S.K. Powers, Effects of short-term endurance exercise training on acute doxorubicin-induced FoxO transcription in cardiac and skeletal muscle, Journal of applied physiology, 117 (2014) 223-230.

[47] A.P. Yu, X.M. Pei, T.K. Sin, S.P. Yip, B.Y. Yung, L.W. Chan, C.S. Wong, P.M. Siu, Acylated and unacylated ghrelin inhibit doxorubicin-induced apoptosis in skeletal muscle, Acta physiologica, 211 (2014) 201-213.

[48] A.J. Smuder, A.N. Kavazis, K. Min, S.K. Powers, Exercise protects against doxorubicin-induced markers of autophagy signaling in skeletal muscle, J Appl Physiol, (2011).

[49] S. Dalal, Lipid metabolism in cancer cachexia, Ann Palliat Med, 8 (2019) 13-23.

[50] P. de Lange, A. Lombardi, E. Silvestri, F. Goglia, A. Lanni, M. Moreno, Peroxisome Proliferator-Activated Receptor Delta: A Conserved Director of Lipid Homeostasis through Regulation of the Oxidative Capacity of Muscle, PPAR Res, 2008 (2008) 172676.

[51] M.A. Tarnopolsky, Myopathies Related to Glycogen Metabolism Disorders, Neurotherapeutics, 15 (2018) 915-927.

[52] M.F. Goody, R.B. Sher, C.A. Henry, Hanging on for the ride: adhesion to the extracellular matrix mediates cellular responses in skeletal muscle morphogenesis and disease, Dev Biol, 401 (2015) 75-91.

[53] L. Lu, J. Barbi, F. Pan, The regulation of immune tolerance by FOXP3, Nature reviews. Immunology, 17 (2017) 703-717.

[54] C.M. Prado, J.R. Lieffers, L.J. McCargar, T. Reiman, M.B. Sawyer, L. Martin, V.E. Baracos, Prevalence and clinical implications of sarcopenic obesity in patients with solid tumours of the respiratory and gastrointestinal tracts: a population-based study, Lancet Oncol, 9 (2008) 629-635.

[55] S.P. Samagh, E.J. Kramer, G. Melkus, D. Laron, B.M. Bodendorfer, K. Natsuhara, H.T. Kim, X. Liu, B.T. Feeley, MRI quantification of fatty infiltration and muscle atrophy in a mouse model of rotator cuff tears, Journal of orthopaedic research : official publication of the Orthopaedic Research Society, 31 (2013) 421-426.

[56] C. Fellner, F. Schick, R. Kob, C. Hechtl, M. Vorbuchner, R. Buttner, O.W. Hamer, C.C. Sieber, C. Stroszczynski, L.C. Bollheimer, Diet-induced and age-related changes in the quadriceps muscle: MRI and MRS in a rat model of sarcopenia, Gerontology, 60 (2014) 530-538.

[57] B.P. Kn, V. Gopalan, S.S. Lee, S.S. Velan, Quantification of abdominal fat depots in rats and mice during obesity and weight loss interventions, PLoS One, 9 (2014) e108979.

[58] C.D. Hines, H. Yu, A. Shimakawa, C.A. McKenzie, T.F. Warner, J.H. Brittain, S.B. Reeder, Quantification of hepatic steatosis with 3-T MR imaging: validation in ob/ob mice, Radiology, 254 (2010) 119-128.

[59] P.M. Siu, S.E. Alway, Id2 and p53 participate in apoptosis during unloading-induced muscle atrophy, Am J Physiol Cell Physiol, 288 (2005) C1058-1073.

[60] M. Van Alstyne, C.M. Simon, S.P. Sardi, L.S. Shihabuddin, G.Z. Mentis, L. Pellizzoni, Dysregulation of Mdm2 and Mdm4 alternative splicing underlies motor neuron death in spinal muscular atrophy, Genes Dev, 32 (2018) 1045-1059.

[61] M.S. Tsai, Y.T. Chiu, S.H. Wang, H.M. Hsieh-Li, H. Li, Abolishing Trp53-dependent apoptosis does not benefit spinal muscular atrophy model mice, Eur J Hum Genet, 14 (2006) 372-375.

[62] P.G. Komarov, E.A. Komarova, R.V. Kondratov, K. Christov-Tselkov, J.S. Coon, M.V. Chernov, A.V. Gudkov, A chemical inhibitor of p53 that protects mice from the side effects of cancer therapy, Science, 285 (1999) 1733-1737.

[63] E. Candi, A. Smirnov, E. Panatta, A.M. Lena, F. Novelli, M. Mancini, G. Viticchie, M.C. Piro, N. Di Daniele, M. Annicchiarico-Petruzzelli, G. Melino, Metabolic pathways regulated by p63, Biochem Biophys Res Commun, 482 (2017) 440-444.

[64] Y. Sasaki, H. Negishi, R. Koyama, N. Anbo, K. Ohori, M. Idogawa, H. Mita, M. Toyota, K. Imai, Y. Shinomura, T. Tokino, p53 family members regulate the expression of the apolipoprotein D gene, J Biol Chem, 284 (2009) 872-883.

[65] S. Strano, O. Monti, N. Pediconi, A. Baccarini, G. Fontemaggi, E. Lapi, F. Mantovani, A. Damalas, G. Citro, A. Sacchi, G. Del Sal, M. Levrero, G. Blandino, The transcriptional coactivator Yes-associated protein drives p73 gene-target specificity in response to DNA Damage, Mol Cell, 18 (2005) 447-459.

[66] N. Furth, Y. Aylon, M. Oren, p53 shades of Hippo, Cell Death Differ, 25 (2018) 81-92.

[67] H. Huang, W. Zhang, Y. Pan, Y. Gao, L. Deng, F. Li, F. Li, X. Ma, S. Hou, J. Xu, P. Li, X. Li, G. Hu, C. Li, H. Chen, L. Zhang, H. Ji, YAP Suppresses Lung Squamous Cell Carcinoma Progression via Deregulation of the DNp63-GPX2 Axis and ROS Accumulation, Cancer Res, 77 (2017) 5769-5781.

[68] X. Feng, Z. Wang, F. Wang, T. Lu, J. Xu, X. Ma, J. Li, L. He, W. Zhang, S. Li, W. Yang, S. Zhang, G. Ge, Y. Zhao, P. Hu, L. Zhang, Dual function of VGLL4 in muscle regeneration, EMBO J, 38 (2019) e101051.

[69] N. Figeac, A.D. Mohamed, C. Sun, M. Schonfelder, D. Matallanas, A. Garcia-Munoz, E. Missiaglia, E. Collie-Duguid, V. De Mello, A.V. Pobbati, J. Pruller, O. Jaka, S.D.R. Harridge, W. Hong, J. Shipley, N. Vargesson, P.S. Zammit, H. Wackerhage, VGLL3 operates via TEAD1, TEAD3 and TEAD4 to influence myogenesis in skeletal muscle, Journal of cell science, 132 (2019).

[70] K. Fraczkowska, M. Bacia, M. Przybylo, D. Drabik, A. Kaczorowska, J. Rybka, E. Stefanko, S. Drobczynski, J. Masajada, H. Podbielska, T. Wrobel, M. Kopaczynska, Alterations of biomechanics in cancer and normal cells induced by doxorubicin, Biomed Pharmacother, 97 (2018) 1195-1203.

[71] O. Gnimassou, M. Francaux, L. Deldicque, Hippo Pathway and Skeletal Muscle Mass Regulation in Mammals: A Controversial Relationship, Frontiers in physiology, 8 (2017) 190.

[72] R.N. Judson, S.R. Gray, C. Walker, A.M. Carroll, C. Itzstein, A. Lionikas, P.S. Zammit, C. De Bari, H. Wackerhage, Constitutive expression of Yes-associated protein (Yap) in adult skeletal muscle fibres induces muscle atrophy and myopathy, PLoS One, 8 (2013) e59622.

[73] K.I. Watt, B.J. Turner, A. Hagg, X. Zhang, J.R. Davey, H. Qian, C. Beyer, C.E. Winbanks, K.F. Harvey, P. Gregorevic, The Hippo pathway effector YAP is a critical regulator of skeletal muscle fibre size, Nature communications, 6 (2015) 6048.

[74] S.R. Iyer, S.B. Shah, C.W. Ward, J.P. Stains, E.E. Spangenburg, E.S. Folker, R.M. Lovering, Differential YAP nuclear signaling in healthy and dystrophic skeletal muscle, Am J Physiol Cell Physiol, 317 (2019) C48-C57.

[75] D.J. Owens, M. Fischer, S. Jabre, S. Moog, K. Mamchaoui, G. Butler-Browne, C. Coirault, Lamin Mutations Cause Increased YAP Nuclear Entry in Muscle Stem Cells, Cells, 9 (2020).
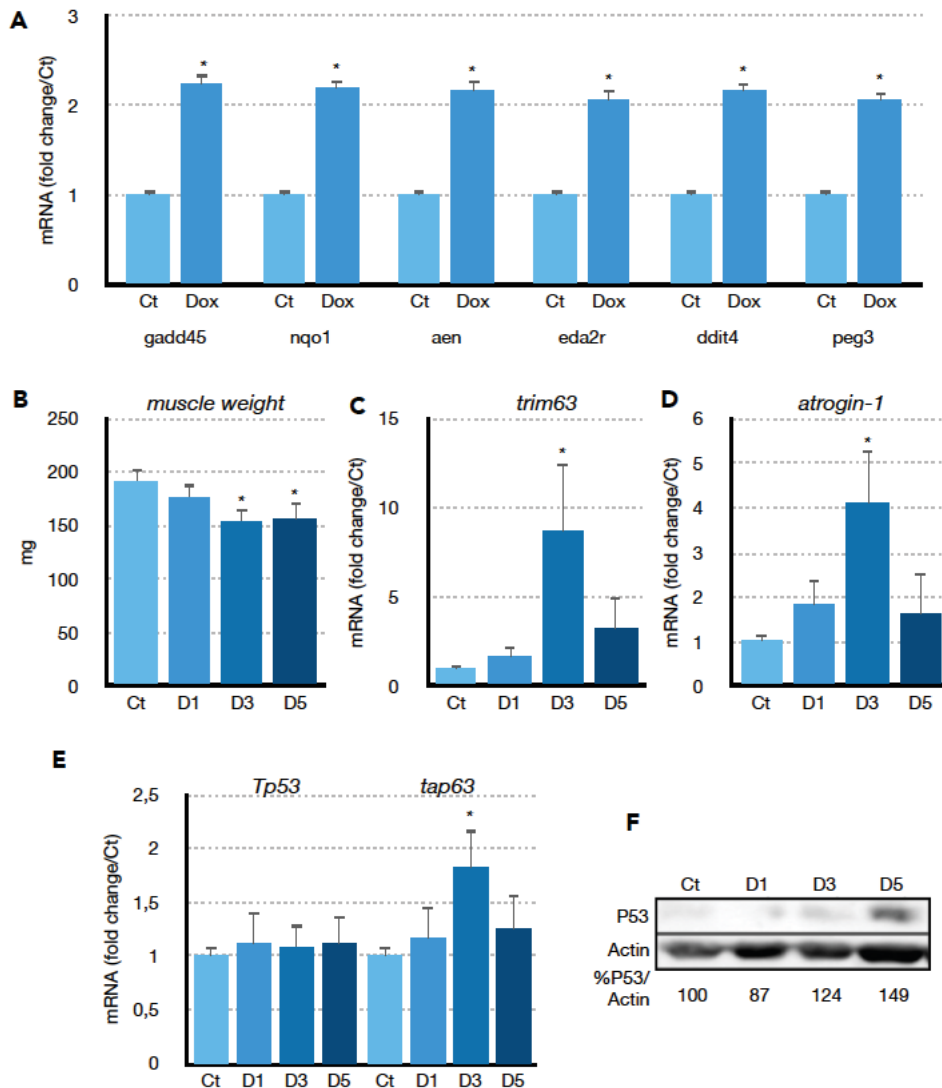
Figure 1
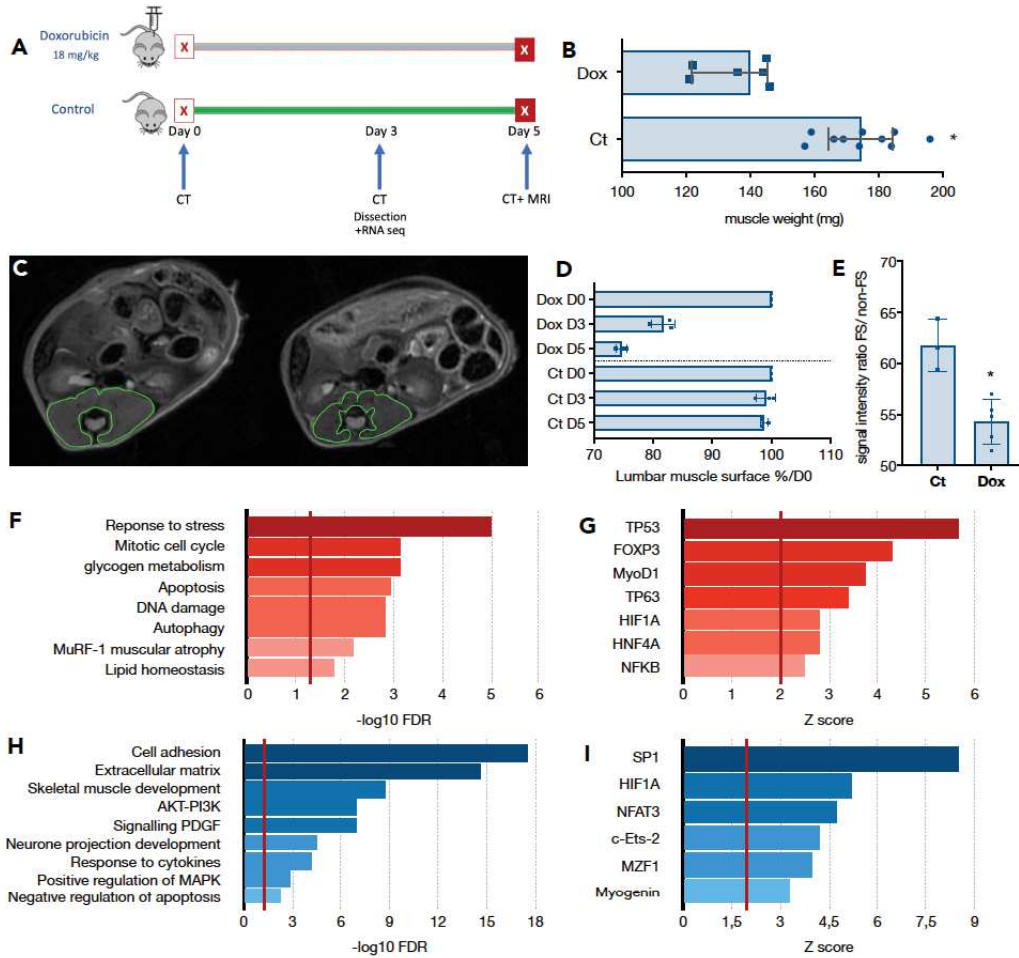
Figure 1. *Gastrocnemius muscle develop a dynamic transcriptomic program in response to the cytotoxicity induced by doxorubicin.* **A.** Schematic representation of the protocol followed to analyze the transcriptome of gastrocnemius of mice treated with doxorubicin (18mg/Kg, single dose). CT=CT scan, MRI=magnetic resonance imaging. **B.** Evolution of non-treated and doxorubicin treated mice weight (mg). * indicates $p < 0.05$ (n=9). **C.** Magnetic resonance imaging (MRI), axial T2-weighted sequence at the level of the renal hilium with manual segmentation of the paravertebral muscles (green) between a doxorubicin-treated mouse at day 5 (right) and a control mouse (left). **D**. Lumbar muscle surface measured by CT scan and represented as percentage of the untreated time (D0). D0= Day 0 before the treatment, D3= 3 days after the treatment, D5= 5 days after the treatment. **E**. Muscle fat content assessed by MRI. **F-I.** Pathways (**F. H.**) and transcription factors-associated genes (**G. I.**) found increased (**F. G.**) or decreased (**H. I.**) enriched upon doxorubicin treatment. Deregulated genes were identified by RNA sequencing. Graphs display -log 10 FDR and z score for indicated deregulated pathways with *adjp* < 0.05. Deregulated pathways were identified using STRING, Reactome, DAVID and Altanalysis software.
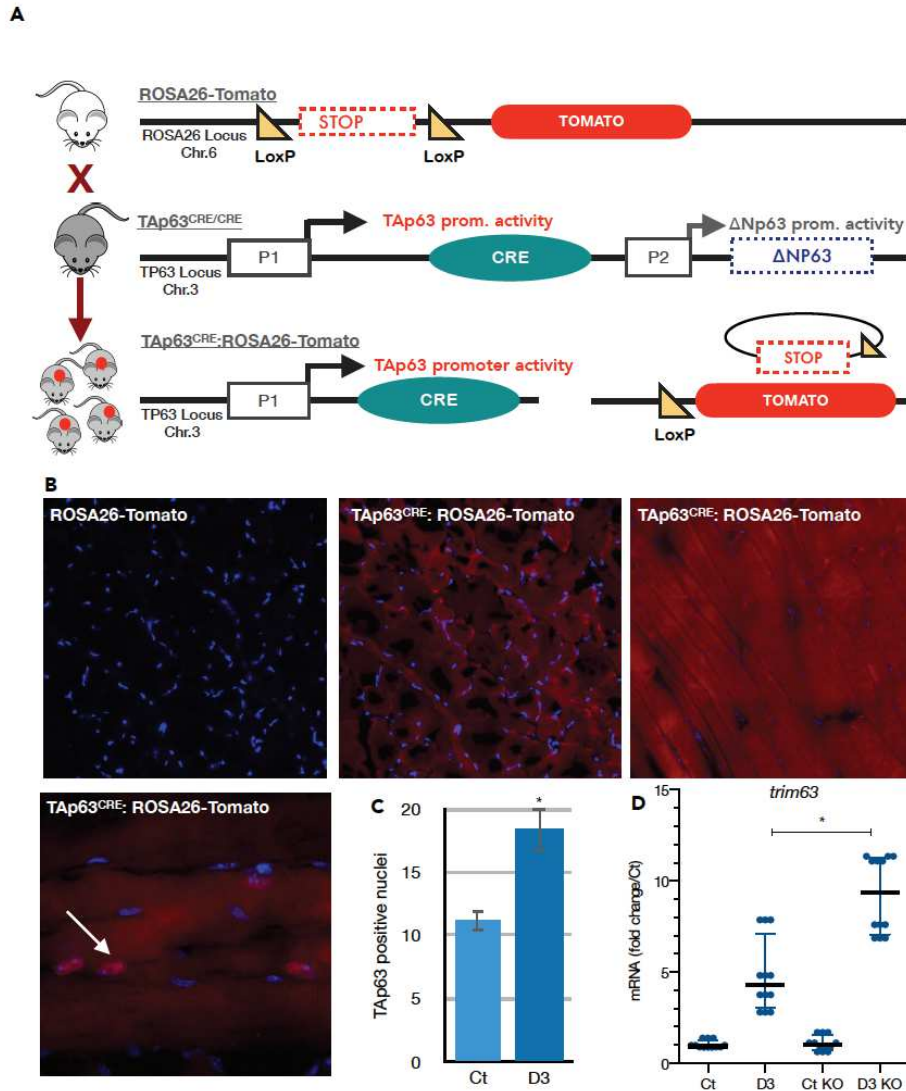
Figure 2. *Doxorubicin induces muscle atrophy markers in muscle tissue.* **A.** Doxorubicin induces expression of p53 family target genes (*gadd45*, *nqo1*, *aen*, *eda2r*, *ddit4* and *peg3*) in gastrocnemius muscles. Graph represent fold change with *adjp* value relative to the control obtained in the RNA sequencing experiment. * indicates p < 0.05 respectively (n=3). **B.** Doxorubicin induces significant loss of mice weight in a time-dependent manner. Mice were weighted before doxorubicin injection (Ct) or 1 day (D1), 3 days (D3) and 5 days (D5) after doxorubicin injection. **C. D. & F.** mRNA level of *trim63* (**C**) and *atrogin1* (**D**) and *tap63* in gastrocnemius muscle (**F**) 3 days (D3) after treatment with doxorubicin. Gastrocnemius muscle were removed, and mRNA were analyzed by qPCR. *tbp* was used as housekeeping gene. Graphs represent means with SD relative to the control. * indicates p < 0.05 respectively (n=3). **E.** Doxorubicin induces the expression of p53 protein time-dependently in gastrocnemius muscle. Skeletal muscle was removed before doxorubicin injection (Ct) or 1 day (D1), 3 days (D3) and 5 days (D5) after doxorubicin treatment and protein level was analyzed by western blot. Actin was used a house-keeping gene.

201

Figure 3

Figure 3. *TAp63 participates in doxorubicin-induced muscle atrophy*. **A.** Schematic representation of the genetic approach used to assess the expression of TAp63 in skeletal muscle. **B.** Muscle tissues of mice treated for 3 days with doxorubicin were labelled for Dapi (blue) and native fluorescence of the Tomato protein was observed (red). A nucleus with high expression of Tomato is indicated by a white arrow. **C.** Doxorubicin induces TAp63 promoter activation in skeletal muscle. Immunoreactive nuclei (white arrow in B) for Tomato (TAp63 activated promoter) were counted in section of gastrocnemius from non-treated (NT) mice or mice treated for 3 days (D3) with doxorubicin. Graphs represent means with SD relative to the control, and * indicates p< 0.05 (n=3). **D.** Doxorubicin induces the upregulation of the pro-atrophic factor *trim63* mRNA in gastrocnemius muscle. Gastrocnemius muscle of wild-type of KO TAp63 mice were isolated before treatment (Ct) or after 3 days (D3) of doxorubicin, were extracted and RT-qPCR were performed on *trim63* mRNA (n=3). Graphs represent means with SD relative to the control and * indicates p< 0.05.
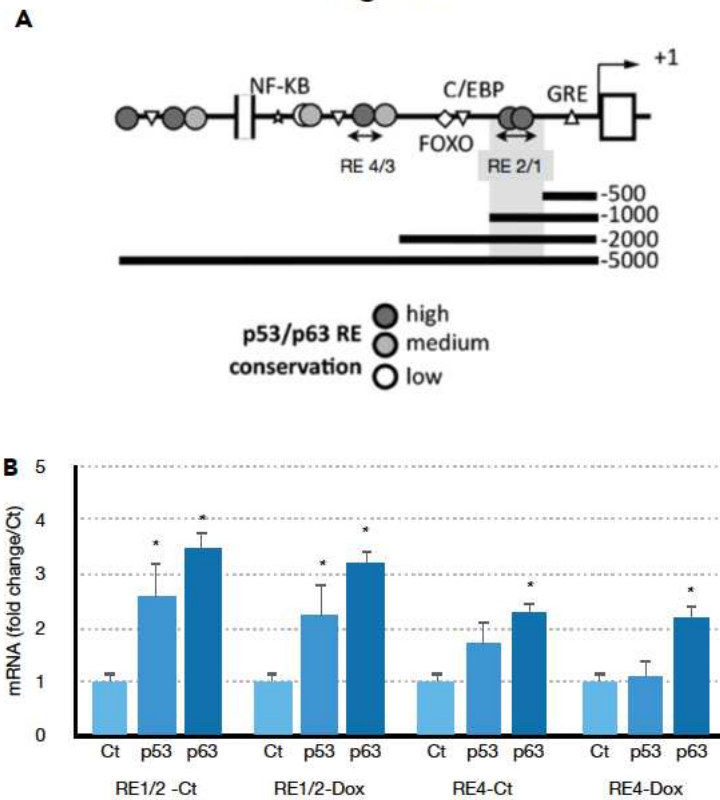
Figure 4
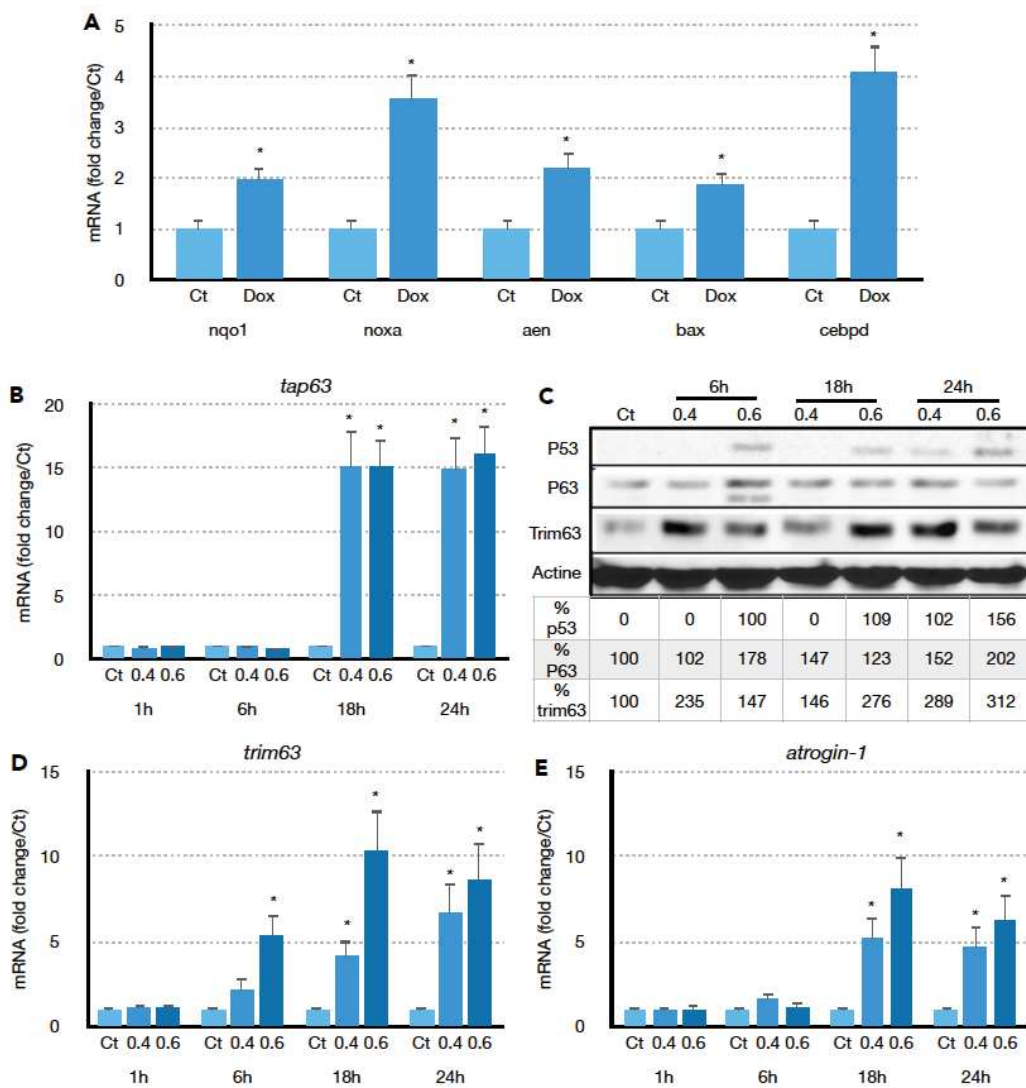
Figure 4. *Doxorubicin induces a correlated upregulation of TAp63 and Trim63 expression in C2C12 myoblastic cells.* **A.** Doxorubicin induces expression of p53 and p63 target genes (*nqo1*, *noxa*, *aen*, *bax* and *cebpd*) in myoblastic cell line C2C12. C2C12 cells were cultured in a non-treated (NT) or 1 day-treated (dox) media and mRNA were analyzed by qPCR. Graphs represent means with SD relative to the control. * indicates p < 0.05 respectively (n=3). **B. D. & E.** Doxorubicin induces an important dose and time-dependent induction of skeletal muscle atrophy mediators. C2C12 cells were cultured in a non-treated media (ct) or doxorubicin-treated media at 0.4 or 0.6µM during 1 hour, 6 hours, 18 hours or 24 hours. mRNA levels were analyzed by qPCR for *tap63* (**B**) *trim63* (**C**) and *atrogin-1* (**E**). **C.** Doxorubicin induces protein level of p53, p63 and Trim63 in C2C12 cells. Proteins were extracted from C2C12 cells in control condition (ct) or after doxorubicin treatment with 0.4 or 0.6µM during 6 hours, 18 hours or 24 hours and p53, p63 and Trim63 protein expression were analyzed by Western blot. Actin was used a house-keeping gene.
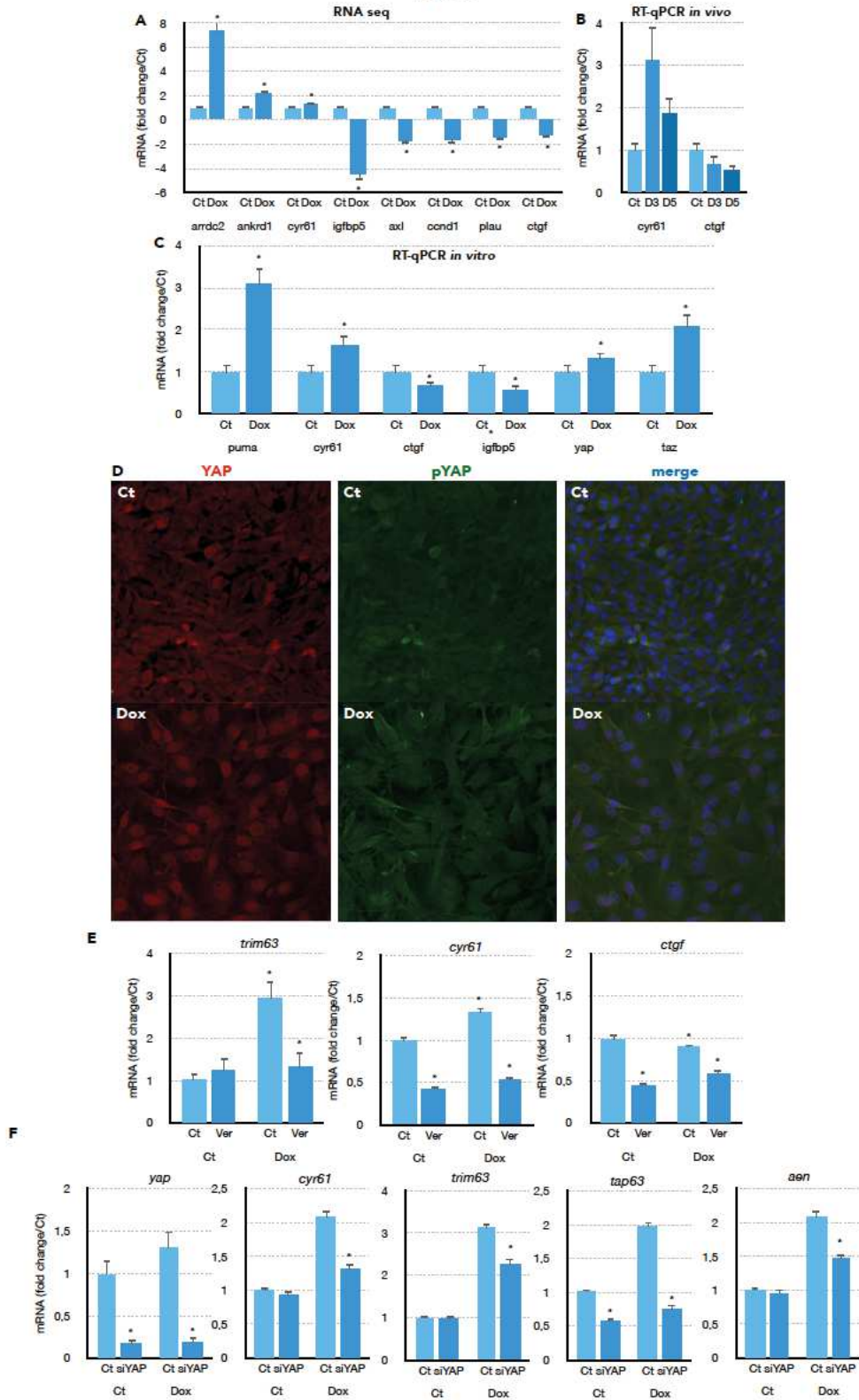
Figure 5
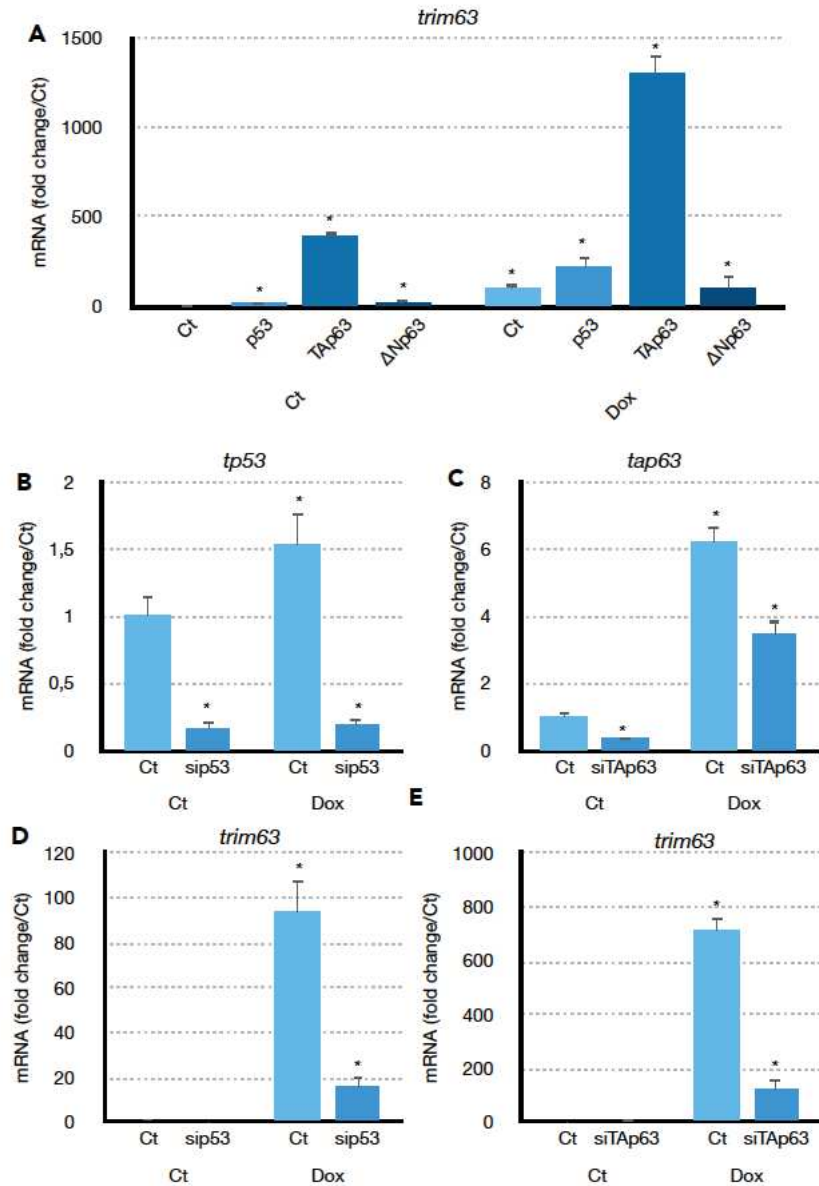
Figure 5. *TAp63 induces trim63 expression in response to doxorubicin*. **A.** Overexpression of p53 family members potentializes doxorubicin-induced *trim63* expression. C2C12 mRNA were extracted after no transfection (ct) or p53 family members overexpression p53, TAp63 or ΔNp63 in non-treated (Ct) or treated for 1 day with doxorubicin (Dox). *trim63* mRNA level was analyzed by qPCR. Graphs represent means with SD relative to the control. * indicates $p < 0.05$ respectively (n=3). *tbp* was used a house-keeping gene. **B-E.** Inhibition of p53 family members negatively induce *trim63* expression in response to doxorubicin. mRNA level of *tp53* (**B**), *tap63* (**C**) and *trim63* (**D & E**) were analyzed after extraction from C2C12 cells transfected by siRNA against p53 (sip53) (**B.&D.**) or TAp63 (siTAp63) (**C.&E.**) or not (ct) before (Ct) or after doxorubicin-treatment (Dox). Graphs represent means with SD relative to the control. * indicates $p < 0.05$ respectively (n=3).

Figure 6. *p53 and p63 bind to the trim63 promoter* **A.** Schematic representation of the *trim63* promoter indicating the location of putative p53/p63 binding sites. **B.** *trim63* promoter regions (RE1/2 and RE4) obtained after chromatin immunoprecipitation (ChIP) using p53 or p63 antibodies were amplified by qPCR. C2C12 cells cultured in normal (Ct) or doxorubicin-treated (Dox). Graphs represent means with SD relative to the control. * indicates $p < 0.05$ respectively (n=3).
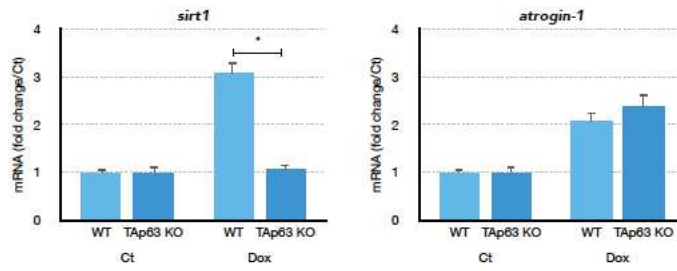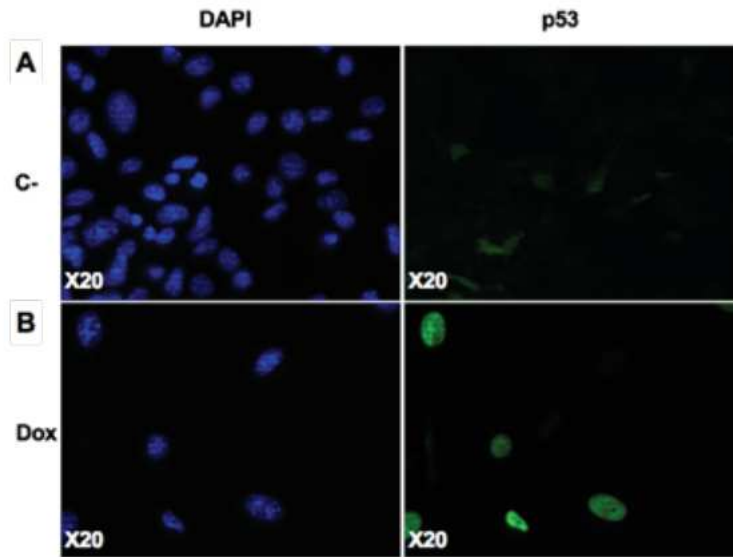
Figure 7

Figure 7. A. Expression fold change of *arrdc2*, *ankrd1*, *cyr61*, *igfbp5*, *axl*, *ccnd1*, *plau* and *ctgf* obtained by RNA sequencing in gastrocnemius muscle of mice treated with doxorubicin. Graphs represent means with *adjp* relative to the control. * indicates p < 0.05 respectively (n=3). **B.** Gastrocnemius muscle were removed in control mice (Ct) or after 3 days (D3) or 5 days (D5) of doxorubicin treatment in mice, and mRNA of YAP target genes (*cyr61* and *ctgf*) were analyzed by RT-qPCR. Graphs represent means with SD relative to the control. * indicates p < 0.05 respectively (n=3). **C.** C2C12 cells were cultured in a non-treated (Ct) or doxorubicin-treated media (Dox) for 1 day and RNA were extracted for RT-qPCR analysis of *puma*, *cyr61*, *ctgf*, *igfbp5*, *yap* and *taz* expression. Graphs represent means with SD relative to the control. * indicates p < 0.05 respectively (n=3). **D.** YAP and pYAP (TAP phosphorylated at serine 127) protein expression and localization was analyzed by immunocytofluorescence, stained with specific YAP and phopho-serine 127-YAP antibodies, and DAPI, in control (Ct) or after doxorubicin treatment (Dox) of C2C12 cells. **E.** Expression of *trim63*, *cyr61* and *ctgf* mRNA were analyzed in normal condition (ct) or YAP inhibition with verteporfin (Ver) in response to doxorubicin (Dox) or not (Ct). Graphs represent means with SD relative to the control. * indicates p < 0.05 respectively (n=3). **F.** Expression of *yap*, cyr61, *trim63*, *tap63* and *aen* were analyzed after RNA extraction from C2C12 cells transfected for 48 hours by siRNA against YAP (siYAP) or not (ct), and treated with doxorubicin for 24 hours (Dox) or not (Ct). Graphs represent means with SD relative to the control. * indicates p < 0.05 respectively (n=3).

Supplementary Figure 1: Effect of doxorubicin on TAp63 KO mice. mRNA were prepared from WT and TAp63 KO mice non-treated or treated for 3 days with doxorubicin (Dox) at 18mg/Kg. RT-qPCR were then performed to measure *sirt1* and *atrogin-1* expression. Graph represent means and error bars (n=6). * indicates p<0.001 as measured by anova and tukey post test.

Supplementary Figure 2: Effect of doxorubicin on p53. C2C12 cells were non-treated (**A**) or treated (**B**) with doxorubicin (0.6 μM) for 24h and p53 was detected by immunohistochemistry. Cells were fixed and stained with antibody against p53 and DNA was stained with DAPI.

A

C- sip53

p53

Actin

B

C- sip63

p63

Actin

C

UCSC Genome Browser on Mouse July 2007 (NCBI37/mm9) Assembly

chr4:133,856,525-133,900,054 43,530 bp

Data CHIP seq TAp63 gamma in ENO2 cells					
chr4	1,34E+08	1,34E+08	MACS_peak_7697	123,8	NM_001039048	Trim63
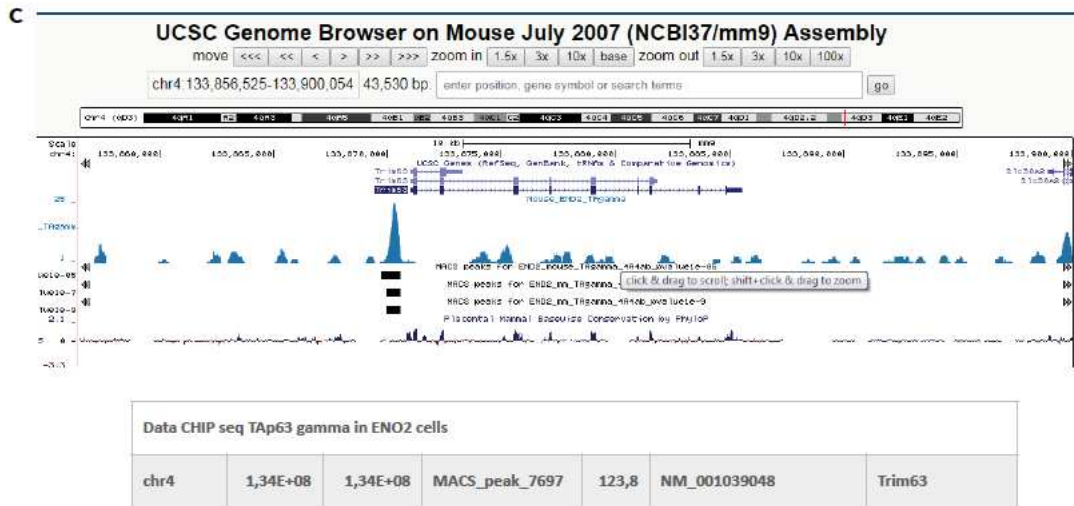
Supplementary Figure 3: Silencing of p53 and p63 on C2C12 cells. P53 and p63 protein expression was detected by Western blot after 48h of transfection with either siRNA control (C-) or siRNA (si) for p53 (**A**) or p63 (**B**).
C. NCBI schematic representation of the TAp63gamma binding sites detected in the Trim63 promoter of the results obtained by CHIP seq performed in ENO2 cells. Data from the ChIP seq are indicated bellow.

209

3. DISCUSSION
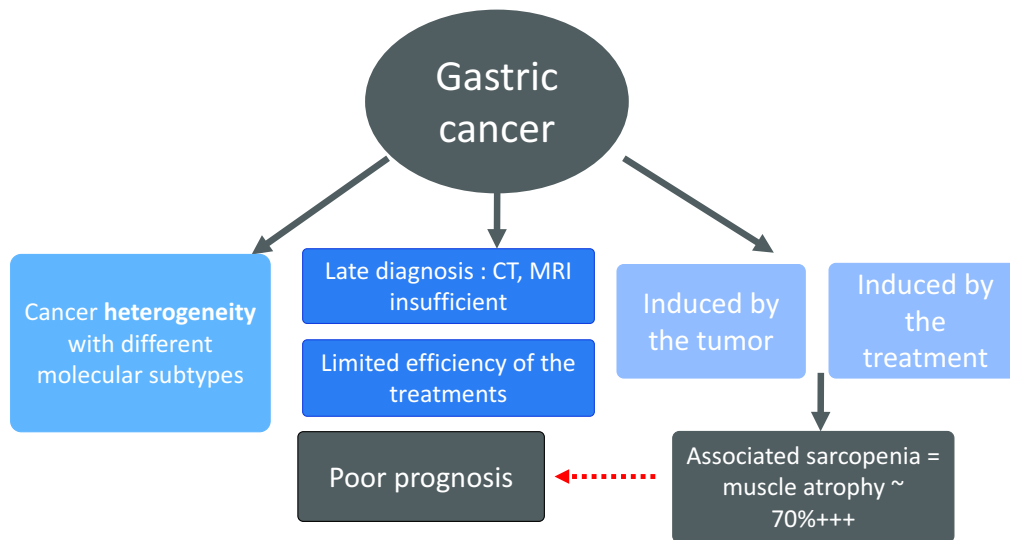
Fifth cancer in terms of worldwide incidence and third in terms of cancer-related deaths, gastric cancer has a poor prognosis, with a very limited overall survival (less than a year) in advanced or metastatic stages. Such a dreadful prognosis has many potential and combined explanations : *i)* gastric cancer is a **heterogeneous disease with multiple subtypes and molecular differences**, *ii)* the poor and **unspecific symptoms of the disease**, often presenting at very advanced stages, *iii)* the **absence of non-invasive diagnosis methods** (for instance, various imaging modalities currently used in clinical routine to diagnose or detect cancers – e.g. hepatocarcinoma, breast, lung cancer – at early stages, are of no use in gastric cancer), *iv)* the **limited treatment options** - where surgery is the only curative option, but is limited to early-stage tumors or good responders to preoperative chemotherapy - and the very high (up to 75%) resistance rate to standard platinum-based chemotherapy agents, with unsatisfactory targeted therapies available for now in clinical routine, *v)* the important proportion of **cancer cachexia and sarcopenia** (50% of digestive tract cancer patients), accounting for around 20 to 25% of cancer mortality. Additionally, the relative low incidence of gastric cancer in industrialized countries may account, at least partially, for the limited effort of investments in research on this field by the pharmacological industry and health care systems. This highlights the progress that remains to be made for its diagnosis and treatment, including the management of tumor/treatment-related complications.

Facing this dramatic situation, the work performed during my thesis led to the establishment of several animal models and a set of experimental protocols useful to address the challenges given by the complexity of gastric cancer. For instance, these studies are laying down the premises for the development of innovative tools to follow tumor growth, variations in the microenvironment constitution (ex. immune landscape) and the impact on the macro-environment (ex. muscles), which are key components to consider for the evaluation of biomarkers for personalized therapy or the activity of novel therapies. In addition, we already somehow applied these protocols with my co-workers to establish the *in vivo* activity of innovative anticancer therapies developed by our laboratory. Altogether, these studies might open new avenues for the development of novel therapeutic protocols or diagnostic tools, including novel imaging protocols.

This is particularly pertinent as compared to other cancer types, with **limited progress made over the last years** for the diagnosis of gastric cancer, **especially regarding its detection at early stages of the disease.** With poor clinical symptoms, mostly presenting at advanced/metastatic stages of the disease, the diagnosis of gastric cancer remains **clinically challenging**. Therefore, it would have been interesting to be able to screen patients with imaging methods (CT, ultrasound or MRI) as it is currently done for other cancers types such breast (screening mammograms) or hepatocarcinoma (α-foeto-protein biological assays, ultrasound, CT/MRI..) or lung (low dose CT or X-rays). Unfortunately, the diagnosis of gastric cancer is not possible on imaging alone and still relies on an invasive method = upper digestive tract endoscopy with biopsies, as no significant progress has been made with the various non-invasive imaging modalities so far. CT remains insufficient for the positive diagnosis and is relegated to the assessment of regional tumor extension and distant metastasis, while MRI is of no use in clinical routine. Therefore, **most gastric cancers are still diagnosed at later stages of the disease**, where curative treatment options are extremely limited. The only curative option remains surgery +/- perioperative chemotherapy, using platinum-based drugs (cisplatin or oxaliplatin). Unfortunately, the survival rate of patients ongoing palliative therapies remains very low, as the **majority (75%) of tumors are chemoresistant at late stages**. As other cancer types, gastric cancer shows inter-patients and intra-tumor variability. Recently, the molecular classification of gastric adenocarcinomas by The Cancer Genome Atlas (TCGA) led to the identification of dysregulated pathways, at which targeted therapies attempts have been made, with unsatisfactory results so far [3]. **Targeted therapies options are still very limited**, as anti-HER2 and anti-PDL1 are the only options potentially available, according to HER2+ or PDL1+ status of the tumor. Hence, taking into account the intratumoral clonal variation and/or the influence of the tumor microenvironment might provide crucial information and lead to new targeted therapies or novel treatment combinations, which might **improve the therapeutic care and find broader therapeutic applications in various cancer types**, in a similar way to trastuzumab, developed for HER2+ breast cancer and which found clinical applications in the therapeutic arsenal of HER2+ gastric cancers.

In preclinical research, to explore the molecular mechanisms supporting tumour growth and their responsiveness to novel anticancer drugs and targeted therapies, animal models such as cell-derived xenografts, patients-derived xenografts, syngeneic models or genetic engineered mice are very helpful. Despite the variety of animal models available, choosing the optimal model remains challenging, as each model bears strengths and weaknesses. One of the most interesting and well-balanced animal model is **patient-derived xenograft**, obtained by implanting a human tumor sample in an athymic immunodeficient mouse (subcutaneously = heterotopic or in the organ of interest = orthotopic) [106-107] PDX models behave their primary human counterpart and can be predictive of the clinical outcome and responses to chemotherapy, therefore appearing as an appealing tool for personalized medicine decisions, by summarizing many of the disease hallmarks observed in cancer patients [135].

For my PhD, **I have developed several models of patient-derived xenografts of gastric cancer with a 21% success rate** (ARTICLE 2). In gastric cancers, there were only a few previous reports of the development and use of gastric cancer PDX models [109-110, 113-114, 126-130]. The success rates of such xenografts in the two major papers was quite low (25% for Choi et al. et and 34% for Zhu et al.), compared to other cancer types, where it can reach 70% (breast, colon…) [109, 114]. With our study,

we confirmed that PDX mouse retain the major characteristics (morphological, genetics…) of the human tumor they originate from and maintain them across passages in various mice generations, reflecting the vast patient and tumor variability and heterogeneity, that is inherent to human cancer [1]. Therefore, PDX mouse appear as one of the best preclinical model to investigate anticancer drugs, tumour growth, mechanisms of drug resistance and to validate targets and positive/negative predictors of responses to therapies.

For instance, regarding the development of new anticancer drugs, **I have been able to validate in vivo the efficacy of a combinatory suberoylanilide hydroxamic acid (SAHA) + cisplatin treatment** in one of the heterotopic PDX mouse model I developed (ARTICLE 3). During this experiment, we also took advantage of the longitudinal follow-up of tumors to compare the accuracy of **ultrasound** imaging in preclinical mouse models (ARTICLE 1). We showed that in addition of being an **efficient measuring device and more accurate than caliper**, especially for non-ellipsoid tumors, the real-time imaging provides the observer with a direct access to tumor morphology and potential treatment-related structural changes, which we confirmed on histology. Even though small animal imaging somehow differs from its human counterpart, every progress that will be made in this field bears potential direct human applications. Over the last years, much progress has been made especially in small animal abdominal oncology, with micro-CT, ultrasound, MRI, PET-CT… and more precise explorations, improved sequences/protocols, better image quality, dedicated coils, reduced imaging time [112, 115, 123]. The scientists' access to small animal imaging platforms has also been greatly improved. In addition to ultrasound, **I also used magnetic resonance imaging (MRI) to characterize our PDX models**. Despite a more complex set-up, MRI enables a morphologically-accurate and precise three-dimensional analysis of tumor volume, structure, vasculature, with a very high spatial resolution [97-98]. Longitudinal time course follow-up of various abdominal tumors and evaluation of distant metastasis, especially to the liver, are also made possible. We showed that our subcutaneous tumors bore different and sometimes distinctive appearances on MR imaging, which correlated to histological differences between tumors.

For our PDX experiments, we used subcutaneous implanted-tumors, which resembled closely morphologically, biologically and biochemically the primary human tumors they are issued from (ARTICLE 1 and 2). Even though their subcutaneous location renders them easy to access, measure and follow-up (ARTICLE 1), the major downfall is that heterotopic xenografts are transplanted tumors, located within an abnormal microenvironment, encircled by a pseudo capsule [130-131]. For future developments, we should aim at **orthotopic implantations** (= directly in the organ of interest) of our tumors, which better mimics the original tumor, reproduces the loco-regional tumor environment and better mimic of metastasis (up to 40%) than subcutaneous xenografts [136-137]. Currently, most orthotopic gastric cancer models (70%) are derived from human gastric cancer cell lines rather than tissue fragments, with variable engraftment rates, ranging from 0 to 100% between studies. Similarly, we aim to develop **genetic engineered mice**. For instance, in gastric cancer researchers developed a model of mixed gastric cancer from combinatorial loss of CDH1 (E-cadherin) and p53 gene, and the acquisition of expression of the pro-oncogenic Kras in gastric parietal cells. In this mode, 100% of the mice develop a thickened and whitened stomach (linea plastic) + lung metastases (100%) and 20% of them liver metastases [135]. The major advantages of such model is that it bores > 25% of **diffuse cells and it is a immune-competent model**. All existing gastric cancer PDX are of intestinal type and, similarly, all our diffuse cancer tissue sample (primary tumor or its metastasis) engraftment attempts

failed [109-110, 113-114]. The other asset of such model is that the cancer will occur directly in the mouse stomach, without any external intervention other than the genetics modifications performed. For instance, orthotopic PDX or genetic engineered mice imaging could aid in improving MRI detection of stomach wall tumors. Additionally, genetic engineered mice could give us an extraordinary imaging insight at the carcinogenesis of the stomach, from very early stages, with imaging studies of the *in situ* development of gastric tumors that could potentially have broad human applications afterwards.

Our perception of cancer and carcinogenesis has greatly evolved by understanding that this pathology does not only involve cancer cells but also their interaction with their **microenvironment**, which represents a therapeutic target (e.g. anti-angiogenic). More recently, particular attention has been paid to the **macro-environment**, which appears to be an important player as well (e.g. the immune system). On this point, our PDX models are not optimal. The tumor microenvironment is influenced by the host immune system (T cells, B cells, infiltrating immune cells, neutrophils...), with which tumor cells are known to interact with during development and growth. In humans, PD-L1 expression varied between tumors and with around 30% of gastric cancer cells and 60% of gastric cancer liver metastasis expressing PD-L1 signal to mimic normal cells and escape elimination [83]. Similarly, **we showed that the expression of immune-check point inhibitor (i.e. PD-L1) can be also very different between PDX models, suggesting that the immune landscape might also be different (ARTICLE 2).** Two PDX models (40%) strongly expressed PD-L1 and there was no significant expression in the remaining 3 models (60%). Additionally, although only done on a small cohort (5 models), we did not see a correlation between p53 expression and PD-L1, in contrast to a recent publication indicating the reverse [138] However, our patient-derived xenografts are developed in athymic immunocompromised NMRI mice, a specific strain of mice with reduced natural killer cell activity, lack of immune system, which renders the model suboptimal, especially for immunotherapies testing. Human lymphoma may potentially occur in xenografts mice, as highlighted by the risk of lymphoproliferation (human proliferative lymphoma, from Epstein Barr Virus-infected human lymphocytes) especially when NOD or NOG mice are used [113]. Therefore, new animal models development should aim at narrowing the microenvironment gap, such as with **humanized model of tumors** [139]. Humanized mice (HM) are highly immunodeficient mouse strains into which human immune systems can be engrafted, results in a xenograft growth within the context of a human immune system and its resulting tumor microenvironment. Recent studies have highlighted all the similarities between human tumors and xenografts in humanized mice, regarding tumor structure, metastasis, and signaling. All in all, humanized mice, despite higher costs, will facilitate the investigation of novel cancer therapies, especially new immunotherapies.

If progress is being made regarding animal models, novel anticancer drugs and small animal imaging, our global perception of cancers is also slowly shifting from an organ-centered disease to a more **global and systemic one.** Cancer cachexia, which is *a progressive loss of adipose tissue and skeletal muscle mass, occurs in* approximately *50% of cancer patients, especially in digestive tract cancers [87]*. The skeletal muscle loss, or *muscle atrophy,* is associated with loss of muscle strength, which altogether define *sarcopenia.* More specifically in gastric cancer, around 30 to 60% of patients develop cancer cachexia, independently of the cancer stage (ARTICLE 6). If late stage diagnosis and limited treatment options partially accounted for the poor prognosis of gastric cancer, cachexia worsens it, especially as its incidence increases after chemotherapy. It is an insidious syndrome that

not only has a dramatic impact on *patients' quality of life,* but also is associated with ***poor responses to therapy (chemotherapy and immunotherapy) and decreased survival.*** It is estimated to account for ***20 to 25% of deaths from cancer***. [92].   Cancer cachexia is also characterized by **systemic inflammation** and negative protein and energy balance. One of the main hypotheses is that cancer-related muscle atrophy is caused by inflammatory processes involving interleukins (such as IL6, TNFα and TWEAK) that are often produced by tumors. Released inflammatory agents could induce mitochondrial decoupling, a failure in the expression of the key components of the electron transport chain, which results in severe mitochondrial dysfunction and a decrease in mitochondrial ATP production [140]. Skeletal muscle dysfunction and the related disrupted capacity for oxidative metabolism, is believed to contribute to patient fatigue, decreased metabolic function, and muscle mass loss [140]. Hence, the detection of IL6 and TNFα in serum have been suggested to assess muscle atrophy in patients, however, inflammation is unspecific of muscle atrophy and therefore introduces an important bias [136]. In addition, functional studies and clinical trials aiming at antagonizing IL6 and TNFα using monoclonal antibodies are disappointing and have not clearly confirmed the importance of these interleukins in cancer-related muscle atrophy. However, the reasons why only some patients are prone to develop cachexia remains largely unknown and cachexia is still largely an ***underestimated and untreated condition.*** Hence, one of the remaining issues is to established the respective contribution of the tumor and the anticancer therapies in cachexia. Unfortunately, ***no therapeutic approach*** can yet efficiently restore ***muscle loss*** and ***strength.*** **We recently showed that** *gastric cancer patients (ARTICLE 5), w***ho benefited from a nutritional support by means of a** *jejunostomy* **before starting chemotherapy, had a better chance of fulfilling the complete 6-weeks rounds of chemotherapy** required for their treatment before surgical removal of the tumor. In addition, we found that a majority of patients **developed muscle atrophy after** *platinum salt-based (***cisplatin or oxaliplatin) chemotherapy (ARTICLE 6)** and that muscle atrophy was drastically reduced for those who underwent jejunostomy. Hence, our results indicate that chemotherapy agents might negatively impact on muscle mass and that jejunostomy might represent a potential therapeutic approach to reduce muscle atrophy in gastric cancer patients. However, jejunostomy is not a risk-free procedure, with around 7 to 12% of postoperative complications and it also did not restore lost muscle mass. Therefore, a better understanding of the underlying mechanisms of cancer-cachexia and sarcopenia are required. For instance, using the anticancer drug doxorubicin, we confirmed that we can **induce muscle atrophy and muscle-related changes** in C57BL/6 mice after three to five days **(ARTICLE 7)**, with increased in muscle atrophy mechanisms, such as the pro-atrophic gene trim63, with the involvement **of** p53 as well as TAp63 regulation of the expression of the pro-atrophic gene trim63 via a direct interaction on its promoter [120]. Currently in cancer patients, muscle atrophy can only be diagnosed at relatively advanced stages, by means of a CT-based surface & density evaluation (abdominal CT with or without contrast, or CT images of PET-CT) of muscle loss, which consists of measuring the surface and the density (in Housefield units) of the muscles (psoas and erector spinae muscles) at the level of the 3rd lumbar vertebra (L3), then normalized to weight and height (BMI) [90-91]. We applied the same measurement method to our drug-induced muscle atrophy mouse model **on micro-CT and MRI (ARTICLE 7)** and we have been able to observe **anticancer drug-induced changes in the morphology and composition of paravertebral muscles in mice.** Doxorubicin induced a progressive and irreversible decrease of paravertebral muscle surface (up to 15% muscle loss within the 5 first days) and such decreased paravertebral muscle surface could also be observed on MRI. **I have been able to observe muscle atrophy in a drug-induced mouse model at rather early stages (day 5)** and MRI also enabled us to observe drug-induced changes in muscle signal intensity on MRI between fat saturated and non-

fat saturated images. Unfortunately, the detection of sarcopenia in humans is currently only possible at rather advanced stages on imaging. Still, there is no recognized means for specifically unmasking early muscle atrophy or patients at risk of developing it during the course of the disease. Blood level of IL6 and TNFα are sometimes used markers for muscle atrophy, but they are not specific and present bias, as they can also be induced by infections or other pathological affections often associated with cancer or anticancer treatments [142]. Unfortunately, no imaging method is able to diagnose or even suspect cancer cachexia and muscle atrophy *at early stages* and future developments should aim this way. One of the dysregulated pathways we observed with our drug-induced muscle atrophy mouse model **(ARTICLE 7)** involved ***metabolism regulations***, such as the ***hypoxia transcription factor HIF1A*** and ***the reactive oxygen species response factor NRF2***. In addition, different muscle-specific genes (TRIM63, Atrogin1 - ubiquitin ligases that favor muscle protein catabolism *via* the ***proteasome...***) also showed a strongly increased expression. On the other hand, some of the muscle-specific genes, whose expression was increased in our transcriptome, have been described as being regulated by ***hypoxia*** and as potential ***early serum markers for muscular atrophy*** (dystrophia). In the near future, we aim to evaluate selective ***PET-CT probes specific*** for ***hypoxia*** such as ^{18}F-AZA (fluoroazomycin arabinofuranoside), ^{18}F-MISO (fluoromisonidazole) - developed by our collaborators from IPHC - for proof of concept that they could be used to detect early muscle atrophy. The hypoxia radio-tracers we are considering, are part of the 2-nitromidazole family and under hypoxic conditions these compounds are sequestered in cells lacking oxygen. ^{18}-F-MISO bears the advantage of being trans-functional with a Marketing Authorization, but suffers from low tumor uptake while ^{18}F-AZA is more hydrophilic, with better specificity, but for clinical trials use only. Similarly, it would be very interesting to apply **phosphorus magnetic resonance spectroscopy and imaging (^{31}P-MRS/MRSI)** to our animal models of muscle atrophy (mouse bearing tumor at advanced stage or doxorubicin-induced muscle atrophy), which offers an offer a very unique window to non-invasively look at tissue metabolism in vivo, especially skeletal muscles, especially as it recently appeared **promising technique to detect skeletal muscle dysfunction at early stages** [140-141].

All in all, **everything we learned about regarding the development and the use of preclinical models in gastric cancer can find broad applications to other cancers and even non-cancerous diseases.** Animal models and their imaging modalities are widely used in preclinical translational research and cancer-cachexia is a global systemic syndrome, overlapping the boundaries between cancer and inflammation. As radiologist, working on such model enables us to have a direct to access organ-related changes and the opportunity to witness cancer development from the very early stages - with a close and reproducible monitoring of normal organs and tumor growth - which is not always feasible with patients. Thus, the search for new biomarkers, the development of new imaging tools and the improvement of existing diagnostic tools is essential for all cancers, with the need to develop more personalized treatments. For this, we need new more realistic mouse models, closer to the characteristics of patients and tumours. The future could be an ***integrated diagnosis***, combining histological features, imaging data, molecular analyzes and genetic characteristics of cancers, with the aim of eventually offering personalized *à la carte* therapies to all cancer patients.

4. REFERENCES

1. Hidalgo, M., Amant, F., Biankin, A. V., Budinská, E., Byrne, A. T., Caldas, C., ... & Roman-Roman, S. (2014). Patient-derived xenograft models: an emerging platform for translational cancer research. *Cancer discovery*, *4*(9), 998-1013.
2. Okines, A., Verheij, M., Allum, W., Cunningham, D., Cervantes, A., & ESMO Guidelines Working Group. (2010). Gastric cancer: ESMO Clinical Practice Guidelines for diagnosis, treatment and follow-up. *Annals of Oncology*, *21*(suppl_5), v50-v54.
3. Kelley, J. R., & Duggan, J. M. (2003). Gastric cancer epidemiology and risk factors. *Journal of clinical epidemiology*, *56*(1), 1-9.
4. Gomceli I et al. Gastric carcinogenesis 2012 and CDU-HGE Abbreviated hepatogastro-enterology and digestive surgery 3rd. edition Chap.27 2015
5. Hartgrink, H. H., Jansen, E. P., van Grieken, N. C., & van de Velde, C. J. (2009). Gastric cancer. *The Lancet*, *374*(9688), 477-490
6. Pharoah, P. D., Guilford, P., Caldas, C., & International Gastric Cancer Linkage Consortium. (2001). Incidence of gastric cancer and breast cancer in CDH1 (E-cadherin) mutation carriers from hereditary diffuse gastric cancer families. *Gastroenterology*, *121*(6), 1348-1353.
7. Fitzgerald, R. C., Hardwick, R., Huntsman, D., Carneiro, F., Guilford, P., Blair, V., ... & Dwerryhouse, S. (2010). Hereditary diffuse gastric cancer: updated consensus guidelines for clinical management and directions for future research. *Journal of medical genetics*, *47*(7), 436-444.
8. Van der Post, R. S., Vogelaar, I. P., Carneiro, F., Guilford, P., Huntsman, D., Hoogerbrugge, N., ... & Bardram, L. (2015). Hereditary diffuse gastric cancer: updated clinical guidelines with an emphasis on germline CDH1 mutation carriers. *Journal of medical genetics*, *52*(6), 361-374.
9. Masciari, S., Dewanwala, A., Stoffel, E. M., Lauwers, G. Y., Zheng, H., Achatz, M. I., ... & Verselis, S. J. (2011). Gastric cancer in individuals with Li-Fraumeni syndrome. *Genetics in Medicine*, *13*(7), 651.
10. Gonzalez, K. D., Buzin, C., Noltner, K. A., Gu, D., Li, W., Malkin, D., & Sommer, S. (2009). High frequency of de novo mutations in Li-Fraumeni syndrome. *Journal of medical genetics*.
11. Tinat, J., Bougeard, G., Baert-Desurmont, S., Vasseur, S., Martin, C., Bouvignies, E., ... & Bonaïti-Pellié, C. (2009). 2009 version of the Chompret criteria for Li Fraumeni syndrome. *J Clin Oncol*, *27*(26), e108-e109.
12. Mankaney, G., Leone, P., Cruise, M., LaGuardia, L., O'Malley, M., Bhatt, A., ... & Burke, C. A. (2017). Gastric cancer in FAP: a concerning rise in incidence. *Familial cancer*, *16*(3), 371-376.
13. Lynch, H. T., & Smyrk, T. (1996). Hereditary nonpolyposis colorectal cancer (Lynch syndrome): an updated review. *Cancer: Interdisciplinary International Journal of the American Cancer Society*, *78*(6), 1149-1167.
14. Brose, M. S., Rebbeck, T. R., Calzone, K. A., Stopfer, J. E., Nathanson, K. L., & Weber, B. L. (2002). Cancer risk estimates for BRCA1 mutation carriers identified in a risk evaluation program. *Journal of the National Cancer Institute*, *94*(18), 1365-1372.
15. Giardiello, F. M., & Trimbath, J. D. (2006). Peutz-Jeghers syndrome and management recommendations. *Clinical gastroenterology and hepatology*, *4*(4), 408-415.
16. Washington, K. (2010). of the AJCC cancer staging manual: stomach. *Annals of surgical oncology*, *17*(12), 3077-3079.
17. Sano, T., Coit, D. G., Kim, H. H., Roviello, F., Kassab, P., Wittekind, C., ... & Ohashi, Y. (2017). Proposal of a new stage grouping of gastric cancer for TNM classification: International Gastric Cancer Association staging project. *Gastric cancer*, *20*(2), 217-225
18. Lauren, P. (1965). The two histological main types of gastric carcinoma: diffuse and so-called intestinal-type carcinoma: an attempt at a histo-clinical classification. *Acta Pathologica Microbiologica Scandinavica*, *64*(1), 31-49.
19. Hu, B., El Hajj, N., Sittler, S., Lammert, N., Barnes, R., & Meloni-Ehrig, A. (2012). Gastric cancer: Classification, histology and application of molecular pathology. *Journal of gastrointestinal oncology*, *3*(3), 251.
20. Sipponen, P., & Correa, P. (2002). Delayed rise in incidence of gastric cancer in females results in unique sex ratio (M/F) pattern: etiologic hypothesis. *Gastric cancer*, *5*(4), 0213-0219.
21. Gravalos, C., & Jimeno, A. (2008). HER2 in gastric cancer: a new prognostic factor and a novel therapeutic target. *Annals of oncology*, *19*(9), 1523-1529.

22. Gravalos, C. (2006). Correlation between Her2/neu overexpression/amplification and clinicopathological parameters sin advanced gastric cancer patients: a prospective study. *J Clin Oncol.*, *24*, 18S.

23. Lee, H. H., Lim, C. H., Park, J. M., Cho, Y. K., Song, K. Y., Jeon, H. M., & Park, C. H. (2012). Low accuracy of endoscopic ultrasonography for detailed T staging in gastric cancer. *World journal of surgical oncology*, *10*(1), 190.

24. Kwee, R. M., & Kwee, T. C. (2007). Imaging in local staging of gastric cancer: a systematic review. *Journal of clinical oncology*, *25*(15), 2107-2116.

25. Seevaratnam R, Cardoso R, McGregor C, Lourenco L, Mahar A, Sutradhar R, et al. How useful is preoperative imaging for tumor, node, metastasis (TNM) staging of gastric cancer? A meta-analysis. Gastric Cancer. 2012;15 Suppl 1:S3-18.

26. Chen, C. Y., Hsu, J. S., Wu, D. C., Kang, W. Y., Hsieh, J. S., Jaw, T. S., ... & Liu, G. C. (2007). Gastric cancer: preoperative local staging with 3D multi–detector row CT—correlation with surgical and histopathologic results. *Radiology*, *242*(2), 472-482.

27. Shimizu, K., Ito, K., Matsunaga, N., Shimizu, A., & Kawakami, Y. (2005). Diagnosis of gastric cancer with MDCT using the water-filling method and multiplanar reconstruction: CT–histologic correlation. *American Journal of Roentgenology*, *185*(5), 1152-1158

28. Kim, H. J., Kim, A. Y., Oh, S. T., Kim, J. S., Kim, K. W., Kim, P. N., ... & Ha, H. K. (2005). Gastric cancer staging at multi–detector row CT gastrography: comparison of transverse and volumetric CT scanning. *Radiology*, *236*(3), 879-885.

29. Leake PA, Cardoso R, Seevaratnam R, Lourenco L, Helyer L, Mahar A, et al. A systematic review of the accuracy and indications for diagnostic laparoscopy prior to curative-intent resection of gastric cancer. Gastric Cancer. 2012;15 Suppl 1:S38-47.

30. Ba-Ssalamah A, Muin D, Schernthaner R et al (2013) Texture-based classification of different gastric tumors at contrast-enhanced CT. Eur J Radiol 82(10):e537–e543

31. Liu S, Liu S, Ji C et al (2017) Application of CT texture analysis in predicting histopathological characteristics of gastric cancers. Eur Radiol 27(12):4951–4959

32. Giganti F, Marra P, Ambrosi A et al (2017) Pre-treatment MDCT-based texture analysis for therapy response prediction in gastric cancer: Comparison with tumor regression grade at final histology. Eur J Radiol 90:129–137

33. Giganti F, Antunes S, Salerno A et al (2017) Gastric cancer: texture analysis from multidetector computed tomography as a potential preoperative prognostic biomarker. Eur Radiol 27(5):1831–1839

34. Yoon SH, Kim YH, Lee YJ et al (2016) Tumor heterogeneity in human epidermal growth factor receptor 2 (HER2)-positive advanced gastric cancer assessed by CT texture analysis: association with survival after trastuzumab treatment. PLoS One 11(8):e0161278

35. Waddell, T., Verheij, M., Allum, W., Cunningham, D., Cervantes, A., & Arnold, D. (2013). Gastric cancer: ESMO–ESSO–ESTRO Clinical Practice Guidelines for diagnosis, treatment and follow-up. *Annals of Oncology*, *24*(suppl_6), vi57-vi63

36. Joo, I., Lee, J. M., Kim, J. H., Shin, C. I., Han, J. K., & Choi, B. I. (2015). Prospective comparison of 3T MRI with diffusion-weighted imaging and MDCT for the preoperative TNM staging of gastric cancer. *Journal of Magnetic Resonance Imaging*, *41*(3), 814-821.

37. Luo M, Song H, Liu G et al (2017) Comparison of DWI and 18F-FDG PET/CT for assessing preoperative N-staging in gastric cancer: evidence from a meta-analysis. Oncotarget 8(48):84473–84488

38. Arslan H, Fatih Özbay M, Çallı İ et al (2017) Contribution of diffusion weighted MRI to diagnosis and staging in gastric tumors and comparison with multi-detector computed tomography. Radiol Oncol 51(1):23–29

39. Liu S, Zheng H, Zhang Y et al (2018) Whole-volume apparent diffusion coefficient-based entropy parameters for assessment of gastric cancer aggressiveness. J Magn Reson Imaging 47(1):168–175

40. Giganti F, Ambrosi A, Chiari D et al (2017) Apparent diffusion coefficient by diffusion-weighted magnetic resonance imaging as a sole biomarker for staging and prognosis of gastric cancer. Chin J Cancer Res 29(2):118–126

41. Liu S, He J, Guan W et al (2014) Preoperative T staging of gastric cancer: comparison of diffusion- and T2-weighted magnetic resonance imaging. J Comput Assist Tomogr 38:544–550

42. Hasbahceci M, Akcakaya A, Memmi N et al (2015) Diffusion MRI on lymph node staging of gastric adenocarcinoma. Quant Imaging Med Surg 5(3):392–400

43. Ma, Q., Xin, J., Zhao, Z., Guo, Q., Yu, S., Xu, W., ... & Zhai, W. (2013). Value of 18F-FDG PET/CT in the diagnosis of primary gastric cancer via stomach distension. *European journal of radiology*, *82*(6), e302-e306.

44. Youn, S. H., Seo, K. W., Lee, S. H., Shin, Y. M., & Yoon, K. Y. (2012). 18F-2-deoxy-2-fluoro-D-glucose positron emission tomography: computed tomography for preoperative staging in gastric cancer patients. *Journal of gastric cancer*, *12*(3), 179-186.

45. Chen, R., Zhou, X., Liu, J., & Huang, G. (2016). Relationship between 18F-FDG PET/CT findings and HER2 expression in gastric cancer. *Journal of Nuclear Medicine*, *57*(7), 1040-1044

46. Lee, D. H., Kim, S. H., Im, S. A., Oh, D. Y., Kim, T. Y., & Han, J. K. (2016). Multiparametric fully-integrated 18-FDG PET/MRI of advanced gastric cancer for prediction of chemotherapy response: a preliminary study. *European radiology*, *26*(8), 2771-2778.

47. Cancer Genome Atlas Research Network. (2014). Comprehensive molecular characterization of gastric adenocarcinoma. *Nature*, *513*(7517), 202.

48. Ajani, J. A., Lee, J., Sano, T., Janjigian, Y. Y., Fan, D., & Song, S. (2017). Gastric adenocarcinoma. *Nature Reviews Disease Primers*, *3*, 17036.

49. Riquelme, I., Saavedra, K., Espinoza, J. A., Weber, H., García, P., Nervi, B., ... & Bizama, C. (2015). Molecular classification of gastric cancer: Towards a pathway-driven targeted therapy. *Oncotarget*, *6*(28), 24750

50. Huscher, C. G., Mingoli, A., Sgarzini, G., Sansonetti, A., Di Paola, M., Recher, A., & Ponzano, C. (2005). Laparoscopic versus open subtotal gastrectomy for distal gastric cancer: five-year results of a randomized prospective trial. *Annals of surgery*, *241*(2), 232.

51. Japanese Gastric Cancer Association. (2017). Japanese gastric cancer treatment guidelines 2014 (ver. 4). *Gastric cancer*, *20*(1), 1-19.

52. Cervantes, A., Roda, D., Tarazona, N., Rosello, S., & Perez-Fidalgo, J. A. (2013). Current questions for the treatment of advanced gastric cancer. *Cancer treatment reviews*, *39*(1), 60-67.

53. Ohtsu A, Ajani JA, Bai YX, et al. Everolimus for previously treated advanced gastric cancer: results of the randomized, double-blind, phase III GRANITE-1 study. *J Clin Oncol.* 2013;31:3935-3943

54. Janku, F., Yap, T. A., & Meric-Bernstam, F. (2018). Targeting the PI3K pathway in cancer: are we making headway?. *Nature Reviews Clinical Oncology*, *15*(5), 273.

55. Polom, K., Marrelli, D., Roviello, G., Pascale, V., Voglino, C., Rho, H., ... & Roviello, F. (2017). Molecular key to understand the gastric cancer biology in elderly patients—The role of microsatellite instability. *Journal of surgical oncology*, *115*(3), 344-350.

56. Tapia, O., Riquelme, I., Leal, P., Sandoval, A., Aedo, S., Weber, H., ... & Roa, J. C. (2014). The PI3K/AKT/mTOR pathway is activated in gastric cancer with potential prognostic and predictive significance. *Virchows Archiv*, *465*(1), 25-33.

57. Gaikwad, S. M., & Ray, P. (2012). Non-invasive imaging of PI3K/Akt/mTOR signalling in cancer. *American journal of nuclear medicine and molecular imaging*, *2*(4), 418.

58. Wadhwa, R., Song, S., Lee, J. S., Yao, Y., Wei, Q., & Ajani, J. A. (2013). Gastric cancer—molecular and clinical dimensions. *Nature Reviews Clinical Oncology*, *10*(11), 643.

59. Chiurillo, M. A. (2015). Role of the Wnt/β-catenin pathway in gastric cancer: An in-depth literature review. *World journal of experimental medicine*, *5*(2), 84.

60. Kang, W., Cheng, A. S., Yu, J., & To, K. F. (2016). Emerging role of Hippo pathway in gastric and other gastrointestinal cancers. *World Journal of Gastroenterology*, *22*(3), 1279.

61. Shi, D.-T., Han, M., Gao, N., Tian, W., and Chen, W. (2014). Association of RASSF1A promoter methylation with gastric cancer risk: a meta-analysis. Tumor Biol. 35, 943–948.

62. Sokolova, O., and Naumann, M. (2017). NF-κB Signaling in Gastric Cancer. Toxins (Basel) 9.

63. Shi, J. (2014). Pathogenetic mechanisms in gastric cancer. World Journal of Gastroenterology 20 , 13804.

64. Katoh, Y., & Katoh, M. (2005). Hedgehog signaling pathway and gastric cancer. *Cancer biology & therapy*, *4*(10), 1050-1054.

65. Wan, J., Zhou, J., Zhao, H., Wang, M., Wei, Z., Gao, H., ... & Cui, H. (2014). Sonic hedgehog pathway contributes to gastric cancer cell growth and proliferation. *BioResearch open access*, *3*(2), 53-59.

66. Ertao, Z., Jianhui, C., Chuangqi, C., Changjiang, Q., Sile, C., Yulong, H., ... & Shirong, C. (2016). Autocrine Sonic hedgehog signaling promotes gastric cancer proliferation through induction of phospholipase Cγ1 and the ERK1/2 pathway. *Journal of Experimental & Clinical Cancer Research*, *35*(1), 63.

67. Lee, D. H., Lee, S. Y., & Oh, S. C. (2017). Hedgehog signaling pathway as a potential target in the treatment of advanced gastric cancer. *Tumor Biology*, *39*(6), 1010428317692266.

68. Levrero, M., De Laurenzi, V., Costanzo, A., Gong, J., Wang, J. Y., & Melino, G. (2000). The p53/p63/p73 family of transcription factors: overlapping and distinct functions. *J Cell Sci*, *113*(10), 1661-1670

69. Ribeiro, J., Malta, M., Galaghar, A., Silva, F., Afonso, L. P., Medeiros, R., & Sousa, H. (2017). P53 deregulation in Epstein-Barr virus-associated gastric cancer. *Cancer letters*, *404*, 37-43.

70. Tannapfel, A., Schmelzer, S., Benicke, M., Klimpfinger, M., Kohlhaw, K., Mössner, J., Engeland, K., and Wittekind, C. (2001). Expression of the p53 homologues p63 and p73 in multiple simultaneous gastric cancer. J. Pathol. 195, 163–170

71. Song, Y., Liu, D., and He, G. (2015). TKTL1and p63 are biomarkers for the poor prognosis of gastric cancer patients. Cancer Biomark 15, 591–597.

72. Wei, J., Zaika, E., and Zaika, A. (2012). p53 Family: Role of Protein Isoforms in Human Cancer.

73. Vilgelm, A.E., Hong, S.-M., Washington, M.K., Wei, J., Chen, H., El-Rifai, W., and Zaika, A.I. (2010). Characterization of ΔNp73 expression and regulation in gastric and esophageal tumors. Oncogene 29, 5861–5868.

74. Vilgelm, A.E., Washington, M.K., Wei, J., Chen, H., Prassolov, V.S., and Zaika, A.I. (2012). Interactions of the p53 protein family in cellular stress response in gastrointestinal tumors. Mol. Cancer Ther. 9, 693–705.

75. Qiang, L., Ji, Z., and Wang, X. (2018). Expression of TAp73α affects the therapy effect of chemotherapy drugs in gastric cancer. Oncol. Res.

76. Ji, Z. P., Qiang, L., & Zhang, J. L. (2018). Transcription activated p73-modulated cyclin D1 expression leads to doxorubicin resistance in gastric cancer. *Experimental and therapeutic medicine*, *15*(2), 1831-1838.

77. Kang, Y. K., Kang, W. K., Shin, D. B., Chen, J., Xiong, J., Wang, J., ... & Philco-Salas, M. (2009). Capecitabine/cisplatin versus 5-fluorouracil/cisplatin as first-line therapy in patients with advanced gastric cancer: a randomised phase III noninferiority trial. *Annals of oncology*, *20*(4), 666-673.

78. Siegel R, Ma J, Zou Z, Jemal A. Cancer statistics, 2014. *CA Cancer J Clin.* 2014;64:9-29.

79. Norguet, E., Dahan, L., & Seitz, J. F. (2012). Targetting esophageal and gastric cancers with monoclonal antibodies. *Current topics in medicinal chemistry*, *12*(15), 1678-1682.

80. Thiel, A., & Ristimäki, A. (2015). Targeted therapy in gastric cancer. *Apmis*, *123*(5), 365-372.

81. Böger, C., Behrens, H. M., Mathiak, M., Krüger, S., Kalthoff, H., & Röcken, C. (2016). PD-L1 is an independent prognostic predictor in gastric cancer of Western patients. *Oncotarget*, *7*(17), 24269.

82. Fuchs, C. S., Doi, T., Jang, R. W., Muro, K., Satoh, T., Machado, M., ... & Garrido, M. (2018). Safety and efficacy of pembrolizumab monotherapy in patients with previously treated advanced gastric and gastroesophageal junction cancer: phase 2 clinical KEYNOTE-059 trial. *JAMA oncology*, *4*(5), e180013-e180013.

83. Shitara, K., Özgüroğlu, M., Bang, Y. J., Di Bartolomeo, M., Mandalà, M., Ryu, M. H., ... & Muro, K. (2018). Pembrolizumab versus paclitaxel for previously treated, advanced gastric or gastro-oesophageal junction cancer (KEYNOTE-061): a randomised, open-label, controlled, phase 3 trial. *The Lancet*, *392*(10142), 123-133.

84. Van Cutsem, E., Kang, Y., Chung, H., Shen, L., Sawaki, A., Lordick, F., ... & Bang, Y. (2009). Efficacy results from the ToGA trial: a phase III study of trastuzumab added to standard chemotherapy in first-line HER2-positive advanced gastric cancer. *J clin oncol*, *27*(18)(suppl), LBA4509.

85. Schauer M, Peiper M, Theisen J, et al. Prognostic factors in patients with diffuse type gastric cancer (linitis plastica) after operative treatment. Eur J Med Res 2011;16:29-33. 10.1186/2047-783X-16-1-29

86. Adachi, Y., Yasuda, K., Inomata, M., Sato, K., Shiraishi, N., & Kitano, S. (2000). Pathology and prognosis of gastric carcinoma: well versus poorly differentiated type. *Cancer: Interdisciplinary International Journal of the American Cancer Society*, *89*(7), 1418-1424.

87. Luu, C., Thapa, R., Woo, K., Coppola, D., Almhanna, K., Pimiento, J. M., ... & Hodul, P. J. (2017). Does histology really influence gastric cancer prognosis?. Journal of gastrointestinal oncology, 8(6), 1026.

88. Cunningham D, Starling N, Rao S, et al. Capecitabine and oxaliplatin for advanced esophagogastric cancer. *N Engl J Med.* 2008;358:36-46.

89. Aoyagi, T.; Terracina, K. P.; Raza, A.; Matsubara, H.; Takabe, K., Cancer cachexia, mechanism and treatment. *World J Gastrointest Oncol* **2015,** *7* (4), 17-29.

90. Cruz-Jentoft AJ, Baeyens JP, Bauer JM, Boirie Y, Cederholm T, Landi F, et al. Sarcopenia: European consensus on definition and diagnosis. Age Ageing. juill 2010;39(4):412-23.

91. Prado, C. M., Lieffers, J. R., McCargar, L. J., Reiman, T., Sawyer, M. B., Martin, L., & Baracos, V. E. (2008). Prevalence and clinical implications of sarcopenic obesity in patients with solid tumors of the respiratory and gastrointestinal tracts: a population-based study. *The lancet oncology*, *9*(7), 629-635.

92. Coss, C. C.; Clinton, S. K.; Phelps, M. A., Cachectic Cancer Patients: Immune to Checkpoint Inhibitor Therapy? *Clin Cancer Res* **2018,** *24* (23), 5787-5789.

93. Huang, D. D., Chen, X. X., Chen, X. Y., Wang, S. L., Shen, X., Chen, X. L., ... & Zhuang, C. L. (2016). Sarcopenia predicts 1-year mortality in elderly patients undergoing curative gastrectomy for gastric cancer: a prospective study. *Journal of cancer research and clinical oncology*, *142*(11), 2347-2356.

94. Voisinet, M., Venkatasamy, A., Alratrout, H., Delhorme, J. B., Brigand, C., Rohr, S., ... & Romain, B. (2020). How to Prevent Sarcopenia Occurrence during Neoadjuvant Chemotherapy for Oesogastric Adenocarcinoma?. *Nutrition and Cancer*, 1-7.

95. Miyamoto, Y.; Hanna, D. L.; Zhang, W.; Baba, H.; Lenz, H. J., Molecular Pathways: Cachexia Signaling-A Targeted Approach to Cancer Treatment. Clin Cancer Res 2016, 22 (16), 3999-4004.

96. Skipworth, R. J.; Stewart, G. D.; Bhana, M.; Christie, J.; Sturgeon, C. M.; Guttridge, D. C.; Cronshaw, A. D.; Fearon, K. C.; Ross, J. A., Mass spectrometric detection of candidate protein biomarkers of cancer cachexia in human urine. *International journal of oncology* **2010,** *36* (4), 973-82.

97. Shahda, S.; Narasimhan, A.; Kays, J.; Perkins, S. M.; Cheng, L.; Hannaford, K. N.; Schloss, D. E. I.; Koniaris, L. G.; Zimmers, T. A., Identification of circulating protein biomarkers for pancreatic cancer cachexia. bioRxiv 2018.

98. Johns, N.; Stretch, C.; Tan, B. H.; Solheim, T. S.; Sorhaug, S.; Stephens, N. A.; Gioulbasanis, I.; Skipworth, R. J.; Deans, D. A.; Vigano, A.; Ross, J. A.; Bathe, O. F.; Tremblay, M. L.; Kaasa, S.; Strasser, F.; Gagnon, B.; Baracos, V. E.; Damaraju, S.; Fearon, K. C., New genetic signatures associated with cancer cachexia as defined by low skeletal muscle index and weight loss. *J Cachexia Sarcopenia Muscle* **2017,** *8* (1), 122-130.

99. Cohen, S.; Nathan, J. A.; Goldberg, A. L., Muscle wasting in disease: molecular mechanisms and promising therapies. Nat Rev Drug Discov 2015, 14 (1), 58-74.

100. von Grabowiecki, Y.; Licona, C.; Palamiuc, L.; Abreu, P.; Vidimar, V.; Coovar, D.; Mellitzer, G.; Gaiddon, C., Regulation of a Notch3-Hes1 pathway and protective effect by a tocopherol-omega alkanol chain derivative in muscle atrophy. J Pharmacol Exp Ther 2014

101. von Grabowiecki, Y.; Abreu, P.; Blanchard, O.; Palamiuc, L.; Benosman, S.; Meriaux, S.; Devignot, V.; Gross, I.; Mellitzer, G.; Gonzalez de Aguilar, J. L.; Gaiddon, C., Transcriptional activator TAp63 is upregulated in muscular atrophy during ALS and induces the pro-atrophic ubiquitin ligase Trim63. *eLife* **2016,** *5*

102. Lee, D. E.; Brown, J. L.; Rosa-Caldwell, M. E.; Blackwell, T. A.; Perry, R. A., Jr.; Brown, L. A.; Khatri, B.; Seo, D.; Bottje, W. G.; Washington, T. A.; Wiggs, M. P.; Kong, B. W.; Greene, N. P., Cancer cachexia-induced muscle atrophy: evidence for alterations in microRNAs important for muscle size. Physiol Genomics 2017, 49 (5), 253-260.

103. Argiles, J. M.; Lopez-Soriano, F. J.; Stemmler, B.; Busquets, S., Novel targeted therapies for cancer cachexia. Biochem J 2017, 474 (16), 2663-2678.

104. Manfredelli, S., Delhorme, J. B., Venkatasamy, A., Gaiddon, C., Brigand, C., Rohr, S., & Romain, B. (2017). Could a feeding jejunostomy be integrated into a standardized preoperative management of oeso-gastric junction adenocarcinoma?. Annals of surgical oncology, 24(11), 3324-3330.

105. Voisinet, M., Venkatasamy, A., Alratrout, H., Delhorme, J. B., Brigand, C., Rohr, S., ... & Romain, B. (2020). How to Prevent Sarcopenia Occurrence during Neoadjuvant Chemotherapy for Oesogastric Adenocarcinoma?. *Nutrition and Cancer*, 1-7.

106. Hidalgo, M., Amant, F., Biankin, A. V., Budinská, E., Byrne, A. T., Caldas, C., ... & Roman-Roman, S. (2014). Patient-derived xenograft models: an emerging platform for translational cancer research. *Cancer discovery*, *4*(9), 998-1013.

107. Siolas, D., & Hannon, G. J. (2013). Patient Derived Tumor Xenografts: transforming clinical samples into mouse models. *Cancer research*, canres-1069.

108. Yu, S., Yang, M., & Nam, K. T. (2014). Mouse models of gastric carcinogenesis. *Journal of gastric cancer*, *14*(2), 67-86.

109. Choi, Y. Y., Lee, J. E., Kim, H., Sim, M. H., Kim, K. K., Lee, G., ... & Noh, S. H. (2016). Establishment and characterisation of patient-derived xenografts as paraclinical models for gastric cancer. *Scientific reports*, *6*, 22172.

110. Huynh, H., Ong, R., & Zopf, D. (2015). Antitumor activity of the multikinase inhibitor regorafenib in patient-derived xenograft models of gastric cancer. *Journal of Experimental & Clinical Cancer Research*, *34*(1), 132.

111. Gengenbacher, N., Singhal, M., & Augustin, H. G. (2017). Preclinical mouse solid tumor models: status quo, challenges and perspectives. *Nature Reviews Cancer*, *17*(12), 751.

112. Lauber, D. T., Fülöp, A., Kovács, T., Szigeti, K., Máthé, D., & Szijártó, A. (2017). State of the art in vivo imaging techniques for laboratory animals. *Laboratory animals*, *51*(5), 465-478.

113. Dieter, S. M., Giessler, K. M., Kriegsmann, M., Dubash, T. D., Möhrmann, L., Schulz, E. R., ... & Heger, U. (2017). Patient-derived xenografts of gastrointestinal cancers are susceptible to rapid and delayed B-lymphoproliferation. *International journal of cancer*, *140*(6), 1356-1363

114. Zhu, Y., Tian, T., Li, Z., Tang, Z., Wang, L., Wu, J., ... & Zou, J. (2015). Establishment and characterization of patient-derived tumor xenograft using gastroscopic biopsies in gastric cancer. *Scientific reports*, *5*, 8542.

115. Dhani, N. C., Lohse, I., Foltz, W. D., Cao, P. J., & Hedley, D. W. (2018). Estimating tumor volume in a primary orthotopic mouse model of human pancreatic cancer using rapid acquisition magnetic resonance imaging. *journal of cancer therapeutics and research*, *3*(1)

116. Hoffman, R. M. (2015). Patient-derived orthotopic xenografts: better mimic of metastasis than subcutaneous xenografts. *Nature Reviews Cancer*, *15*(8), 451.

117. Hiroshima, Y. et al. Patient-derived mouse models of cancer need to be orthotopic in order to evaluate targeted anti-metastatic therapy. Oncotarget **7**, 71696–71702 (2016).

118. Hiroshima, Y. et al. Establishment of a patient-derived orthotopic xenograft (PDOX) model of HER-2-positive cervical cancer expressing the clinical metastatic pattern. PLoS ONE **10**, e0117417 (2015).

119. Till, J. E., Yoon, S. S., & Ryeom, S. (2017). E-cadherin and K-ras: Implications of a newly developed model of gastric cancer. *Oncoscience*, *4*(11-12), 162.

120. Gilliam, L. A., Ferreira, L. F., Bruton, J. D., Moylan, J. S., Westerblad, H., St. Clair, D. K., & Reid, M. B. (2009). Doxorubicin acts through tumor necrosis factor receptor subtype 1 to cause dysfunction of murine skeletal muscle. *Journal of Applied Physiology*, *107*(6), 1935-1942.

121. Goetze, R. G., Buchholz, S. M., Patil, S., Petzold, G., Ellenrieder, V., Hessmann, E., & Neesse, A. (2018). Utilizing high resolution ultrasound to monitor tumor onset and growth in genetically engineered pancreatic cancer models. *JoVE (Journal of Visualized Experiments)*, (134), e56979.

122. Meiburger, K. M. (2017). Quantitative Assessment of Cancer Vascular Architecture by Skeletonization of 3D CEUS Images: Role of Liposomes and Microbubbles. In *Quantitative Ultrasound and Photoacoustic Imaging for the Assessment of Vascular Parameters* (pp. 75-89). Springer, Cham.

123. Lewis, J. S., Achilefu, S., Garbow, J. R., Laforest, R., & Welch, M. J. (2002). Small animal imaging: current technology and perspectives for oncological imaging. *European journal of cancer*, *38*(16), 2173-2188.

124. Ramasamy, K., Dwyer-Nield, L. D., Serkova, N. J., Hasebroock, K. M., Tyagi, A., Raina, K., ... & Agarwal, R. (2011). Silibinin prevents lung tumorigenesis in wild-type but not in iNOS−/− mice: potential of real-time micro-CT in lung cancer chemoprevention studies. *Clinical Cancer Research*, *17*(4), 753-761.

125. Liu, X., & Meltzer, S. J. (2017). Gastric cancer in the era of precision medicine. *Cellular and molecular gastroenterology and hepatology*, *3*(3), 348-358.

126. Yoshiyuki, T. et al. Immunohistochemical demonstration of epidermal growth factor in human gastric cancer xenografts of nude mice. Cancer 65, 953–7 (1990).

127. Kubota, T. et al. Growth of human tumor xenografts in nude mice and mice with severe combined immunodeficiency (SCID). Surg Today 23, 375–7 (1993).

128. Zhang, L. et al. A subset of gastric cancers with EGFR amplification and overexpression respond to cetuximab therapy. Sci Rep 3, 2992 (2013).

129. Wang, H., Lu, J., Tang, J., Chen, S., He, K., Jiang, X., ... & Teng, L. (2017). Establishment of patient-derived gastric cancer xenografts: a useful tool for preclinical evaluation of targeted therapies involving alterations in HER-2, MET and FGFR2 signaling pathways. *BMC cancer*, *17*(1), 191.

130. Kim, J. Y., Kim, W. G., & Kwon, C. H. (2019). Differences in immune contextures among different molecular subtypes of gastric cancer and their prognostic impact. *Gastric Cancer*, *22*(6), 1164-1175.

131. Mutze, K., Langer, R., Becker, K., Ott, K., Novotny, A., Luber, B., ... & Keller, G. (2010). Histone deacetylase (HDAC) 1 and 2 expression and chemotherapy in gastric cancer. *Annals of surgical oncology*, *17*(12), 3336-3343.

132. West, A. C., & Johnstone, R. W. (2014). New and emerging HDAC inhibitors for cancer treatment. *The Journal of clinical investigation*, *124*(1), 30-39.

133. Heider, U., Rademacher, J., Lamottke, B., Mieth, M., Moebs, M., Von Metzler, I., ... & Sezer, O. (2009). Synergistic interaction of the histone deacetylase inhibitor SAHA with the proteasome inhibitor bortezomib in cutaneous T cell lymphoma. *European journal of haematology*, *82*(6), 440-449.

134. Bergamo, A., Gaiddon, C., Schellens, J. H. M., Beijnen, J. H., & Sava, G. (2012). Approaching tumor therapy beyond platinum drugs: status of the art and perspectives of ruthenium drug candidates. *Journal of inorganic biochemistry*, *106*(1), 90-99.

135. Till, J. E., Yoon, S. S., & Ryeom, S. (2017). E-cadherin and K-ras: Implications of a newly developed model of gastric cancer. *Oncoscience*, *4*(11-12), 162.

136. Hoffman, R. M. (2015). Patient-derived orthotopic xenografts: better mimic of metastasis than subcutaneous xenografts. *Nature Reviews Cancer*, *15*(8), 451-452.

137. Reddavid, R., Corso, S., Moya-Rull, D., Giordano, S., & Degiuli, M. (2020). Patient-Derived Orthotopic Xenograft models in gastric cancer: A systematic review. *Updates in Surgery*, 1-16.

138. Jiang, Z., Liu, Z., Li, M., Chen, C., & Wang, X. (2018). Immunogenomics analysis reveals that TP53 mutations inhibit tumor immunity in gastric Cancer. *Translational oncology*, *11*(5), 1171-1187.

139. Morton, J. J., Bird, G., Refaeli, Y., & Jimeno, A. (2016). Humanized mouse xenograft models: narrowing the tumor–microenvironment gap. *Cancer research*, *76*(21), 6153-6158

140. Santos-Díaz, A., & Noseworthy, M. D. (2020). Phosphorus magnetic resonance spectroscopy and imaging (31P-MRS/MRSI) as a window to brain and muscle metabolism: A review of the methods. *Biomedical Signal Processing and Control*, *60*, 101967.

141. Pérez-Rial, S., Barreiro, E., Fernández-Aceñero, M. J., Fernández-Valle, M. E., González-Mangado, N., & Peces-Barba, G. (2020). Early detection of skeletal muscle bioenergetic deficit by magnetic resonance spectroscopy in cigarette smoke-exposed mice. *PloS one*, *15*(6), e0234606

142. Bano, G., Trevisan, C., Carraro, S., Solmi, M., Luchini, C., Stubbs, B., ... & Veronese, N. (2017). Inflammation and sarcopenia: a systematic review and meta-analysis. *Maturitas*, *96*, 10-15.

5. APPENDICES

5.1. APPENDIX 1 : HDAC4 Levels Control Sensibility toward Cisplatin in Gastric Cancer via the p53-p73/BIK Pathway

Article

HDAC4 Levels Control Sensibility toward Cisplatin in Gastric Cancer via the p53-p73/BIK Pathway

Marie-Elodie Spaety [1,2], Alexandre Gries [1], Amandine Badie [1], Aina Venkatasamy [1,3], Benoit Romain [1,4], Christophe Orvain [1], Kazuyoshi Yanagihara [5], Koji Okamoto [5], Alain C. Jung [1,6], Georg Mellitzer [1,6], Sébastien Pfeffer [2] and Christian Gaiddon [1,6,*]

[1] Laboratory STREINTH (Stress Response and Innovative Therapies), Inserm IRFAC UMR_S1113, Université de Strasbourg, 3 av. Molière, 67200 Strasbourg, France; Marie_Elodie_S@hotmail.com (M.-E.S.); alexandre.gries@etu.unistra.fr (A.G.); a.badie@laposte.net (A.B.); aina.vnkt@gmail.com (A.V.); benoit.romain@chru-strasbourg.fr (B.R.); orvain@unistra.fr (C.O.); AJung@strasbourg.unicancer.fr (A.C.J.); mellitzer@unistra.fr (G.M.)
[2] Architecture and Reactivity of RNA, Institut de biologie moléculaire et cellulaire du CNRS, Université de Strasbourg, 15 rue René Descartes, 67084 Strasbourg, France; s.pfeffer@ibmc-cnrs.unistra.fr
[3] Radiology Department, Centre Hospitalier Universitaire (CHU) Hautepierre, 67200 Strasbourg, France
[4] Digestive Surgery department, CHU Hautepierre, 67200 Strasbourg, France
[5] National Cancer Research Center, Tokyo 104_0045, Japan; alefthau@mac.com (K.Y.); kojokamo@ncc.go.jp (K.O.)
[6] Centre de Lutte contre le Cancer Paul Strauss (CLCC), 67065 Strasbourg, France
* Correspondence: gaiddon@unistra.fr

check for updates

Abstract: Gastric cancer (GC) remains a health issue due to the low efficiency of therapies, such as cisplatin. This unsatisfactory situation highlights the necessity of finding factors impacting GC sensibility to therapies. We analyzed the cisplatin pangenomic response in cancer cells and found HDAC4 as a major epigenetic regulator being inhibited. HDAC4 mRNA repression was partly mediated by the cisplatin-induced expression of miR-140. At a functional level, HDAC4 inhibition favored cisplatin cytotoxicity and reduced tumor growth. Inversely, overexpression of HDAC4 inhibits cisplatin cytotoxicity. Importantly, HDAC4 expression was found to be elevated in gastric tumors compared to healthy tissues, and in particular in specific molecular subgroups. Furthermore, mutations in HDAC4 correlate with good prognosis. Pathway analysis of genes whose expression in patients correlated strongly with HDAC4 highlighted DNA damage, p53 stabilization, and apoptosis as processes downregulated by HDAC4. This was further confirmed by silencing of HDAC4, which favored cisplatin-induced apoptosis characterized by cleavage of caspase 3 and induction of proapoptotic genes, such as *BIK*, in part via a p53-dependent mechanism. Altogether, these results reveal HDAC4 as a resistance factor for cisplatin in GC cells that impacts on patients' survival.

Keywords: miR-140; HDAC4; p53; p73; BIK; gastric cancer; cisplatin

1. Introduction

Gastric cancer (GC) is the fifth most common cancer and represents the second highest incidence of cancer-related death worldwide [1]. The first line of treatment is a surgical resection combined with perioperative chemotherapy using platinum-based compounds (cisplatin, oxaliplatin). Unfortunately, only a limited number of tumors respond to the treatment due to intrinsic or acquired resistance [2]. In addition, the lack of early prognosis markers leads to a late diagnosis often occurring at locally advanced or metastasis stage, with a median survival time of only 10 months.

In GC, resistance mechanisms are not well understood, but examples of activation of DNA repair and decrease of the apoptotic response have been reported. One of the cisplatin resistance mechanisms in GC cells is an overexpression or amplification of HER2, which leads to the initiation of epithelial–mesenchymal transition (EMT) correlating with an unfavorable outcome for patients [3]. In addition, patients treated with cisplatin can exhibit an overexpression of ERCC1 and BRCA1, two enzymes implicated in the nucleotide excision repair pathway, which also correlates with a worse prognosis [4]. Furthermore, one major actor of the apoptosis pathway after DNA damage is the p53 protein. p53 is a known tumor suppressor, which is inactivated in more than 60% of GC [5,6] and whose expression is related to the sensitivity of cells to cisplatin [7–9]. Part of the inhibitory impact of p53 mutants on cell death is mediated by their interaction with the two other members of the p53 family: p63 and p73 [10]. These three genes encode for two classes of isoforms, either containing a transactivation domain in the N terminus (p53, TAp63, and TAp73) or not (Δp53, ΔNp63, and ΔNp73). It has been reported that these proteins are involved in many aspects of digestive cancers' progression and aggressiveness [11,12]. For instance, altered expression of TA/ΔNp73 isoforms has been observed in gastric cancers and expression of the ΔNp73 isoform correlates with poor prognosis [13–15].

Another resistance mechanism to chemotherapies involves epigenetic modifications (histone acetylation/deacetylation, histone/DNA methylation) and post-transcriptional regulations (microRNAs) [16,17]. For instance, HDAC enzymes are aberrantly expressed in various cancer types including GC [18]. The HDAC family is composed of 4 classes: the Zn^{2+} dependent class I (HDAC1, 2, 3 and 8), IIa (HDAC4, 5, 7 and 9), IIb (HDAC6 and 10) and IV (HDAC11), and the NAD^+-dependent class III (sirtuin). HDACs remove the acetyl group of lysine residues from histone and nonhistone substrates, leading to chromatin compaction and decreased gene transcription [19]. HDAC1/2 are overexpressed in advanced GC, and their expression level is correlated with poorer patient prognosis [20]. HDAC4 is also overexpressed in GC cell lines and has been implicated in cell growth and apoptosis arrest [21]. Some of the functions of HDAC in cancer progression can be explained by their interaction with p53. Indeed, HDAC1 can interact with p53, reducing its binding capacity to the promoter of the proapoptotic gene *BAX*, thus favoring cancer cell survival [22].

Micro (mi)RNAs are small noncoding RNAs of approximately 22 nucleotides in size, which regulate gene expression through target mRNA translation inhibition or destabilization. Numerous deregulations of miRNAs have been described in gastric cancers, but their functions are not always clear [23]. For instance, the oncomiR miR-21 is overexpressed in 92% of GC, leading to the inhibition of the PTEN tumor suppressor expression [24]. Inversely, genomic loss of the tumor suppressor miR-101 is implicated in cancer progression through EZH2 overexpression [25]. miRNAs often organize in clusters and share common functions. Thus, miR-222-221 and miR-106b-25 are known to be upregulated in GC tissues, increasing the G1/S transition through the activation of CDK2 [26]. In addition, it has also been shown that miRNAs can act on GC cells' chemosensitivity. For instance, miR-143, miR-144, and miR-145 are good prognostic markers for the effectiveness of the chemotherapy [27,28]. Finally, miR-15b and miR-16 are downregulated in multidrug-resistant GC cell lines and their ectopic expression chemo-sensitizes GC cells through the inhibition of the antiapoptotic gene *BCL2* [29].

Here, we investigated the response of cancer cells and healthy digestive tissues to chemotherapies in order to understand the molecular mechanisms underlying chemoresistances and side effects caused by these therapies. To this end, we performed a microarray analysis to identify genes deregulated by cisplatin in cancer cells and identified HDAC4 as a gene inhibited by cisplatin. Strengthened by the finding of Kang et al. that HDAC4 is overexpressed in gastric cancer cell lines [21], we decided to focus our attention on the role of HDAC4 and the underlying molecular mechanisms that are put in place in response to cisplatin in GC cancer.

2. Results

2.1. Loss of HDAC4 Following Cisplatin Treatment of Gastric Cancer Cells

Platinum-based compounds (e.g., cisplatin) are used to treat multiple types of cancer. We previously performed a microarray-based transcriptomic analysis on U87 cancer cells treated with cisplatin for 6 and 24 h [30]. Unsupervised bioinformatics pathway analyses showed that several genes involved in epigenetic regulations were deregulated after 24 h of treatment (Figure 1A). Amongst them, *HDAC4* was significantly repressed by cisplatin at 24 h compared to other HDACs or other epigenetic regulators. Based on this observation, we chose to investigate whether the expression of *HDAC4* was also deregulated in gastric cancer cells upon cisplatin treatment, since cisplatin-based therapy is a standard for the management of this type of cancer.
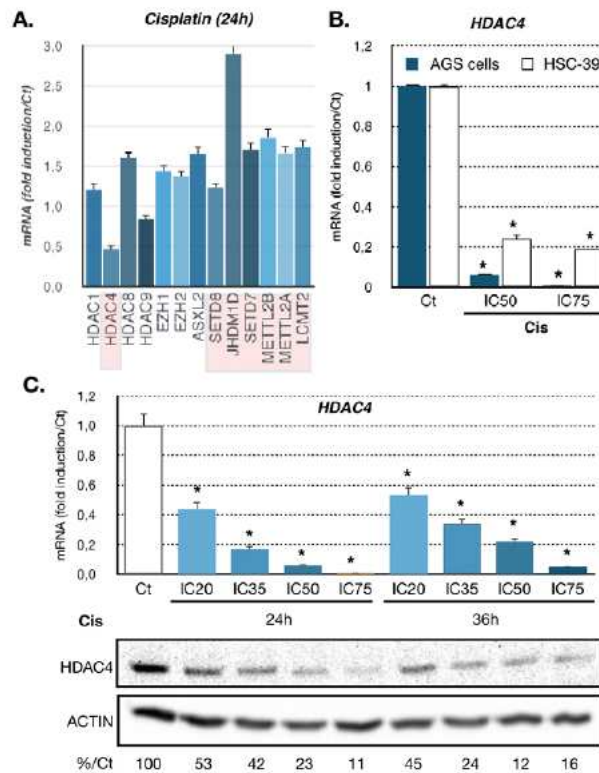
Figure 1. Regulation of *HDAC4* expression in gastric cancer in response to cisplatin. (**A**) Genes encoding epigenetic modulators deregulated in response to cisplatin treatment. The graph represents fold change (treated/not-treated) obtained after microarrays analysis of U87 cells treated for 24 h with cisplatin (IC_{50}) or not treated control ($p < 0.05$). Deregulated genes identified by statistical difference ($p < 0.05$) were analyzed by bioinformatics for unsupervised pathway and mechanism clustering. (**B**) Expression of HDAC4 in gastric cancer cell lines treated with cisplatin. HDAC4 mRNA level was assayed in AGS (Wt p53) and HSC39 (p53 G245S) cells by RT-qPCR. Cells were treated at the IC_{50} and IC_{75} of cisplatin (Cis) for 24 h. Bars are means of fold induction versus the control (Ct) and the indicated cisplatin concentration (μM). *, $p < 0.001$ ($n = 3$), compared with the control, as calculated by one-way ANOVA test followed by a Tukey post-test. (**C**) Expression of HDAC4 in AGS cell line treated with cisplatin

225

for 24 and 36 h. HDAC4 mRNA level was assayed in AGS cells by RT-qPCR. Bars are means of fold induction versus the control (Ct). *, $p < 0.001$ ($n = 3$), compared with the control, calculated by one-way ANOVA followed by a Tukey post-test. Proteins from AGS cells treated or not (Ct) for 24 and 36 h with the indicated concentrations of cisplatin (IC_{50}, IC_{75}) were separated on an SDS PAGE gel and propped with an HDAC4 specific antibody. Numbers at the bottom state in % the quantification of HDAC4 expression under cisplatin treatment (%Ct) compared to not treated AGS cells (Ct) and normalized to actin expression.

We used two different gastric cancer cell lines with different characteristics (AGS and HSC39 cells). AGS cells are of intestinal type (the major type of gastric cancer) and are wild-type p53. The HSC39 cells are of the diffuse type and present a p53 mutation (G245S). The response of these cells to cisplatin was first assessed by monitoring their survival using MTT assay after 48 h of treatment upon increasing concentrations of cisplatin (Supplementary Figure S1). From these curves, we extrapolated the IC_{20}, IC_{35}, IC_{50}, and IC_{75}, which are concentrations of cisplatin that induced 20%, 35%, 50%, and 75% of loss of cell viability, respectively. To validate the impact of cisplatin on HDAC4 expression in gastric cancer cells, we treated the cells with cisplatin at two doses (IC_{50} and IC_{75}) for 24 h. Cisplatin treatment drastically diminished *HDAC4* mRNA level in the two cell lines after 24 h of treatment (Figure 1B). The effect of cisplatin was dose-dependent. Then, we focused on AGS cells that represent the most frequent (>75%) histological type (intestinal) of gastric cancer [1]. We examined in more details the regulation of *HDAC4* expression in AGS cells. Dose-dependent and time-dependent analyses of *HDAC4* mRNA and protein levels were performed (Figure 1C). Cisplatin-dependent downregulation of *HDAC4* expression was detected already with low doses (IC_{20}, IC_{35}) of cisplatin and lasted up to 36 h after treatment. Similarly, immunofluorescence labeling of HDAC4 in AGS cells showed a decreased of HDAC4 expression in all cells following cisplatin treatment after 24 h (Supplementary Figure S3C).

As the transcriptomic analysis revealed deregulation of genes coding for DNA and histone methylation factors (Figure 1A), we tested the possibility that loss of HDAC4 expression was mediated by promoter methylation using decitabine, an inhibitor of DNA methylases. However, decitabine treatment did not abrogate the loss of HDAC4 expression—on the contrary, it rather reinforced it, while indeed increasing the expression of *SFLN11*, a gene known to be regulated by promoter methylation (Figure 2A and Supplementary Figure S1B) [31].
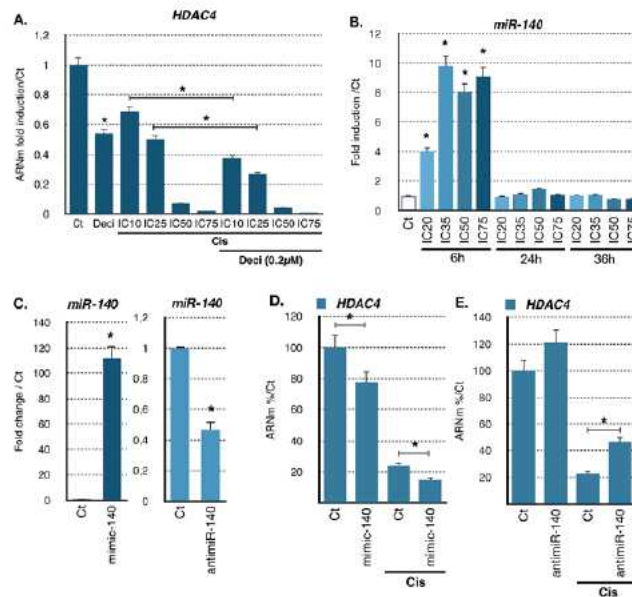
Figure 2. miR140-dependent regulation of HDAC4 expression in gastric cancer cells treated with cisplatin. (**A**) Expression of HDAC4 in the AGS cell line treated with cisplatin and decitabine. HDAC4 mRNA level in AGS cells treated for 24 h was assayed by RT-qPCR. Bars are means of fold induction versus the control (Ct). *, $p < 0.001$ ($n = 3$), compared with the control, calculated by one-way ANOVA followed by a Tukey post-test. (**B**) Expression of miR-140 in AGS cells treated with cisplatin over time at increasing concentrations. miRs levels were assayed by RT-qPCR. Bars are means of fold induction versus the control (Ct) and the indicated cisplatin concentrations. *, $p < 0.001$ ($n = 3$), compared with the control, as calculated by one-way ANOVA followed by a Tukey post-test. (**C**) Expression of *miR-140* in AGS cells transfected 48 h with a miR-140 specific mimic (mimic-140; 100 nM) or antimiR (antimiR-140; 30 nM) specific for miR-140 and treated or not with cisplatin (25 µM, 12 h). MiR-140 was assayed by RT-qPCR. Bars are means of fold induction versus the control (Ct). *, $p < 0.001$ ($n = 3$), compared with the control mimic, and the control antimiR, as calculated by one-way ANOVA followed by a Tukey post-test. (**D,E**) Expression of *HDAC4* in AGS cells transfected 48 h with a miR-140 specific mimic (D. mimic-140; 100 nM) or antimiR (E. antimiR-140; 30 nM) specific for miR-140 and treated or not with cisplatin (25 µM, 12 h). *HDAC4* RNA level was assayed by RT-qPCR. Bars are means of fold induction versus the control (Ct). *, $p < 0.001$ ($n = 3$), compared with the control mimic, and the control antimiR, as calculated by one-way ANOVA followed by a Tukey post-test.

2.2. miR-140 Partly Mediates Cisplatin-Induced HDAC4 Repression

We then hypothesized that cisplatin-induced repression of HDAC4 might be mediated partly by miRNAs. Since HDAC4 mRNA level have been shown to be regulated by multiple miRNAs [32], we assessed their contribution to the effect of cisplatin on HDAC4 mRNA. We analyzed upon cisplatin treatment the expression of previously reported miRNAs targeting HDAC4 and miRNAs found in public databases that might target HDAC4 (Supplementary Figure S2A). Cells were treated for 6, 24, and 36 h at different concentrations of cisplatin (IC_{10} to IC_{75}). Amongst the miRNA tested, we found miR-206, miR-29b, miR-299-5p, and miR-140 to be the most significantly induced by cisplatin in AGS cells (Figure 2B and Supplementary Figure S2B). In particular, cisplatin strongly stimulated (up to 10-fold) miR-140 expression level 6 h after treatment, which reverted to the basal levels after 24 h. Induction of miR-140 level was already occurring at low doses of cisplatin (IC_{20}, IC_{35}).

To further characterize the relationship between HDAC4 and those miRNAs induced by cisplatin, we used mimics and anti-miRNA oligonucleotides to overexpress or block miRNAs in order to assess their importance in *HDAC4* regulation. Amongst the miRNAs tested, only changes in miR-140 levels had a significant impact on HDAC4 mRNA levels. For instance, AGS cells were transfected for 48 h with miR-140 mimics or anti-miRNA and then treated with cisplatin (IC_{50}) for 24 h before *HDAC4* mRNA levels were measured by RT-qPCR. We first verified that the mimics and anti-miRNAs oligonucleotides had the expected effect on miR-140 expression (Figure 2C). Transfection of miR-140 mimics slightly reduced *HDAC4* mRNA level in control condition and more significantly (0.7-fold) in the presence of cisplatin (Figure 2D). Reciprocally, anti-miRNA oligonucleotides directed against miR-140 increased *HDAC4* mRNA level in control condition and even more significantly (1.9-fold) upon cisplatin treatment (Figure 2E). Interestingly, siRNA against DICER, the enzyme that produces miRNAs, did not restore additional HDAC4 mRNA levels upon cisplatin treatment (Figure S2C). We also observed that miR-140 level impact on HDAC4 protein level as shown on HDAC4 mRNA (Figure S3A). Altogether, these results indicated that miR-140 is at least partly involved in the regulation of *HDAC4* RNA level caused by cisplatin treatment.

2.3. Expression Level of HDAC4 Impacts on Cisplatin Cytotoxicity

Since it appeared that cisplatin reduces *HDAC4* expression, we set out to determine whether modulating *HDAC4* expression prior to treatment could impact on the response of gastric cancer cells to cisplatin. To this end, we used gain and loss of function experiments. AGS cells were transfected for 48 h with a plasmid expressing HDAC4, or with a *HDAC4* siRNA that silenced *HDAC4* expression. After 48 h of transfection, cells were then treated with different doses of cisplatin for 48 h, and cell survival was assessed using MTT assay. Overexpression of HDAC4 (Supplementary Figure S3B) resulted in partial protection of AGS cells from cisplatin toxicity (Figure 3A). Reciprocally, silencing of HDAC4 (Supplementary Figure S3C and Figure 5F) resulted in further decreased cell viability caused by cisplatin (Figure 3B). We then used the HDAC4 chemical inhibitor LMK235 [33] and investigated its possible synergy with cisplatin treatment. Combinatory experiments associating increasing doses of cisplatin with increasing doses of LMK235 were performed, and the survival of AGS gastric cancer cells was monitored. Results were analyzed to establish the combinatory indexes (Figure 3C, Supplementary Figure S3D and Supplementary Table S1) [34]. The analysis revealed that LMK235 and cisplatin were acting in synergy to induce cytotoxicity at a lower dose of both drugs (>IC_{50}), further supporting the pro-resistance role of HDAC4 in gastric cancer. In vitro experiments using MC1568, a controversial and poorly soluble inhibitor of HDAC4 [35], confirmed that a combinatory treatment of an HDAC4 inhibitor and cisplatin produces a synergistic response in gastric cancer cells (data not shown). Similar results were obtained on the diffuse type gastric cancer cell line HSC39. Cisplatin reduced HDAC4 protein levels and silencing of HDAC4 or inhibition using LMK235 favored cisplatin cytotoxicity in vitro (Figure 3D and Supplementary Figures S1C and S3C). Furthermore, LMK235 inhibited tubulin acetylation and improved the ability of cisplatin in reducing tumor growth in xenografts in nude mice (Figure 3E). In addition, to further evaluate the importance of miR-140 in cisplatin cytotoxicity and HDAC4 regulation, we transfected AGS cells with miR-140 mimic and measured cell survival after treatment with cisplatin. MiR-140 mimics significantly reduced cell survival in cells treated with increasing doses of cisplatin (Figure S2D), and this effect was additive when combined with HDAC4 siRNA (Figure S2E). These results further support the involvement of a miR-140-HDAC4 axis in the response of gastric cancer cells to cisplatin.

228
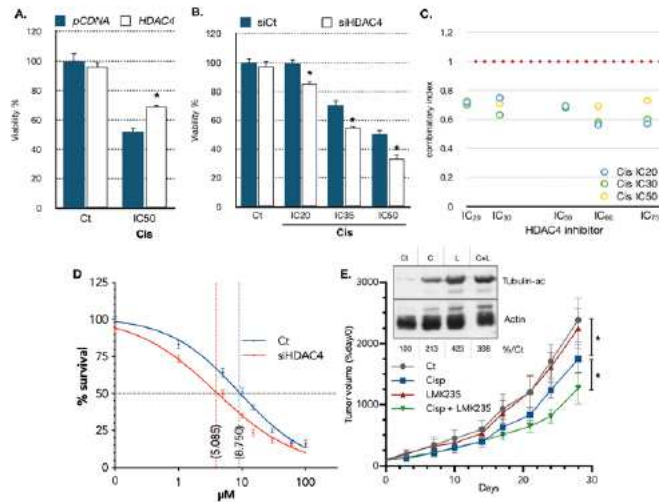
Figure 3. Function of *HDAC4* expression in gastric cancer in response to cisplatin. (**A**) AGS cells were plated in 96-wells plates, transfected with a plasmid (0.05 µg) encoding for HDAC4 (pHDAC4) or an empty vector (pcDNA3, Ct) for 24 h and treated for 48 h with the indicated concentration of cisplatin. The viability of the cells was evaluated using a MTT test. *, $p < 0.001$ ($n = 4$), compared with the control, as calculated by one-way ANOVA test followed by a Tukey post-test. (**B**) AGS cells were plated in 96-well plates and transfected with a siRNA (10 nM) against HDAC4 or luciferase (10 nM, siCt) for 48 h and treated for 48 h with the indicated concentrations of cisplatin. The viability of the cells was evaluated using a MTT test. *, $p < 0.001$ ($n = 4$), compared with the control, as calculated by one-way ANOVA test followed by a Tukey post-test. (**C**) Combinatory indexes of treatment with LMK-235 and cisplatin. AGS cells were treated with a combination of increasing concentration of LMK-235 and cisplatin and the cytotoxicity was evaluated by MTT after 48 h of treatment. The graph represents combination indexes for cisplatin concentration of IC_{20}, IC_{30}, and IC_{50} combined with IC_{20}, IC_{30}, IC_{50}, IC_{60}, and IC_{75} of LMK-235. Combination indexes are inferior to 0.80, indicating a synergistic effect between LMK-235 and cisplatin on AGS cell survival. (**D**) HSC39 cells were plated in 96-well plates and transfected with a siRNA (10 nM) against HDAC4 or luciferase (10 nM, siCt) for 48 h and treated for 48 h with the indicated concentrations of cisplatin. The viability of the cells was evaluated using an MTT test. IC_{50} were statistically different, $p = 0.016$ ($n = 5$), compared with the control, as calculated by the *t*-test. (**E**) HSC39 cells were implanted intradermal in nude mice. Mice were treated when tumor reached 150 mm³ with cisplatin (10 mg/Kg) or LMK235 (5 mg/Kg) or a combination of both once a week. Tumor size was monitored twice a week using a caliper. * indicate $p < 0.05$ as calculated by *t*-test. Inset: Western blot of acetylated tubulin (K40) and actin performed on tumor extracts at 28 days. Ct: Control; C: Cisplatin; L: LMK235.

2.4. Gastric Cancers Harbor HDAC4 Alterations that Impact on Patient Survival

To further characterize the role of HDAC4 in gastric cancer, we analyzed *HDAC4* mRNA levels by RT-qPCR in both tumor and adjacent healthy tissue biopsies from a cohort of 31 gastric cancer patients. Although the *HDAC4* expression pattern showed a strong variation in healthy and tumor tissues, the *HDAC4* mRNA level was significantly higher in gastric cancer biopsies (GC tumors) compared to the adjacent healthy tissues (HT) (Figure 4A). We then analyzed *HDAC4* expression data of the TCGA (The Cancer Genome Atlas) database for gastric cancers and found that HDAC4 expression varied depending on the molecular subgroup of gastric cancer (Figure 4B) [36]. For instance, the genetic stable (GS) subgroup showed the highest level of HDAC4 expression, while the microsatellite instable (MSI) showed the lowest expression. For instance, a two-fold difference (2.4 vs. 5.2) in expression of

HDAC4 exists between the MSI tumors and the GS tumors. This difference is slightly higher to the one observed for the expression of E-cadherin (CDH1) between the GS and MSI subgroups (66 vs. 111), a gene whose expression loss is characteristic of the GS subgroup (Supplementary Figure S4A) [1]. In addition, HDAC4 level are in average lower in the intestinal histological subtype compared to the diffuse subtype (Supplementary Figure S4B). Interestingly, expression of HDAC4 is also reduced in tumors of patients that have been treated with chemotherapies (Supplementary Figure S4C).
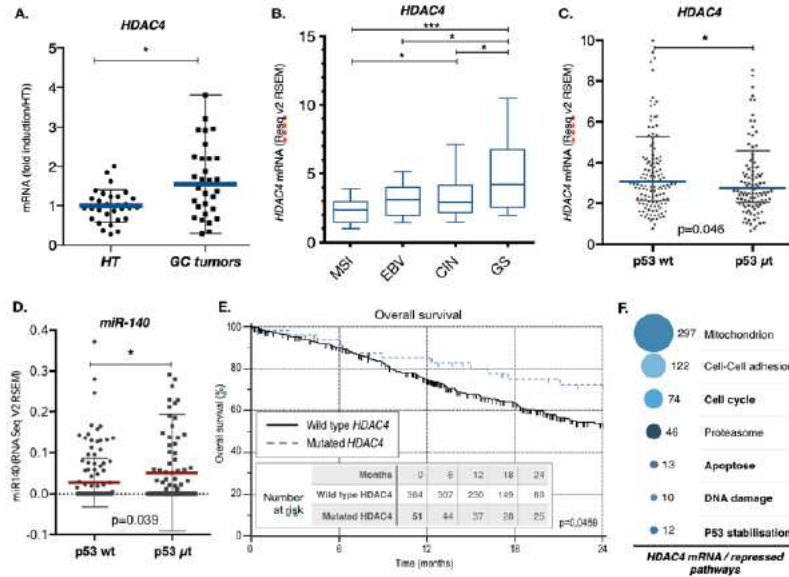
Figure 4. HDAC4 expression and role in gastric cancer patient survival. (**A**) Expression level of HDAC4 in gastric cancers. RNA was extracted from gastric cancer biopsies and adjacent healthy tissue samples obtained from the CARDIA collection of the HUS, Strasbourg. RT-qPCR for HDAC4 was performed and the results were normalized against TBP and G3PDH. The graph represents medians with ranges (*n* = 26). *p* < 0.0069, paired *t*-test. (**B**) *HDAC4* expression level in the gastric tumors of the TCGA based on the molecular subgroups. Expression data for *HDAC4* in gastric tumor were extracted from the TCGA data library and analyzed based on the molecular subgroups (MSI *n* = 58; EBV *n* = 24, CIN *n* = 126, GS *n* = 50). The graph represents mean with 5–95 percentile. *** when *p* < 0.001, * when *p* < 0.05 as determined by ANOVA followed by a Tukey post-test. MSI = microsatellite instable; EBV = Epstein Barr virus; CI*n* = Chromosome Instable; GS = Genetic stable. (**C**,**D**) miR-140 and *HDAC4* expression level in the gastric tumors of the TCGA based on the p53 mutational status. Expression data for miR-140 and *HDAC4* in gastric tumor were extracted from the TCGA data library and analyzed based on the mutational status of p53, either wild type (p53 wt *n* = 141) or mutated (p53 µt *n* = 117). The graph represents mean with standard deviation and analyzed by ANOVA followed by an unpaired *t*-test. (**E**) Kaplan–Meier analysis of patients' overall survival of the 379 patients with wildtype *HDAC4* and 36 patients with either mutated or deleted *HDAC4* and stratified according to HDAC4 mutational status: 0 = no mutation, 1 = mutation or deletion. Mutation or deletion of HDAC4 was a predictor of tumor recurrence (*p* = 0.0383). (**F**) Deregulated signaling pathways and cellular processes that correlated negatively with HDAC4 expression in gastric cancer data of the TCGA. Gene expression data of gastric cancer tumors from the TCGA were analyzed to identify genes with an expression that correlates negatively (Pearson correlation coefficient <−0.3) with the expression of HDAC4 (cBioportal.com). Then, the list of genes was subjected to unsupervised pathways analyses (DAVID: https://david.ncifcrf.gov; https://reactome.org). The graph represents the most relevant deregulated pathways.

As over 50% of GC show p53 mutations, we then assessed the influence of the p53 status on the expression of miR-140 and *HDAC4* in gastric tumors. The HDAC4 mRNA level is lower in tumors with mutated p53 proteins (Figure 4C). Conversely, we found that the expression level of miR-140 is higher in tumors with mutated p53 proteins, which suggested that p53 might directly or indirectly repress miR-140 expression (Figure 4D). This was confirmed by showing that silencing of p53 in AGS cells increases miR-140 level, and, inversely, overexpression of p53 decreases miR-140 levels (Supplementary Figure S7A).

Interestingly, in addition to the elevated expression of *HDAC4*, we observed that 7.7% of gastric cancers available in the TCGA data were shown to have point mutations, frame shift deletion or deep deletion in the *HDAC4* gene that might affect its function (Supplementary Figure S4C). The exact impact of these alterations on HDAC4 properties remains to be established. However, a Kaplan–Meyer analysis showed that the presence of these alterations was associated with a better patients' overall survival (Figure 4E). Importantly, the cancer molecular subtype MSI does not favor patient survival in the same cohort (Supplementary Figure S4D).

Altogether, these results indicate that molecular subgroups of gastric tumors harbor an elevated level of HDAC4 expression based on the p53 status. It also shows that deregulation of HDAC4 impacts on patients' overall survival.

2.5. HDAC4 Regulates Proapoptotic Pathway, Including p53 and TAp73 Expression in Gastric Cancer Cells

We examined the potential molecular mechanisms that might account for the impact of HDAC4 expression on the response of gastric cancer cells to cisplatin. First, we analyzed the TCGA data for gastric cancers by sorting for genes whose expressions are correlated positively or negatively with *HDAC4* expression. An unsupervised bioinformatics pathway analysis of those genes (DAVID: https://david.ncifcrf.gov; https://reactome.org) revealed that several cellular mechanisms are altered Figure 4F and Supplementary Figure S5A,B). This approach gave us an overview on the top ranked pathways potentially affected by the expression level of *HDAC4* in patients with gastric cancer. For instance, the genes whose expression is negatively correlated with *HDAC4* expression are related to a relatively large variety of pathways/mechanisms (Supplementary Figure S5B). Amongst the top 7 ranked pathways/mechanisms anti-correlating with a high expression of *HDAC4* are the cell cycle, apoptosis, DNA damage, and stabilization of p53 (Figure 4F).

These pathways are known to be some of the main targets of the p53 and TAp73 transcription factors, which themselves are key factors in cancer cells' cisplatin response [13–15]. Therefore, we analyzed their expression levels and the induction of apoptosis in AGS cells upon cisplatin treatment. Treatment of AGS cells with cisplatin for 24 h did not induce cleavage of caspase 3, a marker of apoptosis (Figure 5A). Cleavage of caspase 3 after cisplatin treatment occurred after 48 h of treatment (data not shown). However, silencing of HDAC4 by a siRNA accelerated the ability of cisplatin to induce cleavage of caspase 3 after 24 h of treatment. Similar results were obtained using the HDAC4 chemical inhibitor LMK235 (Figure 5B). p53 mRNA was only modestly induced by cisplatin (Supplementary Figure S6A) but p53 protein levels were increased in a dose- and time-dependent manner upon cisplatin treatment (Supplementary Figure S6B). By contrast, both TAp73 mRNA levels and proteins were increased by cisplatin (Supplementary Figure S6A,B). The expression of known p53 and TAp73 target genes that regulate cell survival, such as the proapoptotic gene *PMAIP1* (Noxa) and the cell cycle regulator genes *CDKN1* (p21), *P57* and *AQP3*, were induced by cisplatin (Supplementary Figure S8A–D). Altogether, these results indicated that both p53 and TAp73 are induced by cisplatin in AGS cells, which could lead to the activation of proapoptotic genes such as *PMAIP1*.

231
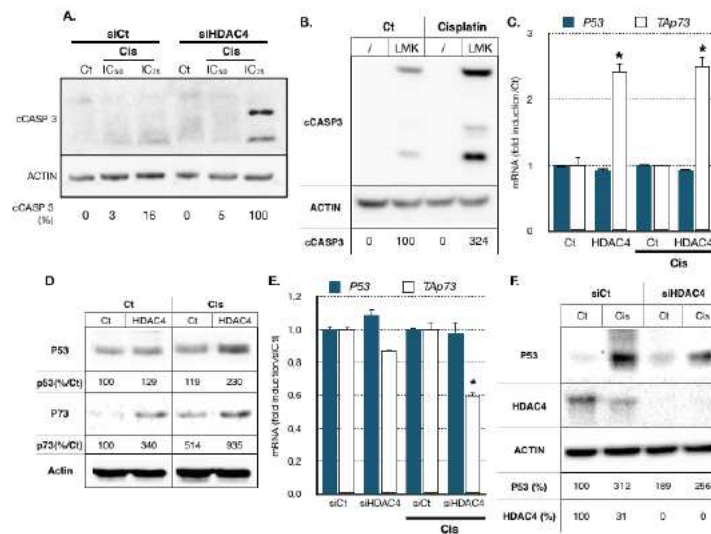
Figure 5. HDAC4 expression correlates with deregulation of cell cycle and proapoptotic pathways regulated by protein of the p53 family. (**A**). Proteins from AGS cells transfected with a siRNA (10 nM) against HDAC4 or luciferase (10 nM, siCtl) for 48 h and treated for 24 h with the indicated concentrations of cisplatin treated or not (Ct) with the indicated concentrations (IC_{50}, IC_{75}) of cisplatin were separated on an SDS PAGE gel. A Western blot experiment was performed using an antibody against cleaved caspase 3 (cCASP3), and actin was using as loading control. Percentage of cleaved Caspase 3 is indicated relative to siHDAC4/Cis(IC_{75}) and corrected with actin level. (**B**). Proteins from AGS cells treated with cisplatin (IC_{50}) and LMK235 (IC_{25}) for 24 h were separated on an SDS PAGE gel. A Western blot experiment was performed using an antibody against cleaved caspase 3, and actin was using as loading control. (**C,D**). AGS cells were transfected with a plasmid encoding for HDAC4 (1μg) or an empty vector (pcDNA3, Ct) for 24 h and then treated for 12 h with cisplatin. Expression of p53 and TAp73 was assayed by RT-qPCR (**A**) and Western blot (**B**). *, $p < 0.001$ ($n = 3$), compared with the control as calculated by one-way ANOVA followed by a Tukey post-test. Percentage of protein is indicated relative to the condition Ct/Ct and corrected with actin level. (**E,F**). AGS cells were transfected with a siRNA (10 nM) against HDAC4 or luciferase (10 nM, siCt) for 48 h and treated with cisplatin for 12 h. Expression of p53 and TAp73 was assayed by RT-qPCR (E). Protein level for p53 and HDAC4 were assayed by Western blot (**F**). *, $p < 0.001$ ($n = 3$), compared with the si control as calculated by one-way ANOVA followed by a Tukey post-test. Percentage of protein is indicated relative to the condition siCt/Ct and corrected with actin level.

We then assessed whether HDAC4 impacts on *P53* and *P73* expression. AGS cells were transfected for 24 h with an expression vector encoding HDAC4. Cells were then treated with cisplatin (IC_{50}) for another 24 h before *P53* and TAp73 isoform RNA and protein levels were measured by RT-qPCR and Western blot, respectively. Overexpression of HDAC4 in AGS cells had no effect on p53 mRNA level (Figure 5C) but induced p53 protein level by two-fold after cisplatin treatment (Figure 5D). Interestingly, HDAC4 induced TAp73 expression both at mRNA and protein levels and in both control and in cisplatin-treated conditions (Figure 5C,D). Reciprocally, HDAC4 siRNA reduced TAp73 mRNA level without significantly affecting p53 mRNA levels (Figure 5E). The effect at the protein level also confirmed the previous experiment in that HDAC4 siRNA reduced p53 protein levels after cisplatin treatment (Figure 5F).

232

2.6. HDAC4 Inhibits BIK and Other Proapoptotic Genes' Expressions in Gastric Cancer Cells: Role of p53

We then investigated the expression levels of proapoptotic genes identified as co-deregulated with HDAC4 in gastric cancer patients (Figure 4F and Supplementary Figure S5A,B). For instance, cisplatin stimulated the expression of several proapoptotic genes *PMAIP1* and *BIK* (Figure 6A) [37,38]. Moreover, the expression of those genes was further elevated when HDAC4 was silenced using siRNA. In addition, the expression of two other proapoptotic genes *CASP8* and *BID* was also slightly elevated upon silencing of HDAC4, although no induction was seen upon cisplatin treatment. Similarly, inhibition of HDAC4 with LMK235 led to increased *BIK* expression in the absence or presence of cisplatin (Figure 6B). In addition, *BIK* expression was significantly reduced upon silencing of p53 using siRNA, suggesting that p53 plays a role in *BIK* expression.
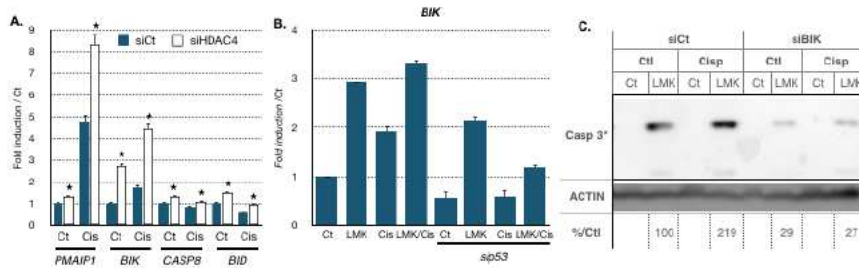
Figure 6. *BIK* expression is involved in caspase 3 cleavage induced by cisplatin and HDAC4 silencing. (**A**). AGS cells were transfected with a siRNA (10 nM) against HDAC4 or luciferase (10 nM, siCt) for 48 h and treated with cisplatin for 12 h. Expression of proapoptotic genes (*PMAIP1, BIK, CASP8, BID*) was assayed by RT-qPCR. *, $p < 0.001$ ($n = 3$), compared with the si control as calculated by one-way ANOVA followed by a Tukey post-test. (**B**). AGS cells were transfected with a siRNA against p53 (30 nM) or luciferase (30 nM, siCt) for 72 h and treated with cisplatin (IC50) of LMK235 (IC25) alone or combined (12 h). Expression of *BIK* was assayed by RT-qPCR. *, $p < 0.001$ ($n = 3$), compared with the si control (siCtl) as calculated by one-way ANOVA followed by a Tukey post-test. (**C**). Proteins from AGS cells transfected with a siRNA (10 nM) against *BIK* or luciferase (10 nM, siCt) for 48 h and treated for 24 h with cisplatin (IC50) of LMK235 (IC25) alone or combined or not (Ct) were separated on an SDS PAGE gel. A Western blot experiment was performed using an antibody against cleaved caspase 3 (cCASP3), and actin was using as loading control.

Then, we assessed if these genes were necessary for the apoptosis induced by inhibition of HDAC4 activity. AGS cells were treated with LMK235 and cisplatin alone or in combination, and in the presence of absence of siRNA directed against BIK. Inhibition of HDAC4 by LMK235 induced cleavage of caspase 3, which was further induced by cisplatin treatment (Figure 6C). Cisplatin further induced caspase cleavage induced by LMK235. By contrast, silencing of BIK significantly reduced the cleavage of caspase 3.

These results indicated that part of HDAC4 function in gastric cancer involves the regulation of apoptosis, in part via BIK and caspase 3, and in part via the activity of proteins of the p53 family.

3. Discussion

Gastric cancer remains a worldwide important health issue, including in western countries, due to a low 5-year survival rate (below 30%). Part of this unfavorable prognosis is due to the poor and variable sensitivity of advanced gastric tumors to perioperative chemotherapy protocols, especially platinum-based therapies. We gathered molecular and clinical evidence indicating that histone deacetylase 4 (*HDAC4*) is a good candidate to explain some of the features leading to a differential sensibility of gastric cancers towards cisplatin. In addition, we identified a regulatory loop in which

HDAC4 functionally interacts with a post-transcriptional regulator, miR-140, and tumor suppressor genes p53 and TAp73 to control proapoptotic gene expression such as BIK.

The role of HDAC4 in the resistance of gastric cancer cells to cisplatin-based chemotherapy is suggested by several observations. Firstly, *HDAC4* expression is elevated in gastric cancer biopsies compared to normal tissues, showing differences between molecular subgroups. In particular, *HDAC4* expression is elevated in the genetic stable (GS) and chromosome instable (CIN) subgroup, as well as in the diffuse versus the intestinal histological subgroup (Figure 4B and Supplementary Figure S4B). Although these differences are not always very strong, they are similar to the ones obtained with genes that are well known to be differently expressed between gastric cancer subgroups, such as E-cadherin (*CDH1*) (Supplementary Figure S4A) [36]. Importantly, mutations or deletions of *HDAC4* in gastric cancers correlate with a better patient survival, and that is even more discriminant than any particular molecular subgroup (e.g., MSI). Secondly, the silencing of *HDAC4* or inhibition of HDAC4 by pharmacological means favor cisplatin cytotoxicity in vitro and cisplatin anticancer activity in vivo. Reciprocally, *HDAC4* overexpression counteracts the activity of cisplatin. Thirdly, in gastric cancer cells treated with cisplatin at a toxic dose, *HDAC4* expression drops dramatically, which is supported by clinical data of the TCGA showing that HDAC4 expression is lower in tumors that have been treated with chemotherapy (Supplementary Figure S4B). Altogether, these data support each other and suggest that HDAC4, according to its expression level and/or mutational status, high vs. low or mutated, dictates in part the sensitivity of cancer cells towards chemotherapy and overall survival. The role of *HDAC4* in chemotherapy resistance is further supported by additional studies showing that high expression of *HDAC4* reduces docetaxel activity [39] and favors the growth of these cells in the absence of treatment [21]. Furthermore, *HDAC4* is overexpressed in esophageal carcinomas and breast cancers and is associated with a poor prognosis [40,41]. Similarly, high expression of HDAC4 is a bad prognosis factor in selected glioblastoma subtypes (proneuronal, mesenchymal) [41]. In epithelial ovarian, colon, and myeloid cancer cells, HDAC4 increases proliferation and migration [42–45]. Although these data suggest that in general, increased HDAC4 expression could be a resistance mechanism in different types of cancers and to several sorts of chemotherapeutic drugs, it is clearly not always the case. Indeed, in the colon cancer cell line HCT116, HDAC4 participates in the resistance to 5-FU (5-fluorouracil) but not to methotrexate [46]. Therefore, the role of HDAC4 in cancer progression and sensitivity to chemotherapy seems complex, and additional information on HDAC4 partners or targets is required to explain how HDAC4 expression can differently impact cancer cells behavior.

The results we obtained established that cisplatin treatment has a significant effect on *HDAC4* expression in gastric cancer cells. Cisplatin-mediated repression of HDAC4 expression occurs at the RNA level and can reach up to a 90% reduction at the protein level upon treatment with high doses of cisplatin (IC_{75}). This reduction of HDAC4 level is functionally relevant as an artificial overexpression of HDAC4 counteracts cisplatin activity. Reciprocally, an amplified inhibition of *HDAC4* expression using siRNA accentuates cisplatin cytotoxicity.

The cisplatin-induced regulation of HDAC4 expression in gastric cancer cells involves complex and balanced mechanisms. One of them involves miR-140. Indeed, miR-140 is rapidly induced by cisplatin (within 6 h) before returning back to basal levels after 24 h of treatment. Artificial overexpression of miR-140 inhibits HDAC4 expression, whereas anti-miRNAs against miR-140 counteract the negative effect of cisplatin on HDAC4 level by even doubling it. In addition, miR-140 expression significantly impacts on gastric cancer cell behavior, as miR-140 mimics favor cisplatin cytotoxicity. However, the role of miR-140 seems to be limited to an early event and cannot explain the long-term downregulation of HDAC4 observed after cisplatin treatment. It seems that miR-140 participates in the initiation of the HDAC4 mRNA downregulation but that other mechanisms ensure that HDAC4 repression is maintained. These mechanisms remain to be identified.

Although the mechanisms leading to miR-140 induction are not known yet, the downregulation of miR-140, including the one occurring after its initial induction at later time points of cisplatin treatment, is partially mediated by p53 and TAp73. Indeed, silencing of p53 using siRNA increased

miR-140 level in control condition and partially restored its level during cisplatin treatment. By doing so, p53 and TAp73 help to maintain *HDAC4* expression to a minimal level, even under cisplatin condition. These in vitro data are confirmed by analyses of the clinical data of the TCGA showing that the expression level of HDAC4 and miR-140 are different depending on the p53 mutational status in gastric tumors. Altogether, this suggests that HDAC4 expression might be necessary to ensure some of p53 functions upon cisplatin treatment. For instance, previous works have suggested that HDAC4 was involved in the p53-dependent repression of G2/M regulators upon DNA damage, such as Cdc2 and Cyclin B2 [47,48]. In addition, HDAC4 has been shown to play a critical role in cell survival by interacting with p53BP1 during the G2/M cell cycle check point [49]. Hence, p53 and TAp73 might contribute to maintaining a minimal HDAC4 protein level to ensure in some cells a functional G2/M cell cycle check point via the repression of miR-140. We were not able to confirm that HDAC4 regulates *CDC2* or *CYCLIN B2* in gastric cancer cells. However, we showed that HDAC4 modulates the expression of two other target genes of the p53 and TAp73 proteins.

Moreover, several genes inhibited by HDAC4, such as *PMAIP1* and *BIK,* are proapoptotic, which could contribute to the resistance mechanism initiated by high HDAC4 expression. This negative effect of HDAC4 on proapoptotic genes also provides mechanistic bases for our observation that silencing or inhibition of HDAC4 favors cisplatin-induced apoptosis. In particular, the expression of BIK appeared to be inhibited in part by HDAC4 and induced by p53 upon cisplatin treatment. This regulation impacts on cisplatin cytotoxicity by favoring caspase 3 cleavage and apoptosis.

4. Materials and Methods

4.1. Biological Materials

AGS and KATOIII cells were obtained from ATCC (ATCC®: LGC Standards S.a.r.l. 6, rue Alfred Kastler BP 83076 F-67123 Molsheim Cedex France: CRL-1739™, HTB-103™). The HSC39 were a gift from Dr. Yanagihira (National Cancer Research Center, 104_0045 Tokyo, Japan). Cells were grown in RPMI (Roswell Park Memorial Institute medium, Dominique DUTSCHER SAS-Head Office: 30, rue de l'Industrie- BP62-67172 BRUMATH cedex, France) with 10% fetal bovine serum (Frankfurter Straye 129 B, Postfach 200152, 64293 Darmstadt, Germany) and 1% penicillin/streptomycin (PAN-Biotech, Am Gewerbepark 13, 94501 Aidenbach, Germany) at 37 °C in a humidified atmosphere and 5% CO_2. Mycoplasma contamination was tested negative using PlasmoTest (Invivogen, 5 Rue Jean Rodier, 31400 Toulouse, France).

Healthy tissue samples, gastric tumor biopsies, and distant normal gastric tissues ($n = 26$) were obtained from the Digestive Surgery department of Hautepierre Hospital (CHU Hautepierre, Strasbourg 67200, France, authorization number: NCT02491840) or the National Cancer Research Center (National Cancer Research Center, 104_0045 Tokyo, Japan). All samples were obtained with patients' informed consent according to the Declaration of Helsinki and approved (EST4: IDRCB2015-A00198-41/PRI2014-HUSn°6042) by the Human Ethics Committee of the Strasbourg University Hospital (CHU Hautepierre, Strasbourg 67200), France.

4.2. Cell survival Assay

A total of 10,000 cells were seeded per well in 96–well microplates (Falcon Multiwell, Dutscher: 30, rue de l'Industrie- BP62, 67170 Brumath, France), 24 h prior to any treatment. Cisplatin was applied for 48 h in fresh medium. MTT assay was performed as previously described by replacing the medium with fresh medium supplemented with 5 mg/L MTT (Sigma, Lyon-Saint Exupéry BP 113, 69125 Lyon, France) for 1 h [50]. Cells were lysed in in DMSO 100% (100 µL/wells). Measurements were performed at 550 nm with the *Tristar*^{2} *Multimode Reader* (Berthold Technologies, Calmbacher Str. 22, 75323 Bad Wildbad, Germany).

235

4.3. Isobologram Assay

A total of 10,000 AGS cells were seeded per well in 96-well microplates (Falcon Mutliwell), 24 h prior to any treatment. A combination of cisplatin and LMK-235 or different concentrations of each drug alone were applied for 48 h in fresh medium. MTT assay was performed as described above. Treatment efficiencies were compared to individual treatment control efficiencies with the Compusyn program (ComboSyn, Inc., Paramus, NJ 07652, USA) which determined the combination indexes. In the present study, when the combination index is superior or equal to 1.20, it indicates an antagonist effect, between 0.80 to 1.20 an additive effect, and when the index is inferior to 0.80, it suggests synergic effects between LMK-235 and cisplatin on cell survival.

4.4. Quantitative RT-PCR

A total of 500,000 cells were seeded per well in 6–well microplates (Falcon Mutliwell), 24 h prior to any treatment. Cells were then treated with indicated drug and time. TRIzol (Invitrogen) was used to extract RNA. One microgram of RNA was used for reverse transcription (High Capacity cDNA Reverse Transcription Kit, Applied Biosystems). cDNAs were diluted five times before being used as described by the provider (4 µL/reaction) with *FastStart Universal SYBR Green PCR Master Mix* or *FastStart Universal Probe Master Mix TaqMan* (Roche, 30, cours de l'Ile Seguin 92650 Boulogne-Billancourt Cedex, France) for qPCR with 20 µL as the total volume for each reaction. For miRNA analysis, we used RT miScript mix, Hi Spec reagent, (Qiagen, 3 avenue du Canada LP 809 91974 Courtaboeuf Cedex; France) and *miScript SYBR Green PCR Kit* (Qiagen) as described by the provider. qPCRs were performed with *7500 Real Time PCR System* (Applied Biosystems, Boulevard Sébastien Brant - F67403 Illkirch Cedex, France). Relative expression levels were normalized to TBP, G3PDH or RNU6 using the $2^{(-\Delta\Delta Ct)}$ method [51]. Primers used are provided in Supplementary Figure S9.

4.5. Western Blot Analyses

Cells or tissues were lysed with LB (125 mM Tris-HCl pH 6.7, NaCl 150 mM, NP40 0.5%, SDS 0.1%, 10% Glycerol). Proteins were denatured and deposited directly (40 µg of proteins) onto SDS PAGE gels. Western blotting was performed using antibodies raised against p53 (rabbit anti-p53, FL-393, Santa Cruz, 10410 Finnell Street, Dallas, TX 75220, USA), p73 (rabbit anti-p73, Ab40658, Abcam, 24 rue Louis Blanc, 75010 Paris, France), HDAC4 (rabbit anti-HDAC4, 607702, Biolegend, France 38 Rue de Berri, 75008 Paris 8, France), acetylated Tubulin K40 (Merck, 201, Rue Carnot Fontenay sous BoisÎle-de-France 94126, France), and cleaved caspase 3 (cCASP3, #9661 Cell Signaling, Cell Signaling Technology Dellaertweg 9b 2316 WZ Leiden, Netherlands). Secondary antibodies (antirabbit NA934V and antimouse NXA931V Horseradish linked) were incubated at 1:10,000. Loading was controlled by analyzing actin protein expression (mouse anti-actin Clone C4, Chemicon, 1:10.000) [52]. Western blot quantifications were performed using the Pxi imager and Genetools (Syngene™, Beacon House Nuffield Road Cambridge CB4 1TF, United Kingdom). The intensity of the bands is indicated as a percentage (%) relative to control when a band is present in the control condition. If not, intensity is indicated as relative to a selected condition as indicated in the figure legends.

4.6. Transfection

Expression vectors for p53, TAp73, and HDAC4 were transfected by polyethylenimmine (PEI) or JetPrim (Polyplus, Strasbourg, France) as previously described [53]. SiRNA transfection was performed using the RNAiMAX protocol as described by the provider (Life Technology, Saint Aubin, France). Sequences of siRNA, miRNA mimic, and anti-miRNA oligonucleotide are provided in Supplementary Figure S9.

4.7. Microarrays Analysis and TCGA Analyses

Files from microarray experiments (GEO accession number: GSE66493) were analyzed individually using AltAnalysis software [54]. Deregulated genes were identified based on 2-fold change expression and *t*-test *p*-value < 0.05. Deregulated genes were then analyzed by GO-Elite with Prune Ontology term using Z score (cutoff 1.96, *p*-value 0.05) and Fisher's exact test for ORA (2000 permutation) for over-representation in selected biological processes in several resources: Gene Ontology, MPhenoOntology, Disease Ontology, GOSlim, PathwayCommons, KEGG, Transcription Factor Targets, miRNA Targets, Domains, BioMarkers, RVista Transcription Sites, DrugBank, BioGrid.

For TCGA analyses, data were downloaded from the cbioportal.org web site and analyzed using the statistical program GraphPad PRISM™. Statistical analyses were performed as indicated in the figures based on distribution of the data toward the Normal (Gaussian) rule.

4.8. Xenografts

Tumors were implanted into BALB/c male nude mice (aged 6–8 weeks; Charles River) by intradermal subcutaneous injection in the lower flank using 5×10^6 cells. Tumors were allowed to grow up to 150 mm^3 before starting the treatment. Two hundred microliters of vehicle or cisplatin (10 mg/Kg) or LMK235 (5 mg/Kg) or a combination of both was administrated intraperitoneally. Tumor volume was measured with calipers until day 28. All experiments were conducted in compliance with project and personal licenses issued under the French and Japanese Animals Committee guidelines for the welfare of animals in experimental procedures. The work was approved by a local ethical review committee (APAFIS #8320).

5. Conclusions

Altogether, this study highlights a complex regulatory loop linking the epigenetic regulators HDAC4 and miR-140 that control in part the response to cisplatin-induced apoptosis via p53 and proapoptotic genes, such as BIK, which might impact on patient survival. This p53/TAp73-miR140-HDAC4-BIK regulatory loop may play a critical role in gastric cancer response to therapy, as both HDAC4 and P73 are expressed at an elevated level in this type of cancer. In addition, p53 is mutated in more than 70% of metastatic gastric cancers. The clinical relevance of this regulatory loop is highlighted by the fact that mutation or deletion of HDAC4 favors the survival of patients with gastric cancer. Hence, the use of selective inhibitor of HDAC4, such as LMK235, in combination with cisplatin may represent a promising therapeutic alternative.

References

1. Mihmanli, M.; Ilhan, E.; Idiz, U.O.; Alemdar, A.; Demir, U. Recent developments and innovations in gastric cancer. *World J. Gastroenterol.* **2016**, *22*, 4307–4320. [CrossRef]

2. Florea, A.M.; Busselberg, D. Cisplatin as an anti-tumor drug: Cellular mechanisms of activity, drug resistance and induced side effects. *Cancers* **2011**, *3*, 1351–1371. [CrossRef]

3. Huang, D.; Duan, H.; Huang, H.; Tong, X.; Han, Y.; Ru, G.; Qu, L.; Shou, C.; Zhao, Z. Cisplatin resistance in gastric cancer cells is associated with HER2 upregulation-induced epithelial-mesenchymal transition. *Sci. Rep.* **2016**, *6*, 20502.

4. Pietrantonio, F.; de Braud, F.; da Prat, V.; Perrone, F.; Pierotti, M.A.; Gariboldi, M.; Fanetti, G.; Biondani, P.; Pellegrinelli, A.; Bossi, I.; et al. A review on biomarkers for prediction of treatment outcome in gastric cancer. *Anticancer Res.* **2013**, *33*, 1257–1266.

5. Grabsch, H.I.; Tan, P. Gastric cancer pathology and underlying molecular mechanisms. *Dig. Surg.* **2013**, *30*, 150–158. [CrossRef]

6. Mahu, C.; Purcarea, A.P.; Gheorghe, C.M.; Purcarea, M.R. Molecular events in gastric carcinogenesis. *J. Med. Life* **2014**, *7*, 375–378.

7. Rivlin, N.; Brosh, R.; Oren, M.; Rotter, V. Mutations in the p53 tumor suppressor gene: Important milestones at the various steps of tumorigenesis. *Genes Cancer* **2011**, *2*, 466–474. [CrossRef]

8. Osman, A.A.; Neskey, D.M.; Katsonis, P.; Patel, A.A.; Ward, A.M.; Hsu, T.K.; Hicks, S.C.; McDonald, T.O.; Ow, T.J.; Alves, M.O.; et al. Evolutionary action score of TP53 coding variants is predictive of platinum response in head and neck cancer patients. *Cancer Res.* **2015**, *75*, 1205–1215. [CrossRef]

9. Oren, M.; Rotter, V. Mutant p53 gain-of-function in cancer. *Cold Spring Harb. Perspect. Biol.* **2010**, *2*, a001107. [CrossRef]

10. Gaiddon, C.; Lokshin, M.; Ahn, J.; Zhang, T.; Prives, C. A subset of tumor-derived mutant forms of p53 down-regulate p63 and p73 through a direct interaction with the p53 core domain. *Mol. Cell Biol.* **2001**, *21*, 1874–1887. [CrossRef]

11. Arrowsmith, C.H. Structure and function in the p53 family. *Cell Death Differ.* **1999**, *6*, 1169–1173. [CrossRef] [PubMed]

12. Zaika, A.I.; El-Rifai, W. The role of p53 protein family in gastrointestinal malignancies. *Cell Death Differ.* **2006**, *13*, 935–940. [CrossRef] [PubMed]

13. Tomkova, K.; Belkhiri, A.; El-Rifai, W.; Zaika, A.I. p73 isoforms can induce T-cell factor-dependent transcription in gastrointestinal cells. *Cancer Res.* **2004**, *64*, 6390–6393. [CrossRef] [PubMed]

14. Tomkova, K.; El-Rifai, W.; Vilgelm, A.; Kelly, M.C.; Wang, T.C.; Zaika, A.I. The gastrin gene promoter is regulated by p73 isoforms in tumor cells. *Oncogene* **2006**, *25*, 6032–6036. [CrossRef] [PubMed]

15. Vilgelm, A.E.; Hong, S.M.; Washington, M.K.; Wei, J.; Chen, H.; El-Rifai, W.; Zaika, A. Characterization of DeltaNp73 expression and regulation in gastric and esophageal tumors. *Oncogene* **2010**, *29*, 5861–5868. [CrossRef]

16. Ellis, L.; Atadja, P.W.; Johnstone, R.W. Epigenetics in cancer: Targeting chromatin modifications. *Mol. Cancer Ther.* **2009**, *8*, 1409–1420. [CrossRef]

17. Hong, L.; Yang, Z.; Ma, J.; Fan, D. Function of miRNA in controlling drug resistance of human cancers. *Curr. Drug Targets* **2013**, *14*, 1118–1127. [CrossRef]

18. Hagelkruys, A.; Sawicka, A.; Rennmayr, M.; Seiser, C. The biology of HDAC in cancer: The nuclear and epigenetic components. *Handb. Exp. Pharmacol.* **2011**, *206*, 13–37.

19. De Ruijter, A.J.; van Gennip, A.H.; Caron, H.N.; Kemp, S.; van Kuilenburg, A.B. Histone deacetylases (HDACs): Characterization of the classical HDAC family. *Biochem. J.* **2003**, *370*, 737–749. [CrossRef]

20. Mutze, K.; Langer, R.; Becker, K.; Ott, K.; Novotny, A.; Luber, B.; Hapfelmeier, A.; Gottlicher, M.; Hofler, H.; Keller, G. Histone deacetylase (HDAC) 1 and 2 expression and chemotherapy in gastric cancer. *Ann. Surg. Oncol.* **2010**, *17*, 3336–3343. [CrossRef]

21. Kang, Z.H.; Wang, C.Y.; Zhang, W.L.; Zhang, J.T.; Yuan, C.H.; Zhao, P.W.; Lin, Y.Y.; Hong, S.; Li, C.Y.; Wang, L. Histone deacetylase HDAC4 promotes gastric cancer SGC-7901 cells progression via p21 repression. *PLoS ONE* **2014**, *9*, e98894. [CrossRef] [PubMed]

22. Juan, L.J.; Shia, W.J.; Chen, M.H.; Yang, W.M.; Seto, E.; Lin, Y.S.; Wu, C.W. Histone deacetylases specifically down-regulate p53-dependent gene activation. *J. Biol. Chem.* **2000**, *275*, 20436–20443. [CrossRef] [PubMed]

23. Riquelme, I.; Letelier, P.; Riffo-Campos, A.L.; Brebi, P.; Roa, J.C. Emerging role of miRNAs in the drug resistance of gastric cancer. *Int. J. Mol. Sci.* **2016**, *17*, 424. [CrossRef] [PubMed]

24. Sekar, D.; Krishnan, R.; Thirugnanasambantham, K.; Rajasekaran, B.; Islam, V.I.; Sekar, P. Significance of microRNA 21 in gastric cancer. *Clin. Res. Hepatol. Gastroenterol.* **2016**. [CrossRef] [PubMed]

25. Ishiguro, H.; Kimura, M.; Takeyama, H. Role of microRNAs in gastric cancer. *World J. Gastroenterol.* **2014**, *20*, 5694–5699. [CrossRef]

26. Kim, Y.K.; Yu, J.; Han, T.S.; Park, S.Y.; Namkoong, B.; Kim, D.H.; Hur, K.; Yoo, M.W.; Lee, H.J.; Yang, H.K.; et al. Functional links between clustered microRNAs: Suppression of cell-cycle inhibitors by microRNA clusters in gastric cancer. *Nucl. Acids Res.* **2009**, *37*, 1672–1681. [CrossRef]

27. Takagi, T.; Iio, A.; Nakagawa, Y.; Naoe, T.; Tanigawa, N.; Akao, Y. Decreased expression of microRNA-143 and -145 in human gastric cancers. *Oncology* **2009**, *77*, 12–21. [CrossRef]

28. Akiyoshi, S.; Fukagawa, T.; Ueo, H.; Ishibashi, M.; Takahashi, Y.; Fabbri, M.; Sasako, M.; Maehara, Y.; Mimori, K.; Mori, M. Clinical significance of miR-144-ZFX axis in disseminated tumour cells in bone marrow in gastric cancer cases. *Br. J. Cancer* **2012**, *107*, 1345–1353. [CrossRef]

29. Xia, L.; Zhang, D.; Du, R.; Pan, Y.; Zhao, L.; Sun, S.; Hong, L.; Liu, J.; Fan, D. miR-15b and miR-16 modulate multidrug resistance by targeting BCL2 in human gastric cancer cells. *Int. J. Cancer* **2008**, *123*, 372–379. [CrossRef]

30. Licona, C.; Spaety, M.E.; Capuozzo, A.; Ali, M.; Santamaria, R.; Armant, O.; Delalande, F.; van Dorsselaer, A.; Cianferani, S.; Spencer, J.; et al. A ruthenium anticancer compound interacts with histones and impacts differently on epigenetic and death pathways compared to cisplatin. *Oncotarget* **2016**. [CrossRef]

31. Nogales, V.; Reinhold, W.C.; Varma, S.; Martinez-Cardus, A.; Moutinho, C.; Moran, S.; Heyn, H.; Sebio, A.; Barnadas, A.; Pommier, Y.; et al. Epigenetic inactivation of the putative DNA/RNA helicase SLFN11 in human cancer confers resistance to platinum drugs. *Oncotarget* **2016**, *7*, 3084–3097. [CrossRef] [PubMed]

32. Di Giorgio, E.; Brancolini, C. Regulation of class IIa HDAC activities: It is not only matter of subcellular localization. *Epigenomics* **2016**, *8*, 251–269. [CrossRef] [PubMed]

33. Marek, L.; Hamacher, A.; Hansen, F.K.; Kuna, K.; Gohlke, H.; Kassack, M.U.; Kurz, T. Histone deacetylase (HDAC) inhibitors with a novel connecting unit linker region reveal a selectivity profile for HDAC4 and HDAC5 with improved activity against chemoresistant cancer cells. *J. Med. Chem.* **2013**, *56*, 427–436. [CrossRef] [PubMed]

34. Chou, T.C. Theoretical basis, experimental design, and computerized simulation of synergism and antagonism in drug combination studies. *Pharmacol. Rev.* **2006**, *58*, 621–681. [CrossRef]

35. Duong, V.; Bret, C.; Altucci, L.; Mai, A.; Duraffourd, C.; Loubersac, J.; Harmand, P.O.; Bonnet, S.; Valente, S.; Maudelonde, T.; et al. Specific activity of class II histone deacetylases in human breast cancer cells. *Mol. Cancer Res.* **2008**, *6*, 1908–1919. [CrossRef]

36. Garattini, S.K.; Basile, D.; Cattaneo, M.; Fanotto, V.; Ongaro, E.; Bonotto, M.; Negri, F.V.; Berenato, R.; Ermacora, P.; Cardellino, G.G.; et al. Molecular classifications of gastric cancers: Novel insights and possible future applications. *World J. Gastrointest. Oncol.* **2017**, *9*, 194–208. [CrossRef]

37. Lopez, I.; Tournillon, A.S.; Martins, R.P.; Karakostis, K.; Malbert-Colas, L.; Nylander, K.; Fahraeus, R. p53-mediated suppression of BiP triggers BIK-induced apoptosis during prolonged endoplasmic reticulum stress. *Cell Death Differ.* **2017**, *24*, 1717–1729. [CrossRef]

38. Li, X.; Zhao, Y.; Xia, Q.; Zheng, L.; Liu, L.; Zhao, B.; Shi, J. Nuclear translocation of annexin 1 following oxygen-glucose deprivation-reperfusion induces apoptosis by regulating Bid expression via p53 binding. *Cell Death Dis.* **2016**, *7*, e2356. [CrossRef]

39. Colarossi, L.; Memeo, L.; Colarossi, C.; Aiello, E.; Iuppa, A.; Espina, V.; Liotta, L.; Mueller, C. Inhibition of histone deacetylase 4 increases cytotoxicity of docetaxel in gastric cancer cells. *Proteomics Clin. Appl.* **2014**, *8*, 924–931. [CrossRef]

40. Zeng, L.S.; Yang, X.Z.; Wen, Y.F.; Mail, S.J.; Wang, M.H.; Zhang, M.Y.; Zheng, X.F.; Wang, H.Y. Overexpressed HDAC4 is associated with poor survival and promotes tumor progression in esophageal carcinoma. *Aging* **2016**, *8*, 1236–1249. [CrossRef]

41. Cohen, A.L.; Piccolo, S.R.; Cheng, L.; Soldi, R.; Han, B.; Johnson, W.E.; Bild, A.H. Genomic pathway analysis reveals that EZH2 and HDAC4 represent mutually exclusive epigenetic pathways across human cancers. *BMC Med. Genom.* **2013**, *6*, 35. [CrossRef] [PubMed]

42. Shen, Y.F.; Wei, A.M.; Kou, Q.; Zhu, Q.Y.; Zhang, L. Histone deacetylase 4 increases progressive epithelial ovarian cancer cells via repression of p21 on fibrillar collagen matrices. *Oncol. Rep.* **2016**, *35*, 948–954. [CrossRef] [PubMed]

43. Amodio, N.; Stamato, M.A.; Gulla, A.M.; Morelli, E.; Romeo, E.; Raimondi, L.; Pitari, M.R.; Ferrandino, I.; Misso, G.; Caraglia, M.; et al. Therapeutic targeting of miR-29b/HDAC4 epigenetic loop in multiple myeloma. *Mol. Cancer Ther.* **2016**. [CrossRef] [PubMed]

44. Vallabhapurapu, S.D.; Noothi, S.K.; Pullum, D.A.; Lawrie, C.H.; Pallapati, R.; Potluri, V.; Kuntzen, C.; Khan, S.; Plas, D.R.; Orlowski, R.Z.; et al. Transcriptional repression by the HDAC4-RelB-p52 complex regulates multiple myeloma survival and growth. *Nat. Commun.* **2015**, *6*, 8428. [CrossRef]

45. Wilson, A.J.; Byun, D.S.; Nasser, S.; Murray, L.B.; Ayyanar, K.; Arango, D.; Figueroa, M.; Melnick, A.; Kao, G.D.; Augenlicht, L.H.; et al. HDAC4 promotes growth of colon cancer cells via repression of p21. *Mol. Biol. Cell* **2008**, *19*, 4062–4075. [CrossRef]

46. Song, B.; Wang, Y.; Xi, Y.; Kudo, K.; Bruheim, S.; Botchkina, G.I.; Gavin, E.; Wan, Y.; Formentini, A.; Kornmann, M.; et al. Mechanism of chemoresistance mediated by miR-140 in human osteosarcoma and colon cancer cells. *Oncogene* **2009**, *28*, 4065–4074. [CrossRef]

47. Imbriano, C.; Gurtner, A.; Cocchiarella, F.; di Agostino, S.; Basile, V.; Gostissa, M.; Dobbelstein, M.; del Sal, G.; Piaggio, G.; Mantovani, R. Direct p53 transcriptional repression: In vivo analysis of CCAAT-containing G2/M promoters. *Mol. Cell Biol.* **2005**, *25*, 3737–3751. [CrossRef]

48. Basile, V.; Mantovani, R.; Imbriano, C. DNA damage promotes histone deacetylase 4 nuclear localization and repression of G2/M promoters, via p53 C-terminal lysines. *J. Biol. Chem.* **2006**, *281*, 2347–2357. [CrossRef]

49. Kao, G.D.; McKenna, W.G.; Guenther, M.G.; Muschel, R.J.; Lazar, M.A.; Yen, T.J. Histone deacetylase 4 interacts with 53BP1 to mediate the DNA damage response. *J. Cell Biol.* **2003**, *160*, 1017–1027. [CrossRef]

50. Gaiddon, C.; de Tapia, M.; Loeffler, J.P. The tissue-specific transcription factor Pit-1/GHF-1 binds to the c-fos serum response element and activates c-fos transcription. *Mol. Endocrinol.* **1999**, *13*, 742–751. [CrossRef]

51. Vidimar, V.; Meng, X.; Klajner, M.; Licona, C.; Fetzer, L.; Harlepp, S.; Hebraud, P.; Sidhoum, M.; Sirlin, C.; Loeffler, J.P.; et al. Induction of caspase 8 and reactive oxygen species by ruthenium-derived anticancer compounds with improved water solubility and cytotoxicity. *Biochem. Pharmacol.* **2012**, *84*, 1428–1436. [CrossRef] [PubMed]

52. Antoine, M.; Gaiddon, C.; Loeffler, J.P. Ca2+/calmodulin kinase types II and IV regulate c-fos transcription in the AtT20 corticotroph cell line. *Mol. Cell Endocrinol.* **1996**, *120*, 1–8. [CrossRef]

53. Benosman, S.; Meng, X.; von Grabowiecki, Y.; Palamiuc, L.; Hritcu, L.; Gross, I.; Mellitzer, G.; Taya, Y.; Loeffler, J.P.; Gaiddon, C. Complex regulation of p73 isoforms after alteration of amyloid precursor polypeptide (APP) function and DNA damage in neurons. *J. Biol. Chem.* **2011**, *286*, 43013–43025. [CrossRef] [PubMed]

54. Emig, D.; Salomonis, N.; Baumbach, J.; Lengauer, T.; Conklin, B.R.; Albrecht, M. AltAnalyze and DomainGraph: Analyzing and visualizing exon expression data. *Nucl. Acids Res.* **2010**, *38*, W755–W762. [CrossRef]
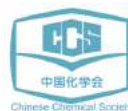
Check for updates

Anticancer activity of ruthenium and osmium cyclometalated compounds: identification of ABCB1 and EGFR as resistance mechanisms†

Cynthia Licona,[a] Jean-Baptiste Delhorme,[a] Gilles Riegel,[a] Vania Vidimar,[a] Ricardo Cerón-Camacho,[b] Bastien Boff,[c] Aina Venkatasamy,[a] Catherine Tomasetto,[d] Priscila da Silva Figueiredo Celestino Gomes,[e] Didier Rognan,[e] Jean-Noel Freund,[a] Ronan Le Lagadec,[b] Michel Pfeffer,[c] Isabelle Gross,[a] Georg Mellitzer[a] and Christian Gaiddon *[a]

Ruthenium and osmium complexes have been shown to bypass several resistance mechanisms of platinum anticancer drugs, suggesting that they might represent therapeutic alternatives. However, the resistance mechanisms that may alter the cytotoxicity of ruthenium and osmium complexes have not been identified yet. Here we investigated the mechanisms governing the variability in the cytotoxicity of two ruthenium cyclometalated compounds and their osmium equivalents. We characterized their anticancer properties *in vitro* and *in vivo*, and we developed a 4-step approach to identify genes involved in their sensibility/resistance by correlating their cytotoxicity measures with transcriptomic data of 60 cancer cell lines. As previously observed for ruthenium complexes, we showed that osmium compounds target the endoplasmic reticulum stress pathway and that their activity was not hindered by mutation in the tumor suppressor gene TP53. Then, we identified multiple sensibility/resistance genes that correlated with the cytotoxicity of cyclometalated compounds. Docking and functional studies demonstrated that inhibition of some of these resistance mechanisms, namely ABCB1 export and EGFR expression, improved the activity of cyclometalated complexes. Interestingly, switching from ruthenium to osmium favored cytotoxicity while reducing sensibility to the ABCB1 export mechanism. In summary, this study represents the first comprehensive investigation of the resistance mechanisms that alter the biological activity of ruthenium or osmium complexes, and identifies some of the chemical determinants that are important for their activity.

Introduction

Ruthenium- and osmium-based compounds are being intensively investigated as potential anticancer drugs encouraged by the intrinsic physico-chemical properties of transition metals and the long-lasting successes of platinum-based drugs.[1–3] Although three Ru-based complexes (KP1039, NAMI-A, and TLD1433) are or have been already tested in clinical trials, the development of Ru-based compounds towards patients is hindered by the diverse and controversial hypotheses on the physico-chemical determinant(s) relevant for their biological activity (ClinicalTrials.gov Identifier: NCT03053635).[4] Indeed, multiple Ru- and Os-based compounds have been designed with different ligands, such as half-sandwich "piano-stool" structures, and different types of bonds between the metal and the ligands (O, S, N, P, C, and Cl).[3,5] This variety leads to a wide range of spatial structures, lipophilicities, metal charges (0 to IV) and redox potentials. The various physico-chemical properties may also explain the diversity of possible direct biological targets (DNA, kinase, and redox proteins) and regulated signaling pathways, such as the TP53 tumor suppressor gene and the endoplasmic reticulum (ER) stress.[6–18] However, the relative contribution of a specific physico-chemical property to a given effect on a direct target or signaling pathway often remains enigmatic. In particular, it is difficult to comprehend the exact contribution of each physico-chemical determinant

[a]*Interface Recherche Fondamentale en Cancérologie, Université de Strasbourg, Inserm UMR_S 1113, 3 av. Molière, 67200 Strasbourg, France.*
E-mail: Gaiddon@unistra.fr; Tel: +33 683525356
[b]*Instituto de Química, UNAM, Circuito Exterior s/n, Ciudad Universitaria, Ciudad de México, 04510, Mexico*
[c]*Institut de Chimie, UMR7177, Laboratoire de Synthèses Métallo-Induites, 4 rue Blaise Pascal, 67000, France*
[d]*IGBMC, Université de Strasbourg, U1258 INSERM UMR-7104 CNRS, Ilkirch, France*
[e]*Laboratoire d'Innovation Thérapeutique, UMR7200 CNRS-Université de Strasbourg, F-67400 Illkirch, France*
†Electronic supplementary information (ESI) available: Fig. S1–S4. See DOI: 10.1039/c9qi01148j

taken individually (*i.e.* redox potential, lipophilicity, and the presence of specific ligands), as by changing a given ligand, several of these characteristics are being modified simultaneously.

In addition, as the mode of action often remains elusive, the biological determinants that drive the sensitivity or resistance of the cancer cells towards these compounds have never been investigated. For instance, original work done on the "piano stool like" Ru complex RM175 showed the requirement of the DNA damage response factor and tumor suppressor gene TP53 for its cytotoxicity.[10] In contrast, we showed that the organoruthenium complex, RDC11, acts *via* the endoplasmic reticulum (ER) stress effector CHOP.[12] More recently, it was shown that two Os structures discriminate between the necessity for the TP53 or ER stress pathway for their cytotoxicity.[14] Importantly, no studies have yet described resistance mechanisms for Ru or Os complexes. In the era of personalized medicine, such information is critical for the development of optimized compounds and for their translation towards clinical use.

In an attempt to address these issues, we searched for the potential resistance mechanisms that might impact the cytotoxicity of Ru and Os complexes by investigating potential candidates, such as TP53, and by using an unbiased transcriptomic approach on 60 different cancer cell lines. For this study we chose 2 pairs of cyclometalated compounds bearing bidentate ligands that have been previously described.[19–22] Within each pair, the complexes have similar ligands but differ by the metal, either Ru or Os, which we expected to change the redox potential of the complex. Both pairs also differ by the ligands (one phenanthroline *vs.* two), which we expected to modulate lipophilicity. Our hypothesis was that by comparing these 4 complexes we would be able to investigate the relative contribution of the redox potential (based on the metal) and the lipophilicity in their biological activity. A comprehensive physico-chemical, molecular, cellular and *in vivo* study was performed on these 4 complexes to evaluate their mode of action and the gene profiles required for their activity in cancer cells.

Results

Exchange of ruthenium to osmium in organometallic complexes favors anticancer properties

Fig. 1a shows the structure of the cyclometalated complexes investigated in this study: the related compounds RDC11/ODC2 and RDC34/ODC3 whose synthesis have been previously described.[19,20] The cytotoxicity of RDC11 and RDC34 has been investigated earlier.[12,13,18,23,24] All the compounds were stable at room temperature in PBS at least for more than 24 hours (Fig. S1†). The replacement of Ru in RDC11 by Os in ODC2 did not significantly affect the spatial structure or the lipophilicity measured by the phase separation assay (log(P_o/w) (Table 1). However, the introduction of Os caused a significant drop in the redox potential ($E^\circ_{1/2}$M(III/II) value) as previously described (Table 1).[19,20]
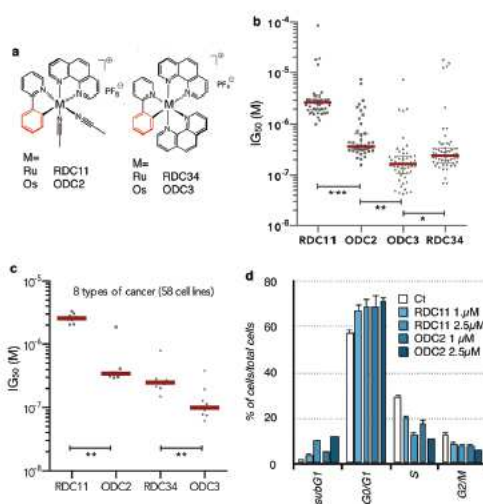
Fig. 1 Growth inhibition and cytotoxic activity of the Ru and Os complexes. (a) Structures of the Ru and Os complexes employed in this study. (b) NCI data of Inhibition Growth 50 (IG_{50}) for the 60 NCI cell lines treated with RDC11, ODC2, RDC34, and ODC3 obtained by SRB were analysed using GraphPad Prism. (c). Mean of IG50 for each of the 8 types of cancer of the NCI panel. (d) Identification of the cell cycle and sub-G1 populations by flow cytometry analysis (FACS) in HCT116 cells treated with RDC11 and ODC2 for 24 h. *, **, and *** indicate statistical differences of 0.05, 0.01 and 0.001 respectively as determined by ANOVA followed by Tukey post-test using GraphPad Prism software.

Table 1 Physico-chemical properties of Ru and Os organometallics. Redox potentials E°(V) of osmium and ruthenium ($M^{III/II}$) *vs.* Ag/AgCl, phosphate buffer 0.075 M pH 7.5, scan rate 10 mV s^{-1}, 25 °C. Lipophilicity was evaluated with log(P_o/w) as described.[19,28]

Complexes	E°/ V (Ag/AgCl)	Log(P_o/w)
ODC2	0.109	1.15 ± 0.05
RDC11	0.423	1.2 ± 0.05
ODC3	0.031	2.34 ± 0.04
RDC34	0.324	2.35 ± 0.05

Earlier studies, including ours, have shown that ruthenium complexes can alter *in vitro* the activity of purified oxidoreductases, such as glucose oxidase, horseradish peroxidase, lactate dehydrogenase or PHD2.[22,24–26] Thus, these redox enzymes can be considered as direct molecular targets of these complexes. To assess how the change in the metal or the ligand could impact the ability of the metalacycles to affect their direct molecular targets, we measured the activity of two purified redox enzymes, glucose oxidase and horseradish peroxidase, in the presence of the organometallic derivatives. The calculation of the k_3 rate constant for the electron transfer between the active site of the enzyme and the complexes, showed that the ability to alter *in vitro* the activity of both puri-

242

Table 2 Biological properties of Ru and Os organometallics. The k_3 value ($(M^{-1} s^{-1}) \times 10^6$) is the rate constant for the electron transfer between the reduced (glucose oxidase, GO) or oxidized (horseradish peroxidase, HRP) form of the active site of the enzymes, and the Ru or Os cyclometalated complexes; *in vitro* cytotoxicity in HCT116 cancer cells is indicated as IC_{50} in µM; *in vivo* activity on xenografted cancer cells is indicated as % of tumor volume relative to the control mice (Ct) treated with vehicle (PBS/cremophore)

| | k_3 ($M^{-1} s^{-1}$) $\times 10^6$ | | Anticancer activity | |
| | | | *In vitro* | *In vivo* |
Complexes	Glucose Ox.	HRP	(IC_{50} µM)	(tumor vol., % Ct)
ODC2	2.9 ± 0.3	2.7	1.2 ± 0.1	55 ± 12
RDC11	1.7 ± 0.2	0.1	1.8 ± 0.1	60 ± 11
ODC3	1.8 ± 0.2	58	0.09 ± 0.01	58 ± 8
RDC34	7.5 ± 0.4	2.3	0.15 ± 0.01	62 ± 9

fied redox enzymes is related to their redox potential (Tables 1 and 2). The addition of a second phenanthroline ligand in RDC34 and ODC3 slightly lowered the redox potential by *ca.* 100 mV, and increased the lipophilicity, as expected due to its extended aromatic system. In addition, these results indicated that the modification of the spatial structure (probable increase of steric effects) may also be responsible for the impact on the ability to affect the redox enzyme function (Tables 1 and 2). For instance, these differences might be visible when comparing the structures of RDC11[27] and ODC2[20] with that of RDC34[22] in which two acetonitrile units have been substituted by a phenanthroline bidendate ligand.

To assess the influence of changing the metal and the ligand on the cellular activity of the complexes, we first compared their cytotoxicity on a panel of human cancer cell lines. The replacement of Ru by Os decreased the IC_{50} values (concentrations reducing viability by 50%) of ODC2 and ODC3 in HCT116 cells measured by MTT [3-(4,5-dimethylthiazol-2-yl)-2,5-diphenyltetrazolium bromide] assay (Table 2, Fig. S2a and b†). The increase in activity was confirmed on various cell lines issued from 8 types of cancers present in the NCI panel, both on the IG50 (50% of growth inhibition, Fig. 1b and c, Fig. S2d and e†) and the LC_{50} (dose inducing 50% of lethality, Fig. S2f and g†). ODC3 displayed a strong anti-proliferative activity in the nanomolar range on cell lines of several types of cancers, suggesting that improving the lipophilicity favors the cytotoxicity, similarly to what we previously described.[19,28]

We then compared the mechanisms that could account for the cytotoxicity of Os and Ru complexes on HCT116 cells using flow cytometry. Treatment of HCT116 cells with RDC11, RDC34, ODC2 and ODC3 increased the number of cells in sub-G1, as well as the number of cells in G0/G1 (Fig. 1d, Fig. S2c†). This suggested that ODC2 and ODC3 can induce both cell cycle arrest in G0/G1 and apoptosis, as pointed out by the presence of a subG1 fraction. In addition, the number of cells in the sub-G1 fraction was slightly more elevated when cells were treated with ODC2 and ODC3 compared to cells treated with their respective ruthenium counterparts (RDC11 and RDC34), suggesting that ODC were slightly more potent to induce apop-

tosis than RDC. To confirm the pro-apoptotic potential of ODC3, we measured the cleavage of PARP1 by western blot, a marker of apoptosis. RDC34 and ODC3 were both able to induce PARP1 cleavage (Fig. S2h†). Of note, quantification of cleaved products indicated that ODC3 was more potent than RDC34 to induce apoptosis, which is consistent with the survival assays. Similarly, ODC3 induced a higher expression of the pro-apoptotic gene *NOXA* (Fig. S2i†). Finally, *in vivo* experiments performed on 3LL lung cancer cells in mice showed that ODC2 and ODC3 tended to be more efficient to reduce tumor growth although the differences were not statistically significant (Table 2, Fig. S2j†).

Osmium cyclometalated complexes enforce the induction of the ER stress pathway

We previously showed that cyclometalated RDC11 and RDC34, bearing one or two phenanthrolines respectively, induced markers of the ER stress pathway.[12,13] This pathway responds to protein misfolding, redox stress and intracellular calcium imbalance.[29,30] We wondered whether their osmium counterparts, ODC2 and ODC3, may have the same properties, especially since an osmium compound (CL2 in this study) that also contained a phenanthroline but lacked the 2-phenylpyridine moiety and the C–metal bond was described as being unable to induce ER stress.[14] Therefore, we evaluated the ability of ODC2 and ODC3 to regulate the expression of ER stress markers, which would assess the importance of 2-phenylpyridine and the C–Os bond in the ability of the complex to induce ER stress markers. ODC2 and ODC3 induced the pro-apoptotic ER stress transcription factor CHOP, while neither the coordinated phenanthroline complex (CL2) nor oxaliplatin displayed any significant effect (Fig. 2a, Fig. S3a†). Similarly, ODC2, but not another platinum-based drug, cisplatin, induced the phosphorylation of EIf2a, one of the early steps in the ER stress pathway (Fig. 2b). Interestingly, ODC2 displayed a stronger ability to induce these markers compared to RDC11, further supporting the higher cytotoxicity of osmium complexes over their ruthenium counterparts, likely mediated by the redox potential difference. These results also indicate that the presence of the cyclometalated 2-phenylpyridine ligand is important to tune osmium complexes' biological activity. Similar results were obtained with ODC3 and RDC34 on CHOP and its target gene *CHAC1* (Fig. S3a and b†). To further understand the role of the ER stress in the biological activity of ODC2, we inhibited two effectors of the ER stress pathway, EIF2a and CHOP. Inhibition of EIF2a by salubrinal did not reduce the biological activity of ODC2 (Fig. S3c†). In contrast, the silencing of CHOP expression diminished the cytotoxicity of ODC2 (Fig. 2c). These results suggest that ODC2 does not require for its activity the PERK1-EIF2a branch of the ER stress pathway, but still needs the expression of the downstream effector CHOP.

Osmium cyclometalated compounds are insensitive towards TP53 mutations

As shown in Fig. 1b, the 60 cell lines of the NCI displayed different sensitivities towards RDCs and ODCs. We decided to

243
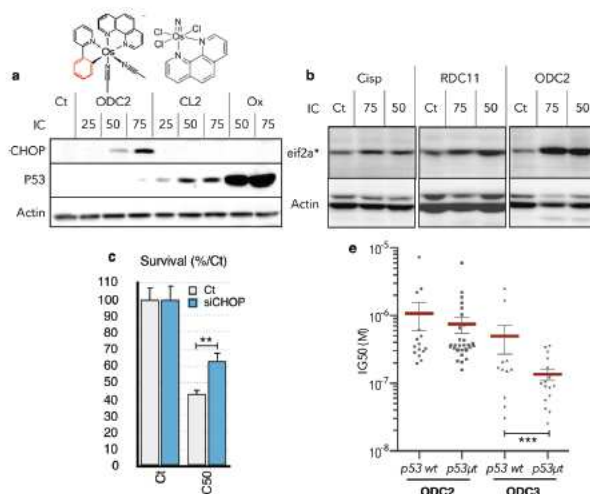
Fig. 2 Role of p53 and ER stress effectors in the cytotoxic activity of the Ru and Os complexes. (a) Western blot of p53 and CHOP in HCT116 cells treated for 24 h with the indicated compounds at $IC_{25 \cdot 50 \cdot 75}$. Ox = oxaliplatin ($IC_{50} = 1$ μM; $IC_{75} = 5$ μM); ODC2 (0, 25; 1; 2;5 μM) CL2 ($IC_{25} = 2$ μM; $IC_{50} = 5$; $IC_{75} = 10$ μM); Ct, DMSO 1%. (b) Western blot of EIF2a phosphorylated (eif2a*) in HCT116 cells treated for 24 h with the indicated compounds. Cisplatin (Cisp; $IC_{50} = 1$ μM, $IC_{75} = 5$ μM), RDC11 ($IC_{50} = 1$ μM; IC_{75}; 2.5 μM) (c) Survival of HCT116 cells treated or not with ODC2 at the IC_{50} and transfected with siRNA directed against CHOP. Cells were transfected for 48 h with the siRNA before treatment for 48 h. Graph shows the mean and standard deviation of % of surviving cells compared to the control condition (Ct) (d) IG50 of ODC2 and ODC3 in the NCI 60 cancer cell line panel as distributed in two groups, cell lines with wild type p53 (p53 wt) ($n = 15$) or cell lines with mutated p53 (p53 µt; $n = 30$). *** indicates statistical differences between the means of the two groups ($p < 0.001$) as determined by ANOVA followed by Tukey post-test using GraphPad Prism software.

investigate the molecular bases accounting for these differences. Based on the frequent mutation of the tumor suppressor gene *TP53* and its role in the activity of some osmium complexes, such as CL2,[14] we analyzed whether mutations in this gene might represent a resistance factor for ODC2 and ODC3 activity. To do so, we classified the cell lines of the NCI into 2 groups. The first group contained cell lines with wild-type p53 (p53 wt) and the second group cell lines with mutated p53 (p53 µt). The means of IG50 of both groups were compared. We first observed that mutation of the p53 tumor suppressor gene in the cancer cell lines did not diminish the cytotoxicity of ODCs and rather increased it (Fig. 2e). This result suggests that TP53 is not necessary for the activities of ODCs.

To further assess the role of TP53 in ODC activity, we analyzed the protein level of p53 by western blot in cells treated with ODCs in comparison with the osmium complex CL2. CL2 was previously described as an inducer of the p53 protein level.[14] Treatment of cancer cells with ODC2 did not increase the p53 protein level (Fig. 2a), in contrast to CL2. We also tested the impact of an inhibitor of p53, pifithrin, on the activity of ODC2. The p53 inhibitor pifithrin did not reduce the cytotoxicity of ODC2 (Fig. S3d†). This set of experiments indicate that the biological activity of ODCs is not dependent on the p53 protein and that mutation in TP53 does not account for the variability and cancer cell sensitivity towards ODCs or RDCs.

Genomic approach identified ABCB1 and EGFR as resistance mechanisms for cyclometalated ruthenium and osmium complexes

As mutation in *TP53* does not account for the variation in ODC and RDC sensitivity in cancer cells, we searched for other mechanisms. To identify potential resistance mechanisms of cyclometalated complexes we used a non-biased strategy based on 4 successive steps that integrated the cytotoxicity data obtained from the NCI, the gene expression levels from Cell Express (http://cellexpress.cgm.ntu.edu.tw), and TCGA (http://www.cbioportal.org). To do so, we focused on RDC11 that generally displayed the lowest activity.

In the first step, we defined two groups of cell lines. The first group contained the 4 most resistant cell lines towards RDC11, namely NCI ADR, CAKI1, HCT15, and UO3, showing a high IG50 for RDC11 (around 10^{-4} M). These cells showed also a low response towards ODC2 (close to 10^{-5} M). The second group contained the most sensitive cell lines, namely HOP92, OVCAR3, NCI H522, and SKMEL5, with a low IG50 close to or below 10^{-6} M. Then, we analyzed the gene expression patterns that might differentiate these two groups of cells using Cell Express (http://cellexpress.cgm.ntu.edu.tw). Among them, 1356 genes presented a p value $< 10^{-3}$, indicating that the biological response of cancer cells towards the complexes might
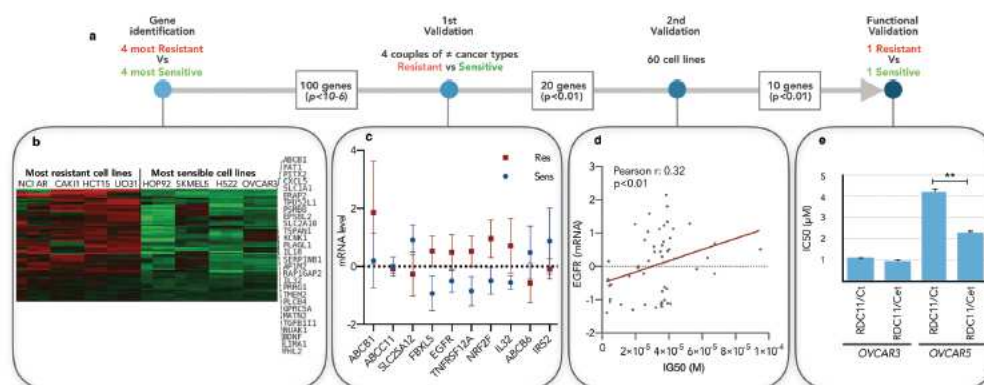
Fig. 3 (a) Multistep selection process for resistant genes against Ru/Os complexes. (b) Heatmap of gene signature identification step using 8 cell lines for CellExpress analysis. 4 sensitive cell lines (HOP92, SKMEL5, H522, and OVCAR3) and 4 resistant cell lines (NCI AR, CAKI1, HCT15, and UO31) for RDC11 were chosen and the genes co-expressed in each group were identified using the CellExpress website. (c) First validation step on 8 cell lines using cBioPortal transcriptomic data. Data of indicated genes for 8 cell lines segregated in two groups (resistant *versus* sensible to RDC11 based on the IG50 from the NCI data) obtained from cBioPortal were analyzed using GraphPad Prism. In each group a cell line from each of the 4 types of cancer is present: HOP92 and NCI ADR for lung cancer, HCT15 and KM12 for colon cancer, BT549 and HS578T for breast cancer, OVCAR3 and OVCAR8 for ovarian cancer. Graph represents means and standard deviations of the relative mRNA level (z score) for the groups of sensitive (Sens) and resistant (Res) cell lines. (d) Second validation step for *EFGR* expression on the 60 cell lines of the NCI and using cBioPortal transcriptomic data. *EGFR* expression is indicated in the relative level (z score). (e) Functional validation step for EGFR using cetuximab (Cet, 0.5 μM), a selective inhibitor of EGFR, on 2 cell lines, with low (OVCAR3) and high (OVCAR5) expression of EGFR. Cetuximab was added 1 h before treatment with RDC11. Cell survival was evaluated by MTT after 48 h of treatment. Graph indicates means ($n = 3$) and standard deviations of IC_{50} obtained in each condition. ** indicates statistical differences of 0.01 as determined by ANOVA followed by Tukey post-test using GraphPad Prism software.

involve numerous pathways (Fig. 3a and b, S4a†). In the second step, we increased the number of cell lines included in the correlation analysis by choosing 4 pairs of cell lines from 4 different types of cancers. This meant that for each cancer type there was one sensitive cell line and one resistant cell line to RDC or ODC: HOP92 and NCI ADR for lung cancer, HCT15 and KM12 for colon cancer, BT549 and HS578T for breast cancer, and OVCAR3 and OVCAR8 for ovarian cancer. This step was used to limit inter-cancer type bias, as for instance, renal cancer cell lines showed less sensibility in general compared to cell lines of other types of cancer. In this second step, we selected out of the 1356 genes initially identified in step 1 the 100 most differently expressed (p value $< 10^{-6}$) genes to further assess whether their expression correlated with the cytotoxicity of cancer cells by using the 4 pairs of cell lines. Out of these 100 genes, only 20 showed a statistically relevant correlation between their expression and the cytotoxicity in cancer cells (p value < 0.01), such as *ABCB1*, *EGFR* or *NRF2F* (Fig. 3c). In the third step, these 20 genes were further validated by correlating their expression to the IG50 of the 60 cell lines of the NCI panel (Fig. 3d). Out of 20 genes only 10 correlated with the IG50 with p value < 0.01, and only 8 with a good correlation ($r = \pm 0.3$) (*ABCB1*, $r = 0.57$; *EGFR*, $r = 0.32$; *IRS2*, $r = -0.31$; *GAS6*, $r = 0.37$; *NR4A2*, $r = 0.3$; *SLC25A2*, $r = -0.4$; *TNFRSF12A*, $r = 0.33$; *NRF2F*, $r = 0.39$).

This strategy allowed us to identify genes that have the most robust correlation between their expression level and the toxi-

city on cancer cell lines of different origins. The final step was to validate their importance in RDC11 cytotoxicity using the loss of function experiments. To do so, we selected *EGFR* and *ABCB1* because both have pharmacological inhibitors with FDA approval for their clinical use. For instance, we investigated the importance of EGFR that is overexpressed in various cancers and that can be inhibited by cetuximab, a monoclonal antibody selectively targeting EGFR. Cell lines with low (OVCAR3; z-score 0.16) and high (OVCAR5; z-score 1.8) expression of EGFR were treated with RDC11 alone or RDC11 with cetuximab (Fig. 3e). Cetuximab inhibition of EGFR signaling was verified by following *AREG* and *EREG* expression (Fig. S4f†), known downstream genes of EGFR signaling.[31] Cetuximab increased by two-fold the cytotoxicity of RDC11 in the OVCAR5 cells, but had no significant effect on OVCAR3 cells. Hence, the elevated expression of EGFR reduced RDC11 cytotoxicity. Altogether, these experiments indicate that the strategy chosen and developed allowed us to identify molecular signatures controlling RDC sensitivity towards specific cancer cells.

ABCB1 as a carrier of cyclometalated complexes

Among the genes identified by our approach, *ABCB1* was the gene whose expression correlated the most with the cytotoxic activity of RDC11 and ODC2 (Fig. 5a, S4b†). *ABCB1* (MDR1, P-gp) encodes a membrane protein that exports compounds outside the cells. Thus, the correlation existing between the

245
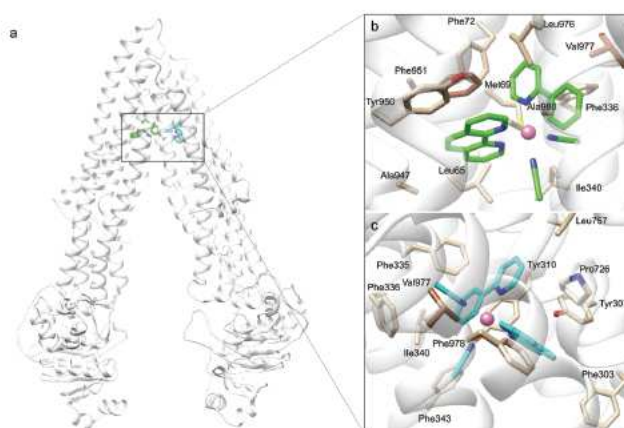
Fig. 4 Binding modes of RDC11 to the human ABCB1 transporter. (a) Overall view of the two adjacent binding modes of RDC11 (green and cyan sticks) to the ABCB1 protein (white ribbons). (b) Close-up of binding site 1. The RDC11 ligands are shown as green sticks, with the Ru atom displayed as a pink sphere. ABCB1 residues lining the binding site are represented by tan sticks, and are labelled at their Cα-atom. (c) Close-up of binding site 2. The RDC11 ligands are shown as cyan sticks, with the Ru atom displayed as a pink sphere. ABCB1 residues lining the binding site are represented by tan sticks, and are labelled at their Cα-atom.
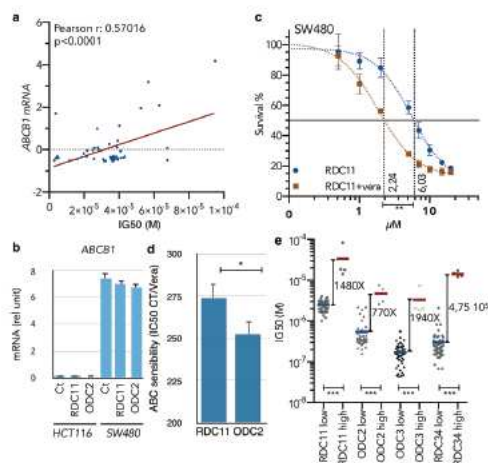
level of *ABCB1* expression and the cytotoxicity of RDC11 and ODC2 suggests that the ABCB1 protein might represent an export mechanism for these two drugs. To test this hypothesis, we first took the opportunity of the existence of an established structure of ABCB1 to perform docking experiments.

The flexible docking of RDC11 into the inner hydrophobic cavity of inward-facing ABCB1 unambiguously proposes two adjacent binding modes to transporter residues known to host several ABCB1 ligands (Fig. 4a). Site 1 corresponds to the location where the absolute lowest binding free energy pose (-7.52 kcal mol^{-1}) of the ligand is found (Fig. 4b). RDC11 is docked in a hydrophobic environment lined by several aromatic residues (Phe72, Phe336, Tyr950, and Phe951) that exhibit either edge-to-face or face-to-face interactions with the two aromatic groups of the RDC11 ligand. No polar interactions with the ligand could be detected, the Ru atom being just used as a tether to optimally orient the 2-phenylpyridine and the 1,10-phenanthroline rings with respect to their aromatic environment. As with most ABCB1 ligands, a second binding site (site 2), adjacent to the first one is found on the upper part of the inner cavity (Fig. 4c) that is particularly rich in aromatic residues.[32–34] The second site corresponds to the preferred location of most docking poses (Fig. 4b) with a slightly lower binding free energy (from -5.18 to -6.76 kcal mol^{-1}). As for site 1, site 2 is lined by a majority of aromatic amino acids (Phe303, Tyr307, Phe335, Phe336, Phe343, and Phe978) exhibiting aromatic interactions to the ligand. Again, no apolar interactions with the transporter are detected in this second binding site. These current docking data clearly suggest that binding of this RDC11 ligand to a nucleotide-free inward-facing conformation of the ABCB1 protein is feasible.

Inhibition of ABCB1 activity increased the cytotoxicity of cyclometalated complexes

Having established that RDC and ODC complexes can be transported by ABCB1, we investigated the impact of *ABCB1* expression on their cytotoxic activity. For this, we selected two colon cancer cell lines with either low (HCT116) or high (SW480) expression for *ABCB1* (Fig. 5b). Importantly, the expression of *ABCB1* or other ABC transporters was not substantially impacted by the treatment with RDCs or ODCs (Fig. S4b and c†). The inhibition of ABC transporters, including ABCB1, was achieved by using verapamil. Verapamil treatment lowered the RDC11's IC$_{50}$ in SW480 cells (high *ABCB1* expression) from 6 μM to 2.2 μM (Fig. 5c). The relative efficacy of RDC11 and ODC2 in the presence and absence of verapamil was calculated for SW480 as percentage relative to the treatment in the absence of verapamil. The ratio showed that the cytotoxicity of RDC11 was increased by about 275% in the presence of verapamil in SW480 (Fig. 5d). Verapamil showed a slightly lesser increase (250%) in the cytotoxic activity of ODC2 in SW480 cells (Fig. 5d). Of note, verapamil did not impact the ODC2 cytotoxicity in HCT116 cells (low *ABCB1* expression; Fig. S4e†). These results confirm that *ABCB1* expression and activity account, at least partially, for the sensitivity of cancer cells towards RDC11 and ODC2, and that RDC11 might be more sensitive to the *ABCB1* expression level.

To further investigate the role of ABCB1 in the activity of the complexes on a larger scale, NCI cell lines were separated into two groups based on *ABCB1* expression as measured by the z-score: the first group with high expression (*ABCB1*

246

Fig. 5 Impact of ABCB1 expression and inhibition on ruthenium- and osmium-based organometallic complexes. (a) Correlation of the *ABCB1* expression level (*z* score) with the cytotoxicity (IG50) of RDC11 in the whole NCI cancer cell line panel (60 cell lines). The correlation coefficient is indicated as calculated by Pearson test and *p* value (*n* = 60). (b) mRNA levels of *ABCB1* in HCT116 and SW480 colon cancer cells measured by RT-qPCR after 24 h of treatment at the IC_{50} (see Fig. 1). mRNA level of *ABCB1* was normalized to the housekeeping gene *TBP*. (c) To test for the impact of the ABC transporter inhibitor verapamil (50 μM), cells were treated for only 1 h with RDC11, and the MTT assay was performed after 48 h. Verapamil was present during the whole experiment. Curves are means of three independent experiments. (d) ABC sensitivity represented as % of IC_{50} difference between cells treated only with RDC11 or ODC2 and cells co-treated with verapamil. *p* < 0.01 (*t* test) (d). (e) Shift of IG50 in the NCI 60 cancer cell lines depending on the expression level (high, *n* = 4; low, *n* = 56) of *ABCB1*. *** indicates statistical differences of 0.001 as determined by ANOVA followed by Tukey post-test using GraphPad Prism software.

expression with a *z* score >2) and the second group with low expression (*z* score < 2). All 4 compounds displayed low cytotoxicity in the high *ABCB1*-expressing group, and higher cytotoxicity in the low *ABCB1*-expressing group (Fig. 5e). Interestingly, the difference of cytotoxicity between the two groups of cell lines was higher with the ruthenium-containing complexes compared to osmium-containing complexes (IG50 ratio of 1480-fold for RDC11 and 770-fold for ODC2; IG50 ratio of 4.75×10^5-fold for RDC34 and 1980-fold for ODC3). This suggests that in average the change of ruthenium for osmium limits ABCB1 resistance mechanisms. Therefore, ABCB1 might contribute to the balance of import and export mechanisms governing organometallic drug concentration in cells.

Discussion

Ruthenium and osmium complexes are being intensively investigated as potential anticancer drugs.[1-3] Multiple Ru- and Os-based compounds have been designed and this variety

leads to a diversity of possible direct biological targets, including DNA, kinase, redox proteins, and regulated signaling pathways, such as p53.[6-18] Three complexes (NAMI-A, KP1039 and TLD1433) are being or have been tested on patients in clinical trials. However, the relative contribution of a specific physicochemical characteristic to a given effect on a direct target or signaling pathway remains often enigmatic for osmium and ruthenium complexes. In addition, the biological determinants that drive the sensitivity or resistance of the cancer cells towards these compounds have never been investigated. To address these questions, we used 2 pairs of metalacycles bearing bidentate ligands that were previously described and that differ either by the metal (Os *versus* Ru) or the number of phenanthroline ligands (1 *versus* 2).[19,20] We expected the metal exchange to modify the redox potential and the number of phenanthrolines to modify the lipophilicity. Using these complexes, we compared *in vitro* and *in vivo* their anticancer properties and we investigated the potential resistance mechanisms that impaired their activity by developing a 4-step strategy that implemented correlations between the cytotoxicity and the genetic signatures of 60 different cancer cell lines.

Osmium and ruthenium cyclometalated complexes as anticancer drugs: role of redox potential and lipophilicity

The 4 complexes exhibited high cytotoxicity on all the 60 cell lines tested. At least part of the cytotoxicity can be linked to apoptosis as several markers were induced, such as the cleavage of PARP1 or induction of *NOXA*. The exchange of ruthenium to osmium in the mono or di-phenanthroline compounds increased the cytotoxicity and the *in vivo* anticancer activity. As the exchange only modifies the redox potential of the complexes, it further illustrates the importance of the redox potential in the biological activity of cyclometalated complexes. It was previously shown that the redox properties of Ru complexes allow them to switch from an inactive Ru(III) state outside the cells into a Ru(II) active state when it entered the cells.[35] However, in this study, we show that the redox potential contributes to the ability of the Os and Ru complexes to modulate the activity of their direct molecular targets, such as redox enzymes. The addition of a second phenanthroline increased also significantly the activity of the metalated complexes, both with ruthenium and osmium. This effect is likely due to the change in lipophilicity brought by the second phenanthroline, but it might also be attributed in part to structural changes.

Osmium cyclometalated complexes induce ER stress effectors

Both ODC2 and ODC3 induced the expression of the ER stress pathway effector CHOP, as well as one of its target gene, *CHAC1*. Interestingly, the osmium complex with one phenanthroline and no Os–C bond did not induce these markers, as previously reported.[14] Hence, the ability of inducing ER stress markers seems to be rather a characteristic of cyclometalated ruthenium and osmium and not a general feature. However, we previously reported that ruthenium complexes with piano-stool structures can also have similar properties on ER stress

markers.[36] Importantly, the activation of the ER stress pathway, or at least of some of its effectors, can account for the cell death induced by these cyclometalated complexes. Indeed, the silencing of CHOP reduced ODC2 cytotoxicity. However, salubrinal which inhibits the PERK-EIF2 pathway did not affect the ability of ODC2 to induce cytotoxicity. Hence, it is likely that the ODC2-regulated expression of CHOP might involve one of the two other components of the ER stress pathway, ATF6 or XBP1s.[37] The exact mechanistic processes that allow cyclometalated compounds to induce the ER stress pathway remains to be established. Interestingly, the ER stress pathway has been shown to be induced by intracellular redox imbalance and abnormal protein oxidation, which may both be altered by the redox properties of cyclometalated compounds, including *via* the deregulation of redox enzyme activities.[29]

ABCB1 and EGFR expression as resistance mechanisms against cyclometalated compounds

To our knowledge, no resistance mechanisms have yet been identified against Ru or Os compounds, despite the fact that their anticancer activity is tested in patients. The 4-step screening process that we developed showed that multiple genes may account for the sensibility of a given cell line towards cyclometalated compounds. The difficulty encountered in validating the 60 cell lines some of the genes identified as sensibility markers in the first step (8 cell lines) highlights the number and the clonal variabilities of the resistance mechanisms that may be involved. The genes initially identified that may, at least in part and in some cell lines, account for the sensibility towards ruthenium and osmium compounds span multiple cellular processes. Similarly, resistance mechanisms are complex and how cancer cells respond to a given drug depends on multiple factors, such as the availability of direct targets, number of off-targets, and expression of generic anti- and pro-apoptotic proteins. Taking advantage of the existence of inactivating drugs, we demonstrated that the overexpression of ABCB1 or EFGR reduced the cytotoxicity of cyclometalated drugs. For instance, ABCB1 may account for an elevated export of the Os and Ru cyclometalated compounds towards the outside of the cell. Surprisingly, these complexes seem to be more sensitive towards *ABCB1* expression compared to cisplatin (Fig. S4b†) or oxaliplatin (data not shown). Alternatively, it may also suggest that Os and Ru complexes are more efficient to overcome other resistance mechanisms, such as the mutation of TP53, favoring the role of *ABCB1*. Besides the use of an inhibitor of ABCB1 transporter to demonstrate its role, docking and modelling analyses support that ABCB1 may export cyclometalated complexes by its binding on two sites, site 1 (Phe72, Phe336, Tyr950, and Phe951) and site 2 (Phe303, Tyr307, Phe335, Phe336, Phe343, and Phe978). As for many existing substrates, we cannot rule out the possibility of a simultaneous occupation of both sites by two molecules of RDC11. The structurally close resemblance between RDC11 and ODC2 indicates that both complexes are fitting into ABCB1. However, the existing modeling tools do not allow us to differentiate possible fitting differences caused by changes

in the electron density surrounding the metal ion that caused the difference in terms of redox potential. Hence, by reducing cyclometalated drug concentration in the cell, cytotoxicity is reduced. This finding represents also one of the very few information on the mechanisms of import/export of Ru or Os complexes in cells. Indeed, besides the report that the import of these Ru complexes into cells is mediated by passive and active mechanisms,[23] so far there is no information that cyclometalated complexes are expelled and subjected to such resistance mechanisms.

Concerning the other gene that seems to partially dictate the sensitivity of cancer cells toward Ru and Os metalacycles, it is likely that EGFR, the receptor for the growth factor EGF, induces proliferative and pro-survival pathways, such as MAPK and AKT, that may partly counteract the pro-apoptotic and cell cycle arrest effects of the metallacycles. This information is to be carefully considered as EGFR over-expression or activating driver mutations are frequent events in several cancer types.[38]

Although the elevated expression of *ABCB1* and *EGFR* is clearly a factor that influences the capacity of cancer cells to respond to Os and Ru metallacycles, their impact on the IC_{50} of these drugs remains below 1 order of magnitude (change in 2- to 3-fold of the IC_{50}). This has to be compared to resistance mechanisms affecting platinum based-drugs or targeted therapies, such as the cetuximab. For instance, the difference of IC_{50} of cisplatin between sensitive and resistant ovarian cancer cells is well above 2 orders of magnitudes.[39] Similarly, the difference in sensitivity for cetuximab between cell lines ranges from 10^{-3} to 10^{24} µM.[31] Therefore, the importance of these resistance mechanisms identified for Os and Ru metallacycles has to be relativized and highlights the anticancer potential of these compounds.

In conclusion, this study is the first report, to the best of our knowledge, that identifies resistance mechanisms against osmium or ruthenium complexes. In particular, we demonstrated that the cytotoxic activity of cyclometalated complexes is reduced by the high expression of *ABCB1* and that the exchange of ruthenium by osmium reduces this effect. Hence, the efficacy of ruthenium and osmium complexes in patients might be improved by cotreatment with inhibitors of ABC transporters, such as verapamil. Furthermore, the insight gained into the role of the redox potential in the biological activity of these compounds constitutes a significant step towards the design of more effective and less expensive small molecules that could target cancer cells more efficiently.

Methods

Chemicals and enzymes

Ruthenium and osmium derived compounds were synthesized and characterized as previously described.[14,19–22] Oxaliplatin and verapamil were purchased from Sigma-Aldrich® and cetuximab was provided by Merck.

Glucose oxidase from *Aspergillus niger* was obtained from Sigma (211 U mg⁻¹), and ᴅ-glucose was obtained from Acros.

All reagents and components of buffer solutions were used as received and solvents were at least HPLC grade. Horseradish peroxidase isoenzyme C (type VI, RZ = 3.1) was purchased from Aldrich. Hydrogen peroxide was standardized by daily measuring the absorbance at 230 nm (ε = 72.8 M^{-1} cm^{-1}). The concentration of the heme group was determined spectrophotometrically using the ratio A_{403}/A_{275} and the HRP activity was measured by the guaiacol assay.

Cell culture, MTT (3-(4,5-dimethylthiazol-2-yl)-2,5-diphenyltetrazolium bromide) test, IC_{50} and NCI IG_{50}

Human colorectal HCT116 and SW480 cells, ovarian OVCAR3 and OVCAR5 were obtained from ATCC and maintained at 37 °C at 20% O_2, 5% CO_2 in DMEM, 1 g L^{-1} glucose (Dulbecco's modified Eagle's medium; Life Technology), supplemented with 10% fetal calf serum (Life Technology), penicillin/streptomycin (100 UI mL^{-1}–100 μg ml^{-1}) and gentamycin (50 mg mL^{-1}). MTT test was performed using 96-well culture plates (Costar).[40] IC_{50} was calculated on extrapolated fit curves based on concentration/effect data analyzed by using GraphPad Prism using the equation: Y = Bottom + (Top-Bottom)/(1 + $10^{((\log IC_{50}-X)}$ × HillSlope)). NCI renamed the IC_{50} into IG50, the concentration that causes 50% growth inhibition, to emphasize the correction for the cell count at time zero; thus, IG50 is the concentration of the test drug where $100 \times (T - T_0)/(C - T_0) = 50$ (dtp.cancer.gov/databases_tools/docs/compare/compare_methodology.htm#specon).

Transfection of siRNA

SiRNA transfection was performed using the RNAiMAX protocol as described by the provider (Life Technology, Saint Aubin, France). Sequences of siRNA for CHOP were previously described.[12]

Electrochemical measurements and calculation of rate constants

Electrochemical measurements were performed on a PC-interfaced potentiostat–galvanostat AUTOLAB PGSTAT 12. A three-electrode setup was used with a BAS working glassy carbon electrode, with Ag/AgCl as a reference electrode and with an auxiliary platinum electrode. Before each measurement, the working electrode was polished with diamond paste, rinsed with water and then with MeOH. The solution was purged with argon or nitrogen. Anodic peak currents (i_o) were obtained from cyclic voltammograms in the absence of the enzyme. Catalytic currents (i_{cat}) were obtained in the presence of GO and D-glucose under nitrogen. The rate constants, k_3, were calculated from the slopes of linear plots of the ratio i_{cat}/i_o against $([GO]/v)^{1/2}$ (v is the scan rate), as described.[41]

Electrochemical simulations were carried out in order to calculate k_3 for HRP, using the DigiElch 4.0 package from ElchSoft Simulation Software & Experience (Kleinromstedt, Germany). The diffusion coefficients were taken as 1 × 10^{-10} cm^2 s^{-1} for HRP,[42] and 1.6 × 10^{-5} cm^2 s^{-1} for H_2O_2.[43] The rate constant for H_2O_2 and HRP of 1.7 × 10^7 M^{-1} s^{-1} was used.[44] The electrode surface was taken as 0.0707 cm^2. The rate constant ks and the transfer coefficient α were first found in the

simulation of separate cyclic voltammograms of the complexes in the absence of H_2O_2 and HRP and then were further used to simulate cyclic voltammograms of osmium and ruthenium compounds in the presence of HRP/H_2O_2 (HRP/H_2O_2 (0.2 μM/1 mM), RDC/ODC (20 μM), phosphate buffer 0.075 M pH 7.6, and scan rate 10 mV s^{-1}, 25 °C). The rate constants k_3 were varied until the best visual match between calculated and experimental cyclic voltammograms was achieved.[45]

Quantitative reverse transcription-PCR (RT-qPCR)

Gene expression was assessed by qPCR using TBP as the normalizing gene.[46] Total RNA was isolated with Tri-reagent (MRC). RNA was quantified using a Nanodrop 2000 spectrophotometer (Thermo Scientific) and cDNA synthesized from 1 μg of total RNA using the High Capacity cDNA synthesis kit (Applied). qPCR was performed in an Applied thermal cycler using the FS Universal SYBR Green Master mix (Roche) or with TaqMan Gene expression assays (Applied Biosystems) and the FS Universal Probe Master mix (Roche). Specificity of the amplification was assessed by performing a melting curve analysis. Nucleotide sequences of the primers are indicated in ESI Material and methods.†

Western blot

Cells were lysed in Laemmli sample buffer 1× (125 mM Tris-HCl, pH 6.7, containing 3.3% SDS, 0.7 M 2-mercaptoethanol, 10% glycerol and 0.02% bromophenol blue) and then boiled for 5 minutes before loading. Equal amounts of total-protein extracts were separated on 10 to 12% PAGE and then electro-transferred to nitrocellulose membranes (Bio-Rad Laboratories). Equal loading was ensured by using an antibody directed against actin (1/2000; Sigma). Immunoprobing was performed with p53 (1/500; BD Transduction Labs), CHOP (1/1000; Novus Biologicals), and Eif2a (1/1000, Abcam). Membranes were then probed with secondary horseradish-peroxidase-conjugated antibody (anti-rabbit, 1/5000 or- mouse 1/1000, Santa Cruz). The antibody reaction was revealed with chemiluminescence detection procedures (Immun-StarTM HRP Chemiluminescence Kits, Bio-Rad Laboratories) and using the Molecular Imager® ChemiDocTM XRS + System (Bio-Rad Laboratories).

In vivo tumor growth

C57BL/6 mice (8-weeks old) were injected subcutaneously with 5 × e^5 3LL cells. Injections of RDC (RDC34 and ODC3 at 4 mmol kg^{-1}; RDC11 and ODC2 at 13.3 mmol kg^{-1}) started when tumors were palpable (100 mm^3) and were performed intraperitoneally twice a week. Tumor volumes were measured using a caliper. Solutions were prepared in PBS/5% Cremophore. Data are representative of two independent experiments (n = 7 animal per group). The control group was injected only with vehicle (PBS/5% Cremophore). Drug effect was statistically different ($p < 0.01$) compared to the control, as calculated by a one-way ANOVA test followed by a Tukey test. Animal experiments have been approved by the regional ethic and animal welfare committee and are performed by author-

249

ized and trained personnel, and hosted in an animal facility with the necessary mandatory administrative authorizations.

Flow cytometry

Hypodiploid DNA was measured as described.[9] Briefly, 5×10^6 cells were centrifuged and fixed in 1 ml of ice-cold 70% ethanol at 4 °C for 1 h, washed once in PBS, 2 mM EDTA, and resuspended in 1 ml of PBS containing 0.25 mg of RNase A, 2 mM EDTA, and 0.1 mg of propidium iodide. After incubation at 37 °C for 30 min, cells were analyzed. The fluorescence of 10 000 cells was analyzed using a FACScan flow cytometer and CellQuest software (BD Biosciences, San Jose, CA).

Abbreviations

ER   Endoplasmic reticulum
MTT   3-(4,5-Dimethylthiazol-2-yl)-2,5-diphenyltetrazolium bromide
GO   Glucose oxidase
HRP   Horseradish peroxidase

Author contributions

The manuscript was written through contributions of all authors. All authors have given approval to the final version of the manuscript.

Funding sources

Conflicts of interest

The authors declare no potential conflicts of interest

Acknowledgements

References

1 M. A. Jakupec, M. Galanski, V. B. Arion, C. G. Hartinger and B. K. Keppler, *Dalton Trans.*, 2008, 183–194, DOI: 10.1039/b712656p.

2 L. Kelland, *Nat. Rev. Cancer*, 2007, 7, 573–584.

3 G. Gasser, I. Ott and N. Metzler-Nolte, *J. Med. Chem.*, 2011, 54, 3–25.

4 A. Bergamo, C. Gaiddon, J. H. Schellens, J. H. Beijnen and G. Sava, *J. Inorg. Biochem.*, 2012, 106, 90–99.

5 M. Hanif, M. V. Babak and C. G. Hartinger, *Drug Discovery Today*, 2014, 19(10), 1640–1648.

6 H. Y. Mei and J. K. Barton, *Proc. Natl. Acad. Sci. U. S. A.*, 1988, 85, 1339–1343.

7 V. Brabec, *Prog. Nucleic Acid Res. Mol. Biol.*, 2002, 71, 1–68.

8 B. M. Zeglis, V. C. Pierre and J. K. Barton, *Chem. Commun.*, 2007, 4565–4579, DOI: 10.1039/b710949k.

9 C. Gaiddon, P. Jeannequin, P. Bischoff, M. Pfeffer, C. Sirlin and J. P. Loeffler, *J. Pharmacol. Exp. Ther.*, 2005, 315, 1403–1411.

10 R. L. Hayward, Q. C. Schornagel, R. Tente, J. S. Macpherson, R. E. Aird, S. Guichard, A. Habtemariam, P. Sadler and D. I. Jodrell, *Cancer Chemother. Pharmacol.*, 2005, 55, 577–583.

11 K. S. Smalley, R. Contractor, N. K. Haass, A. N. Kulp, G. E. Atilla-Gokcumen, D. S. Williams, H. Bregman, K. T. Flaherty, M. S. Soengas, E. Meggers and M. Herlyn, *Cancer Res.*, 2007, 67, 209–217.

12 X. Meng, M. L. Leyva, M. Jenny, I. Gross, S. Benosman, B. Fricker, S. Harlepp, P. Hebraud, A. Boos, P. Wlosik, P. Bischoff, C. Sirlin, M. Pfeffer, J. P. Loeffler and C. Gaiddon, *Cancer Res.*, 2009, 69(13), 5458–5466.

13 V. Vidimar, X. Meng, M. Klajner, C. Licona, L. Fetzer, S. Harlepp, P. Hebraud, M. Sidhoum, C. Sirlin, J. P. Loeffler, G. Mellitzer, G. Sava, M. Pfeffer and C. Gaiddon, *Biochem. Pharmacol.*, 2012, 84, 1428–1436.

14 K. Suntharalingam, T. C. Johnstone, P. M. Bruno, W. Lin, M. T. Hemann and S. J. Lippard, *J. Am. Chem. Soc.*, 2013, 135, 14060–14063.

15 W. H. Ang, A. De Luca, C. Chapuis-Bernasconi, L. Juillerat-Jeanneret, M. Lo Bello and P. J. Dyson, *ChemMedChem*, 2007, 2(12), 1799–1806.

16 S. J. Dougan, A. Habtemariam, S. E. McHale, S. Parsons and P. J. Sadler, *Proc. Natl. Acad. Sci. U. S. A.*, 2008, 105, 11628–11633.

17 B. Gava, S. Zorzet, P. Spessotto, M. Cocchietto and G. Sava, *J. Pharmacol. Exp. Ther.*, 2006, 317, 284–291.

18 M. Klajner, P. Hebraud, C. Sirlin, C. Gaiddon and S. Harlepp, *J. Phys. Chem. B*, 2010, 114, 14041–14047.

19 B. Boff, C. Gaiddon and M. Pfeffer, *Inorg. Chem.*, 2013, 52, 2705–2715.

20 R. Ceron-Camacho, D. Morales-Morales, S. Hernandez, R. Le Lagadec and A. D. Ryabov, *Inorg. Chem.*, 2008, 47, 4988–4995.

21 A. D. Ryabov, V. S. Soukharev, L. Alexandrova, R. Le Lagadec and M. Pfeffer, *Inorg. Chem.*, 2003, 42, 6598–6600.

22 A. D. Ryabov, V. S. Sukharev, L. Alexandrova, R. Le Lagadec and M. Pfeffer, *Inorg. Chem.*, 2001, 40, 6529–6532.

23 M. Klajner, C. Licona, L. Fetzer, P. Hebraud, G. Mellitzer, M. Pfeffer, S. Harlepp and C. Gaiddon, *Inorg. Chem.*, 2014, 53, 5150–5158.

24 V. Vidimar, C. Licona, R. Ceron-Camacho, E. Guerin, P. Coliat, A. Venkatasamy, M. Ali, D. Guenot, R. Le Lagadec, A. C. Jung, J. N. Freund, M. Pfeffer, G. Mellitzer,

G. Sava and C. Gaiddon, *Cancer Lett.*, 2019, 440–441, 145–155.

25 H. Rico Bautista, R. O. Saavedra Diaz, L. Q. Shen, C. Orvain, C. Gaiddon, R. Le Lagadec and A. D. Ryabov, *J. Inorg. Biochem.*, 2016, 163, 28–38.

26 R. O. Saavedra Diaz, R. Le Lagadec and A. D. Ryabov, *J Biol Inorg Chem*, 2013, 18, 547–555.

27 A. D. Ryabov, R. Le Lagadec, H. Estevez, R. A. Toscano, S. Hernandez, L. Alexandrova, V. S. Kurova, A. Fischer, C. Sirlin and M. Pfeffer, *Inorg. Chem.*, 2005, 44, 1626–1634.

28 L. Fetzer, B. Boff, M. Ali, M. Xiangjun, J. P. Collin, C. Sirlin, C. Gaiddon and M. Pfeffer, *Dalton Trans.*, 2011, 40, 8869–8878.

29 S. A. Oakes, *Am. J. Physiol.: Cell. Physiol.*, 2017, 312, C93–C102.

30 F. Sohm, C. Gaiddon, M. Antoine, A. L. Boutillier and J. P. Loeffler, *Oncogene*, 1999, 18, 2762–2769.

31 S. Job, A. de Reynies, B. Heller, A. Weiss, E. Guerin, C. Macabre, S. Ledrappier, C. Bour, C. Wasylyk, N. Etienne-Selloum, L. Brino, C. Gaiddon, B. Wasylyk and A. C. Jung, *Cancers*, 2019, 11(6), pii: E795.

32 S. G. Aller, J. Yu, A. Ward, Y. Weng, S. Chittaboina, R. Zhuo, P. M. Harrell, Y. T. Trinh, Q. Zhang, I. L. Urbatsch and G. Chang, *Science*, 2009, 323, 1718–1722.

33 P. Szewczyk, H. Tao, A. P. McGrath, M. Villaluz, S. D. Rees, S. C. Lee, R. Doshi, I. L. Urbatsch, Q. Zhang and G. Chang, *Acta Crystallogr., Sect. D: Biol. Crystallogr.*, 2015, 71, 732–741.

34 P. H. Palestro, L. Gavernet, G. L. Estiu and L. E. Bruno Blanch, *BioMed Res. Int.*, 2014, 2014, 358425.

35 N. Graf and S. J. Lippard, *Adv. Drug Delivery Rev.*, 2012, 64, 993–1004.

36 M. J. Chow, C. Licona, G. Pastorin, G. Mellitzer, W. H. Ang and C. Gaiddon, *Chem. Sci.*, 2016, 7, 4117–4124.

37 A. Nagelkerke, J. Bussink, F. C. Sweep and P. N. Span, *Biochim. Biophys. Acta*, 2014, 1846, 277–284.

38 R. Roskoski Jr., *Pharmacol. Res.*, 2019, 139, 395–411.

39 S. Dilruba and G. V. Kalayda, *Cancer Chemother. Pharmacol.*, 2016, 77, 1103–1124.

40 C. Gaiddon, M. de Tapia and J. P. Loeffler, *Mol. Endocrinol.*, 1999, 13, 742–751.

41 C. Bourdillon, C. Demaille, J. Moiroux and J.-M. Saveant, *J. Am. Chem. Soc.*, 1993, 115, 1–15.

42 M. Dequaire, B. Limoges, J. Moiroux and J. M. Saveant, *J. Am. Chem. Soc.*, 2002, 124, 240–253.

43 V. G. Prabhu, R. Zarapkar and R. G. Dhaneshwar, *Electrochim. Acta*, 1981, 26, 725.

44 H. B. Dunford, *Heme peroxidases*, John Wiley, New York, 1999.

45 A. D. Ryabov, R. Ceron-Camacho, O. Saavedra-Diaz, M. A. Denardo, A. Ghosh, R. Le Lagadec and T. J. Collins, *Anal. Chem.*, 2012, 84, 9096–9100.

46 S. Benosman, I. Gross, N. Clarke, A. G. Jochemsen, K. Okamoto, J. P. Loeffler and C. Gaiddon, *Cell Death Differ.*, 2007, 14(12), 2047–2057.

5.3. APPENDIX 3 : A redox ruthenium compound directly targets PDH2 and inhibits the HIF1 pathway to reduce tumor angiogenesis independently of p53

Original Articles

A redox ruthenium compound directly targets PHD2 and inhibits the HIF1 pathway to reduce tumor angiogenesis independently of p53

Vania Vidimar[a,c,1], Cynthia Licona[a], Ricardo Cerón-Camacho[d], Eric Guerin[a], Pierre Coliat[a,e], Aina Venkatasamy[a,f], Moussa Ali[b], Dominique Guenot[g], Ronan Le Lagadec[d], Alain C. Jung[a,e], Jean-Noel Freund[g], Michel Pfeffer[b], Georg Mellitzer[a,e], Gianni Sava[c], Christian Gaiddon[a,e,*]

[a] Université de Strasbourg, Inserm IRFAC UMR_S1113, Laboratory Stress Response and Innovative Therapy « Streinth », Strasbourg, 67200, France
[b] UMR 7177 CNRS, Université de Strasbourg, Institut de Chimie, Strasbourg, France
[c] University of Trieste, Department of Life Sciences, Callerio Foundation Onlus, Trieste, Italy
[d] Instituto de Química, UNAM, Circuito Exterior S/n, Ciudad Universitaria, México, D. F. 04510, Mexico
[e] CLCC Paul Strauss, Strasbourg, France
[f] Radiology Department, Hautepierre University Hospital, Strasbourg, France
[g] Université de Strasbourg, Inserm IRFAC UMR_S1113, Laboratory Stem Cell Emergence and Tumor Initiation "SETI", Strasbourg, 67200, France

ABSTRACT

Targeting specific tumor metabolic needs represents an actively investigated therapeutic strategy to bypass tumor resistance mechanisms. In this study, we describe an original approach to impact the cancer metabolism by exploiting the redox properties of a ruthenium organometallic compound. This organometallic complex induced p53-independent cytotoxicity and reduced size and vascularization of patients-derived tumor explants that are resistant to platinum drugs. At the molecular level, the ruthenium complex altered redox enzyme activities and the intracellular redox state by increasing the NAD+/NADH ratio and ROS levels. Pathway analysis pointed to HIF-1 as a top deregulated metabolite pathway. Unlike cisplatin, treatment with the ruthenium complex decreased HIF1A protein levels and expression of HIF1A target genes. The rapid downregulation of HIF1A protein levels involved a direct interaction of the ruthenium compound with the redox enzyme PHD2, a HIF1A master regulator. HIF1A inhibition led to decreased angiogenesis in patient-derived xenografted using fragments of primary human colon tumors. Altogether, our results show that a ruthenium compound impacts metabolic pathways acting as anticancer agents in colon cancer via an original mechanism of action that affects redox enzymes differently than platinum-based drugs.

1. Introduction

The tumor microenvironment is one of the most important determinants of cancer progression together with the accumulation of intrinsic molecular alterations, such as mutations in the p53 tumor suppressor gene [1]. In recent years, multiple studies have highlighted that cancer cells have different metabolic profiles due to the poorly irrigated tumor by blood vessels and reduced oxygenation. To survive, cancer cells shift from oxidative toward glycolytic metabolism [1]. Several molecular mechanisms ensure this shift, such as the HIF1/VEGF and mTOR pathways that respond to reduction in oxygen and other nutrients, and reprogram the cancer cell metabolism by impacting the activity of metabolic redox enzymes [2]. Thus, small molecules (e.g.

rapamycin), or monoclonal antibodies (e.g. anti-VEGF) have been developed to target these pathways. Although these therapies have achieved improvements, clinical data indicate drawbacks mostly linked to their ability to target a single molecule. This limits their use only to a subset of cancers presenting a particular molecular signature, thus favoring the development of resistance by clonogenic expansion [3]. As a consequence, scientists remain challenged to develop new specific drugs directed against novel targets. A complementary and attractive strategy would be to identify anticancer candidates that simultaneously target several key components of the cancer metabolism in order to slow down the development of resistance mechanisms in cells deprived of the drug's single target.

Since the discovery of cisplatin, metal-based drugs turned out to be

---

one of the most active fields in antitumor chemotherapy research. Platinum derivatives exert their cytotoxic properties through the formation of DNA adducts, which activate several signaling transduction pathways leading to cell growth arrest or cell death [4]. This poor selectivity is mostly responsible for the side effects of platinum drugs, such as neurotoxicity [5,6]. Furthermore, tumor cell resistances due to mutations in key signaling pathways, such as in p53, limit their use [7].

Ruthenium complexes have been intensively investigated as potential alternative because of the interesting chemical properties of ruthenium: (a) the availability of 6 coordination sites leading to multiple combinations of ligands, (b) a slow rate of ligand exchange, compatible with a reasonable stability in a biological context and (c) a broad range of redox potentials allowing a potential interference with biological macromolecules [8,9]. Therefore, various structures of ruthenium derivatives have been tested *in vivo* and they seem to offer promising anticancer activities, especially against cisplatin-resistant tumors or even anti-metastatic activity, while presenting a general lower toxicity on healthy tissues compared to cisplatin [8–17]. To date, two ruthenium complexes, namely NAMI-A and KP1019, have entered clinical trials [18].

Even though ruthenium-based compounds have already been tested in humans and largely studied in pre-clinical *in vitro* models, their mode of action remains unclear and most likely involves multiple cellular targets. Indeed, some ruthenium compounds bind DNA, although quite differently from cisplatin [19,20] [21-26]. However, the presence of ruthenium confers also a specific range of redox potentials to the compounds that correlates with their cytotoxicity, and that allows them to be efficient mediators of electron transfer to or from oxidized or reduced active sites of redox enzymes thereby affecting their activity [27–29]. As such, ruthenium derivatives can interact with glutathione (GSH) [30], leading to GSH depletion and increased sensitivity to reactive oxygen species (ROS) [31].

To gain a better understanding of the molecular pathways impacted by ruthenium complexes, we investigated further the mode of action of one of these molecules, RDC11 (ruthenium derived compound 11), which is an organoruthenium compound characterized by a covalent bond between the ruthenium atom and a carbon of a phenylpyridine. RDC11 previously showed interesting anticancer activity *in vivo* in syngeneic models [25,26]. In addition, RDC11 interacts with DNA less efficiently than cisplatin while having a higher cytotoxicity, suggesting that target(s) other than DNA are involved in the ruthenium complexes' cytotoxicity against tumor cells [25,26]. To further understand the signaling pathways involved we performed a transcriptomic approach showing that multiple mechanisms were affected differently than with cisplatin, in particular epigenetic modulators [32]. However, our unsupervised pathway analyses pointed towards additional pathways deregulated by RDC11 treatment, in particular metabolic pathways, suggesting a multimodal mechanism of action. Therefore, we hypothesized that the ability of redox ruthenium-based molecules to interfere with redox enzymes might affect intracellular signaling pathways that are sensitive to the cell metabolism. Hence, we decided to focus on the regulation of one of these pathways, the HIF1 (Hypoxia Inducible Factor 1) pathway, which is strongly connected to the adaptive metabolic response of cancer cells to the hypoxia developing in poorly vascularized tumors [2]. In the current study, we show that alterations of the HIF1 pathway by an organoruthenium compound is an effective strategy to disrupt cancer metabolism and a novel way to bypass mechanisms responsible for platinum drugs' resistance.

2. Materials and methods

2.1. Chemicals

Ruthenium derived compounds were synthesized as previously described [21,28]. Cisplatin was purchased from Mylan Pharmaceuticals, Deferoxamine Mesylate from Sigma-Aldrich® and MG132 from

Calbiochem. ALLM, ALLN and Z-VAD-FMK were obtained from Tocris Bioscience. Glucose oxidase from *Aspergillus niger* was obtained from Sigma (211 U mg^{-1}), and D-glucose was obtained from Acros.

2.2. Cell culture, MTT (3-(4,5-dimethylthiazol-2-yl)-2,5-diphenyltetrazolium bromide) test and NCI IG$_{50}$

Human colorectal adenocarcinoma HCT116 and SW480 cells, obtained from ATCC, were maintained at 37 °C in normoxic (20% O_2, 5% CO_2) or hypoxic (94% N_2, 5% CO_2, 1% O_2, Tri-Gas Incubator, Sanyo) conditions in DMEM, 1 g/L glucose (Dulbecco's modified Eagle's medium; Life Technology), supplemented with 10% fetal calf serum (Life Technology), penicillin/streptomycin (100 UI/mL – 100 μg/ml) and gentamycin (50 mg/mL). HUVEC (Human Umbilical Vein Endothelial Cells, ATTC) were grown in Endothelial Cell Basal Media from Cambrex, supplemented with L-glutamine and 10% FBS. Cell lines are every 6 months tested for mycoplasmas (MycoTOOL, Roche) and are not maintained more than 20 passages. MTT test was performed using 96-well culture plates (Costar) [33]. NCI renamed the IC$_{50}$ into the GI$_{50}$, the concentration that causes 50% growth inhibition, to emphasize the correction for the cell count at time zero; thus, GI$_{50}$ is the concentration of test drug where $100 \times (T-T0)/(C-T0) = 50$ (dtp.cancer.gov/databases_tools/docs/compare/compare_methodology.htm#specon).

2.3. Ruthenium complex-matrix affinity precipitation

Cells were grown in 10 cm plates. Precipitations were performed as previously described [6]. Cells were lysed in 1 mL of NP40 lysis Buffer 1X (125 mM Tris–HCl, pH 6.7, containing 0.1% NP40, 10% glycerol, 150 mM NaCl). Equal amounts of total-protein extracts (3 mg) were incubated for 5 h with 100 μL of 50% slurry RDC11-matrix beads. After 4 washes in NP40 lysis buffer, complexes were either boiled or eluted using RDC11 (5 μM) or cisplatin (5 μM). PHD2 was then detected by Western blot. Matrix-RDC11 was synthesized attaching RDC11 onto a Hypogel 400-COOH (Sigma). Successful synthesis was assessed by spectroscopy.

### 2.4. Quantitative reverse transcription-PCR (RT-qPCR)

Gene expression was assessed by qPCR using *18S* as the normalizing gene [5]. Total RNA was isolated with TRIzol reagent (Invitrogen). RNA was quantified using a Nanodrop 2000 Spectrophotometer (Thermo Scientific) and cDNA synthesized from 1 μg total RNA using the iScript cDNA synthesis kit (Bio-Rad Laboratories). qPCR was performed in Bio-Rad iCycler thermal cycler using iQ SYBR Green supermix (Bio-Rad Laboratories). Specificity of the amplification was assessed by performing a melting curve analysis. Nucleotide sequences of the primers are indicated in supplementary material and methods.

2.5. Intracellular reactive oxygen species (ROS) measurement

5-(and-6)-carboxy-2',7'-dichlorodihydrofluorescein diacetate (carboxy-H2DCFDA) (Molecular Probes) was used to detect intracellular ROS levels according to the manufacturer's instructions and as previously described [34]. For ROS quantification, cells were seeded in 96-well black plates (Greiner Bio-One) and treated with RDC. Afterwards, cells were washed with PBS and incubated with 10 μM carboxy-H2DCFDA in DPBS for 1 h. Cells were then washed with PBS and fluorescence was measured by a plate reader (Perkin Elmer) with an excitation wavelength of 485 nm and an emission wavelength of 535 nm.

2.6. Clonogenic assay

Cells were transfected by control siRNA or HIF1A-directed siRNA
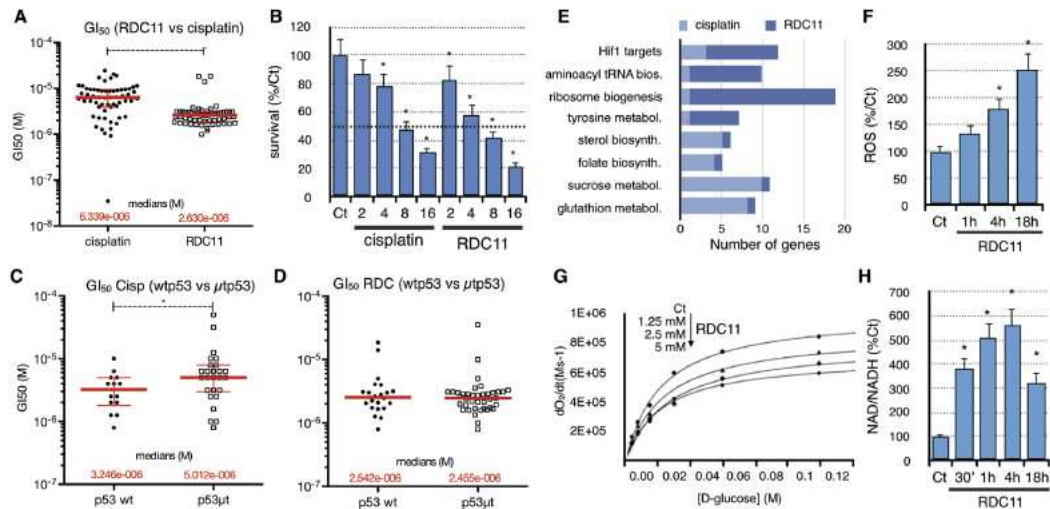
Fig. 1. An organoruthenium compound induces cytotoxicity and regulates cellular metabolism independently of p53.
A, Growth inhibition (GI) caused by the organoruthenium compound and cisplatin on the 60-cancer cell line panel of the NCI. Median GI_{50} (dose for growth inhibition of 50%) for all NCI cell lines is indicated. * indicate $p < 0.05$ as calculated by t-test.
B, Survival dose response of HCT116 colon cancer cells upon of RDC11 and cisplatin treatment. Cells were treated for 48 h at the indicated concentrations (μM) of cisplatin and RDC11 at confluence. Cell viability was determined using the MTT test. Bars are means and asterisks indicate statistically significant difference (* = p = 0.001) compared to control, as calculated by a One-Way ANOVA test followed by a Tukey post-test over the three independent experiments.
C, D, Growth inhibition (GI) caused by the organoruthenium compound and cisplatin on the 60-cancer cell line panel of the NCI classified by expression of wild-type (p53 wt) or mutated (p53 μt) p53 protein. * indicate $p < 0.05$ as calculated by t-test.
E, Graphs represents number of genes in the indicated pathways that are regulated by RDC11 and cisplatin at 24 h. Microarray data were analyzed using AltAnalysis and R bioinformatics tools to identify in KEGG, Gene Ontology, miRNA, transcription factors databanks, the signaling pathways and mechanisms corresponding to the mis-regulated genes.
F, Production of radical oxygen species (ROS) in HCT116 cells treated with RDC11. HCT116 cells grown on coverslips coated with polyornithine were treated with RDC11 (RDC, 5 μM) for the indicated time and labelled with carboxy-H2DCFDA. Fluorescence was quantified with a fluorimeter. Bars are mean and asterisks indicate statistically significant difference ($p < 0.01$) compared to control, as calculated by a one-way ANOVA test followed by a Tuckey post-test over the three independent experiments.
G, RDC11 increases the NAD+/NADH ratio. 2×10^5 HCT116 cells were treated with RDC11 (5 μM) for the indicated time. NAD+ and NADH were subsequently quantified following the manufacturer's protocol **(Supplementary materials and methods)**. Both NAD+ and NADH were calculated from a standard curve (*** = p < 0.001; One-Way ANOVA + Tukey post-test).
H, Measure of O_2 consumption by glucose oxidase in presence of RDC11. Purified glucose oxidase was incubated with increased concentration of glucose and RDC11 (1.25, 2.5 and 5 mM). O_2 was measured using a Clarke electrode and represented as $dO_2/dt(Ms-1)$.

(50 nM, Qiagen™, USA) for 48 h using RNAiMax (Invitrogen™, USA). Cells were then harvested and diluted after treatment, and either 100 or 200 cells were seeded in 6-well microplates. They were then cultured for 12 days, and clones were stained with a methylene blue solution. Surviving positive clones, defined as clones composed of > 50 cells were counted. The plating efficiency (PE) was determined from the number of positive clones obtained when cells were not treated. The percentage of surviving clones in other experimental conditions was calculated by normalizing the number of positive clones with respect to the PE.

2.7. Measure of purified PHD2 activity

Biotinylated peptides derived from the HIF1A Oxygen dependent degradation domain (ODDD: Biotin-DLDLEALAPYIPADDDFQL) were immobilized on NeutrAvidin-coated 96-well plated. 50 ng of purified PHD2 enzyme (Recombinant Human EGLN1/PHD2 Protein; H00054583-P01, Novus Biological) was then incubated at 30 °C for 1 h in a reaction buffer containing 40 mmol/L Tris–HCl, pH 7.4, 4 mmol/L 2-oxoglutarate, 1.5 mmol/L FeSO4, 10 mmol/L KCl, and 3 mmol/L MgCl2 in absence or presence of the ruthenium complexes, deferoxamine or cisplatin [35]. Peptide hydroxylation was detected using a polyclonal rabbit antibody raised against a hydroxylated HIF1A (D43B5, Cell Signaling), followed by addition of a goat anti-rabbit HRP-conjugated secondary antibody.

2.8. In vitro angiogenesis

The anti-angiogenic activity was studied by looking at the generation of a capillary-like network by HUVECs. Briefly, 96-well plates were coated with ECMatrix™ (Millipore) which was allowed to polymerize at 37 °C for 45 min. 5000 cells were then seeded in 200 μL of medium into each well. 1 h later, cells were treated with 200 μL of medium containing cisplatin or RDC11. After 4 h, cells were photographed and tube formation or intersections between cells were scored manually and expressed relative to controls.

2.9. In vivo angiogenesis plug assay

C57BL/6 female mice (6 weeks old) were injected subcutaneously with 600 μl of cold liquid phenol-red free Matrigel (BD Bioscience) supplemented with VEGF (36ng/Matrigel plug; PeproTech), heparin (12 U/Matrigel plug; Sigma), TNF-α (0.72 ng/Matrigel plug; PeproTech), PBS (for controls) or RDC11 (5 μM), near the abdominal
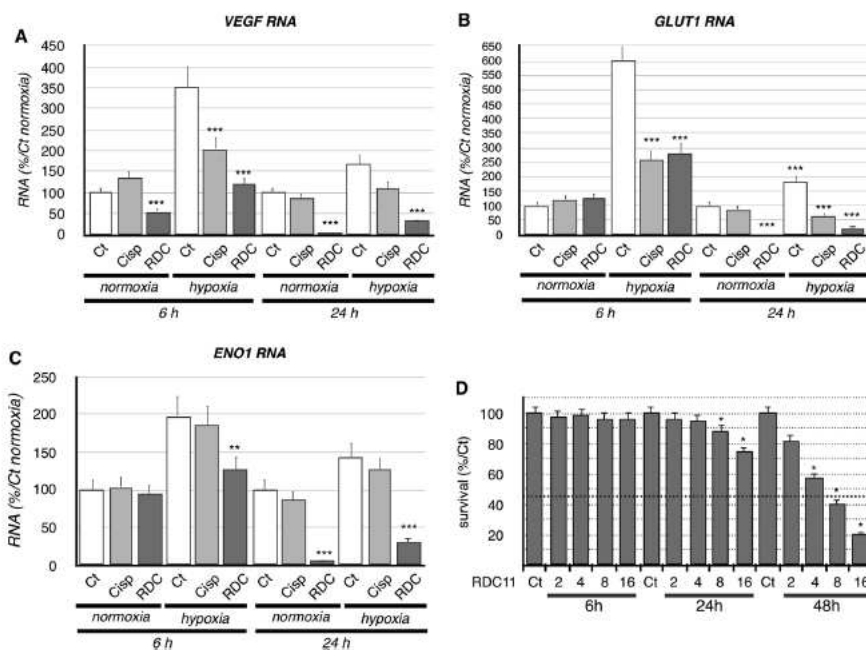
Fig. 2. RDC11 reduces expression of HIF1A target genes.

A–C, HCT116 cells were treated with 5 μM of cisplatin or 5 μM of RDC11 for the indicated time in normoxic (20% O_2) or hypoxic (1% O_2) conditions. RT-qPCR was performed using primers for *VEGF* (A), *GLUT1* (B), *ENO1* (C), and *18S* as housekeeping gene. Data represent relative change in the expression of the different genes in comparison with untreated cells (Ct) and were normalized with *18S*. Columns, means of triplicates; bars, SD. Asterisks indicate statistically significant difference (*** = $p < 0.001$; ** = $p < 0.01$; * = $p < 0.05$) compared to control, as calculated by a One-Way ANOVA test followed by a Tukey post-test over the three independent experiments.

D. Survival dose response of HCT116 colon cancer cells upon of RDC11 treatment. Cells were treated for the indicated time at the indicated concentrations (μM) of RDC11. Cell viability was determined using the MTT test. Bars are means and asterisks indicate statistically significant difference (* = $p < 0.001$) compared to control, as calculated by a One-Way ANOVA test followed by a Tukey post-test over the three independent experiments.

midlines and at the base of the neck. After 4 days, mice were sacrificed and the Matrigel plugs explanted. Matrigel plugs were subsequently washed with PBS, photographed and then weighed. Their hemoglobin content was evaluated with the Drabkin's reagent kit according to the manufacturer's instructions (Sigma).

2.10. In vivo angiogenesis in human xenografted colon tumors

Fragment of a surgical piece of a human colon tumor was subcutaneously implanted and amplified in nude mice. Pre-amplified tumors were extracted and homogenized prior to implantation into novel nude mice. Two homogenous tumor samples (100 μL) were implanted subcutaneously at each side of mice back. Treatments were started once tumors reached 100 mm³ of volume. Tumor volumes and mouse weights were monitored twice a week. Vascularization was monitored by the hemoglobin content measurement by a colorimetric assay and the expression of HIF1 target genes by RT-qPCR. Experiments were conducted in compliance with the French Animals Committee guidelines for the welfare of animals in experimental procedures and approved by a regional ethical review committee.

3. Results

3.1. The organoruthenium compound RDC11 alters redox enzyme activity and metabolic pathways independently of p53

We assessed the activity of the organoruthenium compounds RDC11 on the NCI-60 human tumor cell lines panel (Fig. 1A, Supplementary Table S1). GI$_{50}$, which corresponds to the concentration that inhibit 50% of cell growth as measured by the NCI was used to compared the activity between compounds. We found that the activity of RDC11 (median GI$_{50}$ = 2.63 μM) is higher than that of cisplatin (median GI$_{50}$ = 6.339 μM). A typical difference of the response between cisplatin and RDC11 is shown in the colon cancer cell line HCT116 in Fig. 1B. Importantly, unlike cisplatin, the activity of RDC11 was not affected by the presence of p53 mutations (Fig. 1C and D). This result was confirmed using siRNA against p53 and HCT116 cells in which p53 was deleted [21], which did not alter RDC11 cytotoxic activity (Supplementary Figs. S1C and D). In addition, RDC11 displayed anticancer activity in several different colon cancer cell lines (Supplementary Table S2), while presenting a reduced cytotoxicity on healthy cells (Supplementary Figs. S1A and B).

To identify signaling pathway deregulated by RDC11, we performed an unbiased wide transcriptomic experiment followed by bioinformatics pathway analysis [32]. Amongst the deregulated pathways, several cellular metabolic pathways were present (Fig. 1E). Interestingly, RDC11 and cisplatin displayed different alterations of these

pathways. Notably, RDC11 inhibited the expression of genes regulated by the HIF1 pathway unlike cisplatin (Supplementary Tables S3–5). Interestingly, on HCT116 human colon cancer cells, RDC11 increased the levels of reactive oxygen species (ROS) (Fig. 1F). Use of ROS chelators (NAC: N-acetyl-cysteine) reduced slightly the cytotoxicity of RDC11 (Supplementary Fig. S2C). RDC11 also produced a rapid increase in NAD + levels over NADH (Fig. 1H). Similar results were obtained in SW480 colon cancer cells (Supplementary Figs. S2A and B). The ratio NAD/NADH is of importance in controlling the activity of cellular enzymes critical for cancer development, such as PARP and SIRT [36]. These changes in metabolic markers, suggested that RDC11 has the ability to impact on redox enzymes, as previously described for other complexes [29]. Therefore, we used Clarke electrodes to follow O_2 consumption by the redox enzyme glucose oxidase in presence of increased concentration of glucose and RDC11 (Fig. 1G, Supplementary Fig. S1E). We found that increasing quantity of RDC11 reduced the activity of the glucose oxidase redox enzyme. Taken together, these data suggested that treatment with RDC11 affected the cellular metabolism and the HIF1 pathway.

3.2. Platinum and ruthenium compounds differently impact the HIF1 pathway

HIF1 is a transcription factor composed of two subunits: the constitutively expressed β subunit (HIF1B) and the highly regulated α subunit (HIF1A) [37]. The unsupervised pathway analysis identified the HIF1 pathway as deregulated based on change in the expression of several of its targets genes: VEGFA, GLUT1 (SLC2A1), PSD3, KLF6, NRN1, P4HA2, EGLN3, ENO1, TSC22D (Fig. 1E; Supplementary Table S3). The unsupervised pathway analysis did not identify the HIF1A pathway as deregulated under the cisplatin condition. However, 3 of these genes were also downregulated by cisplatin but with a lower intensity - P4HA2, VEGFA, GLUT1. Because VEGF, involved in angiogenesis, and GLUT1 and ENO1, involved in glucose metabolism are hallmarks of an HIF1A response [38] and resulted in their downregulation by RDC11 in the transcriptomic analysis, we further analyzed their expression. As expected, hypoxia increased the expression of these HIF1 target genes (Fig. 2A–C). After 24 h of treatment, the RDC11 drastically reduced the mRNA level of all 3 genes, both in normoxia and hypoxia. This negative effect was already detected after 6 h. Although cisplatin was able to reduce VEGF and GLUT1 levels in hypoxia, it was clearly less effective than RDC11. Similar results were obtained with additional HIF1A target genes at the mRNA level and the protein level (Supplementary Figs. S3A and B). Importantly, the inhibition of the HIF1 target genes by RDC11 was also observed in the SW480 cells that harbor a mutated p53 protein (p53R273H/P309S). To note, the loss of gene expression was not due to cellular loss/cytotoxicity as we normalized our experiments toward total RNA and reference genes. Furthermore, at 6 h and 24 h there was no significant cytotoxicity detected (Fig. 2D). Altogether, these data indicated that RDC11 was more potent than cisplatin to reduce the activity of HIF1 target gene in colon cancer cells via a p53 independent pathway.

We then monitored the protein levels of HIF1A and HIF1B subunits in HCT116 and SW480 colon cancer cells under the same conditions. As expected HIF1A was not expressed (SW480 cells) or only expressed at low levels (HCT116 cells) in the normoxia condition, due to its O_2-dependent prolyl-hydroxylation with subsequent ubiquitination and proteasomal degradation (Fig. 3A and B). RDC11, unlike cisplatin, strongly reduced HIF1A protein levels in hypoxia in both cell lines and also in normoxia in HCT116 cells, after 6 and 24 h of treatment. HIF1B was constitutively expressed and RDC11 lowered its expression especially after 24 h of treatment in normoxia and hypoxia in both HCT116 and SW480 cells. This inhibition of HIF1A protein level might explain at least in part the cytotoxic activity of the ruthenium compound as the silencing of HIF1A decreased cell survival (Fig. 3C). Inversely, overexpression of HIF1A reduced RDC11 cytotoxicity (Supplementary Fig.
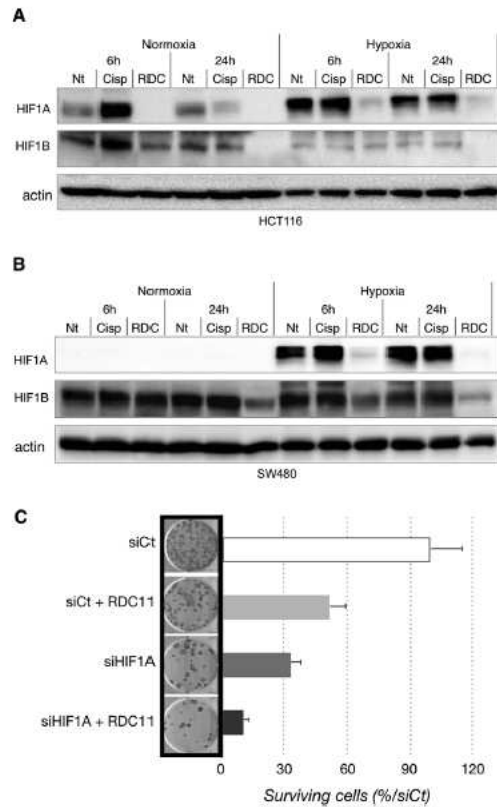

Fig. 3. RDC11 reduces protein levels of HIF1A.
A, B, Western blot analysis of HCT116 (A) and SW480 (B) colorectal cancer cells treated with 5 μM of cisplatin or 5 μM of RDC11 for the indicated time in normoxic (20% O_2) or hypoxic (1% O_2) conditions. Immunoblotting was performed with anti-HIF1A, anti-HIF1B and anti-actin antibodies (Supplementary materials and methods). C, HIF1A silencing reduces cell survival and co-operates with RDC11 cytotoxicity. Graphical representation of a clonogenic survival assay of cancer cells that were treated with 0.5 μM RDC11, with an anti-HIF1A siRNA, or with a combination of both molecules. Non-treated cells, as well as cells transfected with a non-specific scramble siRNA were used as negative controls. The percentage of surviving clones in other experimental conditions was calculated by normalizing the number of positive clones with respect to the PE. Pictures showing representative examples of clonogenic survival assays corresponding to each condition are shown left to the graph.

S2D).

Additionally, RT-qPCR analyses showed that RDC11 was able to strongly reduce HIF1A and HIF1B mRNA after 24 h of treatment in HCT116 cells, which is consistent with its drastic effect on HIF1 protein levels (Supplementary Fig. S3C). However, the lower reduction of HIF1A and HIF1B mRNA observed 6 h after RDC11 treatment suggests the existence of other mechanisms (i.e. independent of mRNA synthesis and degradation) that can contribute to the rapid and dramatic loss of HIF1A protein levels.
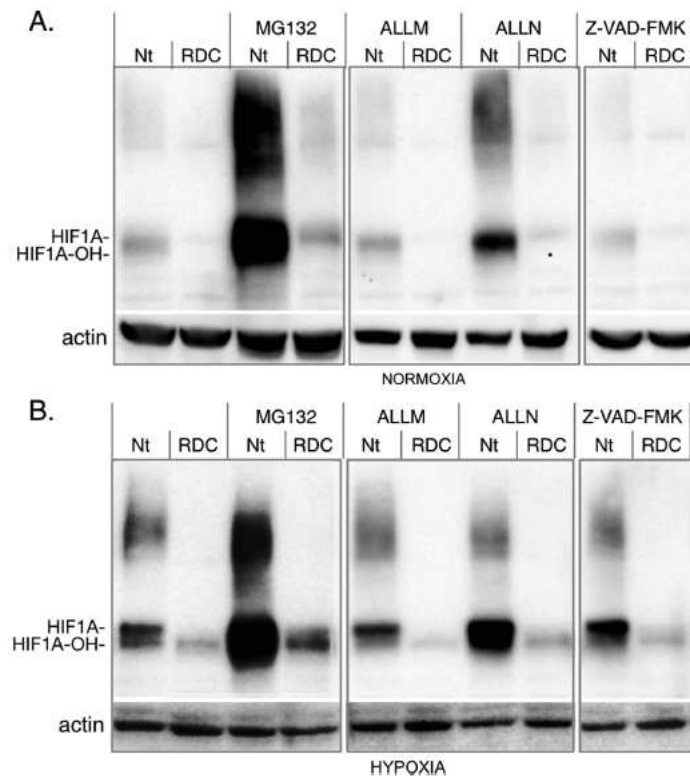
Fig. 4. HIF1A protein reduction involves only partly protease-dependent degradation.
A, B, Western blot analysis of HCT116 colorectal cancer cells treated with 5 μM of RDC11 for 6 h in normoxic (A, 20% O_2) or hypoxic (B, 1% O_2) conditions, in absence or in presence of the indicated protease inhibitors (MG132, 10 μM; ALLM, 10 μM; ALLN, 10 μM; Z-VAD-FMK, 20 μM). Immunoblotting was performed with anti-HIF1A and anti-actin antibodies. Note the presence of two bands for HIF1A, the upper band that correspond to the non-hydroxylated form and the lower band that is the hydroxylated form.

3.3. The ruthenium complex reduces HIF1A protein levels through multiple mechanisms

Degradation of HIF1A by the proteasome after hydroxylation by the iron-containing PHD2 enzyme is one of the important mechanisms regulating its cellular levels [37]. Thus, we assessed whether RDC11 was still able to reduce HIF1A protein levels in the presence of MG132, a potent and reversible proteasome inhibitor. As expected, in absence of RDC11, the MG132 treatment clearly stabilized HIF1A proteins (Fig. 4A and B). Strikingly, the accumulation of HIF1A induced by MG132 was also detected, although to a much lower extent, in the presence of RDC11, both in normoxia and hypoxia. In addition, RDC11 favored the accumulation of hydroxylated HIF1A in hypoxia conditions, suggesting that RDC11 promoted the activity of the hydroxylases such as PHD2. Indeed, *in vitro* treatment of cell extracts with RDC11 stimulated hydroxylation of an HIF1A peptide encompassing the oxygen-dependent degradation domain [39] (Supplementary Fig. S5A). In this assay, deferoxamine (DFO) and inhibitor of PHD2 (N-oxal) reduced the RDC11-dependent hydroxylation of the HIF1A peptide, while cisplatin had no impact. Similar results were obtained with PHD2 siRNA (Supplementary Fig. 4). Altogether, these results indicated that RDC11 stimulated the degradation of HIF1A proteins through the proteasome, but it cannot completely account for the drastic reduction of HIF1A

protein levels, suggesting the involvement of other mechanisms.

3.4. The ruthenium complex interacts with the hydroxylase PHD2

RDC11 promoted the appearance of the hydroxylated form of HIF1A (lower band) during hypoxia (Fig. 4B), suggesting a possible involvement of the PHD2 hydroxylase. To investigate the direct interaction between PHD2 and RDC11, covalently attached RDC11 molecules onto a matrix (Hypogel 400) (RDC11-matrix) were incubated with cellular protein extracts. After several washes, proteins were detached by boiling or by competition with free RDC11 or cisplatin and separated on SDS-PAGE before immunoblotting for PHD2 detection (Fig. 5A). A naked matrix (Matrix-Ø) was used to assess the specificity of the interaction. Incubation of the cellular extracts with the RDC11-matrix pulled PHD2 down. The specificity of the interaction between RDC11 and PHD2 was confirmed by the absence of bands when the naked matrix was used or when proteins were eluted with cisplatin. This represents the first demonstration of a direct interaction between a ruthenium compound and a redox enzyme in cancer cells.

The iron chelator deferoxamine (DFO), which inhibits PHD enzymes, was used to further investigate the role of PHD2 in RDC11 regulation of HIF1A. As expected, DFO induced HIF1A stabilization through the accumulation of its non-hydroxylated form (upper band,

257
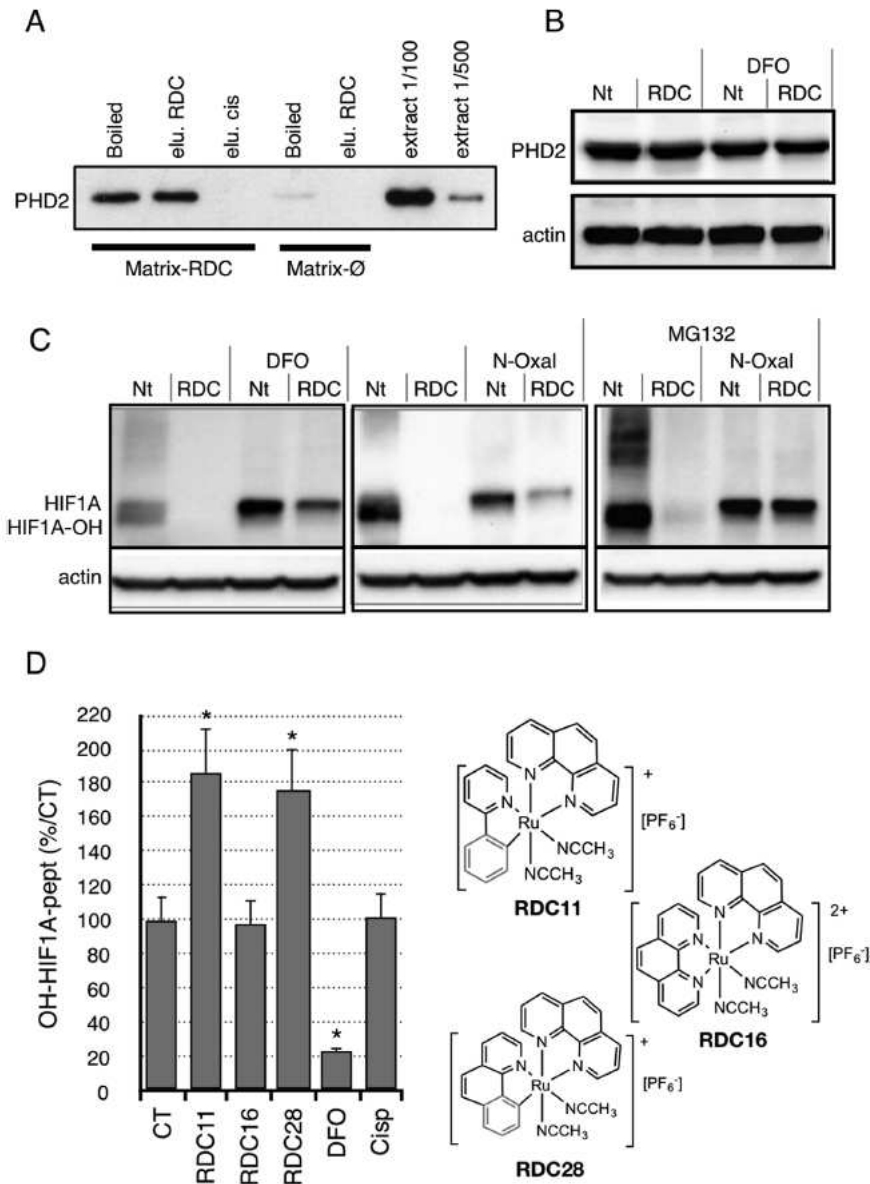
(caption on next page)

Fig. 5C). Upon PHD2 inhibition, RDC11 did not induce the appearance of the lower and hydroxylated band of HIF1A. Similarly, inhibition of PHD2 activity with its selective inhibitor N-oxalilglycine stabilized HIF1A with an accumulation of its non-hydroxylated form. In addition, RDC11 inhibited significantly less HIF1A protein level in both cases, indicating the partial dependence of RDC11 activity on PHD2 function. Although these data suggested that RDC11 might affect HIF1A

hydroxylation, RDC11 had no effect on PHD2 protein levels (Fig. 5B). In addition, the activity of purified PHD2 was increased by RDC11 treatment unlike cisplatin (Fig. 5D). Interestingly, another ruthenium complex with a similar structure (RDC28 [28]) also enhanced PHD2 activity, in contrast to a close structural variant lacking the carbon-ruthenium bond (RDC16 [40]). Hence, these results indicate that RDC11 directly interacts with PHD2 and that this function is important

Fig. 5. RDC11 interact with PHD2 and its activity is dependent upon PHD2 function.

A, HCT116 cells were lysed and 3 mg of protein extract was incubated with RDC11-matrix or empty matrix (Matrix-O) for each indicated condition. After 4 washes, protein complexes were detached by boiling (boiled) or competition with RDC11 (5 μM, elu. RDC11) or cisplatin (5 μM, elu cis). Proteins were then separated on SDS PAGE and immunoblotted with PHD2 antibody.

B, HCT116 cells were treated overnight with deferoxamine mesylate (DFO, 150 μM) to chemically induce hypoxia and subsequently for six hours with RDC11 5 μM. Western blot was done using anti-HIF1A and anti-actin antibodies.

C, HCT116 cells were treated overnight with 5 μM of RDC11 in normoxia (20% O_2) or in chemically-induced hypoxia using deferoxamine mesylate (DFO, 150 μM), or with MG132 10 μM). N-Oxalilglycine (8 μM) was used to inhibit PHD2. Western blot was performed using anti-HIF1A and anti-actin antibodies.

D, Purified PHD2 (50 ng) were incubated with Biotinylated peptides derived from the HIF1A Oxygen dependent degradation domain (ODDD: Biotin-DLDLEALAPYIPADDDFQL) immobilized on NeutrAvidin-coated 96-well plated. Reaction was performed in presence of the indicated compounds (5 μM, RDC11, RDC16, RDC28, Cisp; 150 μM: DFO) for 1 h. Peptide hydroxylation was detected using a polyclonal rabbit antibody raised against a hydroxylated HIF1A followed by addition of a goat anti-rabbit HRP-conjugated secondary antibody. Columns represent average of triplicates with error bars and * indicate p < 0.001 compared to control, as calculated by a One-Way ANOVA test followed by a Tukey post-test.
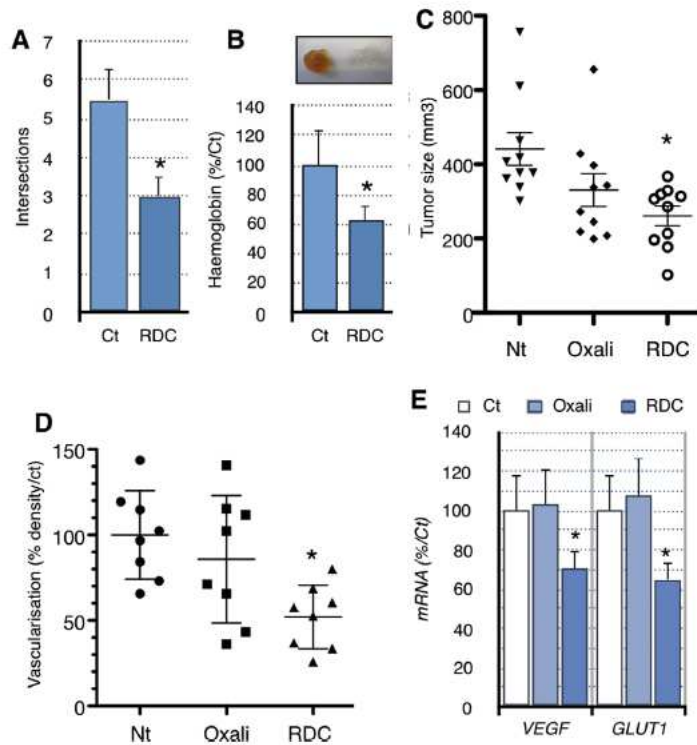

Fig. 6. RDC11 inhibits angiogenesis both *in vitro* and *in vivo*.

A, HUVECs were seeded on ECMatrix™ and 1 h later treated with RDC11 5 μM. After 4 h, cells were photographed and tube formation or intersections between cells were scored manually and expressed relative to controls. (** = p < 0.01; * = p < 0.05 vs Control; One-Way ANOVA + Tukey post-test).

B, C57BL/6 mice (6-week-old) were injected subcutaneously three times with 600 μl of cold liquid Matrigel supplemented with VEGF (36 ng/Matrigel plug), heparin (12 U/Matrigel plug), TNF-α (0.72 ng/Matrigel plug), PBS (for controls) or RDC11 (5 μM). After 4 days, mice were killed and the Matrigel plugs explanted. Quantification of the hemoglobin content was performed with the Drabkin's reagent kit.

C, D, E, pre-amplified homogenized fragments of human colon tumors were subcutaneously implanted in nude mice. Mice were treated with oxaliplatin (11 mole/Kg) or RDC11 (11 μmol/kg) twice a week once the tumor reached 100 mm³. The dose 11 μM/Kg corresponds to the MTD in nude mice. Tumor size was followed (D). Vascularization was estimated by colorimetric assay detection of hemoglobin (C) and expression of HIF-1 target genes (*vegf* and *glut1*) by RT-qPCR 21 days after the first treatment. Bars represented means ± standard deviations (n = 8; * = p < 0.05 vs Control; One-way ANOVA + Tukey post-test).

for RDC11-dependent downregulation of HIF1 protein levels.

3.5. The ruthenium complex reduces angiogenesis both in vitro and in vivo

HIF1A has a critical role in controlling angiogenesis [41]. *In vitro* tests showed that RDC11 was able to reduce the formation of intersections between HUVEC cells 4 h after treatment (Fig. 6A). To evaluate the effect of RDC11 on angiogenesis *in vivo*, we used an assay where angiogenesis was induced by different factors embedded in a Matrigel plug subcutaneously implanted in mice. Four days after implantation, the plugs were extracted and the degree of vascularization was evaluated by assessing the hemoglobin content. The Matrigel plugs containing RDC11 were nearly uncolored, while the control plugs were redder, sign of the presence of small blood-filled channels (Fig. 6B). Quantification of the hemoglobin content confirmed this difference. These results showed that RDC11 was able to exert an anti-angiogenic

effect both *in vitro* and *in vivo*.

RDC11 was active against the growth of primary human colon tumor fragments from a patient tissue xenografted in nude mice. The xenografted mice were treated with RDC11 (11 μmol/kg) or Oxaliplatin (11 μmol/kg). Tumors were analyzed 21 days after the first treatment to ensure the structural integrity of the tumors. RDC11 significantly reduced tumor size (± 45%) as compared to Oxaliplatin (Fig. 6C). We then analyzed the tumors for hemoglobin content and expression of HIF1A target genes (*VEGF* and *GLUT1*). Treatment of the tumors with RDC11 reduced both the vascularization and the expression of HIF1A target genes (Fig. 6D and E). The reduced vascularization was further confirmed by analyzing CD31 staining, a marker for angiogenesis (Supplementary Figs. S5B and C).

152

4. Discussion

The redox properties of ruthenium complexes have made them promising anticancer candidates and potential alternatives to platinum compounds. Indeed, instead of solely targeting DNA like platinum derivatives, ruthenium drugs have been shown to affect the intracellular redox state and activity of metabolic enzymes, which seems to correlate with their cytotoxicity [28] [42] [30] [31] [29]. However, the physiological relevance for their anticancer activity of the functional interaction between redox enzymes and ruthenium drugs is still largely unknown.

This is the first comprehensive study showing a direct link between alteration of redox enzymes by a ruthenium complex (RDC11) and the consequent impact on cancer cell metabolism and tumor growth *in vivo*. Here we demonstrate that the organoruthenium compound RDC11 alters the activity of two redox enzymes involved in the cellular metabolism, namely glucose oxidase and PHD2. Importantly, we report a physical interaction between PHD2 and RDC11 and how this alters PHD2 function, thus affecting the HIF1 pathway, a master regulator of cancer cell survival and tumor angiogenesis. The alteration of these redox enzymes correlates with an increase in ROS and NAD + metabolites. However, it is very likely that the cytotoxicity of RDC11 is not mediated solely by a specific impact on PHD2 and glucose oxidase, but rather on a variety of redox enzymes as well as other types of targets.

The alteration of the metabolism induced by RDC11 might be a direct reflection of the alteration of cellular redox enzymes that have a redox potential in the range of redox potential of the ruthenium compounds [42] [28]. Indeed, PHD2 activity was altered with ruthenium complexes containing a carbon-ruthenium bond and not with a structural equivalent lacking it. These complexes differ only by their redox potential. This multi-targeting property of RDC11 represents an advantage to avoid the development of resistance mechanisms as often seen for selective inhibitors. For instance, RDC11 retains its cytotoxicity on cancer cells that have mutated p53, suggesting that this activity does not depend on the p53 status, which has been recently shown to control cancer cell metabolism [43]. By avoiding the need of the p53 pathway, RDC11 retains its activity on cancer cells with mutated p53 proteins, which represent more than 50% of the tumors.

The RDC11-induced perturbation of the redox enzymes and cellular metabolism affected several metabolic signaling pathways, particularly the HIF1 pathway. Indeed, HIF1A protein levels were dramatically reduced by RDC11 both in normoxia and hypoxia. Interestingly, this effect of RDC11 was much more pronounced than that of cisplatin, pointing out that platinum- and ruthenium-based molecules act differently. The downregulation of both HIF1 subunits correlated with a decrease in the expression of several HIF1 target genes (i.e. *VEGF* and *GLUT1*) linked to angiogenesis or glucose metabolism. Interestingly, multiple studies highlight the role of HIF1 in cancer aggressiveness and platinum resistance [44]. Indeed, silencing of HIF1A decrease cell survival. Hence, the downregulation of HIF1 activity induced by the ruthenium compound might help to bypass tumor resistance and have a double impact on tumor growth by decreasing cancer cell survival and reducing angiogenesis. It is to note that despite inhibiting angiogenesis, RDC11 did not reduce metastasis formation when cancer cells were implanted in the tail's veins of mice (C. Gaiddon; unpublished observations). However, the downregulation of the HIF1 might provide some insights about how ruthenium compounds induce the ER stress pathway [25,45]. Indeed, hypoxia has been shown to induce ER stress [46]. Furthermore, glucose deprivation is a known inducing condition for ER stress activation [47]. Therefore, by acting on the HIF1 pathway, in particular by reducing the expression of glucose transporter GLUT1, ruthenium complexes might favor ER stress.

We identified a PHD2-mediated protein degradation of HIF1A as one of the mechanisms involved in the quick loss of HIF1A proteins observed as early as 6 h after RDC11 treatment. Indeed, RDC11 elevated the level of HIF1A hydroxylation in cells, and blocking the activity of PHD2 with a selective inhibitor affected the ability of RDC11 to reduce HIF1A protein levels. In addition, RDC11 interacted directly with PHD2, an enzyme that controls HIF1A protein levels [37]. Finally, RDC11 induces the activity of purified PHD2 *in vitro*, unlike a non-cytotoxic ruthenium complex. Therefore, we believe that PHD2 is a direct target of RDC11 and that RDC11 might stimulate the activity of PHD2 by a mechanism yet to be discovered but that likely involves the redox potential of the ruthenium complex. However, our results clearly show that mechanisms other than interaction with PHD2 are involved as proteasome inhibitors do not reverse the level of HIF1A protein levels.

For instance, in addition to affecting HIF1A protein degradation, RDC11 drastically decreased *HIF1A* mRNA levels within 24 h, suggesting repression of the *HIF1A* promoter or destabilization of the *HIF1A* mRNA. The exact contribution of these mechanisms in RDC11-induced HIF1A protein loss and its nature remains to be investigated. Destabilization of *HIF1A* mRNA might involve change in expression of miRNA targeting HIF1A. In this respect, our bioinformatic analysis also showed that the aminoacyl tRNA biosynthesis and ribosome biogenesis are affected by RDC11. Both these pathways are known to be deregulated in cancer and linked to mTOR signaling, which is deployed by cancer cells to foster cell survival and proliferation via upregulation of protein biosynthesis [48]. Because RDC11 induces the ER stress pathway [25], which negatively regulates mRNA translation and crosstalk with mTOR [49], we believe that aminoacyl tRNA biosynthesis and ribosome biogenesis could also account for RDC11 anticancer activity. Preliminary results indicate that indeed, RDC11 inhibits the activity of mTOR (V. Vidimar and C. Gaiddon; unpublished observation). However, further investigation is needed to elucidate this.

Nevertheless, by impacting the activity of redox enzymes, the ruthenium compound RDC11 represents an innovative tool to manipulate the cellular metabolism and target cancer cells. Similar observations of inhibition of HIF1A protein levels and activity were done with variants of RDC11, such as RDC34 (C. Licona and C. Gaiddon; unpublished observations) also containing a Ru-C bond and the phenylpyridine and phenanthrolin ligands. This new information on the mode of action of ruthenium compounds is of high interest for anticancer therapy since key actors of tumorigenesis are affected by ruthenium complexes. The HIF1 pathway plays a prominent role in the nutritional status of cancer cells and makes them able to adapt to oxygen deprivation. Our observation that RDC11 reduced VEGF levels and angiogenesis may represent one of the aspects in support of its value for the control of cancer growth. In this respect, the identification of PHD2 as a one of the direct targets of a ruthenium compound alleviate a recurrent unresolved issue in our understanding of the mode of action of these compounds and critical bottleneck in designing more potent and more selective drugs. Interestingly, the regulation of PHD2 seems to be unique to ruthenium complexes with Ru-C bond, as previously shown with other enzymes [42]. Importantly, our results also clearly show that ruthenium complexes do not have a single target. PHD2 and glucose oxidase are not sufficient to explain all the cytotoxicity of RDC11 neither the loss of HIF1A expression. However, this multimodal intracellular action will help to bypass the development of resistances in cancer cells. As PHD2 and other redox enzymes are often ubiquitously present in cancer cells, it is expected that the effects observed in colon cancer cells might also happen in other cancer cell types, although this might have to be confirmed by additional studies.

Finally, when considering ruthenium complexes as a therapeutic alternative, this study highlights two characteristics that can been seen as critical advantages. The first is that platinum and ruthenium complexes clearly display a differential regulation of the HIF1 pathway, which shows that their mode of action differ significantly. Moreover, ruthenium compounds have a more complex mode of action, involving the alteration of the activity of redox enzymes responsible for the cellular metabolism. The fact that ruthenium-based drugs, unlike platinum drugs, target the tumor cells by affecting their metabolic needs, also

provides molecular basis to explain how these drugs can bypass cancer cell resistance mechanisms [21,25,26]. The second important feature is that ruthenium compounds are likely to target simultaneously multiple redox enzymes via their redox potential. This represent an advantage by reducing the ability of the tumors to easily develop resistance mechanisms, as seen when a unique target is aimed. These two properties, independence from p53/DNA damage and simultaneous redox targets, are competitive advantages that point to ruthenium compounds as anticancer drugs.

Conflicts of interest

The authors declare no conflict of interest.

Acknowledgment

Appendix A. Supplementary data

Supplementary data to this article can be found online at https://doi.org/10.1016/j.canlet.2018.09.029.

References

[1] J. Chiche, M.C. Brahimi-Horn, J. Pouyssegur, Tumour hypoxia induces a metabolic shift causing acidosis: a common feature in cancer, J. Cell Mol. Med. 14 (2010) 771–794.

[2] G.L. Semenza, Defining the role of hypoxia-inducible factor 1 in cancer biology and therapeutics, Oncogene 29 (2010) 625–634.

[3] K.I. Block, C. Gyllenhaal, L. Lowe, A. Amedei, A.R. Amin, A. Amin, K. Aquilano, J. Arbiser, A. Arreola, A. Arzumanyan, S.S. Ashraf, A.S. Azmi, F. Benencia, D. Bhakta, A. Bilsland, A. Bishayee, S.W. Blain, P.B. Block, C.S. Boosani, T.E. Carey, A. Carnero, M. Carotenuto, S.C. Casey, M. Chakrabarti, R. Chatuvedi, G.Z. Chen, H. Chen, S. Chen, Y.C. Chen, B.K. Choi, M.R. Ciriolo, H.M. Coley, A.R. Collins, M. Connell, S. Crawford, C.S. Curran, C. Dabrosin, G. Damia, S. Dasgupta, R.J. DeBerardinis, W.K. Decker, P. Dhawan, A.M. Diehl, J.T. Dong, Q.P. Dou, J.E. Drew, E. Elkord, B. El-Rayes, M.A. Feitelson, D.W. Felsher, L.R. Ferguson, C. Fimognari, G.L. Firestone, C. Frezza, H. Fujii, M.M. Fuster, D. Generali, A.G. Georgakilas, F. Giesder, M. Gilbertson, M.F. Green, B. Grue, G. Guha, D. Halicka, W.G. Helferich, P. Heneberg, P. Hentosh, M.D. Hirschey, L.J. Hofseth, R.F. Holcombe, K. Honoki, H.Y. Hsu, G.S. Huang, L.D. Jensen, W.G. Jiang, L.W. Jones, P.A. Karpowicz, W.N. Keith, S.P. Kerkar, G.N. Khan, M. Khatami, Y.H. Ko, O. Kucuk, R.J. Kulathinal, N.B. Kumar, B.S. Kwon, A. Le, M.A. Lea, H.Y. Lee, T. Lichtor, L.T. Lin, J.W. Locasale, B.L. Lokeshwar, V.D. Longo, C.A. Lyssiotis, K.L. MacKenzie, M. Malhotra, M. Marino, M.L. Martinez-Chantar, A. Matheu, C. Maxwell, E. McDonnell, A.K. Meeker, M. Mehrmohamadi, K. Mehta, G.A. Michelotti, R.M. Mohammad, S.I. Mohammed, D.J. Morre, V. Murslidhar, I. Muqbil, M.P. Murphy, G.P. Nagaraju, R. Nahta, E. Niccolai, S. Nowsheen, C. Panis, F. Pantano, V.R. Parslow, G. Pawelec, P.L. Pedersen, B. Poore, D. Poudyal, S. Prakash, M. Prince, I. Raffaghello, J.C. Rathmell, W.K. Rathmell, S.K. Ray, J. Reichrath, S. Rezazadeh, D. Ribatti, L. Ricciardiello, R.B. Robey, F. Rodier, H.P. Rupasinghe, G.L. Russo, E.P. Ryan, A.K. Samadi, I. Sanchez-Garcia, A.J. Sanders, D. Santini, M. Sarkar, T. Sasada, N.K. Saxena, R.E. Shackelford, H.M. Shantha Kumara, D. Sharma, D.M. Shin, D. Sidransky, M.D. Siegelin, E. Signori, N. Singh, S. Sivanand, D. Sliva, C. Smythe, C. Spagnuolo, D.M. Stafforini, J. Stagg, P.R. Subbarayan, T. Sundin, W.H. Talib, S.K. Thompson, P.T. Tran, H. Ungefroren, M.G. Vander Heiden, V. Venkateswaran, D.S. Vinay, P.J. Vlachostergios, Z. Wang, K.E. Wellen, R.L. Whelan, E.S. Yang, H. Yang, X. Yang, P. Yaswen, C. Yedjou, X. Yin, J. Zhu, M. Zollo, Designing a broad-spectrum integrative approach for cancer prevention and treatment, Semin. Canc. Biol. 35 (Suppl) (2015) S276–S304.

[4] F. Bernges, E. Holler, The reaction of platinum(II) complexes with DNA. Kinetics of intrastrand crosslink formation in vitro, Nucleic Acids Res. 19 (1991) 1483–1489.

[5] S. Benosman, I. Gross, N. Clarke, A.G. Jochemsen, K. Okamoto, J.P. Loeffler, C. Gaiddon, Multiple neurotoxic stresses converge on MDMX proteolysis to cause neuronal apoptosis, Cell Death Differ. 14 (12) (2007 Dec) 2047–2057.

[6] S. Benosman, X. Meng, Y. Von Grabowiecki, L. Palamiuc, L. Hritcu, I. Gross, G. Mellitzer, Y. Taya, J.P. Loeffler, C. Gaiddon, Complex regulation of p73 isoforms after alteration of amyloid precursor polypeptide (APP) function and DNA damage in neurons, J. Biol. Chem. 286 (2011) 43013–43025.

[7] M. Galanski, M.A. Jakupec, B.K. Keppler, Update of the preclinical situation of anticancer platinum complexes: novel design strategies and innovative analytical approaches, Curr. Med. Chem. 12 (2005) 2075–2094.

[8] P.C. Bruijnincx, P.J. Sadler, New trends for metal complexes with anticancer

[9] M.A. Jakupec, M. Galanski, V.B. Arion, C.G. Hartinger, B.K. Keppler, Antitumour metal compounds: more than theme and variations, Dalton Trans. (2008) 183–194.

[10] M. Markman, Toxicities of the platinum antineoplastic agents, Expet Opin. Drug Saf. 2 (2003) 597–607.

[11] L. Kelland, The resurgence of platinum-based cancer chemotherapy, Nat. Rev. Canc. 7 (2007) 573–584.

[12] C.S. Allardyce, P.J. Dyson, Ruthenium in medicine: current clinical uses and future prospects, Platin. Met. Rev. 45 (2001) 62.

[13] P.J. Dyson, G. Sava, Metal-based antitumour drugs in the post genomic era, Dalton Trans. (2006) 1929–1933.

[14] B.K. Keppler, W. Balzer, V. Seifried, Synthesis and antitumor activity of triazolium-bis(triazole)-tetrachlororuthenate (III) and bistriazolium-triazolepenta-chlororuthenate (III). Two representatives of a new class of inorganic antitumor agents, Arzneimittelforschung 37 (1987) 770–771.

[15] G. Sava, S. Pacor, S. Zorzet, E. Alessio, G. Mestroni, Antitumour properties of dimethylsulphoxide ruthenium (II) complexes in the Lewis lung carcinoma system, Pharmacol. Res. 21 (1989) 617–628.

[16] S. Fruhauf, W.J. Zeller, New platinum, titanium, and ruthenium complexes with different patterns of DNA damage in rat ovarian tumor cells, Cancer Res. 51 (1991) 2943–2948.

[17] R.E. Morris, R.E. Aird, S. Murdoch Pdel, H. Chen, J. Cummings, N.D. Hughes, S. Parsons, A. Parkin, G. Boyd, D.I. Jodrell, P.J. Sadler, Inhibition of cancer cell growth by ruthenium(II) arene complexes, J. Med. Chem. 44 (2001) 3616–3621.

[18] A. Bergamo, C. Gaiddon, J.H. Schellens, J.H. Beijnen, G. Sava, Approaching tumour therapy beyond platinum drugs Status of the art and perspectives of ruthenium drug candidates, J. Inorg. Biochem. 106 (2012) 90–99.

[19] H.Y. Mei, J.K. Barton, Tris(tetramethylphenanthroline)ruthenium(II): a chiral probe that cleaves A-DNA conformations, Proc. Natl. Acad. Sci. U. S. A. 85 (1988) 1339–1343.

[20] V. Brabec, DNA modifications by antitumor platinum and ruthenium compounds: their recognition and repair, Prog. Nucleic Acid Res. Mol. Biol. 71 (2002) 1–68.

[21] C. Gaiddon, P. Jeannequin, P. Bischoff, M. Pfeffer, C. Sirlin, J.P. Loeffler, Ruthenium (II)-derived organometallic compounds induce cytostatic and cytotoxic effects on mammalian cancer cell lines through p53-dependent and p53-independent mechanisms, J. Pharmacol. Exp. Therapeut. 315 (2005) 1403–1411.

[22] R.L. Hayward, Q.C. Schornagel, R. Tente, J.S. Macpherson, R.E. Aird, S. Guichard, A. Habtemariam, P. Sadler, D.I. Jodrell, Investigation of the role of Bax, p21/Waf1 and p53 as determinants of cellular responses in HCT116 colorectal cancer cells exposed to the novel cytotoxic ruthenium(II) organometallic agent, RM175, Cancer Chemother. Pharmacol. 55 (2005) 577–583.

[23] S. Chatterjee, S. Kundu, A. Bhattacharyya, C.G. Hartinger, P.J. Dyson, The ruthenium(II)-arene compound RAPTA-C induces apoptosis in EAC cells through mitochondrial and p53-JNK pathways, J. Biol. Inorg. Chem. 13 (2008) 1149–1155.

[24] M. Klajner, P. Hebraud, C. Sirlin, C. Gaiddon, S. Harlepp, DNA binding to an anticancer organo-ruthenium complex, J. Phys. Chem. B 114 (2010) 14041–14047.

[25] X. Meng, M.L. Leyva, M. Jenny, I. Gross, S. Benosman, B. Fricker, S. Harlepp, P. Hebraud, A. Boos, P. Wlosik, P. Bischoff, C. Sirlin, M. Pfeffer, J.P. Loeffler, C. Gaiddon, A ruthenium-containing organometallic compound reduces tumor growth through induction of the endoplasmic reticulum stress gene CHOP, Cancer Res. 69 (13) (2009 Jul 1) 5458–5466.

[26] V. Vidimar, X. Meng, M. Klajner, C. Licona, L. Fetzer, S. Harlepp, P. Hebraud, M. Sidhoum, C. Sirlin, J.P. Loeffler, G. Mellitzer, G. Sava, M. Pfeffer, C. Gaiddon, Induction of caspase 8 and reactive oxygen species by ruthenium-derived anticancer compounds with improved water solubility and cytotoxicity, Biochem. Pharmacol. 84 (2012) 1428–1436.

[27] A.D. Ryabov, V.S. Sukharev, L. Alexandrova, R. Le Lagadec, M. Pfeffer, New synthesis and new bio-application of cyclometalated ruthenium(II) complexes for fast mediated electron transfer with peroxidase and glucose oxidase, Inorg. Chem. 40 (2001) 6529–6532.

[28] L. Fetzer, B. Boff, M. Ali, M. Xiangjun, J.P. Collin, C. Sirlin, C. Gaiddon, M. Pfeffer, Library of second-generation cycloruthenated compounds and evaluation of their biological properties as potential anticancer drugs: passing the nanomolar barrier, Dalton Trans. 40 (2011) 8869–8878.

[29] H. Rico Bautista, R.O. Saavedra Diaz, L.Q. Shen, C. Orvain, C. Gaiddon, R. Le Lagadec, A.D. Ryabov, Impact of cyclometalated ruthenium(II) complexes on lactate dehydrogenase activity and cytotoxicity in gastric and colon cancer cells, J. Inorg. Biochem. 163 (2016) 28–38.

[30] F. Wang, J. Xu, A. Habtemariam, J. Bella, P.J. Sadler, Competition between glutathione and guanine for a ruthenium(II) arene anticancer complex: detection of a sulfenato intermediate, J. Am. Chem. Soc. 127 (2005) 17734–17743.

[31] M.A. Jakupec, E. Reisner, A. Eichinger, M. Pongratz, V.B. Arion, M. Galanski, C.G. Hartinger, B.K. Keppler, Redox-active antineoplastic ruthenium complexes with indazole: correlation of in vitro potency and reduction potential, J. Med. Chem. 48 (2005) 2831–2837.

[32] C. Licona, M.E. Spaety, A. Capuozzo, M. Ali, R. Santamaria, O. Armant, F. Delalande, A. Van Dorsselaer, S. Cianferani, J. Spencer, M. Pfeffer, G. Mellitzer, C. Gaiddon, A ruthenium anticancer compound interacts with histones and impacts differently on epigenetic and death pathways compared to cisplatin, Oncotarget 8 (2) (2017 Jan 10) 2568–2584.

[33] C. Gaiddon, M. de Tapia, J.P. Loeffler, The tissue-specific transcription factor Pit-1/GHF-1 binds to the c-fos serum response element and activates c-fos transcription, Mol. Endocrinol. 13 (1999) 742–751.

[34] C. Gaiddon, L. Mercken, C. Bancroft, J.P. Loeffler, Transcriptional effects in GH3 cells of Gs alpha mutants associated with human pituitary tumors: stimulation of adenosine 3',5'- monophosphate response element-binding protein-mediated

261

transcription and of prolactin and growth hormone promoter activity via protein kinase A, Endocrinology 136 (1995) 4331–4338.

[35] J.H. Lim, C. Luo, F. Vazquez, P. Puigserver, Targeting mitochondrial oxidative metabolism in melanoma causes metabolic compensation through glucose and glutamine utilization, Cancer Res. 74 (2014) 3535–3545.

[36] T. Zhang, W.L. Kraus, SIRT1-dependent regulation of chromatin and transcription: linking NAD(+) metabolism and signaling to the control of cellular functions, Biochim. Biophys. Acta 1804 (2010) 1666–1675.

[37] Q. Ke, M. Costa, Hypoxia-inducible factor-1 (HIF-1), Mol. Pharmacol. 70 (2006) 1469–1480.

[38] B.G. Wouters, M. Koritzinsky, Hypoxia signalling through mTOR and the unfolded protein response in cancer, Nat. Rev. Canc. 8 (2008) 851–864.

[39] A. Nandal, J.C. Ruiz, P. Subramanian, S. Ghimire-Rijal, R.A. Sinnamon, T.L. Stemmler, R.K. Bruick, C.C. Philpott, Activation of the HIF prolyl hydroxylase by the iron chaperones PCBP1 and PCBP2, Cell Metabol. 14 (2011) 647–657.

[40] L. Leyva, C. Sirlin, L. Rubio, C. Franco, R. Le Lagadec, J. Spencer, P. Bischoff, C. Gaiddon, J.P. Loeffler, M. Pfeffer, Synthesis of cycloruthenated compounds as potential anticancer agents, Eur. J. Inorg. Chem. (2007) 3055–3066.

[41] D.M. Noonan, R. Benelli, A. Albini, Angiogenesis and cancer prevention: a vision, Recent Results Canc. Res. 174 (2007) 219–224.

[42] A.D. Ryabov, Transition metal chemistry of glucose oxidase, horseradish peroxidase, and related enzymes, Adv. Inorg. Chem. 55 (2004) 201–270.

[43] F. Kruiswijk, C.F. Labuschagne, K.H. Vousden, p53 in survival, death and metabolic health: a lifeguard with a licence to kill, Nat. Rev. Mol. Cell Biol. 16 (2015) 393–405.

[44] Z. Ai, Y. Lu, S. Qiu, Z. Fan, Overcoming cisplatin resistance of ovarian cancer cells by targeting HIF-1-regulated cancer metabolism, Cancer Lett. 373 (2016) 36–44.

[45] M.J. Chow, C. Licona, G. Pastorin, G. Mellitzer, W.H. Ang, C. Gaiddon, Structural tuning of organoruthenium compounds allows oxidative switch to control ER stress pathways and bypass multidrug resistance, Chem. Sci. 7 (2016) 4117–4124.

[46] B. Kong, T. Cheng, W. Wu, I. Regel, S. Raulefs, H. Friess, M. Erkan, I. Esposito, J. Kleeff, C.W. Michalski, Hypoxia-induced endoplasmic reticulum stress characterizes a necrotic phenotype of pancreatic cancer, Oncotarget 6 (2015) 32154–32160.

[47] S.G. de la Cadena, K. Hernandez-Fonseca, I. Camacho-Arroyo, L. Massieu, Glucose deprivation induces reticulum stress by the PERK pathway and caspase-7- and calpain-mediated caspase-12 activation, Apoptosis: Int. J. Program. Cell Death 19 (2014) 414–427.

[48] A. Gentilella, S.C. Kozma, G. Thomas, A liaison between mTOR signaling, ribosome biogenesis and cancer, Biochim. Biophys. Acta 1849 (2015) 812–820.

[49] C. Appenzeller-Herzog, M.N. Hall, Bidirectional crosstalk between endoplasmic reticulum stress and mTOR signaling, Trends Cell Biol. 22 (2012) 274–282.

Aïna VENKATASAMY

Développement et utilisation d'outils d'analyses précliniques pour le traitement du cancer de l'estomac

École Doctorale
des Sciences de la Vie
et de la Santé
S T R A S B O U R G

Université
de Strasbourg

Résumé en français

Le cancer gastrique est un cancer complexe et hétérogène, de mauvais pronostic pour lequel il n'existe pas à l'heure actuelle de thérapie ciblée réellement efficace.

Durant ma thèse, j'ai développé et maintenu 5 xénogreffes dérivées de patients (PDX) différentes, relativement représentatives de la complexité des cancers gastriques (degré de différenciation cellulaire, statut p53/PD-L1..) avec un taux de réussite d'environ 21%. Nous avons ensuite caractérisé nos modèles animaux en imagerie petit animal (échographie, CT et IRM…) avec une comparaison à nos données histologiques et moléculaires appariées. Nous avons utilisé ces modèles pour le développement de nouvelles approches thérapeutiques (HDACi , RDC11…).

Nos résultats ont permis de développer différents modèles animaux et plusieurs protocoles expérimentaux qui seront utiles pour relever les défis posés par la complexités des cancers et notamment du cancer gastrique. Cela pose les prémisses du développement d'outils innovants pour le suivi de la croissance tumorale, l'étude des variations de la constitution du microenvironnement (ex. paysage immunitaire) et sur les tissus environnants (ex. les muscles), qui sont des éléments clés à considérer pour le développement de biomarqueurs, notamment our évaluer l'activité de nouvelles biothérapies ciblées, débouchant sur des prise en charges plus personnalisées de nos patients.

Mots clefs : cancer gastrique, modèles animaux, xénogreffes dérivées de patients, échographie, IRM, atrophie musculaire, paysage immunitaire, PD-L1

English summary

Gastric cancer is a complex and heterogeneous cancer with a poor prognosis, for which there is currently no truly effective targeted therapy. During my thesis, I have developed and maintained 5 different patient-derived xenografts (PDX), which are somehow representative of the complexity of gastric cancers (degree of cell differentiation, p53/PD-L1 status ..) with a success rate around 21%. We then characterized them with small animal imaging (ultrasound, CT and MRI, etc.) and compared them to paired histological and molecular data. The overall idea behind the development of such novel animal models is to use them for the development of new therapeutic approaches and innovant molecules, some of which we have already tested in our laboratory (HDACi, RDC11…). The development of different animal models and several experimental protocols will be useful to meet some of the challenges issued from the complexities of cancers and gastric ones especially. This lays the foundations for the development of innovative tools to monitor tumor growth, study variations in the tumor microenvironment (e.g. immune landscape) and in surrounding tissues (e.g. muscles), which are keys elements to consider for the development of biomarkers designed to evaluate of the activity of new targeted biotherapies, leading to more personalized care for our patients.

Keywords : gastric cancer, mouse models, patient-derived xenografts, MRI, ultrasound, muscle atrophy, immune checkpoint, PD-L1